DOC.20070822.0003

QA: QA

MDL-NBS-HS-000010 REV 03

August 2007

Site-Scale Saturated Zone Transport

Prepared for:
U.S. Department of Energy
Office of Civilian Radioactive Waste Management
Office of Repository Development
1551 Hillshire Drive
Las Vegas, Nevada 89134-6321

Prepared by:
Sandia National Laboratories
OCRWM Lead Laboratory for Repository Systems
1180 Town Center Drive
Las Vegas, Nevada 89144

Under Contract Number
DE-AC04-94AL85000

DISCLAIMER

This report was prepared as an account of work sponsored by an agency of the United States Government. Neither the United States Government nor any agency thereof, nor any of their employees, nor any of their contractors, subcontractors or their employees, makes any warranty, express or implied, or assumes any legal liability or responsibility for the accuracy, completeness, or any third party's use or the results of such use of any information, apparatus, product, or process disclosed, or represents that its use would not infringe privately owned rights. Reference herein to any specific commercial product, process, or service by trade name, trademark, manufacturer, or otherwise, does not necessarily constitute or imply its endorsement, recommendation, or favoring by the United States Government or any agency thereof or its contractors or subcontractors. The views and opinions of authors expressed herein do not necessarily state or reflect those of the United States Government or any agency thereof.

QA: QA

Site-Scale Saturated Zone Transport

MDL-NBS-HS-000010 REV 03

August 2007

Model Signature Page/Change History

Complete only applicable items.

1. Total Pages: 422

2. Type of Mathematical Model

☒ Process Model ☐ Abstraction Model ☐ System Model

Describe Intended Use of Model

The purpose of the site-scale SZ transport model is to simulate transport in saturated porous rock and alluvium.

3. Title

Site-Scale Saturated Zone Transport

4. DI (including Revision No. and Addendum No.):

MDL-NBS-HS-000010 REV 03

	Printed Name	Signature	Date
5. Originator	S. Kelkar	Sharad Kelkar	8/16/2007
6. Independent Technical Reviewer	M. Zhu		8/16/07
7. Checker	A. Eddebbarh		8/16/07
8. QCS/Lead Lab QA Reviewer	S. Kassabian-Darnell	Sonnia K. Darnell	08/17/07
9. Responsible Manager/Lead	B. Arnold for	Kenneth Rehfeldt	08/17/07
10. Responsible Manager	S. Kuzio		08/17/07

11. Remarks

Change History

12. Revision No. and Addendum No.	13. Description of Change
REV 00	Initial issue
REV 01	Revision includes additional data and parameters. No change bars were used because of the extensive nature of the changes.
REV 01 Errata 001	Response to CR 1162
REV 01 Errata 002	Response to CR 821 and CR 2019
REV 02	Increased transparency in response to the regulatory-focused evaluation performed by the Regulatory Integration Team. Entire model documentation was revised. Side bars are not used because the changes were too extensive to use Step 5.8f)1) per AP-SIII.10Q, REV 02, ICN 07.

REV 03	This revision incorporates the revised SZ site scale flow model and revised K_d distributions in response to *Technical Work Plan For: Saturated Zone Analysis and Model Report Integration* (BSC 2006 [DIRS 177375]. This model report addresses the Condition Reports (CR) associated with previous versions as follows: • CR 5600 (action 5600-007) identified direct inputs for which the specific part of the source was not identified in DIRS. In the present revision, specific parts of direct inputs are identified. • CR 8670 (action 8670-002) identified errors in Table A-4 which have now been corrected. • CR 10668 identified errors in four tables in Appendices A, G, and I, which have now been corrected. The entire model documentation was revised and, because of the extensive nature of the changes, change bars were not used in this revision.

CONTENTS

Page

CONTENTS (Continued)

Page

CONTENTS (Continued)

Page

CONTENTS (Continued)

Page

FIGURES

Page

FIGURES (Continued)

Page

FIGURES (Continued)

Page

FIGURES (Continued)

Page

FIGURES (Continued)

Page

FIGURES (Continued)

Page

FIGURES (Continued)

Page

FIGURES (Continued)

Page

TABLES

Page

TABLES (Continued)

Page

ACRONYMS AND ABBREVIATIONS

ATC	(Nye Country) Alluvial Testing Complex
BTC	breakthrough curve
CDF	cumulative distribution function
CNWRA	Center for Nuclear Waste Regulatory Analysis
DIRS	Document Input Reference System
DO	dissolved oxygen
DTN	Data Tracking Number
EWDP	Early Warning Drilling Program
FEHM	Finite Heat-Mass Transfer
FEPs	features, events, or processes
LANL	Los Alamos National Laboratory
M	moles per liter
NC-EWDP	Nye County Early Warning Drilling Program
NNWSI	Nevada Nuclear Waste Storage Investigations
NRC	U.S. Nuclear Regulatory Commission
NTS	Nevada Test Site
ORP	oxidation/reduction potential
PFBA	pentafluorobenzoic acid
QA	quality assurance
QAM	Quality Assurance Manual
SHE	standard hydrogen electrode
SME	subject matter expert
SNL	Sandia National Laboratory
STN	software tracking number
SZ	saturated zone
TSPA	total system performance assessment
TWP	technical work plan
XRD	X-ray diffraction
YMP	Yucca Mountain Project
YMRP	*Yucca Mountain Review Plan, Final Report*

INTENTIONALLY LEFT BLANK

1. PURPOSE

This work provides a process-level site-scale transport model for calculating radionuclide transport in the saturated zone at Yucca Mountain and for use in the saturated zone (SZ) flow and transport abstraction model in support of total system performance assessment (TSPA). The purpose of this model report is to provide documentation for the components of the site-scale SZ transport model in accordance with SCI-PRO-006, *Models*.

The model report has been revised in accordance with *Technical Work Plan For: Saturated Zone Analysis and Model Report Integration* (BSC 2006 [DIRS 177375], Sections 2.1.4 and 2.2.4) to incorporate the revised SZ site-scale flow model (SNL 2007 [DIRS 177391], Sections 4 and 6) and revised sorption coefficient (K_d) distributions (Appendices A and C). Although this TWP was prepared before transition to the Lead Laboratory, it was considered appropriate for developing this report because it was prepared in compliance with LP-2.29Q-BSC, *Planning for Science Activities* (a BSC procedure (predecessor)), which corresponds to SCI-PRO-002, *Planning for Science Activities* (the Lead Laboratory procedure). This report deviates from *Technical Work Plan For: Saturated Zone Analysis and Model Report Integration* (BSC 2006 [DIRS 177375], Section 2.2.4.1) by excluding validation activities item #3. This item was not needed because the kinetics-based colloid transport has not been incorporated into the compliance model. This report documents: (1) the advection-dispersion transport model including matrix diffusion (Sections 6.3 and 6.4); (2) a description and validation of the transport model (Sections 6.3 and 7); (3) the numerical methods for simulating radionuclide transport (Section 6.4); (4) the parameters K_d and their uncertainty distributions used for modeling radionuclide sorption (Appendices A and C); (5) the parameters used for modeling colloid-facilitated radionuclide transport (Table 4-1, Section 6.4.2.6, and Appendix B); and (6) alternative conceptual models and their dispositions (Section 6.6).

The intended use of this model is to simulate transport in saturated fractured porous rock and alluvium. The particle-tracking method of simulating radionuclide transport is incorporated in the finite-volume heat and mass transfer numerical analysis (FEHM) computer code, (FEHM V2.24-01, STN: 10086-2.24-01 [DIRS 179419]) and is described in Section 6.4. FEHM is a three-dimensional, finite-volume, finite-element, heat and mass flow-and-transport code.

This report documents the features and capabilities of the site-scale transport model for calculating radionuclide transport in the saturated zone at Yucca Mountain in support of the TSPA. Correlative flow-model calculations using FEHM are carried out and documented in *Saturated Zone Site-Scale Flow Model* (SNL 2007 [DIRS 177391], Sections 6, 7 and 8). The velocity fields are calculated by the flow model independent of the transport processes and supplied as a part of the output package from the flow model, which is then used as inputs to the transport model. Several SZ reports provide information and data needed as feed-ins for this report, and this report in turn provides technical product outputs that feed into other SZ reports. The details of inputs to the site-scale transport model are provided in Section 4.

Figure 1-1 shows the relationship of this report to other model reports that also pertain to flow and transport in the saturated zone and also shows the flow of key information among the SZ reports. Figure 1-1 does not contain a complete representation of the data and parameter inputs and outputs, nor does it show inputs external to this suite of SZ reports. The primary input

model to this report is the SZ site-scale flow model. In addition, several other reports provide the technical basis for the conceptual models of radionuclide transport in fractured and porous media and in association with groundwater colloids. Table 4-1 provides a complete listing and justification of the input data. The output model from this report is the SZ site-scale transport model, which forms the basis of the abstraction models for use in the TSPA. Table 8.2-1 lists outputs from this report.

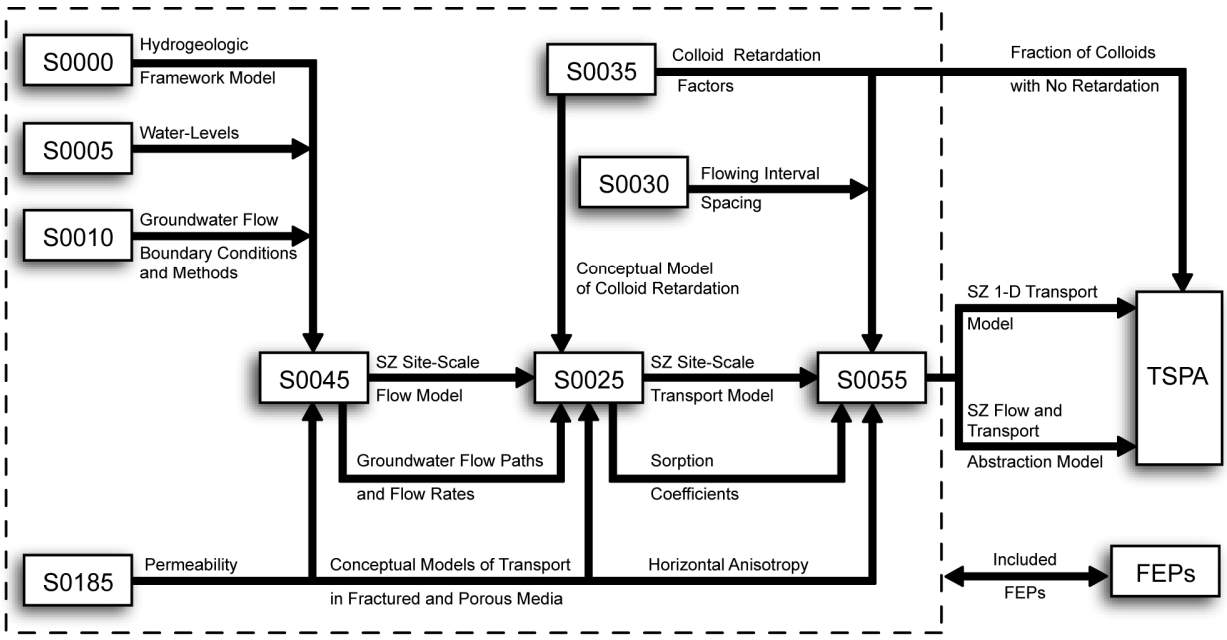

Legend

S0000 - Hydrogeologic Framework Model	MDL-NBS-HS-000024
S0005 - Water-Level Data Analysis	ANL-NBS-HS-000034
S0010 - Recharge and Lateral Groundwater Flow Boundary Conditions	ANL-NBS-MD-000010
S0025 - Site-Scale Saturated Zone Transport	MDL-NBS-HS-000010
S0030 - Probability Distribution for Flowing Interval Spacing	ANL-NBS-MD-000003
S0035 - Saturated Zone Colloid Transport	ANL-NBS-HS-000031
S0045 - Site-Scale Saturated Zone Flow Model	MDL-NBS-HS-000011
S0055 - Saturated Zone Flow and Transport Model Abstraction	MDL-NBS-HS-000021
FEPs - Features, Events, and Processes in SZ Flow and Transport	DTN: MO0706SPAFEPLA.001
S0185 - Saturated Zone In-Situ Testing	ANL-NBS-HS-000039

00438DC_001e.ai

Figure 1-1. A Schematic of the Flow of Information Among Saturated Zone Reports

The geohydrologic setting to be modeled is complex, with multifaceted and diverse geochemical interactions possible between the groundwater, solutes, and geological materials. Also, the intended use by the TSPA requires a computationally efficient model that is amenable to repeated runs for stochastic simulations. The approach taken in this report is to construct a plausible conceptual model of transport that represents the important SZ transport processes and also supports the TSPA. Alternate conceptual models and the implications of these models for transport predictions are evaluated relative to the base-case model. A number of relevant features, events, and processes (FEPs) are included in this report (Section 6.2). The manner of their inclusion is described in various sections of this report. The FEPs are discussed in the LA

FEP List (Data Tracking Number (DTN): MO0706SPAFEPLA.001 [DIRS 181613], filename: *FEPs_be.mdb, Table 7.1-1*) The transport of chemical species in groundwater generally leads to retardation of the transported species with respect to the bulk movement of the groundwater. The radionuclide transport times can be several orders of magnitude longer than those for the bulk water. The processes of importance to the site-scale SZ transport model are advection, radionuclide dispersion, diffusion into the porous rock matrix and subsequent radionuclide sorption onto matrix surfaces, and colloid-facilitated radionuclide transport. These processes are included in the site-scale SZ transport model. Justification for the model including detailed references, along with a discussion of alternate conceptual models is presented in Sections 6.3, 6.4 and 6.6. The sorption of radionuclides onto fracture surfaces is not included in this model as a conservative approach.

The process of radionuclide adsorption within the rock matrix is represented using a sorption coefficient (K_d) approach, which is presented in this report with justification for its use (Sections 6.3, 6.4, 6.6, and Appendix A). Probability distributions for the K_d values for radionuclides of interest are derived based on data from the field, laboratory, and literature; models of sorption reactions; and expert judgment. The probability distributions are designed to include expected variations in environmental parameters that can influence the sorption behavior of the radionuclides of interest. To make the transport calculations more efficient computationally, the approach taken is to use two separate single-valued sorption coefficients to calculate transport rates in the volcanic and alluvial portions of the flow path in the saturated zone. The justification for this approach is provided in this report (Appendices A and C). Also, the process of colloid-facilitated radionuclide transport is represented using the colloid partition coefficient (K_c) approach. This modeling approach and its justification are presented in this report (Sections 6.3, 6.4, 6.6, and Appendix B).

The methodology for computing the transport of radionuclides within the saturated zone has been revised to capture a variety of different processes. This document presents the conceptual, mathematical, and computational aspects of a radionuclide transport model for the saturated zone and satisfies a requirement of the Yucca Mountain Project (YMP) to produce scientifically defensible transport predictions. The numerical techniques required to implement the method are described in Section 6.4.

Model validation activities presented in this report provide increased confidence that the model is a reasonable representation of the transport at Yucca Mountain near the repository site (Section 7). Because of the time and spatial scales involved and the fact that radionuclides cannot be used as tracers in field experiments, postdevelopment validation is limited to two activities involving naturally occurring geochemical constituents, and confidence-building activities during model development are also documented in the validation section of this report. Recognizing that the model is being used to perform probabilistic calculations in which parameter uncertainties are propagated through the model, the intent of this validation is to confirm that radionuclide parameters and processes included in the site-scale SZ transport model are adequately represented with sufficient accuracy. Confidence building during model development (Section 7.1) is carried out by a series of different approaches that include: (1) comparison to analogue sites, (2) submodel-data comparisons, (3) model-data comparisons, and (4) comparison with data published in referenced journals. The data used in confidence building for the relevant transport parameters (e.g., sorption coefficients), submodel processes

(e.g., advection, sorption), and site-scale model processes (e.g., flow pathways, transit times) are based on laboratory testing, field tests, natural analogue sites, and expert elicitations. Postdevelopment validation (Section 7.2) is carried out by comparison of model predictions with inferences based on geochemical data. By demonstrating that the parameters and processes selected have an experimental or observational basis, the model is validated for use in a stochastic analysis that establishes ranges of potential behavior of the SZ transport system.

The technical output of this report is composed of the site-scale SZ transport model and associated input and output files (base-case transport files); and SZ distribution coefficients (K_ds) data for uranium, neptunium, plutonium, cesium, americium, protactinium, strontium, thorium, radium, carbon, technetium, iodine, tin and selenium (Table C-14). The output breakthrough curves (BTC) and transport times will be integrated into the SZ flow and transport abstractions model for use in the TSPA calculations.

When using the site-scale SZ transport model for calculations, limitations are:

- *Input parameter values/ranges*. The transport model is intended for use with stochastic simulations using large uncertainty ranges for particular parameters such as specific discharge, flowing interval spacing and aperture, diffusion coefficient, and sorption coefficients. Care should be exercised in interpreting individual simulations for single sets of parameter values. Also, care should be exercised if the parameters that are used fall outside the range of parameter values (Table 4-2) or outside the range established by model validation (Section 7.3).

- *Sufficient number of input particles for particle tracking*. Radionuclide transport is implemented in the site-scale SZ transport model using particle tracking with a random walk method (Sections 6.4.2.3 and 6.4.2.4). To obtain reproducible results, a sufficient number of particles must be input into the model. The base-case transport model utilizes 500 input particles (output DTN: LA0702SK150304.001), considered on the basis of expert judgment and previous experience to be sufficient for obtaining a smooth BTC at the boundary of the accessible environment at 18 km (Figure 6.5-1). However, a larger number of input particles may be required, depending on the purpose of the model use.

Note that the six-digit numerical identifier following each reference callout is the YMP Document Input Reference System (DIRS) number, the purpose of which is to assist in locating a specific reference in the reference list in Section 9 and in the DIRS database.

2. QUALITY ASSURANCE

The Yucca Mountain Quality Assurance (QA) program applies to the development of this technical product. *Technical Work Plan for Saturated Zone Flow and Transport Modeling* (BSC 2006 [DIRS 177375], Sections 2.1.4 and 2.2.4) determined this activity to be subject to *Quality Assurance Requirements and Description* (QARD) (DOE 2007 [DIRS 182051]) requirements. The site-scale SZ transport model development and model validation was conducted under this TWP. Approved QA procedures identified in the technical work plan have been used to conduct and document the activities described in this model report. The electronic management of data was accomplished in accordance with the controls specified in the TWP (BSC 2006 [DIRS 177375], Section 8) and the Lead Laboratory procedure, IM-PRO-002, *Control of the Electronic Management of Information*. This model report provides a validated site-scale SZ transport model that is important in demonstrating compliance with the postclosure performance objectives prescribed in 10 CFR 63.113 [DIRS 180319]. Therefore, the saturated zone is classified in *Q-List* (BSC 2005 [DIRS 175539], Table A-1) as "SC" (safety category), reflecting its importance to waste isolation.

INTENTIONALLY LEFT BLANK

3. USE OF SOFTWARE

3.1 SOFTWARE TRACKED BY CONFIGURATION MANAGEMENT

The computer software code used as the basis to model SZ transport in this report is FEHM. This version of the code includes the particle-tracking algorithm described in this report and was obtained from Software Configuration Management. The other codes listed in Table 3-1 were used in the analysis described in the appendices. All were obtained from Software Configuration Management, used only within the range of validation as required by IM-PRO-003, *Software Management*, Revision 1, and are appropriate for the application in this report. Input and output files for this report are listed in Section 8.2.2 and identified in the respective discussions in Sections 6, 7, and 8.

Table 3-1. Computer Software and Routines

Software Title/Version Number	Software Tracking Number	Code Usage	Computer: Type, Platform, and Location	References
FEHM V 2.24-01-00	10086-2.24-01	Used for calculations throughout this model report. The FEHM V 2.24-01 application is based on a finite-volume/ finite-element heat- and mass-transfer code that simulates nonisothermal, multiphase, multicomponent flow and solute transport in porous media.	Sun, PC Sun OS 5.9, Microsoft Windows 2000, 2003 and XP, Red Hat Linux 2.4.21, Location: LANL	[DIRS 179419]
FEHM V2.20	10086-2.20-00	Used for calculations in Appendix C of this model report. The FEHM V 2.20 application is based on a finite-volume/ finite-element heat- and mass-transfer code that simulates nonisothermal, multiphase, multicomponent flow and solute transport in porous media.	Sun, PC Sun OS 5.7 & 5.8, Windows 2000, RedHat, Linux 7.1 Location: LANL	[DIRS 161725]
cr8sptr.c V 2.0	10927-2.0-00	Used to create an input file for sptr macro in FEHM.	Sun, Sun OS 5.7, Location: LANL	[DIRS 163836]
calc_cdf.c V 1.0	10924-1.0-00	Used to calculate the cumulative distribution function of the stochastic distributions of K_d.	Sun, Sun OS 5.7, Location: LANL	[DIRS 149117]
GS2FEHM.C V 1.0	10923-1.0-00	Used to create an input file for the perm macro in FEHM.	Sun, Sun OS 5.7, Location: LANL	[DIRS 163837]
GSLIB V1.0GAMV3V1.201	10398-1.0GAM V3V1.201-00	Used to calculate a three dimensional variogram of input data.	Sun, Sun OS 5.5.1, Location: LANL	[DIRS 153099]
GSLIB V2.0MSISIMV2.0	10098-2.0MSI SIMV2.0-00	Used to generate a stochastic distribution of parameters, such as K_d and permeability.	Sun, UNIX, Location: LANL	[DIRS 149114]

Table 3-1. Computer Software and Routines (Continued)

Software Title/Version Number	Software Tracking Number	Code Usage	Computer: Type, Platform, and Location	References
PHREEQC V 2.3	10068-2.3-01	Calculates surface complexation reactions for radionuclides.	PC Windows 2000 Location: LANL	[DIRS 157837]
RELAP V2.0	10551-2.0-00	Generate BTCs	PC, Windows 2000/NT Location : LANL	[DIRS 159065]
FRACT_p V1.0	11009-1.0-00	Calculates data that correlate concentrations with time for transport in the fractured media.	PC, LINUX 2.4.18, Location: LANL	[DIRS 164509]
fehm2post V.1.0	11031-1.0-00	Software is a set of perl scripts used to automate the repetitive series of steps required to make multiple runs of FEHM and post-process the output data.	WINDOWS 2000, SUN O.S 5.8&5.7, Redhat Linux 2.4.18	[DIRS 165754]
fehm2post V.1.0	11031-1.0-01	Software is a set of perl scripts used to automate the repetitive series of steps required to make multiple runs of FEHM and post-process the output data.	SUN O.S 5.9	[DIRS 181225]
EarthVision 5.1	10174-5.1-00	This software was used for plotting and visualization of data	Silicon Graphics Octane workstation running IRIX 6.5	[DIRS 167994]

LANL = Los Alamos National Laboratory; OS = operating system; PC = personal computer.

3.2 EXEMPT SOFTWARE

Commercial, off-the-shelf software used in support of this model report is listed in Table 3-2. This software is exempt from the requirements of IM-PRO-003, *Software Management*.

Table 3-2. Exempt Software

Software Name and Version	Description	Computer and Platform Identification
Microsoft Excel 2000	Used for preparing spreadsheets of data and plotting graphs. No data analysis was done with this software. Only built-in standard functions in this software were used. No software routines or macros were used with this software to prepare this report. The output was visually checked for correctness.	PC, Microsoft Windows 2000/NT

Table 3-2. Exempt Software(Continued)

Software Name and Version	Description	Computer and Platform Identification
Tecplot 360	Used for plotting and visualization of analysis results in figures shown in this report. No data analysis was done with this software. Only built-in standard functions in this software were used. No software routines or macros were used with this software to prepare this report. The output was visually checked for correctness.	PC, Microsoft Windows 2000/NT, Sun with UNIX OS, FORTRAN
BestFit V4.5 (a subset of @RISK V 4.5 STN 600806-4.5-00), Serial # 11874954, March 2000, Palisade Corporation, 798 Cascadilla Street, Ithaca, NY 14850	A statistic program that finds the distribution that best fits given data. Output of this program was used only as a guide for the selection of the distribution functions. Only built-in standard functions in this software were used. No software routines or macros were used with this software to prepare this report. The output was visually checked for correctness.	PC, Microsoft Windows 2000/NT

PC = personal computer.

INTENTIONALLY LEFT BLANK

4. INPUTS

4.1 DIRECT INPUTS

This section identifies all input data and parameters that are used in this modeling activity. The data providing input for the development of parameters used in the modeling activities documented in this report are listed in Table 4-1. Several SZ reports provide information and data needed as feed-ins for this report, and this report in turn provides technical product outputs that feed into other SZ reports. This flow of information is shown schematically in Figure 1-1. The base-case SZ site-scale flow model (DTN: SN0612T0510106.004 [DIRS 178956]) forms the starting point data for this transport model. The development of this flow model, including the conceptual model, various alternate conceptual models, the choice of parameter values for base-case flow model, and the appropriateness of data and technical information used in this model are discussed in detail in *Saturated Zone Site-Scale Flow Model* (SNL 2007 [DIRS 177391], Sections 4 and 6). For a number of parameters that are needed in the transport model, the selection of ranges of values and uncertainty distributions are presented in *Saturated Zone Flow and Transport Model Abstraction* (SNL 2007 [DIRS 181650]). Where available, sorption coefficient data for radionuclides of interest on rock and water samples from Yucca Mountain were used for developing the K_d distributions that are used in this model report, as described in detail in Appendix A. These sorption coefficient data were augmented by technical information available in the literature on systems with similar geochemical characteristics and qualified as appropriate. Mineralogic composition data are available on core samples taken from boreholes in the Yucca Mountain area. Since these data are site specific, they were considered the most appropriate data for use in stochastic analysis of K_d distributions described in Appendix C. These input data and technical information and their sources are provided in Table 4-1. The range of values for the specific discharge multiplier and flowing interval spacing were developed in *Saturated Zone Flow and Transport Model Abstraction* (SNL 2007 [DIRS 181650], Section 6.5.2[a]). Parameters needed for modeling colloid-facilitated transport (Table 4-2) were developed in *Saturated Zone Colloid Transport* (BSC 2004 [DIRS 170006], Sections 6.4, 6.5, and 6.6) and *Waste Form and In-Drift Colloids-Associated Radionuclide Concentrations: Abstraction and Summary* (SNL 2007 [DIRS 177423], Section 6.3). Justification for the choice of data and technical information for selecting the range of values (presented in Table 4-2) of all other parameters needed for the site-scale SZ transport model is given in detail in *Saturated Zone Flow and Transport Model Abstraction* (SNL 2007 [DIRS 181650], Section 6.5.2). The qualification of DTNs: LA0310AM831341.001 [DIRS 165865] and LA0305AM831341.001 [DIRS 163789] is presented in Appendix H, and the qualification of water composition as documented by Ogard and Kerrisk (1984 [DIRS 100783]) is presented in Appendix I. The qualification status of the remaining input sources is provided in the Technical Data Management System. A discussion of the selection of the range of values for each model parameter using the available data is presented in Section 4.1.2.

Table 4-1. Input Data and Technical Information

Data Description	Source/ Data Tracking Number
Data and Technical Information for Uncertainty Distribution of Parameters	
Uncertainty distribution for parameters used in the saturated zone transport abstractions model	SN0310T0502103.009 [DIRS 168763], *DTN-SN0310T0502103.009.zip\Table 6-8_updated.doc,* SN0706INPUTSZF.000 [DIRS 182007], file *updated_SZ_inputs_table.doc*
Data and Technical Information for Base-Case Flow Model	
FEHM V2.24 files for base-case saturated zone site-scale flow model	SN0612T0510106.004 [DIRS 178956], *SZ Flow Model.zip*
Data and Technical Information for Sorption Coefficient Data	
Thermodynamic database for PHREEQC modeling calculation of radionuclide sorption coefficient	MO0604SPAPHR25.001[DIRS 176868], *phreeqcDATA025.dat*
Americium, protactinium, plutonium, and thorium sorption coefficients on silica and surface area for silica sample	Allard et al. 1983 [DIRS 162982], pp. 6, 9, 10, 12; Allard et al. 1980 [DIRS 104410], p. 478; Beall et al. 1986 [DIRS 162983], entire document. See Appendix L, Sections L1 and L2 for justification of the use of the data
Density of sorption sites on the solid surface; uranium and neptunium surface complexation binding constants on silica	Pabalan et al. 1998 [DIRS 162987], p. 124 See Appendix L, Section L3 for the justification of the use of the data
Batch sorption coefficient data for barium on Yucca Mountain tuffs in representative water compositions	LA0407AM831341.001 [DIRS 170623], *BARIUM(RIT).xls*
Batch sorption coefficient data for cesium on Yucca Mountain tuffs in representative water compositions	LA0407AM831341.002 [DIRS 170621]
Batch sorption coefficient data for strontium on Yucca Mountain tuffs in representative water compositions	LA0407AM831341.003 [DIRS 170626], *STRONTIUM(RIT).xls*
Batch sorption coefficient data for neptunium on Yucca Mountain tuffs in representative water compositions	LA0407AM831341.004 [DIRS 170622], *NEPTUNIUM(RIT).xls*
Batch sorption coefficient data for plutonium on Yucca Mountain tuffs in representative water compositions	LA0407AM831341.005 [DIRS 170625], *PLUTONIUM(RIT).xls*
Batch sorption coefficient data for uranium on Yucca Mountain tuffs in representative water compositions	LA0407AM831341.006 [DIRS 170628], *URANIUM(RIT).xls*
Neptunium, uranium, plutonium, barium, strontium, sorption coefficients on Yucca Mountain tuffs	LA0305AM831341.001 [DIRS 163789] (Data are qualified in Appendix H) *Am Sorption Rations.xls, Ba Sorption Rations.xls, Np Sorption Rations.xls, Pa Sorption Rations.xls, Pu Sorption Rations.xls, Sr Sorption Rations.xls, Th Sorption Rations.xls, U Sorption Rations.xls* LA0302MD831341.003 [DIRS 163784], *Np-237.txt* LA0302MD831341.004 [DIRS 163785], *U-233.doc*

Table 4-1. Input Data and Technical Information (Continued)

Data Description	Source/ Data Tracking Number
Data and Technical Information for Sorption Coefficient Data (Continued)	
Sorption/desorption measurements of cesium on Yucca Mountain tuff	LA0310AM831341.001 [DIRS 165865] (Data are qualified in Appendix H), *Cs Sorption Ratios_new.xls* and *Cs Sorption Ratios.xls*
Water chemistry for J-13 water and pH in p#1 water	MO0007MAJIONPH.011 [DIRS 151524]
FLUORINE ABUNDANCE DATA FROM UE-25 P#1 TAKEN ON FEBRUARY 09,1983	SN0705FLUORINE.001 [DIRS 182006] (data qualified in appendix M)
Deprotonation constants and binding constants for aluminum and silica	Dixit and Van Cappellen 2002 [DIRS 162985], p. 2,565 See Appendix L, Section L5 for the justification of the use of the data
Binding constants for sodium on silica	Marmier et al. 1999 [DIRS 162986], p. 228 See Appendix L, Section L6 for the justification of the use of the data
Binding constants for neptunium on silica	Turner et al. 1998 [DIRS 162989], p. 264 See Appendix L, Section L4 for the justification of the use of the data
Water compositions for samples from wells J-13 and p#1	Ogard and Kerrisk 1984 [DIRS 100783] Data are qualified in Appendix I
Se (selenium) and Sn (tin) sorption on Yucca Mountain rock samples.	LA0702AM831341.001[DIRS 179306], *Se Sn DTN.R1.xls*
Colloid retardation factors for the Saturated Zone Alluvium	LA0303HV831352.004 [DIRS 163559], *Alluvium_retardation.txt*
Boundary of the Accessible Environment at 18 km	
Boundary of the accessible environment	10 CFR 63.302 [DIRS 180319] See NOTES for the justification of the use of the data
Data and Information for Stochastic Modeling of K_d	
Mineralogic data for Yucca Mountain.	LASC831321AQ98.001 [DIRS 109047], Table S98084_002
XRD data describing mineralogic composition of core samples from wells	Chipera et al. 1995 [DIRS 111081], entire document LA000000000086.002 [DIRS 107144], Table S97218_001
XRD data describing mineralogic composition of core samples from wells	LAJC831321AQ98.005 [DIRS 109004], Table S97218_001 LASC831321AQ98.001 [DIRS 109047], Table S98084_002 LADV831321AQ99.001 [DIRS 109044], Tables S99203_001, and S99203_002 MO0408K8313211.000 [DIRS 171437], *zz_sep_252605.zip, zz_sep_252606.zip, zz_sep_252607.zip, zz_sep_252608.zip, zz_sep_252609.zip, zz_sep_252610.zip*
XRD data describing mineralogic composition of core samples from wells	MO0101XRDMINAB.001 [DIRS 163796], MO0106XRDDRILC.003 [DIRS 163797], MO0101XRDDRILC.002 [DIRS 163795]

Table 4-1. Input Data and Technical Information (Continued)

Data Description	Source/ Data Tracking Number
Data and Information for Stochastic Modeling of K_d (Continued)	
Values of diffusion coefficients used for stochastic analysis	LA0003JC831362.001 [DIRS 149557], Table S00230_001 (Data qualified in Appendix K)
Hydraulic gradient used in stochastic modeling on a 550-m block	LA0511SK831214.001 [DIRS 175769], *hydraulic.zip*

NOTES: The accessible environment is any point outside of the controlled area, which must not extend farther south than 36°40'13.6661" North latitude, in the predominant direction of ground-water flow" in 10 CFR 63.302 [DIRS 180319]. This latitude is approximately 18 km south of the southern boundary of the repository footprint. It is refered to as the 'boundary to the accessible environment at 18 km' in this report, and it is used as an input to the site-scale SZ transport model for calculating BTCs. Any radionuclides crossing the vertical east-west plane across the entire site-scale SZ flow model, 18 km downstream from the repository footprint, are counted as breakthrough particles. This boundary is established by 10 CFR 63.302 [DIRS 180319], which, as a code of federal regulations, is judged to be an established fact.

EWDP = Early Warning Drilling Program; XRD = X-ray diffraction.

4.1.2 Parameters and Parameter Uncertainty

The range of values for each input parameter is presented in Table 4-2 and discussed in Sections 4.1.2.1 to 4.1.2.18 and in Appendix A. The ranges of sorption coefficient values presented in Table 4-2 encompass all the radionuclides of interest since the intent of this report is to present a site-scale SZ transport model that can be used by the TSPA with any of these radionuclides. The distributions for individual radionuclides are presented in Table C-14. The base transport model presents the case of non-sorbing radionuclides. The non-sorbing radionuclides in solution travel faster than the sorbing radionuclides since the movement of the later is retarded due to their tendency to bind to rock surfaces, as discussed in Section 6.3. An exception to this is the case of colloid facilitated transport of sorbing radionuclides, which tend to experience much less matrix diffusion in the fractured volcanic formations. Such colloid facilitated transport is considered explicitly, as discussed in Section 6.4.2.6. Base-case values for most parameters were chosen to be the median values for the distributions except for sorption coefficients, which were taken to be 0 to represent a nonsorbing radionuclide, and the horizontal permeability anisotropy ratio was taken to be 5 from the SZ site scale flow model (DTN: SN0612T0510106.004 [DIRS 178956]).

Table 4-2. Input Parameters and Range of Values for the Site-Scale Saturated Zone Transport Model

Parameter	Base-Case Value(s)	Uncertainty Range	Units	Variable Type	Source/DTN
Specific discharge multiplier [a]	1 [b]	0.112 to 8.933	NA	Stochastic	SN0706INPUTSZF.000 [DIRS 182007], file *updated_SZ_inputs_table.doc*

Table 4-2. Input Parameters and Range of Values for the Site-Scale Saturated Zone Transport Model (Continued)

Parameter	Base-Case Value(s)	Uncertainty Range	Units	Variable Type	Source/DTN
Permeability horizontal anisotropy ratio (north-south/east-west)	5 [n]	0.05 to 20	NA	Stochastic	SN0310T0502103.009 [DIRS 168763], file *Table 6-8_updated.doc* SN0612T0510106.004 [DIRS 178956] , file *SZ Flow Model.zip*
Bulk density in alluvium	1,910 [b]	1,669 to 2,151 [d]	kg/m^3	Stochastic	SNL 2007 [DIRS 181650], Section 6.5.2 SN0310T0502103.009 [DIRS 168763], *DTN-SN0310T0502103.009.zip\Table 6-8_updated.doc*
Sorption coefficient in alluvium	0.0 [e]	0 to 10,000	mL/g	Stochastic	Appendices A and C of this report
Effective porosity in the alluvium, fraction	0.18 [b]	0.02 [j] to 0.3	NA	Stochastic	SNL 2007 [DIRS 181650], Section 6.5.2 SN0310T0502103.009 [DIRS 168763], *DTN-SN0310T0502103.009.zip\Table 6-8_updated.doc*
Colloid retardation factor in alluvium for irreversible colloids	1 [f]	8 to 5,195	NA	Stochastic	SNL 2007 [DIRS 170006] LA0303HV831352.004 [DIRS 163559]
Colloid retardation factor in alluvium for nonsorbing radionuclides	1 [g]	NA	NA	NA	NA
Flowing interval porosity, fraction [i]	0.001 [i]	0.00001 to 0.1	NA	Stochastic	SNL 2007 [DIRS 181650], Section 6.5.2 SN0310T0502103.009 [DIRS 168763], *DTN-SN0310T0502103.009.zip\Table 6-8_updated.doc*
Flowing interval spacing	25.773 [b]	1.860 to 80.0	m	Stochastic	SN0706INPUTSZF.000 [DIRS 182007], file *updated_SZ_inputs_table.doc*
Matrix porosity in volcanics, fraction	0.15 to 0.25 [h]	NA	NA	Assigned value for each unit; not a stochastic parameter	SNL 2007 [DIRS 181650], Section 6.5.2 SN0310T0502103.009 [DIRS 168763], *DTN-SN0310T0502103.009.zip\Table 6-8_updated.doc*

Table 4-2. Input Parameters and Range of Values for the Site-Scale Saturated Zone Transport Model (Continued)

Parameter	Base-Case Value(s)	Uncertainty Range	Units	Variable Type	Source/DTN
Effective diffusion coefficient in volcanics	5.0×10^{-11} [b]	5.0×10^{-12} to 5.0×10^{-10}	m^2/s	Stochastic	SNL 2007 [DIRS 181650], Section 6.5.2 SN0310T0502103.009 [DIRS 168763], *DTN-SN0310T0502103.009.zip\Table 6-8_updated.doc*, parameter DCVO
Matrix sorption coefficient in volcanics	0.0 [e]	0 to 10,000	mL/g	Stochastic	Appendices A and C
Colloid retardation factor in volcanics for irreversible colloids	1 [f]	6.0 to 794 [k]	NA	Stochastic	BSC 2004 [DIRS 170006] LA0303HV831352.002 [DIRS 163558]
Colloid retardation factor in volcanics related to nonsorbing radionuclides	1 [g]	N/A	NA	NA	NA
Groundwater concentration of colloids	N/A [f]	10^{-9} to 2×10^{-4} [l]	g/mL	Stochastic	SNL 2007 [DIRS 177423], Section 6.3, MO0701PAGROUND.000 [DIRS 179310]
Groundwater concentration of colloids related to nonsorbing radionuclides	0 [g]	NA	g/mL	NA	NA
Sorption coefficient onto colloids	0 [f]	1 to 1.0×10^7	mL/g	Stochastic	SNL 2007 [DIRS 177423], Section 6.3 DTNs: MO0701PAKDSUNP.000 [DIRS 180392] and MO0701PASORPTN.000 [DIRS 180391]
Sorption coefficient onto colloids for nonsorbing radionuclides	0 [g]	NA	mL/g	NA	NA
Fraction of colloids transported unretarded	1 [f]	0.00034 [m] to 0.0017 [m]	NA	Stochastic	BSC 2004 [DIRS 170006]
Fraction of colloids transported unretarded related to nonsorbing radionuclides	0 [g]	NA	NA	NA	NA
Dispersivity, longitudinal	10.0	0.10 to 2,000	m	Stochastic	Section 4.1.2.16
Dispersivity, transverse, horizontal	0.05	0.0005 to 10	m	Stochastic	Section 4.1.2.17

Table 4-2. Input Parameters and Range of Values for the Site-Scale Saturated Zone Transport Model (Continued)

Parameter	Base-Case Value(s)	Uncertainty Range	Units	Variable Type	Source/DTN
Dispersivity, transverse, vertical	0.0005	0.000005 to 0.1	m	Stochastic	Section 4.1.2.18

[a] The boundary fluxes, recharge rates and permeabilities were multiplied by this factor to vary the specific discharge. (The value of specific discharge is not directly input to the transport model, it is implicit in the flow fields. It has a base-case value of 0.36 m/yr from the repository to a distance of 5 km, as shown in SNL 2007 [DIRS 177391], Section 6.5.2.4.)

[b] Median value, given as the 0.5 probability value in the source data tracking number (DTN).

[c] Median value, interpolated to the 0.5 probability from the data given in the source DTN, *Table 6-8_updated.doc*, entry for parameter HAVO.

[d] Range derived from the normal distribution given in SNL 2007 [DIRS 181650], Figure 6-17.

[e] Base case is taken to be the value for nonsorbing radionuclides.

[f] These do not apply to the site-scale SZ transport model base case because the base case considers only the nonsorbing radionuclides and hence also excludes colloid facilitated transport.

[g] Base-case colloid sorption parameters are set to 0, and retardation factors set to 1, to simulate the base case of nonsorbing radionuclides.

[h] Each hydrostratigraphic unit was assigned a fixed value within this range.

[I] Flowing interval porosity is referred to as the "Fracture porosity in volcanic units," parameter FPVO, in DTN: SN0310T0502103.009 [DIRS 168763], *Table 6-8_updated.doc*.

[j] As discussed in Section 4.1.2.5, this value differs from that given in the reference DTN, but this is a conservative choice that avoids potential numerical problems.

[k] The value given here is lower than the value of 800 given in the source/DTN. This is a conservative choice.

[l] Note that the numbers in the source/DTN are in units of mg/L, which are converted to the units of this table, g/mL by multiplying by 10^{-6}.

[m] The lower limit given here is somewhat higher than the one given in the source/DTN and the upper limit given here is somewhat higher than that given in the source/DTN. This is a conservative choice.

[n] Value given in DTN: SN0612T0510106.004 [DIRS 178956].

4.1.2.1 Specific Discharge Multiplier

Field values of groundwater-specific discharge in the saturated zone have been estimated from the tracer testing at the Alluvial Testing Complex as shown in *Saturated Zone In-Situ Testing* (SNL 2007 [DIRS 177394], Section 6.5.5) to be in the range of 0.46 to 9.4 m per year. This information is combined with the recommendations presented in *Saturated Zone Flow and Transport Expert Elicitation Project* (CRWMS M&O 1998 [DIRS 100353], p. 3-43) using Bayesian updating to create a distribution of the specific discharge multiplier in the range of 0.112 to 8.933 (SNL 2007 [DIRS 181650], Table 6-7[a]). All the permeabilities in the base-case flow model are multiplied by this factor, and all the recharge values and boundary fluxes input to the model are also multiplied by this factor to preserve the calibration of the base-case SZ flow model, as discussed in *Saturated Zone Site-Scale Flow Model* (SNL 2007 [DIRS 177391], Section 6.6; Tables 6-8 and 6-4[a]). The effect of the range of uncertainty in this parameter on the output BTCs is presented in Section 6.7.1. The base-case multiplier for the site-scale SZ transport model is chosen to be 1, corresponding to the median value used in the base-case SZ site-scale flow model.

4.1.2.2 Horizontal Anisotropy in Permeability

Field estimates of the horizontal permeability anisotropy ratio in the north-south/east-west direction were obtained from the long-term pumping test conducted at the C-wells complex presented in *Saturated Zone In-Situ Testing* (SNL 2007 [DIRS 177394], Section 6.2.6). These data were used to obtain a distribution of the anisotropy ratio in the range of 0.05 to 20 (DTN: SN0310T0502103.009 [DIRS 168763]). More details of this analysis are presented in *Saturated Zone Flow and Transport Model Abstraction* (SNL 2007 [DIRS 181650], Section 6.5.2). The effect of the range of uncertainty in this parameter on the output BTCs is presented in Section 6.7.2. The base-case ratio is chosen to be 5 as given in the SZ site-scale flow model DTN: SN0612T0510106.004 [DIRS 178956].

4.1.2.3 Bulk Density in Alluvium

Borehole gravimeter data (DTN: MO0105GPLOG19D.000 [DIRS 163480]) from the well NC-EWDP-19D1 was used in conjunction with laboratory grain-density measurements (USGS n.d. [DIRS 154495]) in estimating the uncertainty distribution of the bulk density. These data yielded a normal distribution with a mean of 1,910 kg/m^3 and standard deviation of 78 kg/m^3 (DTN: SN0310T0502103.009 [DIRS 168763]). More details of this analysis, including a graphical representation, are presented in *Saturated Zone Flow and Transport Model Abstraction* (SNL 2007 [DIRS 181650], Section 6.5.2.7 and Figure 6-17). From this graph, a lower bound of 1,669 kg/m^3 and an upper bound of 2,151 kg/m^3 are estimated. The effect of the range of uncertainty in this parameter on the output BTCs is presented in Section 6.7.3. The base-case value is chosen to be the median value of 1,910 kg/m^3.

4.1.2.4 Sorption Coefficient in Alluvium

Sorption coefficient measurements for neptunium and uranium on core samples from the alluvium to the south of Yucca Mountain are available (Sections A.7.3.3 and A.7.11.3 of Appendix A). For the radionuclides of americium, cesium, plutonium, protactinium, radium, strontium and thorium, the data on devitrified tuff samples from the Yucca Mountain area are used, since devitrified tuff makes up a major portion of the alluvium (Sections A.7.1.1, A.7.2.1, A.7.4.1, A.7.5.1, A.7.6.1, A.7.8.1, and A.7.9.1 of Appendix A). These data and the analysis to obtain stochastic uncertainty distributions for the sorption coefficient are presented in detail in Appendix A. Uncertainty distributions with wide ranges were selected to account for the uncertainty in the sorption coefficient rising from the uncertainties associated with the conceptual model (Section 6), geochemical conditions, and the in situ rock mineralogy (output DTN: LA0702AM150304.001 (TBV)). The sensitivity of the BTCs for each radionuclide to the uncertainty in its K_d values is presented in *Saturated Zone Flow and Transport Model Abstraction* (SNL 2007 [DIRS 181650], Section 6.6). In this report only the overall uncertainty range that encompasses all the radionuclides, 0 to 10,000 mL/g (Table 4-2), is considered. The effect of the range of uncertainty in this parameter on the output BTCs is presented in Section 6.7.4. A base-case value of 0 is chosen to represent the case of nonsorbing radionuclides.

4.1.2.5 Effective Porosity in Alluvium

The study by Bedinger et al. (1989 [DIRS 129676], p. A18, Table 1) on the hydraulic characteristics of alluvium within the Southwest Basin and Range Province is relevant to the local basin fill conditions and provides an uncertainty distribution for effective porosity. Further information is available from the following sources:

- Single-point, site-specific, effective porosity data from the well NC-EWDP-19D1 presented in *Saturated Zone In-Situ Testing* (SNL 2007 [DIRS 177394], Section G.4.2.4) with a value of 0.1

- Total porosity data from the CAMBRIC study (Burbey and Wheatcraft 1986 [DIRS 129679], pp. 23 to 24) with an average value of 0.34

- Total porosity data presented in *Regional Groundwater Flow and Tritium Transport Modeling and Risk Assessment of the Underground Test Area, Nevada Test Site, Nevada* (DOE 1997 [DIRS 103021], Tables 8-1 and 8-2) with values of 0.36 and 0.35.

All these data are used as supporting information to develop an uncertainty distribution with an upper bound of 0.3, median value of 0.18 and lower limit of 0 (DTN: SN0310T0502103.009 [DIRS 168763]) for the effective porosity. More details of this analysis are presented in *Saturated Zone Flow and Transport Model Abstraction* (SNL 2007 [DIRS 181650], Section 6.5.2.3). The lower limit given in this report (Tables 4.2 and 6.4-2) is 0.02, a conservative choice that avoids potential numerical problems with the value 0. The effect of the range of uncertainty in this parameter on the output BTCs is presented in Section 6.7.5. The base-case value is chosen to be the median value of 0.18.

4.1.2.6 Retardation Factor in Alluvium for Irreversible Colloids

The development of colloid retardation factors based on experimental data specific to Yucca Mountain as well as field studies of bacteriophage transport in alluvial material is presented in *Saturated Zone Colloid Transport* (BSC 2004 [DIRS 170006], Section 6.5). An uncertainty distribution with a range of 8 to 5,188 and a median value of 33.9 is presented. More details of this analysis are presented in *Saturated Zone Flow and Transport Model Abstraction* (SNL 2007 [DIRS 181650], Section 6.5.2.11). The effect of the range of uncertainty in this parameter on the output BTCs is presented in Section 6.7.6. The base-case value is set to 1 to simulate the transport of nonsorbing radionuclides.

4.1.2.7 Flowing Interval Porosity

At Yucca Mountain, a flowing interval is defined as the region in which significant groundwater flow occurs at a well. The flowing interval porosity characterizes these flowing intervals rather than individual fractures. Data from tests in unsaturated tuff in the Exploratory Studies Facility were used to estimate the uncertainty distribution with a range of 0.00001 to 0.1 and a median value of 0.001, using gas flow as presented in *Analysis of Hydrologic Properties Data* (BSC 2004 [DIRS 170038], Section 6.1.3.2); water flow (BSC 2004 [DIRS 170038], Section 6.1.3.4); cross-hole tracer tests at the C-Wells complex given in *Report of Results of Hydraulic and*

Tracer Tests at the C-Holes Complex (CRWMS M&O 1997 [DIRS 100328], pp. 2 to 4 and 28); Nevada Environmental Restoration Project tests presented in *Regional Groundwater Flow and Tritium Transport Modeling and Risk Assessment of the Underground Test Area, Nevada Test Site, Nevada* (DOE 1997 [DIRS 103021], p. 5-14); and laboratory measurements on core from the wells USW G-1, USW G-3, USW G-4, and UE-25 a#1, where a parallel-plate fracture geometry model was used (Wilson et al. 1994 [DIRS 100191], Volume 1, Chapter 7, Table 7-19, p. 7-30). More details of this analysis are presented in *Saturated Zone Flow and Transport Model Abstraction* (SNL 2007 [DIRS 181650], Section 6.5.2.5). The flowing interval porosity enters the transport model indirectly through the flowing interval aperture parameter, which is computed as a product of the porosity and the spacing. The effect of the range of uncertainty in the flowing interval aperture on the output BTCs is presented in Section 6.7.8. The base-case value of the flowing interval porosity is taken to be the median value of 0.001.

4.1.2.8 Flowing Interval Spacing

An uncertainty distribution with a range of 1.86 m to 80.0 m and a median value of 25.773 m was developed in *Saturated Zone Flow and Transport Model Abstraction* (SNL 2007 [DIRS 181650]; Table 6-7[a]). The borehole flow meter survey data and analysis presented in *Probability Distribution for Flowing Interval Spacing* (BSC 2004 [DIRS 170014], Section 6.5) were used in the above-referenced analysis. The flowing interval spacing enters the transport model indirectly through the flowing interval aperture parameter, which is computed as a product of the porosity and the spacing. The effect of the range of uncertainty in the flowing interval aperture on the output BTCs is presented in Section 6.7.8. The base-case value of the flowing interval spacing was taken to be the median of the distribution, 25.773 m.

4.1.2.9 Matrix Porosity in Volcanics

The matrix porosity in volcanic units is treated as a nonstochastic parameter, although it is allowed to vary from unit to unit (DTN: SN0310T0502103.009 [DIRS 168763]). It is acceptable to treat this parameter as a nonstochastic parameter because it enters the site-scale SZ transport model through a combination with the distribution coefficient (Section 6.4.2.4.1, Equation 57) or with the diffusion coefficient (Equations 64 and 74, Section 6.4.2.4.1), and both these coefficients are being treated as stochastic variables with wide ranges (Sections 4.1.2.10 and 4.1.2.11). Values in the range of 0.15 to 0.25 are assigned on a unit-by-unit basis. Values were chosen based on *Rock Properties Model* (BSC 2004 [DIRS 170032], Table 6.4-2) and porosity data from Boreholes UE-25 p#1, USW H-3, USW SD-7, USW G-3, USW H-1, USW G-4, USW H-5, and USW H-6 (DTNs: SN0004T0501399.003 [DIRS 155045], MO0109HYMXPROP.001 [DIRS 155989], and MO0010CPORGLOG.002 [DIRS 155229]). More details of this analysis are presented in *SZ Flow and Transport Model Abstraction* (SNL 2007 [DIRS 181650], Section 6.5.2.18).

4.1.2.10 Effective Diffusion Coefficient in Volcanics

Matrix diffusion is a process in which diffusing particles move, via Brownian motion, through both mobile and immobile fluids. Diffusion is a Fickian process. Diffusing species move from high to low concentrations. It depends on the free water molecular diffusion coefficient for individual constituents and the characteristics of the flow path in which the diffusing species

passes. Because diffusion through porous media is less than free water molecular diffusion, it is quantitatively defined as the effective diffusion coefficient, D_e. The variability in D_e in saturated media is caused by the variability in: (1) the individual constituents' size (atom, ion, or molecule) and charge; (2) fluid temperature; and (3) the unique properties of a porous media's lithology at a microscopic scale, including the tortuosity of the media.

Reimus et al. reported diffusion cell measurements on numerous rock samples from the vicinity of Yucca Mountain (2002 [DIRS 162956], Tables 3-2 to 3-8; 2002 [DIRS 163008], Tables 2-4 and 2-5). These measurements give a correlation between the measured effective diffusion coefficient, sample porosity, and sample permeability. The range of values is corroborated by the site-specific values reported by Triay et al. (1993 [DIRS 145123], Tables 1 and 2) and Rundberg et al. (1987 [DIRS 106481]). The correlation given by Reimus et al. (2002 [DIRS 163008], Equation 2.5, p. 2.25) was used to develop a range of values appropriate for the porosities and permeabilities of various units as reported by Flint (1998 [DIRS 100033], p. 89). These were scaled to account for the uncertainty and variation in the effective diffusion coefficient based on the species size and charge, leading to the final uncertainty range of 5×10^{-12} to 5×10^{-10} m^2/s, with a median value of 5.0×10^{-11} m^2/s (DTN: SN0310T0502103.009 [DIRS 168763]). Details of this analysis are presented in *Saturated Zone Flow and Transport Model Abstraction* (SNL 2007 [DIRS 181650], Section 6.5.2.6). The effect of the range of uncertainty in this parameter on the output BTCs is presented in Section 6.7.9. The median value of 5.0×10^{-11} m^2/s was taken to be the base-case value.

4.1.2.11 Matrix Sorption Coefficient in Volcanics

Sorption coefficients were measured on devitrified and zeolitic tuff samples from the Yucca Mountain area for the radionuclides americium, barium, cesium, neptunium, plutonium, protactinium, radium, strontium, thorium, and uranium. These data and analyses were used to obtain stochastic uncertainty distributions for the sorption coefficients presented in detail in Appendix A. These measurements represent a spatial scale on the order of centimeters. A stochastic scaling procedure was used to obtain from these distributions the uncertainty distributions on the scale of 500 m. This analysis was considered acceptable even though the scale of the grid blocks used in the site-scale SZ transport model is 250 m (SNL 2007 [DIRS 177391] Section 6.1), as explained in Appendix C. This stochastic analysis is presented in detail in Appendix C of this report. Stochastic analysis was combined with expert judgment (Appendix C, Section C-2) to develop uncertainty distributions with wide ranges. These were selected to account for the uncertainty in the sorption coefficient rising from the uncertainties associated with the conceptual model (Section 6), geochemical conditions, and the in situ rock mineralogy (output DTN: LA0702AM150304.001). The resulting distributions for individual radionuclides are given in Table C-14 and output DTN: LA0702AM150304.001). The overall uncertainty range that encompasses all the radionuclides is 0 to 10,000 mL/g (Table C-14). The effect of the range of uncertainty in this parameter on the output BTCs is presented in Section 6.7.10. A base-case value of 0 was chosen to represent the case of nonsorbing radionuclides such as ^{14}C.

4.1.2.12 Retardation Factor in Volcanics for Irreversible Colloids

Saturated Zone Colloid Transport describes the development of colloid retardation factors for fractured tuff from field and experimental data (BSC 2004 [DIRS 170006], Section 6.4). More details of this analysis are presented in *Saturated Zone Flow and Transport Model Abstraction* (SNL 2007 [DIRS 181650], Section 6.5.2.11) leading to an uncertainty distribution with a range of 6 to 800 and a median value of 26 (DTN: LA0303HV831352.002 [DIRS 163558]). The effect of the range of uncertainty in this parameter on the output BTCs is presented in Section 6.7.11. Base-case value for the site-scale SZ transport model is set to 1 to simulate the transport of nonsorbing radionuclides.

4.1.2.13 Groundwater Concentrations of Colloids

The uncertainty distribution was developed in *Waste Form and In-Drift Colloids-Associated Radionuclide Concentrations: Abstraction and Summary* (SNL 2007 [DIRS 177423], Section 6.3, DTN: MO0701PAGROUND.000 [DIRS 179310]) A range of 10^{-9} to 2×10^{-4} g/mL with a median value of 10^{-7} g/mL is given. This parameter enters the site-scale SZ transport model indirectly through the coefficient for reversible sorption onto colloids shown in *Saturated Zone Flow and Transport Model Abstraction* (SNL 2007 [DIRS 181650], Section 6.5.2.12). The effect of the range of uncertainty in this parameter on the output BTCs is presented in Section 6.7.12. The value of this parameter in the base-case transport model is set to 0 to simulate the transport of nonsorbing radionuclides.

4.1.2.14 Sorption Coefficient onto Colloids

The uncertainty distributions for the coefficient of sorption of plutonium, americium, thorium, protactinium, and cesium onto colloids were developed in *Waste Form and In-Drift Colloids-Associated Radionuclide Concentrations: Abstraction and Summary* (SNL 2007 [DIRS 177423], Section 6.3) and DTNs: MO0701PAKDSUNP.000 [DIRS 180392] and MO0701PASORPTN.000 [DIRS 180391]). A range of 1 (uranium and cesium on iron oxide corrosion production colloids) to 10^7 (americium on smectite colloids) mL/g was used with a median value of 5×10^5 mL/g (DTNs: MO0701PASORPTN.000 [DIRS 180391], Table 1-3, and MO0701PAKDSUNP.000 [DIRS 180392], Table 1-2). This parameter enters the site-scale SZ transport model indirectly through the coefficient for reversible sorption onto colloids. The effect of the range of uncertainty in this parameter on the output BTCs is presented in Section 6.7.12. The value of this parameter in the base-case transport model is set to 0 to simulate the transport of nonsorbing radionuclides.

4.1.2.15 Fraction of Colloids Transported Unretarded

A discussion of the fraction of colloids transported with no retardation is in *Saturated Zone Colloid Transport* (BSC 2004 [DIRS 170006], Section 6.6). The range of uncertainty distribution of this fraction is taken to be 0.00034 to 0.0017 with a median value of 0.0005. This parameter is applied in the TSPA calculations after the BTCs are calculated from the site-scale SZ transport model; hence, the influence of the uncertainty in this parameter on the BTCs is not discussed in this report. The base-case value is set to 0 to simulate the transport of nonsorbing radionuclides.

4.1.2.16 Dispersivity, Longitudinal

As explained in *Saturated Zone Flow and Transport Model Abstraction* (SNL 2007 [DIRS 181650], Section 6.5.2.9), the uncertainty distribution for longitudinal dispersivity was taken to be truncated lognormal with the mean of 2 and the standard deviation of 0.75 (in the log space) (DTN: SN0310T0502103.009 [DIRS 168763]). The basis used in *SZ Flow and Transport Model Abstraction* for this distribution was expert elicitation (CRWMS M&O 1998 [DIRS 100353], pp. 3-10, 3-11, and LG-12). Graphically, the estimated range of this distribution is 1 m to 20,000 m with a median value of 100 m, as discussed in *Saturated Zone Flow and Transport Model Abstraction* (SNL 2007 [DIRS 181650], Figure 6-18). As explained in *SZ Flow and Transport Model Abstraction*, these dispersivity values are on the scale of the site-scale SZ transport model and correspond to dispersivity values smaller by a factor of 10 when represented on the scale of 500 m, comparable to the scale of computational grid blocks (250 m) shown in *Saturated Zone Flow and Transport Model Abstraction* (SNL 2007 [DIRS 181650], Section 6.5.2.9 and Figure 6-19). Hence, the range of uncertainty for this parameter given in Table 4-2 is 0.1 to 2,000 m. The effect of the range of uncertainty in this parameter on the output BTCs is presented in Section 6.7.13. The base-case value is taken to be the median value on the 500-m scale, 10 m.

4.1.2.17 Dispersivity, Transverse, Horizontal

As explained in *Saturated Zone Flow and Transport Model Abstraction*, the transverse horizontal dispersivity values were determined by dividing the longitudinal dispersivity by a factor of 200 (SNL 2007 [DIRS 181650], Section 6.5.2.9). The basis used in *Saturated Zone Flow and Transport Model Abstraction* for the use of this factor was expert elicitation given in *Saturated Zone Flow and Transport Expert Elicitation Project* (CRWMS M&O 1998 [DIRS 100353], pp. 3-11, LG-11, and LG-14). The range of values is 0.0005 to 10 m. The base-case value is taken to be 0.05 m, calculated as the median value of the longitudinal dispersivity (Section 4.1.2.16) of 10 m divided by 200.

4.1.2.18 Dispersivity, Transverse, Vertical

As explained in *Saturated Zone Flow and Transport Model Abstraction*, the transverse vertical dispersivity values were determined by dividing the transverse horizontal dispersivity by a factor of 100 (SNL 2007 [DIRS 181650], Section 6.5.2.9). The basis used in *Saturated Zone Flow and Transport Model Abstraction* for the use of this factor was expert elicitation discussed in *Saturated Zone Flow and Transport Expert Elicitation Project* (CRWMS M&O 1998 [DIRS 100353], pp. 3-11, LG-11, and LG-14). The range of values is 0.000005 m to 0.1 m. The base-case value is taken to be 0.0005 m, calculated as the base value of the transverse horizontal dispersivity (Section 4.1.2.17) of 0.05 m divided by 100.

4.1.3 Accuracy, Precision, and Representativeness

The site-scale SZ transport model is a theoretical framework involving a number of transport parameters that reflect the properties of the saturated zone, incorporated into a computer code using numerical methods. This model is intended for making TSPA predictions using stochastic methods with a wide range of values that reflect uncertainty in the input parameters. The

accuracy and precision of the output results depend upon the accuracy and precision of the input parameter values, the theoretical model and the numerical model. As seen in Table 4-2, the uncertainty ranges for all input parameters (except the matrix porosity in volcanics, which is a deterministic value per each lithologic unit) are at least 25% or more of the base-case value, and in most cases they are several orders of magnitude larger than the base-case value. The theoretical and mathematical methods selected for the computational transport model, as described in detail in Section 6, are well established in the literature and are sufficiently accurate to deal with these wide parameter ranges. The approach taken in this report is to select a range of values for each input parameter as described in Section 4.1.2 and evaluate the propagation of this uncertainty range to the output BTCs as described in Section 6.7. Confidence in the representativeness of the model output is developed through the validation activities of comparison against field data and independent models, and other confidence-building activities described in detail in Section 7.

4.2 CRITERIA

General requirements to be satisfied by the TSPA are stated in 10 CFR 63.114 [DIRS 180319]. The acceptance criteria that will be used by the NRC to determine whether the technical requirements have been met are identified in *Yucca Mountain Review Plan, Final Report* (YMRP) (NRC 2003 [DIRS 163274]). The requirements to be satisfied by this document are identified in *Technical Work Plan For: Saturated Zone Analysis and Model Report Integration* (BSC 2006 [DIRS 177375], Table 5). Table 4-3 summarizes the pertinent requirements and criteria for this report.

Table 4-3. Project Requirements and Acceptance Criteria Applicable to This Model Report

Requirement Title[a]	10 CFR 63 Link[a]	YMRP Acceptance Criteria[b]
Requirements for performance assessment	10 CFR 63.114 (a) to (c) and (e) to (g)	Criteria 1(1), 1(2),1(3), 1(5), 1(6), 2 (1), 2(3), 3(1), 3(2), 3(4), 3(5), 3(6), 4(1), 4(2),4(3), and 4(4) for radionuclide transport in the saturated zone

[a]From 10 CFR 63 [DIRS 180319].

[b]From NRC 2003 [DIRS 163274].

The acceptance criteria identified in Section 2.2.1.3.9.3 of the YMRP (NRC 2003 [DIRS 163274]) are included below. In cases where subsidiary criteria are listed in the YMRP (NRC 2003 [DIRS 163274]) for a given criterion, only the subsidiary criteria addressed by this scientific analysis are listed below. How the acceptance criteria and the subsidiary criteria are addressed in this report is presented in Section 8.4.

Acceptance Criteria from Section 2.2.1.3.9.3, *Radionuclide Transport in the Saturated Zone*

Acceptance Criterion 1: System Description and Model Integration Are Adequate

(1) Total system performance assessment adequately incorporates important design features, physical phenomena, and couplings, and uses consistent and appropriate assumptions throughout the radionuclide transport in the saturated zone abstraction process.

(2) The description of the aspects of hydrology, geology, geochemistry, design features, physical phenomena, and couplings that may affect radionuclide transport in the saturated zone is adequate. For example, the description includes changes in transport properties in the saturated zone from water-rock interaction. Conditions and assumptions in the abstraction of radionuclide transport in the saturated zone are readily identified and consistent with the body of data presented in the description.

(3) The abstraction of radionuclide transport in the saturated zone uses assumptions, technical bases, data, and models that are appropriate and consistent with other related U.S. Department of Energy abstractions. For example, assumptions used for radionuclide transport in the saturated zone are consistent with the total system performance assessment abstractions of radionuclide release rates and solubility limits, and flow paths in the saturated zone (Sections 2.2.1.3.4 and 2.2.1.3.8 of the Yucca Mountain Review Plan, respectively). The descriptions and technical bases provide transparent and traceable support for the abstraction of radionuclide transport in the saturated zone.

(5) Sufficient data and technical bases for the inclusion of features, events, and processes related to radionuclide transport in the saturated zone in the total system performance assessment abstraction are provided; and

(6) Guidance in NUREG–1297 and NUREG–1298 (Altman et al. 1988 [DIRS 103597]; [DIRS 103750]), or other acceptable approaches for peer review and data qualification is followed.

Acceptance Criterion 2: Data Are Sufficient for Model Justification

(1) Geological, hydrological, and geochemical values used in the license application are adequately justified (e.g., flow path lengths, sorption coefficients, retardation factors, colloid concentrations, etc.). Adequate descriptions of how the data were used, interpreted, and appropriately synthesized into the parameters are provided;

(3) Data on the geology, hydrology, and geochemistry of the saturated zone, including the influence of structural features, fracture distributions, fracture properties, and stratigraphy, used in the total system performance assessment abstraction, are based on appropriate techniques. These techniques may include laboratory experiments, site-specific field measurements, natural analog research, and process-level modeling studies. As appropriate, sensitivity or uncertainty analyses used to support the U.S. Department of Energy total system performance assessment abstraction are adequate to determine the possible need for additional data.

Acceptance Criterion 3: Data Uncertainty Is Characterized and Propagated Through the Model Abstraction

(1) Models use parameter values, assumed ranges, probability distributions, and bounding assumptions that are technically defensible, reasonably account for uncertainties and variabilities, and do not result in an under-representation of the risk estimate.

(2) For those radionuclides where the total system performance assessment abstraction indicates that transport in fractures and matrix in the saturated zone is important to waste isolation: (i) estimated flow and transport parameters are appropriate and valid, based on techniques that may include laboratory experiments, field measurements, natural analog research, and process-level modeling studies conducted under conditions relevant to the saturated zone at Yucca Mountain; and (ii) models are demonstrated to adequately predict field transport test results. For example, if a sorption coefficient approach is used, the assumptions implicit in that approach are validated.

(4) Parameter values for processes, such as matrix diffusion, dispersion, and groundwater mixing, are based on reasonable assumptions about climate, aquifer properties, and ground-water volumetric fluxes (Section 2.2.1.3.8 of the Yucca Mountain Review Plan);

(5) Uncertainty is adequately represented in parameter development for conceptual models, process-level models, and alternative conceptual models considered in developing the abstraction of radionuclide transport in the saturated zone. This may be done either through sensitivity analyses or use of conservative limits.

(6) Where sufficient data do not exist, the definition of parameter values and conceptual models is based on appropriate use of other sources, such as expert elicitation conducted in accordance with NUREG-1563 (Kotra et al. 1996 [DIRS 100909]). If other approaches are used, the U.S. Department of Energy adequately justifies their use.

Acceptance Criterion 4: Model Uncertainty Is Characterized and Propagated Through the Model Abstraction

(1) Alternative modeling approaches of features, events, and processes are considered and are consistent with available data and current scientific understanding, and the results and limitations are appropriately considered in the abstraction.

(2) Conceptual model uncertainties are adequately defined and documented, and effects on conclusions regarding performance are properly assessed.

(3) Consideration of conceptual model uncertainty is consistent with available site characterization data, laboratory experiments, field measurements, natural analogue information, and process-level modeling studies; and the treatment of conceptual model uncertainty does not result in an under-representation of the risk estimate.

(4) Appropriate alternative modeling approaches are consistent with available data and current scientific knowledge, and appropriately consider their results and limitations using tests and analyses that are sensitive to the processes modeled. For example, for radionuclide transport through fractures, the U.S. Department of Energy adequately considers alternative modeling approaches to develop its understanding of fracture distributions and ranges of fracture flow and transport properties in the saturated zone.

4.3 CODES, STANDARDS, AND REGULATIONS

No codes, standards, or regulations other than those identified in *Technical Work Plan For: Saturated Zone Analysis and Model Report Integration* (BSC 2006 [DIRS 177375], Section 3) and determined to be applicable (Table 4-3) were used in this analysis.

INTENTIONALLY LEFT BLANK

5. ASSUMPTIONS

A list of the assumptions used in this model report is provided in Table 5-1. Subsections where assumptions are used are identified in the table.

Table 5-1. Assumptions

Number	Assumption	Rationale	Location in this Report
1	It is assumed that sorption on individual fracture surfaces need not be included in the site-scale SZ transport model	Sorption on individual fracture surfaces can result in significant retardation of radionuclide transport even for small values of fracture sorption coefficients (Robinson 1994 [DIRS 101154], Figure 7). However, the sorption coefficient onto fracture surfaces is a strong function of the minerals coating the fracture surfaces. Because of the lack of sufficient data, there is uncertainty about the nature of the fracture coatings in the volcanics along the potential transport pathways in the saturated zone. Hence, as a conservative approach, no credit is taken for sorption on individual fracture surfaces in the saturated zone. This assumption requires no further justification.	Section 6.3
2	The derivation of the probability distribution for the sorption coefficients assumes that conditions are oxidizing in the groundwater in the saturated zone	Available measurements show that the waters in the saturated zone at Yucca Mountain along the potential transport pathways downstream of the repository footprint (Appendix F, Table F-1) are mostly in oxidizing conditions or in transition between oxidizing-reducing conditions, with some of the deeper waters being in reducing condition. There is insufficient data to completely characterize in detail the oxidation state of the water along the expected transport pathways (Figures 7-9a and 7-9b) in the saturated zone. Further, the assumption of oxidizing conditions leads to predictions of lower values of sorption coefficients. Hence, as a conservative approach, it is assumed that conditions are oxidizing in the groundwater in the saturated zone. This assumption requires no further justification.	Appendix A, Section A7; Appendix F

Table 5-1. Assumptions (Continued)

Number	Assumption	Rationale	Location in this Report
3	For the radionuclides americium, cesium, plutonium, protactinium, strontium, and thorium, sorption coefficients in alluvium are assumed to be those corresponding to the values measured on samples of devitrified crushed tuff	There is insufficient data on the sorption coefficients of the radionuclides americium, cesium, plutonium, protactinium, strontium, and thorium in alluvium. Alluvium along the potential transport pathways is composed largely of disaggregated tuffaceous materials. Sources of data on aquifer matrix compositions in the saturated zone are provided in Table C-1. These data have been incorporated into a site mineralogic model, *Mineralogic Model (MM3.0) Report (*BSC 2004 [DIRS 170031]). There are two dominant rock types in the saturated zone along potential flow paths in volcanics to the 18-km boundary: devitrified tuff and zeolitic tuff. Because devitrified tuff makes up a major portion of the volcanic units exposed at the surface, it should be a major component in alluvium. In addition, clays and other secondary minerals are enriched in alluvial materials. These characteristics would result in higher sorption coefficients for alluvial materials compared to intact devitrified tuff. Also, the sorption coefficients onto zeolitic tuffs are higher than those on devitrified tuffs. Hence, as a conservative approach, it is assumed that, for the radionuclides americium, cesium, plutonium, protactinium, strontium, and thorium, sorption coefficients in alluvium are given by the corresponding values measured on samples of devitrified crushed tuff. This assumption needs no further justification.	Appendix A, Section A7
4	Transport of colloid particles is not affected by the radionuclides attached to them	Colloids are microscopic particles that are much larger than solute molecules. Solute molecules can absorb onto the colloid particles and be transported along with them. Because the colloidal particles are much larger in size and mass than the radionuclides that sorb onto them, the radionuclides do not affect the transport of the colloid particles.	Section 6.3

6. MODEL DISCUSSION

This section presents a discussion of the site-scale SZ transport model. Section 6.1 summarizes the objectives of this modeling activity, a description of the problem, and model inputs and outputs. Section 6.2 lists the FEPs included in TSPA and relevant to this model report. The FEPs are given in DTN: MO0706SPAFEPLA.001 [DIRS 181613], file *FEPs_be.mdb*, Table 7.1-1. The base-case conceptual model is presented in Section 6.3. The mathematical formulation of the base-case conceptual model is presented in Section 6.4, and the base-case model results are given in Section 6.5. Alternative conceptual models are discussed and evaluated along with their dispositions in Section 6.6. Model uncertainties and propagation of input uncertainties to output results are presented in Section 6.7. In Section 6.8, a description of the saturated zone as a barrier to transport of radionuclides is given.

6.1 MODELING OBJECTIVES

As summarized in Section 1, the objective of the site-scale SZ transport model is to simulate the transport of radionuclides in the saturated, fractured volcanic rock and alluvium near Yucca Mountain. The geohydrologic setting to be modeled is multifaceted with complex and diverse geochemical interactions possible between the groundwater, solutes, and the geological materials. Also, the intended use requires a computationally efficient model that is amenable to repeated runs for stochastic simulations. The approach taken here is to construct a plausible conceptual model of transport that incorporates the main SZ transport processes and is amenable to efficient computation (Sections 6.3 and 6.4). Alternate conceptual models and the implications of these models for transport predictions are evaluated relative to this base-case model (Section 6.6).

This transport model takes the calibrated flow model (DTN: SN0612T0510106.004 [DIRS 178956]) described in detail in *Saturated Zone Site-Scale Flow Model* (SNL 2007 [DIRS 177391], Sections 6.5, 6.6) as the starting point. The dependence of the flow field on various material and fluid properties, such as permeability and viscosity, is discussed in the SZ site-scale flow model report. Using the steady-state flow-velocity field supplied by the flow model, this transport model incorporates the transport processes of advection, dispersion, diffusion, retardation, and colloid-facilitated transport to compute the downstream radionuclide BTCs. Input parameters to the transport model are dispersivities in the volcanics, matrix porosity, matrix diffusion coefficient, the sorption distribution coefficient K_d in the matrix, flowing interval porosity, flowing interval spacing, flowing interval aperture, retardation factor in the flowing interval, bulk density of the alluvium, effective porosity of the alluvium, dispersivities in the alluvium, and the K_d in the alluvium. These are listed along with the base case and range of values in Table 6.4-2 in Section 6.4.3 and in Table 4-2 in Section 4. The site-scale SZ transport model generates BTCs for a unit point source, and the radionuclide release locations for various scenarios are discussed in *Saturated Zone Flow and Transport Model Abstraction* (SNL 2007 [DIRS 181650], Sections 6.3.3 and 6.5.2.13). The output from the transport model consists of radionuclide BTCs at the boundary of the accessible environment at 18 km for nonsorbing transport as well as radionuclides subject to reactive transport. The reactive transport includes dissolved species and colloid-facilitated transport. Breakthrough curves for aqueous species are calculated including the retardation due to sorption onto rock surfaces (Section 6.4.2.5). Breakthrough curves are generated for transport of radionuclides

attached reversibly to the colloids using modified transport parameters (Section 6.4.2.6.2). Breakthrough curves for the radionuclides attached irreversibly to the colloids are generated using retardation factors for colloids (Section 6.4.2.6.1). A small fraction of colloids travels with the groundwater unretarded and is handled using the BTCs for nonsorbing radionuclides without the process of matrix diffusion.

A variety of laboratory and field data supports the understanding of the transport processes of importance included in the transport model. The cross-hole tracer tests conducted at the C-wells complex support the use of a dual-porosity fracture flow and transport model of advection and dispersion coupled with a matrix-diffusion and matrix-sorption model (*Saturated Zone In-Situ Testing*, SNL 2007 [DIRS 177394], Sections 6.3.3 and 6.3.4). Additionally, several laboratory-scale colloid-facilitated plutonium transport experiments conducted in fractured volcanic rocks support the use of a colloid-facilitated transport model in the volcanics (Kersting and Reimus 2003 [DIRS 162421], Chapter 7; and DTNs: LA0301PR831361.003 [DIRS 162435] and LA0301PR831361.004 [DIRS 162436]). The model of transport in the alluvium with advection, dispersion, sorption, and colloid-facilitated transport is supported by the single-well tracer tests at the Nye County Alluvial Testing Complex (ATC) wells as presented in *Saturated Zone In-Situ Testing* (SNL 2007 [DIRS 177394], Section 6.5). Laboratory column transport experiments in Yucca Mountain alluvium have indicated that sorption should be included in the alluvium transport model *Saturated Zone In-Situ Testing* (SNL 2007 [DIRS 177394], Section 6.5.6). Likewise, colloid-facilitated plutonium transport experiments in laboratory-scale columns packed with Yucca Mountain alluvium (DTN: LA0301AA831352.001 [DIRS 162433]) have indicated that colloid-facilitated transport is a valid process to include in the alluvium transport model. These models are supported also by information available from analogue studies at the Nevada Test Site (NTS) (see Sections 7.1.1 and 7.1.2.6). The overall site-scale transport model is validated by comparison against transit times and flow paths deduced from hydrochemistry data (Section 7.2).

The site-scale SZ transport model is used directly in *Saturated Zone Flow and Transport Model Abstraction* (SNL 2007 [DIRS 181650]) for generating a set of radionuclide BTCs at the accessible environment for use in the TSPA simulations of radionuclide release to the biosphere. The outputs from the transport model are transit times, flow paths, and BTCs at the boundary of the accessible environment at 18 km for various radionuclides of concern. The results for the base case are given in Section 6.5.

6.2 FEATURES, EVENTS, AND PROCESSES

As stipulated in *Technical Work Plan for: Saturated Zone Analysis and Model Report Integration* (BSC 2006 [DIRS 177375]), this report addresses the saturated zone FEPs pertaining to the site-scale SZ transport that are included for TSPA (Table 6.2-1). Saturated zone FEPs for TSPA are given in DTN: MO0706SPAFEPLA.001 ([DIRS 181613], file *FEPs_be.mdb*, Table 7.1-1). Table 6.2-1 provides a list of FEPs that are relevant to this model analysis in accordance with their assignment in the LA FEP list. Specific reference to the various sections within this document where issues related to each FEP are addressed is provided in the table.

Table 6.2-1. Features, Events, and Processes Included in TSPA and Relevant to This Model Report

FEP No.	FEP Name	Sections That Support Disposition	FEP Topic Addressed in Other Saturated Zone Analysis or Model Reports
1.2.02.01.0A	Fractures	6.3, 6.4.2.4	Upstream Feeds[a] –SNL 2007 [DIRS 177391] Corroborating[b] –BSC 2004 [DIRS 170014], SNL 2007 [DIRS 177394], SNL 2007 [DIRS 174109], Section 6
1.2.02.02.0A	Faults	6.3, 6.4.2.1, 6.4.2.4	Upstream Feeds[a] – SNL 2007 [DIRS 177391] Corroborating[b] –SNL 2007 [DIRS 177394], SNL 2007 [DIRS 174109], Section 6
1.3.07.02.0A	Water table rise affects saturated zone	6.6, Appendix E	Upstream Feeds[a] –SNL 2007 [DIRS 177391] Corroborating[b] –BSC 2004 [DIRS 170009]
2.2.03.01.0A	Stratigraphy	6.3	Upstream Feeds[a] –SNL 2007 [DIRS 177391] Corroborating[b] –BSC 2004 [DIRS 174109], Section 6, BSC 2004 [DIRS 170014], SNL 2007 [DIRS 177394]
2.2.03.02.0A	Rock properties of host rock and other units	4.1.2, 6.3, 6.6, 7.1	Upstream Feeds[a] –SNL 2007 [DIRS 177391] Corroborating[b] –SNL 2007 [DIRS 177394], SNL 2007 [DIRS 174109], Section 6, BSC 2004 [DIRS 170014]
2.2.07.12.0A	Saturated groundwater flow in the geosphere	4.1.2, 6.3, 6.4, 6.6, 7.	Upstream Feeds[a] –SNL 2007 [DIRS 177391] Corroborating[b]–SNL 2007 [DIRS 177391], SNL 2007 [DIRS 177394], BSC 2004 [DIRS 170014], BSC 2004 [DIRS 170015]
2.2.07.13.0A	Water-conducting features in the saturated zone	4.1.2, 6.3, 6.6	Upstream Feeds[a]–SNL 2007 [DIRS 177391] Corroborating[b]–BSC 2004 [DIRS 170014], SNL 2007 [DIRS 177394], SNL 2007 [DIRS 174109], Section 6
2.2.07.15.0A	Advection and dispersion in the saturated zone	6.3 (Items 2 and 6), 6.4.2.2, 6.4.2.3, 4.1.2.1, 4.1.2.16, 7.1	Upstream Feeds[a]–SNL 2007 [DIRS 177391] Corroborating[b] –SNL 2007 [DIRS 177394], BSC 2004 [DIRS 170015]
2.2.07.16.0A	Dilution of radionuclides in groundwater	6.3, 6.4	Upstream Feeds[a]–N/A Corroborating[b]–N/A
2.2.07.17.0A	Diffusion in the saturated zone	6.3 (Item 3), 6.4.2.4, 4.1.2.10, 7.1	Upstream Feeds[a]–N/A Corroborating[b]–BSC 2004 [DIRS 170006], SNL 2007 [DIRS 177394], BSC 2004 [DIRS 170014]
2.2.08.01.0A	Chemical characteristics of groundwater in the saturated zone	6.3 (Items 4 and 7), Appendix A (A.3 and A.7)	Upstream Feeds[a] –N/A Corroborating[b]–SNL 2007 [DIRS 177391]
2.2.08.06.0A	Complexation in the saturated zone	6.4.2.4.1, 6.4.2.5, 6.4.2.6, Appendices A (A.7 and A.8) and B	Upstream Feeds[a]–N/A Corroborating[b]–N/A
2.2.08.08.0A	Matrix diffusion in the saturated zone	6.3 (Item 3), 6.4.2.4, 4.1.2.10, 7.1	Upstream Feeds[a]–N/A Corroborating[b]–BSC 2004 [DIRS 170014], SNL 2007 [DIRS 177394], BSC 2004 [DIRS 170006]
2.2.08.09.0A	Sorption in the saturated zone	6.3 (Items 4 and 7), 6.4.2.4, 6.4.2.5, 7.1, Appendix A (A.7, A.8)	Upstream Feeds[a]–N/A Corroborating[b] –BSC 2004 [DIRS 170006]
2.2.08.10.0A	Colloidal transport in the saturated zone	6.4.2.6, 7.1, Appendix B	Upstream Feeds[a]–BSC 2004 [DIRS 170006] Corroborating[b]–SNL 2007 [DIRS 177394]

Table 6.2-1. Features, Events, and Processes Included in TSPA and Relevant to This Model Report (Continued)

FEP No.	FEP Name	Sections That Support Disposition	FEP Topic Addressed in Other Saturated Zone Analysis or Model Reports
2.2.10.03.0A	Natural geothermal effects on flow in the saturated zone	6.1	Upstream Feeds[a]–SNL 2007 [DIRS 177391] Corroborating[b] –N/A
2.2.12.00.0B	Undetected features in the saturated zone	Appendix A, Appendix C	Upstream Feeds[a]–SNL 2007 [DIRS 177391] Corroborating[b]–SNL 2007 [DIRS 174109], Section 6, BSC 2004 [DIRS 170014], SNL 2007 [DIRS 177394]

[a] Upstream Feeds–Aspects of the saturated zone FEP dispositions adopted in this report are a result of saturated zone analyses performed in a directly upstream saturated zone model or analysis.

[b] Corroborating–Corroborative aspect(s) of the FEP topic is (are) discussed in a saturated zone analysis or model report.

6.3 BASE-CASE CONCEPTUAL MODEL

The transport of chemical species in the groundwater involves a variety of processes such as advection, dispersion, diffusion, sorption, and colloid-facilitated transport. These processes, in general, lead to retardation of the migration of transported species with respect to the bulk movement of the groundwater. Hence, the radionuclide transport times can be several orders of magnitude longer than the transport times of groundwater. Given the complex geohydrologic setting and the computational constraints imposed by the TSPA methodology, the approach taken here is to construct a plausible conceptual transport model that incorporates the main saturated zone transport processes and is amenable to efficient computation. Alternate conceptual models and the implications of these models for transport predictions are evaluated relative to this base-case model.

The base-case conceptual model of saturated zone transport begins in the neighborhood of the repository footprint at the water table, where the radionuclides enter the water table, and ends at the downstream boundary of the model. This model boundary is located to the south of, and downstream from the regulatory boundary of the accessible environment at 18 km downstream from the repository footprint. The flow path from the repository to the proposed boundary of the accessible environment at 18 km begins in the volcanic tuffs but ends in the alluvium, and different transport processes operate in the volcanic tuffs and the alluvium.

The components of the conceptual model are schematically illustrated in Figure 6.3-1. They are: (1) Radionuclides enter the saturated zone via fluids percolating through the unsaturated zone below the repository site. Within the saturated zone, they are transported with the groundwater that flows subhorizontally in a southerly or southeasterly direction. (2) The radionuclides advect and disperse with the groundwater through the fractured portions of the tuffs near the water table. (3) Fluid flow occurs preferentially within the flowing intervals, whereas stagnant fluid resides in the rock matrix. Solutes diffuse in and out of fluid within the rock matrix that is essentially stagnant. (4) Sorption reactions occur in volcanics between the rock matrix and some of the radionuclides, tending to retard the transport of these radionuclides. (5) Radionuclides can undergo colloid-facilitated transport in the volcanics. (6) The radionuclides advect and disperse with the groundwater through the alluvium. (7) Sorption reactions occur in alluvium between

the rock and some of the radionuclides, tending to retard the transport of these radionuclides. (8) Radionuclides can undergo colloid-facilitated transport in alluvium.

The boundary to the accessible environment is taken at 18 km downstream (10 CFR 63.302 [DIRS 180319]) of the repository footprint. As discussed above, the flow direction is generally southwards downstream from the repository. The southern boundary of the SZ site-scale flow model, which is also taken to be the southern boundary of the transport model, is more than 18 km downstream of the repository footprint (SNL 2007 [DIRS 177391], Section 6.3.1.6). Thus the site-scale SZ transport model encompasses the boundary to the accessible environment. The radionuclides reaching the model boundary are removed from the model, providing a boundary condition necessary for modeling the transport.

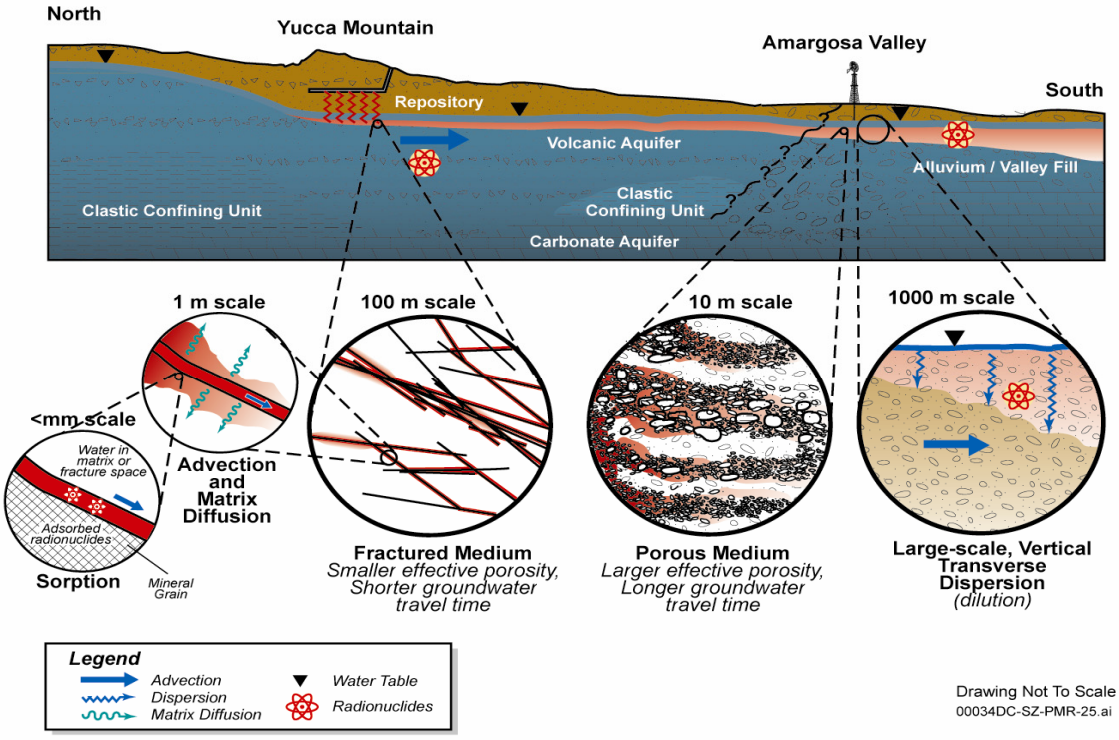

NOTE: This figure is for conceptual purposes only–the relative positions of the various geological units and locations shown here are not meant to accurately represent the actual settings. For the sake of clarity, the following processes are not explicitly indicated in this figure: dispersion and colloid-facilitated transport in the volcanics; and advection, longitudinal dispersion, sorption, and colloid-facilitated transport in the alluvium.

Figure 6.3-1. Schematic Illustration of the Conceptual Model of Transport Processes in the Volcanic Tuffs and the Alluvium

A discussion of each model component follows:

1. *Radionuclides enter the SZ via fluids percolating through the UZ below the repository site.* The source of radionuclides in the site-scale SZ transport model is provided by the UZ transport model. The nature of this source term and its relationship to various release scenarios is discussed in *Saturated Zone Flow and Transport Model*

Abstraction (SNL 2007 [DIRS 181650], Sections 6.3.3 and 6.5.2.13). The site-scale SZ transport model generates BTCs for a unit point source. The conceptual model of site-scale SZ transport is suitable for a range of locations of the source term, and the mathematical and computational model is designed to handle such variations. Thus, the SZ transport component of the site-scale SZ model is developed independently from a transport model for the unsaturated zone. As discussed in *Saturated Zone Flow and Transport Model Abstraction* (SNL 2007 [DIRS 181650], Section 6.3.3), this approach leads to results that are generally conservative with respect to radionuclide concentrations and transport times.

As shown in *Saturated Zone Site-Scale Flow Model* (SNL 2007 [DIRS 177391], Section 6.3.1.3), the general flow direction starting at the repository footprint is to the south. The flow lines remain shallow and subhorizontal within the saturated zone. Thus, fluid flow occurs within the fractured volcanics immediately below and downstream of the repository footprint, entering the alluvium further downstream, and continuing through the alluvium to the boundary of the accessible environment at 18 km.

2. *The radionuclides advect and disperse with the groundwater through the fractured portions of the tuffs near the water table*. Flow occurs within the fractured portions of the tuffs near the water table. Flow intervals identified in well tests correlate with fracture locations (Erickson and Waddell 1985 [DIRS 105279], p. 18), the extent of fracturing correlates reasonably well with the degree of welding (Waddell et al. 1984 [DIRS 101064], p. 26), and the degree of welding is one of the criteria used to define the submembers within a lithologic unit. In the SZ flow model, such lithologic members are represented as single zones, each represented by homogeneous hydrologic properties (SNL 2007 [DIRS 177391], Tables 6-2 and 6-10). This representation is also used in the transport model; however, the influence of heterogeneities within a permeability zone is incorporated into the model via dispersion and matrix diffusion as discussed below.

   A distinction must be made between fracture zones and individual fractures. Fracture zones are typically spaced tens of meters apart, with thicknesses on the order of meters, and contain broken-up matrix blocks and many intersecting fractures that are conduits to flow and to diffusion and retardation. Individual fractures, on the other hand, tend to be spaced as close as a meter or less, have thicknesses on the order of fractions of millimeters, and may or may not contribute to the flow of groundwater.

   The conceptual model is that high-permeability regions are offset by low-permeability regions due to the extensive faulting and fracturing observed in the volcanics (Luckey et al. 1996 [DIRS 100465], pp. 8 to 12) in the model domain. These low-permeability regions effectively will act as large-scale heterogeneities that give rise to large-scale macroscopic dispersion due to the tortuous nature of flow over the scale of hundreds of meters to kilometers. Field studies of transport and dispersion at a variety of length scales (from meters to kilometers) presented in *Saturated Zone In-Situ Testing* (SNL 2007 [DIRS 177394], Figures E-39 and E-40) and Neuman (1990 [DIRS 101464], Figure 1) show a trend toward larger apparent dispersion coefficients for transport

over longer distances. The estimates of dispersivities from the C-wells tracer tests presented in *Saturated Zone In-Situ Testing* (SNL 2007 [DIRS 177394], Section E.4.1) fall within the range of values from other sites, suggesting that transport in the fractured tuffs exhibits similar dispersive characteristics.

In an equivalent-continuum dispersion model, hydrogeologic features that may be present at scales smaller than the size of a typical grid cell are simulated as averages. The equivalent-continuum model averages the concentration variations within a grid block into a single value for the block. Concentration differences at scales smaller than the grid cell, if present, are not resolved. Whether this distinction is important depends on specific performance criteria and scenarios for exposure to humans or plants. Because the site-scale SZ flow and transport model is used to calculate radionuclide mass reaching the accessible environment at 18 km, which is then used to calculate groundwater concentrations in a representative volume of 3000 acre-feet in accordance with 10 CFR 63.312 [DIRS 180319), the above approach is considered appropriate.

3. *Fluid flow occurs preferentially within the flowing intervals, whereas stagnant fluid resides in the rock matrix*. Solutes diffuse in and out of fluid within the rock matrix that is essentially stagnant. Current hydrologic evidence supports the model of fluid flow within fracture zones in the moderately to densely welded tuffs of the saturated zone (e.g., Waddell et al. 1984 [DIRS 101064], Table 2, pp. 17 to 22). Hydraulic conductivities measured for core samples in the laboratory are orders of magnitude higher when the sample is fractured (Peters et al. 1984 [DIRS 121957], p. 60). Also, there generally is a positive correlation between fractures, identified using acoustic televiewer or borehole television tools, and zones of high transmissivity (Erickson and Waddell 1985 [DIRS 105279], Figure 3; Karasaki et al. 1990 [DIRS 148309], p. 811). The fluid travels preferentially within regions of large apertures with large sections of the fracture surface containing stagnant fluid or no fluid where the faces are in contact.

   Matrix materials conduct no fluid under natural groundwater flow conditions but are physically connected to the fracture fluid through the pore network. When a dissolved species travels with the fluid within a fracture, it can migrate by molecular diffusion into the stagnant fluid in the rock matrix. The Brownian motion of the solute molecules becomes dominant, and the effect of advection resumes when the solute re-enters the fracture. The result is a delay of the delivery of the solute to a downgradient location from what would be predicted if the solute had remained in the fracture.

   Several theoretical, laboratory, and field studies have demonstrated the validity of the matrix-diffusion model. Sudicky and Frind (1981 [DIRS 148342], pp. 161 to 163) developed a model of flow in an aquifer with diffusion into a surrounding aquitard to show that the movement of ^{14}C can be much slower than predicted if only movement with the flowing water is considered. Maloszewski and Zuber (1985 [DIRS 148312], pp. 353 to 354) reached a similar conclusion with a model for ^{14}C transport that consists of uniform flow through a network of equally spaced fractures with diffusion into the surrounding rock matrix between the joints. Maloszewski and Zuber present

analyses of several interwell tracer experiments that show that their matrix diffusion model can be used to provide simulations of these tests that are consistent with the values of matrix porosity obtained in the laboratory and aperture values estimated from hydraulic tests. In all cases, the results are superior when compared to previous analyses that did not include matrix diffusion effects. Finally, a data set of great relevance to the saturated zone beneath Yucca Mountain is the C-wells reactive tracer test presented in *Saturated Zone In-Situ Testing* (SNL 2007 [DIRS 177394], Section 6.3.), which demonstrated that models incorporating matrix diffusion provide more reasonable fits to the tracer experiment data than those that use a single continuum. The calculated transport times of saturated zone fluids determined from ^{14}C data (SNL 2007 [DIRS 177391], Table A6-11) are on the order of hundreds to thousands of years. As demonstrated in Figures 6.8-2a, 6.8-2b, and 6.8-3, model transit times without matrix diffusion are only on the order of several hundred years but become comparable with transit times estimated from the geochemical data when retardation due to matrix diffusion is included in the model. Thus, the ^{14}C ages are consistent with the conceptual model of interchange of solutes between fractures and matrix found in the matrix diffusion model.

Matrix diffusion is characterized using an abstracted model of uniform flow and transport in equally spaced, parallel fractures. This treatment represents a considerable simplification of the complex fracture network observed in volcanic rocks. It is acceptable because the particle-tracking model is intended to be used in large-scale simulations. The size of a typical computational grid block in the SZ flow and transport model is 250 m by 250 m. Average flowing intervals are subvertical with an average spacing of 20 m, order of magnitude smaller than the grid block size. In such circumstances, the use of an abstracted dual-porosity model with equally spaced, parallel fractures to capture the transport behavior is reasonable. In numerical modeling studies, such uncertainties are commonly addressed through the use of simpler conceptual models, such as this one, combined with sensitivity analyses to assess the importance of the uncertain parameters to the final model result. Therefore, a broad range of flowing interval spacings is used (Table 4-2), and the influence on the final results is quantified (Section 6.7).

4. *Sorption reactions occur in volcanics between the rock matrix and some of the radionuclides, tending to retard the transport of these radionuclides*. Radionuclide-rock interactions can potentially occur on the surfaces of fractures and within the rock matrix. Sorption reactions are chemical reactions that involve the distribution of chemical constituents between water and solid surfaces. Measurements show that the majority of water samples from the Yucca Mountain saturated zone (Appendix F and Table A-2b) are in oxidizing conditions or in transition between oxidizing-reducing conditions. Further, other factors being equal, oxidizing conditions lead to lower values of sorption coefficients (Appendix A). Hence, this conceptual model takes the geochemical conditions along the entire flow path to be oxidizing.

   Although the radionuclide-rock reactions can be complex in detail, they are represented in the transport model by a constant called the sorption coefficient K_d (Freeze and Cherry 1979 [DIRS 101173], p. 403, Equation 9.13). The use of the K_d

model requires that the reactions must be in equilibrium, instantaneous (kinetics), linear, and reversible. The validity of these requirements at Yucca Mountain and their implications for the transport model are discussed in Section 6.6 on alternate conceptual models. The surface-area to fluid-volume ratio and the mineral distributions are probably different in the fractures as compared to the matrix. As a conservative approach, sorption on individual fracture surfaces is not included in the transport model.

Maloszewski and Zuber (1985 [DIRS 148312], pp. 353 to 354) show that, at several sites, models that include the effect of chemical exchange reactions in the matrix lead to greater agreement with the field data than the models that do not include these effects. Of particular relevance to Yucca Mountain, the lithium tracer in the C-wells reactive tracer experiment (SNL 2007 [DIRS 177394], Section 6.3; and Robinson 1994 [DIRS 101154], pp. 86 to 93, Figures 5 and 8) was modeled using a matrix diffusion model with the sorption coefficient as an additional adjustable parameter. The fact that the early lithium response had the same timing as that of the nonsorbing tracers, but with a lower normalized peak concentration, is consistent with matrix diffusion coupled with sorption in the matrix (Robinson 1994 [DIRS 101154], Figure 7).

5. *Radionuclides can undergo colloid-facilitated transport in the volcanics*. Colloids are microscopic particles that are much larger than solute molecules. Solute molecules can absorb onto the colloid particles and be transported along with them. Because the colloidal particles are much larger in size and mass than the radionuclides that sorb onto them, the radionuclides do not affect the transport of the colloid particles. A discussion of colloid-facilitated transport is found in Section 6.4.2.6 and presented in *Saturated Zone Colloid Transport* (BSC 2004 [DIRS 170006]), Section 6.4). The colloids in the saturated zone can be of several types including natural colloids (typically clay or silica), waste-form colloids resulting from degradation of spent nuclear fuel or glass, and iron-oxyhydroxide colloids resulting from degradation of the waste container presented in *Waste Form and In-Drift Colloids-Associated Radionuclide Concentrations: Abstraction and Summary* (SNL 2007 [DIRS 177423], Section 6.3.1). The transport of colloids themselves in groundwater, as well as the mechanisms of sorption of radionuclides onto these colloid particles, needs to be included in the transport model for the saturated zone. The irreversibly sorbed radionuclides are taken to transport identically to the colloids to which they are sorbed.

   Mechanisms for transport of colloid particles in groundwater are distinct from those appropriate for the solute molecules and are considered in detail in *Saturated Zone Colloid Transport* BSC (2004 [DIRS 170006], Section 6.4). In the transport, movement of colloids is taken to occur within fractures only. Because of the relatively large size of the colloids, matrix diffusion of these particles is taken to be negligible. Several field observations have suggested that a small percentage of colloids transport with essentially no retardation in groundwater (Kersting et al. 1999 [DIRS 103282], p. 56, 58; Penrose et al. 1990 [DIRS 100811], p. 228), whereas the majority undergo either reversible or irreversible filtration, which can be described by a retardation factor. The retardation factor is dependent on several factors such as

colloid size, colloid type, and geochemical conditions (e.g., pH, Eh, and ionic strength). Details are presented in *Saturated Zone Colloid Transport* (BSC 2004 [DIRS 170006], Section 6).

The radionuclides that are reversibly absorbed onto colloids are modeled using the K_c model. This model represents the equilibrium partitioning of radionuclides between the aqueous phase and the colloidal phase with the distribution coefficient (Appendix B, Equations B-2 through B-7). Based on the estimated rate constants and the range of transport times being considered for transport through saturated fractured tuffs, it is shown in *Saturated Zone Colloid Transport* (BSC 2004 [DIRS 170006], Section 6.7) that the equilibrium partitioning is valid for all but the shortest transport times and overestimates transport mobility of radionuclides for the shortest transport times. The distribution coefficient K_c is modeled as a function of radionuclide sorption properties, colloid substrate properties, aqueous chemistry, and colloid concentration, but independent of the properties of the immobile media through which transport occurs (Appendix B). The radionuclides that are irreversibly absorbed onto the colloids are modeled to transport in a manner identical to the colloids onto which they are sorbed. The transport of the colloids is simulated using the advection-dispersion equation.

Colloid-facilitated transport is not included in the base-case site-scale SZ transport model because it represents the extreme case of nonsorbing radionuclides.

6. *The radionuclides advect and disperse with the groundwater through the alluvium*. Alluvium is valley-fill material consisting of heterogeneous deposits of sand and gravel interbedded with mud and clay-sized materials (Waddell et al. 1984 [DIRS 101064], p. 27). This material is not well consolidated and tends to exhibit a more porous, less-fractured nature. Because of the heterogeneous nature of the medium, flow occurs through the more permeable regions within the alluvium, and the lower-permeability regions act as flow barriers. This characteristic tends to reduce the amount of porosity actually available to flow and transport as compared to the total large-scale porosity of the alluvium. To account for this, the effective flow porosity of the alluvium is considered to be a stochastic variable with a range of input values presented in *Saturated Zone Flow and Transport Model Abstraction* (SNL 2007 [DIRS 181650], Section 6.5.2.3). Dispersion is caused by heterogeneities at all scales, from the scale of individual pore spaces to the scale of the thickness of individual strata and the length of structural features such as faults. The spreading and dilution of radionuclides that result from these heterogeneities could be important to the performance of the repository. The largest heterogeneities are represented explicitly in *Saturated Zone Site-Scale Flow Model* (SNL 2007 [DIRS 177391], Section 6.3.1.9). For dispersion at smaller scales, the advective-dispersion model is used with dispersion characterized using a dispersion coefficient tensor.

7. *Sorption reactions occur in alluvium between the solid surfaces and some of the radionuclides, tending to retard the transport of these radionuclides*. In contrast to the fractured tuffs, there are no cross-hole, field-scale tracer transport tests in the alluvium south of Yucca Mountain to confirm the in situ sorption characteristics. However, the

transport of sorbing solutes in porous media that is not controlled by fractures has been well studied (e.g., Freeze and Cherry 1979 [DIRS 101173], Chapter 9, pp. 385 to 457). Sorption coefficients onto alluvium from the Nye County wells have been measured for a few key radionuclides. For the remaining radionuclides, sorption coefficients have been estimated based on the corresponding values measured for crushed tuff (Appendix A). Radionuclides could also precipitate in the saturated zone, forming solid phases on the rock surfaces. The most credible mechanism for this effect to occur is through a different redox condition in the saturated zone. If the conditions were significantly more reducing, the valence states of actinides, such as neptunium, uranium, and plutonium, and fission products, such as technetium and iodine, could be lowered. Typically, in these groundwaters, this situation results in much lower solubilities of the radionuclides and hence, precipitation. This effect is an extreme form of retardation that renders the bulk of the radionuclide plume virtually immobile. The base-case model takes the conditions to be oxidizing, which results in higher solubilities and lower sorption coefficients than would be the case if reducing conditions were selected. Therefore, the base-case model produces more rapid transport of some radionuclides than would have resulted if lower valence states for these radionuclides were used.

8. *Radionuclides can undergo colloid-facilitated transport in alluvium*. The conceptual model for colloid-facilitated transport in the alluvium is essentially the same as in fractured tuffs in that colloids are modeled as transported only by advective water (no diffusion into stagnant water or into grains), and colloid attachment and detachment onto alluvial surfaces are described by first-order rate expressions. Because the colloidal particles are much larger in size and mass than the radionuclides that sorb onto them, the radionuclides do not affect the transport of the colloid particles. The irreversibly sorbed radionuclides are taken to transport identically to the colloids to which they are sorbed. A discussion of colloid-facilitated transport is found in Section 6.4.2.6 and in *Saturated Zone Colloid Transport* (BSC 2004 [DIRS 170006], Section 6.5). Laboratory site-specific data for colloid transport in the alluvium along with literature data are used to obtain distributions and bounds for attachment and detachment rate constants as given in *Saturated Zone Colloid Transport* (BSC 2004 [DIRS 170006], Section 6.5). Based on the estimated rate constants and the range of transport times being considered, it was shown in *Saturated Zone Colloid Transport* (BSC 2004 [DIRS 170006], Section 6.7) that the equilibrium partitioning is valid for all but the shortest transport times and overestimates transport mobility of radionuclides for the shortest transport times.

6.4 MATHEMATICAL AND COMPUTATIONAL FORMULATION OF BASE-CASE CONCEPTUAL MODEL

6.4.1 Overview of Model Formulation

The mathematical model formulation of the conceptual model presented in Section 6.3 is described below. The advection-dispersion equation is stated in Section 6.4.2.1, and the form of the dispersion tensor used in this work is given in Section 6.4.2.2. A random-walk particle-tracking method for implementing advection-dispersion in a numerical code is presented

in Section 6.4.2.3. A mathematical formulation to treat matrix diffusion in volcanics is presented next in Section 6.4.2.4, followed by a mathematical description of sorptive transport in alluvium in Section 6.4.2.5 and colloid-facilitated transport in Section 6.4.2.6. The computer implementation of the mathematical models in the code FEHM is verified with a suite of example problems using published examples, analytical and semianalytical solutions and examples run with different codes. These are documented in the verification report for FEHM (LANL 2003 [DIRS 166306]).

6.4.2 Mathematical Model Description

6.4.2.1 Advective Dispersive Transport

The fundamental mass transport equation for transport of a nonreactive, dilute species in a saturated porous medium (with no sources or sinks) has the form (e.g., Bear 1972 [DIRS 156269], p. 617, Equation 10.5.2):

$$\frac{\partial C}{\partial t} + \nabla \cdot (\bar{v} C) - \nabla \cdot (D' \nabla C) = 0 \qquad \text{(Eq. 1)}$$

where

- C denotes the solute concentration in units of moles per liter
- t is time
- $\bar{v}$ designates the porewater velocity vector
- D' denotes the dispersion tensor.

This equation serves as the starting point for all subsequent development below, and the sorbing and colloid-facilitated transport described later on. The porewater velocity is obtained from the flow field presented by the flow model (SNL 2007 [DIRS 177391], Section 6.5), taken to be independent of the transport model. The dispersion tensor D' appearing in Equation 1 is the sum of the mechanical dispersion tensor (D) for the flow system and the coefficient of molecular diffusion (D_0) in porous media. The effects of molecular diffusion are significant only at low flow velocities (Bear 1972 [DIRS 156269], p. 581). The following discussion deals with D for the sake of simplicity. The effects of molecular diffusion can be accounted for by adding in the term D_0 to the diagonal components of the displacement tensor.

6.4.2.2 Form of the Dispersion Tensor for Axisymmetric Media

Generally, the porewater velocity and the dispersion tensor vary spatially and temporally. Experimental studies of transport in groundwater have determined the nature of the dispersion tensor and the appropriate values of the dispersivity parameter. Gelhar (1997 [DIRS 145122], p. 164, Figure 8) showed that distinct values of the longitudinal dispersivity, the transverse dispersivity in the horizontal direction, and the transverse dispersivity in the vertical direction can be identified based on available field transport studies. The general conceptual model underlying the use of these three terms is one of horizontal flow with tortuous fine-scale flow through heterogeneous media. The details of transport through the heterogeneous media give

rise to the spreading of solute in the direction of flow and, to a lesser extent, transverse to the direction of flow. Of course, groundwater flow, though generally horizontal, exhibits vertical velocities locally in regions of upward or downward gradients, such as in areas of recharge or discharge or when the flow is subject to variability in hydraulic conductivity that diverts water vertically.

In practice, it is difficult, from available data, to propose more complex forms of the dispersion process and to determine the alternate dispersivity values from field observations. Nevertheless, it is quite possible that more complex forms are more representative, given the complexity and variety of different heterogeneities present in nature. An important conclusion from the available field data is that longitudinal dispersion is a strong function of scale, that is, the travel length of a solute plume in the medium (e.g., Neuman 1990 [DIRS 101464], Figure 1). In a typical groundwater flow model at the scale of a flow basin, characteristic flow distances of tens to hundreds of meters vertically may be present, compared to hundreds to thousands of meters horizontally. Given the difference in scale, it is not clear that the longitudinal dispersivity in the vertical direction should be set equal to that in the horizontal direction. In addition, in stratified porous media containing heterogeneities such as irregularly shaped beds or clay lenses, the characteristic scale of the heterogeneity encountered by a solute will be different in the horizontal and vertical directions, yielding potentially different values for longitudinal dispersion. This was the motivation for deriving a general form of the dispersion tensor for an axisymmetric medium (a medium that displays rotational symmetry about an axis) as presented by Lichtner et al. (2002 [DIRS 163821], Equations 1 and 47). This form of the dispersion tensor allows the longitudinal dispersivity in the vertical direction to be different from that in the horizontal direction. While quite general, this formulation requires the specification of four independent parameters, limiting the use of this approach in practical problems.

Burnett and Frind (1987 [DIRS 130526], Equations 6a to 6f) proposed a dispersion tensor for axisymmetric media, hereafter designated as D_{BF} and referred to as the BF-dispersion tensor. One attractive feature of the BF-dispersion tensor is that it involves only three independent parameters. These refer to longitudinal dispersion (α_L) and transverse horizontal (α_T^H) and vertical (α_T^V) dispersion. This form of the dispersion tensor was derived for isotropic media to account for different transverse dispersivities in the horizontal and vertical directions as observed in natural stratified media with flow along the bedding plane. For example, Zheng and Bennett (1995 [DIRS 154702], pp. 45 to 46) have used the Burnett-Frind tensor to model dispersion in axisymmetric media.

Burnett and Frind (1987 [DIRS 130526], Equations 6a to 6f) write the dispersion tensor as a matrix of coefficients in the form:

$$\overline{D}_{BF} = \begin{pmatrix} \alpha_L \frac{v_1^2}{v} + \alpha_T^H \frac{v_2^2}{v} + \alpha_T^V \frac{v_3^2}{v} & \left(\alpha_L - \alpha_T^H\right)\frac{v_1 v_2}{v} & \left(\alpha_L - \alpha_T^V\right)\frac{v_1 v_3}{v} \\ \left(\alpha_L - \alpha_T^H\right)\frac{v_2 v_1}{v} & \alpha_T^H \frac{v_1^2}{v} + \alpha_L \frac{v_2^2}{v} + \alpha_T^V \frac{v_3^2}{v} & \left(\alpha_L - \alpha_T^V\right)\frac{v_2 v_3}{v} \\ \left(\alpha_L - \alpha_T^V\right)v\frac{v_3 v_1}{v} & \left(\alpha_L - \alpha_T^V\right)\frac{v_3 v_2}{v} & \alpha_T^V \frac{v_1^2 + v_2^2}{v} + \alpha_L \frac{v_3^2}{v} \end{pmatrix} \quad \text{(Eq. 2)}$$

The main limitation with the form of the BF-dispersion tensor is that there is only one coefficient for longitudinal dispersion, which is, therefore, the same for flow in both the vertical and horizontal directions, i.e., parallel and perpendicular to the axis of symmetry, contrary to what one would expect for nonisotropic porous media. Nonetheless, for flow perpendicular to the axis of symmetry, the BF-tensor agrees with the more general form given by Lichtner et al. (2002 [DIRS 163821], Section 2.6). And for small values of vertical velocity, v_3, the generalized form of the dispersion tensor reduces to the form given by Burnett and Frind (1987 [DIRS 130526], Equations 6a to 6f). Hence, in situations where the axis of symmetry is vertical and the flow fields are horizontal to subhorizontal, as is the case at Yucca Mountain presented in *Saturated Zone Site-Scale Flow Model* (SNL 2007 [DIRS 177391], Section 6.5), this form of the dispersion tensor is adequate. This is the form that is used in the calculations presented in this report.

6.4.2.3 Random-Walk Particle-Tracking Method

Given a steady-state velocity field generated, for example, for an arbitrary permeability field, a random walk is superimposed on the flow field to describe dispersion and molecular diffusion. The general approach used in particle tracking is to replace the partial differential equation for the solute concentration, C, generally expressed by Equation 1, with random-walk displacements defined in differential form by the Langevin equation for position vector $x(t)$ (Gardiner 1997 [DIRS 145116], p. 80):

$$dx = A(x,t)dt + B(x,t)dW(t) \quad \text{(Eq. 3)}$$

The matrix A represents the deterministic background displacement determined by $\bar{v}$ and, in addition, contains contributions from the dispersion tensor. The displacement matrix B refers to a stochastic random-walk process that incorporates molecular diffusion and dispersion. The differential $dW(t)$ represents a Wiener process describing Brownian motion with the properties:

$$< dW >= 0 \quad \text{(Eq. 4)}$$

and

$$< dW(t)dW(t) >= Idt \quad \text{(Eq. 5)}$$

where the angular brackets represent the ensemble mean.

The equivalent Fokker-Planck equation corresponding to the Langevin equation for the conditional probability $P(x,t|x_0,t_0)$ is given by (Gardiner 1997 [DIRS 145116], p. 97):

$$\frac{\partial P}{\partial t} = -\nabla \cdot \left[A(x,t)P\right] + \nabla : \nabla \left[\frac{1}{2} B\tilde{B}P\right] \quad \text{(Eq. 6)}$$

where $\tilde{B}$ represents the transpose of the B matrix. The Fokker-Planck equation may be written in the form of the transport equation by rearranging Equation 6 to obtain:

$$\frac{\partial P}{\partial t} = -\nabla \cdot \left[\left(A(x,t) - \frac{1}{2}\nabla \cdot B\tilde{B}\right)P\right] + \nabla \cdot \left[\frac{1}{2} B\tilde{B}\nabla P\right] \quad \text{(Eq. 7)}$$

Comparing this modified Fokker-Planck equation with the continuum-based transport equation given in Equation 1 yields the identifications:

$$P(x,t \mid x_0,t_0) = \frac{N_A}{N} C(x,t), \quad \text{(Eq. 8)}$$

where N represents the number of particles and N_A denotes Avogadro's number,

$$A(x,t) = \vec{v} + \nabla \cdot D \quad \text{(Eq. 9)}$$

and

$$\frac{1}{2} B\tilde{B} = D \quad \text{(Eq. 10)}$$

Therefore, it is necessary to obtain the displacement matrix B based on the dispersion tensor D. To do this, the approach used by Tompson et al. (1987 [DIRS 145195], Appendix A) is followed in which a transformation that diagonalizes the dispersion tensor is carried out. By construction, the eigenvectors of the dispersion tensor depend only on the components of the flow velocity but not on the dispersivity values themselves. One eigenvector always points in the direction of the flow velocity. The other two eigenvectors are perpendicular to the direction of flow. The eigenvalue problem for D reads:

$$De_\lambda = \lambda \bar{e}_\lambda \quad \text{(Eq. 11)}$$

with eigenvalue λ and eigenvector $\bar{e}_\lambda$. Because the dispersion tensor is symmetric (Bear 1972 [DIRS 156269], p. 611), there exists an orthogonal transformation U that diagonalizes D (Tompson et al. 1987 [DIRS 145195], p. 106, Equation A-3):

$$\tilde{U}DU\tilde{U}e_\lambda = \lambda \tilde{U}\bar{e}_\lambda \quad \text{(Eq. 12)}$$

where $\widetilde{U}$ is the transpose of U, with:

$$\widetilde{U}DU = \hat{D} \quad \text{(Eq. 13)}$$

where $\hat{D}$ is a diagonal matrix, and U satisfies the relations:

$$U\widetilde{U} = \widetilde{U}U = I \quad \text{(Eq. 14)}$$

Expressing $\hat{D}$ in the form:

$$\hat{D} = Q\widetilde{Q} \quad \text{(Eq. 15)}$$

with Q diagonal, then gives:

$$2D = 2U\hat{D}\widetilde{U} = 2UQ\widetilde{Q}\widetilde{U} = B\widetilde{B} \quad \text{(Eq. 16)}$$

From this relation it follows that the displacement matrix B is given by (Tompson et al. 1987 [DIRS 145195], p. 107, Equation A-10):

$$B = \sqrt{2}UQ \quad \text{(Eq. 17)}$$

The implementation of the particle-tracking model requires a finite difference form of Equation 3 at time step *n*, which in this model is given by:

$$X_i^n = X_i^{n-1} + A_i\Delta t + \sqrt{\Delta t}\sum_j B_{ij}Z_j \quad \text{(Eq. 18)}$$

with

$$dW_j = Z_j\sqrt{\Delta t} \quad \text{(Eq. 19)}$$

for a time step Δt, where Z_j represents a uniform random number occurring with unit probability over the interval $-\frac{1}{2}$ to $\frac{1}{2}$.

The final step in the derivation is to determine the form of the displacement matrix B. It is given below for the Burnett and Frind tensor given above in Equation 2 (Lichtner et al. 2002 [DIRS 163821], Equation 66).

$$B = \begin{pmatrix} \frac{v_1}{v}\sqrt{2(\alpha_L v + D_0)} & -\frac{v_1 v_3 \sqrt{2(\alpha^v{}_T v + D_0)}}{v\sqrt{v_1^2 + v_2^2}} & -\frac{v_2\sqrt{2[\alpha_T^H (v_1^2 + v_2^2) + \alpha_T^v v_3^2]/v + 2D_0)}}{\sqrt{v_1^2 + v_2^2}} \\ \frac{v_2}{v}\sqrt{2(\alpha_L v + D_0)} & -\frac{v_2 v_3 \sqrt{2(\alpha^v{}_T v + D_0)}}{v\sqrt{v_1^2 + v_2^2}} & \frac{v_1\sqrt{2[\alpha_T^H (v_1^2 + v_2^2) + \alpha_T^v v_3^2]/v + 2D_0)}}{\sqrt{v_1^2 + v_2^2}} \\ \frac{v_3}{v}\sqrt{2(\alpha_L v + D_0)} & \sqrt{2\frac{v_1^2 + v_2^2}{v^2}(\alpha^v{}_T v + D_0)} & 0 \end{pmatrix} \quad \text{(Eq. 20)}$$

In summary, the particle trajectory is computed by a finite difference technique expressed in Equation 18. The first displacement term of this equation ($A\Delta t$) is deterministic, with A defined in Equation 9. This expression captures the movement of particles in the streamlines defined by the flow field. The term $\nabla \cdot D\Delta t$ is required to reproduce the transport equation correctly for cases in which there are gradients in velocity or dispersion coefficient. It reduces to zero for uniform flow fields and constant dispersivity. What is retained in this case is transport along the flow streamline governed by the flow field. The last term in Equation 18 is a stochastic random-walk term to simulate dispersion, with the form of the matrix B derived for the Burnett and Frind dispersion coefficient tensor in Equation 20.

Determination of the advection portion of the deterministic term $A\Delta t$ requires that the velocity at the particle location be determined. In this version of the code FEHM, the method is restricted to orthogonal finite-element grids. This simplification means that the control volume associated with each grid point is a brick-shaped element. Velocity interpolation within a cell is then determined quickly and easily using the velocity interpolation scheme first derived by Pollock (1988 [DIRS 101466], Equations 4a to 5c). Using that scheme, the code determines, for a given particle at a given location within the cell, the time required to exit the cell and the location where it leaves. If this time is greater than the time step Δt, the particle location within the cell is computed. If the time is less than the time step Δt, the particle is forced to stop at this location and then proceed in another step within the adjoining cell. This process is repeated until the ending time Δt is reached. At the end of this time step, the term $\nabla \cdot D\Delta t$ is used to move the particle deterministically to correct for gradients in the dispersion coefficient. A differencing scheme on the finite-element grid using a trilinear interpolation analogous to the method described by LaBolle et al. (1996 [DIRS 105039], pp. 587 to 588) is used to compute these terms, with the modification that the interpolated quantity is the local Darcy flux rather than the fluid velocity. This modification yields smoother results in situations such as those encountered at volcanic rock-alluvium interfaces, where local porosity can change by several orders of magnitude from a node to its neighbor. Finally, the random-walk term is applied (the final term in Equation 18) using the B matrix derived above (Equation 20).

For this method to work properly, the time step must be selected such that, on average, a particle takes several time steps within each cell. In a system with large variations in porewater velocity due to permeability and porosity differences from cell to cell, the appropriate time step can vary greatly throughout the domain. In FEHM, this factor is accounted for by dynamically determining the characteristic time step in an approach similar to that developed by Wen and Gomez-Hernandez (1996 [DIRS 130510], p. 137). In a given cell, the magnitude of the velocity in the cell is used to scale the time step. The time required to traverse the cell completely in each

of the three coordinate directions is computed, and the minimum is determined. Then a user-defined parameter called the Courant factor is multiplied by this minimum time to obtain the time step for the particle within the cell. This approach ensures that several steps are taken by a particle within a cell but minimizes computational time by tailoring each time step to the characteristic velocities within the cells.

Applying the random-walk method on grids and flow fields, it was found that the theoretically simple inclusion of the $\nabla \cdot D$ term to correct for velocity gradients may not be sufficient to account for regions with highly variable velocity fields. In short, computation of $\nabla \cdot D$ on the scale of the finite-element grid may not be sufficient to capture the magnitude of this term adequately. For example, in high-permeability zones immediately adjacent to confining units of low permeability, the gradient is not captured sufficiently accurately to prevent the artificial meandering of a small number of particles into the low-permeability region. As a result, some particles are held up for an unrealistically long time in these zones, resulting in a nonconservative tailing of the solute BTC at a downstream location. To correct this problem, a user-defined velocity-scaling parameter can be defined to prohibit particles from entering the low-velocity domain by random-walk processes. If the ratio of the velocity before and after the random-walk jump is less than this parameter, the code prohibits the jump, and the particle is returned to the original position where another jump is taken with a different set of random numbers.

The particle tracking method presented here, as discussed by Lichtner et al. (2002 [DIRS 163821]), has the advantage that solute mass is automatically conserved as long as the number of particles is tracked in the numerical implementation, and the method is free from numerical convergence and numerical dispersion problems encountered by the methods that use the approach of solving discretized forms of the advection dispersion equation (Equation 1). Further, the boundary conditions described in Section 6.3 are easily implemented by removing from further computations any particles that reach a model boundary.

To report the results of a particle-tracking simulation, two options are available. The first requires the definition of a zone consisting of a set of finite-element grid points representing a portion of the model domain where transport results are desired. For example, a “boundary of the accessible environment” compliance boundary, which is a given distance from the repository, can be defined by listing all of the nodes in the boundary. Then the code determines the first arrival time of each particle at any node in this fence and reports the cumulative arrival time distribution for all particles. This arrival-time distribution can then be converted to a groundwater concentration using a representative volume of 3,000 acre-feet in accordance with 10 CFR 63.312 [DIRS 180319], and the resulting curve can be used as the input to the performance assessment analysis. Alternatively, the concentration of particles at any cell in the finite-element domain can be reported as the number of particles residing in the cell divided by the fluid mass in the cell. Concentrations computed in this way represent the in situ concentration in response to the injection of a pulse of solute at time zero. To obtain the cumulative BTC, a time integration of these results may be performed, yielding the in situ concentration BTC at the node in response to a step change in concentration.

6.4.2.4 Matrix Diffusion in Fractured Geological Media

To incorporate the influence of sorption and matrix diffusion, the residence time transfer function particle-tracking method outlined in the FEHM models and methods document (Zyvoloski et al. 1997 [DIRS 110491], pp. 41 to 42) has been adapted to the particle-tracking algorithm. In this method, adjustments to the transport time of a particle are made to account for the influence of physicochemical processes such as sorption and matrix diffusion. During its path along a streamline, the particle transport time is governed by a transfer function describing the probability of the particle spending a given length of time on that portion of its path. For a cumulative probability distribution function of particle residence times, the transport time of a particle along this portion of its path is computed by generating a random number between 0 and 1 and determining the corresponding residence time. On average, if a large number of particles travel through this portion of the model domain, the cumulative residence time distribution of particles will reproduce the shape of the transfer function. The form of the transfer function is derived from an analytical or numerical solution to capture the appropriate processes being considered. A suite of type curves were generated for numerically implementing the transfer function.

6.4.2.4.1 Mathematical Description of Matrix Diffusion and Sorption

In this particle-tracking algorithm, the schematic model depicted in Figure 6.4-1 is used to provide a transfer function for the case of fracture flow and diffusion between equally spaced fractures. In this model:

z = spatial coordinate along the fracture
t = time
$2b$ = fracture aperture
$2B$ = mean fracture spacing
v = linear groundwater velocity in the fracture
θ = porosity of the matrix
q = diffusive flux from fracture to matrix
K_d = distribution coefficient in the fracture
k'_d = distribution coefficient in the matrix
R' = retardation factor in the matrix
R = retardation factor in the fracture
ρ_b = bulk density of the matrix
ρ_w = density of water
D' = matrix effective diffusion coefficient
D = dispersion coefficient in the fracture
c = concentration at z along the fracture
c_0 = source concentration at $z = z_0$.

The equations describing the radionuclide transport in the fractures and matrix are (Robinson 1994 [DIRS 101154], p. 81, Equations 1 and 2):

$$\frac{\partial c}{\partial t} + \frac{v}{R}\frac{\partial c}{\partial z} - \frac{D}{R}\frac{\partial^2 c}{\partial z^2} + \frac{q}{bR} = 0 \qquad \text{(Eq. 21a)}$$

and in the matrix:

$$\frac{\partial c}{\partial t} - \frac{D'}{R'}\frac{\partial^2 c}{\partial x^2} = 0 \qquad \text{(Eq. 21b)}$$

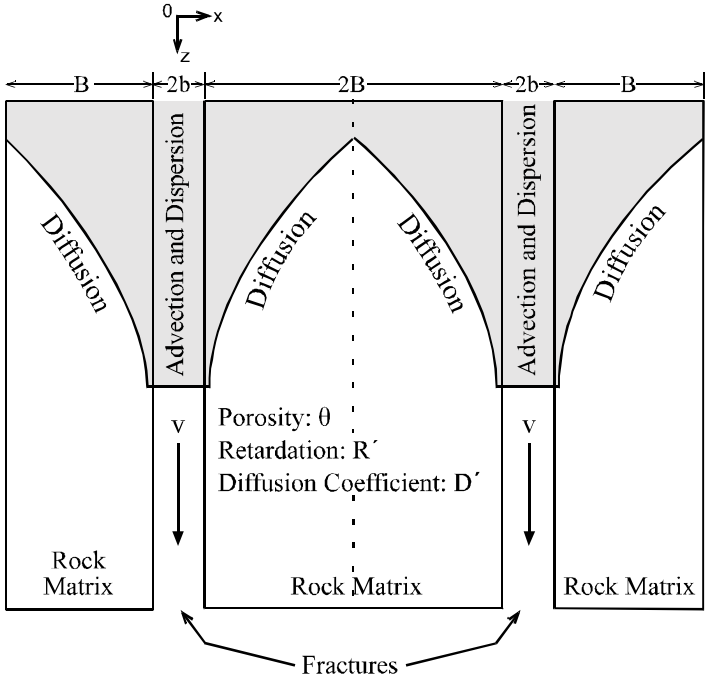

Figure 6.4-1. Schematic of the Matrix Diffusion Submodel

The distribution coefficient and the retardation factor are related by (Freeze and Cherry 1979 [DIRS 101173], p. 404, Equation 9.14):

$$R' = 1 + \frac{\rho_b}{\theta} k'_d \qquad \text{(Eq. 22)}$$

The transient solution for contaminant transport with $D = 0$ in parallel fractures, for $c = c_0$ at the inlet end with $z = 0$, and $\partial c/\partial x = 0$ at the center line between the fractures at $x = B$ (Figure 6.4-1) is given by Sudicky and Frind (1982 [DIRS 105043], p. 1637, Equation 28):

$$\frac{c}{c_0} = 0, T^0 \le 0 \qquad \text{(Eq. 23)}$$

$$\frac{c}{c_0} = \frac{1}{\pi}\exp\left(\frac{R\lambda z}{v}\right)\int_0^{\infty} \frac{\varepsilon}{\lambda^2 + \varepsilon^4/4}\exp(\varepsilon_R{}^0)\left[\exp(-\lambda T^0)\left\{\frac{\varepsilon^2}{2}\sin(\varepsilon_I{}^0) - \lambda\cos(\varepsilon_I{}^0)\right\} + \frac{\varepsilon^2}{2}\sin(\Omega_I{}^0) + \lambda\cos(\Omega_I{}^0)\right] d\varepsilon, \quad T^0 > 0 \qquad \text{(Eq. 24)}$$

where λ is the radioactive decay constant for the element under consideration, ε is an integration variable, and

$$T^0 = t - \frac{Rz}{v} \qquad \text{(Eq. 25)}$$

$$\varepsilon_R{}^0 = -\frac{\omega\varepsilon}{2}\left(\frac{\sinh(\sigma\varepsilon) - \sin(\sigma\varepsilon)}{\cosh(\sigma\varepsilon) + \cos(\sigma\varepsilon)}\right) \qquad \text{(Eq. 26)}$$

$$\varepsilon_I{}^0 = \frac{\varepsilon^2 T^0}{2} - \frac{\omega\varepsilon}{2}\left(\frac{\sinh(\sigma\varepsilon) + \sin(\sigma\varepsilon)}{\cosh(\sigma\varepsilon) + \cos(\sigma\varepsilon)}\right) \qquad \text{(Eq. 27)}$$

$$\Omega_I{}^0 = \frac{\omega\varepsilon}{2}\left(\frac{\sinh(\sigma\varepsilon) + \sin(\sigma\varepsilon)}{\cosh(\sigma\varepsilon) + \cos(\sigma\varepsilon)}\right) \qquad \text{(Eq. 28)}$$

with

$$\omega = \frac{\theta(R'D')^{1/2} z}{bv} \qquad \text{(Eq. 29)}$$

$$\sigma = (R'/D')^{1/2}(B - b) \qquad \text{(Eq. 30)}$$

Using the transformation variables:

$$\tau_0 = \frac{z}{v} \qquad \text{(Eq. 31)}$$

$$\varepsilon_1 = \varepsilon\tau_0^{1/2} \qquad \text{(Eq. 32)}$$

Equations 23 through 30 can be rewritten as:

$$\frac{c}{c_0} = 0, \; T_1^0 \le 0 \qquad \text{(Eq. 33)}$$

$$\frac{c}{c_0} = \frac{1}{\pi}\exp(R\lambda\tau_0)\int_0^{\infty} \frac{\varepsilon_1}{\lambda^2\tau_0^2 + \varepsilon_1^4/4}\exp(\varepsilon_R{}^0)\left[\exp(-\lambda\tau_0 T_1^0)\left\{\frac{\varepsilon_1^2}{2}\sin(\varepsilon_I{}^0) - \lambda\tau_0\cos(\varepsilon_I{}^0)\right\} + \frac{\varepsilon_1^2}{2}\sin(\Omega_I{}^0) + \lambda\tau_0\cos(\Omega_I{}^0)\right] d\varepsilon_1, \quad T_1^0 > 0 \qquad \text{(Eq. 34)}$$

where

$$T_1^0 = \frac{t}{\tau_0} - R \quad \text{(Eq. 35)}$$

$$\varepsilon_R{}^0 = -\frac{\omega_1 \varepsilon_1}{2}\left(\frac{\sinh(\sigma_1\varepsilon_1) - \sin(\sigma_1\varepsilon_1)}{\cosh(\sigma_1\varepsilon_1) + \cos(\sigma_1\varepsilon_1)}\right) \quad \text{(Eq. 36)}$$

$$\varepsilon_I{}^0 = \frac{\varepsilon_1^2 T_1^0}{2} - \frac{\omega_1 \varepsilon_1}{2}\left(\frac{\sinh(\sigma_1\varepsilon_1) + \sin(\sigma_1\varepsilon_1)}{\cosh(\sigma_1\varepsilon_1) + \cos(\sigma_1\varepsilon_1)}\right) \quad \text{(Eq. 37)}$$

$$\Omega_I{}^0 = \frac{\omega_1 \varepsilon_1}{2}\left(\frac{\sinh(\sigma_1\varepsilon_1) + \sin(\sigma_1\varepsilon_1)}{\cosh(\sigma_1\varepsilon_1) + \cos(\sigma_1\varepsilon_1)}\right) \quad \text{(Eq. 38)}$$

with

$$\omega_1 = \frac{\theta(R'D'\tau_0)^{1/2}}{b} \quad \text{(Eq. 39)}$$

$$\sigma_1 = \left(\frac{R'}{D'\tau_0}\right)^{1/2}(B-b) \quad \text{(Eq. 40)}$$

For the case of no radioactive decay ($\lambda = 0$):

$$\frac{c}{c_0} = \frac{1}{\pi}\int_0^\infty \frac{2}{\varepsilon_1}\exp(\varepsilon_R{}^0)\left[\sin(\varepsilon_I{}^0) + \sin(\Omega_I{}^0)\right]d\varepsilon_1 \quad \text{(Eq. 41)}$$

Therefore, to implement this model, the algorithm requires the input of transport parameters defined in Equations 39 and 40. With the transport parameters and the unretarded transport time τ_0 within a given portion of the path known from the advection part of the particle, values of ω_1 and σ_1 are computed, thereby fully defining the transfer function for this portion of the particle's travel path. Given these parameters, the model returns a value of the delayed transport time of the particle from Equation 35 that is consistent with the matrix diffusion model. To implement this model in FEHM, a series of type curves were generated (output DTN: LA0302RP831228.001) at specified values of ω_1 and σ_1 using a code FRACT_p V1.0 (FRACT_p V1.0, STN: 11009-1.0-00) (LANL 2003 [DIRS 164509]). For given values of the parameters, the code performs a linear interpolation between the nearest type curves to obtain the result. This approach of tabulating the results of the analytical solution is much more computationally efficient than computing the values through integration at run time. Under limiting conditions of low diffusion and/or large fracture spacing, the infinite spacing solution of Tang et al. (1981 [DIRS 101160], p. 559, Eq. 35) implemented in the cell-based particle-tracking algorithm of FEHM can be used instead of the finite spacing model. A provision in the code allows the Tang solution to be invoked in this particle-tracking model as well, but it should be

used only when the characteristic diffusion time to the centerline between the fractures (of order B^2/D') is much greater than the time of the simulation.

The final step of the model development is to integrate the matrix diffusion model with the random-walk transport model developed in Section 6.4.2.3. Specifically, the time intervals over which the time delays are applied must be set in a manner that allows for computationally efficient and accurate solutions to be obtained. In this model, the time delay is applied to a particle at the time at which it exits a cell, after having determined the cumulative time the particle spent in advective transport through the cell. Within a cell, the transport properties of diffusion and sorption are, by definition, uniform, so that a unique set of transport dimensionless parameters can be defined. Alternatively, the time delay could be applied at each segment of the particle path, resulting in potentially many time delays for a particle within each cell as it is transported by advection and random-walk dispersion. However, in initial prototype testing using this approach, it was determined that the technique, although theoretically equivalent to the application of time delay once per cell, showed that practical limitations of reduced accuracy and reduced computational efficiency resulted. Therefore, the code was developed with the time delay applied only at the time the particle exits the cell, which can occur either by advection or by random-walk dispersion.

To apply the time delay, the particle is held at that location until the time the simulation run catches up to the time of that particle, after which the particle is allowed to resume its transport. Finally, it is noted that for sorption without matrix diffusion, the time delay is computed deterministically by computing a retardation factor based on the sorption coefficient K_d, but otherwise, the method is identical to the matrix-diffusion method. Alternatively, this particular case could have been handled through a simple adjustment of the transport velocity, but the implementation using the time-delay method was simpler because it is consistent with the matrix-diffusion method just described.

6.4.2.5 Mathematical Description of Sorptive Transport in Alluvium

Equation 1 for advective-dispersive transport can be generalized to include sorption onto the rock surfaces as follows (Freeze and Cherry 1979 [DIRS 101173], Equations 9.9 and A10.14):

$$\frac{\partial C}{\partial t} + \nabla \cdot (\vec{v} C) - \nabla \cdot (D \nabla C) = \frac{\rho_b}{\theta} \frac{\partial S}{\partial t} \quad \text{(Eq. 42)}$$

where S is the mass of the transported species adsorbed on the solid per unit bulk dry mass of the porous medium. For linear, reversible, equilibrium sorption, the K_d model can be used, and S and C are related as follows (Freeze and Cherry 1979 [DIRS 101173], Equation 9.12):

$$S = K_d C \quad \text{(Eq. 43)}$$

6.4.2.6 Colloid-Facilitated Transport

Radionuclides can attach to the colloids either reversibly or irreversibly. The radionuclides that are attached to the colloids reversibly are partitioned between the colloids, rock surfaces and the aqueous phase. On the other hand, the radionuclides that are irreversibly attached to the colloids

stay attached to the particles for the entire duration of the transit through the saturated zone to the boundary of the accessible environment at 18 km. The colloid-facilitated transport of the radionuclides follows different mechanisms for the two different types of attachments, which are summarized in Table 6.4-1 and described below.

Table 6.4-1. Colloid-Facilitated Transport of Radionuclides

Radionuclides Attached Reversibly to Colloids	**Radionuclides Attached Irreversibly to Colloids (Transport in a Manner Identical to Colloids)**	
Radionuclides spend part of the time attached to the colloids and part of the time in the aqueous phase or attached to rock surfaces.	Radionuclides are embedded in the colloids, mostly those derived from the waste form degradation. This is discussed in *Saturated Zone Colloid Transport* (BSC 2004 [DIRS 170006], Sections 6.3 and 6.6). The radionuclides travel in a manner identical to the colloids.	
	Normal (Fraction that Undergoes Reversible Filtration)	**Fast (Fraction That Does Not Undergo Reversible Filtration)**
Radionuclides are treated in the site-scale SZ transport model using equations similar to those for aqueous phase transport (Appendix B) but with modified parameters. The diffusion coefficient in volcanics is reduced with respect to that for aqueous transport. This is given by Equation 45a in Section 6.4.2.6.2. The equation is derived in *Saturated Zone Flow and Transport Model Abstraction* (SNL 2007 [DIRS 181650], Section 6.5.1.1). The sorption coefficient is modified and given in Equation 46, Section 6.4.2.6.2 and derived in *Saturated Zone Flow and Transport Model Abstraction* (SNL 2007 [DIRS 181650], Section 6.5.1.1). K_c needed in Equation 45a and 46 is given in Equation 45b. The groundwater concentration of colloids and the sorption coefficient onto colloids are summarized in Table 4-2 and taken from *Waste Form and In-Drift Colloids-Associated Radionuclide Concentrations: Abstraction and Summary* (SNL 2007 [DIRS 177423], Section 6.3.1). Section 7.1.2.5.2 gives confidence-building arguments for this process based on laboratory data and theoretical considerations from literature. The transport of these radionuclides is simulated in the site-scale SZ transport model using the same approach as the aqueous species but with modified diffusion coefficient and K_d as described above.	The colloids undergo "reversible filtration." This is discussed in *Saturated Zone Colloid Transport* (BSC 2004 [DIRS 170006], Section 6.4) where field and laboratory data are analyzed to get "attachment rate constants" and "detachment rate constants." These lead to a retardation factor for the colloids (Equation 44). The same retardation factor applies to the fraction of radionuclides absorbed irreversibly onto colloids. The range of values for this fraction is given in *Waste Form and In-Drift Colloids-Associated Radionuclide Concentrations: Abstraction and Summary* SNL 2007 [DIRS 177423], Section 6.3). Section 7.1.2.5.1 gives confidence-building arguments for "colloid filtration" based on C-wells data. The transport of these radionuclides is simulated in the site-scale SZ transport model using the same approach as the aqueous species but with zero diffusion coefficient and colloid retardation factor as explained above.	A small fraction of colloids travels with the groundwater without any retardation. The radionuclides sorbed onto this fraction also travel without any retardation. The transport times for this fraction are the same as those for nonsorbing radionuclides. The range of values of this fraction is given in Table 4-2 and discussed in *Waste Form and In-Drift Colloids-Associated Radionuclide Concentrations: Abstraction and Summary (*SNL 2007 [DIRS 177423], Section 6.3). Section 7.1.1.1.3 gives confidence-building arguments for the occurrence of this process based on NTS data. The BTCs for these radionuclides are simulated without sorption and matrix diffusion.

6.4.2.6.1 Radionuclides Attached Irreversibly to the Colloids

These radionuclides are embedded in the colloids and travel in a manner identical to the colloids themselves. This fraction of radionuclides does not experience any matrix diffusion and is transported at the same rate as the colloid particles .The majority of the colloid particles undergo filtration during transport through the saturated zone; however, a small fraction travels with the movement of the bulk water without any retardation. The transport of colloid particles is included in the site-scale SZ transport model using the process of reversible filtration shown in *Saturated Zone Colloid Transport* (BSC 2004 [DIRS 170006] Sections 6.4 and 6.5). The transport of the colloids is simulated using the advection-dispersion equation, and colloids are taken not to diffuse. Filtration of the colloids can be described by a retardation factor, R_{col}. The value of R_{col} is dependent on several factors such as colloid size, colloid type, and geochemical conditions (e.g., pH, Eh, and ionic strength) as shown in *Saturated Zone Colloid Transport* (BSC 2004 [DIRS 170006], Section 6.3). These factors are folded into the distribution of R_{col} that has been developed from field and experimental data collected under varying geochemical conditions with different colloid types and sizes as discussed in *Saturated Zone Colloid Transport* (BSC 2004 [DIRS 170006], Tables 6-2 and 6-3). Attachment rate constants, K_{att}, and detachment rate constants, K_{det}, of colloids to the rock matrix have been measured, and R_{col} distributions have been developed for the fractured volcanics and alluvium. The relationship between R_{col}, K_{att}, and K_{det} is given by (BSC 2004 [DIRS 170006], Equation 6-3):

$$R_{\text{col}} = 1 + \frac{K_{\text{att}}}{K_{\text{det}}} \qquad \text{(Eq. 44)}$$

The attachment rate constant is also used to determine the fraction of the colloids that transport with no retardation. Specifically, colloids for which one over the attachment rate constant is smaller than the transport time through the system will transport with no retardation. The fraction of colloids that transport unretarded is documented in *Saturated Zone Colloid Transport* (BSC 2004 [DIRS 170006], Table 6-4).

6.4.2.6.2 Radionuclides Attached Reversibly to the Colloids

Radionuclides cannot diffuse into the matrix while attached to colloids because the colloid particles themselves cannot diffuse into the matrix (Section 6.3). Hence the fraction of radionuclides that are reversibly attached onto the colloids experiences a reduction in the diffusion process because this fraction can diffuse into the matrix only while unattached to the colloids. In the volcanics, this is implemented through a reduction in the effective diffusion coefficient for the radionuclides attached reversibly to colloids, given by the following equation given in *Saturated Zone Flow and Transport Model Abstraction* (SNL 2007 [DIRS 181650], Equation 6-9):

$$D_e^{adjusted} = \frac{D_e}{(1 + K_c)^2} \qquad \text{(Eq. 45a)}$$

where

$D_e^{adjusted}$ is the effective diffusion coefficient of the radionuclide adjusted for the effect of reversible attachment to colloids,

D_e is the effective diffusion coefficient of the radionuclide in the matrix, and

K_c is the distribution parameter expressing the relative amount of radionuclide residing on the colloids with respect to that in the aqueous phase, given by (Appendix B, Equation B-4):

$$K_c = C_c * K_{d-c} \quad \text{(Eq. 45b)}$$

where

C_c is the colloid concentration in the groundwater, and

K_{d-c} is the sorption coefficient for the radionuclide onto the colloids.

The alluvium is modeled as a single porosity medium; hence matrix diffusion is not included. However, the sorption coefficient for the radionuclide onto the alluvium is modified due to the competition with the colloids as follows, shown in *Saturated Zone Flow and Transport Model Abstraction* (SNL 2007 [DIRS 181650], Section 6.5.1.1, Equation 6-5):

$$K_d^{adjusted} = \frac{K_d^{original}}{(1 + K_c)} \quad \text{(Eq. 46)}$$

where

$K_d^{original}$ is the sorption coefficient for the radionuclide in the alluvium in the absence of colloids, and

$K_d^{adjusted}$ is the sorption coefficient for the radionuclide in the alluvium in the presence of reversible attachment to colloids.

Equation 46 does not apply to the transport of radionuclides in the volcanic matrix. This is because the conceptual model of transport in the site scale saturated zone is that the groundwater in the volcanic matrix is stagnant and the colloids being transported with the groundwater in the flowing intervals do not diffuse into the volcanic matrix.

As a simplifying assumption in the derivation of the Equations 45a and 46, the filtration of the colloids themselves is not considered. Thus the adjusted parameters $D_e^{adjusted}$ and $K_d^{adjusted}$ tend to underpredict the amount of retardation that might be experienced by the radionuclides in actuality.

6.4.3 Base-Case Model Inputs

The base-case flow model, *Saturated Zone Site-Scale Flow Model* (SNL 2007 [DIRS 177391], Section 6.5; DTN: SN0612T0510106.004 [DIRS 178956]), was used directly as an input to the base-case transport model. The flow model provides the numerical grid with geometric coefficients and the groundwater flow velocity field, which are used by the transport

model. Modifications were made to the input file to include base-case transport parameter values. These modifications do not impact the results of the flow calculations. The parameters modified are rock bulk density, rock bulk porosity, effective porosity in alluvium, flowing-interval porosity, matrix porosity in volcanics, effective diffusion coefficient in the volcanic matrix, and flowing-interval spacing in volcanics. Table 6.4-2 provides a list of input parameters for the base-case transport model. This table gives the parameter name, its description and intended use, base-case value, type of uncertainty and the source DTN. Additional parameters that are not included in the base-case model but are needed for the flow and transport abstractions analysis (SNL 2007 [DIRS 181650]) and subsequent feed to the TSPA are listed in Table 6.4-3. The values of all of these parameters involve uncertainties. For each parameter, the rationale for the selection of the range of value, probability distribution, and expected value is summarized in Section 4.1.2 and details are given in Appendix A and in *Saturated Zone Flow and Transport Model Abstraction* (SNL 2007 [DIRS 181650], Sections 6.5.2 and 6.5.2[a]). The transport base case reported in this section focuses on providing, as output, a single case of the transport model calculations. The ranges of input uncertainties are listed in Table 4-2. For most parameters, the base-case value was chosen to be the median of the uncertainty distribution, except for the sorption coefficient, which was assigned a value of 0 for the base case, leading to faster transit times for the base case than the stochastic simulations. The propagation of the uncertainties to the output BTCs (output DTNs: LA0703SK150304.002 to LA0703SK150304.006) is documented in Section 6.7.

Table 6.4-2. Base-Case Model Inputs

Input Name (Name of the Variable in the FEHM Code)	Input Description and Intended Use	Base-Case Value	Units	Type of Uncertainty	Source/DTN
DENRD in the control statement “rock”	Bulk density in alluvium needed for retardation calculations in Equation 22	1,910	kg/m^3	Epistemic [a]	SNL 2007 [DIRS 181650 SN0310T0502103.009 [DIRS 168763], file *DTN-SN0310T0502103.009.zip\Table 6-8_updated.doc*
K_d in the control statement “sptr”	Sorption coefficient in alluvium needed for retardation calculations in Equation 22	0.0	mL/g	Epistemic	Appendix A. Output DTN: LA0702AM150304.001
For alluvium, PSD in the control statement “rock”	Effective porosity in the alluvium needed for converting Darcy flux to fluid velocity and retardation calculations in Equation 22	0.18	-	Epistemic	SNL 2007 [DIRS 181650] SN0310T0502103.009 [DIRS 168763], file *DTN-SN0310T0502103.009.zip\Table 6-8_updated.doc*

Table 6.4-2. Base-Case Model Inputs (Continued)

Input Name (Name of the Variable in the FEHM Code)	Input Description and Intended Use	Base-Case Value	Units	Type of Uncertainty	Source/DTN
For volcanics, PSD in the control statement "rock"	Flowing interval porosity needed for a) converting Darcy flux to fluid velocity and b) diffusion and retardation calculations	0.001	-	Epistemic	SNL 2007 [DIRS 181650] SN0306T0502103.007 [DIRS 168763], file *DTN-SN0310T0502103.009.zip\Table 6-8_updated.doc*
Flowing interval spacing in volcanics, this is not a direct parameter in FEHM.	Enters indirectly via the Flowing Interval Aperture through the relation[b] Porosity = (Aperture/Spacing), needed for converting a) Darcy flux to fluid velocity and b) diffusion and retardation calculations	25.773	m	Epistemic	SN0706INPUTSZF.000 [DIRS 182007], file *updated_SZ_inputs_table.doc*
APERTURE in the control statement "sptr"[b]	Flowing interval aperture needed for converting a) Darcy flux to fluid velocity and b) diffusion calculations	0.2	m	Epistemic	Obtained as the product of flowing interval porosity and flowing interval spacing given this table.
POR_MATRIX in the control statement "sptr," fraction	Matrix porosity in volcanics, needed for a) diffusion calculation in Equation 22, and b) diffusion calculations in Equation 29.	0.15 to 0.25	-	Epistemic	SNL 2007 [DIRS 181650] SN0306T0502103.007 [DIRS 168763], file *DTN-SN0310T0502103.009.zip\Table 6-8_updated.doc*
DIFM in the control statement "sptr"	Effective diffusion coefficient in volcanics, needed for diffusion calculations in Equation 29	5.0×10^{-11}	m^2/s	Epistemic	SNL 2007 [DIRS 181650] SN0310T0502103.009 [DIRS 168763], file *DTN-SN0310T0502103.009.zip\Table 6-8_updated.doc*
K_d in the control statement "sptr"	Matrix sorption coefficient in volcanics, needed for retardation calculations in Equations 22 and 29	0.0	mL/g	Epistemic	Output DTN: LA0702AM150304.001
AL in the control statement "sptr"	Dispersivity, longitudinal, needed for dispersion calculations in Equations 1 and 20	10.0	m	Epistemic	Section 4.1.2.16
ATH in the control	Dispersivity, transverse, horizontal, needed for	0.05	m	Epistemic	Section 4.1.2.17

Table 6.4-2. Base-Case Model Inputs (Continued)

Input Name (Name of the Variable in the FEHM Code)	Input Description and Intended Use	Base-Case Value	Units	Type of Uncertainty	Source/DTN
statement “sptr”	dispersion calculations in Equations 1 and 20.				
ATV in the control statement “sptr”	Dispersivity, transverse, vertical, needed for dispersion calculations in Equations 1 and 20.	0.0005	m	Epistemic	Section 4.1.2.18

Source: Output DTN: LA0702SK150304.001.

[a] Epistemic uncertainty is defined as uncertainty in the parameter space of a conceptual model for which some knowledge is obtainable as given in BSC 2002 [DIRS 158794], Section 4.1.1.

[b] Input listed in Table 4-2 for flowing-interval porosity was multiplied by flowing interval spacing to obtain flowing interval aperture.

Table 6.4-3. Additional Parameters Needed for Abstraction Analysis

Input Name (Variable Name and the Control Statement where it Appears in the FEHM Code)	Input Description	Base-Case Value(s)	Units	Type of Uncertainty	Source/DTN
Multiplying factor[a] for SKD in control statement “flow”	Specific discharge multiplication factor	1	-	Stochastic	SN0706INPUTSZF.000 [DIRS 182007], file *updated_SZ_inputs_table.doc*
SCALEX[c], SCALEY[c] in control statement “fper,” ratio	Permeability horizontal anisotropy (HAVO) [c]	5[c]	-	Stochastic	SN0612T0510106.004 [DIRS 178956], file *SZ Flow Model.zip*
RD_FRAC in the control statement “sptr,” ratio	Colloid retardation factor in volcanics for irreversible colloids	1	-	Epistemic	Table 4-2
Groundwater concentration of colloids Not a direct parameter in FEHM.	Needed in Equations 45 and 46 for calculating the relative concentration of radionuclide on colloids, which is in turn needed for colloid- facilitated reversible transport	0	g/mL	Epistemic	Table 4-2
Sorption coefficient onto colloids Not a direct parameter in FEHM.	Needed in Equations 45 and 46 for calculating the relative concentration of radionuclide on colloids, which is, in turn, needed for colloid- facilitated reversible transport	0	mL/g	Epistemic	Table 4-2

Table 6.4-3. Additional Parameters Needed for Abstraction Analysis

Input Name (Variable Name and the Control Statement where it Appears in the FEHM Code)	Input Description	Base-Case Value(s)	Units	Type of Uncertainty	Source/DTN
Fraction of colloids transported unretarded . Not a direct parameter in FEHM.	In TSPA calculations, used for post processing the BTCs generated by the transport model.	0.0005[b]	-	Epistemic	BSC 2004 [DIRS 170006], Section 6.6
Colloid retardation factor in alluvium and volcanics for irreversible colloids . Not a direct parameter in FEHM.	Used for calculating colloid sorption coefficient using Equation 22, which is in turn input as the variable K_d in the control statement "sptr," ratio	1	-	Epistemic	Table 4-2

[a] Base-case permeabilities and recharge and boundary fluxes are multiplied by this factor to vary specific discharge without affecting the flow calibration.
[b] This value is different from the base-case value given in Table 4-2. This parameter does not enter the base-case transport model directly. It is used in TSPA calculations for postprocessing the BTCs output from this report.
[c] Geometric mean of the permeability is preserved, thus the relationships used for calculating SCALEX and SCALEY From HAVO are : SCALEX=1/sqrt(HAVO) and SCALEY=sqrt(HAVO).

Infiltration rates enter the transport model only indirectly through the velocity field that is provided by the flow model. *Saturated Zone Site Scale Flow Model* (SNL 2007 [DIRS 177391], Section 6.4.3.9) notes that the increase in the updated infiltration estimates forms only 13% of the infiltration budget, and only 1% of the flow through lateral boundaries. An increased infiltration flux in the vicinity of the repository area can be expected to lead to higher specific discharge values in the volcanics, resulting in shorter travel times for the portions of the flow paths that reside in volcanics formation, thus leading to somewhat shorter overall travel times.

6.5 BASE-CASE MODEL RESULTS

The base-case model results (output DTN: LA0703SK150304.001) are discussed in this section. The conceptual and mathematical model described in Sections 6.3 and 6.4 was implemented in the numerical code FEHM V 2.24-01, a finite-volume/finite-element heat- and mass-transfer code that simulates nonisothermal, multiphase, multicomponent flow and solute transport in porous media. The details of this code, its usage and verification example are given in *Validation Test Plan (VTP) for the FEHM Application Version 2.24-01* (DOE 2007 [DIRS 181096]). The calibrated base-case site-scale SZ flow model (DTN: SN0612T0510106.004 [DIRS 178956]), which is described in detail in *Site-Scale Saturated Zone Flow Model* (SNL 2007 [DIRS 177391], Section 6.5), was used as the starting input.

The purpose of this model report is to provide a site-scale SZ transport model to be used as the starting point for the SZ abstraction model presented in *Saturated Zone Flow and Transport Model Abstraction* (SNL 2007 [DIRS 181650], Section 6.3) for use in the TSPA calculations. For this purpose, a single base-case transport model is presented here along with its outputs. The propagations of uncertainties in the input parameters to the output BTCs are presented in

Section 6.7 by documenting the BTCs at the boundary of the accessible environment at 18 km (10 CFR 63.302 [DIRS 180319]) for minimum and maximum values of the various parameters. The barrier capabilities of the saturated zone transport are presented in Section 6.8, where the influence of key parameters on the radionuclide breakthrough is discussed.

The base case serves as a reference point for exploring the role of processes and features of the system in subsequent simulations. The input transport parameter values and the sources for these values for the base-case model are given in Table 6.4-2. The particle source location was chosen near the middle of the anticipated repository footprint at the water table (SNL 2007 [DIRS 181650], Section 6.5.2.13). Calculations were performed for an instantaneous release of particles at the source location. The BTC at the boundary of the accessible environment at 18 km was calculated by starting 500 particles and by outputting the cumulative number of particles crossing an east-west vertical plane across the entire width and depth of the model. This is the BTC for a conservative, nonsorbing radionuclide in the absence of radioactive decay. Output of this model is shown in Figure 6.5-1 where normalized cumulative mass is plotted on the *y*-axis and the time in years on the log scale on the *x*-axis. The solid red curve in Figure 6.5-1 shows the BTC at the 18-km boundary, which can also be thought of as an arrival time distribution for transport through the saturated zone. Breakthrough times on the order of hundreds of years are predicted for the bulk of the mass arriving at the water table, with transport times extending into the thousands of years for the slowest moving 20% of the mass. This BTC in Figure 6.5-1 corresponds to a breakthrough time at 50% concentration of 810 years.

For comparison, also shown in Figure 6.5-1 by the green curve is the BTC for base case with initial number of particles being 1,000 instead of 500. As expected, although this curve is smoother than the BTC for 500 particles, they compare reasonably well with each other. The results presented in this report are single realizations of parameter values intended for conceptual illustration of the model behavior. Based on experience, 500 particles are judged adequate for the rest of the model runs reported in this model report. These model runs are not used directly in downstream analysis. In TSPA modeling, multiple realizations are conducted by stochastic sampling of the entire range of the distributions of various parameters.

A similar model calculation was performed where the number of input tracer particles was changed (from 500 in the base case) to nine particles spread over the repository footprint, and the output option was changed to produce detailed particle tracks as they moved from the source location to the boundary of the accessible environment at 18 km. These are plotted against a shaded relief map of the SZ site-scale model area in Figure 6.5-2. Note that there is very minimal transverse spreading of the flow paths due to the small value of transverse dispersivities (Table 6.4-2). The flow paths in Figure 6.5-2 appear to converge toward the southern portion of the model due to the large-scale heterogeneities that are explicitly included in the hydrologic framework model shown in *Saturated Zone Site-Scale Flow Model* (SNL 2007 [DIRS 177391], Section 6.3.1.9). The flow paths shown here are consistent with those presented in *Zone Site-Scale Flow Model* (SNL 2007 [DIRS 177391], Figure 6-17).

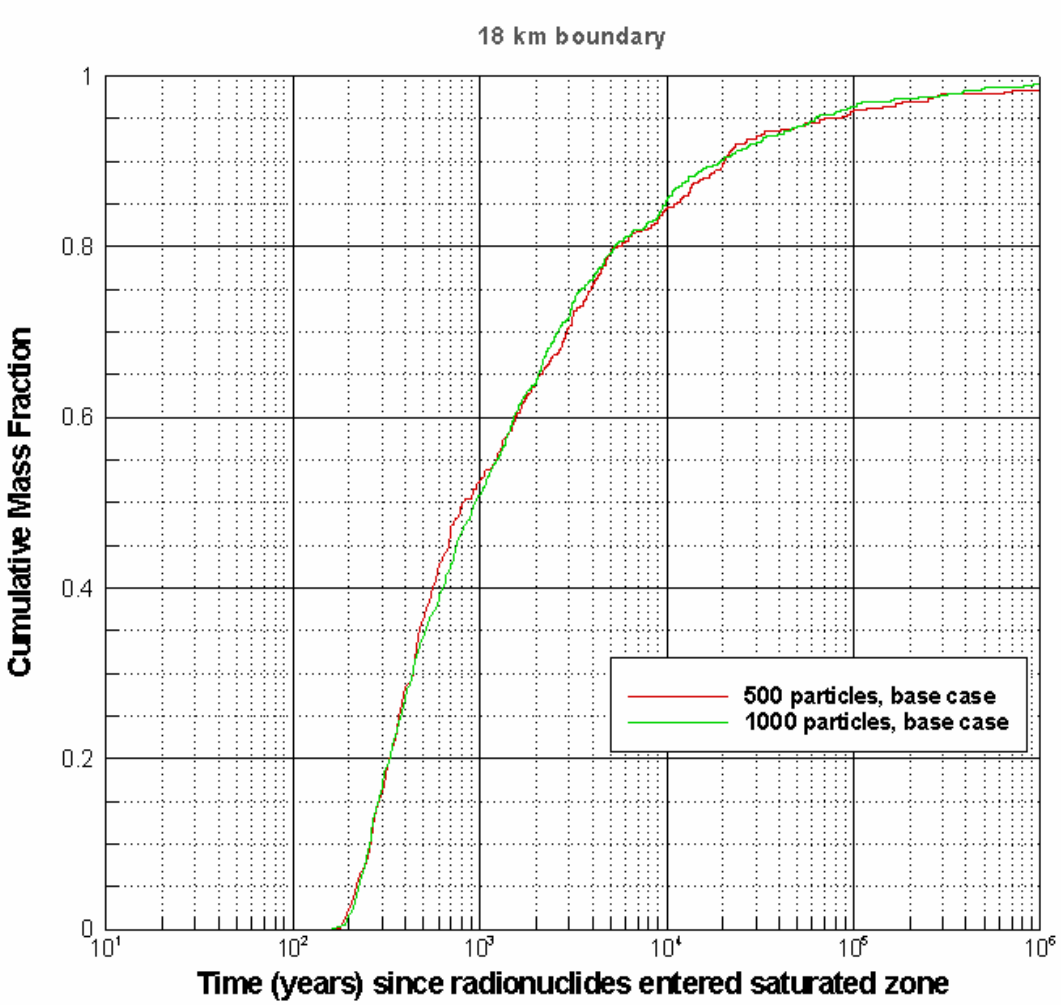

Output DTN: LA0703SK150304.001.

NOTE: Mass BTCs and median transport times are for an instantaneous source, present-day climate, and do not include radionuclide decay. Particle source location was near the middle of the anticipated repository footprint.

Figure 6.5-1. Breakthrough Curves at the 18-km Boundary for the Transport Base Case (500 particles for a Conservative, Nonsorbing Radionuclide) with 1000 Particle Case for Comparison

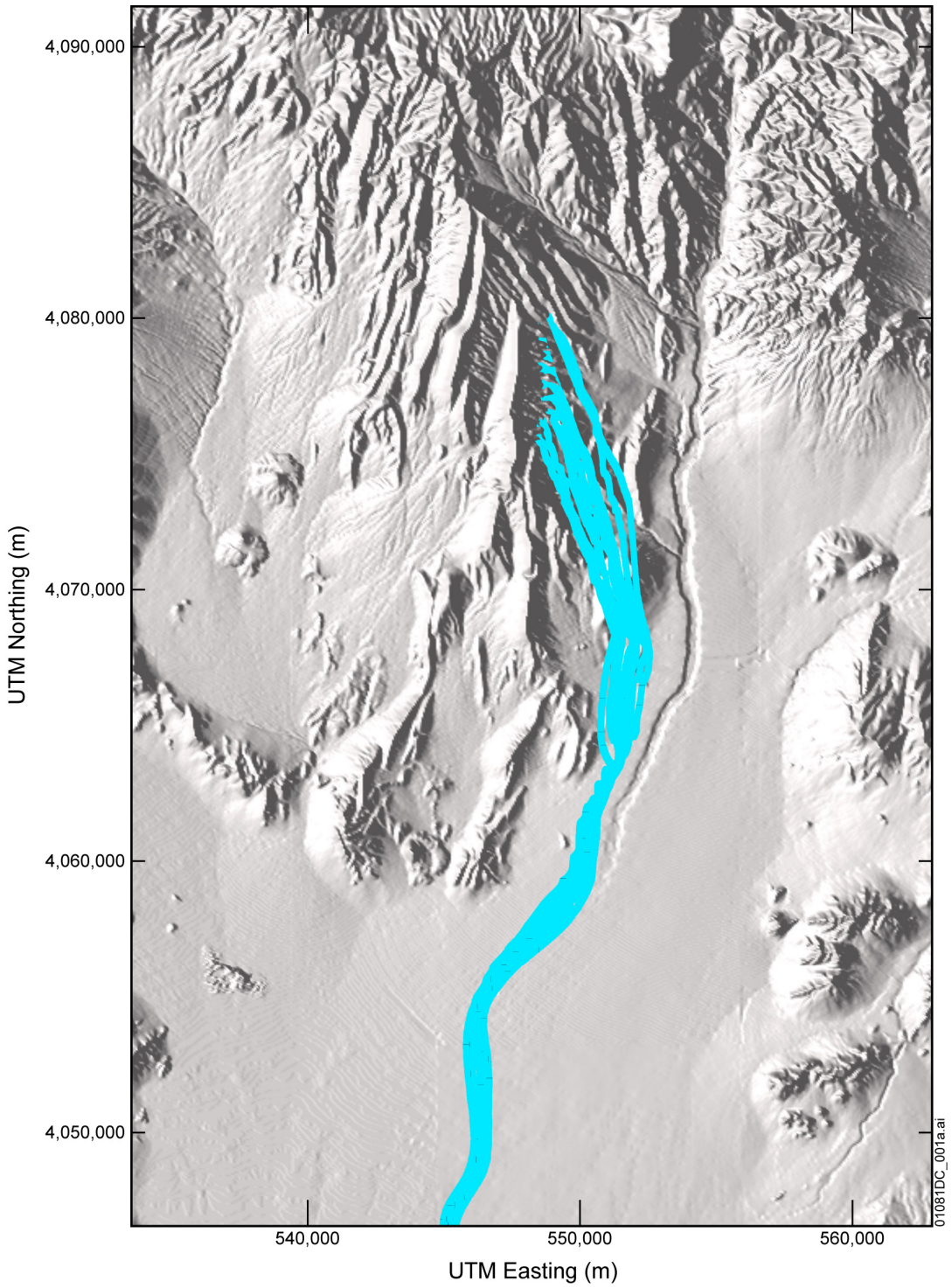

Output DTN: LA0703SK150304.001.

NOTE: The base-case transport calculations were performed for an instantaneous source, present-day climate, without radionuclide decay. Particle source locations were distributed over the anticipated repository footprint.

Figure 6.5-2. Particle Tracks Resulting from the Site-Scale Saturated Zone Base-Case Transport Model

6.6 ALTERNATIVE CONCEPTUAL MODELS

Credible alternatives to the conceptual model of SZ transport presented in Section 6.3 were evaluated in regards to their impact on the radionuclide transit times from the repository footprint to the boundary of the accessible environment at 18 km. The alternative conceptual models fall into two classes. One class consists of the alternative conceptual models that are excluded from further consideration because they lead to transit times greater than those calculated by the site-scale SZ transport model. The key components of each of these alternative conceptual models, and the basis for the disposition are presented in Table 6.6-1a. The other class consists of alternative conceptual models that can be accommodated within the current mathematical model framework by modifying the uncertainty distributions of the effective parameters (such as effective sorption coefficients and effective porosities) used in the model. The key components of each of these alternative conceptual models and the basis for the disposition are presented in Table 6.6-1b.

Table 6.6-1a. Key Components and Basis for the Alternative Conceptual Models Excluded from Further Consideration Because They Lead to Transit Times Greater than the Base-Case Results

Item	Alternative Conceptual Model	Key Components	Basis
1	Fluid flow in matrix blocks	The matrix material in the intervening space between the flowing intervals in the volcanics has significant permeability and transmits significant amounts of fluid by advection for the flow conditions in the saturated zone	There are three situations possible: (1) flow occurs from the fractures into the matrix, (2) flow occurs from the matrix into the fractures, and (3) flow occurs independently within matrix blocks. In the first case, flow out of the fractures into the matrix would enhance the effects of the matrix diffusion, leading to transit times greater than those calculated by this model. In the second case, considering the steady-state nature of the flow system as presented in *Saturated Zone Site-Scale Flow Model* (SNL 2007 [DIRS 177391], Section 6.1), if some flow is occurring out of the matrix into the fractures, then equivalent flow must also occur from fractures into the matrix blocks. Thus, the matrix diffusion effects will be negated in some areas and enhanced in others, and the overall effect on the effective diffusion coefficient will be small. In the third case, an effective porosity would have to be used that is larger than that being used for the fractured flowing intervals, thus leading to transit times greater than those calculated by this model.

Table 6.6-1a. Key Components and Basis for the Alternative Conceptual Models Excluded from Further Consideration Because They Lead to Transit Times Greater than the Base-Case Results (Continued)

Item	Alternative Conceptual Model	Key Components	Basis
2	Irreversible sorption	Rate of desorption of radionuclides from the rock surfaces is slower than the rate of absorption	Available data show that rate of desorption of U and Np from the rock surfaces is slower than the rate of absorption (Appendix J). Sorption reactions that are not fully reversible result in rates of transport that are slower than would be the case for fully reversible reactions. Therefore, using sorption coefficients based on data such as that reported in Appendix J would result in diminished total radionuclide mass breakthrough from the saturated zone, compared to the breakthrough based on using the values recommended in Appendices A and C. A potential scenario for which this simplification could lead to enhanced radionuclide mass breakthrough is when deposition of radionuclides takes place under the ambient geochemical conditions, and later, because of geochemical changes, the deposited radionuclides re-enter the aqueous phase and are transported downstream as a pulse. On the basis of available geochemical and mineralogical data, this situation is not considered likely. It is being addressed as a FEP (DTN: MO0706SPAFEPLA.001 [DIRS 181613], file *FEPs_be.mdb*, Table 7.1-1).
3	Radionuclide precipitation	Radionuclides could precipitate in the saturated zone, forming solid phases on the rock surfaces	Thermodynamically, chemical species in supersaturation possess a driving force that favors the formation of solid phases. The result for a radionuclide would be an extreme form of retardation that renders the bulk of the radionuclide plume virtually immobile. Given that most radionuclides reaching the saturated zone would need to transport there in aqueous solution, thermodynamic conditions along the flow path would have to change (relative to the unsaturated zone) for species to precipitate. The most credible mechanism for this to occur would be through a different redox condition in the saturated zone. If the conditions were significantly more reducing, the valence state of actinides, such as neptunium, uranium, and plutonium, and fission products, such as technetium and iodine, could be lowered. Typically, in these groundwaters, this condition would result in much lower solubilities of the radionuclides and hence, precipitation. There are insufficient measurements and data concerning the redox behavior of these radionuclides to warrant including redox behavior in model calculations. In all cases, the radionuclides in question have been assigned to their highest valence state, which results in higher solubilities and lower sorption coefficients than would be the case if the lower valence state were selected. A potential scenario for which this simplification could be less straightforward is when deposition of radionuclides takes place under the ambient geochemical conditions, and later, because of geochemical changes, the deposited radionuclides re-enter the aqueous phase and are transported downstream as a pulse. On the basis of available geochemical and mineralogical data, this situation is not considered likely. It is being addressed as a FEP (DTN: MO0706SPAFEPLA.001 [DIRS 181613], file *FEPs_be.mdb*, Table 7.1-1).

Table 6.6-1a. Key Components and Basis for the Alternative Conceptual Models Excluded from Further Consideration Because They Lead to Transit Times Greater than the Base-Case Results (Continued)

Item	Alternative Conceptual Model	Key Components	Basis
4	Water table rise	Future water table rise could elevate the water table, leading to radionuclide transport through geological horizons currently considered outside of the saturated zone	Wetter, glacial climatic conditions could occur in the future at the Yucca Mountain site within the regulatory period. These changes in the climate relative to present conditions would affect groundwater flow in the saturated zone in the saturated zone by increasing the amount of recharge to the regional groundwater flow system. These regional and local increases in recharge will tend to increase the groundwater flux through the saturated zone system and lead to a rise in the water table beneath Yucca Mountain. In previous analyses, the effect of this on the saturated zone BTCs was modeled using a scaling factor representing the alternative climate state as given in *Saturated Zone Flow and Transport Model Abstraction* (SNL 2007 [DIRS 181650], Section 6.5). The scaling factor used in this approach is the ratio of average saturated zone groundwater flux under the future climatic conditions to the flux under present conditions. However, this approach uses the same flow paths for radionuclide transport through the saturated zone under wetter climatic conditions of the future. Alternatively, the rise in the water table due to climatic changes could be included in the model with potentially different flow paths through different hydrogeologic units in the saturated zone. *Saturated Zone Site-Scale Flow Model* (SNL 2007 [DIRS 177391], Section 6.6.4) presents a modeling exercise that adapts the site-scale SZ flow model to include the effects of estimated water table rise. The results of particle-tracking simulations using this adapted model to the simple flux-scaling approach are presented in Appendix E. Figures E-1 and E-2 present results indicating that the model with the higher water table results in longer simulated transport times for the nonsorbing species and for neptunium. The simplified approach of scaling the BTCs from the SZ site-scale transport model with the present water-table elevations is, thus, an acceptable representation of transport in the saturated zone under wetter, glacial climatic conditions relative to the adapted model that incorporates water-table rise associated with future conditions. The reason for the longer transport times using the water-table-rise model relates to the hydrogeologic units encountered by a radionuclide plume arriving at the water table. Transport must occur through lower-permeability confining units, and the flow-path distance through the alluvium is predicted to be longer for the water-table-rise model.
5	Diffusion into low-permeability zones	Within alluvium, solutes can diffuse into low-permeability zones, later diffusing out into the flow, which leads to a long tail for the radionuclide BTC	This phenomenon was not observed to occur in the single-hole tracer tests conducted at the ATC presented in *Saturated Zone In-Situ Testing* (SNL 2007 [DIRS 177394], Section 6.5, Figures G-18 and G-19). On a larger scale, this scenario will lead to lower concentrations at breakthrough and longer times for reaching 50% breakthrough concentrations. Thus, the conceptual model presented in this model report is acceptable.

Table 6.6-1b. Key Components and Basis for Alternative Conceptual Models Implicitly Included in the Site-Scale Saturated Zone Transport Model

Alternative Conceptual Model	Key Components	Basis
Sorption reactions are not instantaneous	Reaction rates for sorption kinetics are slow compared to the rates of solute transport	Among the radionuclides of concern, plutonium has the slowest reaction kinetics (Appendix A). Calculations of the Damköhler number (*Da*) (Appendix D) for reaction rates, and analysis of laboratory data (presented in Appendix G) for plutonium indicate that, for typical transport times through the saturated zone, the local equilibrium approach is valid. However, in localized areas, flow rates may be fast enough for kinetic limitations to be a factor for plutonium (Appendix A). The possibility of the sorption reaction rate being slow relative to the flow rate would lead to in situ sorption experienced locally by the radionuclides being less than that estimated on the basis of equilibrium K_d values. Thus the effective K_d experienced by the radionuclide over entire flow path would be lower than the equilibrium values measured in the laboratory. Accommodation is made for this by biasing the sorption-coefficient distributions downward for the radionuclides of interest that appear to have slow sorption kinetics (Appendices A and C).
Nonlinear sorption	Sorption reactions have to be modeled using nonlinear isotherms	The K_d model is based on treating the concentration of the radionuclides absorbed onto the rock surface as a linear function of the concentration of that species in the aqueous solution. This treatment is valid at low concentrations, but at higher concentrations, as absorption sites start getting saturated, the absorbed concentration starts falling below the value predicted by this linear relationship. This effect results in a lower apparent value of K_d at higher concentrations. Thus the in situ K_d experienced by the radionuclides will be lower locally in the areas where the concentrations might be high, resulting in a lower value of the effective K_d experienced over the entire flow path. This is accounted for in the model by biasing the K_d distributions at low values (Appendix A).

Table 6.6-1b. Key Components and Basis for Alternative Conceptual Models Implicitly Included in the Site-Scale Saturated Zone Transport Model (Continued)

Alternative Conceptual Model	Key Components	Basis
Locally varying sorption parameters	Sorption parameters are strong functions of local water chemistry, rock mineralogy, and solute concentrations. The properties have to be calculated locally at each node along the travel path	The approach taken in this model report is to use linear transport equations with transport parameters appearing in the equations being treated as "effective" stochastic variables appropriate for the model scale. Transport parameters such as the K_d coefficients depend on type and concentration of the species, rock mineralogy, and groundwater composition including pH and Eh. As discussed in appendix A3, the range of groundwater compositions expected to occur in the saturated zone is taken into account in developing the small scale uncertainty distributions for K_ds. Given the current level of data available, water pH data are being treated as spatially random along the transport path, and oxidizing conditions are taken as a conservative approach, as justified in Section 6.3. To evaluate the effect of variations in rock mineralogy and scale on the K_d distributions, calculations were performed to calculate upscaled K_d distributions for the radionuclides uranium, neptunium, cesium, and plutonium. It was observed that the effective K_d distributions calculated for a single 500-m × 500-m grid block were narrower than the input K_d distributions. As discussed in appendix C2, the subject matter expert added a bias towards lower values to the CDFs. During performance assessment modeling studies, calculations will be made through multiple runs, each with a distinct K_d value sampled from the above-mentioned effective K_d distribution. This approach is more approximate than assigning K_d values on a node basis, as the latter approach will lead to breakthrough behavior that can be described by an even narrower distribution than the effective K_d distributions.
Channeling in alluvium	In alluvium, high-permeability channels exist that can provide preferential pathways for flow and transport	The conceptual model presented in this model report uses the effective-continuum approach, using effective values averaged over the grid block sizes on the order of 250 m × 250 m × 50 m for the parameters of interest, such as porosity. The effective porosity for alluvium being used in the TSPA calculations is represented by a normal distribution with the expected value of 0.18 and a value of 0.027 at 3 standard deviations below the mean shown in *Saturated Zone Flow and Transport Model Abstraction* (SNL 2007 [DIRS 181650], Section 6.5.2.3). Thus, the TSPA calculations allow for the eventuality that all the flow is concentrated within a small fraction of the alluvium, corresponding to the low effective porosity of 0.027. The conceptual and numerical model presented in this model report is appropriate for these ranges of values.

6.7 MODEL UNCERTAINTIES

Model-form uncertainty as presented in *Guidelines for Developing and Documenting Alternative Conceptual Models, Model Abstractions, and Parameter Uncertainty in the Total System Performance Assessment for the License Application* (BSC 2002 [DIRS 158794], Section 4.1.1)

in regards to the transport model is unavoidable given the sparseness of observed data and the limited amount of information available to corroborate or refute alternative models. This form of uncertainty is explicitly addressed by discussing alternative conceptual models in Section 6.6. The discussion and screening of the alternative conceptual models is based on available understanding and data. As discussed in Section 6.6, several of the alternative conceptual models can be accommodated within the current mathematical model framework by modifying the uncertainty distributions of the effective parameters (such as effective sorption coefficients and effective porosities) used in the model. Although the model is meant to represent the saturated zone transport accurately, for the case of those alternative conceptual models that could not be included in the model, the transport model was selected such that it resulted in transit times faster than those expected for the alternative conceptual model.

There are uncertainties associated with scaling parameter values from the scale of measurements to the scale of interest. Much of the data used for deriving parameter values in this report are from laboratory or field experiments conducted on spatial and temporal scales much smaller than those in the site-scale SZ model. Most of the measurements are done on sample sizes less than 1 m, with the exception of the C-wells and ATC field tests, which were conducted on the scale of tens of meters. This scale is still several orders of magnitude smaller than the site scale. Because the objective here is to calculate cumulative BTCs at a boundary of the accessible environment, large grid spacing (250 m × 250 m) is used in the numerical model. This leads to significant averaging of properties in the model calculations, thereby reducing the sensitivity of the output results to the stochastic variations in the parameter values. This is well demonstrated by the analysis presented in Appendix C for upscaling the distribution of the K_d values from a 4-m to a 500-m scale. These calculations demonstrate that the resulting 500-m-scale K_d distribution is actually narrower, for example, as shown in Table C-11 for uranium, with a standard deviation of 0.61 mL/g (and a mean of 6.61 mL/g) than the two starting 4-m-scale K_d distributions, shown in Table C-4, with mean and standard deviations of 2.0 mL/g and 0.6 mL/g, respectively in devitrified tuff, and 12.0 mL/g and 3.6 mL/g in zeolitic tuff, respectively. However, geological formations are inherently inhomogeneous, and they incorporate fractures, faults, and other heterogeneities on a variety of scales. Spatial correlations over some length scales often exist. Thus, it is difficult to extrapolate the measurements on a small scale to the SZ site scale.

As presented in *Guidelines for Developing and Documenting Alternative Conceptual Models, Model Abstractions, and Parameter Uncertainty in the Total System Performance Assessment for the License Application* (BSC 2002 [DIRS 158794], Section 4.1.1), there is epistemic uncertainty in the parameter space of the base-case conceptual model. This form of uncertainty is explicitly described by using probability distributions for appropriate model parameters. Expected uncertainty ranges for the various transport parameters are discussed in Section 4.1.2 and summarized in Table 4-2. The development and discussion of the K_d parameters needed for modeling reactive transport and the K_c parameters needed for modeling colloid-facilitated transport are presented in Appendices A, B, and C. The probability distributions for all other model parameters are presented and discussed in *Saturated Zone Flow and Transport Model Abstraction* (SNL 2007 [DIRS 181650], Sections 6.5.2 and 6.5.2[a]). These uncertainties are propagated through the model to the output BTCs, presented in Section 6.7.1. Radionuclide transit times are most sensitive to groundwater-specific discharge. This is because increasing the specific discharge not only increases the advective velocity but also reduces the time available

for matrix diffusion to be effective. In assessing the sensitivity of breakthrough times to the specific discharge through the model, permeabilities of the various units are scaled along with the specific discharge to preserve the model calibration. Other parameters of importance to the breakthrough times are matrix diffusion, the sorption coefficient in the volcanics as well as the alluvium, the effective flowing interval porosity in the volcanics (as reflected in the flowing interval aperture and spacing), the effective porosity in the alluvium, and the sorption coefficients for reversible colloids and retardation factor for irreversible colloids in the volcanics and alluvium. The volcanic retardation factors are important since the distribution contains large values that result in significant retardation even though transport times in the volcanics are shorter than the transport times in the alluvium. The contaminants spend the majority of the time in the alluvium; therefore, any retardation in the alluvium results in large effects in the overall transport time. Although the time for 50% breakthrough shows only a moderate sensitivity to the value of longitudinal dispersivity (Figure 6.7-14), the leading and tailing edges of the BTC are significantly affected for dispersivity values near the upper limit. Thus, dispersivity could be an important parameter to consider in situations where the first and last arrival times for radionuclides play an important role. Quantification of the sensitivity of the model output BTCs for various radionuclides of concern to parameter uncertainties are further evaluated in *Saturated Zone Flow and Transport Model Abstraction* (SNL 2007 [DIRS 181650], Sections 6.6, 6.7, and 8).

6.7.1 Propagation of Uncertainty in the Input Parameter Values to the Output

Starting with the SZ site-scale base-case transport model, sensitivity of the output BTCs to each of the uncertain input parameters was investigated by considering the upper and lower levels of each parameter individually (Table 6.7-1). The results presented here are limited to demonstrating the response of the model output to the extreme values of the input parameters given below.

Table 6.7-1. Effect of Parameter Ranges on 50-Percent Breakthrough Times

	Parameter	Base-case Value(s)	Uncertainty Range (Units)	Output Range, Time (Years) for 50% Breakthrough
1	Specific discharge multiplication factor[a]	1	0.112 to 8.933	31 to 52,840
2	Permeability horizontal anisotropy (north-south/east-west)	5	0.05 to 20 (ratio)	1,314 to 2,100
3	Bulk density in alluvium	1,910	1,669 to 2,151 kg/m^3	9,528 to 11,581
4	Sorption coefficient in alluvium	0.0	0 to 10,000 (mL/g)	810 to >106
5	Effective porosity in the alluvium	0.18	0. 02 to 0.3 (fraction)	709 to 986
6	Colloid retardation factor in alluvium for irreversible colloids	1	8 to 5,188 [e] (ratio)	1,859 to 688,357
7	Adjusted sorption coefficient for reversible sorption onto colloids in alluvium[b]	0	0 to 10,000 (mL/g)	245 to 7,023

Table 6.7-1. Effect of Parameter Ranges on 50 Percent Breakthrough Times (Continued)

	Parameter	Base-case Value(s)	Uncertainty Range (Units)	Output Range, Time (Years) for 50% Breakthrough
8	Flowing interval aperture[c] (holding Flowing Interval Porosity fixed at the base-case value of 0.001)	0.025773 (m)	1.86×10^{-5} to 8.0[d] (m)	166 to 6,653
9	Flowing Interval Porosity (holding the Flowing Interval Aperture fixed at the base-case value of 0.025773 m)	10^{-3}	10^{-5} to 10^{-1}	132 to 9,008
9	Effective diffusion coefficient in volcanics	5.0×10^{-11}	5.0×10^{-12} to 5.0×10^{-10} (m^2/s)	245 to 6,324
10	Matrix sorption coefficient in volcanics	0.0	0 to 10,000 (mL/g)	810 to $>10^6$
11	Colloid retardation factor in volcanics for irreversible colloids	1	6 to 794 (ratio)	4,600 to 28,519
12	Adjusted sorption coefficient for radionuclides with reversible sorption onto colloids in volcanics	0	0 to 10,000 (mL/g)	165 to $>10^6$
13	Dispersivity, longitudinal	10.0	0.10 to 2,000 (m)	671 to 5,900

[a] Base-case permeabilities and the recharge and boundary fluxes are multiplied by this factor to vary specific discharge without affecting the flow calibration.

[b] See Equations 45 and 46 in Section 6.4.2.6.

[c] Flowing interval aperture is the product of the flowing interval porosity and flowing interval spacing.

[d] This value is made to address the case when flowing interval spacing is very large.

[e] The value used here is slightly lower than that given in Table 4-2.

6.7.1.1 Specific Discharge Multiplier

The results from simulations that evaluate the effect of changes in the specific discharge are shown in Figure 6.7-1. In these simulations, the base-case flow model was modified to scale the input recharge fluxes by the same factor as the rock permeabilities to preserve the model calibration. The results show that output is very sensitive to the level of uncertainty in this parameter. For the case of upper limit of specific discharge multiplier where the base-case fluxes are multiplied by a factor of 8.933, time to 50% breakthrough is 31 years (with extremely fast fluid flow such as would be expected for the very unlikely case of a high-permeability channel going continuously over the distance of 18 km in a highly faulted region). The lower limit of specific discharge multiplier, a factor of 0.112, leads to a breakthrough time of 52,840 years. This indicates that information that helps reduce the uncertainty of this parameter will greatly improve the ability of the model to predict the results.

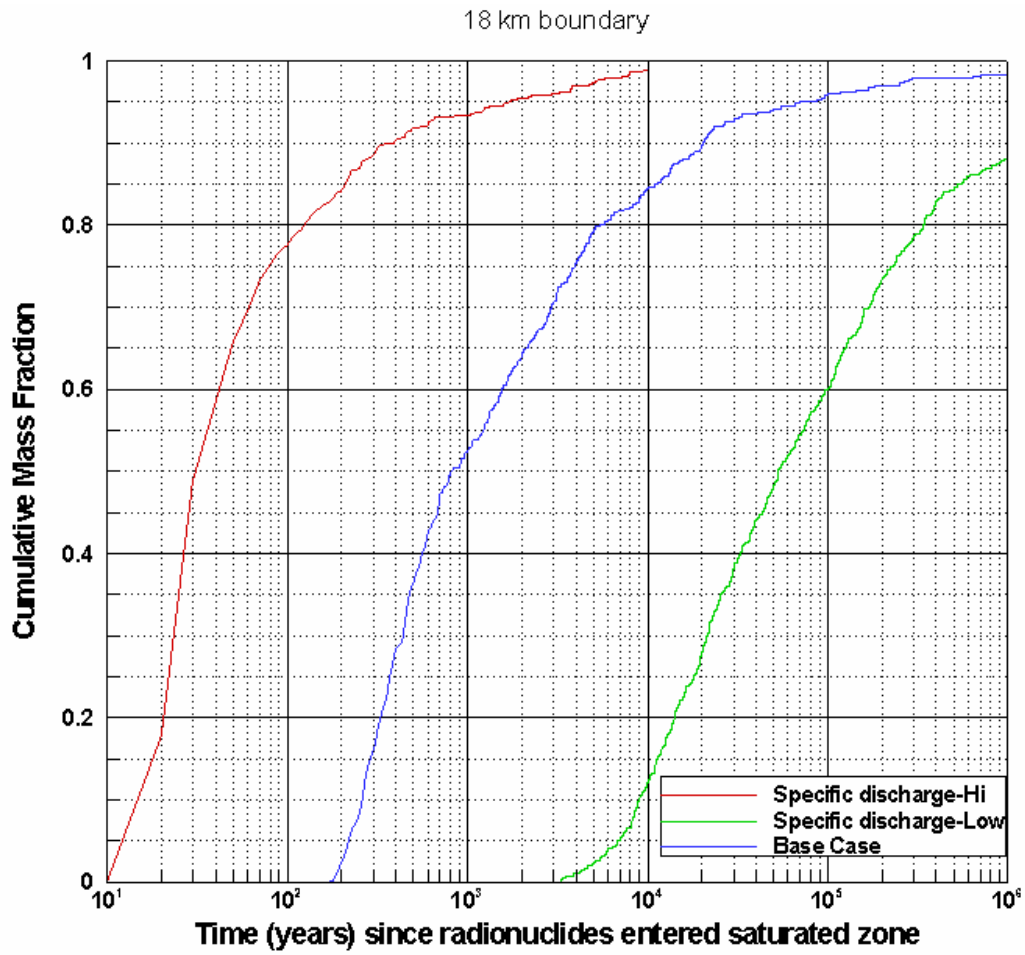

Output DTNs: LA0703SK150304.001; LA0703SK150304.002.

NOTE: Mass BTCs and median transport times are for an instantaneous source, present-day climate, and do not include radionuclide decay. Particle source location was near the middle of the anticipated repository footprint.

Figure 6.7-1. Propagation of Input Uncertainty in the Specific Discharge to the Output Breakthrough Curves at the 18-km Boundary

6.7.1.2 Horizontal Permeability Anisotropy

The results from simulations that evaluate the effect of changes in the ratio of horizontal permeability anisotropy (north-south/east-west) are shown in Figure 6.7-2a. The base-case flow model (with a horizontal permeability anisotropy ratio of 5) was modified to include the permeability ratios; however, note that the flow model was not recalibrated for the different values of permeability. The output shows a moderate level of variation resulting from the uncertainty limits of this parameter (0.05 to 20, Table 6.7-1) with the time for 50% breakthrough varying between 1,314 to 2,100 years. This variation results mainly from the variation in the flow paths due to the changed velocity fields corresponding to the different ratios of the east-west versus the north-south permeabilities.

The results presented here are limited to demonstrating the response of the model output to the extreme values of the ratio of horizontal permeability anisotropy. It is noted that the BTC for the

base case lies outside the range bracketed by the BTCs for high and low anisotropy cases. The horizontal anisotropy is a parameter that modifies the flow field and thus, indirectly affects the transport model. Variations in this parameter can be expected to lead to monotonic and smooth variations in the flow field in the case of a simple uniform hydrologic model. However, the hydrogeology underlying the site-scale flow model is complex, and permeabilities can vary abruptly by several orders of magnitude from unit to unit (SNL 2007 [DIRS 177391], Section 6.5). Thus changes in this parameter may lead to abrupt changes in the flow paths as well as velocities. As seen in Figure 6.7-2b, the flow paths for anisotropy extremes are deeper and more tortuous, especially for the case of low anisotropy ratio. Further, velocities from case to case can differ even along the same flow paths since the pressure gradients can be expected to differ, considering that the flow fields are not recalibrated for the different anisotropy cases. The transit times are governed not only by advection but also by diffusion in the volcanic rock matrix (see Section 6.7.1.10), and this effect is a non-linear function of the advective flow velocity. A combination of these complicating factors is likely the cause of the behavior of the BTCs noted above. The results presented in this report are single realizations of parameter values intended for conceptual illustration of the model behavior; they are not used directly in downstream analysis. In TSPA modeling multiple realizations are conducted by stochastic sampling of the entire range of distribution of various parameters.

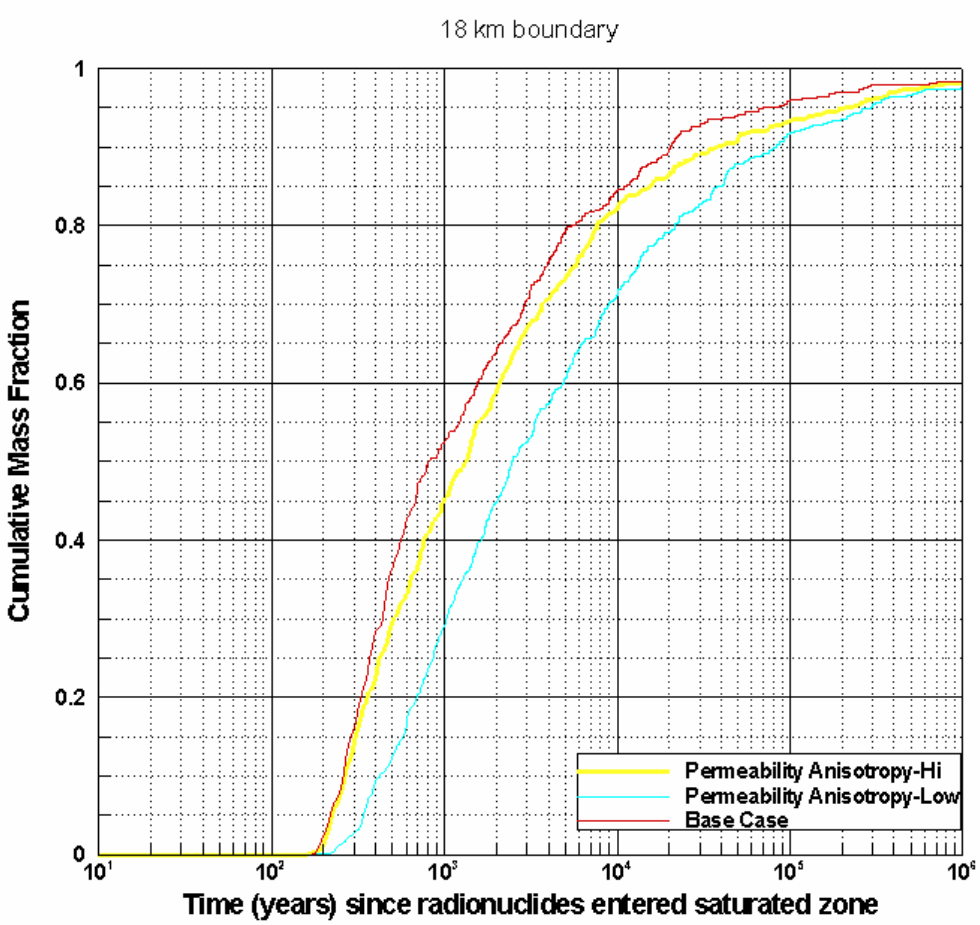

Output DTNs: LA0703SK150304.001, LA0703SK150304.002.

NOTE: Mass BTCs and median transport times are for an instantaneous source, present-day climate, and do not include radionuclide decay. Particle source location was near the middle of the anticipated repository footprint.

Figure 6.7-2a. Propagation of Input Uncertainty in the Horizontal Permeability Anisotropy Ratio to the Output Breakthrough Curves at the 18-km Boundary

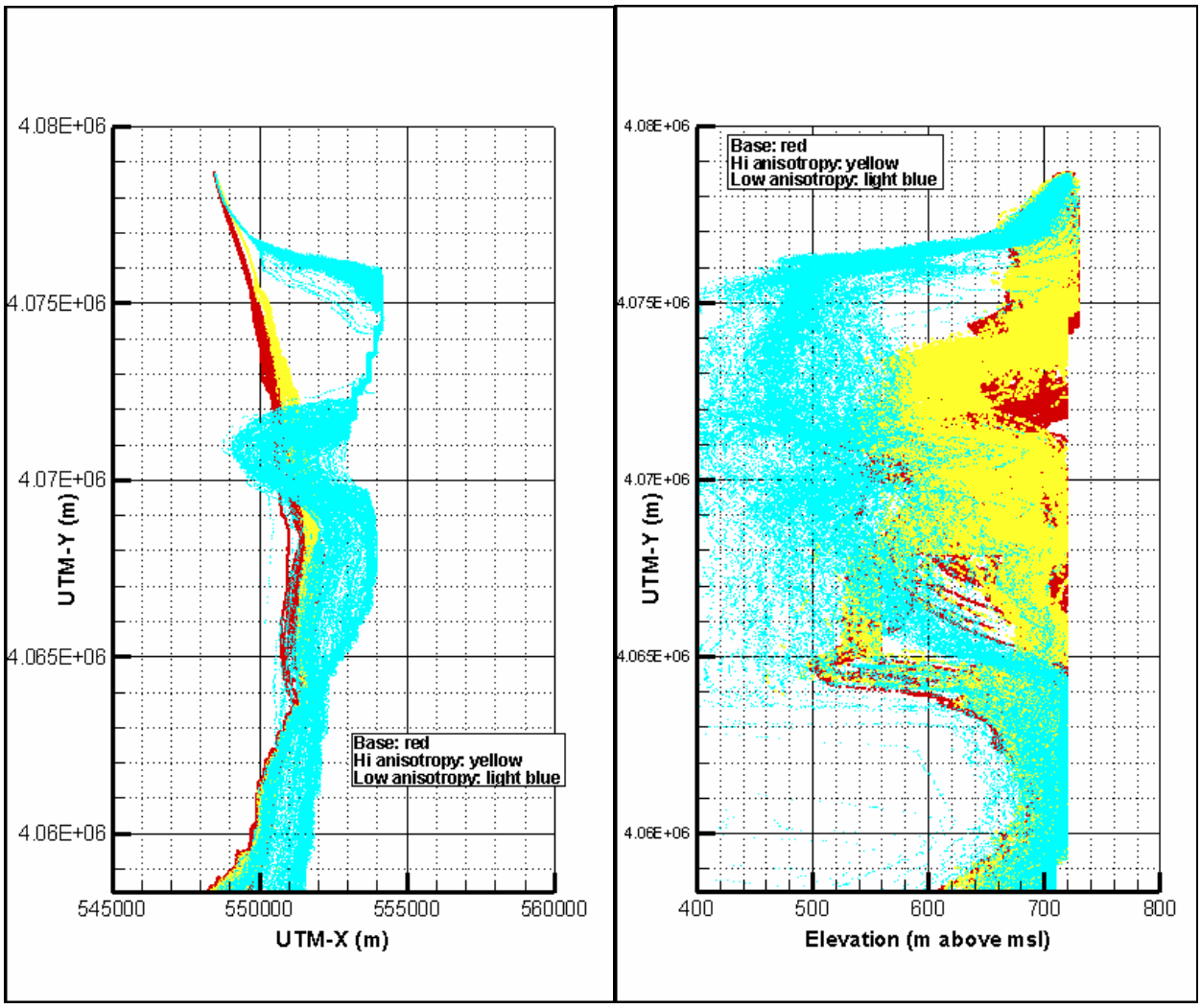

Output DTNs: LA0703SK150304.001, LA0703SK150304.002.

NOTES: Transport simulations are for an instantaneous source, present-day climate, and without radionuclide decay. Particle source location was near the middle of the anticipated repository footprint. The left panel shows the plan view; the right panel, the vertical cross section.

Figure 6.7-2b. Flow Paths For High And Low Extremes Of The Horizontal Anisotropy, Compared With The Base Case Flow Paths

6.7.1.3 Bulk Density in Alluvium

The results from simulations that evaluate the effect of changes in the bulk density in the alluvium are shown in Figure 6.7-3. Because the bulk density enters the transport calculations only through the retardation factor as given in Equation 22, these simulations were done with a K_d = 6.3 mL/g, corresponding to a mildly sorbing radionuclide. Also shown for comparison is the BTC for K_d = 6.3 mL/g but all other parameters having base-case values. The BTCs are seen to be mildly sensitive to this parameter, the 50% breakthrough time changing from 9,538 years to 11,578 years as the bulk density is varied from 1,669 kg/m^3 to 2,151 kg/m^3.

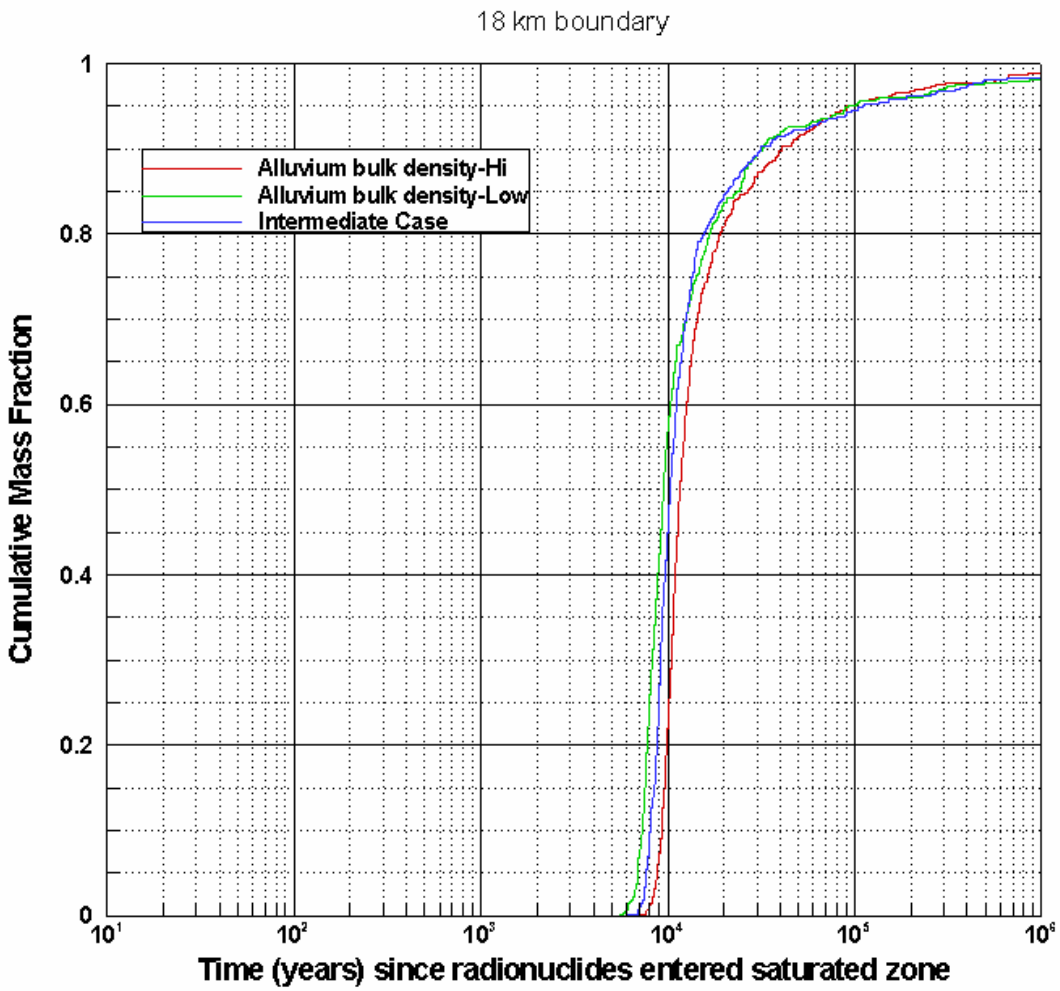

Output DTNs: LA0703SK150304.001, LA0703SK150304.003.

NOTE: Mass BTCs and median transport times are for an instantaneous source, present-day climate, and do not include radionuclide decay. Particle source location was near the middle of the anticipated repository footprint.

Figure 6.7-3. Propagation of Input Uncertainty in the Bulk Density of Alluvium to the Output Breakthrough Curves at the 18-km Boundary

6.7.1.4 Sorption Coefficient in Alluvium

The results from simulations that evaluate the effect of changes in sorption coefficient in alluvium on the output BTCs are shown in Figure 6.7-4. The results indicate that when the sorption coefficient is high (10,000 mL/g), no breakthrough of the tracers is observed in 10^6 years. Thus, the alluvium could form a very effective barrier for sorbing radionuclides. The base-case simulation is the same as for the low-sorption case because the base-case value of the sorption coefficient is 0, meant to represent the behavior of a nonsorbing radionuclide. For comparison, the green line in Figure 6.7-4 shows the breakthrough results for an intermediate value of the sorption coefficient of 6.3 mL/g, meant to represent a weakly sorbing radionuclide like neptunium. Since the base case does not have any retardation, transit times for both the extreme cases are higher than that for the base case.

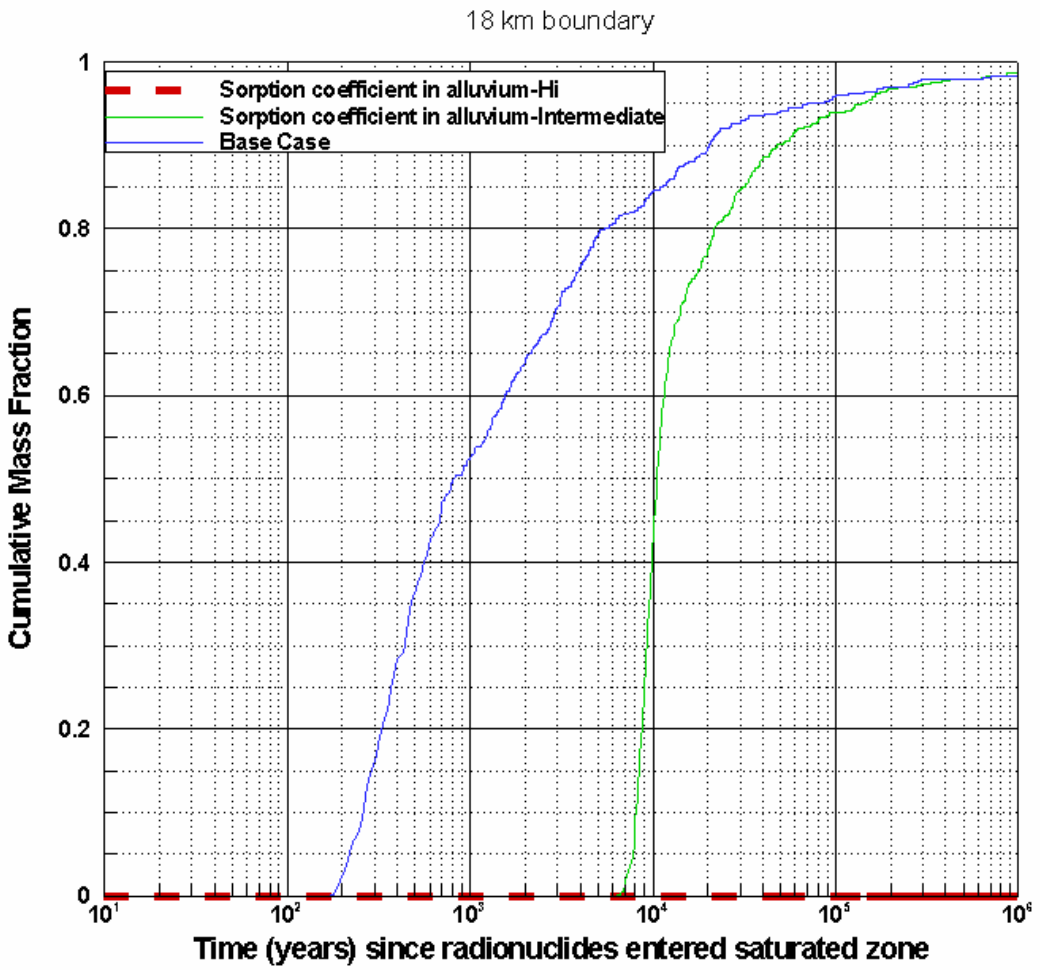

Output DTNs: LA0703SK150304.001, LA0703SK150304.006.

NOTE: Mass BTCs and median transport times are for an instantaneous source, present-day climate, and do not include radionuclide decay. Particle source location was near the middle of the anticipated repository footprint.

Figure 6.7-4. Propagation of Input Uncertainty in the Sorption Coefficient in Alluvium to the Output Breakthrough Curves at the 18-km Boundary

6.7.1.5 Effective Porosity in Alluvium

The results from simulations that evaluate the effect of changes in the effective porosity in the alluvium are shown in Figure 6.7-5. Note that in these simulations, the influence of the alluvium porosity on the retardation factor (Equation 22) does not show up because the base case does not include sorption. Thus, the effect shown in Figure 6.7-5 is that resulting from the effect of porosity on the fluid velocity through the relation:

$$\bar{v} = \frac{\bar{u}}{\theta} \qquad \text{(Eq. 47)}$$

where

$\overline{u}$ is the Darcy velocity obtained from the base-case flow model
$\overline{v}$ is the fluid velocity
θ is the porosity.

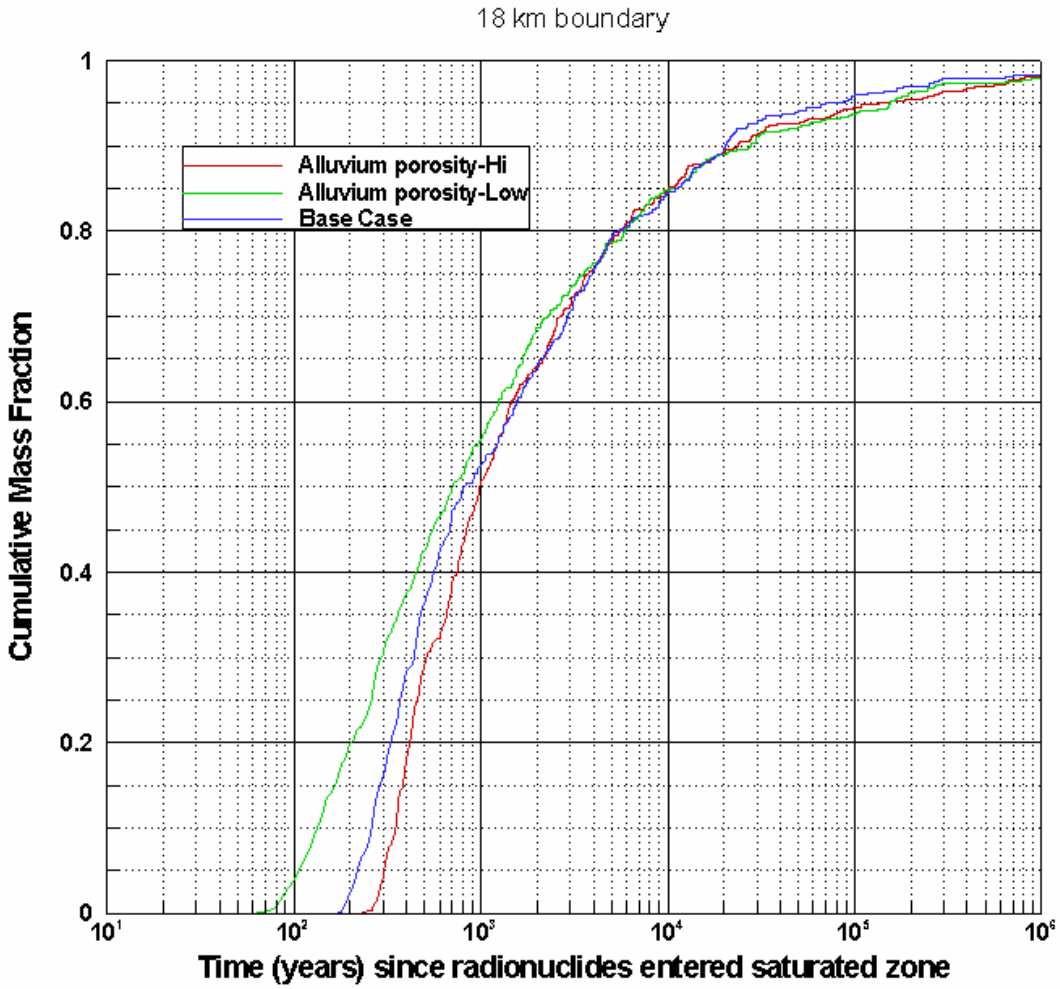

Output DTNs: LA0703SK150304.001, LA0703SK150304.003.

NOTE: Mass BTCs and median transport times are for an instantaneous source, present-day climate, and do not include radionuclide decay. Particle source location was near the middle of the anticipated repository footprint.

Figure 6.7-5. Propagation of Input Uncertainty in the Effective Porosity of Alluvium to the Breakthrough Curves at the 18-km Boundary

A moderate sensitivity is seen in Table 6.7-1 with the 50% breakthrough time spanning 709 to 986 years for the input range of values from 0.02 to 0.3.

The late time behavior of the BTCs is governed by matrix diffusion effects in the volcanic formations and dispersion throughout the flow domain; hence it is reasonable that the three curves tend to converge at long times. Since these processes are represented by random walk with a limited number of particles, some noise is seen in these curves.

6.7.1.6 Retardation Factor in Alluvium for Radionuclides Attached Irreversibly to Colloids

The results from simulations that evaluate the effect of changes in the colloid retardation factor in the alluvium are shown in Figure 6.7-6. As discussed in Section 6.4.2.6, these results include the retardation of the colloid particles due to reversible filtration in the porous media. The radionuclides attached irreversibly to the colloids do not diffuse into the volcanic matrix due to the large size of the colloids. Thus, the matrix diffusion coefficient is set to 0 in these simulations. The effect of colloids transported unretarded is applied in the TSPA calculations after the BTCs are calculated from the site-scale SZ transport model, and hence it is not considered here. Note that the retardation arises from the reversible filtration of the colloids in the alluvium. The range of uncertainty in the retardation factor of 8 to 5,188 translates into an output uncertainty range of 1,859 years to 688,357 years for the 50% breakthrough time. Recall that breakthrough time for the base case is 810 years.

For comparison, the base case, which considers nonsorbing radionuclides without any retardation, but includes matrix diffusion in the volcanic portion of the flow path, is shown. It is not surprising that the base-case curve crosses that for the colloids, which do not have matrix diffusion, since the effect of matrix diffusion is to give the BTC a tail for long times. To emphasize this point, BTC for the case with a very low value (10^{-50} m^2/s) of the dispersion coefficient is also shown – it is seen to be approximately parallel to the colloid BTCs.

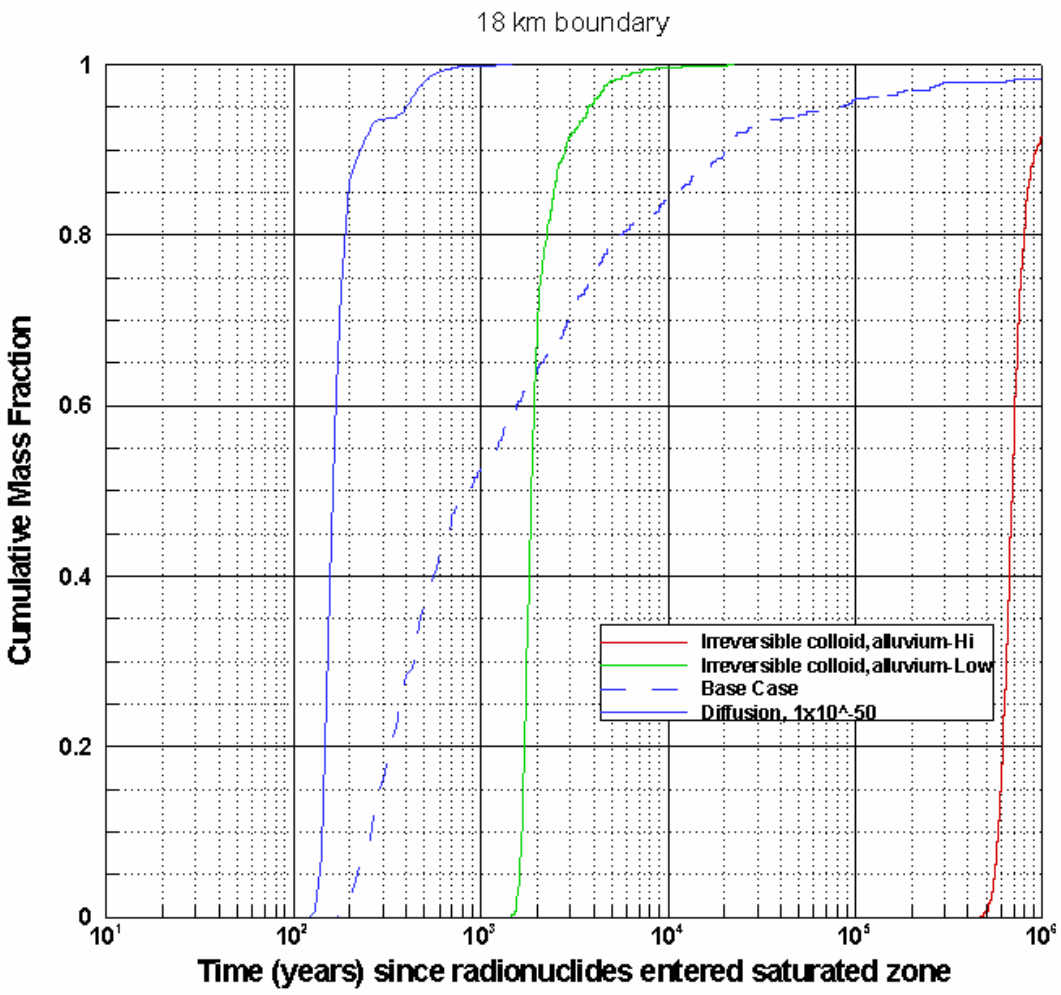

Output DTNs: LA0703SK150304.001, LA0703SK150304.004.

NOTE: Mass BTCs and median transport times are for an instantaneous source, present-day climate, and do not include radionuclide decay. Particle source location was near the middle of the anticipated repository footprint.

Figure 6.7-6. Propagation of Input Uncertainty in the Colloid Retardation Factor in Alluvium for Irreversible Colloids to the Breakthrough Curves at the 18-km Boundary

6.7.1.7 Reversible Sorption onto Colloids in the Alluvium

The results from simulations that evaluate the effect of changes in distribution parameters for reversible sorption onto colloids in alluvium are shown in Figure 6.7-7. The lower limit of the colloid concentration in groundwater (C_c) is 1.0×10^{-9} g/mL (Table 4-2). The minimum value for sorption onto colloids ($K_{d\text{-}c}$), 1.0 mL/g, occurs for uranium on iron oxide corrosion production colloids (Table 4-2), leading to the value of 10^{-9} for K_c. A minimum value of sorption coefficient (K_d) of 0.0 mL/g is used here as a conservative choice. The minimum value of the diffusion coefficient given in Table 4-2 is 5.0×10^{-12} m^2/s. For this case the minimum value of the adjusted effective diffusion coefficient ($D_e^{adjusted}$) in volcanics, computed using Equations 45a and 45b, is also 5.0×10^{-12} m^2/s, since K_c is much smaller than 1. This case is identical to the

low diffusion coefficient case presented in Figure 6.7-10, shown here in Figure 6.7-7 by the solid light-blue curve, labeled "Reversible colloid alluvium-Low." For comparison, the base case, which considers nonsorbing radionuclides without any retardation but includes matrix diffusion in the volcanic portion of the flow path, is shown by the dashed blue line. Note that the dashed blue curve crosses the red one, as expected, since the later has a much lower value of the diffusion coefficient.

The upper limiting value for sorption onto colloids ($K_{d\text{-}c}$), 1.0×10^{7} mL/g, occurs for the case of Am onto hematite colloids. The upper limit of the colloid concentration in groundwater (C_c) is 2.0×10^{-4} g/mL (Table 4-2), leading to the value of 2.0×10^{3} for K_c. The upper limit of sorption coefficient onto rocks ($K_d^{original}$, both volcanics and alluvium) for americium is 10,000 mL/g (Table C-14). Using Equations 45a, 45b, and 46, this value for the adjusted sorption coefficient onto rocks ($K_d^{adjusted}$) in alluvium becomes 5.0 mL/g. Using the minimum value of 5.0×10^{-12} m^2/s for the diffusion coefficient from Table 4-2, the adjusted minimum effective diffusion coefficient ($D_e^{adjusted}$) in volcanics for this case has value 1.25×10^{-18} m^2/s. This is the high curve (labeled "Reversible colloid alluvium-Hi") in Figure 6.7-7. This case includes diffusion and retardation in volcanics as well. It is seen that the time for 50% of the mass to breakthrough at the 18-km boundary is 7,023 years.

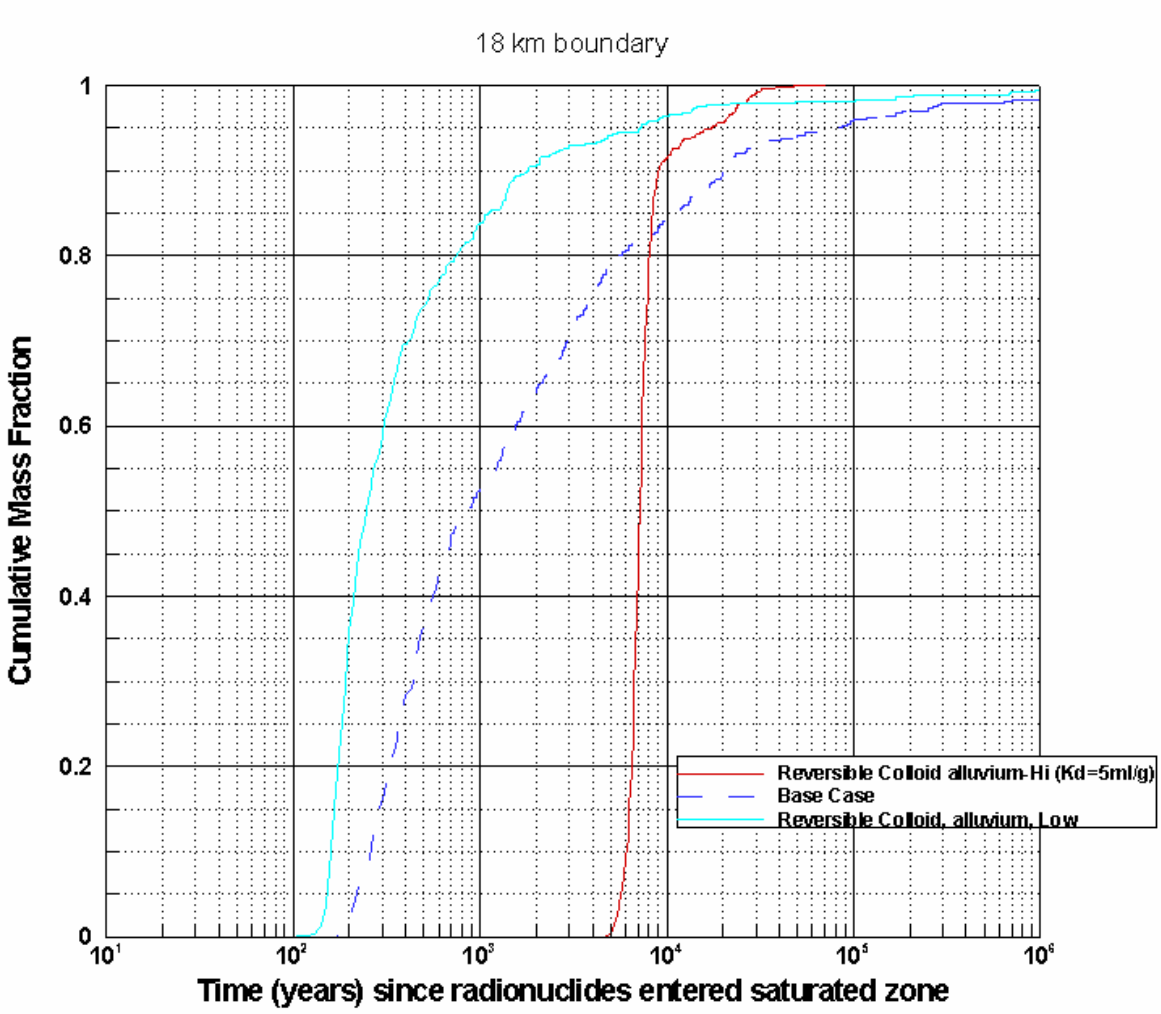

Output DTNs: LA0703SK150304.001, LA0703SK150304.006.

NOTE: Mass BTCs and median transport times are for an instantaneous source, present-day climate, and do not include radionuclide decay. Particle source location was near the middle of the anticipated repository footprint.

Figure 6.7-7. Propagation of Input Uncertainty in the Colloid Retardation Factor in Alluvium for Reversible Colloids to the Output Breakthrough Curves at the 18-km Boundary

6.7.1.8 Flowing Interval Aperture in Volcanics

The results from simulations that evaluate the effect of changes in flowing interval aperture in volcanics (holding flowing interval porosity fixed at the base-case value of 0.001) on the BTCs are shown in Figure 6.7-8. When the flow aperture is at the lower end of the parameter distribution, 1.86×10^{-5} m (Table 6.7-1), the retardation due to matrix diffusion is amplified so much that it overtakes the effects of increased velocities in the flowing interval. This results in more than an order of magnitude increase in the time for 50% mass breakthrough. The reverse is true for the upper limit of the aperture, 8 m, where there is very little diffusion, and breakthrough occurs somewhat earlier than in the base case.

For the case of high value of the aperture, the effect of diffusion is expected to be very small, as seen by comparing the red and the dashed-black curves in Figure 6.7-8. On the other hand, the case of low value of the aperture is expected to behave similar to a single porosity medium but with a larger value of the porosity, as seen from the fact that the green curve in the figure is delayed but approximately parallel to the red curve.

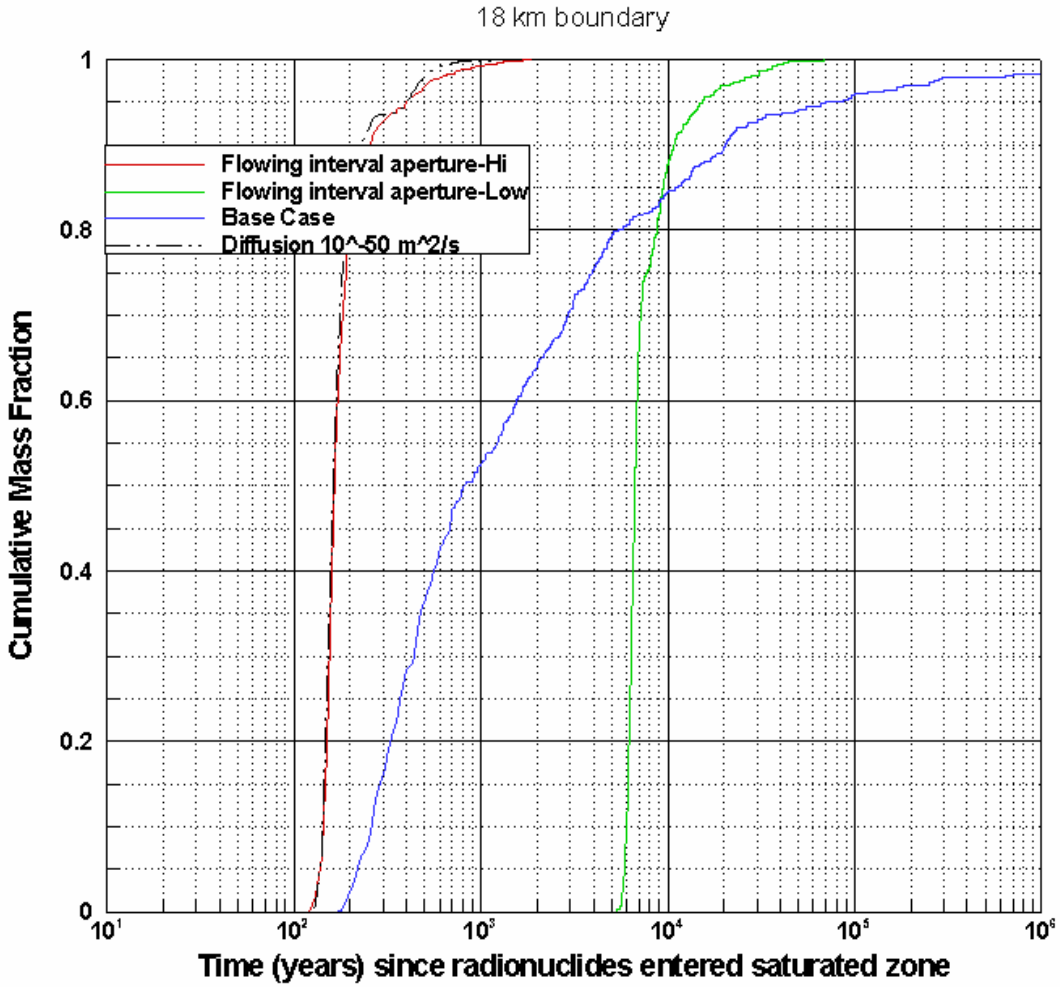

Output DTNs: LA0703SK150304.001, LA0703SK150304.005.

NOTE: Mass BTCs and median transport times are for an instantaneous source, present-day climate, and do not include radionuclide decay. Particle source location was near the middle of the anticipated repository footprint.

Figure 6.7-8. Propagation of Input Uncertainty in the Flowing Interval Aperture in Volcanics to the Breakthrough Curves at the 18-km Boundary

6.7.1.9 Flowing Interval Porosity in Volcanics

The results from simulations that evaluate the effect of changes in flowing interval aperture in volcanics (holding flowing interval aperture fixed at the base-case value of 25.773×10^{-5} m) on the BTCs are shown in Figure 6.7-9.

For the case of low value of the porosity, the effect of diffusion is expected to be small, as seen by comparing the green and the base case (blue) curves in Figure 6.7-8. On the other hand, the case of high value of the porosity is expected to behave similar to a single porosity medium but with a longer transit time, as seen from the fact that the red curve in the figure is delayed but approximately parallel to the green curve.

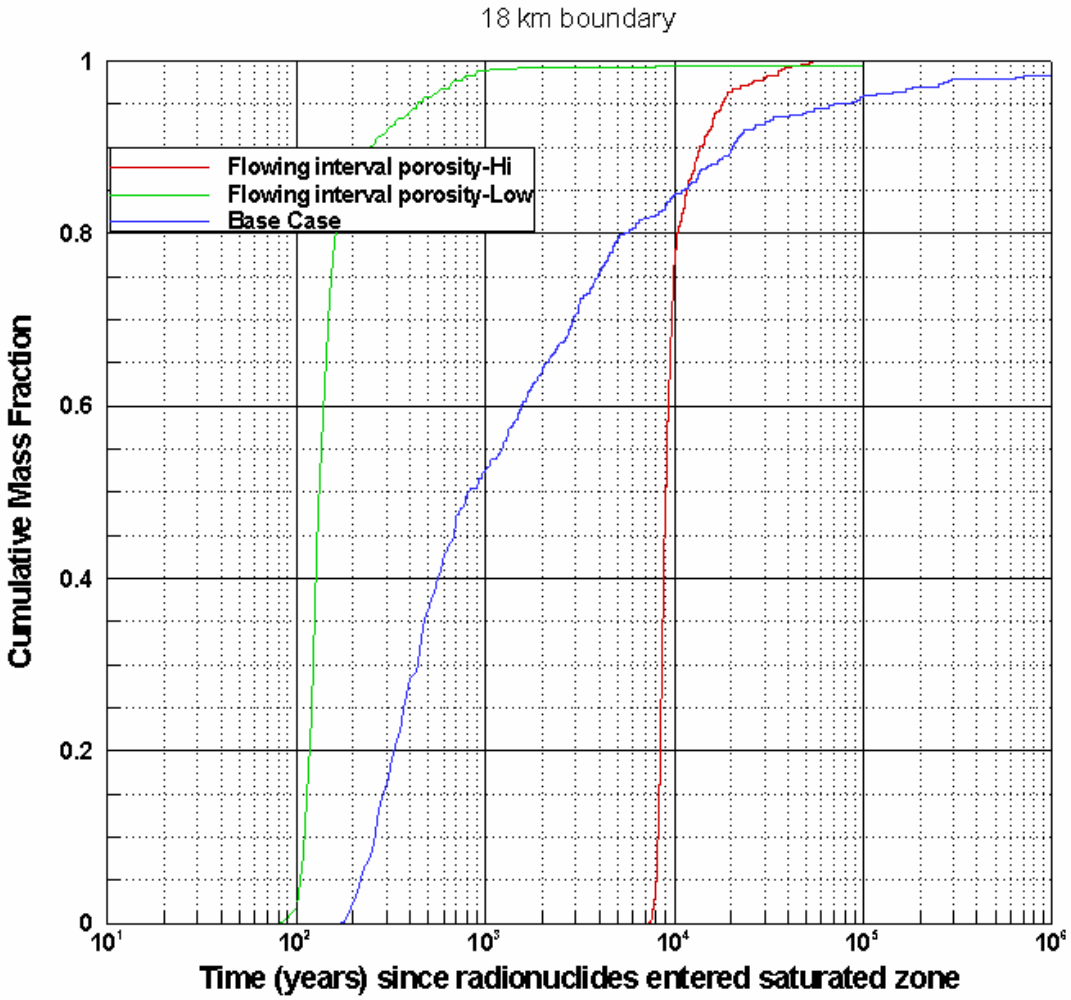

Output DTNs: LA0703SK150304.001, LA0703SK150304.005.

NOTE: Mass BTCs and median transport times are for an instantaneous source, present-day climate, and do not include radionuclide decay. Particle source location was near the middle of the anticipated repository footprint.

Figure 6.7-9. Propagation of Input Uncertainty in the Flowing Interval Porosity in Volcanics to the Breakthrough Curves at the 18-km Boundary

6.7.1.10 Effective Diffusion Coefficient in Volcanics

The results from simulations that evaluate the effect of changes in effective diffusion coefficient in volcanics on the BTCs are shown in Figure 6.7-10. Also shown in the figure for comparison is the BTC for practically zero diffusion (diffusion coefficient of 10^{-50} m^2/s). The range of 5.0×10^{-12} to 5.0×10^{-10} (m^2/s) in the input value results in the range of 245 to 6,324 years for output (50% breakthrough time). Considering that this parameter affects only the transport through the volcanics and not through that in the alluvium, it has a significant impact on the output.

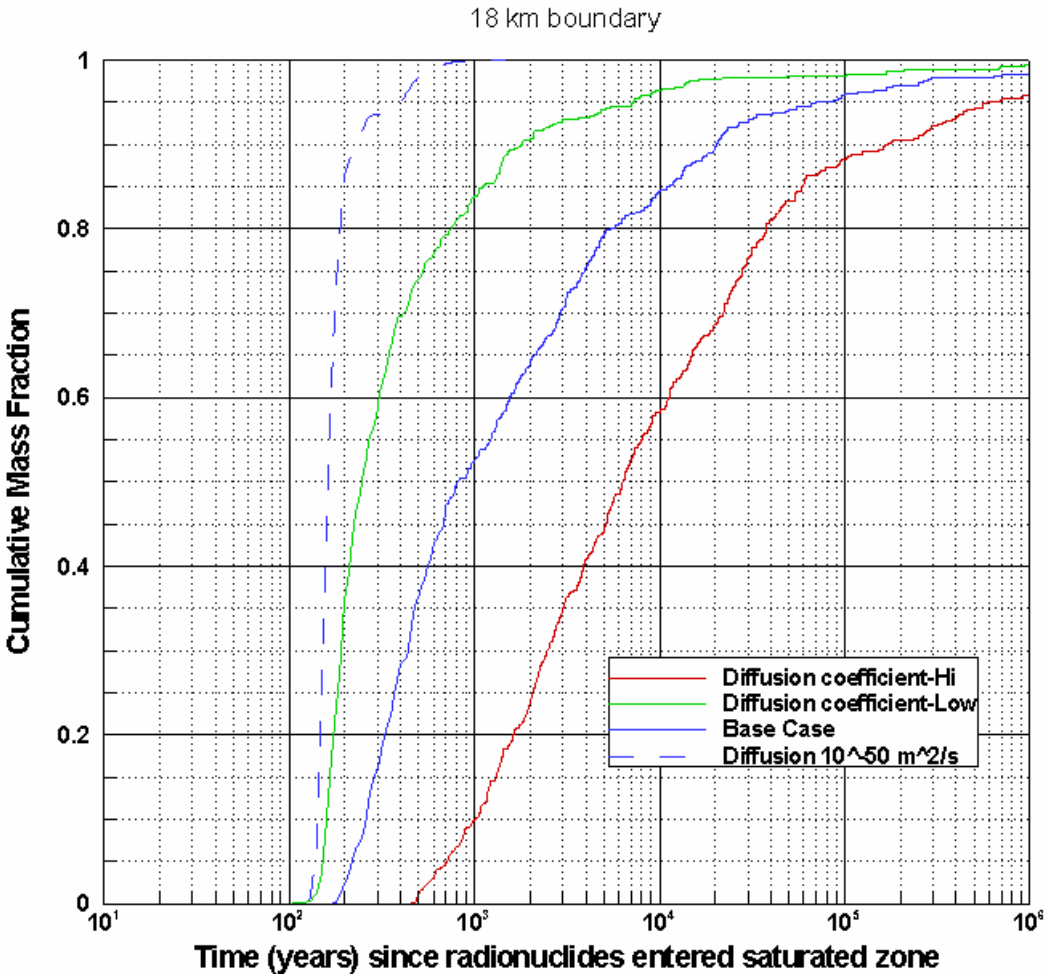

Output DTNs: LA0703SK150304.001, LA0703SK150304.003.

NOTE: Mass BTCs and median transport times are for an instantaneous source, present-day climate, and do not include radionuclide decay. Particle source location was near the middle of the anticipated repository footprint.

Figure 6.7-10. Propagation of Input Uncertainty in the Effective Diffusion Coefficient in Volcanics to the Output Breakthrough Curves at the 18-km Boundary

6.7.1.11 Matrix Sorption Coefficient in Volcanics

The results from simulations that evaluate the effect of changes in matrix sorption coefficient in volcanics on the output BTCs are shown in Figure 6.7-11. The results indicate that when the sorption coefficient is high (10,000 mL/g), no breakthrough of the tracers is observed in one million years. Thus, the volcanics could form a very effective barrier for those radionuclides that diffuse and adsorb in the matrix. The base-case simulation is the same as for the low-sorption case because the base-case value of the matrix sorption coefficient is 0, which is the same as the lower limit value. For comparative purposes, also plotted in the figure is the breakthrough for an intermediate case with the matrix sorption coefficient equal to 1.5 mL/g. It is seen that even this moderate value is sufficient to cause a delay by thousands of years.

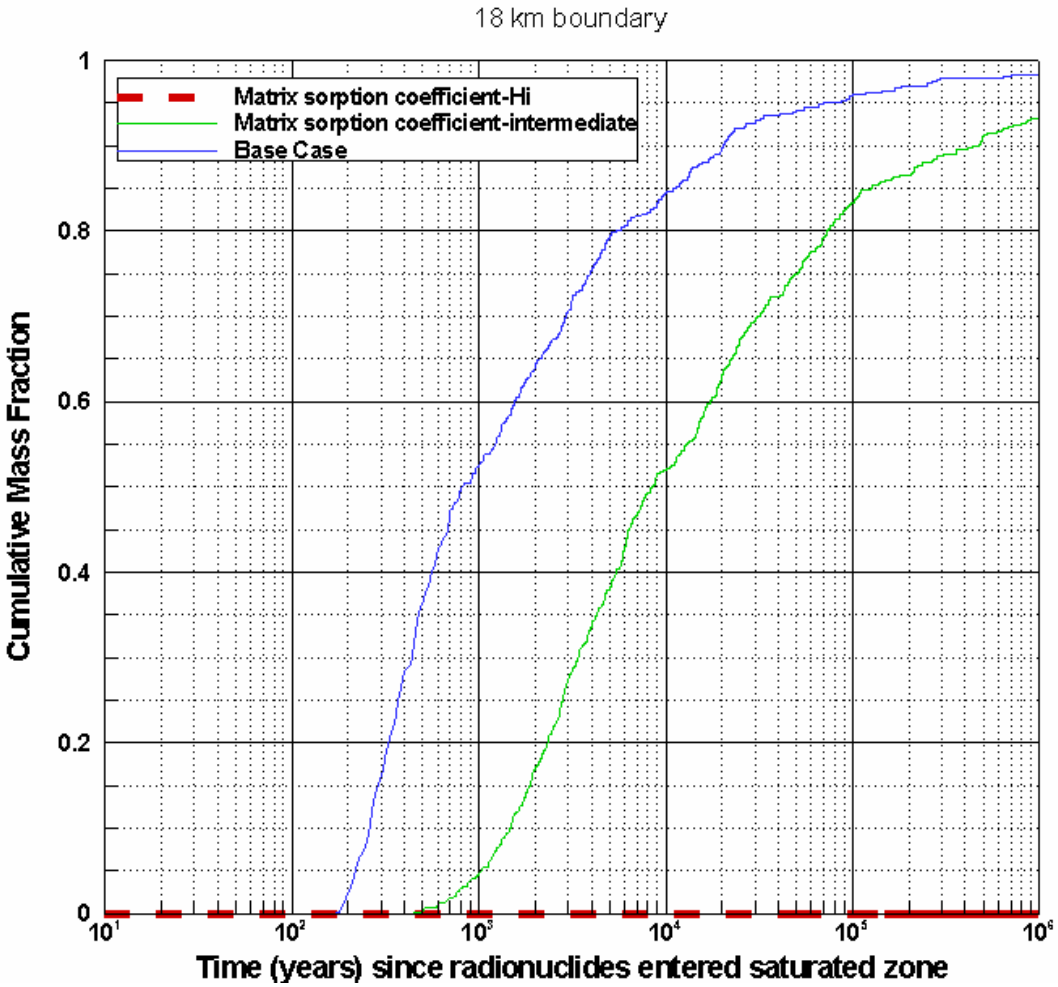

Output DTNs: LA0703SK150304.001, LA0703SK150304.004.

NOTE: Mass BTCs and median transport times are for an instantaneous source, present-day climate, and do not include radionuclide decay. Particle source location was near the middle of the anticipated repository footprint.

Figure 6.7-11. Propagation of Input Uncertainty in the Matrix Sorption Coefficient in Volcanics to the Output Breakthrough Curves at the 18-km Boundary

6.7.1.12 Retardation Factor in Volcanics for Radionuclides Attached Irreversibly to Colloids

The results from simulations that evaluate the effect of changes in the colloid retardation factor on the transport of irreversibly sorbed radionuclides in volcanics on the output BTCs are shown in Figure 6.7-12. As discussed in Section 6.4.2.6, these results include the retardation of the colloid particles due to reversible filtration in the fractured flowing intervals in the volcanics. The radionuclides attached irreversibly to the colloids do not diffuse into the volcanic matrix due to the large size of the colloids. Thus, the matrix diffusion coefficient is set to 0 in these simulations. The effect of colloids transported unretarded is applied in the TSPA calculations after the BTCs are calculated from the site-scale SZ transport model, and hence it is not considered here. For comparison, the base case, which considers nonsorbing radionuclides without any retardation but includes matrix diffusion in the volcanic portion of the flow path, is also shown. Note that the retardation arises from the reversible filtration of the colloids in the alluvium. The range of uncertainty in the retardation factor of 6 to 794 translates into an output uncertainty range of 4,600 to 28,519 years for the 50% breakthrough time. Recall that breakthrough time for the base case is 810 years.

Blue curve shows the base case, which considers nonsorbing radionuclides without any retardation but includes matrix diffusion in the volcanic portion of the flow path. It is not surprising that this curve crosses that for the low value of retardation factor since the effect of matrix diffusion is to give the BTC a tail for long times.

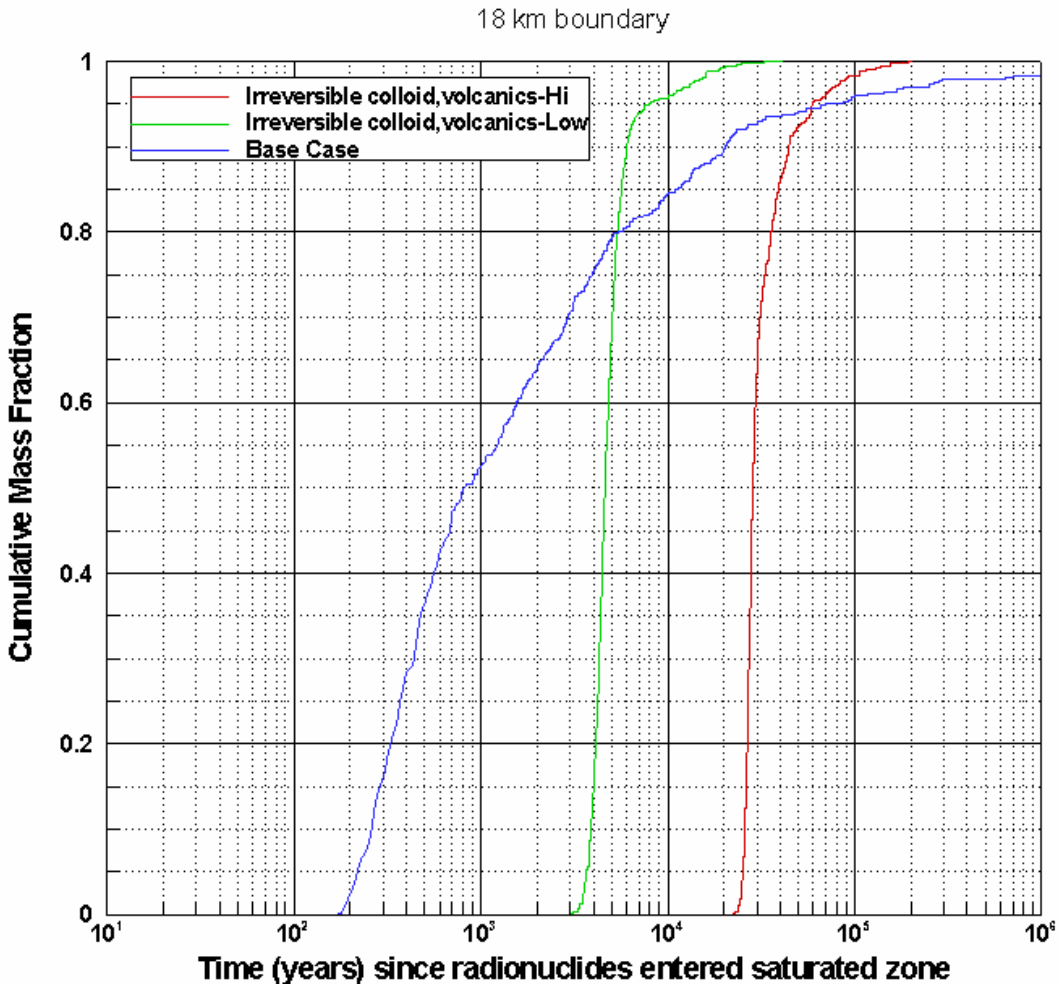

Output DTNs: LA0703SK150304.001, LA0703SK150304.004.

NOTE: Mass BTCs and median transport times are for an instantaneous source, present-day climate, and do not include radionuclide decay. Particle source location was near the middle of the anticipated repository footprint.

Figure 6.7-12. Propagation of Input Uncertainty in the Colloid Retardation Factor in Volcanics for Irreversible Colloids to the Output Breakthrough Curves at the 18-km Boundary

6.7.1.13 Reversible Sorption onto Colloids in the Volcanics

The process of colloid facilitated transport of radionuclides attached reversibly to colloids through volcanics is somewhat complicated, in that the effective diffusion ($D_e^{adjusted}$) is a function of the distribution parameter K_c, as given in Equations 45a, and 45b. The K_c in turn is a product of the concentration of colloids in the groundwater and the sorption coefficient for the radionuclide onto the colloids. The results from simulations that evaluate the effect of changes in the distribution parameter K_c for reversible sorption onto colloids in the volcanics are shown in Figure 6.7-13.

The lower limit of the colloid concentration in groundwater (C_c) is 1.0×10^{-9} g/mL (Table 4-2). The minimum value for sorption onto colloids ($K_{d\text{-}c}$), 1.0 mL/g, occurs for uranium on oxide corrosion production colloids (Table 4-2), and the minimum value of sorption coefficient onto

volcanic rocks of 0.0 mL/g also occurs for uranium (Table C-14). For this case the minimum value of the adjusted effective diffusion coefficient ($D_e^{adjusted}$), computed using Equations 45a, and 45b is 5.0×10^{-12} m^2/s. This is identical to the green curve in Figure 6.7-10, reproduced here for comparison, labeled in Figure 6.7-13 as "Reversible colloids, Volcanics, Low." However, if the lower limit of the colloid concentration in groundwater (1.0×10^{-9} g/mL) is considered with the upper limit of the sorption coefficient onto colloids (for the case of americium onto hematite colloids), 1.0×10^{7} mL/g, with the upper limit of the sorption coefficient onto to rock matrix is 10,000 mL/g. This value, along with the median value of the diffusion coefficient, will lead to the almost identical result as the dashed red line in Figure 6.7-11, with no breakthrough within 1 million years. It is shown here also by the dashed red curve, labeled "Reversible colloids,Volcanics, Upper limit."

The impact of the effective diffusion ($D_e^{adjusted}$) upon travel time is complicated due its dependence on the colloid concentration in groundwater (C_c) and coefficient of sorption onto colloids ($K_{d\text{-}c}$),. For example, faster breakthroughs can be obtained for colloid facilitated transport in volcanics than the green curve labeled in Figure 6.7-13 as "Reversible colloids, Volcanics, Low". To see this, consider the upper limiting value for sorption onto colloids ($K_{d\text{-}c}$), 1.0×10^{7} mL/g, for the case of americium onto hematite colloids. Consider the upper limit of the colloid concentration in groundwater (C_c) is 2.0×10^{-4} g/mL (Table 4-2). Using Equations 45a and 45b, the adjusted minimum effective diffusion coefficient ($D_e^{adjusted}$) for this case has value 1.25×10^{-18} m^2/s. Due to this very small value, there is very small degree of radionuclide diffusion into the volcanic rock matrix; thus using even a robust value of 5.0 mL/g for the sorption coefficient onto rock matrix (K_d) does not lead to any significant retardation. As seen in Figure 6.7-13, the brown curve, labeled "Reversible colloids, Volcanics, rapid breakthrough," illustrates that short transit times result for this case.

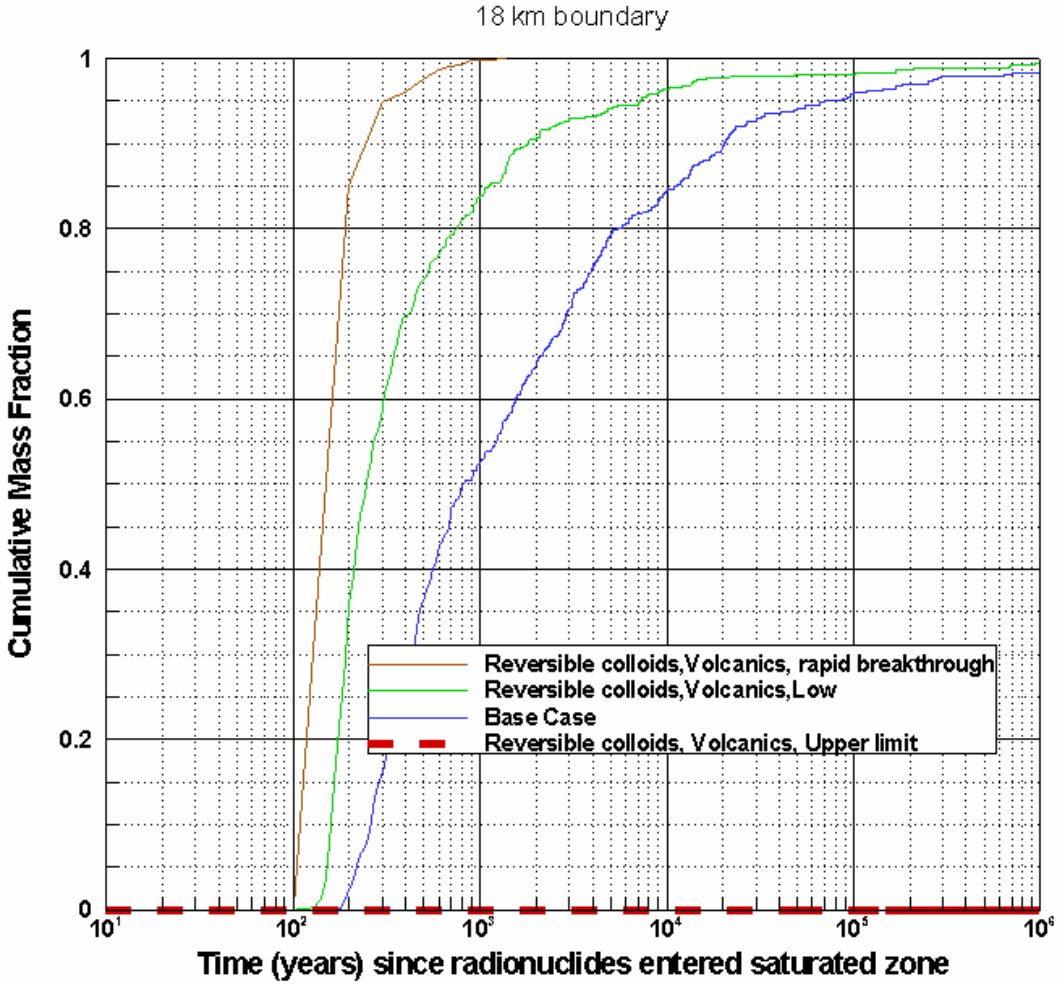

Output DTNs: LA0703SK150304.001, LA0703SK150304.006.

NOTE: Mass BTCs and median transport times are for an instantaneous source, present-day climate, and do not include radionuclide decay. Particle source location was near the middle of the anticipated repository footprint.

Figure 6.7-13. Propagation of Input Uncertainty in the Distribution Parameter K_c in Volcanics for Reversible Colloids to the Output Breakthrough Curves at the 18-km Boundary

6.7.1.14 Longitudinal Dispersivity

The results from simulations that evaluate the effect of changes in longitudinal dispersivity on the output BTCs are shown in Figure 6.7-14. In these simulations, the same longitudinal dispersivity values were applied to both the volcanics and the alluvium together. At the minimum value of dispersivity (0.1 m), the results with a breakthrough time of 671 years are only slightly different from the base case value of 813 years (which has a dispersivity value of 10 m). This is because at low values of dispersivity, the effects of diffusion tend to mask the effects of dispersion. At maximum values of dispersivity (2,000 m), an earlier low-concentration breakthrough is observed, which continues at a lower concentration relative to the base case for

the duration of the simulation. The 50% breakthrough is delayed to 5,900 years. The high dispersivity case has an overall longer release time (start to end of release) than the other cases.

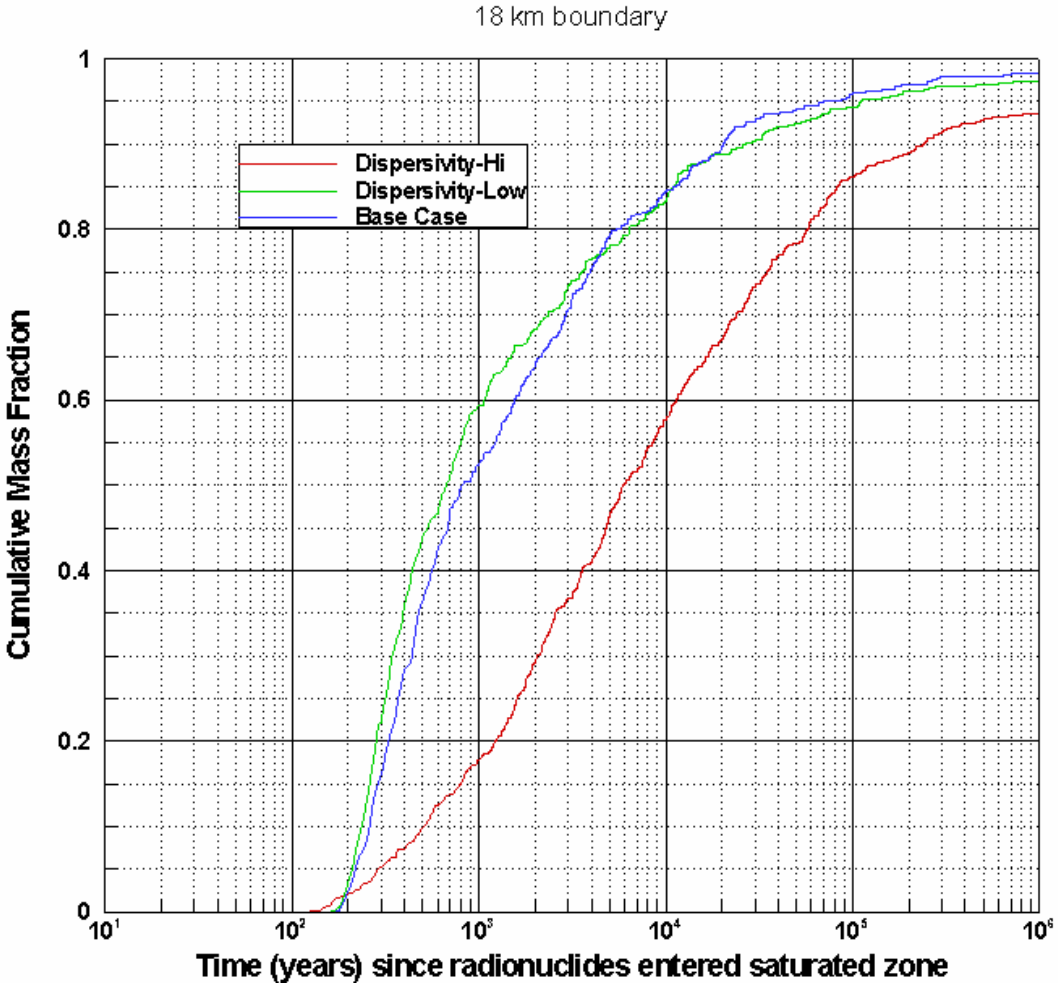

Output DTNs: LA0703SK150304.001, LA0703SK150304.003.

NOTE: Mass BTCs and median transport times are for an instantaneous source, present-day climate, and do not include radionuclide decay. Particle source location was near the middle of the anticipated repository footprint.

Figure 6.7-14. Propagation of Input Uncertainty in the Longitudinal Dispersivity to the Output Breakthrough Curves at the 18-km Boundary

6.8 BARRIER CAPABILITY

6.8.1 Introduction

This section presents transport model calculations designed to illustrate the function of the saturated zone barrier. These simulations explore in greater detail some of the key aspects of the system, important uncertain model parameters, physical properties, and boundaries to illustrate the functioning of the saturated zone as a barrier to radionuclide migration. Combined with the validation section (Section 7) and the analysis of model uncertainties (Section 8.3), this section

describes the technical basis for the saturated zone barrier in the context of the Yucca Mountain waste disposal system.

In its simplest form, the saturated zone performs two functions in its role as a barrier to radionuclide migration: (1) it delays the transport of radionuclides from beneath the repository to the boundary of the accessible environment at 18 km, and (2) it attenuates the concentration of radionuclides in the mobile water. By examining the processes of matrix diffusion, advection, and dispersion for various ranges of parameters, the role of various processes on the delay and dilution of radionuclides is presented. Also presented are intermediate BTCs at the contact between the fractured volcanic tuffs and the alluvium to assess the relative importance of the two key hydrostratigraphic rock types. Because all parameters are estimated rather than known with certainty, a few key parameters in this section are varied to complement the results from Section 8.3. Finally, transport simulations for the fraction of radionuclides bound to colloids are also examined because of the importance of this process to radionuclide transport predictions in the saturated zone.

6.8.2 Saturated Zone Subsystem Performance: Sorption in Volcanics and Alluvium

Most radionuclides are expected to sorb to the rock, which should delay their arrival at the boundary of the accessible environment at 18 km. Figure 6.8-1a also shows several simulations of sorbing radionuclides. The curve labeled "Matrix sorption" allows sorption in the matrix continuum of the volcanic tuffs and reflects a small matrix sorption coefficient of 1.3 mL/g. Including only this process yields a BTC similar to the base-case BTC but with significantly delayed transport times. The final curve in the figure shows the influence of sorption in the alluvium along with the fractured volcanics. Travel times largely in excess of 10,000 years are predicted in the saturated zone alone for a sorption coefficient of 6.3 mL/g, meant to fall in the range of K_d values for weakly sorbing radionuclides such as neptunium. It is seen from these curves that sorption in the alluvium can increase the transport time by orders of magnitude of even the weakly sorbing radionuclides such as neptunium (the results presented in Figure 6.8-1a do not include the effects of colloid-facilitated transport; those are discussed in Section 6.8.5).

6.8.3 Saturated-Zone Subsystem Performance: Fractured Volcanic Tuffs and Alluvium

To illustrate in more detail the function of the saturated zone, BTCs were computed at an intermediate location in the model at a boundary defined by the transition from fractured volcanic tuffs to alluvium. Figure 6.8-1b shows BTCs for the base-case and matrix sorption scenarios at the volcanic/alluvium boundary, which is approximately 11 km south of the southern boundary of the repository footprint. Comparing these simulations to the equivalent curves in Figure 6.8-1a, it is observed that the early parts of the BTCs differ from each other, but the latter parts are very close to each other. This shows that alluvium plays a significant role for short transport times. By contrast, the tails of the BTCs are due primarily to transport through fractures and matrix diffusion. Therefore, while the fractured volcanic tuffs provide significant delay for a fraction of the mass, the fastest moving portion of a radionuclide is controlled by transport through the alluvium. The reason for this result is that the continuum flow and transport through the bulk medium characterizes alluvium transport, in contrast to the fracture transport characterized by dual-porosity in the volcanics. Finally, based on the matrix sorption

BTC in Figure 6.8-1b, sorption in the fractured tuffs is expected to provide significant transport-time delays, even without considering the subsequent transport through the alluvium.

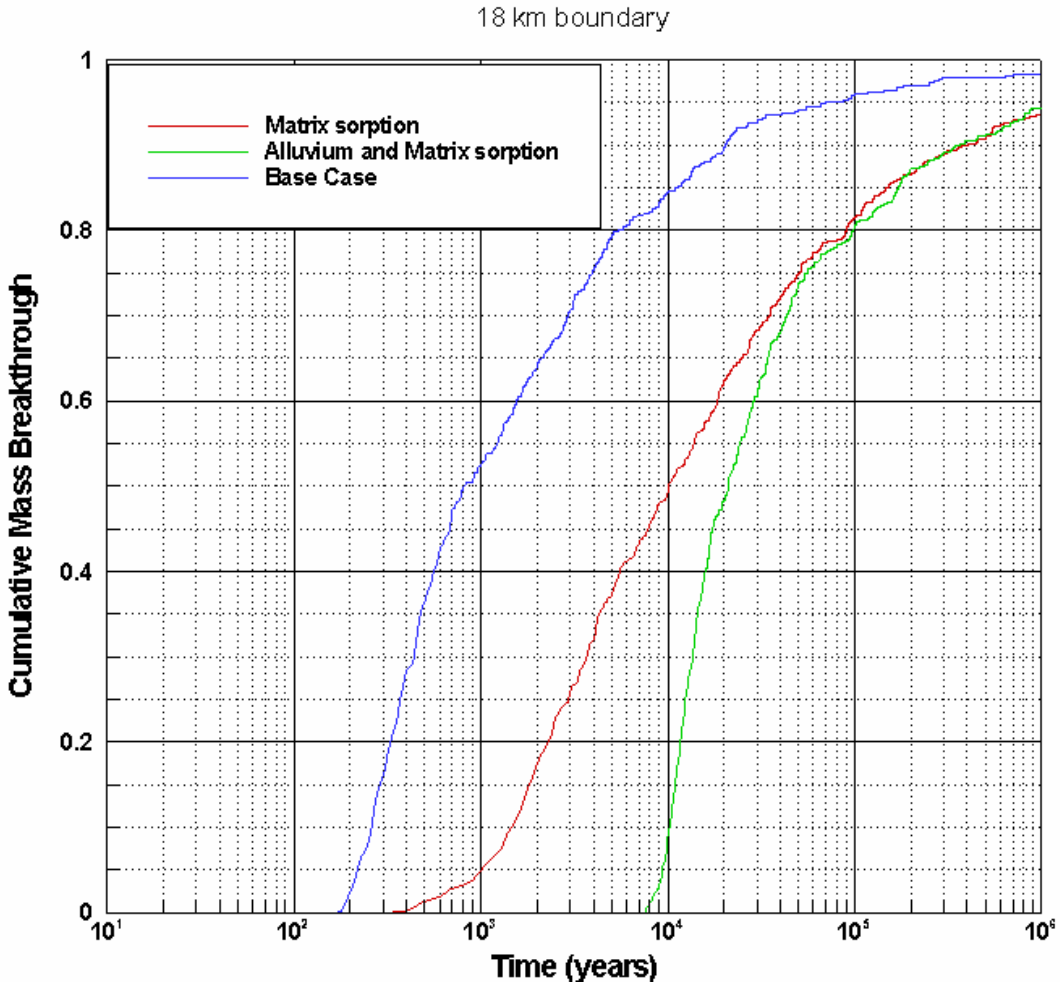

Output DTNs: LA0703SK150304.001, LA0703SK150304.007.

NOTE: Mass BTCs and median transport times are for an instantaneous source, present-day climate, and do not include radionuclide decay. Particle source location was near the middle of the anticipated repository footprint.

Figure 6.8-1a. Breakthrough Curves for the Base Case, Conservative Radionuclide, and Sorbing Radionuclides: 18-km Boundary

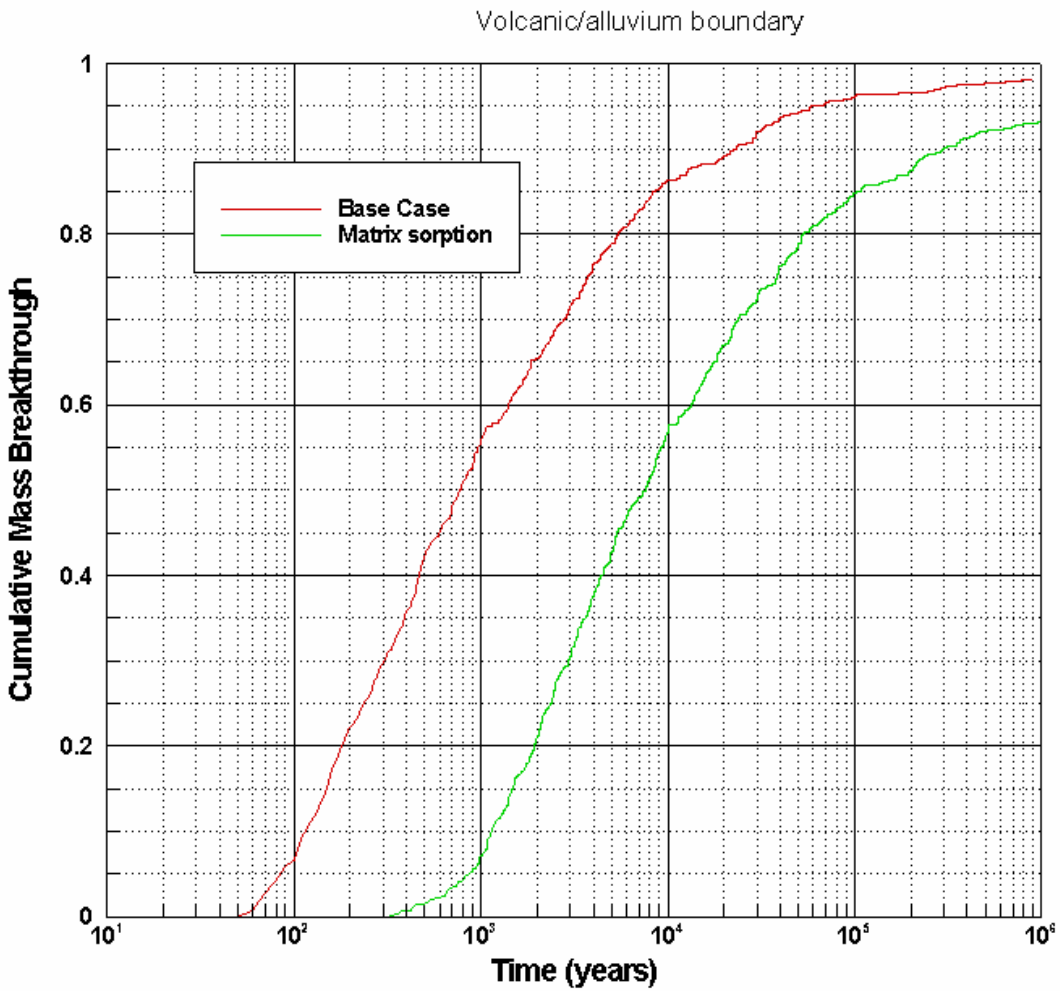

Output DTNs: LA0703SK150304.001, LA0703SK150304.009.

NOTE: Mass BTCs and median transport times are for an instantaneous source, present-day climate, and do not include radionuclide decay. Particle source location was near the middle of the anticipated repository footprint.

Figure 6.8-1b. Breakthrough Curves for the Base Case, Conservative Radionuclides, and Sorbing Radionuclides: Volcanic/Alluvium Boundary

6.8.4 Saturated-Zone Sensitivity Analyses: Advection, Diffusion, and Dispersion

The processes of advection, dispersion, and diffusion into the rock matrix all play key roles in the prediction of saturated zone barrier performance. In this section, the importance of these processes is illustrated by examining BTCs for a variety of scenarios in which one or more parameters are changed to isolate a particular process. These results are presented in the context of saturated zone transport barrier performance, focusing on results relevant to the arrival times and dispersion of radionuclides. Figures 6.8-2a (18-km boundary) and 6.8-2b (volcanic/alluvium contact) show the BTCs for a conservative radionuclide for the base case, a case with matrix diffusion but with a very small value (10^{-50} m) of longitudinal hydrodynamic dispersion (referred to in this section and in Figures 6.8-2a and 6.8-2b as "nondispersive"), and a case with dispersion but no diffusion. Both diffusion and dispersion result in the spreading of BTCs at the

18-km boundary (or the volcanic/alluvium contact). The implication for radionuclide dilution is that any sharp pulse of high concentration reaching the saturated zone would be attenuated due to diffusion and dispersion by the time that mass reached the boundary of the accessible environment at 18 km. Additional discussion of this point is provided in Section 6.8.6.

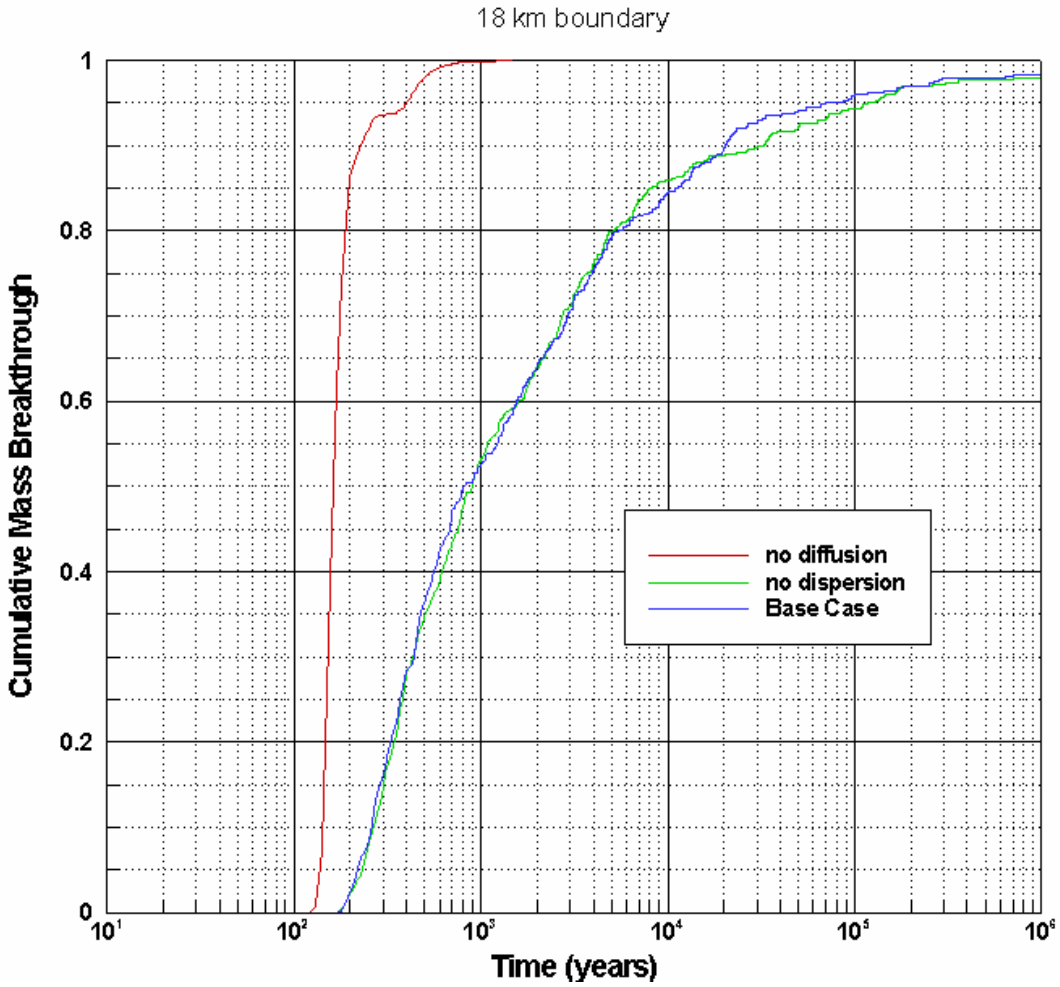

Output DTNs: LA0703SK150304.001, LA0703SK150304.008.

NOTE: Mass BTCs and median transport times are for an instantaneous source, present-day climate, and do not include radionuclide decay. Particle source location was a point near the middle of the repository footprint.

Figure 6.8-2a. Breakthrough Curves Comparing the Base Case, Nondispersive, and Nondiffusive Cases: 18-km Boundary

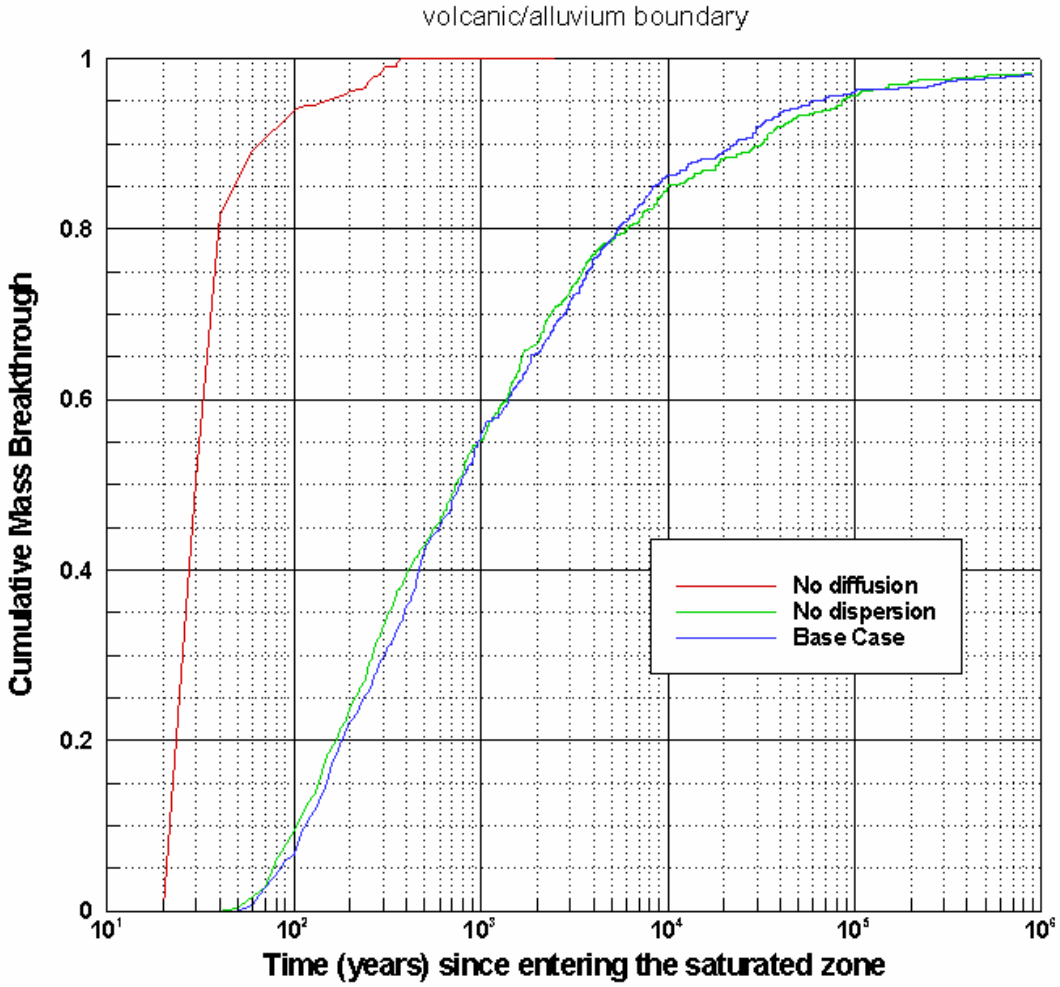

Output DTNs: LA0703SK150304.001, LA0703SK150304.009.

NOTE: Mass BTCs and median transport times are for an instantaneous source, present-day climate, and do not include radionuclide decay. Particle source location was a point near the middle of the repository footprint.

Figure 6.8-2b. Breakthrough Curves Comparing the Base Case, Nondispersive, and Nondiffusive Cases: Volcanic/Alluvium Boundary

Regarding the relative importance of diffusion and dispersion in spreading the arrival time distribution, Figures 6.8-2a and 6.8-2b suggest that as long as diffusion in the volcanics matrix occurs, the additional spreading afforded by a dispersion mechanism is very small (note the close similarity of the base-case and "no dispersion" curves). By contrast, the no-diffusion BTC deviates significantly from the base case, showing the role of diffusion both for dispersing the mass and delaying the arrival times. One important factor to consider is that the dispersion being examined in this sensitivity analysis is only the hydrodynamic dispersion that occurs at scales smaller than the model grid block, as parameterized with the random-walk dispersion model. Larger-scale heterogeneities (e.g., hydrostratigraphic units of contrasting permeabilities, faults) are explicitly incorporated in the model. Therefore, because these large-scale dispersion mechanisms are "built into" the model, they are not turned off in the low dispersion simulations presented here. Nevertheless, the BTC comparisons show the importance of diffusion as a

mechanism for both delaying the transport times and spreading the distribution of the arrival times. Small-scale dispersion is relatively unimportant.

Another factor requiring examination is the spatial distribution of the contaminant source term. These BTCs have been generated for a point release of contaminants. If the radionuclide source term occurs due to the failure of only one or a few waste packages, the source term at the saturated zone would more closely resemble a point source. Figure 6.8-3 examines the role of the contaminant source in controlling the BTC by comparing the distributed source with one in which all particles are introduced at a single location near the center of the repository footprint. A greater spreading of arrival times is caused by the different starting locations of the particles, especially if there is a wide range of permeabilities and fluid fluxes directly beneath the repository. The BTC at the 18-km boundary for the case without diffusion is sharper for the point source than the one for the distributed source, and the difference between the curves is more pronounced at later times. This suggests that the spreading at early arrival times for nondiffusive transport is caused by the distributed source. However, diffusion into the rock matrix becomes more important at later times, suggesting that the details of the release location(s) at the repository footprint should have a noticeable but minor effect on the predicted BTC.

Regarding advection, specific discharge is one of the most important uncertain parameters in the site-scale SZ transport model, owing to its first-order influence on solute velocity and the fact that available data and models can only provide relatively wide bounds on its estimated value. Figures 6.8-4 shows the predicted BTCs for a conservative radionuclide over a broad range of values of specific discharge (this figure is identical to Figure 6.7-1, reproduced here for convenience).

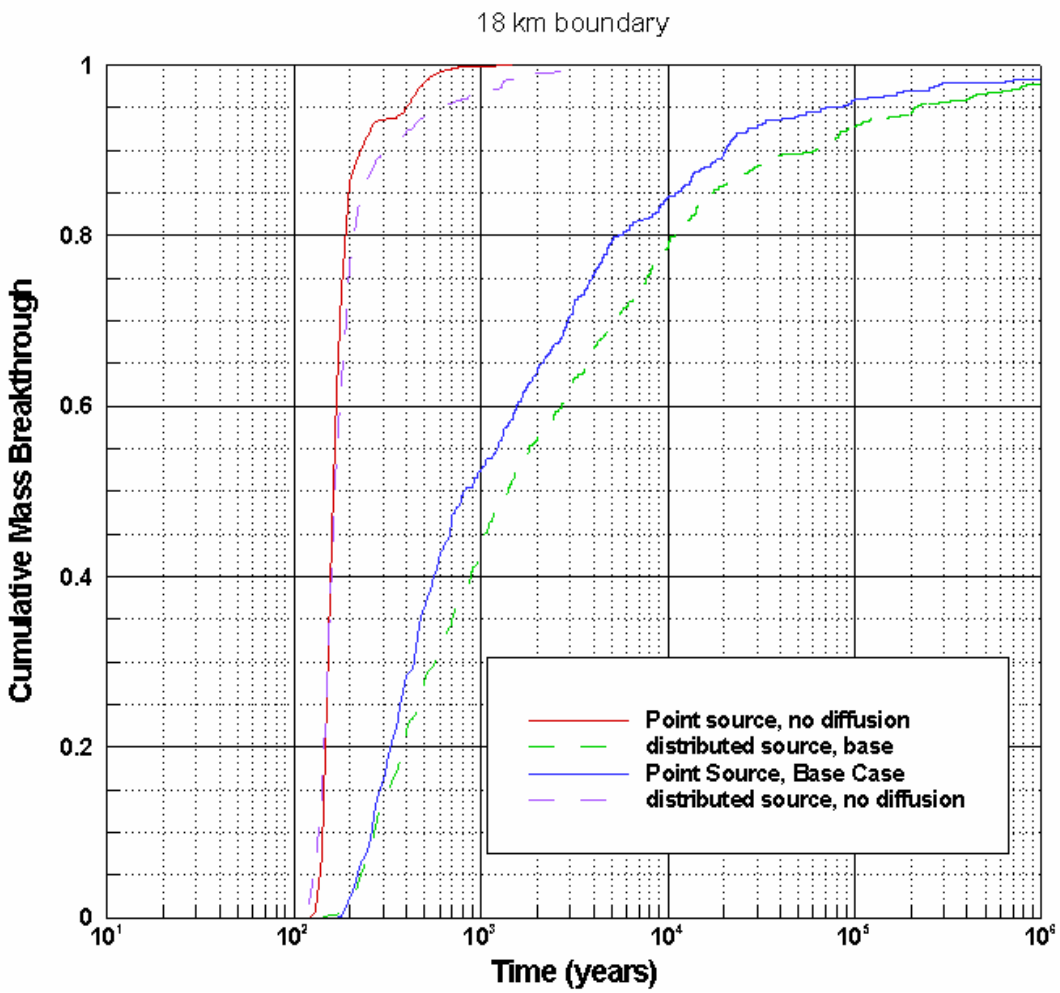

Output DTNs: LA0703SK150304.001, LA0703SK150304.008, LA0703SK150304.010.

NOTE: Mass BTCs and median transport times are for an instantaneous source, present-day climate, and do not include radionuclide decay. Particle source location was a point near the middle of the repository footprint.

Figure 6.8-3. Breakthrough Curves for the Base-Case Parameters with Point Source and Distributed Source for Input to the Saturated Zone: 18-km Boundary

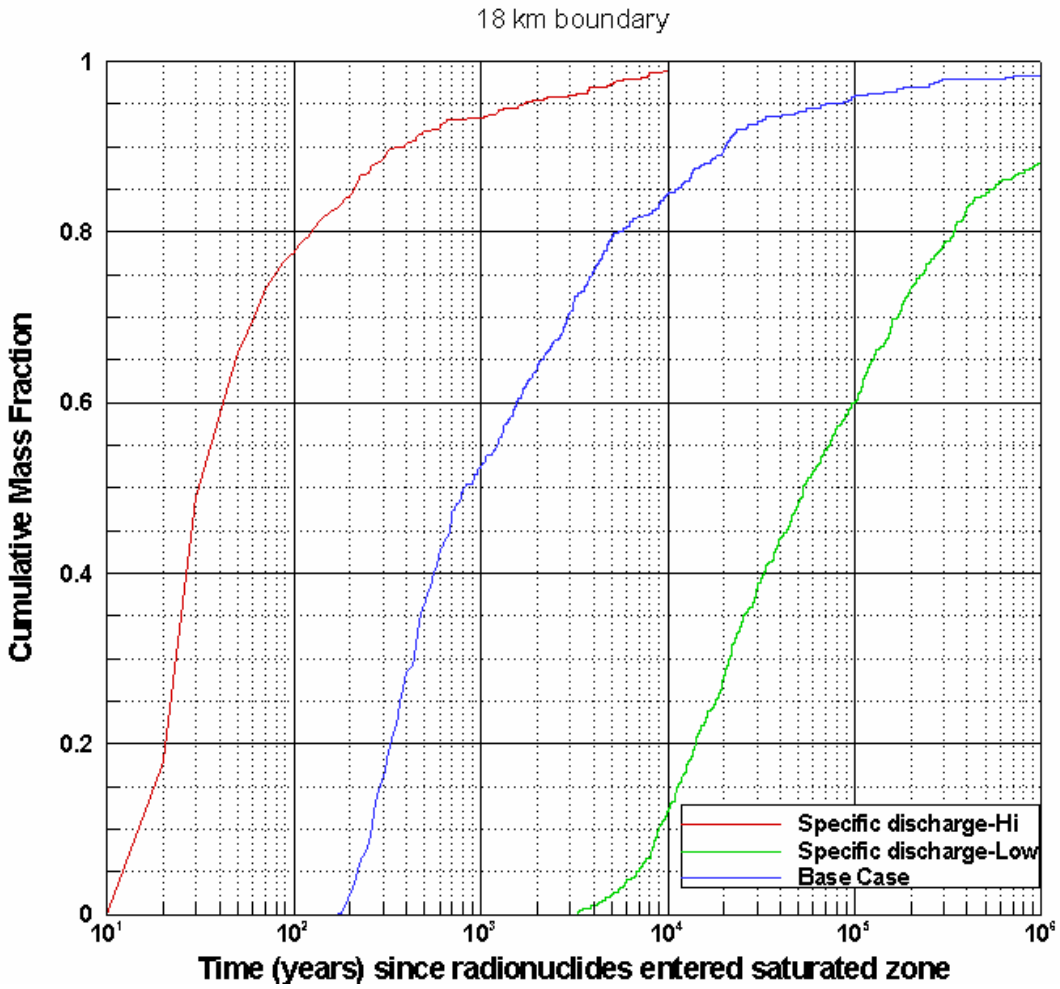

Output DTNs: LA0703SK150304.001, LA0703SK150304.002.

NOTE: Mass BTCs and median transport times are for an instantaneous source, present-day climate, and do not include radionuclide decay. Particle source location was a point near the middle of the repository footprint.

Figure 6.8-4. Breakthrough Curves for the Base Case and Cases with Lower and Higher Specific Discharge: 18-km Boundary

6.8.5 Colloid-Facilitated Transport in the Saturated Zone

In the final set of simulations of this section, calculations are presented that illustrate the performance of the saturated zone barrier to retard the migration of radionuclides bound to colloids. Given that the most deleterious colloid-related effect on saturated zone performance is likely to be the mobility of otherwise immobile radionuclides via colloids, the focus of this section is on that process. For this reason, attention is also restricted to radionuclides irreversibly attached to colloids (termed "irreversible colloids" in the figures). These radionuclides do not diffuse into the volcanic matrix due to the large size of the colloids. Thus, the matrix diffusion coefficient is set to 0 in this simulation. Retardation occurs due to the reversible filtration of the colloids themselves in the alluvium and in the fractures within the volcanic units, modeled using a retardation factor that will be treated as a stochastic parameter in TSPA calculations. The small fraction of the colloids that travels unretarded is considered explicitly in the TSPA calculations and is not considered here. The colloid retardation factor distributions for the

volcanics and the alluvium were constructed from numerous laboratory and field experiments. The construction of these distributions is described in detail in *Saturated Zone Colloid Transport* (BSC 2004 [DIRS 170006], Sections 6.4 and 6.5). Median values for the colloid retardation factor in alluvium of 33.9 and in the volcanics of 26 are used in the simulation, as given in *Saturated Zone Flow and Transport Model Abstraction* (SNL 2007 [DIRS 181650], Table 6-8; DTN: SN0310T0502103.009 [DIRS 168763]). Figure 6.8-5 shows the expected behavior of colloidal-species transport compared to the base-case aqueous species transport. Most of the inventory will arrive at the boundary of the accessible environment at 18 km in 4,000 to 10,000 years. However, if larger specific discharge values were used, as would be the case for a future, wetter climate, the entire BTC would shift to earlier transport times. The difference between the aqueous and colloid BTCs is attributable to reversible filtration of the colloids. Thus, the modeling suggests that for the fraction of the radionuclide inventory that reaches the saturated zone within the compliance time period, the saturated zone is expected to impart a significant transport-time delay, but perhaps not sufficient to prevent some of these radionuclides from reaching the biosphere.

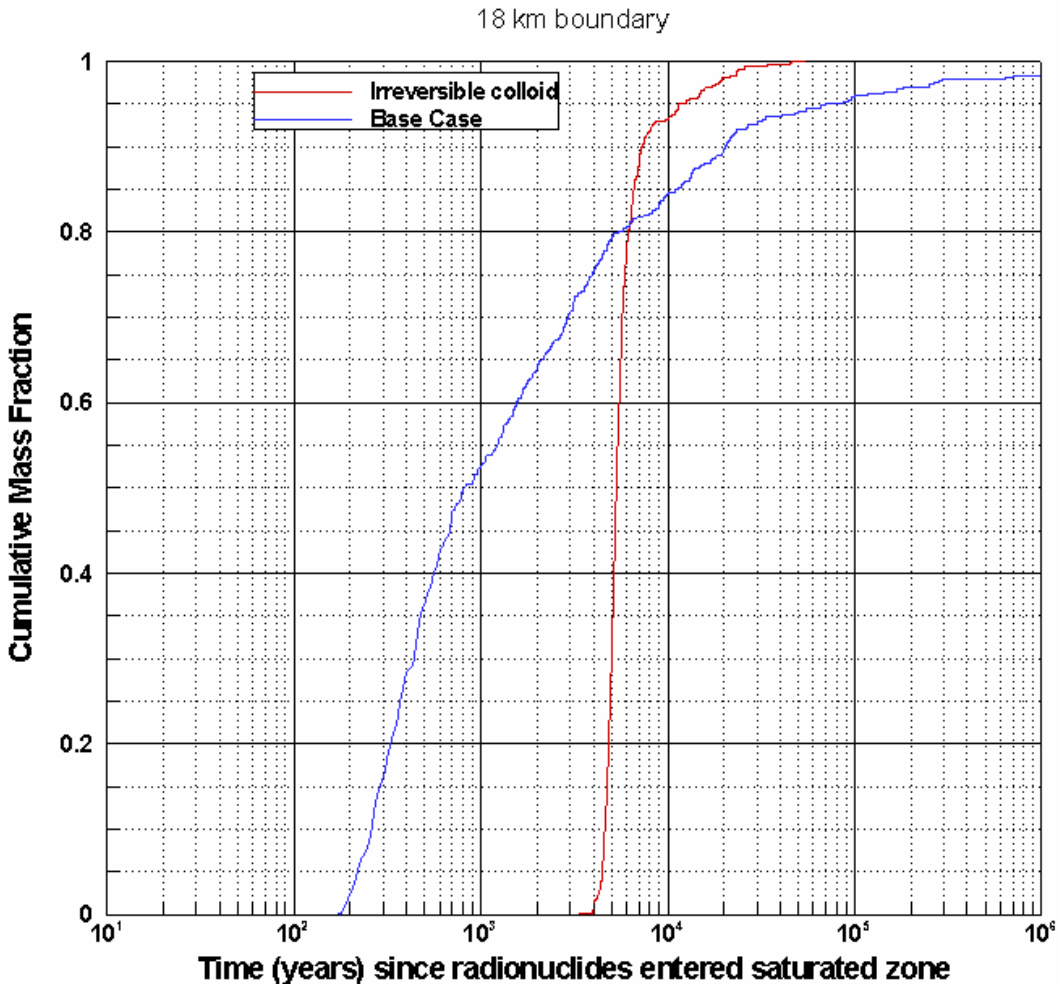

Output DTNs: LA0703SK150304.001, LA0703SK150304.010.

NOTE: Mass BTCs and median transport times are for an instantaneous source, present-day climate, and do not include radionuclide decay. Particle source location was a point near the middle of the repository footprint.

Figure 6.8-5. Comparison of Breakthrough Curves for the Base Case and Radionuclides Irreversibly Attached to Colloids: 18-km Boundary

6.8.6 Discussion of Saturated-Zone Barrier Performance

The two functions of the saturated zone barrier, which are the ability to delay the arrival and attenuate the radionuclides via the mechanisms of dispersion, diffusion and sorption, have been demonstrated in this section through a series of model simulations. The results and the discussion presented here are for the case of present day climate without water table rise (effects of alternate conceptual models resulting from water table rise due to possible future climate changes are discussed in Table 6.6-1a). The results presented here are for base-case transport property values (Table 6.4-2) unless explicitly noted otherwise. It is seen that sorption in the alluvium can increase the transport time by orders of magnitude of even the weakly sorbing radionuclides such as neptunium. Thus, for the base-case site-scale SZ transport model with the inclusion of sorption in the alluvium, transport times in excess of 10,000 years are expected within the saturated zone for all but the most weakly or nonsorbing radionuclides. For nonsorbing species, transport times on the order of 1,000 years are expected. Radionuclides

irreversibly bound to colloids may be delayed by several thousand years, but the actual value is quite uncertain due to the multiplicative impact of uncertainties in the specific discharge and the effective filtration retardation factor of colloids. Transport times for radionuclides irreversibly bound to the fast fraction of colloids are expected to be on the order of 1,000 years, the same as those for the nonsorbing case. In essence, the saturated zone barrier provides a transport-time delay on the order of or greater than the regulatory time period of interest for many radionuclides, but not for those expected to travel without significant retardation due to sorption or colloid filtration.

To understand the role played by the saturated zone barrier in attenuating radionuclides, the spread of arrival times at the boundary of the accessible environment at 18 km in the form of cumulative arrival-time distributions was examined, rather than simulating the groundwater concentrations. The justification for this approach relates to the regulatory framework in which the modeling is being performed. Radionuclide mass flux is calculated by assuming that the entire annual radionuclide mass reaching the accessible environment is captured (10 CFR 63.332 (b)(2) [DIRS 180319]). The concentration is then calculated by assuming that this mass is uniformly distributed in the representative volume of groundwater that would be withdrawn annually (3,000 acre-feet per year as defined by 10 CFR 63.332(a)(3) [DIRS 180319]). Therefore, in situ concentrations are not relevant to barrier performance. The mass flux of radionuclides divided by the representative volume is the concentration of interest. Radionuclide mass flux at a boundary of the accessible environment at 18 km is a common metric used in studies of contaminant transport in groundwater (e.g., Dagan et al. 1992 [DIRS 163800], pp. 1,369 to 1,370). The approach taken here is patterned after the well-known solute mass flux approach. Hence, it is acceptable to use the particle-tracking model, although it has limitations requiring the use of a large number of input particles in applications where in situ concentrations are needed.

Nevertheless, attenuation of radionuclides during their transit from beneath the repository to the boundary of the accessible environment at 18 km can be treated qualitatively by recognizing that the spread of the arrival-time distribution is related to the ability of the saturated zone to dilute radionuclide concentrations. The approximate duration over which relative concentration in the BTCs rise from 0 to 1 can be compared to the duration of a transient pulse of high concentration. If the latter is smaller than the former, then the saturated zone barrier will dilute the input pulse of high concentration to a lower value through the process of hydrodynamic dispersion and matrix diffusion. Thus, based on the BTCs provided in this section, short-duration pulse of radionuclides of duration of about 100 years or less would become spread out in time within the saturated zone alone, to a high degree of certainty. Instantaneous output concentrations resulting from such a pulse will be significantly lower compared to the initial concentrations even though the cumulative mass breakthrough may be the same. This characteristic of the SZ barrier has implications on how the system is modeled for TSPA. Specifically, it implies that short-time-scale, high-concentration pulses need not be simulated explicitly as long as the correct overall radionuclide mass is input into the model.

For reasons related to the discussion above, transverse dispersion, though included in the site-scale SZ transport model, was not examined in sensitivity studies of barrier performance because it is not likely to be important to the function of the barrier. Small transverse dispersivity values estimated for the saturated zone will spread radionuclides a short distance

orthogonal to the principal transport direction. This would have a significant influence on the in situ concentration but not on the overall flow path through which the plume travels. Therefore, the mass flux reaching the boundary of the accessible environment will not be affected significantly.

INTENTIONALLY LEFT BLANK

7. VALIDATION

The site-scale SZ transport model is designed to provide an analysis tool that facilitates understanding of solute transport in the aquifer beneath and down gradient from the repository. It is also a computational tool for performing radionuclide migration predictions in the saturated zone. For these predictions to be creditable, it must be demonstrated that the site-scale SZ transport model has been validated for its intended use, which means there is established "confidence that a mathematical or numerical model and its underlying conceptual model adequately represents with sufficient accuracy the phenomenon, process, or system in question" (SCI-PRO-006, Attachment 1).

The validation activities for the site-scale SZ transport model are carried out according to *Technical Work Plan For: Saturated Zone Analysis and Model Report Integration* (BSC 2006 [DIRS 177375], Sections 2.1.4 and 2.2.4). The technical work plan (TWP) specifies level II validation. The BSC Level II validation is equivalent to Level I validation as described in SCI-PRO-002. Nevertheless, the site-scale SZ transport model was validated to Level II requirements. The Level II validation includes the six steps of confidence building during model development as described in SCI-PRO-002 and at least two post-development activities as described in SCI-PRO-006, Section 6.3.2. These validation activities do not generate a separate DTN.

To satisfy the model validation requirements, the following two postdevelopment validation activities (BSC 2006 [DIRS 177375], Section 2.2.4) were performed:

- Quantitative comparison of simulated transit times from beneath the repository to the accessible environment with those derived from isotopic data. Validation will be considered acceptable if the range of model results falls within the uncertainty estimates for groundwater ages from near the repository and from near the boundary of the accessible environment.

- Qualitative comparison of simulated flow paths with flow paths inferred from hydrochemistry and isotopic data. The model is considered valid if its flowpaths fall within those estimated by hydrochemical analyses.

This report deviates from *Technical Work Plan For: Saturated Zone Analysis and Model Report Integration* (BSC 2006 [DIRS 177375], Section 2.2.4.1) by excluding validation activity item #3. This item addresses the development of kinetics-based colloid transport model which was excluded from the scope of the work presented here. The purpose of the proposed kinetics-based colloid transport model was to reduce conservatism in the SZ transport model by using a more detailed model of the reversible filtration of the colloids with irreversibly attached radionuclides. Since the transport times predicted by the SZ transport model are longer than those expected to result from the kinetic based model, this exclusion is considered acceptable.

As a result of the time and spatial scales involved and the fact that radionuclides cannot be used as tracers in field experiments, validation and confidence building for the site-scale SZ transport model relies on indirect data and inferences derived from technically related laboratory and field tests and natural analogues. Recognizing that the model is being used to perform probabilistic

calculations in which parameter uncertainties are propagated through the model, the intent of the validation and confidence-building activities is to confirm that radionuclide parameters and processes operative at the Yucca Mountain site are adequately represented with sufficient accuracy in the site-scale SZ transport model. This confirmation is accomplished by a series of different approaches that include comparisons to analogue sites, model-data comparisons, and comparison with data published in referenced journals.

The validation exercises performed here demonstrate that the parameters and processes selected have an experimental or observational basis and that the model-derived flow paths and transit times are consistent with field data. The model is validated for use in a stochastic analysis that establishes ranges of potential behavior of the saturated zone transport system. The site-scale SZ transport model is valid for simulating radionuclide transport in the saturated zone resulting in generation of radionuclide BTCs several kilometers downstream from the source region. This model is intended for use with stochastic simulations using large uncertainty ranges for certain parameters such as specific discharge, flowing interval spacing and aperture, diffusion coefficient, and sorption coefficients. Care should be exercised in interpreting individual simulations for a single set of parameter values. Also, care should be exercised if the parameters used fall outside the range of parameter values given in this report.

7.1 CONFIDENCE BUILDING DURING MODEL DEVELOPMENT TO ESTABLISH SCIENTIFIC BASIS AND ACCURACY FOR INTENDED USE

Confidence building during model development was based on the available laboratory and analogue data as well as comparison with an independent site-scale groundwater flow model for the Yucca Mountain saturated zone (Winterle et al. 2003 [DIRS 163823], pp. 152 to 153). These data were not used for postdevelopment model validation, and only the comparison with the field hydrochemical and isotopic data were used as a postdevelopment method for satisfying the validation criteria as detailed in Section 7.2.

Level II model validation was planned in the TWP (BSC 2006 [DIRS 177375], Section 2.2.4.2). That model validation plan, developed under LP-2.29Q-BSC, also meets the requirements for Level I model validation in SCI-PRO-002, Attachment 3. The development of the site-scale SZ transport model was conducted according to the following criteria (italicized). The paragraphs following each criterion describe how it was satisfied.

1. *Evaluate and select input parameters and/or data that are adequate for the model's intended use* [SCI-PRO-002 Attachment 3, Level I (1)].

   All direct inputs to the site-scale SZ transport model have been qualified (Table 4.1), including discussion about selection of input and design parameters (Sections 4.1.2.1 through 4.1.2.18). Confidence building in submodel components of the site-scale SZ transport model was conducted through comparison of the conceptual model of SZ transport with the results of field tests conducted at YMP and analog sites to support transport parameters. These are presented in Section 7.1.2. Additional studies of input parameters based on observations at analogue sites are presented in Section 7.1.1, leading to increased confidence in the processes and parameters that are used in the transport model presented in this report. Thus, this requirement is considered satisfied.

2. *Ensure simulation conditions have been designed to span the range of intended use and avoid inconsistent outputs or that those inconsistencies can be adequately explained and demonstrated to have little impact on results* [SCI-PRO-002, Attachment 3 Level I (5)].

   The site-scale SZ transport model uses the calibrated SZ site-scale flow model (DTN: SN0612T0510106.004 [DIRS 178956]) as a starting point. The SZ flow model is calibrated to available head data in the vicinity of Yucca Mountain. However, the radionuclide transport model itself has been developed in the absence of direct data on which to base predictions of radionuclide transport over the length and time scales of interest. Therefore, the transport model development does not include formal, numerical model calibration to data beyond that used for calibration of the flow model. Nevertheless, there are numerous lines of evidence available to provide confidence that the model, with associated parameters and uncertainty ranges, captures the range of uncertainty in radionuclide transport predictions from beneath the repository to the 18-km compliance boundary. Most field data sets provide confidence that the conceptual model for transport in the fractured volcanic tuff and the alluvium are appropriate for use in predicting saturated zone transport behavior. These tests and their use in building confidence in the model are presented in Sections 7.1.1 through 7.1.3.

   The site-scale SZ transport model generates BTCs for a unit instantaneous source. Section 6.3, item 1 discusses the source term for the transport model. Section 6.3 and Section 6.4.2.3 discuss the transport boundary conditions downstream of the repository footprint. Sections 6.5 and 6.8 provide detailed discussion of various model results. As discussed in Section 6.4.2.3, particle tracking method of solving the advective-dispersion equation conserves mass and the method is free from the numerical convergence problems and numerical dispersion errors. Thus, this requirement is considered satisfied.

3. *Represent important future state (aleatoric), parameter (epistemic), and alternative model uncertainties to an appropriate degree commensurate with the model's intended use. Ensure that model predictions (performance parameters) adequately represent the range of possible outcomes, consistent with important uncertainties and modeling assumptions, conceptualizations, and implementation*. [SCI-PRO-002 Attachment 3 Level 1 (4) and (6)].

   Discussion of model uncertainties is provided in Sections 6.7 and 8.3. Sensitivity of the output BTCs to each of the uncertain input parameters is discussed in Sections 6.7.1.1 through 6.7.1.13.

4. *Formulate defensible assumptions and simplifications that are adequate for the model's intended use* [SCI-PRO-002 Attachment 3 Level I (2)].

   Discussion of assumptions and simplifications are provided in Sections 5 and 6.3. The conceptual model of transport in the saturated zone and the components of the model are discussed in Section 6.3. As discussed in detail in Section 7.1.2, further confidence building in submodel components of the site-scale SZ transport model was conducted

through comparison of the conceptual model of saturated zone transport with the results of field tests conducted at the C-wells complex, the ATC, and the CAMBRIC site on the NTS. Thus, this requirement is considered satisfied.

5. *Ensure consistency with physical principles, such as conservation of mass, energy, and momentum, to an appropriate degree commensurate with the model's intended use* [SCI-PRO-002 Attachment 3 Level I (3)].

   Consistency with physical principles is demonstrated by the conceptual and mathematical formulation in Sections 6.3 and 6.4, and the selection and use of the FEHM code in Section 3. The flow model is based on the principles of conservation of mass and energy, and Darcy's law. The transport model (Equation 1) is based on the principle of conservation of mass of the solutes. Thus, this requirement is considered satisfied.

7.1.1 Analogue Studies to Support Transport Parameters

The study of radionuclide transport parameters based on observations at analogue sites leads to increased confidence in the parameters that are used in the transport model presented in this report. The transport parameter values and processes for radionuclides of concern are sensitive to the site-specific geological and geochemical conditions. However, the site-scale SZ transport model is intended for use in making TSPA predictions using a wide range of parameter input values that reflect uncertainty in the input. The analogue studies provide a qualitative comparison of the information with the parameters used in this model report. The analogue studies considered here are the NTS and uranium analogue sites—Uranium Mill Tailings Remedial Action sites and Los Alamos in the United States; El Borrocal in Spain; Palmottu, Finland; Alligator Rivers in Australia; Pocos de Caldas in Brazil; and Cigar Lake in Canada. Consistency between the transport parameters from the site-scale SZ transport model and those derived from analogue studies lead to increased confidence in the selection and choice of ranges for the transport parameters.

7.1.1.1 Studies Performed at the Nevada Test Site

Discussed in this section are relevant information and insights gained from radionuclide migration studies performed at the NTS, which is the United States continental nuclear weapons testing site. As shown in Figure 7-1, Yucca Mountain and the NTS are near each other. The NTS results are relevant because the NTS geology and geochemistry are similar to those at Yucca Mountain. Between 1951 and 1992, 828 underground tests were conducted at the NTS at locations indicated in Figure 7-1 (Wolfsberg et al. 2002 [DIRS 162688]). Many of the tests were conducted near or below the water table, making radionuclide migration information potentially important to consider for the site-scale SZ transport model. Tests in Yucca Flat and Frenchman Flat were principally situated in Quaternary-aged alluvium, analogous to the alluvium downgradient from Yucca Mountain. In contrast, tests beneath Pahute Mesa were generally conducted in volcanic-rock aquifers, which is a useful analogue for the fractured volcanic tuffs beneath Yucca Mountain. Therefore, observations of radionuclide migration from these tests are useful corroborative information relevant to the main rock types in the flow path from beneath Yucca Mountain to the boundary of the accessible environment.

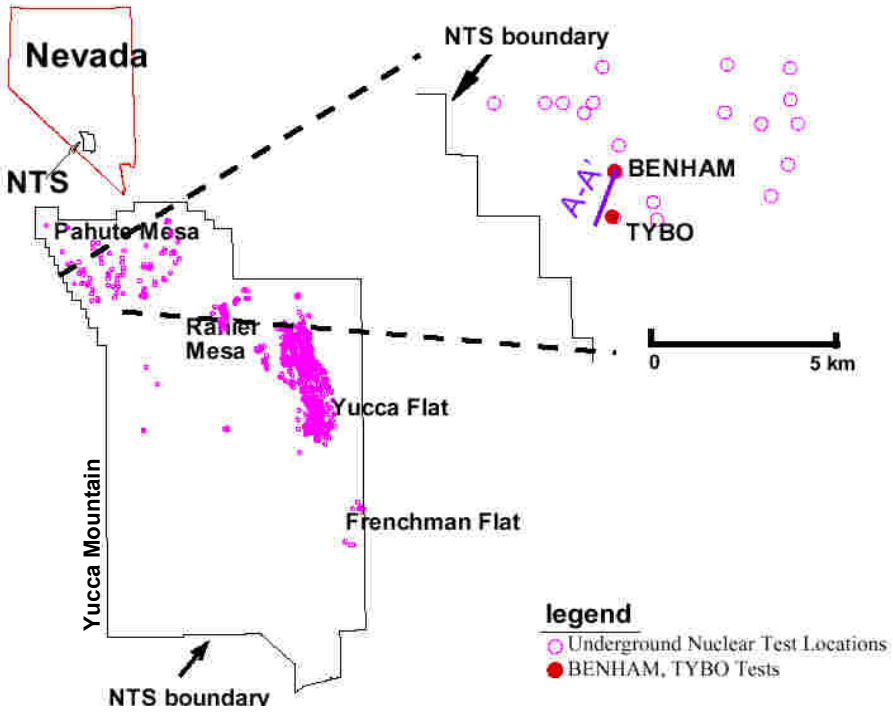

Source: Wolfsberg et al. 2002 [DIRS 162688], Figure 1-1.

Figure 7-1. Locations of Underground Nuclear Tests and the Specific Locations of the TYBO and BENHAM Tests at the Nevada Test Site

For several decades, radiological data have been gathered to examine the potential migration of radionuclides in groundwater away from underground nuclear tests. Smith (2002 [DIRS 162687]) summarizes the radiochemical investigations performed by the DOE Defense and Environmental Management Programs to characterize the current and potential future migration rates of radionuclides from these tests. In addition to general conclusions about the relative mobility of radionuclides at the NTS, there are more site-specific results in both alluvium and volcanic-rock aquifers that provide points of reference for large-scale mobility under hydrogeologic conditions similar to the Yucca Mountain saturated zone. The next section summarizes the general conclusions, followed by detailed discussions on observations and testing at the CAMBRIC site and the ER-20-5 wells adjacent to the TYBO-BENHAM site. For the latter discussions, the NTS results are compared to the saturated zone transport conceptual model to demonstrate consistency with NTS data and analyses.

7.1.1.1.1 General Conclusions from NTS Investigations

To understand the similarities and differences between potential transport in the saturated zone beneath Yucca Mountain and migration away from an underground nuclear test, a brief conceptual description derived from Smith (2002 [DIRS 162687], pp. 20 to 23) is provided. Transport from a nuclear test occurs in two steps: (1) a "prompt transport" occurring over time scales of the nuclear detonation, and (2) groundwater transport occurring over a scale of years to centuries, depending on the flow regime. Prompt processes are generally thought to be as a plasma or gas through localized zones of failure in the rock. After this initial period, the system typically reverts over a period of years to a more ambient condition. However, the near-field

system is permanently changed as a result of the nuclear detonation. Generally, a cavity is created containing a large inventory of radionuclides in the form of solidified glass. The interaction of the glass with groundwater results in a long-term source for radionuclides in the groundwater. Above the cavity, a chimney of hydrologic-affected rock exists as a result of the underground explosion. If this chimney is of higher permeability than the surrounding rock, residual heat from the detonation can create a thermally buoyant water flow and radionuclide transport pathway up the chimney to zones of permeable rock in the aquifer. Then, groundwater flow under natural conditions transports radionuclides in the prevailing direction and at a velocity governed by the aquifer flow conditions.

Only the far-field flow and transport from underground tests are directly relevant to Yucca Mountain saturated zone transport. Therefore, data from downgradient wells provide the most useful information for the present study. However, the far-field observations contain inherent uncertainties due to the other transport processes (e.g., prompt transport and buoyant transport in the chimney). Additional indirect evidence on radionuclide mobility is also available by comparing the radionuclide concentrations in the cavity, chimney, and far-field fluids collected and summarized by Smith (2002 [DIRS 162687]). Caution must be exercised with cavity and chimney data because they can have unique thermal and geochemical conditions that could influence the speciation and sorption characteristics of the radionuclides. As a result, including radionuclide concentrations from cavities and chimneys could potentially introduce data that were collected under conditions that are not representative of the saturated zone beneath and downgradient of Yucca Mountain. Despite these limitations, the following summarizes Smith's (2002 [DIRS 162687], p. 31) conclusions on the relative mobility of radionuclides derived from cavity, chimney, and far-field radionuclide measurements.

- The most mobile radionuclides at the NTS, traveling essentially unretarded compared to tritiated water (^{3}H), are ^{14}C, ^{36}Cl, ^{85}Kr, ^{99}Tc, and ^{129}I.

- By contrast, ^{90}Sr, ^{137}Cs, ^{152}Eu, ^{154}Eu, and ^{239}Pu are relatively immobile, appearing in the cavity and chimney waters but generally not in the far field.

- Despite this conclusion, several radionuclides generally considered immobile, such as plutonium, sorb to natural colloids and appear to migrate over significant distances. For example, Kersting et al. (1999 [DIRS 103282], p. 59) showed that the concentration of plutonium observed in wells significantly downstream from the source was very small (approximately 10^{-14} M) and, therefore, concluded that only a very limited fraction of the plutonium associated with the test was mobile. Additional details are provided in Section 7.1.1.1.3.

- Wolfsberg et al. (2002 [DIRS 162688], Section 7.7.3) report that cesium, strontium, and europium isotopes were also found in these wells in the presence of colloids.

- Finnegan and Thompson (2002 [DIRS 162695], pp. 13 to 14) detected ^{237}Np in the same wells listed above.

These results are qualitatively consistent with the site-scale SZ transport model conceptualization and parameter distributions. Sorption coefficients are set to zero for radionuclides found to be mobile at the NTS, most notably ^{14}C, ^{36}Cl, ^{99}Tc, and ^{129}I. The saturated zone base-case transport model represents the case of these radionuclides. For less-mobile radionuclides, such as ^{90}Sr and ^{137}Cs, as discussed in Appendix A, relatively large sorption coefficients are recommended, and hence, significant retardation. The available CAMBRIC data, based on a lack of arrival of the radionuclides, can only lead to general conclusions regarding a plausible lower bound on K_d. But the data do not contradict the lower bound being higher, which is what is derived from the Lab data in Appendix A. Colloid-facilitated transport is included in the site-scale saturated zone transport model. Also it is not possible to draw any conclusions from these data on following items: (1) upper limits on K_ds and (2) differences in the K_ds for different radionuclides. In general, the relative mobility of the different radionuclides included in the site-scale SZ transport model is consistent with the data available from the NTS radiological measurements.

7.1.1.1.2 Radionuclide Transport in Alluvium (CAMBRIC Test)

Transport from the CAMBRIC test, conducted in 1965 in the alluvium in Frenchman Flat, has been extensively studied in subsequent years to understand the rates of radionuclide migration in groundwater. Wells were drilled to obtain radionuclide concentrations in both the near field and far field, and a 16-yr aquifer pump test was conducted to determine the migration rates through the alluvium from the test cavity to the pumping well under forced-gradient conditions. The pumping well RNM-2S was drilled 91 m south of the CAMBRIC test and screened from 16 m to 41 m below the bottom of the CAMBRIC cavity (Smith 2002 [DIRS 162687], p. 7). After about two years of pumping, essentially simultaneous breakthrough of ^{3}H, ^{85}Kr, ^{36}Cl, ^{129}I, ^{106}Ru, and ^{99}Tc were observed. A tritium BTC published in Tompson et al. shows a peak concentration about 5.5 years after pumping started and a slow decline in concentrations thereafter, until the end of the test (1999 [DIRS 162686], Figure 35). By contrast, cations ^{90}Sr, ^{137}Cs, ^{152}Eu, ^{154}Eu, and ^{239}Pu, though present in the cavity fluids, were not observed in the well during the 16 years of pumping (Smith 2002 [DIRS 162687], p. 7).

The lack of arrival of less-mobile radionuclides at the pumping well allows a lower bound to be placed on the retardation factor. As an order-of-magnitude estimate, lack of arrival after 16 years when the first arrival of tritium was about two years led to retardation factors of at least 8. Using the range of porosities of 0.1 to 0.38 reported in Thompson et al. (1999 [DIRS 162686], Table 20), this value of the retardation factor leads to K_d values between 5 and 10 mL/g, which are consistent with the ranges given in Appendix A for these radionuclides. Complications include a time-varying flow rate and analytical detection limit issues for plutonium (Tompson et al. 1999 [DIRS 162686], p. 152). Nevertheless, this minimum value of 8 can be compared to the retardation factors exceeding 1,000 based on models and laboratory data for ^{90}Sr and ^{137}Cs (Tompson et al. 1999 [DIRS 162686], Table 25). In short, breakthrough was not expected based on laboratory data and sorption models, and it did not occur in the field, which lends credence to the concept of retardation by sorption in the alluvium. However, a tight bound on the actual retardation factor is not possible from this field test.

7.1.1.1.3 Radionuclide Transport in the Volcanics (TYBO-BENHAM Study)

The interpretations presented in this section were obtained from a report by Wolfsberg et al., who performed a comprehensive analysis of transport at the NTS (2002 [DIRS 162688], Chapter 1). Underground tests called BENHAM (in 1968) and TYBO (in 1975) were conducted at Pahute Mesa in volcanic rocks beneath the water table (Figure 7-1). Subsequently, to investigate the potential migration of radionuclides, observation wells ER-20-5 #1 and ER-20-5 #3 were drilled and completed in the Topopah Spring welded tuff approximately 300 m southwest of TYBO. Topopah Spring is the same unit in which the TYBO test was carried out (Pawloski 1999 [DIRS 162685], p. 20). Sampling of these observation wells between 1996 and 1998 indicates elevated concentrations of isotopes of hydrogen, carbon, chlorine, strontium, technetium, iodine, cesium, cobalt, europium, americium, and plutonium (Wolfsberg et al. 2002 [DIRS 162688], Tables 1-1 and 1-2). Kersting et al. studied the low levels of plutonium found in the two observation wells in greater detail (1999 [DIRS 103282], p. 56). Plutonium was detected in ER-20-5 #3 at approximately the elevation of the BENHAM working (detonation) point and in ER-20-5 #1, approximately 500 m above the lava (Figure 7-2). The plutonium in both wells was found associated with colloidal material, and isotopic fingerprinting by Kersting et al. showed that the plutonium originated at BENHAM rather than TYBO, despite the closer proximity of the ER-20-5 wells to TYBO (1999 [DIRS 103282], p. 58).

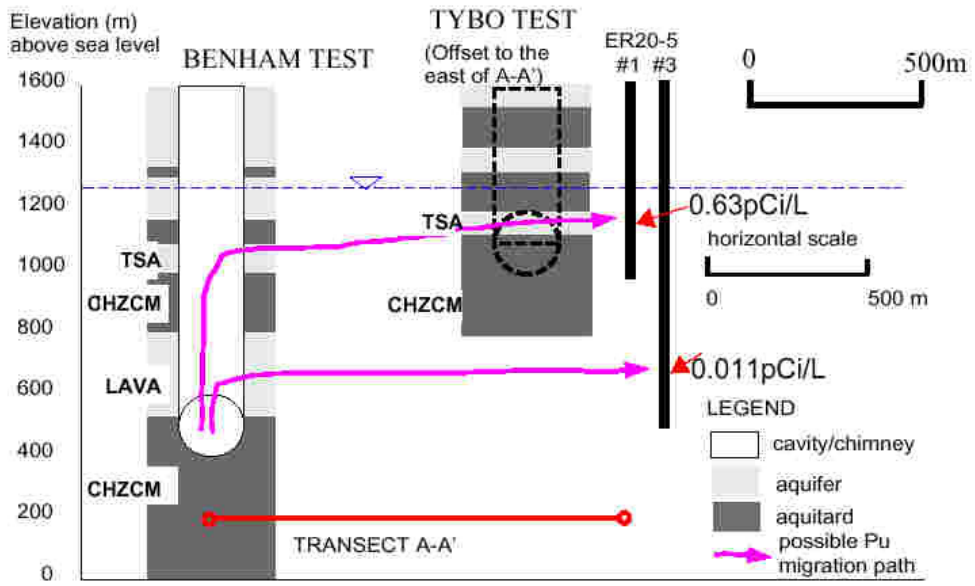

Source: Wolfsberg et al. 2002 [DIRS 162688], Figure 1-2.

Figure 7-2. Schematic of Possible Pathways from the BENHAM Test to the ER-20-5 Observation Wells

This observation suggests that plutonium, typically considered to be relatively immobile, migrated 500 m vertically and 1,300 m horizontally. Kersting et al. point out that it is unlikely that plutonium from BENHAM was transported via prompt injection (at the time of detonation) over the distances necessary for observation at the two separate ER-20-5 wells (1999 [DIRS 103282], p. 58). Further, because the plutonium detected in the ER-20-5 wells was

entirely associated with colloids, plutonium migration via colloid-facilitated transport in groundwater is the most likely explanation. Wolfsberg et al. constructed an integrated model of the system based on the conceptual model depicted in Figure 7-2 (2002 [DIRS 162688], Chapter 1). That study concluded that for expected values for parameters, migration of small amounts of plutonium from BENHAM to the observation points is plausible in less than 30 years (Wolfsberg et al. 2002 [DIRS 162688], p. 8-3). Their colloid-facilitated transport model employed a kinetic model for the sorption of plutonium onto colloids. It was found that slow desorption of plutonium from the colloids is required to allow a small fraction of the mass to travel via colloids. In the site-scale SZ transport model, two mechanisms of colloid-facilitated transport are incorporated: one is a reversible sorption model, and the other is an irreversible sorption model for radionuclide attachment onto colloids. The only retardation mechanism for the latter is retardation of the colloids by filtration, which is modeled using a retardation-factor-type parameter. This latter approach is consistent with the field observation from the TYBO-BENHAM and ER-20-5 wells that a fraction of the inventory of otherwise immobile radionuclides is transported via colloids.

Although it is not possible to fingerprint the source of the other radionuclides detected at these observation wells using isotope ratios, the plutonium observations pointing to a BENHAM source can be used to hypothesize that the other radionuclides cited above also migrated 1,300 m horizontally from BENHAM, given that a groundwater transport pathway is implied by the plutonium data. For some of these other radionuclides, such as americium, colloid-facilitated transport is a likely mechanism; this explanation is adopted in the site-scale SZ transport model by treating americium using a colloid-facilitated transport model. Others, such as ^{90}Sr and ^{137}Cs, are normally considered to be aqueous, sorbing radionuclides. Based on the available information, it is not possible to choose among the following explanations: (1) colloids are also responsible for migration; (2) sorption is not effective due to limited contact with the rock during fracture flow; or (3) the source of these radionuclides is not BENHAM, but TYBO, and transport distances are much shorter. The site-scale SZ transport model includes wide uncertainty distributions for the values of fracture flow parameters and specific discharge, as well as those for sorption coefficient of strontium and cesium, thus allowing for relatively rapid transport of these radionuclides. The data reported here from the TYBO-BENHAM study are inconclusive on the issue of cesium being transported as a radionuclide that attaches reversibly to colloids

7.1.1.2 Transport of Uranium at Natural Analogue Sites

This section briefly summarizes information on transport of uranium from different analogue sites to determine their relevance to conditions present at Yucca Mountain. Based on monitoring programs at Uranium Mill Tailings Remedial Action sites across the U.S., under oxidizing conditions representative of the transport path in the saturated zone, uranium transports are considered as nonsorbing to weakly sorbing contaminants as shown in *Natural Analogue Synthesis Report* (BSC 2004 [DIRS 169218], Section 12.3). This finding is consistent with the conceptual and mathematical model presented in Section 6 and the ranges of K_d values developed for uranium in Appendix A.

A study of natural uranium ore bodies at El Berrocal in Spain as shown in *Natural Analogue Synthesis Report* (BSC 2004 [DIRS 169218], Section 12.4.2.1) and a study of radionuclide migration in fractured gneisses and migmatites at Palmottu, Finland, *Natural Analogue Synthesis*

Report (BSC 2004 [DIRS 169218], Section 12.4.2.2) led to the conclusion that effects of matrix diffusion are seen in up to several tens of millimeters of rock matrix adjacent to fracture surfaces. These studies also showed that reactive processes between the radionuclides and the rock matrix effectively immobilized the radionuclides.

In studies at Cigar Lake, Canada; Alligator Rivers, Australia; and Pocos de Caldas, Brazil, it was found that uranium, thorium, and rare-earth elements transported in association with colloids as shown in *Natural Analogue Synthesis Report* (BSC 2004 [DIRS 169218], Section 12.4.3). Similar conclusions were reached in studies at the Nevada Test Site and Los Alamos in the United States as presented in *Natural Analogue Synthesis Report* (BSC 2004 [DIRS 169218], Section 12.4.3). These studies support the inclusion of colloid facilitated transport in the site-scale SZ transport model.

7.1.2 Submodel Components

Confidence building in submodel components of the site-scale SZ transport model was conducted through comparison of the conceptual model of saturated zone transport with the results of field tests conducted at the C-wells complex, the ATC, and the CAMBRIC site on the NTS. At the C-wells complex, which is located approximately 2 km southeast of the high-level radioactive waste repository footprint at Yucca Mountain, a series of conservative and reactive tracer tests were conducted in the various hydrogeologic units, principally fractured volcanic tuffs. Tracer tests were conducted separately in Bullfrog Tuff and Prow Pass Tuff units to study contaminant transport in different fractured volcanic media presented in *Saturated Zone In-Situ Testing* (SNL 2007 [DIRS 177394], Section 6.3). The tracer tests conducted at the C-wells are used to identify the important transport processes for the fractured volcanics. Conceptualization of transport processes for the alluvium was also based on field tests conducted at the NC-EWDP-19D1 wells and at the CAMBRIC site on the NTS. At the NC-EWDP-19D1 wells, three single-well, injection-withdrawal tests were conducted in the saturated alluvium. In each of the three tracer tests, two nonsorbing solute tracers with different diffusion coefficients were simultaneously injected. Detailed information on the identification of the various transport processes is provided in *Saturated Zone In-Situ Testing* (BSC 2003 [DIRS 177394], Sections 6.3 and 6.5). Summary level discussions of the conceptual model elements follow in Sections 7.1.2.1 to 7.1.2.9. More lengthy discussions in Section 6 give added detail to the inclusion of the following in the site-scale SZ transport model:

- Advection in the volcanics (see Section 6.3, item number 2)
- Dispersion in the volcanics (see Section 6.3, item number 2)
- Matrix diffusion in the volcanics (see Section 6.3, item number 3)
- Sorption in the volcanics (see Section 6.3, item number 4)
- Colloid-facilitated transport in the volcanics (see Section 6.3, item number 5)
- Advection in the alluvium (see Section 6.3, item number 6)
- Diffusion and dispersion in the alluvium (see Section 6.3, item number 6)
- Sorption in the alluvium (see Section 6.3, item number 7)
- Colloid-facilitated transport in the alluvium (see Section 6.3, item number 8).

7.1.2.1 Advection Through Fractures in the Volcanics

Figure 7-3 shows the results of a cross-hole tracer test in the Bullfrog Tuff member of the Crater Flat Group for the three soluble tracers: penta-fluorobenzoic acid (PFBA), bromide, and lithium (a weakly sorbing tracer). The injection and production wells were separated by approximately 30 m at the test depth as presented in *Saturated Zone In-Situ Testing* (SNL 2007 [DIRS 177394], Table C-6). The fractional recovery for PFBA and bromide was 0.69 and for lithium was 0.39 as shown in *Saturated Zone In-Situ Testing* (SNL 2007 [DIRS 177394], Appendix D4.5). This is consistent with the interpretation of lithium as a sorbing tracer. Tracer BTCs are plotted as normalized concentration versus time (normalization is performed by dividing by the tracer mass injected) at the production well so that they can be compared directly to one another. The most prevalent feature in these BTCs is the presence of multiple peaks. This result was due to the presence of two advective pathways between the wells and the particular means for injecting the tracer mixture, which gave rise to two distinct flow paths of overlapping transport times. This feature is a site-specific detail due to the local hydrologic conditions. The general behavior of the system implied by the BTCs in Figure 7-3 is that advection occurs primarily in the fractures. Rapid travel velocities between the wells (solute breakthrough within the first 10 hours of the test) are consistent with the conceptual model element of fracture flow through the volcanics. This test was conducted under forced gradient conditions discussed in *Saturated Zone In-Situ Testing* (SNL 2007 [DIRS 177394], Sections D.4.3 and D.4.5) and the solute velocities were expected to be much higher than the natural gradient conditions. By contrast, advection in the matrix would have resulted in much longer transport times. Therefore, these observations lend strong support to the use of a fracture-flow model for advection in the volcanics.

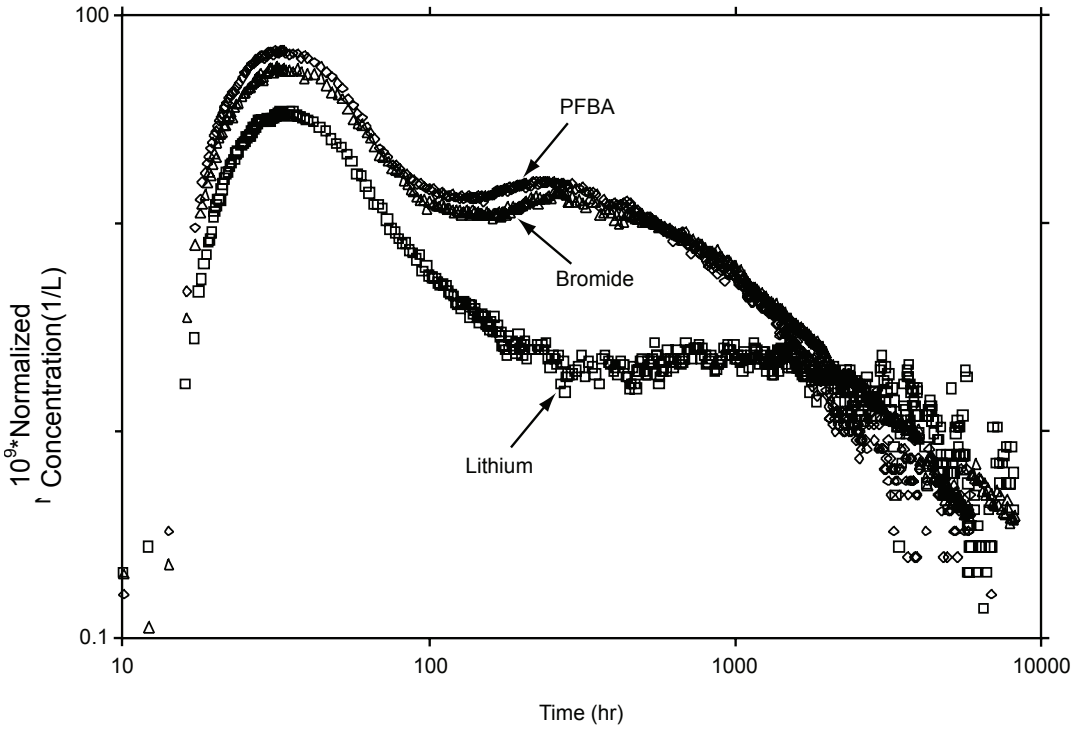

Source: SNL 2007 [DIRS 177394], Figure D-19.

NOTE: Log-log scales are used for the axes so that the bimodal nature of the tracer responses can be seen more clearly.

Figure 7-3. Normalized Tracer Concentrations versus Time in the Bullfrog Tuff Tracer Test Conducted from October 1996 to September 1997

7.1.2.2 Dispersion in the Volcanics

A computer modeling analysis of the C-wells test has been used to derive field-scale transport parameters for longitudinal dispersivity. A plot of the longitudinal dispersivity values as a function of test scale for several NTS fractured-rock, tracer-test programs is shown in Figure 7-4. The plot indicates that the longitudinal dispersivity increases with test scale, the range of the test scale going from less than 1 m to more than 100 m (Leap and Belmonte 1992 [DIRS 156838], pp. 87 to 95). Figure 7-5 shows the range of longitudinal dispersivities as a function of scale derived from the C-wells multiple-tracer tests (darkened area) superimposed on a plot of dispersivity versus scale prepared by Neuman (1990 [DIRS 101464], Figure 3). Note that the lower end of the range of length scales associated with the darkened area corresponds to the interwell separation in the tracer tests and the upper end corresponds to the test interval thickness (used as an upper bound for the transport distance). The range of longitudinal dispersivities derived from the C-wells tests and the scale dependence of longitudinal dispersivity in the tests plotted in Figure 7-4 are consistent with the understanding developed in the literature. This result lends strong support to the use of a longitudinal dispersivity model.

There is no site-specific information available to select the transverse dispersivity in the fractured volcanics. Values were chosen based on *Saturated Zone Flow and Transport Expert Elicitation Project* (CRWMS M&O 1998 [DIRS 100353], pp. 3-11 and LG-11 to LG-14).

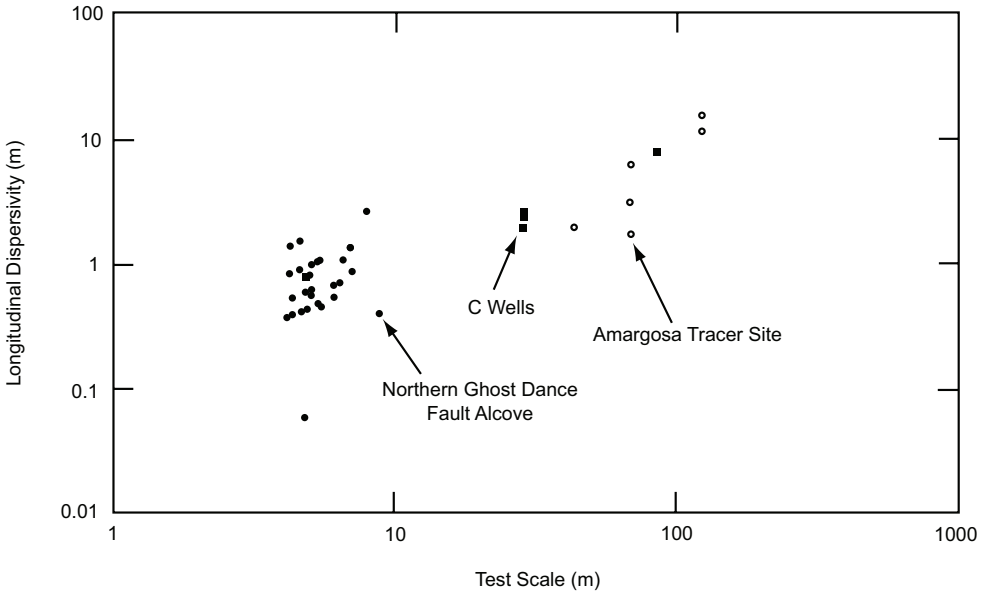

Source: SNL 2007 [DIRS 177394], Figure E-39.

Figure 7-4. Longitudinal Dispersivity as a Function of Test Scale in Several Tracer Tests Conducted in the Vicinity of Yucca Mountain

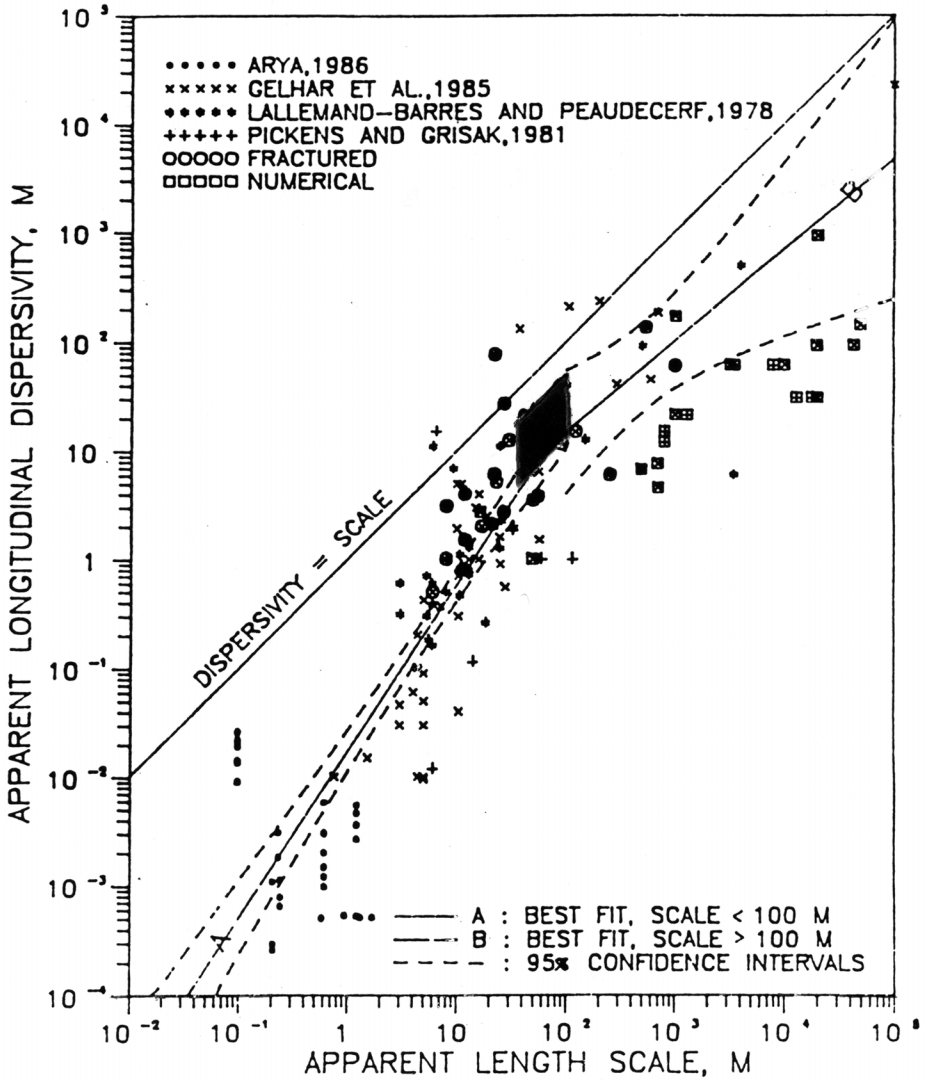

Source: SNL 2007 [DIRS 177394], Figure E-40.

NOTE: The darkened box shows the range of values derived from the multiple-tracer tests. The right edge of the box corresponds to the interwell separation distance, and the left edge of the box corresponds to the test interval thickness (taken to be the upper limit of transport distance).

Figure 7-5. Plot of Longitudinal Dispersivity versus Length Scale Showing the Range of C-Wells Values Derived from Interpretations of the Prow Pass and Bullfrog Multiple-Tracer Tests

7.1.2.3 Matrix Diffusion in the Volcanics

For the purposes of validating the matrix-diffusion model for the fractured volcanics, the critical result from the C-wells tests is the relative heights of the peaks for the various tracers shown in Figure 7-3. For the conservative tracers, the fact that PFBA, the tracer with the lower molecular diffusion coefficient (SNL 2007 [DIRS 177394], Table D-4), exhibited a higher peak concentration is consistent with the dual-porosity model in which tracer travels in the fractures but also diffuses into the rock matrix.

When using a dual-porosity medium as was done in this study, nonuniqueness of tracer test interpretations is an issue. For instance, long tails in tracer responses can be interpreted as being the result of either large longitudinal dispersion or significant matrix diffusion. In addition, at short time and distance scales, there may be a significant influence of diffusion into stagnant-free water within fractures in addition to "true" matrix diffusion. Thus, matrix-diffusion parameters obtained from laboratory tracer experiments should be used cautiously when predicting contaminant migration at larger scales in fractured media. Nevertheless, in the multiple-tracer tests, nonuniqueness of interpretations was minimized by simultaneously fitting the tracer responses using known ratios of diffusion coefficients as constraints on the relative matrix diffusion of different tracers. The method of interpreting the field test data is given in detail in *Saturated Zone In-Situ Testing* (SNL 2007 [DIRS 177394], Section 6.3.) and the parameter values obtained from the data fit are reported in *Saturated Zone In-Situ Testing* (SNL 2007 [DIRS 177394], Tables D-2, D-3, D-7, and D-10). The mass transfer coefficients and fracture aperture values given in the above reference along with the base-case matrix porosity given in Table 4-2 (0.15 to 0.25) lead to matrix diffusion coefficient values in the range of 1.6×10^{-8} m^2/s to 8×10^{-13} m^2/s, which overlaps with the range given in Table 4-2. Rationale for the selection of the range of diffusion coefficient values given in Table 4-2 is provided in Section 4.1.2.10 and in *Saturated Zone Flow and Transport Model Abstraction* (SNL 2007 [DIRS 181650], Section 6.5.2.6).

The intent of the present discussion is to build confidence in the conceptual model of diffusive mass transfer in the volcanics. All the C-wells test results discussed in *Saturated Zone In-Situ Testing* (SNL 2007 [DIRS 177394], Section 6.3) are consistent with diffusive mass transfer having a strong influence on the migration of solutes in fractured volcanic tuffs. Therefore, the field evidence strongly supports the use of a matrix-diffusion model as opposed to a single-continuum model for transport in the fractured volcanics.

7.1.2.4 Sorption in the Volcanics

As with matrix diffusion, sorption can also be observed in the C-wells tests by examining the reactive tracer shown in Figure 7-3. Lithium, the sorbing tracer, exhibits further attenuation but a similar arrival time as the two conservative tracers. A matrix-diffusion model explains this observation more completely than a single-continuum model, which would predict delayed arrival times for a sorbing tracer in addition to attenuation. Using the dual-porosity equivalent continuum model, sorption within fractures leads to a delayed peak time along with attenuation, whereas sorption in matrix but not within fractures leads to the same peak arrival time but with attenuated response (Robinson 1994 [DIRS 101154], Figure 7). Thus, the field observed response of lithium is indicative of sorption within the volcanic matrix and not within the fractures on the scale of the C-wells test (tens of meters). Sorption coefficients were measured in the laboratory and compared to field-estimated values of K_d. The lithium K_d values estimated from the field tracer tests are in the same range but consistently higher than the corresponding K_d values measured at the lowest lithium concentrations in the laboratory. These results suggest that the use of laboratory-derived K_d values to predict sorbing species transport in the saturated fractured tuffs near the C-wells location would tend to under-predict the amount of sorption experienced by the species in the field. The fact that the field K_d values tended to be greater than the laboratory K_d values suggests that lithium may have come into contact with alteration minerals in the field that were not present or were depleted in the lab rock samples. Any loosely

adhering alteration minerals (e.g., clays) that may have been present in the core samples would very likely have been lost during crushing and sieving of the material when it was prepared for the batch-sorption experiments given in *Saturated Zone In-Situ Testing* (SNL 2007 [DIRS 177394], Section D.4.8.4). Nevertheless, given the consistency of the BTCs with sorption and the field estimates of K_d yielding similar values to those in the laboratory (which are considered conservative for performance assessment because the values from the field tests are generally higher), the available data strongly support the use of a K_d-based matrix sorption model for the fractured volcanics. Broad ranges of values for K_d are being used in the TSPA (Appendix C, Table C-14) to account for the uncertainties in determining this parameter.

7.1.2.5 Colloid-Facilitated Transport in the Volcanics

The approach used in the site-scale SZ transport model for colloid-facilitated transport is presented in Section 6.4.2.6 and Table 6.4-1.

7.1.2.5.1 Radionuclides Attached Irreversibly to the Colloids

The radionuclides attached irreversibly to colloids transport in a manner identical to the colloids. Tests were conducted at the C-wells to study the transport of colloids. In addition to the conservative and reactive tracers, 360-nm-diameter carboxylate-modified polystyrene microspheres were injected in the Bullfrog tracer test to examine how finite-sized particles transport through the fractured tuffs. These microspheres are meant to provide insight into the potential behavior of colloids transporting in the groundwater. Figure 7-6 shows a comparison of the microsphere BTC with the PFBA tracer. Microspheres do indeed transport through the medium at the scale of this test, but the concentrations are attenuated compared to a conservative solute. The fractional recovery of the microspheres is 0.145 compared to 0.69 for the PFBA as discussed in *Saturated Zone In-Situ Testing* (SNL 2007 [DIRS 177394], Section D.4.5). This result is probably due to filtration effects in the medium, although the possibility of settling cannot be ruled out. The site-scale SZ transport model applies a reversible-filtration model to simulate colloid-facilitated transport. The retardation factors estimated from the colloid attachment and resuspension rates (for tests that showed measurable microsphere recovery) given in Tables D-8 and D-9 of *Saturated Zone In-Situ Testing* (SNL 2007 [DIRS 177394]) are in the range of about 6 to 794, which is the range given in Table 4-2. The data in Figure 7-6 strongly support the concept of a filtration component of the conceptual model.

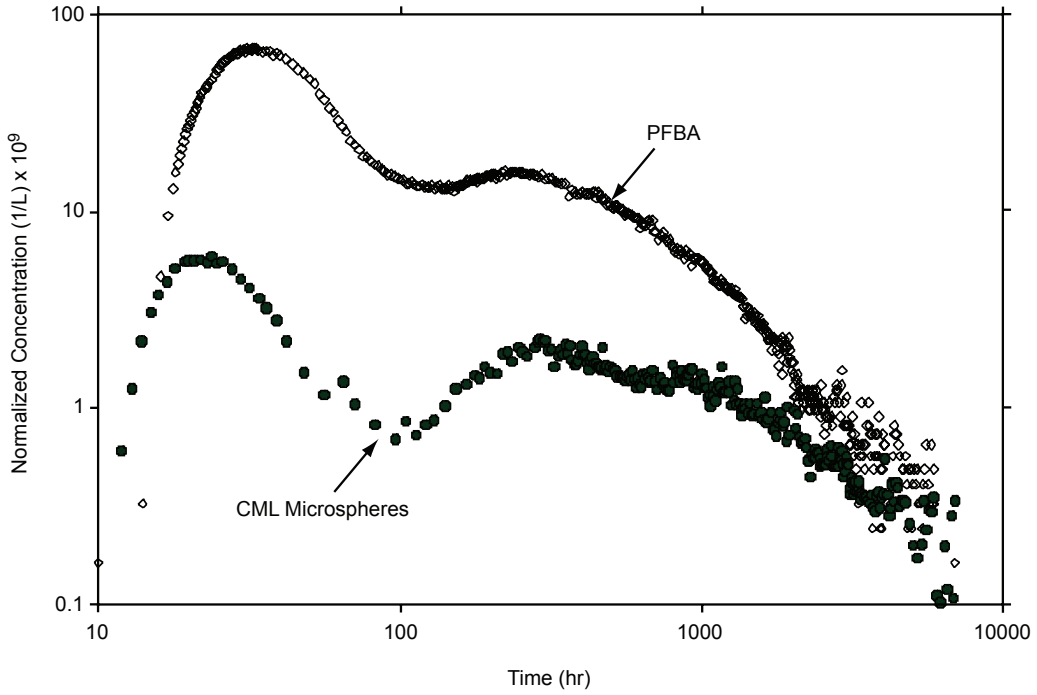

Source: SNL 2007 [DIRS 177394], Figure D-20.

NOTE: Log-log scales are used for the axes so that the bimodal nature of the tracer responses can be seen more clearly.

Figure 7-6. Normalized Concentrations of PFBA and 360-nm-Diameter Carboxylate-Modified Polystyrene Latex Microspheres in the Bullfrog Tuff Tracer Test

7.1.2.5.2 Radionuclides Attached Reversibly to the Colloids

Published work from literature is described in this section to build confidence in the conceptual model for the transport of the radionuclides attached reversibly to the colloids. Early models considered equilibrium partitioning of contaminants between the solute phase, colloid surfaces, and media surfaces (Hwang et al. 1989 [DIRS 165931], p. 600; Smith and Degueldre 1993 [DIRS 144658], pp. 145 to 150; and Grindrod 1993 [DIRS 165928], pp. 171 to 175). These efforts focused on describing transport through fractured media. Corapcioglu and Jiang (1993 [DIRS 105761], pp. 2,217 to 2,221) introduced a numerical model with first order reversible rate expressions describing colloid attachment and detachment to media surfaces. Their model (with some adjustments) was later used to describe ^{137}Cs transport facilitated by silica colloids through glass bead columns (Noell et al. 1998 [DIRS 106920], pp. 48 to 52). Ibaraki and Sudicky (1995 [DIRS 109297], pp. 2,948 to 2,951; and 1995 [DIRS 165930], pp. 2,961 to 2,964) were the first to implement kinetic expressions in a model to explicitly describe colloid-facilitated contaminant transport in discrete fractures and fracture networks, although their approach was essentially mathematically identical to that of Corapcioglu and Jiang (1993 [DIRS 105761], pp. 2,217 to 2,221). Oswald and Ibaraki (2001 [DIRS 165961], pp. 217 to 218) later extended the model to account for matrix diffusion of colloids, a phenomenon that was observed in laboratory experiments conducted in a fractured saprolite of high matrix porosity (the exclusion of this phenomenon from the site-scale SZ transport model, as discussed in Section 6.3, leads to potentially shorter transit time predictions).

7.1.2.6 Advection in the Alluvium

7.1.2.6.1 Alluvial Tests at NC-EWDP-19D1 and NC-EWDP Site 22

NC-EWDP-19D1

Three single-well injection-withdrawal tracer tests were conducted in the saturated alluvium at NC-EWDP-19D1 between December 2000 and April 2001. In each of the three tracer tests, two nonsorbing solute tracers with different diffusion coefficients were simultaneously injected (a halide and a fluorinated benzoic acid dissolved in the same solution). The three tests were conducted in essentially the same manner except for the time that was allowed to elapse between the cessation of tracer and chase-water injection and the initiation of pumping—that is, the "rest" or "shut-in" period. The rest period was systematically varied from approximately 0.5 hour to approximately 2 days and to approximately 30 days in the tests to vary the time allowed for tracers to diffuse into stagnant water in the flow system and for the tracers to migrate with the natural groundwater flow. Test interpretations were based on comparing the responses of the different tracers in the same test as well as the responses of similar tracers in the different tests. Differences in the responses of the two tracers injected in the same test provided information on diffusion into stagnant water in the system, whereas differences in the responses of tracers injected in different tests (after correcting for the effects of diffusion) provided information on tracer drift during the rest periods of the tests. Because the three tracer tests used different drift durations, a comparison of the results, combined with an idealized model of the groundwater flow behavior near the well, could be used to estimate the specific discharge. Values ranging from 1.2 to 9.4 m/y, depending on conceptual model and parameter uncertainties, were obtained from *Saturated Zone In-Situ Testing* (SNL 2007 [DIRS 177394], Table G-8). This range is consistent with the range of input values used in this report (Table 4-2). The site-scale SZ transport model is intended for use in making TSPA predictions using a wide range of parameter input values that reflect uncertainty in the input. Hence, a comparison of the range of values is considered sufficient. This result lends strong support to the process of advection in the alluvium.

NC-EWDP Site 22

Two single-well injection-withdrawal tracer tests and two cross-hole tracer tests were conducted in the alluvium in the second interval from the surface at Site 22 between December 2004 and October 2005. This interval ranges from approximately 54 m to 89 m (178 ft to 293 ft) below the water table. The two single-well tests were conducted in essentially identical manner except the rest periods (the times the tracers were allowed to drift with ambient groundwater flow in the formation) were approximately 3 days and 30 days. These tests yielded specific discharge estimates ranging from 0.47 to 5.4 m/yr (depending on the assumed flow porosity and the analysis method) (SNL 2007 [DIRS 177394], Table 6.5-6). Specific discharge at NC-EWDP Site 22 was also estimated from the analysis of changes in tracer concentrations after a 159-day flow interruption that occurred between the end of the first cross-hole tracer test and the start of the second cross-hole tracer test. This analysis yielded an estimated range of specific discharges from 0.46 to 2.8 m/yr (again depending on the assumed flow porosity) (SNL 2007 [DIRS 177394], Table 6.5-6), which is in good agreement with the estimates obtained from the single-well tracer tests. The analysis of the cross-hole tracer test responses also indicated a general

north-to-south direction of the ambient groundwater flow based on the changes in concentrations of tracers injected into different wells that were oriented in orthogonal directions from the pumping well (SNL 2007 [DIRS 177394], Table 6.5-6). The north-to-south flow direction is in good agreement with the flow direction inferred from water levels in NC-EWDP wells and also with that predicted by the calibrated SZ site-scale flow model (SNL 2007 [DIRS 177391], Section 6.5.2.3). The specific discharge estimates at Site 22 are somewhat lower than those predicted by the site-scale flow model at Site 22 (~20 m/yr), although these differences may be attributable to the significant differences in the scale of the two estimates, which are on the order of 10 m or so for the tracer tests and several hundred meters for the flow model.

7.1.2.6.2 CAMBRIC (NTS)

Velocities of movement under forced-gradient conditions used in the CAMBRIC experiment are not directly relevant to natural-gradient flow and transport at Yucca Mountain. However, modeling analyses performed by Tompson et al. (1999 [DIRS 162686], Chapter 10) for the NTS Environmental Restoration (ER) Project provide information on relevant hydrologic and transport parameter estimates for alluvium at the site. Using a heterogeneous distribution of permeability and constant porosities ranging from 0.1 to 0.38 (Tompson et al. 1999 [DIRS 162686], Table 20), Tompson showed that a continuum model, after calibration, was able to match the tritium BTC well (Tompson et al. 1999 [DIRS 162686], Figure 40). This range of porosities compares favorably with the uncertainty range of 0.02 to 0.3 for the effective alluvium porosity in Table 4-2. In a simulation of tracer migration in which the fluid extraction rate is specified, the key parameters controlling the BTC are the effective porosity, which controls the mean arrival time, and the correlation length of the heterogeneity, which controls the macrodispersive spreading of the BTC. In the site-scale SZ transport model, porosity and permeability are taken to be uniform within hydrogeologic units, and a macrodispersion model governs the dispersion. The NTS and YMP models are both continuum models, so the mean arrival time is controlled by the effective porosity. The models handle dispersion differently, which does not affect the mean arrival time. The fact that both are continuum models means that effective porosity values derived by Tompson et al. (1999 [DIRS 162686], Table 20) should be relevant to the site-scale SZ transport model. The CAMBRIC test and modeling of Tompson et al. (1999 [DIRS 162686], Chapter 10), therefore, confirms that a continuum model with porosity values of the same order of magnitude as the small-scale, measured porosity of the alluvial material is valid.

7.1.2.7 Diffusion and Dispersion in the Alluvium

Figure 7-7 shows a representative result from one of the single-well injection-withdrawal tracer experiments. The normalized tracer responses for two solutes and microspheres are shown. The two solute tracers had essentially identical responses (within experimental error) in this test (and other similar tests carried out in this interval). Flow interruptions during the tailing portions of the two longer tests (not shown) provided additional evidence for minimal diffusive mass transfer in the aquifer. The results here suggest that, in contrast to the fractured tuffs, the alluvium exhibits more of a continuum model behavior with less diffusion into stagnant fluid, such as the pore water of low-permeability material. This result may be scale-dependent such that, over longer transport times, diffusion becomes a more important factor. Nevertheless, these

results support the conservative conceptual model of single-continuum transport with little or no diffusion into stagnant regions.

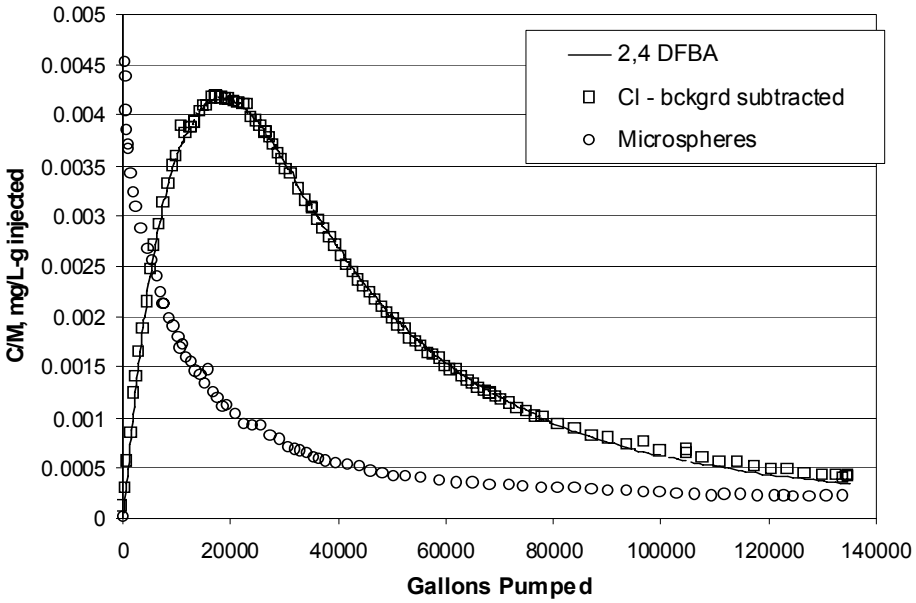

Source: SNL 2007 [DIRS 177394], Figure G-18.

NOTE: Microspheres were 640-nm-diameter carboxylate-modified polystyrene latex spheres tagged with an ultraviolet-excited fluorescent dye for detection. The normalized concentration is the observed outlet tracer concentration in mg/L divided by the tracer injection mass in grams.

Figure 7-7. Normalized Concentrations of Tracers in Production Water from NC-EWDP-19D1 as a Function of Gallons Pumped After a Rest Period of Approximately 0.5 Hour

Using a semianalytical method, data from the NC-EWDP-19D1 test were used to provide an estimate of 5 m for the longitudinal dispersivity shown in *Saturated Zone In-Situ Testing* (SNL 2007 [DIRS 177394], Section G4.2.4) along with a porosity of 10% and a transverse dispersivity of 2 m, the scale of the test being estimated around 8 m. Also, the literature is full of information on dispersivity values in alluvial aquifers. Neuman (1990 [DIRS 101464], Figures 1 to 3) compiles a comprehensive list of dispersivity values in porous media including alluvium at different scales (Figure 7-5). Using scientific judgment, one can infer that values for dispersivity from the literature are applicable to the alluvial system at Yucca Mountain. All these considerations lend strong support to the conceptual model of dispersion in the alluvium. Broad ranges of values for dispersivities are being used in the TSPA and presented in *Saturated Zone Flow and Transport Model Abstraction* (SNL 2007 [DIRS 181650], Section 6.5.2.9) to account for the uncertainties in determining this parameter.

7.1.2.8 Sorption in the Alluvium

Field testing using single-well and cross-well tracer tests have confirmed the occurrence of sorption in alluvium downgradient of Yucca Mountain (SNL 2007 [DIRS 177394], Section 6.5.5 and Appendix G5.4.3). Laboratory-scale experimental results are also available. Figure 7-8 presents the results of several column transport experiments using groundwater and alluvium obtained from the site of the ATC Well NC-EWDP-19D1. These experiments involved injecting

lithium bromide as pulses at three different concentrations spanning the range of lithium concentrations expected in the field.

Examination of the results (Figure 7-8) indicates that the data are consistent with a model that includes sorption. This result suggests that sorption is occurring in the columns. The issue of lack of site-specific field evidence is mitigated by two considerations. First, transport field tests using sorbing tracers in similar hydrogeologic settings have shown that sorption does occur in such systems (LeBlanc et al. 1991 [DIRS 163781], p. 905; Hess et al. 2002 [DIRS 163780], pp. 36-6 and 36-14; Thorbjarnarson and Mackay 1994 [DIRS 163782], pp. 413 to 414). Second, as demonstrated earlier, the fractured volcanic tuffs were shown to sorb tracers in the C-wells tracer experiments. These rocks have a similar mineralogic content as the alluvium and a similar fluid geochemistry. Therefore, demonstrated sorption in the fractured tuffs provides a line of site-specific field evidence in favor of sorption in the alluvium. All of these considerations lend strong support to the validity of the conceptual model of sorption in the alluvium. Broad ranges of values for sorption coefficients in alluvium are being used in TSPA as discussed in *Saturated Zone Flow and Transport Model Abstraction* (SNL 2007 DIRS 181650], Section 6.5.2.8) to account for the uncertainties in determining this parameter.

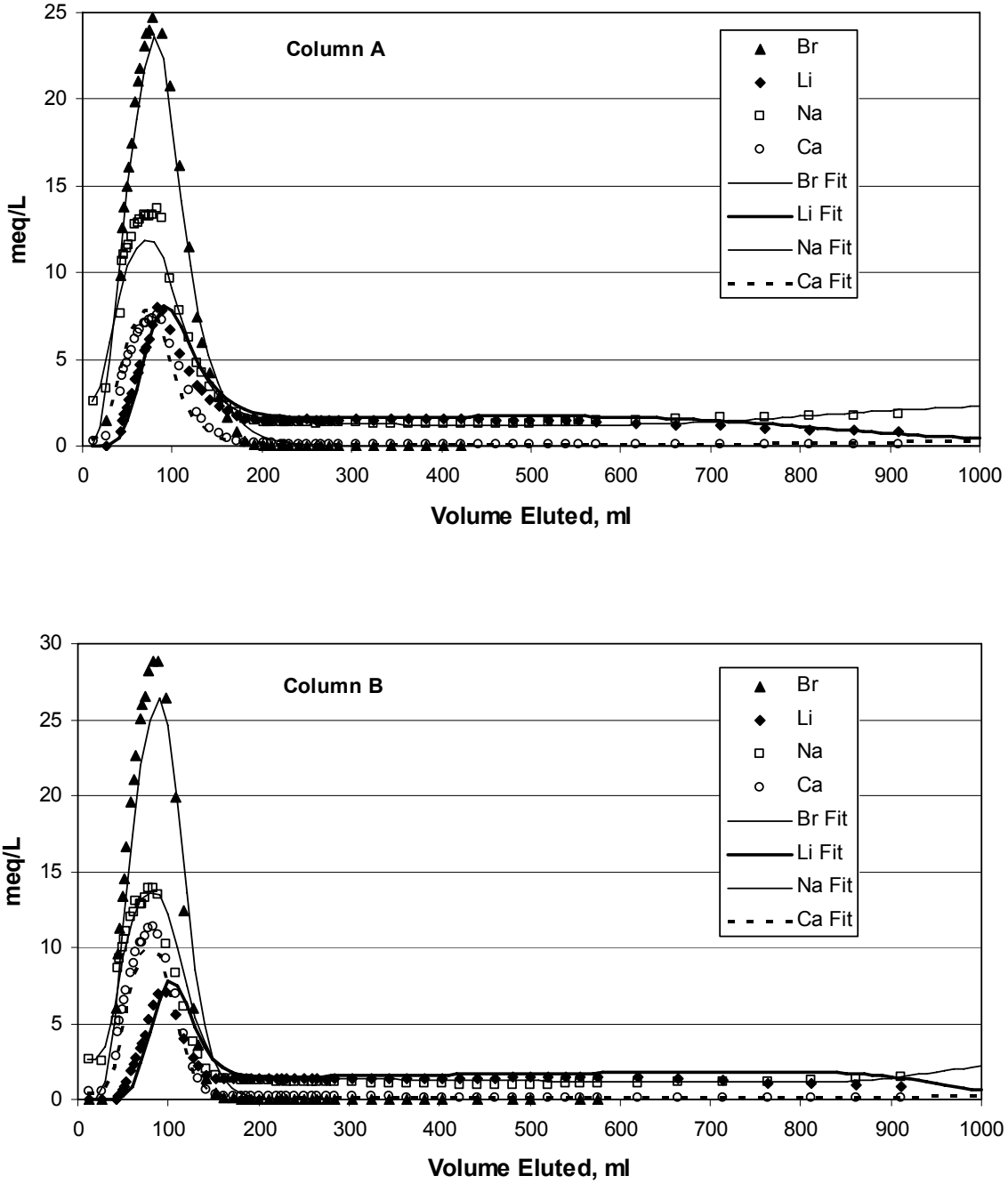

Source: SNL 2007 [DIRS 177394], Figure H-4 (model).

Figure 7-8. Column Data (concentration in the units of milli-equivalent/liter) and MULTRAN Fits for Experiments with a LiBr Injection Concentration of 0.0275 M

7.1.2.9 Colloid-Facilitated Transport in the Alluvium

The approach used in the site-scale SZ transport model for colloid-facilitated transport is presented in Section 6.4.2.6 and Table 6.4-1.

7.1.2.9.1 Radionuclides Attached Irreversibly to the Colloids

The radionuclides attached irreversibly to colloids get transported along with the colloid particles. Tests were conducted at the C-wells to study the transport of colloids in fractured volcanics. Also, the microsphere results for well NC-EWDP-19D1 shown in Figure 7-7 provide information on colloid filtration and detachment rates in the alluvial flow system. Qualitatively, compared to the conservative aqueous tracers, a much earlier breakthrough of microspheres in the withdrawal portion of the test was observed, followed by a very long tail. These observations are consistent with a model in which colloidal-sized particles undergo filtration in the alluvium. Filtration holds some microspheres up very close to the borehole. Upon pumping the aquifer, those microspheres close to the borehole are produced, essentially, instantly. Borehole effects could influence the early return of the microspheres as well. The fraction of microspheres that traveled farther into the medium undergoes filtration during their return, resulting in the long tail. The tail could be influenced by plume drift and aquifer heterogeneities. This qualitative evidence lends support to the conceptual model of filtration of colloids in the alluvium.

7.1.2.9.2 Radionuclides Attached Reversibly to the Colloids

The discussion in Section 7.1.2.5.2 also applies to the alluvium.

7.1.3 Comparison of Flow Paths and Transit Times Against Those Computed by an Independent Site-Scale Model

The NRC developed an independent site-scale groundwater flow model of the Yucca Mountain saturated zone (Winterle et al. 2003 [DIRS 163823]). Two different flow models of the flow system were considered. They differed in the material geometries, the number of material zones, and the permeability values assigned to each material type. Each model was calibrated to the measured heads by a trial and error process. Particle flow paths and transport times to the boundary of the accessible environment at 18 km (10 CFR 63.302 [DIRS 180319]) were computed from the model using advection only, excluding dispersion, diffusion, and retardation. The first model predicted flow paths starting to the east but shortly turning southward and traveling more or less directly southward (Winterle et al. 2003 [DIRS 163823], Figure 4). The particle transport times predicted by this model ranged from 1,800 to 110,000 years (Winterle et al. 2003 [DIRS 163823], Figure 5). The second model showed flow paths moving farther east before swinging south (Winterle et al. 2003 [DIRS 163823], Figure 8). This model predicted flow times in the range of 7,100 to 205,000 years (Winterle et al. 2003 [DIRS 163823], p. 153).

The general trend of flow paths reported by Winterle et al. (2003 [DIRS 163823], Figures 4 and 8), starting eastward and then moving southward to the boundary of the accessible environment, compares favorably with the flow paths in Figure 7-9b, although the latter show a more westward component in the southern part of the model compared to the study by Winterle et al. (2003 [DIRS 163823], Figure 8). Although the model described in this report does not predict the upper end of the transport times reported by Winterle et al. (2003 [DIRS 163823], p.153), the range of transit times reported here overlaps with those reported by them. This result corroborates the site-scale SZ transport model.

7.2 POSTDEVELOPMENT VALIDATION TO SUPPORT THE SCIENTIFIC BASIS OF THE MODEL

Numerical results from the site-scale SZ transport model have been compared to data and to independent models to provide confidence that, when combining the submodels with appropriate geologic-, hydrologic-, and boundary-condition information, the overall model is consistent with available observational data. Specifically, the flow pathways from the model are compared to hydrochemistry data (Section 7.2.1), and the transit times computed from the site-scale SZ transport model are compared to ^{14}C data at the field scale (Section 7.2.2).

7.2.1 Comparison of Flow Paths Against Those Deduced from Hydrochemistry Data

Flow paths of tracer particles were calculated for the base-case transport model. The particles were started in the vicinity of the repository footprint and allowed to transport downstream to the boundary of the accessible environment at 18 km. The transport parameter values used in this model calculation are given in Table 6.4-2. The results are shown in Figure 7-9b. Flow paths deduced from the hydrochemistry data are shown in Figure 7-9 (a and b) and are given in *Saturated Zone Site-Scale Flow Model* (SNL 2007 [DIRS 177391], Section A6.3.11 and Figure B6-15). Chemical and isotopic compositions were measured for groundwater samples taken from a number of wells in the area of the site-scale SZ flow model. As explained in detail in *Saturated Zone Site-Scale Flow Model* (SNL 2007 [DIRS 177391], Section A6.3.11), graphical analysis was done of the variations in the hydrochemical concentrations and isotopic ratios to estimate plausible flow lines. Of particular interest are the flow paths labeled # 2 and #7 in Figure 7-9 (a and b) from this analysis. Flow path 7, which is derived from hydrochemistry data, originates in the vicinity of the repository footprint and generally overlaps the model-calculated flow paths as seen in Figure 7-9b. Flow path 2 is also of interest here, although it originates northeast of the repository, because it closely bounds flow path #7 to the east. Note that the flow path 9 (shown by broad dashed line in Figure 7-9a going from east to west), which appears to cut across the flow paths 2 and 7 in the two-dimensional figure, actually represents regional underflow in the deep carbonate aquifer that underlies the volcanics and the alluvium in the saturated zone model area, and thus does not interfere with the flow paths 2 and 7.

Flow path 2 traces the movement of groundwater from the Fortymile Canyon area southward along the axis of Fortymile Wash into the Amargosa Desert. This pathway is drawn on the basis of similar anion and cation concentrations along the flow path and dissimilarities to regions to the east and west. Further details are presented in *Saturated Zone Site-Scale Flow Model* (SNL 2007 [DIRS 177391], Section A6.3.11).

Flow path 7 traces the movement of groundwater from northern Yucca Mountain southeastward toward wells in the Dune Wash area and then southwestward along the western edge of the Fortymile Wash shown in *Saturated Zone Site-Scale Flow Model* (SNL 2007 [DIRS 177391], Section A6.3.11). High $^{234}U/^{238}U$ activity ratios and low Cl^-, SO_4^{2-}, δD and $\delta^{18}O$ values characterize this flow path. A detailed discussion is presented in *Saturated Zone Site-Scale Flow Model* (SNL 2007 [DIRS 177391], Section A6.3.11).

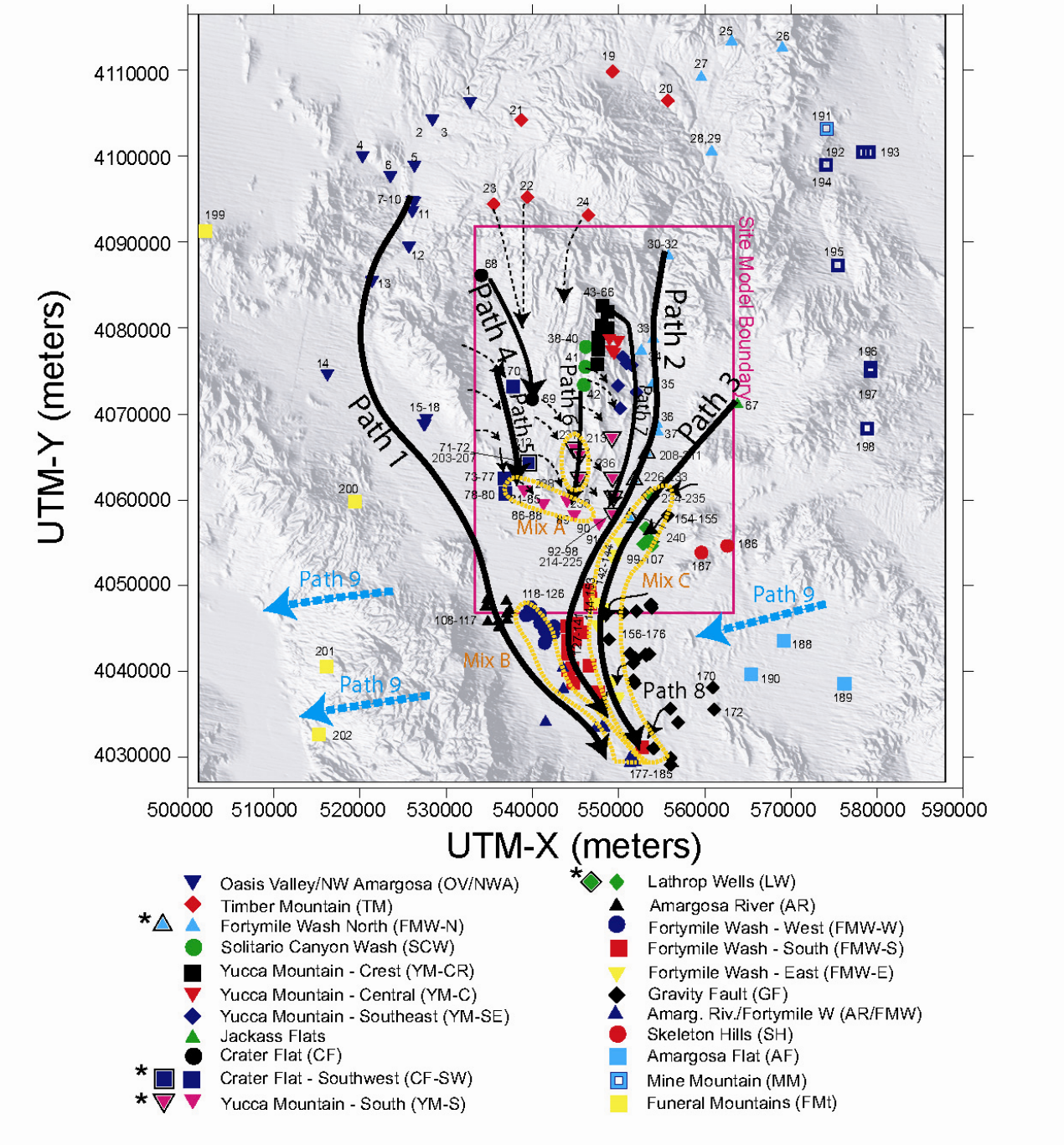

Source: SNL 2007 [DIRS 177391], Figure B6-15.

NOTES: [1]Colored symbols in the figure represent details of geochemical data, not directly relevant to the present discussion. Hence, for the sake of clarity, the detailed legend is not included here; see the source of the figure for details.
[2]Flow path 9 shown by broad dotted blue arrows pointing easterly is flow through deep regional aquifer and does not interfere with the flow paths 1 through 8 in the shallow volcanics and alluvium.

Figure 7-9a. Transport Pathways Deduced from Hydrochemistry

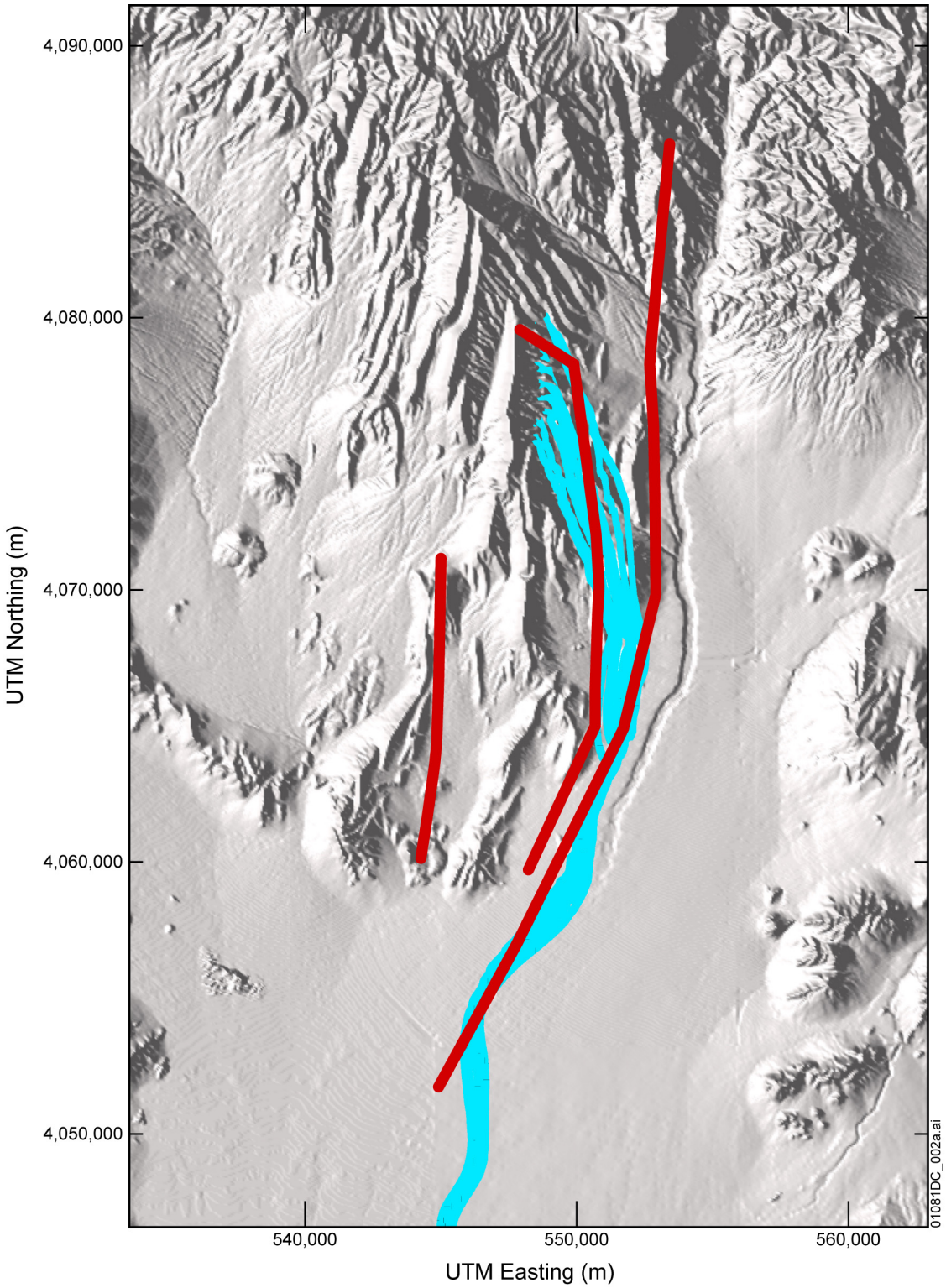

Source: Output DTN: LA0703SK150304.001.

Figure 7-9b. Transport Pathways Deduced from Hydrochemistry Data (in red, enlarged from Figure 7-9a) Overlaying Flow Paths Calculated from the Site-Scale Saturated Zone Transport Model (in black) for Tracer Particles Starting at the Repository Footprint

The flow paths deduced from the geochemistry data are qualitative in nature and denote broad areas of flow continuity inferred from available data, rather than specific streamlines. They are meant to represent broad flow directions and not the detailed variations that can be seen in a streamline computed from the model. It is seen in Figure 7-9b that the model streamlines originating at the repository footprint follow the general orientation and remain within the flow regions defined by the Flow paths 7 and 2 deduced from the geochemistry data. Hence, this validation is considered acceptable as defined in the TWP (BSC 2006 [DIRS 177375], Section 2.2.4.1, second bullet)

7.2.2 Comparison of Transit Times Against Those Deduced from ^{14}C Data

The radioactive isotope of carbon, ^{14}C, is produced in the atmosphere primarily by the interaction of cosmic rays with the atmospheric ^{14}N. ^{14}C decays with a half-life of 5,730 years. ^{14}C is rapidly incorporated into the atmospheric CO_2 and becomes available for terrestrial processes including that of dissolution into atmospheric precipitation as presented in *Saturated Zone Site-Scale Flow Model* (SNL 2007 [DIRS 177391], Section A6.3.1.2.2). ^{14}C enters the saturated zone groundwater through recharge and is transported principally as bicarbonate as a nonsorbing species. Estimates of groundwater age, obtained from the measured ^{14}C activity, corrected for possible water/rock interactions, are given in *Saturated Zone Site-Scale Flow Model* (SNL 2007 [DIRS 177391], Section A6.3.6.6.2). In interpreting these age estimates, it must be noted that the possibility of a fraction of younger water mixing with older water leading to the apparent age as determined from the ^{14}C activity cannot be ruled out. Radiometric dates in geochemically open systems are mixed dates that can be used for estimating upper and lower bounds of the groundwater ages.

Data from water samples taken from 7 wells in the vicinity of Yucca Mountain were analyzed for ^{14}C activity as shown in *Saturated Zone Site-Scale Flow Model* (SNL 2007 [DIRS 177391], Section A6.3.6.6.2) and the resulting ages are reported to lie in the range of 11,430 years to 16,390 years (SNL 2007 [DIRS 177391], Table A6-7). These ages reflect the time from atmospheric precipitation to the present and thus include transport time through the unsaturated zone as well as the saturated zone, along with the residence time within saturated zone. Thus, they are not direct indicators of transit times in the saturated zone, but they do provide a plausible upper bound on the saturated zone transit time.

Groundwater transit times can also be inferred from measured ^{14}C activity from water samples taken from wells that are inferred to lie along a flow path and where the geochemical compositions of waters suggests that flow paths exist between the two wells (SNL 2007 [DIRS 177391], Section A6.3.9). Data from two wells were used: UE-25 WT#3 and NC-EWDP-19D, both of which are downstream of the repository footprint, and lie on the interpreted flow path 7 that starts at Yucca Mountain and moves downstream in an overall southwardly direction (Figure 7-9a). The approximate distance between the two wells is 15 km (SNL 2007 [DIRS 177391], Section A6.3.9.1). The ^{14}C transport times lie in the range of 0 (or negative values) years to 3,110 years over the sampled depths (SNL 2007 [DIRS 177391], Section A6.3.9.1, Table A6-11). The data are clustered around two ranges corresponding to different sampling intervals: one in the interval of 188 to 535 years and the other in the interval of 1,601 to 3,110 years. For the interwell distance of 15 km, these ranges translate into groundwater velocity ranges of 80 to 28 m/yr and 9.4 to 4.8 m/yr. Using a nominal distance of 18 km from

the repository footprint to the boundary of the accessible environment at 18 km and taking constant velocities along the flow path, these velocities lead to transit time ranges of 226 to 643 years and 1,915 to 3,750 years. In interpreting these transit time estimates, it must be noted that the possibility of a fraction of younger water mixing with older water leading to the apparent age as determined from the ^{14}C activity cannot be ruled out with complete certainty. Hence, the values obtained from ^{14}C activity data should be interpreted as representing the likely range of groundwater transport times, without excluding a small probability of groundwater ages having values outside the indicated range.

There are two simplifications built into the above estimates (in addition to the ^{14}C data interpretation as discussed in *Saturated Zone Site-Scale Flow Model* (SNL 2007 [DIRS 177391], Sections A6.3.9, A6.3.1.2.2, and A6.3.6.6.2): one is that in calculating velocities from the transport time estimates, a nominal travel distance is used equal to the well separation, and the second is that a constant velocity is used along the entire flow path. Regarding the first simplification, using a nominal distance instead of the distance along the actual flow path, details of the tortuousness of the flow path are neglected. In actuality, the distance along the flow path will be somewhat greater than the interwell spacing, and thus the calculated velocity will be somewhat less than the actual velocity. However, the influence of this simplification on the estimated transport time to the 18-km boundary is somewhat offset by the fact that the actual travel distance along the flow path (including the segment beyond the well UE-25 WT#3) is also replaced by the somewhat lower value of 18 km, thus a ratio is taken of two numbers that are both somewhat lower than the actual values in the field. Secondly, in using a constant velocity along the flow path from the well UE-25 WT#3 to the boundary of the accessible environment at 18 km, an average of velocities in the volcanics and the alluvium is applied to the additional distance of 3 km that is traveled within the alluvium from the well NC-EWDP-19D to the boundary of the accessible environment. Considering that the porosity in alluvium is many orders of magnitude greater than the volcanic rocks, the effect of this simplification could be quite large. This would result in the estimated upper limit of 3,750 years being an underestimation of the actual transport time.

Transport model simulations were conducted to evaluate the propagation of uncertainty in the input parameter values to the output BTCs, as documented in Section 6.7. Starting with the base-case parameter values (Section 6), scenarios were constructed by considering one parameter at a time, using the upper and lower limit of each parameter value (Table 6.7-1). The parameters considered include specific discharge, horizontal anisotropy ratio in permeability, effective porosity in the alluvium, flowing interval aperture in the volcanics, effective diffusion coefficient in the volcanics, and the longitudinal dispersivity. Reactive transport parameters considered in the analysis described in Section 6.7 are not considered here, as they are not relevant to ^{14}C transport. The time at which 50% of the injected particles broke through the boundary of the accessible environment at 18 km downstream from the repository footprint is given in Table 6.7-1.

It can be seen from Table 6.7-1 that most of the nonsorbing cases considered here (Case numbers 1, 2, 3, 5, 8, 9, and 13) predict transport times within the range estimated on the basis of the ^{14}C hydrochemistry data discussed on the previous page of 226 to 3,750 years. The base-case transport model leads to a transit time of 705 years, well within the range predicted by hydrochemistry data. This validation is considered acceptable, as defined in the TWP (BSC

2006 [DIRS 177375], Section 2.2.4.1, first bullet of validation criteria) (reference to the previous version of the TWP has been retained because it specifies the validation criteria to which this work was done). (These criteria are not reproduced in the new version.) There are three outlier cases—using the limits of data interpretation discussed in the first paragraph of this section, and as discussed below, that are considered to be within the requirements of the model validation criteria:

- The case of maximum specific discharge leads to a transport time of 31 years, which is lower than the lower limit of 226 years calculated above This case is within the criteria specified in the TWP (BSC 2006 [DIRS 177375], Section 2.2.4.1, first bullet of validation criteria) (Reference to the previous version of the TWP has been retained because it specifies the validation criteria to which this work was done. These criteria are not reproduced in the new version.)

- The case of minimum specific discharge leads to a transport time of 52,840 years, which is greater than the upper limit of 3,750 years calculated from the ^{14}C data. This discrepancy can be readily explained as follows: 1) as noted in the first paragraph of this section, the value of 3,600 years is an estimate of the upper bound in the range of inferred transit times, and 2) longer transport times cannot be completely excluded from consideration, based on the available data.

- A transit time of 3,750 years would result from a specific discharge multiplier of 0.216 approximately (~0.078 m/year at 5km). The rationale for choosing a lower value of 0.04 m/year as the bounding value of the uncertainty distribution is discussed in *Saturated Zone Flow and Transport Model Abstraction* (SNL 2007 [DIRS 181650], Section 6.5.2.1). The uncertainty distribution at the low values of the specific discharge multiplier tapers off to 0 at a value of 0.112, and the cumulative probability of finding a value of specific discharge multiplier less than 0.216 (corresponding to the approximate transport time of 3,750 years) is low (less than 3%), and only a few stochastically sampled values are expected to fall below the factor of 1/4.

- The case of a minimum value of flowing-interval aperture leads to a transit time of 6,653 years, which is greater than the upper limit of 3,750 years calculated from the ^{14}C data. As noted in the first paragraph of this section, the value of 3,750 years is an estimate of the upper bound in the range of inferred transit times, and longer transport times cannot be completely excluded from consideration based on the available data.

A transit time of 3,750 years would result from a flowing-interval aperture of approximately 2×10^{-4} m. The flowing interval aperture is calculated as the product of the flowing interval spacing and the flowing interval porosity. The rationale for choosing the lower limits of the uncertainty distributions for these parameters is discussed in detail in *Saturated Zone Flow and Transport Model Abstraction* (SNL 2007 [DIRS 181650], Sections 6.5.2.4 and 6.5.2.5). As seen in Figure 6-13 of that report, the uncertainty distribution at the low values of the porosity tapers off to zero at about 10^{-5}, and the interval spacing tapers off to zero at about 1.86 m. Hence, the probability of finding a value of aperture less than 2×10^{-4} m (corresponding to the approximate transport time of 3,750 years) is low, less than approximately 5%. Thus, only a few

stochastically sampled values are expected to fall below the validated lower limit of about 2×10^{-4} m.

- The case of maximum value of flowing interval porosity leads to a transit time of 9008 years, which is greater that the upper limit of 3,750 years calculated from the ^{14}C data.

7.3 VALIDATION SUMMARY

The site-scale SZ transport model has been validated by applying acceptance criteria based on an evaluation of the model's relative importance to the potential performance of the repository system. The validation requirements defined in *Technical Work Plan for: Saturated Zone Flow and Transport Modeling and Testing* (BSC 2006 [DIRS 177375], Section 2.2.4.1, bullets 1 and 2) have been fulfilled, including corroboration of model results with field data. Activities requirements for confidence building during model development have also been satisfied. The model development activities and postdevelopment validation activities described establish the scientific bases for the site-scale SZ transport model. Therefore, the site-scale SZ transport model used in this model report is considered to be sufficiently accurate and adequate for the intended purpose and to the level of confidence required by the model's relative importance to the potential performance of the repository.

8. CONCLUSIONS

The site-scale SZ transport model is the culmination of efforts incorporating geologic, hydrologic, and geochemistry data from laboratory and field-testing with theoretical models of radionuclide transport into a coherent representation of transport through the saturated zone near Yucca Mountain (Sections 6.3 and 6.4). This model uses as its basis the calibrated SZ site-scale flow model, described in *Saturated Zone Site-Scale Flow Model* (SNL 2007 [DIRS 177391], Section 6.5).

The site-scale SZ transport model matches field data both quantitatively and qualitatively. These data include transit times derived from ^{14}C (Section 7.2.2) and flow paths inferred from Cl^- and SO_4^{-2} hydrochemical data (Section 7.2.1). The base-case transport model (for present-day climate, not including radionuclide decay, for an instantaneous source) leads to the BTC (Figure 6.5-1) at the boundary of the accessible environment at 18 km (10 CFR 63.302 [DIRS 180319]), corresponding to a breakthrough time at 50% concentration of 705 years.

The analysis of K_d data (Appendix A) and the modeling to upscale these data to a 500-m grid (Appendix C), combined with expert judgment (Appendix C), lead to the K_d distributions presented in Table C-14.

When using the site-scale SZ transport model for TSPA calculations, there are limitations that must be noted with regard to the following:

- *Input parameter values/ranges*. The transport model is intended for use with stochastic simulations using large uncertainty ranges for particular parameters such as specific discharge, flowing interval spacing and aperture, diffusion coefficient, and sorption coefficients. Care should be exercised in interpreting individual simulations for single sets of parameter values. Also, care should be exercised if the parameters used fall outside the range of parameter values (Table 4-2) or outside the range established by model validation (Section 7.2).

- *Sufficient number of input particles for particle tracking*. Radionuclide transport is implemented in the site-scale SZ transport model, using particle tracking with a random-walk method (Sections 6.4.2.3 and 6.4.2.4). In order to obtain reproducible results, a sufficient number of particles must be input to the model. The base-case transport model utilizes 500 input particles (output DTN: LA0703SK150304.001), visually judged as sufficient for obtaining a reasonably smooth BTC at the boundary of the accessible environment at 18 km (Figure 6.5-1). However, a larger number of input particles may be required depending on the purpose of the model use.

8.1 SUMMARY OF MODELING ACTIVITIES

Available hydrogeology, hydrochemistry, field, and laboratory data on transport processes were reviewed to form a conceptual model of the transport processes of importance to the site-scale SZ region (Sections 6.3 and 7.1). Available data on sorption of radionuclides were synthesized to develop distributions for sorption parameters (Appendices A and C). A mathematical formulation of the conceptual model was developed (Section 6.5) and incorporated in the FEHM

numerical code. A calibrated numerical model of groundwater flow, the SZ site-scale flow model (SNL 2007 [DIRS 177391], Section 6.5) was taken as the basis for transport calculations. A series of validation and confidence-building activities was completed (Section 7). Finally, results of this model were provided (output DTN: LA0306SK831231.001), and the associated uncertainties were discussed (Sections 6.7.1 and 8.3).

8.1.1 Hydrogeologic Setting and Conceptual Flow Model

The discussion of hydrogeologic setting and the conceptual flow model in this subsection is presented for the case of completeness only. Details are given in SNL 2007 [DIRS 177391]. Yucca Mountain is located about 150 km northwest of Las Vegas, Nevada, in the Great Basin section of the Basin and Range province. Yucca Mountain consists of a group of north-trending block-faulted ridges composed of volcanic rocks bounded by basins composed of volcanic rocks, alluvium, underlain by a thick carbonate aquifer. Yucca Mountain is part of the Alkali Flat-Furnace Creek subbasin of the Death Valley groundwater basin. The water table in the vicinity of the repository footprint is deep, as much as 750 m below the surface. The saturated zone occurs in thick ash-flow and ash-fall tuffs, underlain by the regional carbonate aquifer.

The general conceptual model of saturated zone flow in the model area is that groundwater flows southward from recharge areas in the north and at higher elevations, through the Tertiary volcanic rocks, toward the Amargosa Desert. Water inputs to the site-scale model include inflow along the northern boundary, recharge from precipitation at higher elevations, and recharge from surface runoff in the Fortymile Wash area. In the northern portion of the model, the flow occurs through the fractured volcanic rocks underlain by the carbonate aquifer. Toward the southern portion of the model area, the flow enters the valley-fill alluvium. Discharge from the model occurs via the alluvium, across the model boundary to the south and southeast, and through pumping of wells in the Amargosa Valley.

The overall groundwater flow is modeled as a three-dimensional steady-state system. A confined aquifer solution is used for the flow model. The dual-porosity, effective-continuum approach is used to model flow and transport, which averages fracture and surrounding rock properties in a given grid block, with the modification that several of the important fault zones are included as explicit features.

8.1.2 Conceptual Model of Transport

The flow paths from the repository site to the boundary of the accessible environment at 18 km begin in the volcanic tuffs below the repository footprint and end in the alluvium of the Amargosa Valley (Figure 6.5-2). Within the saturated zone, radionuclides are transported in the upper-few-hundred meters below the water table with pore water that flows subhorizontally in a southwardly direction through the highly fractured portions of the tuff, leading to the alluvium in the south (Section 6.3). The components of the conceptual model are: (1) radionuclides enter the saturated zone via fluids percolating through the unsaturated zone below the repository site. Within the saturated zone, they are transported with the groundwater that flows subhorizontally in a southerly or southeasterly direction; (2) the radionuclides advect and disperse with the groundwater through the fractured portions of the tuffs near the water table; (3) fluid flow occurs preferentially within the flowing intervals, whereas stagnant fluid resides in the rock matrix.

Solutes diffuse in and out of fluid within the rock matrix that is essentially stagnant; (4) sorption reactions occur in volcanics between the rock matrix and some of the radionuclides, tending to retard the transport of these radionuclides; (5) radionuclides can undergo colloid-facilitated transport in the volcanics; (6) the radionuclides advect and disperse with the groundwater through the alluvium; (7) sorption reactions occur in alluvium between the rock and some of the radionuclides, tending to retard the transport of these radionuclides; (8) radionuclides can undergo colloid-facilitated transport in alluvium; and (9) the radionuclides reaching the model boundary, which is downstream from the boundary to the accessible environment at 18 km downstream of the repository footprint are removed from the model. It is assumed that: a) sorption on individual fracture surfaces need not be included in the site-scale SZ transport model; b) the groundwaters in the saturated zone are in oxidizing conditions; and c) for the radionuclides americium, cesium, plutonium, protactinium, strontium, and thorium, sorption coefficients in alluvium are those corresponding to the values measured on samples of devitrified crushed tuff.

The mathematical basis (and the associated numerical approaches) of the site-scale SZ transport model is designed to incorporate the important transport processes in an efficient numerical code to compute radionuclide BTCs and transit times for use in TSPA simulations (Section 6.4). A particle-tracking approach is used to compute solute trajectories and transport times, combined with a random-walk model to incorporate dispersion. A semianalytical method is used for including retardation due to diffusion and sorption, as well as colloid-facilitated transport in the random-walk model.

8.1.3 Model Validation and Confidence Building

Recognizing that the site-scale SZ transport model is being used to perform probabilistic calculations in which parameter uncertainties are propagated through the model, the intent of validation was to confirm the radionuclide parameters and processes included in the model. Confidence in the results of the model was built by a series of different approaches (Section 7.1) that included: (1) comparisons to analogue sites, (2) model-data comparisons, (3) comparison with data published in referenced journals, and (4) comparison to an independent site-scale groundwater flow model for the Yucca Mountain saturated zone. The data used in the confidence building for the relevant transport parameters (e.g., sorption coefficient), submodel processes (e.g., advection, sorption), and site-scale model processes (e.g., flow pathways, transit times) were based on laboratory testing, field tests, natural analogue sites, and expert elicitations. The model was validated by postdevelopment comparison of model transit times with those inferred from ^{14}C data (Section 7.2.2) and qualitative comparison of flow paths predicted by the model and those inferred from the hydrochemistry and isotopic data (Section 7.2.1).

8.2 OUTPUTS

8.2.1 Technical Output

The technical output of this report is composed of (1) the site-scale SZ transport model and associated input and output files (base-case transport files); and (2) saturated zone distribution coefficients (K_ds) data for uranium, neptunium, plutonium, cesium, americium, protactinium, strontium, thorium, radium, selenium, tin, carbon, technetium, and iodine (Table C-14). The

site-scale SZ transport model files and uncertainty distributions for sorption coefficients will be integrated into the SZ flow and transport abstractions model for use in the TSPA calculations.

8.2.2 Developed Output Listed by Data Tracking Number

The outputs associated with the site-scale SZ transport model are listed in Table 8.2-1.

Table 8.2-1. Output Data

Transport Model		
Data Description	**Source**	**Data Tracking Number**
Probability Distribution Functions and Correlations for Sorption Coefficient Probability Distributions in the saturated zone for U, Np, Pu, Cs, Am, Pa, Sr, Th, Ra, Sn, and Se	Appendices A and C	LA0702AM150304.001
Type curve data for FEHM macro 'sptr' based on Sudicky and Frind solution	Section 6	LA0302RP831228.001
Modeling calculations of the radionuclides Am, U, Np, and Pu sorption via surface-complexation reactions	Appendix A	LA0702MD831232.001
FEHM V 2.24-01 Input Files for Base Case Transport Model	Section 6.6	LA0702SK150304.001
For the radionuclides Am, U, Np, and Pu- input data sets for PHREEQC modeling calculation of radionuclide sorption on Yucca Mountain volcanic tuff	Appendix A	LA0702MD831232.002
Files for FEHM V 2.24-01 for site-scale SZ transport model, FEHM files for base case	Section 6.4.3 and Section 6.5	LA0703SK150304.001
Files for FEHM V 2.24-01, Input Uncertainty Propagation, specific discharge multiplier and horizontal permeability anisotropy ratio	Section 6.7	LA0703SK150304.002
Files for FEHM V 2.24-01, Input Uncertainty Propagation, dispersivity, effective diffusion coefficient in volcanics, matrix sorption coefficient in volcanics, effective porosity in alluvium, bulk density in alluvium	Section 6.7	LA0703SK150304.003
Files for FEHM V 2.24-01, Input Uncertainty Propagation, colloid retardation factor for irreversible colloids in alluvium and volcanics	Section 6.7	LA0703SK150304.004
Files for FEHM V 2.24-01, Input Uncertainty Propagation, flowing interval aperture and porosity in volcanics	Section 6.7	LA0703SK150304.005
Files for FEHM V 2.24-01, Input Uncertainty Propagation, sorption coefficient in alluvium, reversible sorption onto colloids in volcanics and alluvium	Section 6.7	LA0703SK150304.006
Files for FEHM V 2.24-01 for evaluating barrier capabilities – Part 1	Section 6.8	LA0703SK150304.007
Files for FEHM V 2.24-01 for evaluating barrier capabilities – Part 2	Section 6.8	LA0703SK150304.008
Files for FEHM V 2.24-01 for evaluating barrier capabilities – Volcanic/Alluvium	Section 6.8	LA0703SK150304.009

Table 8.2-1. Output Data (Continued)

Transport Model		
Data Description	**Source**	**Data Tracking Number**
Boundary files for FEHM V 2.24-01 for evaluating barrier capabilities – Part 3	Section 6.8	LA0703SK150304.010
Files for FEHM V 2.24-01 for water table rise due to future climate change	Appendix E	LA0703SK150304.011
Files for GSLIB for generating stochastic realizations of rock types from mineralogic data	Appendix C	LA0309RP831321.001
Files FEHM V 2.20 for calculation of effective K_d distribution for U	Appendix C	LA0309RP831341.004
Files FEHM V 2.20 for calculation of effective K_d distribution for Cs	Appendix C	LA0309RP831341.001
Files FEHM V 2.20 for calculation of effective K_d distribution for Np	Appendix C	LA0309RP831341.002
Files FEHM V 2.20 for calculation of effective K_d distribution for Pu	Appendix C	LA0309RP831341.003

In addition, DTN: MO0707SURFCOMP.000 was developed to support surface complexation modeling in Appendix A3 to document K_d distributions.

8.3 OUTPUT UNCERTAINTY

Model-form uncertainty is explicitly addressed by discussing alternative conceptual models in Section 6.6. There are uncertainties associated with scaling parameter values from the scale of measurements to the scale of interest. Much of the data used for deriving parameter values in this report are from laboratory or field experiments conducted on spatial and temporal scales much smaller than those in the site-scale SZ model. Geological formations are inherently inhomogeneous, and they embed fractures, faults, and other heterogeneities on a variety of scales. Spatial correlations over some length scales often exist. Thus, it is difficult to extrapolate the measurements on a small scale to the SZ site scale. Accommodations are made for these uncertainties by choosing wide distributions of input parameters (Table 4-2) for TSPA analysis (SNL 2007 [DIRS 181650], Sections 6.5.2 and 6.5.2[a]).

Epistemic uncertainty is explicitly described by using probability distributions for appropriate model parameters. Expected uncertainty ranges for the various transport parameters are discussed in Section 4.1.2 and summarized in Table 4-2. The development and discussion of the K_d parameters needed for modeling reactive transport and the K_c parameters needed for modeling colloid-facilitated transport are presented in Appendices A, B, and C. The probability distributions for all other model parameters are presented and discussed in *Saturated Zone Flow and Transport Model Abstraction* (SNL 2007 [DIRS 181650], Sections 6.5.2 and 6.5.2[a]). These uncertainties are propagated through the model to the output BTCs, presented in Section 6.7. Radionuclide transit times are most sensitive to groundwater-specific discharge. Other parameters of importance to the breakthrough times are matrix diffusion, the sorption coefficient in the volcanics as well as the alluvium, the effective flowing interval in the volcanics (as reflected in the flowing interval aperture and spacing), the effective porosity in the

alluvium, and the sorption coefficients for reversible colloids and retardation factor for irreversible colloids in the volcanics and alluvium. Quantification of the sensitivity of the model output BTCs for various radionuclides of concern to parameter uncertainties are further evaluated in *Saturated Zone Flow and Transport Model Abstraction* (SNL 2007 [DIRS 181650], Sections 6.6, 6.7, and 8).

8.4 HOW THE ACCEPTANCE CRITERIA ARE ADDRESSED

The following information describes how this analysis addresses the acceptance criteria in the YMRP (NRC 2003 [DIRS 163274], Section 2.2.1.3.9.3). Only those acceptance criteria that are applicable to this report (Section 4.2) are discussed. In most cases, the applicable acceptance criteria are not addressed solely by this report; rather, the acceptance criteria are fully addressed when this report is considered in conjunction with other analysis and model reports that describe flow and transport in the saturated zone. Compliance with the procedures was determined through QA audits and other oversight activities.

Acceptance Criteria from Section 2.2.1.3.9.3, *Radionuclide Transport in the Saturated Zone*

Acceptance Criterion 1: System Description and Model Integration Are Adequate

Subcriterion (1): The model described in this report incorporates or considers known Yucca Mountain physical phenomena and couplings affecting radionuclide transport through the saturated zone. Sections 6.1 through 6.8 describe the main saturated zone transport processes that were included to construct an efficient model to be used in the abstraction process and TSPA. The primary assumptions incorporated in the model (Section 5) are: (1) sorption on individual fracture surfaces is not included; (2) sorption coefficients assume that conditions are oxidizing in groundwater; and (3) for americium, cesium, plutonium, protactinium, strontium, and thorium, sorption coefficients are assumed to be those corresponding to the values measured on samples of devitrified crushed tuff. These assumptions are consistent with the model (Section 6.3) and with those made in reports supporting other abstractions prepared for Yucca Mountain, and the assumptions are appropriate for describing a conservative model of transport in the saturated zone (Sections 5 and 6.3).

Subcriterion (2): This report provides extensive descriptions of the aspects of hydrology, geology, geochemistry, physical phenomena, and couplings that are considered and/or included in the site-scale model (see Sections 6.2 for FEPs and 6.3 for model development). Conditions and assumptions supporting the abstraction of radionuclide transport in the saturated zone are readily identified in Sections 5, 6.3, 6.4, and 6.6, and they are consistent with the body of data incorporated in the report (Section 4.1). Changes in transport due to aspects of sorption and matrix diffusion are considered and are either specifically included in the model or discarded due to nonconservatism (Sections 6.2, 6.3, and 6.6).

Subcriterion (3): The assumptions, technical bases, data, and models employed in this site-scale model are appropriate due to their inclusion of major factors affecting transport of radionuclides in the saturated zone (Sections 4.1, 6.1, 6.3, and 6.6) and are consistent with other related Yucca Mountain abstractions. The site-scale SZ model described in this report is used directly in *Saturated Zone Flow and Transport Model Abstraction* (SNL 2007 [DIRS 181650]) for

generating a set of radionuclide BTCs at the accessible environment for use in TSPA simulations of radionuclide release to the biosphere. The descriptions and technical bases in this report (detailed in Sections 6 and 7) provide transparent and traceable support for the abstraction of radionuclide transport in the saturated zone through detailed descriptions of assumptions, phenomena affecting transport, and numerical methods employed.

Subcriterion (5): This report addresses the saturated zone FEPs pertaining to the site-scale SZ transport that are included for TSPA (Table 6.2-1). Saturated zone FEPs for TSPA are described in the LA FEP List (DTN: MO0706SPAFEPLA.001 [DIRS 181613], file *FEPs_be.mdb*, Table 7.1-1) Table 6.2-1 provides a list of FEPs that are relevant to this model analysis in accordance with their assignment in the LA FEP list.

Subcriterion (6): This report was developed using processes and procedures consistent with the QARD, which commits to these NUREGs and with SCI-PRO-006, which implements those commitments for model reports.

Acceptance Criterion 2: Data Are Sufficient for Model Justification

Subcriterion (1): Input parameters to this transport model are radionuclide release locations, dispersivities in the volcanics, matrix porosity, matrix diffusion coefficient, sorption distribution coefficient K_d in the matrix, flowing interval porosity, flowing interval spacing, retardation factor in the flowing interval, effective porosity of the alluvium, dispersivities in the alluvium, and the K_d value in the alluvium. Their base-case values and range of values are listed in Table 6.4-2 in Section 6.4.3 and in Table 4-2 in Section 4. Adequate justifications for the average or range of values chosen and descriptions of how the data comprising these values were interpreted and used are presented in detail in Sections 6.3 and 6.4.

Subcriterion (3): Data employed in this model and results were developed from Yucca Mountain borehole data, Yucca Mountain and other related field experiments, laboratory experiments, natural analogue research, and current, accepted technical information as shown in Table 4-1. The documents cited as sources in Table 4-1 provide detailed descriptions of the methods used in generating the data. Discussions of model uncertainties are included in Section 6.7. Sensitivity of the output BTCs to each of the uncertain input parameters is discussed in Sections 6.7.1.1 through 6.7.1.13.

Acceptance Criterion 3: Data Uncertainty Is Characterized and Propagated Through the Model Abstraction

Subcriterion (1): Base case values for site-scale SZ transport model parameters are listed in Table 6.4-2 and Table 4-2, and the uncertainty ranges for these parameters are given in Table 4-2. Sections 6.3, 6.4, and 6.6 provide technically defensible arguments for their adoption in this model. Those sections also discuss uncertainties in the parameters and nonconservatisms that might be introduced if other parameters or approaches were adopted. Also, the formulation of the model incorporates numerous conservative approaches that should prevent an underestimate of the risk estimate. This conclusion is supported by the validation process that employed analogue studies (Section 7.2) to support the chosen transport parameters and the submodel components.

Subcriterion (2): Sources of flow and transport parameters for various nuclides important to waste isolation are given in Table 4-1 (Section 4.1). These parameters are based on Yucca Mountain borehole data, Yucca Mountain and other related field experiments, laboratory experiments, natural analogue research, and current, accepted technical information as shown in Table 4-1 and in assumption number 3 in Table 5-1 for the sorption coefficients of radionuclides americium, cesium, plutonium, protactinium, strontium, and thorium in alluvium. The model was validated by various methods including: (1) analogue studies from the NTS (Section 7.1.1.1) and uranium transport at natural analogue sites (Section 7.1.1.2); (2) comparison of flow paths against those deduced from hydrochemistry data (Section 7.2.1); and (3) comparison of transit times against those deduced from ^{14}C data (Section 7.2.2). The submodel components were validated by numerous methods described in Sections 7.1.2.1 through 7.1.2.9.

Subcriterion (4): Effective diffusion coefficients, matrix sorption coefficients, dispersivity coefficients, and colloid retardation factors in volcanics and alluvium employed in this model are consistent with aquifer properties. Their parametric values and data sources are shown in Table 4-2. These sources are primarily documents describing Yucca Mountain aquifer characteristics taken from borehole data and field and laboratory experiments. Further, the above parameters are taken to be stochastic variables sampled from broad distributions to allow for uncertainties in the aquifer characteristics and the influence of these uncertainties on the parameter values.

Subcriterion (5): Uncertainty in representation of radionuclide transport is adequately represented by adopting conservative positions on mechanisms and alternate models included in this site-scale SZ transport model. An example is that sorption on individual fracture surfaces was not included in the model because it would tend to retard radionuclide transport and the mineral distributions in fractures as opposed to the matrix are not well known. Another example is oxidizing conditions were included along the entire flow path because they tend to lead to lower values of sorption coefficients (Section 6.3, Item 4). Models that lead to transit times greater than those calculated by the site-scale SZ transport model are considered less conservative because they predict delay and possible lowering of the concentrations of radionuclides reaching the accessible environment. Section 6.6 discusses alternative conceptual models that were screened out on this basis. Discussions of model uncertainties are included in Section 6.7. Sensitivity of the output BTCs to each of the uncertain input parameters is discussed in Sections 6.7.1.1 through 6.7.1.13.

Subcriterion (6): Sufficient data did not exist; hence the process of expert elicitation was used for determining the range of values of the specific discharge multiplier (Section 4.1.2.1) and dispersivities (Sections 4.1.2.16, 4.1.2.17, and 4.1.2.18), as well as the distribution functions for sorption coefficients of various radionuclides (Appendix C). Further, because of the time and spatial scales involved and the fact that radionuclides cannot be used as tracers in field experiments, confidence-building activities during model development (Section 7.1) as well as postdevelopment validation (Section 7.2) were conducted to support the definition of parameter values and the conceptual models (Sections 6.3 and 6.4) used in this report.

Acceptance Criterion 4: Model Uncertainty Is Characterized and Propagated Through the Model Abstraction

Subcriterion (1): Alternative conceptual models are discussed in detail in Section 6.6. The alternative conceptual models fall into two classes: (1) those that are screened out because they lead to transit times greater than those calculated by the site-scale SZ transport model (Table 6.6-1a). Models that lead to transit times greater than those calculated by the site-scale SZ transport model are considered less conservative because they predict delay and possible lowering of the concentrations of radionuclides reaching the accessible environment; and (2) alternative conceptual models that are implicitly included in the site-scale SZ transport model through the range of uncertainty in parameter values (see Table 6.7-1). The key components, screening assessment, and basis for the assessment are presented in Tables 6.6-1a and 6.6-1b. The screening assessment and basis discuss the model approach, assumptions, results, and whether the alternative conceptual model is included implicitly or explicitly in the model supporting the abstraction of saturated zone radionuclide transport.

Subcriterion (2): Discussions of conceptual model uncertainties are included in Section 6.6 and 6.7. Sensitivity of the output BTCs to each of the uncertain input parameters is discussed in Sections 6.7.1.1 through 6.7.1.13. Expected uncertainty ranges for transport parameters are discussed in Sections 4.1 and 6.7. Although the model is meant to represent the saturated zone transport accurately, for the case of those alternative conceptual models that could not be included in the model, the transport model was selected such that it resulted in transit times faster than those expected for the alternative conceptual model (Section 6.6). Uncertainties associated with scaling parameter values from the scale of measurements to the scale of interest are discussed in Section 6.7. Sensitivity of the output BTCs to each of the uncertain input parameters was investigated by considering the upper and lower levels of each parameter individually (see Section 6.7 and Table 6.7-1).

Subcriterion (3): The uncertainties related to the K_d parameters needed for modeling reactive transport, the K_c parameters needed for modeling colloid-facilitated transport, and the probability distributions for all other model parameters are propagated through the model to the output BTCs, presented in Section 6.7. Through analysis of sensitivity of the output BTCs to each of the uncertain input parameters (see Section 6.7 and Table 6.7-1), the uncertainty of the site characterization data, experiments, measurements, and studies is incorporated. The model formulation results in conservative choices of parameters and approaches that result in relatively faster transit times for transport of radionuclides than otherwise would exist. Therefore, this model does not contribute to an under-representation of the risk estimate.

Subcriterion (4): Alternative conceptual models are discussed in detail in Section 6.6 and are consistent with available and current scientific knowledge. The results and limitations of each of the models and approaches are presented in Tables 6.6-1a and 6.6-1b. The screening assessment and basis in those tables discuss approach, assumptions, supporting data, and scientific knowledge associated with the model. For example, “water table rise” considers potential future glacial climatic conditions that could occur and is discussed in the Table 6.6-1a. Supporting information on other implicitly included alternative conceptual models in Table 6.6-1b is provided in Appendices A through J.

INTENTIONALLY LEFT BLANK

9. INPUTS AND REFERENCES

The following is a list of the references cited in this document. The six digit numerical identifier preceding each reference in this section is the Document Input Reference System number, which is placed in the rest of the text following the reference callout (e.g., BSC 2004 [DIRS 161340]). The purpose of these numbers is to assist in locating a specific reference. Multiple sources by the same author (e.g., BSC 2004) are sorted alphabetically by title.

9.1 DOCUMENTS CITED

147235 Allard, B. and Beall, G.W. 1979. "Sorption of Americium on Geologic Media." *Journal of Environmental Science and Health. Part A Environmental Science and Engineering, A14,* (6), 507-518. New York, New York: Marcel Dekker. TIC: 224102.

104410 Allard, B.; Beall, G.W.; and Krajewski, T. 1980. "The Sorption of Actinides in Igneous Rocks." *Nuclear Technology, 49,* (3), 474-480. La Grange Park, Illinois: American Nuclear Society. TIC: 245772.

162982 Allard, B.; Olofsson, U.; Torstenfelt, B.; and Kipatsi, H. 1983. *Sorption Behaviour of Well-Defined Oxidation States.* SKB TR-83-61. Stockholm, Sweden: Svensk Kärnbränsleförsörjning A.B. TIC: 206122.

103750 Altman, W.D.; Donnelly, J.P.; and Kennedy, J.E. 1988. *Qualification of Existing Data for High-Level Nuclear Waste Repositories: Generic Technical Position.* NUREG-1298. Washington, D.C.: U.S. Nuclear Regulatory Commission. TIC: 200652.

103597 Altman, W.D.; Donnelly, J.P.; and Kennedy, J.E. 1988. *Peer Review for High-Level Nuclear Waste Repositories: Generic Technical Position.* NUREG-1297. Washington, D.C.: U.S. Nuclear Regulatory Commission. TIC: 200651.

144539 Bahr, J.M. and Rubin, J. 1987. "Direct Comparison of Kinetic and Local Equilibrium Formulations for Solute Transport Affected by Surface Reactions." *Water Resources Research, 23,* (3), 438-452. Washington, D.C.: American Geophysical Union. TIC: 246894.

162983 Beall, G.W.; Lee, W.W.-L.; and Van Luik, A.E. 1986. "Americium Speciation and Distribution Coefficients in a Granitic Ground Water." *Scientific Basis for Nuclear Waste Management IX, Symposium held September 9-11, 1985, Stockholm, Sweden.* Werme, L.O., ed. *50,* 501-508. Pittsburgh, Pennsylvania: Materials Research Society. TIC: 203664.

156269 Bear, J. 1972. *Dynamics of Fluids in Porous Media.* Environmental Science Series. Biswas, A.K., ed. New York, New York: Elsevier. TIC: 217356.

129676 Bedinger, M.S.; Sargent, K.A.; Langer, W.H.; Sherman, F.B.; Reed, J.E.; and Brady, B.T. 1989. *Studies of Geology and Hydrology in the Basin and Range Province, Southwestern United States, for Isolation of High-Level Radioactive Waste—Basis of Characterization and Evaluation*. U.S. Geological Survey Professional Paper 1370-A. Washington, D.C.: U.S. Government Printing Office. ACC: NNA.19910524.0125.

101036 Benson, L.V. and McKinley, P.W. 1985. *Chemical Composition of Ground Water in the Yucca Mountain Area, Nevada, 1971-84.* Open-File Report 85-484. Denver, Colorado: U.S. Geological Survey. ACC: NNA.19900207.0281.

144728 Berry, J.A.; Hobley, J.; Lane, S.A.; Littleboy, A.K.; Nash, M.J.; Oliver, P.; Smith-Briggs, J.L.; and Williams, S.J. 1989. "Solubility and Sorption of Protactinium in the Near-Field and Far-Field Environments of a Radioactive Waste Repository." *Analyst, 114,* 339-347. Cambridge, England: Royal Society of Chemistry. TIC: 247004.

100023 Broxton, D.E.; Warren, R.G.; Hagan, R.C.; and Luedemann, G. 1986. *Chemistry of Diagenetically Altered Tuffs at a Potential Nuclear Waste Repository, Yucca Mountain, Nye County, Nevada.* LA-10802-MS. Los Alamos, New Mexico: Los Alamos National Laboratory. ACC: MOL.19980527.0202.

158794 BSC (Bechtel SAIC Company) 2002. *Guidelines for Developing and Documenting Alternative Conceptual Models, Model Abstractions, and Parameter Uncertainty in the Total System Performance Assessment for the License Application*. TDR-WIS-PA-000008 REV 00 ICN 01. Las Vegas, Nevada: Bechtel SAIC Company. ACC: MOL.20020904.0002.

170038 BSC 2004. *Analysis of Hydrologic Properties Data.* ANL-NBS-HS-000042 REV 00. Las Vegas, Nevada: Bechtel SAIC Company. ACC: DOC.20041005.0004; DOC.20050815.0003.

170031 BSC 2004. *Mineralogic Model (MM3.0) Report.* MDL-NBS-GS-000003 REV 01. Las Vegas, Nevada: Bechtel SAIC Company. ACC: DOC.20040908.0006.

169218 BSC 2004. *Natural Analogue Synthesis Report.* TDR-NBS-GS-000027 REV 01. Las Vegas, Nevada: Bechtel SAIC Company. ACC: DOC.20040524.0008.

170014 BSC 2004. *Probability Distribution for Flowing Interval Spacing.* ANL-NBS-MD-000003 REV 01. Las Vegas, Nevada: Bechtel SAIC Company. ACC: DOC.20040923.0003.

170015 BSC 2004. *Recharge and Lateral Groundwater Flow Boundary Conditions for the Saturated Zone Site-Scale Flow and Transport Model*. ANL-NBS-MD-000010 REV 01. Las Vegas, Nevada: Bechtel SAIC Company. ACC: DOC.20041008.0004.

170032 BSC 2004. *Rock Properties Model.* MDL-NBS-GS-000004 REV 01. Las Vegas, Nevada: Bechtel SAIC Company. ACC: DOC.20040915.0011; DOC.20050214.0003.

170006 BSC 2004. *Saturated Zone Colloid Transport.* ANL-NBS-HS-000031 REV 02. Las Vegas, Nevada: Bechtel SAIC Company. ACC: DOC.20041008.0007; DOC.20051215.0005.

170009 BSC 2004. *Water-Level Data Analysis for the Saturated Zone Site-Scale Flow and Transport Model.* ANL-NBS-HS-000034 REV 02. Las Vegas, Nevada: Bechtel SAIC Company. ACC: DOC.20041012.0002; DOC.20050214.0002.

174566 BSC 2005. *Dissolved Concentration Limits of Radioactive Elements.* ANL-WIS-MD-000010 REV 05. Las Vegas, Nevada: Bechtel SAIC Company. ACC: DOC.20050713.0006; DOC.20051006.0002.

175539 BSC 2005. *Q-List.* 000-30R-MGR0-00500-000-003. Las Vegas, Nevada: Bechtel SAIC Company. ACC: ENG.20050929.0008.

180708 BSC 2006. *Data Qualification Report: Qualification of Hydraulic Gradient at Yucca Mountain for the Purpose of Stochastic Modeling for Derivation of Composite Upscale K_d Distributions*. TDR-NBS-HS-000018 REV 00. Las Vegas, Nevada: Bechtel SAIC Company. ACC: DOC.20060221.0007.

177375 BSC 2006. *Technical Work Plan for Saturated Zone Flow and Transport Modeling.* TWP-NBS-MD-000006 REV 02. Las Vegas, Nevada: Bechtel SAIC Company. ACC: DOC.20060519.0002.

129679 Burbey, T.J. and Wheatcraft, S.W. 1986. *Tritium and Chlorine-36 Migration from a Nuclear Explosion Cavity.* DOE/NV/10384-09. Reno, Nevada: University of Nevada, Desert Research Institute, Water Resources Center. TIC: 201927.

130526 Burnett, R.D. and Frind, E.O. 1987. "Simulation of Contaminant Transport in Three Dimensions, 2. Dimensionality Effects." *Water Resources Research, 23,* (4), 695-705. Washington, D.C.: American Geophysical Union. TIC: 246359.

102495 Castor, S.B.; Tingley, J.V.; and Bonham, H.F., Jr. 1994. "Pyritic Ash-Flow Tuff, Yucca Mountain, Nevada." *Economic Geology, 89,* 401-407. El Paso, Texas: Economic Geology Publishing. TIC: 234278.

101374 Chipera, S.J. and Bish, D.L. 1989. *Quantitative X-Ray Diffraction Analyses of Samples Used for Sorption Studies by the Isotope and Nuclear Chemistry Division, Los Alamos National Laboratory*. LA-11669-MS. Los Alamos, New Mexico: Los Alamos National Laboratory. ACC: NNA.19890414.0062.

111081 Chipera, S.J.; Vaniman, D.T.; Carlos, B.A.; and Bish, D.L. 1995. *Mineralogic Variation in Drill Core UE-25 UZ#16, Yucca Mountain, Nevada.* LA-12810-MS. Los Alamos, New Mexico: Los Alamos National Laboratory. ACC: NNA.19940427.0099.

105761 Corapcioglu, M.Y. and Jiang, S. 1993. "Colloid-Facilitated Groundwater Contaminant Transport." *Water Resources Research, 29,* (7), 2215-2226. Washington, D.C.: American Geophysical Union. TIC: 222362.

101584 Cotton, F.A. and Wilkinson, G. 1980. *Advanced Inorganic Chemistry: A Comprehensive Text.* 4th Edition. New York, New York: John Wiley & Sons. TIC: 217739.

100328 CRWMS M&O 1997. *Report of Results of Hydraulic and Tracer Tests at the C-Holes Complex.* Deliverable SP23APM3. Las Vegas, Nevada: CRWMS M&O. ACC: MOL.19971024.0074.

100353 CRWMS M&O 1998. *Saturated Zone Flow and Transport Expert Elicitation Project.* Deliverable SL5X4AM3. Las Vegas, Nevada: CRWMS M&O. ACC: MOL.19980825.0008.

163800 Dagan, G.; Cvetkovic, V.; and Shapiro, A. 1992. "A Solute Flux Approach to Transport in Heterogeneous Formations 1. The General Framework." *Water Resources Research, 28,* (5), 1369-1376. Washington, D.C.: American Geophysical Union. TIC: 254598.

105803 Daniels, W.R.; Wolfsberg, K.; Rundberg, R.S.; Ogard, A.E.; Kerrisk, J.F.; Duffy, C.J.; Newton, T.W.; Thompson, J.L.; Bayhurst, B.P.; Bish, D.L.; Blacic, J.D.; Crowe, B.M.; Erdal, B.R.; Griffith, J.F.; Knight, S.D.; Lawrence, F.O.; Rundberg, V.L.; Skyes, M.L.; Thompson, G.M.; Travis, B.J.; Treher, E.N.; Vidale, R.J.; Walter, G.R.; Aguilar, R.D.; Cisneros, M.R.; Maestas, S.; Mitchell, A.J.; Oliver, P.Q.; Raybold, N.A.; and Wanek, P.L. 1982. *Summary Report on the Geochemistry of Yucca Mountain and Environs.* LA-9328-MS. Los Alamos, New Mexico: Los Alamos National Laboratory. ACC: NNA.19870406.0243.

153651 Degueldre, C.; Triay, I.; Kim, J-I; Vilks, P.; Laaksoharju, M.; and Miekeley, N. 2000. "Groundwater Colloid Properties: A Global Approach." *Applied Geochemistry, 15,* (7), 1043-1051. New York, New York: Pergamon Press. TIC: 249340.

164737 Ding, M.; Reimus, P.W.; Ware, S.D.; and Meijer, A. 2003. "Experimental Studies of Radionuclide Migration in Yucca Mountain Alluvium." *Proceedings of the 10th International High-Level Radioactive Waste Management Conference (IHLRWM), March 30-April 2, 2003, Las Vegas, Nevada.* Pages 126-135. La Grange Park, Illinois: American Nuclear Society. TIC: 254559.

162985 Dixit, S. and Van Cappellen, P. 2002. "Surface Chemistry and Reactivity of Biogenic Silica." *Geochimica et Cosmochimica Acta, 66,* (14), 2559-2568. New York, New York: Pergamon. TIC: 254531.

103021 DOE (U.S. Department of Energy) 1997. *Regional Groundwater Flow and Tritium Transport Modeling and Risk Assessment of the Underground Test Area, Nevada Test Site, Nevada*. DOE/NV-477. Las Vegas, Nevada: U.S. Department of Energy. ACC: MOL.20010731.0303.

182051 DOE 2007. *Quality Assurance Requirements and Description.* DOE/RW-0333P, Rev. 19. Washington, D. C.: U.S. Department of Energy, Office of Civilian Radioactive Waste Management. ACC: DOC.20070717.0006.

181096 DOE 2007. *User Information Document for: FEHM V2.24-01.* Document ID: 10086-UID-2.24-01-00. Las Vegas, Nevada: U.S. Department of Energy, Office of Repository Development. ACC: MOL.20070309.0037.

105279 Erickson, J.R. and Waddell, R.K. 1985. *Identification and Characterization of Hydrologic Properties of Fractured Tuff Using Hydraulic and Tracer Tests--Test Well USW H-4, Yucca Mountain, Nye County, Nevada*. Water-Resources Investigations Report 85-4066. Denver, Colorado: U.S. Geological Survey. ACC: NNA.19890713.0211.

162695 Finnegan, D.L. and Thompson, J.L. 2002. *Laboratory and Field Studies Related to Radionuclide Migration at the Nevada Test Site in Support of the Underground Test Area and Hydrologic Resources Management Projects*. LA-13919-MS. Los Alamos, New Mexico: Los Alamos National Laboratory. ACC: MOL.20030926.0011.

100033 Flint, L.E. 1998. *Characterization of Hydrogeologic Units Using Matrix Properties, Yucca Mountain, Nevada.* Water-Resources Investigations Report 97-4243. Denver, Colorado: U.S. Geological Survey. ACC: MOL.19980429.0512.

101173 Freeze, R.A. and Cherry, J.A. 1979. *Groundwater.* Englewood Cliffs, New Jersey: Prentice-Hall. TIC: 217571.

145116 Gardiner, C.W. 1997. *Handbook of Stochastic Methods for Physics, Chemistry and the Natural Sciences.* 2nd Edition. 442. New York, New York: Springer-Verlag. TIC: 247770.

145122 Gelhar, L.W. 1997. "Perspectives on Field-Scale Application of Stochastic Subsurface Hydrology." *Subsurface Flow and Transport: A Stochastic Approach.* Dagan, G. and Neuman, S.P., eds. Pages 157-176. New York, New York: Cambridge University Press. TIC: 247805.

165928 Grindrod, P. 1993. *The Impact of Colloids on the Migration and Dispersal of Radionuclides within Fractured Rock.* 13. 1-4. 167-181. New York, New York: Elsevier. TIC: 222399.

163780 Hess, K.M.; Davis, J.A.; Kent, D.B.; and Coston, J.A. 2002. "Multispecies Reactive Tracer Test in an Aquifer with Spatially Variable Chemical Conditions, Cape Cod, Massachusetts: Dispersive Transport of Bromide and Nickel." *Water Resources Research, 38,* (8), 36-1 to 36-17. Washington, D.C.: American Geophysical Union. TIC: 254599.

161904 Hummel, W.; Berner, U.; Curti, E.; Pearson, F.J.; and Thoenen, T. 2002. *Nagra/PSI Chemical Thermodynamic Data Base 01/01.* Parkland, Florida: Universal Publishers. TIC: 253421.

165931 Hwang, Y.; Chambré, P.L.; Lee, W.W.-L.; and Pigford, T.H. 1989. "Analytic Studies of Colloid Transport in Fractured Porous Media." *Scientific Basis for Nuclear Waste Management XIII, Symposium held November 27-30, 1989, Boston, Massachusetts.* Oversby, V.M. and Brown, P.W., eds. *176,* 599-605. Pittsburgh, Pennsylvania: Materials Research Society. TIC: 203658.

109297 Ibaraki, M. and Sudicky, E.A. 1995. "Colloid-Facilitated Contaminant Transport in Discretely Fractured Porous Media 1. Numerical Formulation and Sensitivity Analysis." *Water Resources Research, 31,* (12), 2945-2960. Washington, D.C.: American Geophysical Union. TIC: 245719.

165930 Ibaraki, M. and Sudicky, E.A. 1995. "Colloid-Facilitated Contaminant Transport in Discretely Fractured Porous Media 2. Fracture Network Examples." *Water Resources Research, 31,* (12), 2961-2969. Washington, D.C.: American Geophysical Union. TIC: 252318.

148309 Karasaki, K.; Landsfeld, M.; and Grossenbacher, K. 1990. "Building of a Conceptual Model at the UE25-c Hole Complex." High Level Radioactive Waste Management, Proceedings of the International Topical Meeting, Las Vegas, Nevada, April 8-12, 1990. 2, 811-817. La Grange Park, Illinois: American Nuclear Society. TIC: 202058.

106313 Keeney-Kennicutt, W.L. and Morse, J.W. 1985. "The Redox Chemistry of $Pu(V)O^{+}_{2}$ Interaction with Common Mineral Surfaces in Dilute Solutions and Seawater." *Geochimica et Cosmochimica Acta, 49,* (12), 2577-2588. New York, New York: Pergamon. TIC: 237000.

103282 Kersting, A.B.; Efurd, D.W.; Finnegan, D.L.; Rokop, D.J.; Smith, D.K.; and Thompson, J.L. 1999. "Migration of Plutonium in Ground Water at the Nevada Test Site." *Nature, 397,* (6714), 56-59. London, England: Macmillan Journals. TIC: 243597.

162421 Kersting, A.P. and Reimus, P.W., eds. 2003. *Colloid-Facilitated Transport of Low-Solubility Radionuclides: A Field, Experimental, and Modeling Investigation.* UCRL-ID-149688. Livermore, California: Lawrence Livermore National Laboratory. TIC: 254176.

100909 Kotra, J.P.; Lee, M.P.; Eisenberg, N.A.; and DeWispelare, A.R. 1996. *Branch Technical Position on the Use of Expert Elicitation in the High-Level Radioactive Waste Program.* NUREG-1563. Washington, D.C.: U.S. Nuclear Regulatory Commission. TIC: 226832.

105039 LaBolle, E.M.; Fogg, G.E.; and Tompson, A.F.B. 1996. "Random-Walk Simulation of Transport in Heterogeneous Porous Media: Local Mass-Conservation Problem and Implementation Methods." *Water Resources Research, 32,* (3), 583-593. Washington, D.C.: American Geophysical Union. TIC: 245563.

100051 Langmuir, D. 1997. *Aqueous Environmental Geochemistry.* Upper Saddle River, New Jersey: Prentice Hall. TIC: 237107.

147527 Langmuir, D. and Herman, J.S. 1980. "The Mobility of Thorium in Natural Waters at Low Temperatures." *Geochimica et Cosmochimica Acta, 44,* 1753-1766. New York, New York: Pergamon Press. TIC: 237029.

171444 LANL (Los Alamos National Laboratories) 1984. *Quality Assurance Audit of Los Alamos National Laboratories (LANL) Nevada Nuclear Waste Storage Investigations (NNWSI) Project.* Los Alamos, New Mexico: Los Alamos National Laboratories. ACC: NNA.19870317.0482.

166306 LANL 2003. *Validation Test Plan (VTP) for the FEHM Application Version 2.21.* 10086-VTP-2.21-00. Los Alamos, New Mexico: Los Alamos National Laboratory. ACC: MOL.20031031.0264; MOL.20031031.0265.

156838 Leap, D.I. and Belmonte, P.M. 1992. "Influence of Pore Pressure on Apparent Dispersivity of a Fissured Dolomitic Aquifer." *Ground Water, 30,* (1), 87-95. Worthington, Ohio: Water Well Journal Publishing. TIC: 239275.

163781 LeBlanc, D.R.; Garabedian, S.P.; Hess, K.M.; Gelhar, L.W.; Quadri, R.D.; Stollenwerk, K.G.; and Wood, W.W. 1991. "Large-Scale Natural Gradient Tracer Test in Sand and Gravel, Cape Cod, Massachusetts 1. Experimental Design and Observed Tracer Movement." *Water Resources Research, 27,* (5), 895-910. Washington, D.C.: American Geophysical Union. TIC: 254593.

163821 Lichtner, P.C.; Kelkar, S.; and Robinson, B. 2002. "New Form of Dispersion Tensor for Axisymmetric Porous Media with Implementation in Particle Tracking." *Water Resources Research, 38,* (8), 21-1 through 21-16. Washington, D.C.: American Geophysical Union. TIC: 254597.

106684 Lieser, K.H. and Muhlenweg, U. 1988. "Neptunium in the Hydrosphere and in the Geosphere, I. Chemistry of Neptunium in the Hydrosphere and Sorption of Neptunium from Groundwaters on Sediments Under Aerobic and Anaerobic Conditions." *Radiochimica Acta, 43,* 27-35. Munchen, Germany: R. Oldenbourg Verlag. TIC: 236783.

106685 Lindberg, R.D. and Runnells, D.D. 1984. "Ground Water Redox Reactions: An Analysis of Equilibrium State Applied to Eh Measurements and Geochemical Modeling." *Science, 225,* 925-927. Washington, D.C.: American Association for the Advancement of Science. TIC: 224111.

171445 Los Alamos Scientific Laboratories 1979. *Audit of Los Alamos Scientific Laboratories Quality Assurance Program Plan for Nevada Nuclear Waste Storage Investigations.* Audit 79-5. Los Alamos, New Mexico: Los Alamos Scientific Laboratories. ACC: HQZ.19880629.5531.

100465 Luckey, R.R.; Tucci, P.; Faunt, C.C.; Ervin, E.M.; Steinkampf, W.C.; D'Agnese, F.A.; and Patterson, G.L. 1996. *Status of Understanding of the Saturated-Zone Ground-Water Flow System at Yucca Mountain, Nevada, as of 1995.* Water-Resources Investigations Report 96-4077. Denver, Colorado: U.S. Geological Survey. ACC: MOL.19970513.0209.

148312 Maloszewski, P. and Zuber, A. 1985. "On the Theory of Tracer Experiments in Fissured Rocks with a Porous Matrix." *Journal of Hydrology, 79,* 333-358. Amsterdam, The Netherlands: Elsevier. TIC: 222390.

162986 Marmier, N.; Delisée, A.; and Fromage, F. 1999. "Surface Complexation Modeling of Yb(III) and Cs(I) Sorption on Silica." *Journal of Colloid and Interface Science, 212,* (2), 228-233. New York, New York: Academic Press. TIC: 254530.

101464 Neuman, S.P. 1990. "Universal Scaling of Hydraulic Conductivities and Dispersivities in Geologic Media." *Water Resources Research, 26,* (8), 1749-1758. Washington, D.C.: American Geophysical Union. TIC: 237977.

155218 Nitsche, H.; Gatti, R.C.; Standifer, E.M.; Lee, S.C.; Müller, A.; Prussin, T.; Deinhammer, R.S.; Maurer, H.; Becraft, K.; Leung, S.; and Carpenter, S.A. 1993. *Measured Solubilities and Speciations of Neptunium, Plutonium, and Americium in a Typical Groundwater (J-13) from the Yucca Mountain Region.* LA-12562-MS. Los Alamos, New Mexico: Los Alamos National Laboratory. ACC: NNA.19930507.0136.

100163 Nitsche, H.; Roberts, K.; Prussin, T.; Muller, A.; Becraft, K.; Keeney, D.; Carpenter, S.A.; and Gatti, R.C. 1995. *Measured Solubilities and Speciations from Oversaturation Experiments of Neptunium, Plutonium and Americium in UE25p#1 Well Water from the Yucca Mountain Region*. LA-12563-MS. Los Alamos, New Mexico: Los Alamos National Laboratory. ACC: MOL.19951006.0171.

106920 Noell, A.L.; Thompson, J.L.; Corapcioglu, M.Y.; and Triay, I.R. 1998. "The Role of Silica Colloids on Facilitated Cesium Transport Through Glass Bead Columns and Modeling." *Journal of Contaminant Hydrology, 31,* (1-2), 23-56. Amsterdam, The Netherlands: Elsevier. TIC: 245510.

181692 NRC (U.S. Nuclear Regulatory Commission) 1989. *Nuclear Regulatory Commission Staff Safety Evaluation of U.S. Department of Energy Quality Assurance Program Description for the Office of Civilian Radioactive Waste Management*. Washington, D.C.: U.S. Nuclear Regulatory Commission. ACC: HQX.19910618.0038.

163274 NRC 2003. *Yucca Mountain Review Plan, Final Report.* NUREG-1804, Rev. 2. Washington, D.C.: U.S. Nuclear Regulatory Commission, Office of Nuclear Material Safety and Safeguards. TIC: 254568.

100783 Ogard, A.E. and Kerrisk, J.F. 1984. *Groundwater Chemistry Along Flow Paths Between a Proposed Repository Site and the Accessible Environment.* LA-10188-MS. Los Alamos, New Mexico: Los Alamos National Laboratory. ACC: HQS.19880517.2031.

165961 Oswald, J.G. and Ibaraki, M. 2001. "Migration of Colloids in Discretely Fractured Porous Media: Effect of Colloidal Matrix Diffusion." *Journal of Contaminant Hydrology, 52,* (1-4), 213-244. New York, New York: Elsevier. TIC: 255089.

162987 Pabalan, R.T.; Turner, D.R.; Bertetti, F.P.; and Prikryl, J.D. 1998. "Uranium^{VI} Sorption onto Selected Mineral Surfaces, Key Geochemical Parameters." *Adsorption of Metals by Geomedia.* Jenne, E.A., ed. Pages 99-130. New York, New York: Academic Press. TIC: 239504.

142177 Parkhurst, D.L. 1995. *User's Guide to PHREEQC—A Computer Program for Speciation, Reaction-Path, Advective-Transport, and Inverse Geochemical Calculations*. Water-Resources Investigations Report 95-4227. Lakewood, Colorado: U.S. Geological Survey. TIC: 248314.

162685 Pawloski, G.A. 1999. *Development of Phenomenological Models of Underground Nuclear Tests on Pahute Mesa, Nevada Test Site—BENHAM and TYBO.* UCRL-ID-136003. Livermore, California: Lawrence Livermore National Laboratory. ACC: MOL.20030926.0012.

100811 Penrose, W.R.; Polzer, W.L.; Essington, E.H.; Nelson, D.M.; and Orlandini, K.A. 1990. "Mobility of Plutonium and Americium Through a Shallow Aquifer in a Semiarid Region." *Environmental Science & Technology, 24,* 228-234. Washington, D.C.: American Chemical Society. TIC: 224113.

121957 Peters, R.R.; Klavetter, E.A.; Hall, I.J.; Blair, S.C.; Heller, P.R.; and Gee, G.W. 1984. *Fracture and Matrix Hydrologic Characteristics of Tuffaceous Materials from Yucca Mountain, Nye County, Nevada.* SAND84-1471. Albuquerque, New Mexico: Sandia National Laboratories. ACC: NNA.19900810.0674.

101466 Pollock, D.W. 1988. "Semianalytical Computation of Path Lines for Finite-Difference Models." *Ground Water, 26,* (6), 743-750. Worthington, Ohio: National Water Well Association. TIC: 226464.

162956 Reimus, P.W.; Haga, M.J.; Humphrey, A.R.; Counce, D.A.; Callahan, T.J.; and Ware, S.D. 2002. *Diffusion Cell and Fracture Transport Experiments to Support Interpretations of the BULLION Forced-Gradient Experiment.* LA-UR-02-6884. Los Alamos, New Mexico: Los Alamos National Laboratory. TIC: 253859.

163008 Reimus, P.W.; Ware, S.D.; Benedict, F.C.; Warren, R.G.; Humphrey, A.; Adams, A.; Wilson, B.; and Gonzales, D. 2002. *Diffusive and Advective Transport of ^{3}H, ^{14}C, and ^{99}Tc in Saturated, Fractured Volcanic Rocks from Pahute Mesa, Nevada*. LA-13891-MS. Los Alamos, New Mexico: Los Alamos National Laboratory. TIC: 253905.

101154 Robinson, B.A. 1994. "A Strategy for Validating a Conceptual Model for Radionuclide Migration in the Saturated Zone Beneath Yucca Mountain." *Radioactive Waste Management and Environmental Restoration, 19,* (1-3), 73-96. Yverdon, Switzerland: Harwood Academic Publishers. TIC: 222513.

100416 Robinson, B.A.; Wolfsberg, A.V.; Viswanathan, H.S.; Bussod, G.Y.; Gable, C.W.; and Meijer, A. 1997. *The Site-Scale Unsaturated Zone Transport Model of Yucca Mountain.* Milestone SP25BM3. Los Alamos, New Mexico: Los Alamos National Laboratory. ACC: MOL.19980203.0570.

101355 Rundberg, R.S.; Ogard, A.E.; and Vaniman, D.T., eds. 1985. *Research and Development Related to the Nevada Nuclear Waste Storage Investigations, April 1–June 30, 1984.* LA-10297-PR. Los Alamos, New Mexico: Los Alamos National Laboratory. ACC: NNA.19920922.0018.

106481 Rundberg, R.S.; Partom, I.; Ott, M.A.; Mitchell, A.J.; and Birdsell, K. 1987. *Diffusion of Nonsorbing Tracers in Yucca Mountain Tuff.* Milestone R524. Los Alamos, New Mexico: Los Alamos National Laboratory. ACC: NNA.19930405.0074.

162687 Smith, D.K. 2002. *Evaluation of the Radiochemistry of Near-Field Water Samples at the Nevada Test Site Applied to the Definition of a Hydrologic Source Team*. UCRL-ID-149049. Livermore, California: Lawrence Livermore National Laboratory. ACC: MOL.20030926.0013.

144658 Smith, P.A. and Degueldre, C. 1993. "Colloid-Facilitated Transport of Radionuclides Through Fractured Media." *Journal of Contaminant Hydrology, 13,* 143-166. Amsterdam, The Netherlands: Elsevier. TIC: 224863.

174109 SNL (Sandia National Laboratories) 2007. *Hydrogeologic Framework Model for the Saturated Zone Site-Scale Flow and Transport Model.* MDL-NBS-HS-000024 REV 01. Las Vegas, Nevada: Sandia National Laboratories. ACC: DOC.20070411.0003.

177424 SNL 2007. *Radionuclide Screening.* ANL-WIS-MD-000006 REV 02. Las Vegas, Nevada: Sandia National Laboratories. ACC: DOC.20070326.0003.

181650 SNL 2007. *Saturated Zone Flow and Transport Model Abstraction.* MDL-NBS-HS-000021 REV 03 AD 01. Las Vegas, Nevada: Sandia National Laboratories.

177394 SNL 2007. *Saturated Zone In-Situ Testing.* ANL-NBS-HS-000039 REV 02. Las Vegas, Nevada: Sandia National Laboratories. ACC: DOC.20070608.0004.

177391 SNL 2007. *Saturated Zone Site-Scale Flow Model.* MDL-NBS-HS-000011 REV 03. Las Vegas, Nevada: Sandia National Laboratories. ACC: DOC.20070626.0004.

177423 SNL 2007. *Waste Form and In-Drift Colloids-Associated Radionuclide Concentrations: Abstraction and Summary.* MDL-EBS-PA-000004 REV 03. Las Vegas, Nevada: Sandia National Laboratories.

100829 Stumm, W. and Morgan, J.J. 1981. *Aquatic Chemistry, An Introduction Emphasizing Chemical Equilibria in Natural Waters.* 2nd Edition. New York, New York: John Wiley & Sons. TIC: 208448.

148342 Sudicky, E.A. and Frind, E.O. 1981. "Carbon 14 Dating of Groundwater in Confined Aquifers: Implications of Aquitard Diffusion." *Water Resources Research, 17,* (4), 1060-1064. Washington, D.C.: American Geophysical Union. TIC: 247712.

105043 Sudicky, E.A. and Frind, E.O. 1982. "Contaminant Transport in Fractured Porous Media: Analytical Solutions for a System of Parallel Fractures." *Water Resources Research, 18,* (6), 1634-1642. Washington, D.C.: American Geophysical Union. TIC: 217475.

101160 Tang, D.H.; Frind, E.O.; and Sudicky, E.A. 1981. "Contaminant Transport in Fractured Porous Media: Analytical Solution for a Single Fracture." *Water Resources Research, 17,* (3), 555-564. Washington, D.C.: American Geophysical Union. TIC: 225358.

163782 Thorbjarnarson, K.W. and Mackay, D.M. 1994. "A Forced-Gradient Experiment on Solute Transport in the Borden Aquifer. 3. Nonequilibrium Transport of the Sorbing Organic Compounds." *Water Resources Research, 30,* (2), 401-419. Washington, D.C.: American Geophysical Union. TIC: 252320.

159212 Ticknor, K.V.; Vandergraaf, T.T.; McMurry, J.; Boisvenue, L.; and Wilkin, D.L. 1996. *Parametric Studies of Factors Affecting Se and Sn Sorption.* AECL-TR-723. Pinawa, Manitoba, Canada: Atomic Energy of Canada Limited, Whiteshell Laboratories. TIC: 223923.

162686 Tompson, A.F.B.; Bruton, C.J.; and Pawloski, G.A., eds. 1999. *Evaluation of the Hydrologic Source Term from Underground Nuclear Tests in Frenchman Flat at the Nevada Test Site: The CAMBRIC Test*. UCRL-ID-132300. Livermore, California: Lawrence Livermore National Laboratory. ACC: MOL.20030926.0014.

145195 Tompson, A.F.B.; Vomvoris, E.G.; and Gelhar, L.W. 1987. *Numerical Simulation of Solute Transport in Randomly Heterogeneous Porous Media: Motivation, Model Development, and Application*. UCID 21281. Livermore, California: Lawrence Livermore National Laboratory. ACC: MOL.19950131.0007.

145123 Triay, I.R.; Birdsell, K.H.; Mitchell, A.J.; and Ott, M.A. 1993. "Diffusion of Sorbing and Non-Sorbing Radionuclides." High Level Radioactive Waste Management, Proceedings of the Fourth Annual International Conference, Las Vegas, Nevada, April 26-30, 1993. 2, 1527-1532. La Grange Park, Illinois: American Nuclear Society. TIC: 208542.

101023 Triay, I.R.; Cotter, C.R.; Huddleston, M.H.; Leonard, D.E.; Weaver, S.C.; Chipera, S.J.; Bish, D.L.; Meijer, A.; and Canepa, J.A. 1996. *Batch Sorption Results for Neptunium Transport Through Yucca Mountain Tuffs.* LA-12961-MS. Los Alamos, New Mexico: Los Alamos National Laboratory. ACC: MOL.19980924.0050.

101024 Triay, I.R.; Furlano, A.C.; Weaver, S.C.; Chipera, S.J.; and Bish, D.L. 1996. *Comparison of Neptunium Sorption Results Using Batch and Column Techniques.* LA-12958-MS. Los Alamos, New Mexico: Los Alamos National Laboratory. ACC: MOL.19980924.0049.

104129 Triay, I.R.; Meijer, A.; Cisneros, M.R.; Miller, G.G.; Mitchell, A.J.; Ott, M.A.; Hobart, D.E.; Palmer, P.D.; Perrin, R.E.; and Aguilar, R.D. 1991. "Sorption of Americium in Tuff and Pure Minerals Using Synthetic and Natural Groundwaters." *Radiochimica Acta, 52/53,* 141-145. München, Germany: R. Oldenbourg Verlag. TIC: 222704.

100422 Triay, I.R.; Meijer, A.; Conca, J.L.; Kung, K.S.; Rundberg, R.S.; Strietelmeier, B.A.; and Tait, C.D. 1997. *Summary and Synthesis Report on Radionuclide Retardation for the Yucca Mountain Site Characterization Project.* Eckhardt, R.C., ed. LA-13262-MS. Los Alamos, New Mexico: Los Alamos National Laboratory. ACC: MOL.19971210.0177.

164633 Turin, H.J.; Groffman, A.R.; Wolfsberg, L.E.; Roach, J.L.; and Strietelmeier, B.A. 2002. "Tracer and Radionuclide Sorption to Vitric Tuffs of Busted Butte, Nevada." *Applied Geochemistry, 17,* (6), 825-836. New York, New York: Pergamon. TIC: 254046.

162989 Turner, D.R.; Pabalan, R.T.; and Bertetti, F.P. 1998. "Neptunium(V) Sorption on Montmorillonite: An Experimental and Surface Complexation Modeling Study." *Clays and Clay Minerals, 46,* (3), 256-269. Boulder, Colorado: Clay Minerals Society. TIC: 254532.

154495 USGS (U.S. Geological Survey) n.d. Bulk Density. Denver, Colorado: U.S. Geological Survey. ACC: NNA.19940406.0076.

144579 Valocchi, A.J. 1985. "Validity of the Local Equilibrium Assumption for Modeling Sorbing Solute Transport Through Homogeneous Soils." *Water Resources Research, 21,* (6), 808-820. Washington, D.C.: American Geophysical Union. TIC: 223203.

101064 Waddell, R.K.; Robison, J.H.; and Blankennagel, R.K. 1984. *Hydrology of Yucca Mountain and Vicinity, Nevada-California--Investigative Results Through Mid-1983.* Water-Resources Investigations Report 84-4267. Denver, Colorado: U.S. Geological Survey. ACC: NNA.19870406.0343.

130510 Wen, X-H. and Gomez-Hernandez, J.J. 1996. "The Constant Displacement Scheme for Tracking Particles in Heterogeneous Aquifers." *Ground Water, 34,* (1), 135-142. Worthington, Ohio: Water Well Journal Publishing. TIC: 246656.

100191 Wilson, M.L.; Gauthier, J.H.; Barnard, R.W.; Barr, G.E.; Dockery, H.A.; Dunn, E.; Eaton, R.R.; Guerin, D.C.; Lu, N.; Martinez, M.J.; Nilson, R.; Rautman, C.A.; Robey, T.H.; Ross, B.; Ryder, E.E.; Schenker, A.R.; Shannon, S.A.; Skinner, L.H.; Halsey, W.G.; Gansemer, J.D.; Lewis, L.C.; Lamont, A.D.; Triay, I.R.; Meijer, A.; and Morris, D.E. 1994. *Total-System Performance Assessment for Yucca Mountain – SNL Second Iteration (TSPA-1993).* SAND93-2675. Executive Summary and two volumes. Albuquerque, New Mexico: Sandia National Laboratories. ACC: NNA.19940112.0123.

163823 Winterle, J.R.; Claisse, A.; and Arlt, H.D. 2003. "An Independent Site-Scale Groundwater Flow Model for Yucca Mountain." *Proceedings of the 10th International High-Level Radioactive Waste Management Conference (IHLRWM), March 30-April 2, 2003, Las Vegas, Nevada.* Pages 151-158. La Grange Park, Illinois: American Nuclear Society. TIC: 254559.

162688 Wolfsberg, A.; Glascoe, L.; Lu, G.; Olson, A.; Lichtner, P.; McGraw, M.; Cherry, T.; and Roemer, G. 2002. *TYBO/BENHAM: Model Analysis of Groundwater Flow and Radionuclide Migration from Underground Nuclear Tests in Southwestern Pahute Mesa, Nevada*. LA-13977. Los Alamos, New Mexico: Los Alamos National Laboratory. ACC: MOL.20030926.0009.

154702 Zheng, C. and Bennett, G.D. 1995. *Applied Contaminant Transport Modeling, Theory and Practice.* New York, New York: Van Nostrand Reinhold. TIC: 249865.

110491 Zyvoloski, G.A.; Robinson, B.A.; Dash, Z.V.; and Trease, L.L. 1997. *Summary of the Models and Methods for the FEHM Application—A Finite-Element Heat- and Mass-Transfer Code.* LA-13307-MS. Los Alamos, New Mexico: Los Alamos National Laboratory. TIC: 235587.

9.2 CODES, STANDARDS, REGULATIONS, AND PROCEDURES

176567 10 CFR 50. 2006. Energy: Domestic Licensing of Production and Utilization Facilities. Internet Accessible.

180319 10 CFR 63. 2007. Energy: Disposal of High-Level Radioactive Wastes in a Geologic Repository at Yucca Mountain, Nevada. Internet Accessible.

IM-PRO-002, *Control of the Electronic Management of Information*.

IM-PRO-003, *Software Management*.

LP-2.29Q-BSC, *Planning For Science Activities*.

SCI-PRO-001, *Qualification of Unqualified Data*.

SCI-PRO-002, *Planning For Science Activities*.

SCI-PRO-006, *Models*.

9.3 SOURCE DATA, LISTED BY DATA TRACKING NUMBER

162910 GS010308312322.002. Chemical and Isotopic Data from Wells in Yucca Mountain Area, Nye County, Nevada, Collected between 12/11/98 and 11/15/99. Submittal date: 03/29/2001.

154734 GS010308312322.003. Field, Chemical and Isotopic Data from Wells in Yucca Mountain Area, Nye County, Nevada, Collected Between 12/11/98 and 11/15/99. Submittal date: 03/29/2001.

163555 GS010908312332.002. Borehole Data from Water-Level Data Analysis for the Saturated Zone Site-Scale Flow and Transport Model. Submittal date: 10/02/2001.

162911 GS011108312322.006. Field and Chemical Data Collected between 1/20/00 and 4/24/01 and Isotopic Data Collected between 12/11/98 and 11/6/00 from Wells in the Yucca Mountain Area, Nye County, Nevada. Submittal date: 11/20/2001.

179422 GS040108312322.001. Field and Chemical Data Collected Between 10/4/01 and 10/3/02 and Isotopic Data Collected Between 5/19/00 and 5/22/03 from Wells in the Yucca Mountain Area, Nye County, Nevada. Submittal date: 06/07/2004.

145763 GS930208318523.001. Temperature and Thermal Conductivity in Wells Near Yucca Mountain. Submittal date: 02/16/1993.

145530 GS930308312323.001. Chemical Composition of Groundwater and the Locations of Permeable Zones in the Yucca Mountain Area. Submittal date: 03/05/1993.

145404 GS930908312323.003. Hydrochemical Data from Field Test and Lab Analyses of Water Samples Collected at Field Stations: USW VH-1, JF3, UE-29 UZN#91, Virgin Spring, Nevares Spring, UE-25 J#12, UE-25 J#13, UE-22 ARMY#1, and USW UZ-14. Submittal date: 09/30/1993.

148114 GS950808312322.001. Field, Chemical, and Isotopic Data Describing Water Samples Collected in Death Valley National Monument and at Various Boreholes in and Around Yucca Mountain, Nevada, Between 1992 and 1995. Submittal date: 08/16/1995.

145606 GS960308312133.001. Water Quality Data from Samples Collected in the Fortymile Wash Watershed, Yucca Mountain Area, Nevada, Water Year 1995. Submittal date: 03/27/1996.

182207 GS970700012847.002. Water-Quality Data from a Sample Collected at Well UE-25 C#3 on 5/18/95. Submittal date: 07/02/1997.

182209 GS970708312314.004. Water Chemistry Data from Three Samples Collected at Well UE-25 C#3, 12/4/96, 2/19/97, and 6/12/97. Submittal date: 07/16/1997.

149980 GS971000012847.004. Water Quality Data Collected from Springs and Wells in the Yucca Mountain Region from May 6, 1997 to May 15, 1997. Submittal date: 10/23/1997.

182212 GS980308312314.001. Water-Quality Data from a Suite of Samples Collected at UE-25 C #3 on 10/21/97. Submittal date: 03/26/1998.

145412 GS980908312322.008. Field, Chemical, and Isotopic Data from Precipitation Sample Collected Behind Service Station in Area 25 and Ground Water Samples Collected at Boreholes UE-25 C #2, UE-25 C #3, USW UZ-14, UE-25 WT #3, UE-25 WT #17, and USW WT-24, 10/06/97 to 07/01/98. Submittal date: 09/15/1998.

145611 GS990608312133.001. Ground-Water Quality Data. Submittal date: 06/09/1999.

107144 LA000000000086.002. Mineralogic Variation in Drill Core UE-25 UZ#16 Yucca Mountain, Nevada. Submittal date: 03/28/1995.

149557 LA0003JC831362.001. Preliminary Matrix Diffusion Coefficients for Yucca Mountain Tuffs. Submittal date: 4/10/2000.

156870 LA0109MD831341.001. Adsorption of NP-237 in Three Types of Alluvium as a Function of Time and Stratigraphic Position. Submittal date: 09/14/2001.

160051 LA0206AM831234.001. Eh-pH Field Measurements on Nye County EWDP Wells. Submittal date: 06/21/2002.

163852 LA0206AM831234.002. Geochemical Field Measurements on Nye County EWDP Wells. Submittal date: 06/21/2002.

162433 LA0301AA831352.001. Experiments on Pu(V)-Colloid Transport in Columns Packed with Material from Nye County Borehole 19D, Zone 4. Submittal date: 01/23/2003.

162435 LA0301PR831361.003. Breakthrough Curves of Tritium, Plutonium, and Various Colloids in Saturated UE20C Fractured Cores from the Nevada Test Site. Submittal date: 01/22/2003.

162436 LA0301PR831361.004. Breakthrough Curves of Tritium, Plutonium, and Various Colloids in Saturated PM-1 and PM-2 Fractured Cores from the Nevada Test Site. Submittal date: 01/22/2003.

163783 LA0302HV831361.001. A Study of Kinetic Reaction Rates for Plutonium Sorption in Devitrified Tuffs. Submittal date: 02/10/2003.

164956 LA0302MD831341.001. Iodine-129 Sorption in Alluvium from NCEWDP Wells 19IM1A, 10SA, and 22SA Under Ambient Conditions. Submittal date: 02/13/2003.

164957 LA0302MD831341.002. Technetium-99 Sorption in Alluvium from NCEWDP Wells 19IM1A, 10SA, and 22SA Under Ambient Conditions. Submittal date: 02/11/2003.

163784 LA0302MD831341.003. Neptunium-237 Sorption in Alluvium from NC-EWDP Wells 19IM1A, 10SA, and 22SA Under Ambient Conditions. Submittal date: 02/11/2003.

163785 LA0302MD831341.004. Uranium Sorption in Alluvium from NC-EWDP Wells 19IM1A, 10SA, and 22SA Under Ambient Conditions. Submittal date: 02/11/2003.

163558 LA0303HV831352.002. Colloid Retardation Factors for the Saturated Zone Fractured Volcanics. Submittal date: 03/31/2003.

163559 LA0303HV831352.004. Colloid Retardation Factors for the Saturated Zone Alluvium. Submittal date: 03/31/2003.

163789 LA0305AM831341.001. 1977 to 1987 Sorption Measurements of AM, BA, CS, NP, PU, PA, SR, TH, and U with Yucca Mountain Tuff Samples. Submittal date: 05/21/2003.

165865 LA0310AM831341.001. Sorption/Desorption Measurements of Cesium on Yucca Mountain Tuff. Submittal date: 10/21/2003.

166068 LA0311EK831232.001. Hydrochemical Data Obtained from GEOCHEM.02 Database. Submittal date: 11/06/2003.

180903 LA0401MD831322.001. Quantitative X-Ray Diffraction Analyses of Mineral Abundances for Alluvium Samples from NC-EWDP-19D and 19P Wells. Submittal date: 01/21/2004.

180904 LA0401MD831322.002. Quantitative X-Ray Diffraction Analyses of Mineral Abundances for Alluvium Samples from NC-EWDP-19IM1A, 10SA, and 22SA Wells. Submittal date: 01/21/2004.

180905 LA0401MD831322.003. Quantitative X-Ray Diffraction Analyses of Mineral Abundances for Alluvium Samples from NC-EWDP-02D, 09SX and 3S Wells. Submittal date: 01/21/2004.

166696 LA0401MD831361.001. U-233 Column Tests Performed on Alluvium from NC-EWDP Wells 19IM1A, 10SA, and 22SA Under Ambient Conditions. Submittal date: 01/08/2004.

166726 LA0401PR831361.001. Column Studies Using G4-268 Devitrified Tuff with J-13 Well Water and Radionuclides (H-3 and Pu-239). Submittal date: 01/13/2004.

170623 LA0407AM831341.001. Batch Sorption Coefficient Data for Barium on Yucca Mountain Tuffs in Representative Water Compositions. Submittal date: 07/12/2004.

170621 LA0407AM831341.002. Batch Sorption Coefficient Data for Cesium on Yucca Mountain Tuffs in Representative Water Compositions. Submittal date: 07/12/2004.

170626 LA0407AM831341.003. Batch Sorption Coefficient Data for Strontium on Yucca Mountain Tuffs in Representative Water Compositions. Submittal date: 07/12/2004.

170622 LA0407AM831341.004. Batch Sorption Coefficient Data for Neptunium on Yucca Mountain Tuffs in Representative Water Compositions. Submittal date: 07/12/2004.

170625 LA0407AM831341.005. Batch Sorption Coefficient Data for Plutonium on Yucca Mountain Tuffs in Representative Water Compositions. Submittal date: 07/12/2004.

170628 LA0407AM831341.006. Batch Sorption Coefficient Data for Uranium on Yucca Mountain Tuffs in Representative Water Compositions. Submittal date: 07/12/2004.

180913 LA0408MD831341.001. Uranium-233 Sorption in Alluvium from NCEWDP Wells 19IM1A and 22SA Under Ambient Conditions Using 19D Zone 4 Water. Submittal date: 08/11/2004.

180727 LA0408MD831341.002. Kinetic of Uranium-233 Sorption in Alluvium from NCEWDP Well 19IM1A Under Ambient Conditions. Submittal date: 08/11/2004.

180728 LA0408MD831341.003. Kinetic of Uranium-233 Sorption in Alluvium from NCEWDP Well 10SA Under Ambient Conditions. Submittal date: 08/11/2004.

180729 LA0408MD831341.004. Kinetic of Uranium-233 Sorption in Alluvium from NCEWDP Well 22SA Under Ambient Conditions. Submittal date: 08/11/2004.

180917 LA0408MD831341.005. Multistep Batch Desorption Experiments of Sorbed Uranium-233 in Alluvium from NC-EWDP Wells 19IM1A and 10SA Under Ambient Conditions. Submittal date: 08/16/2004.

180927 LA0408MD831341.007. Neptunium-237/Tritium Flow through Column Experiment Performed on Saturated Alluvium from NC-EWDP-19D Well (Test #1). Submittal date: 08/16/2004.

181187 LA0408PR831341.001. Analyses Conducted to Explain Early Column Breakthroughs of Np and U. Submittal date: 08/02/2004.

180928 LA0409MD831341.001. Neptunium-237/Tritium Flow through Column Experiment Performed on Saturated Alluvium from NC-EWDP-19D Well (Test #2) (Flow Rate: 3 ML/H). Submittal date: 09/07/2004.

180929 LA0409MD831341.002. Neptunium-237/Tritium Flow through Column Experiment Performed on Saturated Alluvium from NC-EWDP-19D Well (Test #3) (Flow Rate: 0.6 ML/H). Submittal date: 09/07/2004.

180930 LA0409MD831341.003. Neptunium-237/Tritium Flow through Column Experiment Performed on Saturated Alluvium from NC-EWDP-19D Well (Test #4) (Flow Rate: 10 ML/H). Submittal date: 09/07/2004.

180925 LA0409MD831341.004. Neptunium-237/Tritium Flow through Column Experiment Performed on Saturated Alluvium from NC-EWDP-03S Well (Test #1) (Flow Rate: 2 ML/H). Submittal date: 09/07/2004.

180926 LA0409MD831341.005. Neptunium-237/Tritium Flow through Column Experiment Performed on Saturated Alluvium from NC-EWDP-03S Well (Test #2, Flow Rate: 2 ML/H). Submittal date: 09/07/2004.

180743 LA0410AM831232.002. Field Saturated Zone Water Chemistry Investigations: In-Situ Measurements. Submittal date: 10/07/2004.

182089 LA0410MD831341.001. Continue Flow Desorption Experiments of Sorbed Uranium-233 in Alluvium from NC-EWDP Wells 19IM1A and 10SA Under Ambient Conditions. Submittal date: 09/30/2004.

180906 LA0412MD831341.001. Specific Surface Area of Yucca Mountain Alluvium. Submittal date: 12/01/2004.

180908 LA0412MD831341.002. Neptunium Adsorption onto Alluvium in 19D Ground Water and Nano Pure Water. Submittal date: 12/01/2004.

180911 LA0412MD831341.003. Neptunium Adsorption onto Alluvium in Solutions with Different Ionic Strength. Submittal date: 12/03/2004.

181078 LA0412MD831341.004. Neptunium Adsorption in 19D Alluvium as a Function of Time. Submittal date: 12/03/2004.

175769 LA0511SK831214.001. Hydraulic Gradient at Yucca Mountain for the Purpose of Stochastic Modeling for Derivation of Compsite Upscaled KD Distributions. Submittal date: 11/17/2005.

179438 LA0612RR150304.003. Geochemical and Isotopic Data for Selected NC-EWDP Wells, Phases II, III and IV. Submittal date: 01/02/2007.

179306 LA0702AM831341.001. Se (Selenium) and Sn (Tin) Sorption on Yucca Mountain Rock Samples. Submittal date: 12/14/2006.

181314 LA0702CS150304.001. Model Fits of Fraction Sorbed vs. Time Curves from Np-237 Long-Term Column Desorption from Yucca Mountain Alluvium. Submittal date: 05/08/2007.

181313 LA0702CS150304.002. Calculation of Effective Kd Values from Column Desorption of Np-237 from Yucca Mountain Alluvium. Submittal date: 05/09/2007.

181312 LA0702CS150304.003. Model Fits of Fraction Sorbed vs. Time Curves from U-233 Long-Term Column Desorption from Yucca Mountain Alluvium. Submittal date: 05/09/2007.

181311 LA0702CS150304.004. Calculation of Effective Kd Values from Column Desorption of U-233 from Yucca Mountain Alluvium. Submittal date: 05/09/2007.

181762 LA0705CS150304.001. Results of Quantitative X-Ray Diffraction Analysis of Alluvium (Sieved and Recombined <75 Micrometers to 2000 Micrometers Size Fraction from SPC01022965, SPC01022975, SPC01022984). Submittal date: 05/31/2007

181309 LA0705MD150304.001. Constituents Concentrations in Groundwaters Collected from NE-EWDP-19P and NE-EWDP-03S Wells. Submittal date: 05/17/2007.

149209 LA9907AM831234.009. Flow-through Cell Measurements for NC-EWDP-01S, NC-EWDP-03S, NC-EWDP-09SX, 5/17/99, 5/18/99, 5/19/99, 5/20/99. Submittal date: 01/27/2000.

149212 LA9907AM831234.011. Flow-Through Cell Measurements for AD-2, 10-Jun-99. Submittal date: 01/27/2000.

149520 LAAM831311AQ98.007. Flow-Thru Cell and Static Measurements at UE-25 WT#3, 22-Jun-98. Submittal date: 09/14/1998.

149522 LAAM831311AQ98.010. Static Measurements for UE-25 WT#17, 01 Jul 98. Submittal date: 09/14/1998.

109044 LADV831321AQ99.001. Quantitative XRD Results for the USW SD-6 and USW WT-24 Drill Core Samples. Submittal date: 04/16/1999.

109004 LAJC831321AQ98.005. Quantitative XRD Results for Drill Core USW SD-7, USW SD-9, USW SD-12 and UE-25 UZ#16. Submittal date: 10/27/1998.

109047 LASC831321AQ98.001. Results of Real-Time Analysis for Erionite in Drill Hole USWWT-24, Yucca Mountain, Nevada. Submittal date: 02/10/1998.

151029 MO0006J13WTRCM.000. Recommended Mean Values of Major Constituents in J-13 Well Water. Submittal date: 06/07/2000.

151524 MO0007MAJIONPH.011. Major Ion Content of Groundwater from Selected Yucca Mountain Project Boreholes Extracted from ANL-NBS-HS-000021, Geochemical and Isotopic Constraints on Groundwater Flow Directions, Mixing and Recharge at Yucca Mountain, Nevada. Submittal date: 07/27/2000.

155229 MO0010CPORGLOG.002. Calculated Porosity from Geophysical Logs Data from "Old 40" Boreholes. Submittal date: 10/16/2000.

163795 MO0101XRDDRILC.002. XRD Analyses of Drill Core from Boreholes UE-25 A#1 and USW G-2. Submittal date: 01/26/2001.

163796 MO0101XRDMINAB.001. XRD Analyses of Drill Core from Boreholes UE-25B#1, USW G-1, USW G-3, USW GU-3, and USW G-4. Submittal date: 01/26/2001.

163480 MO0105GPLOG19D.000. Geophysical Log Data from Borehole NC EWDP 19D. Submittal date: 05/31/2001.

163797 MO0106XRDDRILC.003. XRD Analyses of Drill Core from Borehole USW H-6. Submittal date: 06/08/2001.

155989 MO0109HYMXPROP.001. Matrix Hydrologic Properties Data. Submittal date: 09/17/2001.

171437 MO0408K8313211.000. Mineralogic Variation in Drill Holes. Submittal date: 08/27/2004.

176868 MO0604SPAPHR25.001. PHREEQC Data 0 Thermodynamic Database for 25 Degrees C - File: PHREEQCDATA025.DAT. Submittal date: 04/10/2006.

180723 MO0608DOE19MZ1.000. Column Desorption of Np-237 from Alluvium NC-EWDP-19IM1A in 19D Zone 1 Groundwater. Submittal date: 08/28/2006.

180724 MO0608DOENP2Z4.000. Column Desorption of Np-237 from Alluvium NC-EWDP-22SA in 19D Zone 4 Groundwater. Submittal date: 08/28/2006.

180726 MO0608DOENPMZ4.000. Column Desorption of Np-237 from Alluvium NC-EWDP-19IM1A in 19D Zone 4 Groundwater. Submittal date: 08/28/2006.

180725 MO0608DOENPSZ1.000. Column Desorption of Np-237 from Alluvium NC-EWDP-22SA in 19D Zone 1 Groundwater. Submittal date: 08/28/2006.

180720 MO0608DOEU19Z1.000. Column Desorption of U-233 from Alluvium NC-EWDP-19IM1A in 19D Zone 1 Groundwater. Submittal date: 08/28/2006.

180719 MO0608DOEU19Z4.000. Column Desorption of U-233 from Alluvium NC-EWDP-19IM1A in 19D Zone 4. Submittal date: 08/28/2006.

180718 MO0608DOEU22Z1.000. Column Desorption of U-233 from Alluvium NC-EWDP-22SA in 19D Zone 1 Groundwater. Submittal date: 08/28/2006.

180717 MO0608DOEU22Z4.000. Column Desorption of U-233 from Alluvium NC-EWDP-22SA in 19D Zone 4 Groundwater. Submittal date: 08/28/2006.

180721 MO0608DOEUS10S.000. Column Desorption of U-233 from Alluvium NC-EWDP-10SA in 10S Groundwater. Submittal date: 08/28/2006.

179310 MO0701PAGROUND.000. Groundwater Colloid Concentration Parameters. Submittal date: 01/18/2007.

180392 MO0701PAKDSUNP.000. Colloidal KdS for U, Np, Ra and Sn. Submittal date: 04/17/2007.

180391 MO0701PASORPTN.000. Colloidal Sorption Coefficients for Pu, Am, Th, Cs, and Pa. Submittal date: 04/17/2007.

181613 MO0706SPAFEPLA.001. FY 2007 LA FEP List and Screening. Submittal date: 06/20/2007.

155045 SN0004T0501399.003. Statistical Summary of Porosity Data. Submittal date: 04/13/2000.

168763 SN0310T0502103.009. Revised Saturated Zone Transport Abstraction Model Uncertain Inputs. Submittal date: 10/09/2003.

178956 SN0612T0510106.004. Saturated Zone (SZ) Site-Scale Flow Model Pest and FEHM Files Using HFM2006. Submittal date: 01/17/2007.

179575 SN0702T0510106.006. Saturated Zone (SZ) Site-Scale Flow Model with “Water Table Rise” Alternate Conceptual Model - FEHM Files Using HFM2006. Submittal date: 02/19/2007.

182006 SN0705FLUORINE.001. Fluorine Abundance Data from UE-25 P#1 Taken on February 09,1983. Submittal date: 07/17/2007.

182007 SN0706INPUTSZF.000. Updated or New Inputs Used In the SZ Flow and Transport Abstraction Model and the SZ One-Dimensional Transport Model. Submittal date: 07/17/2007.

9.4 OUTPUT DATA, LISTED BY DATA TRACKING NUMBER

LA0702AM150304.001. Probability Distribution Functions and Cross-Radionuclide Correlations for Sampling of Sorption Coefficient Probability Distributions in the SZ at the YM. Submittal date: 08/16/2007.

LA0302RP831228.001. Type Curve Data for FEHM Macro "SPTR" Based on Sudicky and Frind Solution. Submittal date: 02/11/2003.

LA0702MD831232.001. Input Data Sets for Modeling Calculation of Radionuclide Sorption on Yucca Mountain Volcanic Tuff. Submittal date: 07/26/2007.

LA0702SK150304.001. SZ Transport Model, FEHM Input Files for Base Case. Submittal date: 02/07/2007.

LA0702MD831232.002. Modeling Calculation of Radionuclide Sorption on Yucca Mountain Volcanic Tuff. Submittal date: 07/26/2007.

LA0703SK150304.001. Base Case SZ Transport Model. Submittal date: 07/05/2007.

LA0703SK150304.002. Input Uncertainty Propagation, SZ Transport Model, FEHM Input & Output Files: Specific Discharge Multiplier and Horizontal Permeability Anisotropy Ratio. Submittal date: 07/05/2007.

LA0703SK150304.003. Input Uncertainty Propagation, SZ Transport Model, FEHM Input & Output Files: Dispersivity, Effective Diffusion Coefficient in Volcanics, Matrix Sorption Coefficient in Volcanics, Effective Porosity in Alluvium and Bulk Density in Alluvium. Submittal date: 07/05/2007.

LA0703SK150304.004. Input Uncertainty Propagation, SZ Transport Model, FEHM Input & Output Files: Colloid Retardation Factor for Irreversible Colloids in Alluvium and Volcanics. Submittal date: 04/20/2007.

LA0703SK150304.005. Input Uncertainty Propagation, SZ Transport Model, FEHM Input & Output Files: Flowing Interval Aperture and Porosity in Volcanics. Submittal date: 04/20/2007.

LA0703SK150304.006. Input Uncertainty Propagation, SZ Transport Model, FEHM INPUT & Output Files: Sorption Coefficient in Alluvium, Reversible Sorption onto Colloids and Reversible Colloids with High Filtration in Volcanics. Submittal date: 07/05/2007.

LA0703SK150304.007. Performance of SZ as a Natural Barrier: Part 1. Submittal date: 07/05/2007.

LA0703SK150304.008. Performance of SZ as a Natural Barrier: Part 2. Submittal date: 07/05/2007.

LA0703SK150304.009. SZ Transport, Breakthrough Curves at Volcanic/Alluvium Boundary. Submittal date: 07/05/2007.

LA0703SK150304.010. Performance of SZ as a Natural Barrier: Part 3. Submittal date: 04/20/2007.

LA0703SK150304.011. Water Table Rise due to Future Climate Change. Submittal date: 04/20/2007.

LA0309RP831321.001. Calculation of the Rock Type Distributions, SZ Transport Model. Submittal date: 09/23/2003.

LA0309RP831341.004. Calculation of Kd Distributions for Uranium. Submittal date: 09/29/2003.

LA0309RP831341.001. Calculation of Kd Distributions for Cesium. Submittal date: 09/29/2003.

LA0309RP831341.002. Calculation of Kd Distributions for Neptunium. Submittal date: 09/30/2003.

LA0309RP831341.003. Calculation of Kd Distributions for Plutonium. Submittal date: 09/30/2003.

9.5 DEVELOPED DATA, LISTED BY DATA TRACKING NUMBER

MO0707SURFCOMP.000. Sensitivity of Surface Complexation Model Using PHREEQC to DO, Fe, and Mn Concentrations. Submittal date: 07/30/2007.

9.6 SOFTWARE CODES

149117 calc_cdf.c V. 1.0. 2000. SUN O.S. 5.7. STN: 10924-1.0-00.

163836 cr8sptr.c V. 2.0. 2002. SUN, SunO.S. 5.7. 10927-2.0-00.

167994 EARTHVISION V. 5.1. 2000. IRIX 6.5. STN: 10174-5.1-00.

161725 FEHM V. 2.20. 2003. SUN 9.S. 5.7 & 5.8, Windows 2000, RedHat Linux 7.1. STN: 10086-2.20-00.

179419 FEHM V. 2.24-01. 2007. WIN2003, 2000, & XP, Red Hat Linux 2.4.21, OS 5.9. STN: 10086-2.24-01-00.

165754 fehm2post V. 1.0. 2003. WINDOWS 2000, SUN O.S. 5.8&5.7, Redhat Linux 2.4.18. STN: 11031-1.0-00.

181225 fehm2post V. 1.0. 2005. OS 5.9. STN: 11031-1.0-01.

164509 FRACT_p V. 1.0. 2003. PC, LINUX 2.4.18. 11009-1.0-00.

163837 GS2FEHM.C V. 1.0. 2002. SUN, SunO.S. 5.7. 10923-1.0-00.

153099 GSLIB V. 1.0GAMV3V1.201. 2000. SUN w/Unix OS. 10398-1.0GAMV3V1.201-00.

149114 GSLIB V2.0 MSISIM V. 2.0. 2000. 10098-2.0MSISIMV2.0-00.

157837 PHREEQC V. 2.3. 2002. PC. 10068-2.3-01.

159065 RELAP V. 2.0. 2002. PC, Windows 2000/NT. 10551-2.0-00.

APPENDIX A
TECHNICAL BASIS FOR SORPTION-COEFFICIENT PROBABILITY DISTRIBUTION FUNCTIONS

APPENDIX A: TECHNICAL BASIS FOR SORPTION-COEFFICIENT PROBABILITY DISTRIBUTION FUNCTIONS

A1. INTRODUCTION

This appendix provides the bases for the derivation of sorption-coefficient probability distributions used in the saturated zone (SZ) transport model. These distributions (Table A-4) in conjunction with the analysis presented in Appendix C lead to the recommended composite distributions for K_ds (Table C-14) and correlations for sampling sorption coefficient probability distributions (Table A-6) that form a technical product output of this report (Output DTN: LA0702AM150304.001). The data needed as inputs to the analysis presented in this appendix are treated as being "direct input" to the site-scale SZ transport model. The sorption-coefficient data on which the distributions are based were obtained in laboratory experiments in which representative rock samples from the Yucca Mountain site were contacted with groundwaters (or simulated groundwaters) representative of the site, spiked with one or more of the elements of interest. Sorption experiments were carried out as a function of rock type, time, element concentration, atmospheric composition, grain size, and temperature. In some cases, the solids remaining from sorption experiments were contacted with unspiked groundwater in desorption experiments. The sorption and desorption experiments together provide information on the equilibration rates of the sorption reactions.

For elements that sorb primarily through surface-complexation reactions, the experimental data are augmented with the results of modeling calculations using PHREEQC (PHREEQC V2.3, STN: 10068-2.3-01, [DIRS 157837]) with the thermodynamic input data file *PHREEQCDATA025.DAT* (DTN: MO0604SPAPHR25.001 [DIRS 176868]). The inputs for the modeling calculations include groundwater compositions, rock surface areas, binding constants for the elements of interest, and thermodynamic data for solid and solution species (Table 4-1). These modeling calculations provide a basis for interpolation and extrapolation of the experimentally derived sorption-coefficient data set.

The primary controls on sorption behavior of the elements of interest in the saturated zone at Yucca Mountain include the detailed characteristics of mineral surfaces in the rock units through which water flows in the saturated zone, the detailed chemistry of groundwater in the saturated zone, the sorption behavior of each element, and the concentrations of the various radionuclides in the waters. These parameters will be discussed in the following sections.

As noted in *Saturated Zone Flow and Transport Model Abstraction* (SNL 2007 [DIRS 181650]), the SZ transport model uses a stochastic approach to calculate the transport rates of radionuclides of interest. In this approach, each realization (i.e., calculation involving a single radionuclide) selects a single value for the "equivalent" sorption coefficient of each radionuclide from a probability distribution that reflects the uncertainty in "equivalent" sorption-coefficient values in the saturated volcanic section or the alluvial section. The "equivalent" sorption coefficient is a sorption coefficient that would result in a breakthrough curve with characteristics similar to the breakthrough curve that would be obtained if separate sorption coefficient values were derived (reflecting local conditions) for each node in the SZ transport calculation. This appendix provides probability distributions for each element of interest on the two major rock types (devitrified and zeolitic tuff) found in the saturated volcanic section. It also provides probability

distributions for sorption coefficients in alluvium. The impact of possible variations in water chemistry, radionuclide concentrations, and variations in rock surface properties within the major rock types and alluvium were incorporated into the probability distributions. The distribution types selected were based in part on actual experimental data and in part on professional judgment regarding the impact of variables not considered in the experimental program. For example, there are potential impacts from variations in water and rock compositions outside those addressed in the experimental program (e.g., pH, Eh, variations in surface areas, variations in mineralogical composition, etc.). In the case of mineralogical composition, an attempt was made to emphasize those experiments that used samples closest to the average composition of the hydrologic units as defined in the transport model. Thus, experimental data points for devitrified tuff samples containing significant quantities of clays were discounted.

This analysis of sorption coefficients focuses on room temperature conditions. Available data show little statistical variation in the sorption coefficient values up to 80°C (DTNs: LA0407AM831341.002 [DIRS 170621], LA0407AM831341.003 [DIRS 170626]). Temperatures in the saturated zone are expected to be in the neighborhood of 35°C (DTN: GS930208318523.001 [DIRS 145763]). Hence, sorption coefficient values at elevated temperatures are not discussed in this model report.

A2. AQUIFER MATRIX COMPOSITIONS ALONG MOST PROBABLE TRANSPORT PATHWAYS

Sources of data on aquifer matrix compositions in the saturated zone are provided in Table C-1. These data have been incorporated into *Mineralogic Model (MM3.0) Report* (BSC 2004 [DIRS 170031]). There are two dominant rock types in the saturated zone along potential flow paths in volcanics to the 18-km boundary: devitrified tuff and zeolitic tuff. Devitrified tuff is composed primarily of silica (quartz and cristobalite) and alkali feldspar. It may also contain minor to trace amounts of mica, hematite, calcite, tridymite, kaolinite, and hornblende and minor amounts (less than 25%) of smectite and/or zeolite. For the purposes of this analysis, sorption-coefficient distributions for devitrified tuff are based on data obtained on samples that are composed primarily of silica phases and feldspar with only trace amounts of other minerals. Although devitrified tuff samples that contain significant amounts (more than 5%) of clays or zeolites generally have higher sorption coefficients than samples that do not, the distribution of these types of altered rocks along the flow path is not well enough established to reliably incorporate results for these rock types into the sorption-coefficient probability distributions. Sorption-coefficient distributions for zeolitic tuff use only samples that contain more than 20% zeolite, with the balance made up of silica phases, alkali feldspar, clays, and/or glass.

The total number of samples of each rock type used in this analysis included 38 devitrified tuffs and 34 zeolitic tuffs, of which not all were obtained from the saturated zone. Nonetheless, these samples are representative of devitrified and zeolitic tuffs in the saturated zone at Yucca Mountain.

As explained further, surface areas for the sorption substrates are an input to PHREEQC calculations. Table A-1 presents surface-area analyses for 20 tuff samples from *Batch Sorption Results for Neptunium Transport Through Yucca Mountain Tuffs* (Triay et al. 1996 [DIRS 101023], p. 62). A 2.8-m^2/g surface area was used in the PHREEQC modeling. This

value is at the lower end of the range of values represented in the table. The use of a lower end value for the surface area leads to conservative estimates of the sorption coefficients, since a larger surface area would lead to larger sorption coefficients. Similarly, a representative value of 28 m^2/g is used for zeolitic tuff, which is at the lower end of the range of values for zeolitic tuff as presented in Table A-1.

Table A-1. Surface Areas (m^2/g) for Yucca Mountain Tuffs

Borehole	Not Crushed	Dry Sieved	Wet Sieved With J-13 Well Water	Wet Sieved With UE-25 p#1 Water
Devitrified Tuffs				
USW G1-732	2.1	2.7	2.6	3.3
USW G1-1936	4.5	4.9	3.6	3.7
USW G4-270	2	6.4	5.1	5
USW G4-275	2.9	4.5	—	—
USW G4-2570	2.8	3.6	2.9	2.8
USW GU3-747	2.2	2.9	2.8	2.8
USW GU3-2325	1.8	2.5	2.2	2.5
Average	**2.6**	**3.9**	**3.2**	**3.4**
Zeolitic Tuffs				
USW G1-1405	32	28	26	31
USW G2-1813	—	—	34	—
USW G2-1951	—	—	66	—
USW GU3-1992	—	—	32	—
USW G4-1506	22	30	27	25
USW G4-1529	37	21	22	31
USW G4-1530	40	41	—	—
USW G4-1625	28	27	28	33
USW G4-1772	23	22	23	23
USW G4-2077	19	18		
Average	**28.7**	**26.7**	**32.3**	**28.6**
Vitric Tuffs				
USW G2-767	0.89	1.1	0.62	0.87
USW GU3-1249	0.52	0.92	0.99	0.87
USW GU3-1407	1.7	3.3	3	3.2
Average	**1.0**	**1.8**	**1.5**	**1.6**

Source: Triay et al. 1996 [DIRS 101023], p. 62.

The list of radionuclides for which sorption-coefficient data are required was derived in *Radionuclide Screening* (SNL 2007 [DIRS 177424], Tables 6-7 and 6-8). The list includes isotopes of americium, cesium, neptunium, protactinium, plutonium, radium, selenium, strontium, thorium, tin, and uranium. Because different isotopes of a given (heavy) element behave the same in chemical reactions, this discussion will focus on this list of elements.

Sorption coefficients for the radionuclides-of-interest are often a function of the concentrations of the radionuclides present in solution (i.e., sorption isotherms are often non-linear). Thus, sorption experiments have been carried out as a function of radionuclide concentration. As the

radionuclide concentrations are increased in the experiments, an upper limit is eventually reached for most elements-of-interest where a pure phase incorporating the element of interest becomes oversaturated and could precipitate out of solution. This concentration is known as the solubility limit for the element of interest in the experimental system. Because sorption experiments have been carried out by the Yucca Mountain Project (YMP) up to and, in some cases above, the solubility limit for most elements-of-interest, the ranges of sorption coefficients obtained reflect this dependency. The only elements-of-interest for which the experimental concentrations did not approach solubility limits were cesium and selenium. The solubilities of cesium and selenium are very high (Sections A7.2 and A7.7) relative to the concentrations used in the sorption experiments.

A sorption experiment in which the final concentration of a radionuclide-of-interest in solution is in excess of a solubility limit should not be used to derive a sorption coefficient. The reason for this is that the concentration of the radionuclide-of-interest in the solid phase in this situation could represent a combination of the amount sorbed onto the solid phase (i.e., rock) and the amount of the pure phase precipitated out of solution. A sorption coefficient is supposed to reflect only sorption reactions.

As part of the evaluation of the sorption coefficient data obtained by the YMP for the various elements-of-interest and water/rock combinations, the calculated final solution concentrations of the radionuclide-of-interest in each sorption experiment was compared against a solubility limit that reflected the experimental conditions (i.e., water composition, temperature, atmosphere). Experiments in which calculated final solution concentrations of the radionuclide-of-interest exceeded these solubility limits were not used in the derivation of sorption coefficient probability distribution functions. The solubility limits used in this analysis were either obtained from solubility experiments carried out by the YMP or from calculations using the geochemical code PHREEQC.

For solubility limits obtained from solubility experiments using waters from the site, i.e., UE-25 J-13 (J-13) and UE-25 p#1 (p#1), this approach is adequate. For the solubility limits not based on solubility experiments with site waters, a potential problem can arise with this approach. The problem results from the fact that the waters used in the sorption experiments (i.e., J-13, p#1) contain natural concentrations of some of the elements-of-interest. For example, J-13 well and p#1 waters contain background concentrations of the elements-of-interest barium, cesium, protactinium, selenium, strontium, thorium, tin, and uranium. During sorption experiments, this background is sorbed to the solid phase along with the radioactive isotopes used in the experiments. Thus, the actual concentrations of these elements-of-interest were higher in these sorption experiments than the concentrations calculated only on the basis of the activity of the radioactive isotopes used in the experiments. The problem arises mainly in sorption experiments carried out at final solution concentrations that were just below the solubility limit based only on the concentration of the radioactive isotope. When the natural element concentrations are added to the concentrations of the radioactive isotope, some of these solutions could actually have been oversaturated with a pure solid phase of the element-of-interest.

Normally, it would be expected that the precipitation of a pure phase would result in a higher sorption coefficient than would be the case if such a phase had not precipitated. However, as discussed below in the sections on individual elements, the experimental data do not reflect this

expectation. In fact, experiments in which final solution concentrations exceeded solubility limits (i.e., oversaturated solutions) generally resulted in lower sorption coefficients than experiments with undersaturated solutions. A likely reason for this observed behavior is that the nucleation and/or precipitation rates of the appropriate pure solid phases were slow enough under the conditions used in the experiments so that no solid precipitates were formed. Alternatively, the pure-phase precipitates did form but were too fine-grained to be removed from solution by the techniques used to separate the solid and liquid phases at the end of each experiment. The overall conclusion here is that the problem with oversaturation is probably not as important as it may seem.

A3. WATER COMPOSITIONAL RANGES ALONG TRANSPORT PATHWAYS

The chemistry of water in the saturated zone along potential flow paths to the accessible environment is discussed in *Saturated Zone Site-Scale Flow Model* (SNL 2007 [DIRS 177391], Table A6-1). In the saturated zone, there are two rather distinct water types in the ambient system. One is typified by water from the well J-13, located on the east side of Fortymile Wash. The other is from the well p#1, located near the southern entrance to the Exploratory Shaft Facility. The J-13 well and p#1 waters were used in sorption experiments as end-member compositions intended to bracket the impact of water composition on sorption coefficients. Table A-2a presents these data for a sample from the well J-13, a composite water sample from the volcanic portion of the well p#1, and a carbonate portion of p#1. Comparative information on range of concentrations of the same chemical constituents from other wells in the area is presented in Table A-2b. It can be seen from these tables that for most constituents, the J-13 well and p#1 water compositions approximately bracket the compositions of other wells both in volcanics and alluvium along the potential flow paths to the accessible environment. The pH of the waters from alluvium wells ranges outside that given by J-13 well and p#1; however, this is accommodated in the experiments, as seen in Section A7, where water pH ranged up to 9.0. The water compositions used in modeling studies were those reported in Table A-2a.

In addition to the major chemical constituents listed in Table A-2a (and qualified for use in Appendix I), concentrations of dissolved oxygen and the trace elements aluminum, iron, and manganese are also included in the surface complexation modeling (output DTN: LA0702MD831232.001):

- A value of 5.7 mg/L for dissolved oxygen (Ogard and Kerrisk 1984 [DIRS 100783], Table II) is specified in the model inputs for both groundwaters to define oxidizing conditions in J-13 groundwater. However, this value is only a placeholder and does not control the dissolved oxygen concentration of the modeled groundwater. Rather, the input file implements the assumption that the modeled concentration (and, hence, the redox condition) is controlled by equilibrium with the atmosphere, with the partial pressure for oxygen set at 10^{-7} atm. This assumption is consistent with the upper bound for oxidizing groundwater as discussed in Appendix F, and *Aqueous Environmental Geochemistry* (Langmuir 1997 [DIRS 100051], p. 409). Hence, the values of initial dissolved oxygen concentration do not require further justification.

- The trace element aluminum is assigned a value of 0.03 mg/L in J-13 well water and 0.1 mg/L in p#1 water (Ogard and Kerrisk 1984 [DIRS 100783], Table I). However, the initial aluminum concentrations given in the input files are only placeholders and do not control the aluminum concentrations used in the modeling calculations. Rather, the input file implements the condition that the concentration of this element is controlled by equilibrium with kaolinite (SNL 2007 [DIRS 177391], Section A6.3.5 and Figure A6-33). Hence, the values of initial aluminum concentration do not require further justification.

- For the trace elements iron and manganese, values of 0.04 and 0.001 mg/L are used, respectively, as reported by Ogard and Kerrisk (1984 [DIRS 100783], Table I). The acceptability of using these data in the model was evaluated by comparing them against appropriate USGS groundwater data available in the TDMS. Recently drilled wells were excluded from consideration. For wells that tap the volcanic aquifer in, near, or down-gradient from Yucca Crest, iron concentrations range from 0.003 to 0.100 mg/L and manganese concentrations range from < 0.001 to 0.130 mg/L (DTNs: GS011108312322.006 [DIRS 162911], GS040108312322.001 [DIRS 179422], GS950808312322.001 [DIRS 148114], GS960308312133.001 [DIRS 145606], GS970700012847.002 [DIRS 182207], GS970708312314.004 [DIRS 182209], GS971000012847.004 [DIRS 149980], GS980308312314.001 [DIRS 182212], GS980908312322.008 [DIRS 145412], GS990608312133.001 [DIRS 145611]). The values used are within these ranges. Further justification is provided by modeling results that confirm that iron and manganese do not significantly participate in the reactions of interest for the surface complexation model. This finding is demonstrated by the sensitivity analysis performed for output K_d values of americium, neptunium, and uranium in J-13 well water using an upper limit of 0.100 mg/L for iron and 0.130 mg/L for manganese (Developed DTN: MO0707SURFCOMP.000). The calculated K_d values vary by less that 1% for americium and neptunium, and by less than 1.5% for uranium, as compared to the original cases (Output DTN: LA0702MD831232.002). Hence the values of iron and manganese used in this analysis are considered acceptable for the intended use in this report.

As will become evident in the discussions of the sorption behavior of individual elements given below, variations in water chemistry can have a significant impact on the sorption behavior of a limited number of elements, particularly uranium and neptunium. To constrain these potential impacts, modeling studies with PHREEQC with the thermodynamic input data file *PHREEQCDATA025.DAT* (DTN: MO0604SPAPHR25.001 [DIRS 176868]) were carried out as discussed further.

Because carbonate water from the p#1 well was not available to the experimental program at all times, a synthetic p#1 water was developed. This water (Table A-2b) was primarily intended to have a bicarbonate concentration similar to that found in UE-25 p#1 (carbonate). It was used in experiments with uranium, neptunium, and plutonium because the solution and sorption behavior of these elements is sensitive to the bicarbonate and carbonate concentrations in solution (Nitsche et al. 1993 [DIRS 155218], pp. 54, 60, and 78; 1995 [DIRS 100163], p. 39). Modeling studies to simulate the results of the sorption experiments (for uranium, neptunium, and plutonium) with PHREEQC used similarly composed water to that from the volcanic portion of

p#1 (Table A-2a) and modified to have the sodium and bicarbonate compositions of this synthetic p#1 water (Table A-2b).

Table A-2a. Compositions of Waters from UE-25 J-13 and UE-25 p#1

Chemical Constituent	UE-25 J-13 Well Water[a] (mg/L)	UE-25 p#1 (Volcanics) Water[b] (mg/L)	UE-25 p#1 (Carbonate) Water[a] (mg/L)
Ca^{2+}	11.5	37	87.8
Mg^{2+}	1.76	10	31.9
Na^{+}	45	92	171
K^{+}	5 .3	5.6	13.4
SiO_2	64.2	49	37.3[d]
Cl^{-}	6.4	13	37
F^{-}	2.1	3.4[c]	3.5
SO_4^{2-}	18.1	38	129
HCO_3^{-}	143	344	698
pH	6.9	6.8	6.7

Sources: [a]Ogard and Kerrisk 1984 [DIRS 100783].
[b] DTN: MO0007MAJIONPH.011 [DIRS 151524].
[c] DTN: SN0705FLUORINE.001 [DIRS:182006].
[d] value derived from Table III of Ogard and Kerrisk 1984 [DIRS 100783].

Table A-2b. Comparative Information on the Range of Concentrations from Wells in the Saturated Zone Transport Model Area

Chemical Constituent	Range of Concentrations in Downgradient Wells in Volcanics[a] (mg/L)	Range of Concentrations in Downgradient Wells in Alluvium[a] (mg/L)	Synthetic p#1 Water (mg/L)
Ca^{2+}	0.8 to 37	0.8 to 20.3	
Mg^{2+}	< 0.1 to 10	0.0 to 7.7	
Na^{+}	38 to 120	57.9 to 180.5	261[b]
K^{+}	1.1 to 8.9	1.8 to 5.5	
SiO_2	36 to 57	40.5 to 61	
Cl^{-}	6.0 to 13	5.6 to 18	
F^{-}	1.0 to 6.7	1.6 to 4.2	
SO_4^{2-}	14 to 38	18.7 to 61.7	
HCO_3^{-}	107 to 344	110 to 255.5	691[b]
CO_3^{2-}	0.0	0.0 to 23.5	
pH	6.8 to 8.4	7.5 to 8.9	
Eh	-	128 to 197 mv	-

Sources: [a]SNL 2007 [DIRS 177391], Table A6-1.
[b]Triay et al. 1996 [DIRS 101024], p. 4.

A4. EXPERIMENTAL TECHNIQUES

The basic technique for the laboratory determination of sorption coefficients involved the contact of a groundwater sample, spiked with the radionuclide of interest, with a crushed sample of tuff or alluvium (Daniels et al. 1982 [DIRS 105803]). The rock sample was generally obtained as a core sample. The core was crushed in a jaw crusher and subsequently sieved to a selected grain-size fraction. The sieving process was usually carried out under water. Initially, several

different grain-size fractions were used in the experiments. With experience, it was concluded that the 75- to 500-μm fraction was the most appropriate for use in these types of experiments. Results for samples that included all sizes below a certain grain size (e.g., less than 35 μm) tended to produce higher sorption-coefficient values than the 75- to 500-μm fraction.

Mineral fractionation is the process by which certain minerals, such as clays, may become enriched in a very fine-grain size fraction due to sieving effects. Mineralogic analysis of different mineral fractions, including fines, indicates some mineral fractionation has occurred (Chipera and Bish 1989 [DIRS 101374], Appendix A). Thus, this fractionation may be the cause of the enhanced sorption observed in the fractions that include fines.

One gram of crushed rock material (usually the 75- to 500-μm fraction) was added to a test tube with 20 mL groundwater spiked with the radionuclide(s) of interest. The test tube was put on a shaker table for a predetermined period (days to weeks) to allow reaction to occur. After the predetermined time had passed, the solution was separated from the solid phase by either centrifugation or filtration. Centrifugation was preferred for those elements thought to have an affinity for the filter medium. The separations were not always perfect due to various experimental constraints. In some cases, the concentration in the solid fraction was determined separately from that in the solution. A sorption coefficient was usually calculated from the difference between the initial and final solution concentrations. Corrections were generally made for sorption onto the surface of the test tube during the equilibration (shaking) period.

Some potential sources of errors and experimental artifacts that may pertain to the sorption coefficient experiments include weighing errors, counting errors, errors resulting from solutions being oversaturated with the element of interest, errors from imperfect solid/liquid separations, errors from inaccurate correction for sorption onto container walls, recording errors, transcription errors, inadvertent laboratory errors, and calculation errors. These errors cannot be quantitatively assessed. However, their existence will become apparent in the scatter of the data on diagrams presented in Section A7.

A5. APPROACH TO THE DERIVATION OF SORPTION-COEFFICIENT RANGES FOR MAJOR ROCK TYPES IN THE YUCCA MOUNTAIN FLOW SYSTEM

The derivation of sorption-coefficient probability distributions for the elements of interest on the major rock types in Yucca Mountain involves an evaluation of available experimental data, sorption modeling, and professional judgment. Experimental data are used to evaluate the impact of variations in (1) rock sorption properties (within each of the two major groupings), (2) radionuclide concentrations, (3) sorption kinetics, and (4) water chemistry, on sorption coefficients for the elements of interest.

The radionuclides of interest are divided into three groups of radioelements. For the first group, including americium, neptunium, plutonium, and uranium, experimental data are used to evaluate the impact of radionuclide concentrations, sorption kinetics, and variations in water chemistry on sorption coefficients. Surface-complexation modeling is used to further evaluate the impact of variations in water chemistry on sorption coefficients. The surface-complexation models used in this analysis are based on the code PHREEQC, using the thermodynamic input data file *PHREEQCDATA025.DAT* (DTN: MO0604SPAPHR25.001 [DIRS 176868]). The

binding constants required for surface-complexation modeling are either obtained from the literature or derived from experimental data involving sorption of the radioelement on silica.

In the second group of elements, including cesium, protactinium, radium, selenium, strontium, and tin, sorption-coefficient distributions for the major rock types are derived more directly from the available experimental data and the ranges for environmental variables expected in the transport system. Although it would be preferable to have theoretical models to evaluate the impacts of variations in water chemistry and rock chemistry on sorption coefficients for these radionuclides, there were not sufficient data available to properly constrain such a model.

For the third group, including carbon, iodine, and technetium, the sorption coefficient is taken to be zero in the volcanic rocks and in the alluvium. This approach leads to model breakthrough times shorter than would be the case if transport processes not currently included, such as reduction of technetium in the saturated zone, were included in the model.

A6. SURFACE-COMPLEXATION MODELING

The PHREEQC surface-complexation model used in this analysis is a nonelectrostatic model (Parkhurst 1995 [DIRS 142177], pp. 10 to 11). Inputs required for modeling include deprotonation constants, binding constants for elements of interest, total site concentrations, water chemistry, and a thermodynamic database for solution species and solids. Because the tuffs contain up to 76 wt % silica (Broxton et al. 1986 [DIRS 100023], p. 39), a silica surface was used to represent the mineral surfaces in the tuffs. The surface-complexation models included the effects of competition from common constituents in the rock such as calcium, magnesium, sodium, potassium, and aluminum. Deprotonation constants for silica were obtained from Dixit and Van Cappellen (2002 [DIRS 162985], p. 2,565). Binding constants were obtained from Dixit and Van Cappellen (2002 [DIRS 162985], p. 2,565) for aluminum on silica, and from Marmier et al. (1999 [DIRS 162986], p. 228) for sodium on silica. The total site concentrations were obtained from surface areas (Section A2 and Table A-1), and a site density of 2.3 sites/nm^2 was used as recommended by Pabalan et al. (1998 [DIRS 162987], p. 124). Pabalan et al. (1998 [DIRS 162987]) was also the source for uranium binding constants on silica. The binding constants were used in surface complexation modeling calculations to evaluate the impact of variations in water chemistry on uranium sorption coefficients. The thermodynamic data used for the modeling was from file *PHREEQCDATA025.DAT* (DTN: MO0604SPAPHR25.001 [DIRS 176868]).

A7. DISCUSSIONS AND ANALYSIS OF EXPERIMENTAL SORPTION-COEFFICIENT DATA AND SURFACE-COMPLEXATION MODELING

The data and modeling results for each element are discussed in separate sections, arranged in alphabetical order.

A7.1 AMERICIUM

According to Nitsche et al. (1993 [DIRS 155218], p. 78), the solubility of americium in J-13 well water is controlled by $AmOHCO_3$.

At 25°C and a pH of 8.5, the reported solubility of $AmOHCO_3$ in J-13 well water is 2.4 (± 1.9) $\times 10^{-9}$ M. At 25°C and a pH of 7.0, the reported solubility is 1.2 (± 0.3) $\times 10^{-9}$ M.

A7.1.1 Devitrified Tuff

Sorption coefficients (K_d) measured on devitrified tuffs are plotted versus calculated final solution concentrations in Figure A-1. The points identified by the term "sorption" refer to experiments in which J-13 well water spiked with americium was contacted with devitrified tuff. The points identified by the term "desorption" refer to experiments in which the solid remaining after the "sorption" step was contacted with unspiked J-13 well water. The steep negative slopes evident at the higher concentrations for individual samples reflect a mass balance constraint. That is, the final solution concentration is calculated using the starting solution concentration and the measured sorption coefficient. For a given starting concentration, this approach will produce a linear relationship between the sorption coefficient and the final solution concentration. The offsets between the linear trends in Figure A-1 primarily reflect different starting concentrations.

As shown in Figure A-1, the calculated final solution concentrations were higher than the reported solubility of $AmOHCO_3$ in J-13 well water in numerous experiments with samples JA-32 and YM-54. Thus, the results for these experiments will not be used in the derivation of sorption coefficient probability distributions because the solid phase may have contained $AmOHCO_3$. For the remaining experiments, the sorption coefficients range from 1,000 to more than 10,000 mL/g. In one sample (GU3-688), americium concentrations were analyzed by isotope dilution mass spectrometry (Triay et al. 1991 [DIRS 104129], pp. 142 to 144). This technique has higher sensitivity than the (radioactivity) counting techniques normally used, thereby allowing the use of lower americium concentrations. It also has smaller analytical errors than the counting techniques normally used in batch sorption experiments. Thus, the result obtained for this sample is judged to be more reliable than those obtained with counting techniques. It is at the high end of the range of values obtained for the other samples.

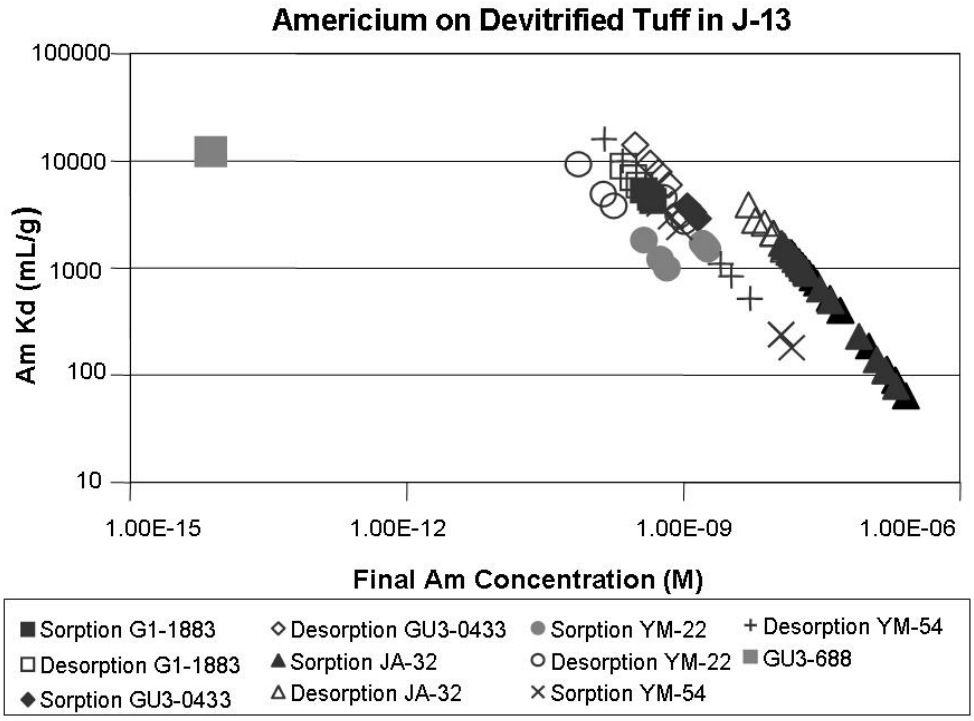

Source: DTN: LA0305AM831341.001 [DIRS 163789].

Figure A-1. Americium Sorption Coefficients on Devitrified Tuff versus Calculated Final Americium Concentration in Solution

Americium sorption coefficients are plotted versus duration of the sorption and desorption experiments in Figure A-2. The trend in the data (ignoring data from samples JA-32 and YM-54 because of the over-saturation problem) suggests that americium sorption-coefficient values are not very sensitive to the duration of the experiments except in those experiments with very short durations. Thus, the kinetics of the americium sorption reactions appear to be relatively fast. This implies that the linear trends shown in Figure A-1 are not due primarily to sorption kinetics.

A more likely cause for these trends is imperfect separation of liquid and solid phases at the end of the sorption experiments. When sorption coefficients are large, as in this case, final solution concentrations are quite small and any colloid-sized material that remains in the liquid phase following centrifugation will increase the final "solution" concentration and lower the apparent K_d. Note that oversaturation with a "pure" americium phase would lead to nearly constant final solution concentrations. Thus, the trends shown for oversaturated samples JA-32 and YM-54 cannot be explained as due to oversaturation with a "pure" americium phase.

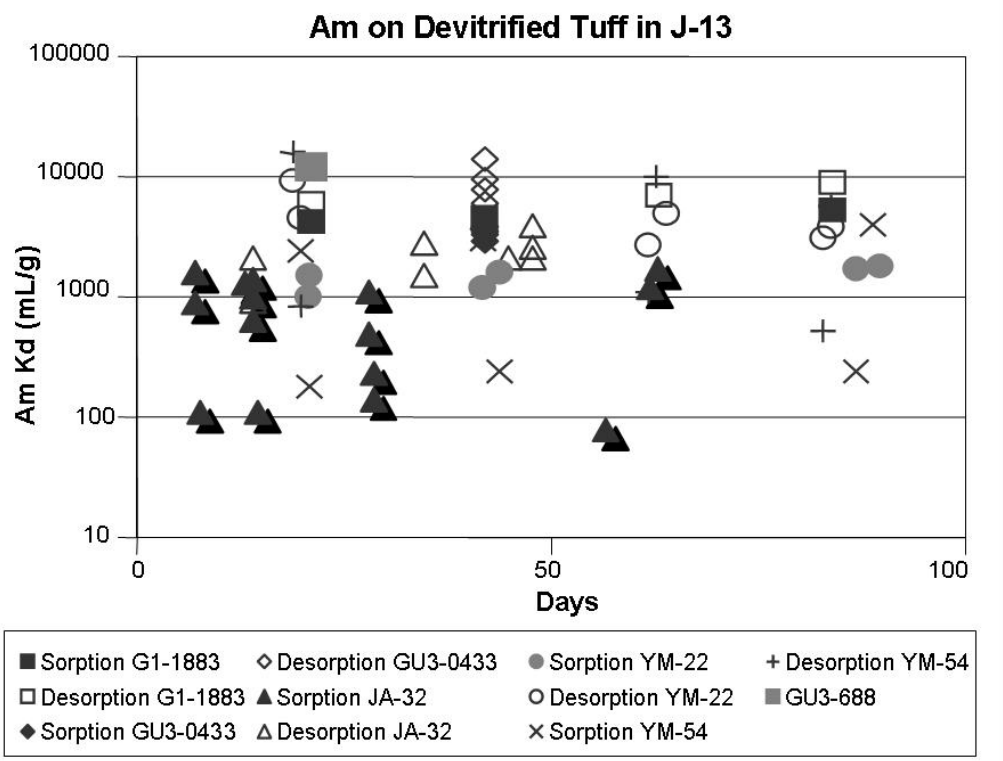

Source: DTN: LA0305AM831341.001 [DIRS 163789].

Figure A-2. Americium Sorption Coefficients for Devitrified Tuff as a Function of Experiment Duration

The effects of variations in water chemistry on americium sorption coefficients have not been tested experimentally except for variations in solution pH. All the americium sorption and desorption experiments carried out with Yucca Mountain samples used J-13 well water. Americium sorption and desorption coefficients in J-13 well water are plotted versus pH in Figure A-3. It is evident that there is no clear trend among the data points plotted. The variations in sorption coefficients observed in multiple experiments with the same rock sample could reflect differences in solution concentrations, (radioactivity) counting statistics, long-term stability of the counting equipment, sorption kinetics, imperfect separation of the solid and liquid phases, adsorption of americium to the walls of the experimental containers, and other factors. Errors due to counting statistics are generally a small percentage of the measured sorption coefficient. The other factors cannot be quantified with the available data.

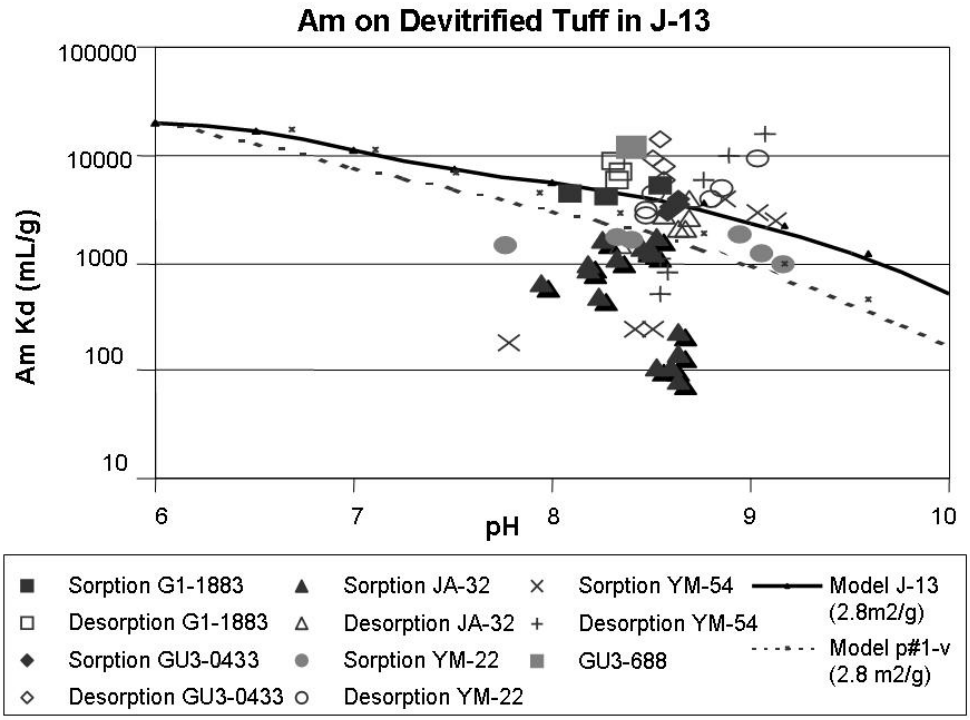

Sources: DTNs: LA0305AM831341.001 [DIRS 163789]

NOTE: Model curves derived with PHREEQC surface-complexation modeling are also shown (Output DTN: LA0702MD831232.002 file *output_07.xls*, worksheets *Amsij13.pun.xls* and *Amsip1.pun.xls*

Figure A-3. Americium Sorption Coefficients on Devitrified Tuff versus pH

To gauge the potential impact of variations in water chemistry on americium sorption coefficients, surface complexation modeling was carried out with PHREEQC with the thermodynamic input data file *PHREEQCDATA025.DAT* (DTN: MO0604SPAPHR25.001 [DIRS 176868]). In the modeling, surface sites on devitrified tuff were taken to be equivalent to surface sites on silica. Surface complexation reaction constants for americium species on silica were derived by fitting experimental data presented by Beall et al. (1986 [DIRS 162983], p. 502) for the sorption of americium onto quartz (Allard et al. 1980 [DIRS 104410], p. 478) in Oak Ridge National Laboratory Standard Water (Allard and Beall (1979 [DIRS 147235], p. 511). This water is similar in composition to J-13. Allard et al. (1980 [DIRS 104410]) was the source for the surface area (2.8 m^2/g) of silica samples used in experiments reported by Beall et al. (1986 [DIRS 162983]).

As shown in Figure A-4, the sorption coefficients for americium on quartz (Beall et al. 1986 [DIRS 162983], p. 502) as a function of pH could be fit very well using two surface reactions, chosen using expert judgment involving an americium sulfate complex and an americium carbonate complex, with the choice of log k values given in Table A-3. These reactions are listed in Table A-3.

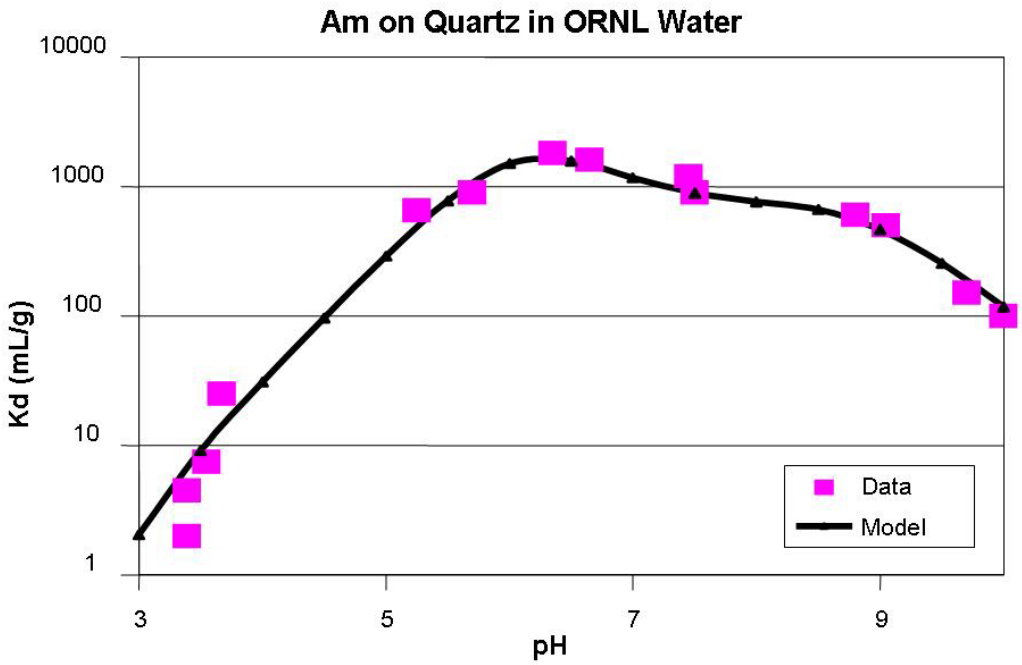

Source: Beall et al. 1986 [DIRS 162983].

Output DTN: LA0702MD831232.002, *output_07.xls*, worksheet *Amornl5.pun.xls*.

Figure A-4. Americium Sorption Coefficients on Quartz from Beall et al. and Model Fit

Table A-3. Surface Complexation Reactions for Americium

Reaction	Log *K*
$SiOH + Am^{3+} + SO_4^{2-} \leftrightarrow SiOAmSO_4 + H^+$	5.5
$SiOH + Am^{3+} + CO_3^{2-} \leftrightarrow SiOAmCO_3 + H^+$	6.5

Source: Output DTN: LA0702MD831232.001.

Using a surface area of 2.8 m^2/g, americium sorption coefficients were calculated for "devitrified tuff" in J-13 well water as a function of pH. The model curves are shown in Figure A-3. The fact that the model sorption coefficient for J-13 well water at a pH value of 8.5 lies in the middle of the range of experimental values provides some confidence that the model is reasonable. The model curves move up or down linearly with surface area. Thus, at least part of the range of experimental values could reflect variations in devitrified tuff surface areas.

The model curves shown in Figure A-3 suggest that sorption coefficients for americium will increase with decreasing pH in the pH range from 7.0 to 9.0. Thus, in terms of pH, the experimentally derived sorption coefficients shown in Figure A-3 are at the low end of the range of coefficients to be expected in the saturated zone. The effect of variation in major ion chemistry of groundwater is shown by the curve calculated using the p#1 groundwater composition. Americium sorption coefficients calculated using p#1 water are similar to those calculated using J-13 well water over the pH range of interest (7.0 to 8.5). Thus, variations in water chemistry are not expected to have a major impact on americium sorption coefficients.

On the basis of the experimental data and model curves plotted in Figure A-3, the range of americium sorption coefficients expected for devitrified tuffs in the saturated volcanic section at Yucca Mountain is selected as 1,000 to 10,000 mL/g. The probability distribution type selected is a truncated normal distribution with a mean of 5,500 mL/g and standard deviation of 1,500 mL/g. The data for JA-32 and YM-54 were not included in the derivation of the distribution because the final solutions in the experiments with these samples were oversaturated with $AmOHCO_3$.

A7.1.2 Zeolitic Tuff

The measured sorption coefficients for zeolitic tuff are plotted versus calculated final solution concentrations in Figure A-5. The calculated final solution concentrations were higher than the solubility of $AmOHCO_3$ in essentially all the experiments with sample JA-18. Therefore, the sorption coefficients obtained for this sample will not be used in the derivation of the sorption-coefficient probability distribution for americium on zeolitic tuff. Sorption experiments with sample G4-1952 were close to saturation with $AmOHCO_3$. The sorption coefficients obtained for this sample will be used in the derivation of the distribution.

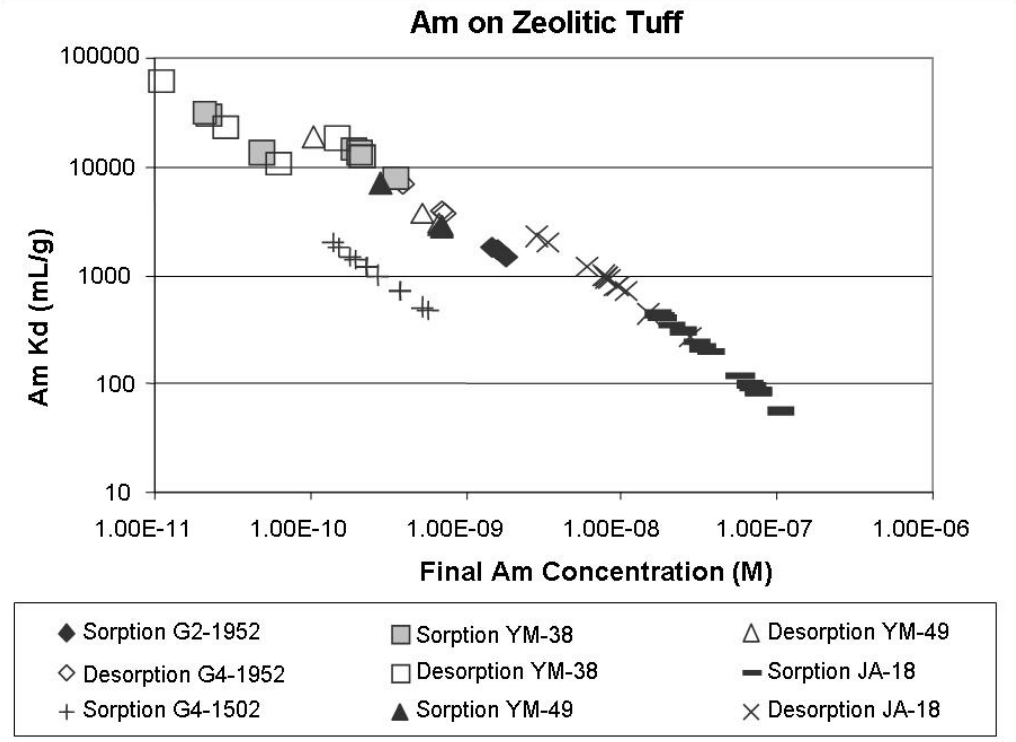

Source: DTN: LA0305AM831341.001 [DIRS 163789].

Figure A-5. Americium Sorption Coefficients on Zeolitic Tuff versus Calculated Final Americium Concentration in Solution

Americium sorption coefficients for zeolitic tuff are plotted versus duration of the sorption and desorption experiments in Figure A-6. As with the devitrified tuffs, the trend in the data (excluding sample JA-18) suggests americium sorption-coefficient values obtained in experiments with solutions undersaturated with $AmOHCO_3$ are not very sensitive (< 10 times) to

the duration of the experiments except in those experiments with short durations (e.g., sample G4-1502). Thus, the kinetics of the americium sorption reactions on zeolitic tuff appear to be relatively fast.

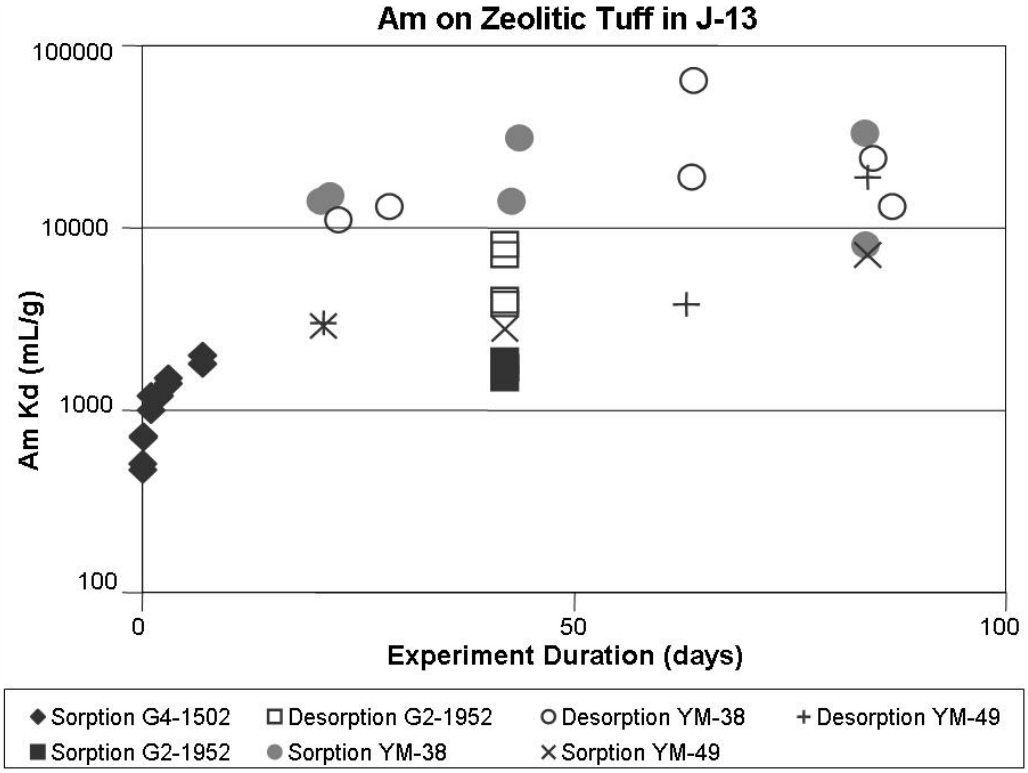

Source: DTN: LA0305AM831341.001 [DIRS 163789].

Figure A-6. Americium Sorption Coefficients for Zeolitic Tuff as a Function of Duration of Sorption and Desorption Experiments

As with devitrified tuff, sorption coefficient experiments were only carried out with J-13 well water. To investigate the impact of variations in water chemistry on sorption coefficients for americium on zeolitic tuffs, a surface complexation model was developed. The surface complexation model for zeolitic tuff is similar to the model developed for devitrified tuff except that a surface area of 28 m^2/g was used as a representative value (Table A-1 of this report). The model sorption coefficient at a pH of 8.5 lies at the high end of the range of experimental values (Figure A-7). It might be expected that the sorption coefficients for zeolitic tuffs would be on the order of 10 times larger than those for devitrified tuffs to reflect the factor of 10 increase in surface area. Although some samples reflect this expectation, most do not. This suggests not all the surface area in the zeolitic tuffs may be accessible to americium. Alternatively, the binding sites in the interior of zeolite crystals may not have a high affinity for americium species.

As with devitrified tuff, the model curves for zeolitic tuffs shown in Figure A-7 indicate that sorption coefficients for americium will increase with decreasing pH in the pH range from 7.0 to 9.0. Thus, in terms of pH, the experimentally derived sorption coefficients are at the low end of the range of coefficients to be expected in the saturated zone. The effect of variation in major ion chemistry of groundwater is shown by the curve calculated for Borehole p#1 groundwater. It

is evident in Figure A-7 that americium sorption coefficients calculated using p#1 water are similar in value to the coefficients calculated using J-13 well water. Thus, variation in water chemistry will not have a major impact on americium sorption coefficients in the saturated zone.

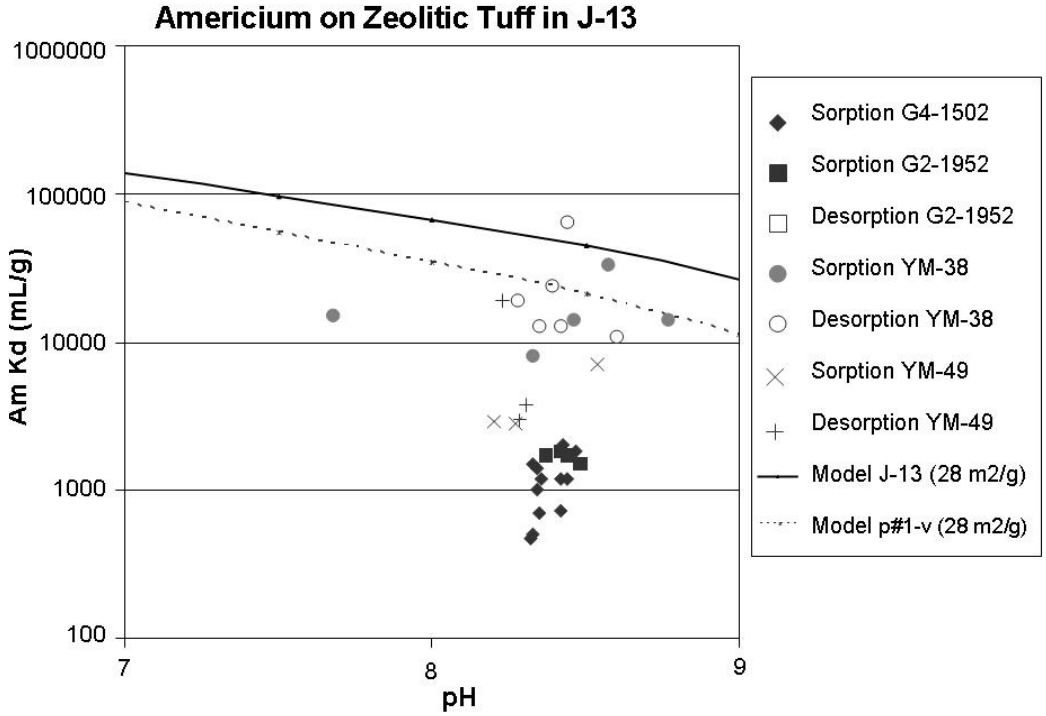

Sources: DTN: LA0305AM831341.001 [DIRS 163789] and Output DTN: LA0702MD831232.002, file *output_07.xls*, worksheets *Amzeoj13.pun.xls* and *Amzeop1.pun.xls*

NOTE: Model curves derived with PHREEQC surface-complexation modeling are also shown (Output DTN: LA0702MD831232.002).

Figure A-7. Americium Sorption Coefficient Data and Modeling Results for Zeolitic Tuff as a Function of pH

On the basis of the experimental data and model curves plotted in Figure A-7, the range of americium sorption coefficients selected for zeolitic tuffs in the saturated volcanic section at Yucca Mountain is 1,000 to 10,000 mL/g. The probability distribution type selected is a truncated normal distribution with the mean of 5,500 mL/g and the standard deviation of 1,500 mL/g. The upper end of this distribution could have been set at 100,000 mL/g instead of 10,000 mL/g based on the available data and modeling results. However, the 10,000 mL/g value is large enough to effectively keep americium from being transported over the regulatory time frame. In addition, by using an upper limit of 10,000 mL/g, the same distribution can be used for devitrified and zeolitic tuffs. The data for sample JA-18 were not included in the derivation of the distribution because the final solutions in the experiments with this sample were oversaturated with $AmOHCO_3$.

A7.1.3 Alluvium

The probability distribution for devitrified tuff will be used as a default for the americium sorption-coefficient probability distribution in alluvium. Alluvium along the flow path is

composed largely of disaggregated tuffaceous materials. Because devitrified tuff makes up a major portion of the volcanic units exposed at the surface, it should be a major component in alluvium. In addition, clays and other secondary minerals are enriched in alluvial materials. These characteristics should result in higher sorption coefficients for alluvial materials compared to intact devitrified tuff.

A7.2 CESIUM

The solubility of cesium in J-13 well water at 25°C is very high. In fact, cesium concentrations in Yucca Mountain groundwaters will not have a solubility limitation (BSC 2005 [DIRS 174566], Section 6.17).

A7.2.1 Devitrified Tuff

Experimentally derived sorption coefficients for cesium on devitrified tuff are plotted against the calculated final cesium concentrations of the experiments in Figure A-8. The data points are separated into groups on the basis of when the experiments were carried out (before May 1989 = "old" and after May 1989 = "new"), water type, and on whether the sorption coefficient was determined from a sorption or a desorption experiment. In May 1989 NRC issued *Nuclear Regulatory Commission Staff Safety Evaluation of U.S. Department of Energy Quality Assurance Program Description of the Office of Civilian Radioactive Waste Management* (NRC 1989 [DIRS 181692]). Data collected after this date fall under YMP's QA program. Data collected prior to this date fall under different quality assurance programs; hence, the distinction is made in most figures.

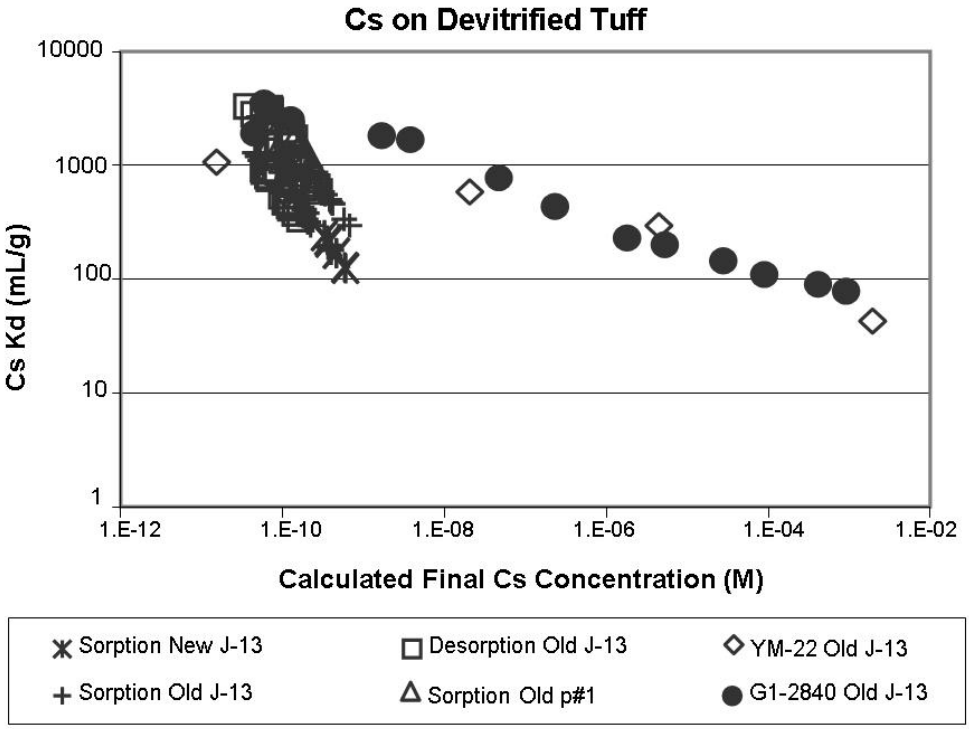

Sources: DTNs: LA0310AM831341.001 [DIRS 165865] (Column B and Column N were used to generate the graph); LA0407AM831341.002 [DIRS 170621] (Column N and Column P were used to generate the graph).

NOTE: In the legend, 'old' stands for data collected before May 1989, 'new' stands for data collected after May 1989.

Figure A-8. Cesium Sorption Coefficients on Devitrified Tuff versus Calculated Final Cesium Concentration in Solution

Sorption coefficients obtained in "new" experiments lie within the range defined by the "old" experiments at similar cesium concentrations. This indicates the experimental procedures and techniques used in the "old" experiments were comparable to those used in the "new" experiments. The scatter of cesium K_d values for experiments with final solution concentrations of less than 10^{-9} M most likely reflects variability in ion exchange capacities of the rock samples used in the experiments. Nonlinear sorption isotherms were obtained for samples YM-22 and G1-2840 in J-13 well water. The data for sample G1-2840 were fit using a Freundlich equation as shown in Figure A-9. The nonlinear isotherm indicates that cesium sorption coefficients on devitrified tuff in the saturated zone will be a function of concentration.

Sorption coefficients obtained in experiments with p#1 water fall in the middle of the cluster of points in Figure A-8 near 1×10^{-10} M. Thus, there is little or no impact of variations in water chemistry on cesium sorption coefficients on devitrified tuff.

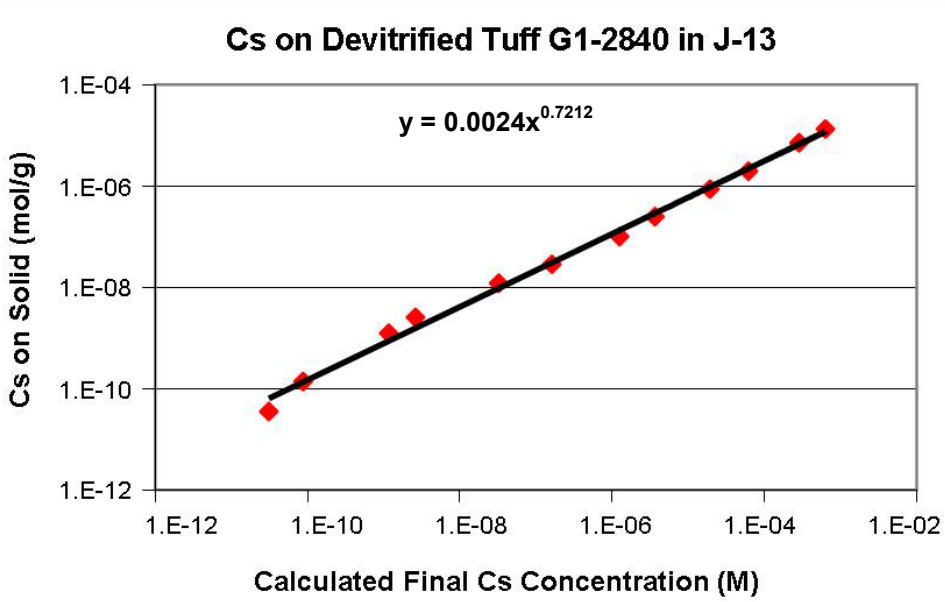

Source: DTN: LA0310AM831341.001 [DIRS 165865] (Column B and Column N were used to generate the graph).

Figure A-9. Freundlich Isotherm Fit to Sorption-Coefficient Data for Cesium on Devitrified Tuff Sample G1-2840 in J-13 Well Water

The effects of experiment duration on the cesium sorption coefficients for devitrified tuff are shown in Figure A-10. The large range in sorption coefficients obtained at a given duration (e.g., 21 days) mainly reflects variations in cesium solution concentrations, although variations in ion-exchange capacities also contribute to the range. The range of sorption-coefficient values is fairly constant with duration when the results for samples YM-22 and G1-2840 are excluded. This range extends from just above 100 mL/g to above 1,000 mL/g. The constancy indicates cesium sorption reactions are fast.

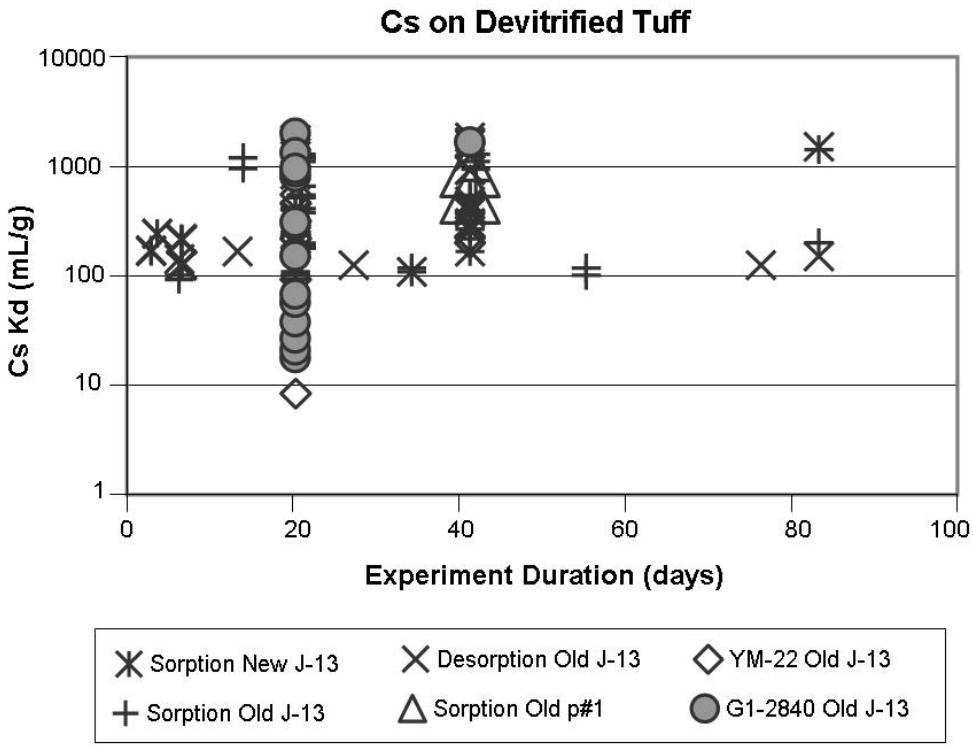

Sources: DTNs: LA0310AM831341.001 [DIRS 165865]; LA0407AM831341.002 [DIRS 170621].

NOTE: In the legend, 'old' stands for data collected before May 1989, 'new' stands for data collected after May 1989. The results for experiments which included the "fines" fraction were not included in the figure.

Figure A-10. Cesium Sorption Coefficients on Devitrified Tuff versus Experiment Duration for Sorption (Forward) and Desorption (Backward) Experiments

The cesium sorption-coefficient probability distribution derived for devitrified tuff in the saturated zone is a truncated normal distribution with a range of 100 mL/g to 1,000 mL/g, mean value of 728 mL/g, and a standard deviation of 464 mL/g. The low end of the chosen range was selected based on the minimum value observed in experiments with solution concentrations less than 10^{-7} M. The upper end of the distribution was chosen as a minimum upper limit given the potential impacts of low cesium solution concentrations and high ion-exchange capacities.

A7.2.2 Zeolitic Tuff

Experimentally derived sorption coefficients for cesium on zeolitic tuff are plotted against the calculated final cesium concentrations of the experiments in Figure A-11. The data points are separated into groups on the basis of when the experiments were carried out (before May 1989 = "old" and after May 1989 = "new"), water type, and on whether the sorption coefficient was determined from a sorption or a desorption experiment. The range of measured cesium sorption coefficients for zeolitic tuffs is 3,500 to 72,000 mL/g. A sorption isotherm was obtained for sample YM-38 in J-13 well water. As shown in Figure A-12, the isotherm is nearly linear (i.e., the exponent is close to 1.0). Thus, variations in cesium concentrations do not have a major impact on sorption coefficient values in zeolitic tuffs at concentrations below approximately 10^{-5} M. This suggests the trend in the data points below 10^{-11} M primarily reflects variations in rock properties such as ion exchange capacities and mineral compositions. Sorption coefficients

obtained in experiments with Borehole p#1 water fall at the lower end of the range of values obtained for experiments with J-13 well water (Figure A-11). Thus, there is some impact of variations in water chemistry on cesium sorption coefficients on zeolitic tuff, although this impact is minor (approximately a factor of 2).

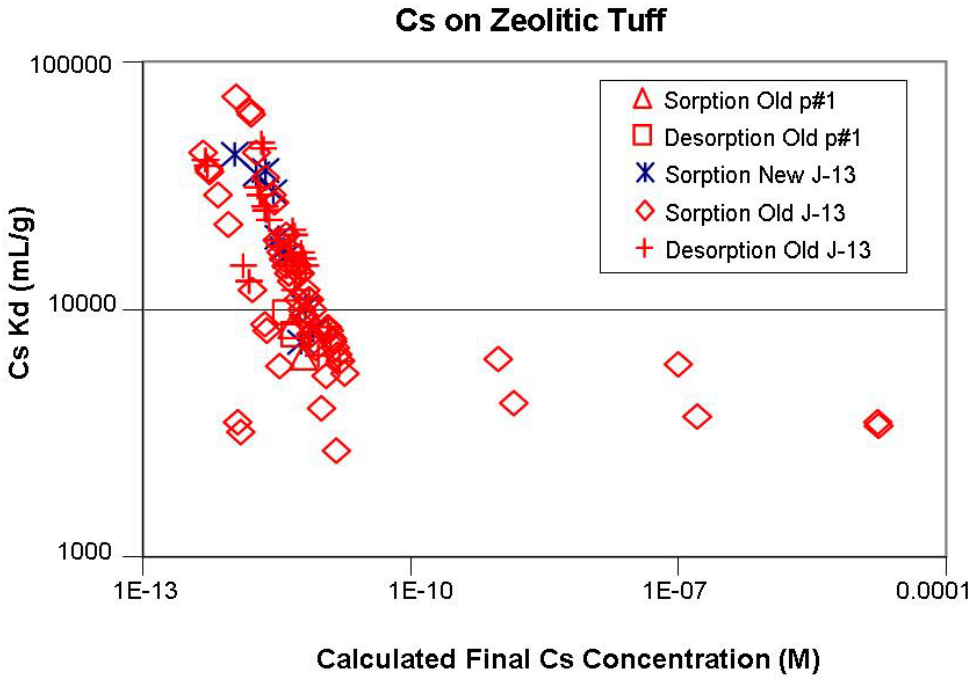

Sources: DTNs: LA0310AM831341.001 [DIRS 165865]; LA0407AM831341.002 [DIRS 170621].

NOTE: In the legend, 'old' stands for data collected before May 1989, 'new' stands for data collected after May 1989.

Figure A-11. Cesium Sorption Coefficients on Zeolitic Tuff versus Calculated Final Cesium Concentration in Solution

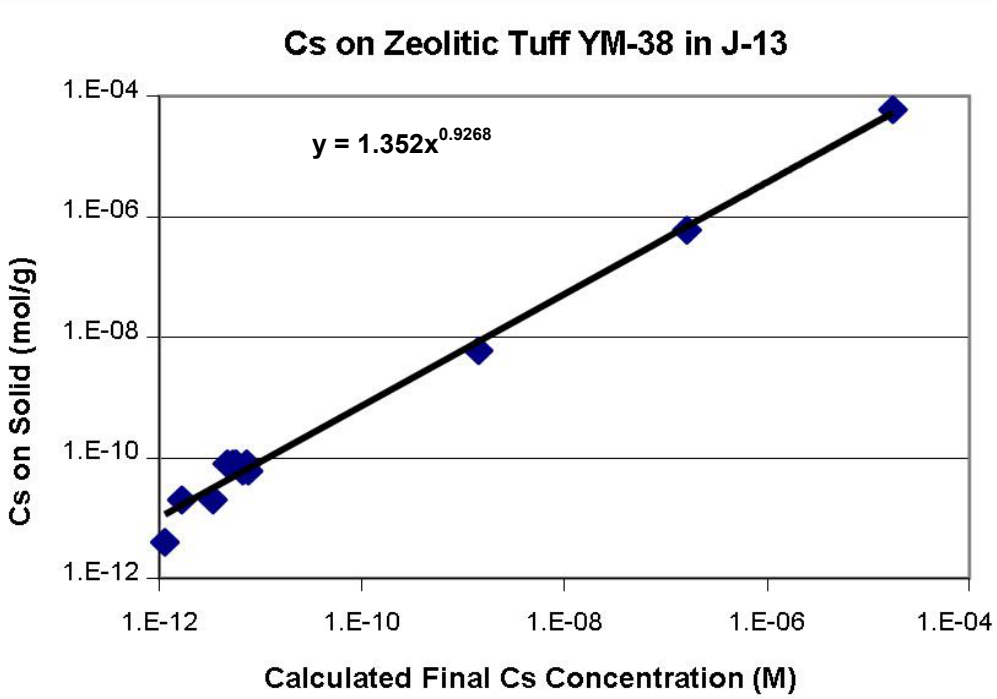

Source: DTN: LA0310AM831341.001 [DIRS 165865].

Figure A-12. Freundlich Isotherm Fit to Sorption-Coefficient Data for Sample YM-38 in J-13 Well Water

The effects of experiment duration on the value of K_d for cesium on zeolitic tuff are shown in Figure A-13. The large range in sorption coefficients obtained at a given duration mainly reflects variations in ion-exchange capacities and mineral compositions of the zeolitic tuff samples used in the experiments. The range of sorption-coefficient values is fairly consistent with duration. For example, the range of sorption-coefficient values for the 3.6-day experiments is similar to the range for the 42-day experiments. This result indicates the sorption reaction kinetics are fast.

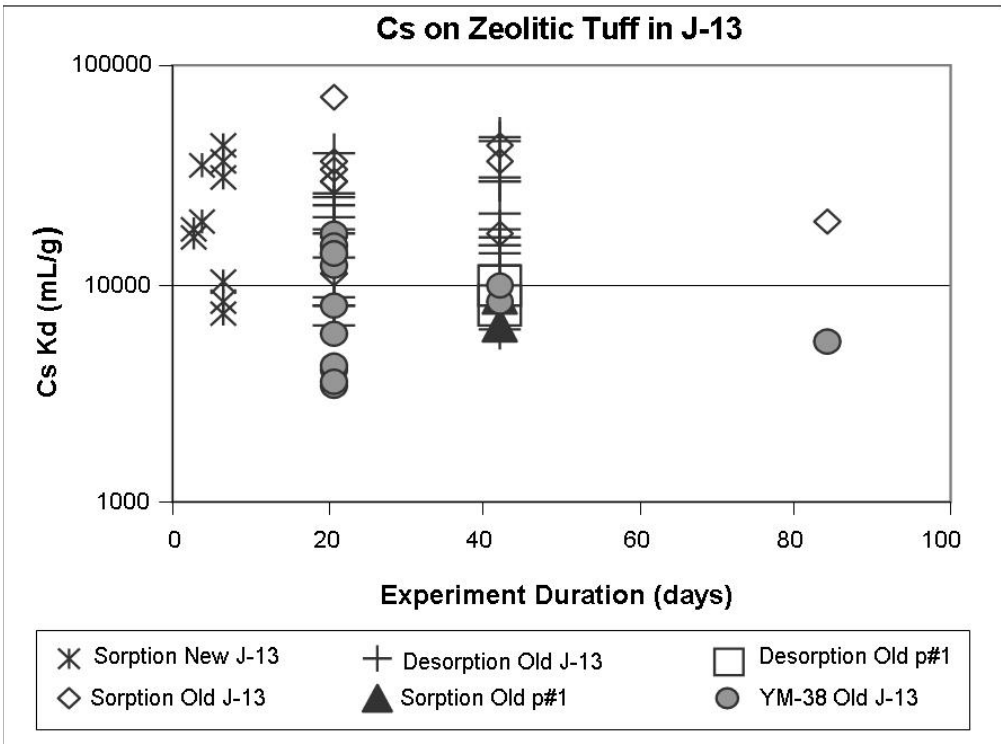

Sources: DTNs: LA0310AM831341.001 [DIRS 165865]; LA0407AM831341.002 [DIRS 170621].

NOTES: In the legend, 'old' stands for data collected before May 1989, 'new' stands for data collected after May 1989. The results for experiments which included the "fines" fraction were not included in the figure.

Figure A-13. Cesium Sorption Coefficients on Zeolitic Tuff versus Experiment Duration for Sorption (Forward) and Desorption (Backward) Experiments

The cesium sorption-coefficient probability distribution selected for zeolitic tuff in the saturated zone is an exponential distribution with a range of 4,000 to 42,000 mL/g, a mean of 16,942 mL/g, and a standard deviation of 14,930 mL/g. The low end of the chosen range was selected based on the minimum value observed in the available experiments, including those with p#1 water. The upper end of the distribution was chosen as a minimum upper limit given the potential impacts of variations in mineral compositions and ion-exchange capacities beyond those encountered in the experimental program.

A7.2.3 Alluvium

The probability distribution for devitrified tuff will be used as a default for the cesium sorption-coefficient probability distribution in alluvium. Alluvium along the flow path is composed largely of disaggregated tuffaceous materials. Because devitrified tuff makes up a major portion of the volcanic units exposed at the surface, it should be a major component in alluvium. In addition, clays and other secondary minerals are enriched in alluvial materials. These characteristics should result in higher sorption coefficients for alluvial materials compared to intact devitrified tuff.

A7.3 NEPTUNIUM

According to Nitsche et al. (1993 [DIRS 155218], Table VI), the solubility of neptunium in J-13 well water at 25°C and a pH of 8.5 is 4.4×10^{-5} M, and the solubility-controlling solid is Np_2O_5 under oxidizing conditions (Eh > 180 mV) (Eh is the oxidation/reduction potential normalized to the standard hydrogen electrode). At a pH of 6.9, the solubility is higher at 1.3×10^{-4} M under oxidizing conditions (Eh > 250 mV). The solubility of neptunium in Borehole p#1 water at 25°C at a pH of 8.5 is 7.0×10^{-6} M and 4.7 (± 0.4) $\times 10^{-5}$ M at a pH of 7.0, according to Nitsche et al. (1995 [DIRS 100163], Table A).

A7.3.1 Devitrified Tuff

The results of sorption experiments with devitrified tuff are shown in Figure A-14. Some of the experiments with J-13 well water had final neptunium concentrations above 7.0×10^{-6} M. Thus, the results for these experiments will not be used in the derivation of sorption coefficient probability distributions because the experiments could have been oversaturated with Np_2O_5. All but four of the experiments with synthetic p#1 water had final neptunium solution concentrations less than 2.5×10^{-5} M. The results for the four experiments with oversaturated final solutions will not be used in the derivation of sorption coefficient probability distributions. The remaining data points, plotted in Figure A-15, are suggestive of a dependence of the sorption coefficient on the final neptunium solution concentration. The two datapoints for "new sorption p#1" experiments with high K_d values (18-30 mL/g) are outliers and probably not reliable. Most of the "new sorption p#1" datapoints have values less than 2.0.

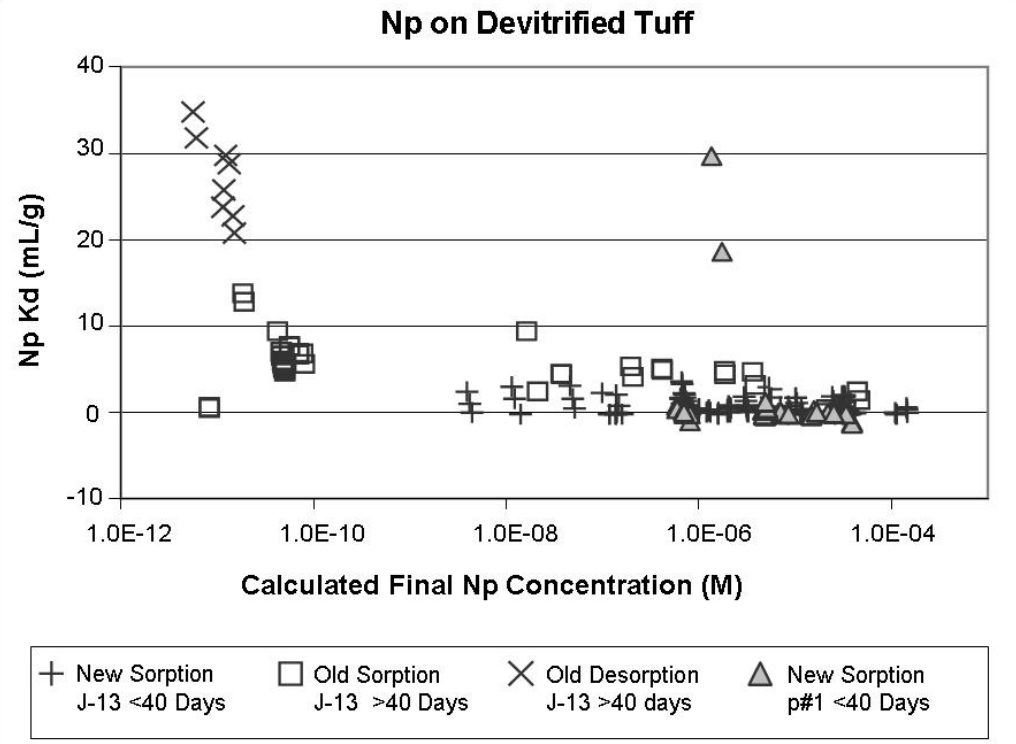

Sources: DTNs: LA0305AM831341.001 [DIRS 163789]; LA0407AM831341.004 [DIRS 170622].

NOTE: In the legend, 'old' stands for data collected before May 1989, 'new' stands for data collected after May 1989.

Figure A-14. Neptunium Sorption Coefficients on Devitrified Tuff versus Calculated Final Neptunium Concentration in Solution

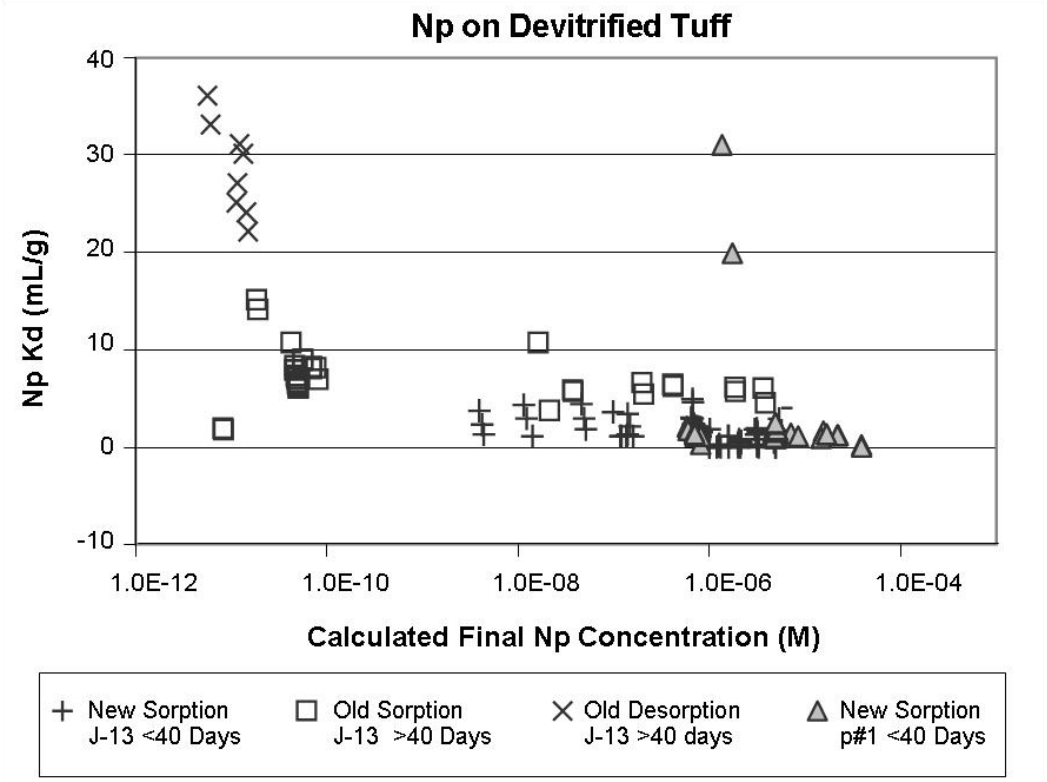

Sources: DTNs: LA0305AM831341.001 [DIRS 163789]; LA0407AM831341.004 [DIRS 170622].

NOTE: In the legend, 'old' stands for data collected before May 1989, 'new' stands for data collected after May 1989. Experiments oversaturated with Np_2O_5 have been omitted.

Figure A-15. Neptunium Sorption Coefficients on Devitrified Tuff versus Calculated Final Neptunium Concentration in Solution

Neptunium sorption experiments carried out as a function of experiment duration are shown in Figure A-16. There is a significant difference between the results for "old" and "new" experiments with the "old" results generally having higher values than the "new" results. The most straightforward explanation for this difference is that neptunium sorption kinetics are relatively slow. This would cause longer term experiments ("old") to have higher sorption coefficient values than short term experiments ("new"). Within the "old" sorption data points, the sorption-coefficient values appear to reach a steady-state level after approximately 40 days. However, the fact that sorption-coefficient values obtained in "old" desorption experiments are substantially higher than those obtained in "old" sorption experiments suggests that to reach equilibrium may take substantially more than 40 days. Thus, the sorption kinetics for neptunium are relatively slow on devitrified tuffs compared to the sorption kinetics of elements such as cesium.

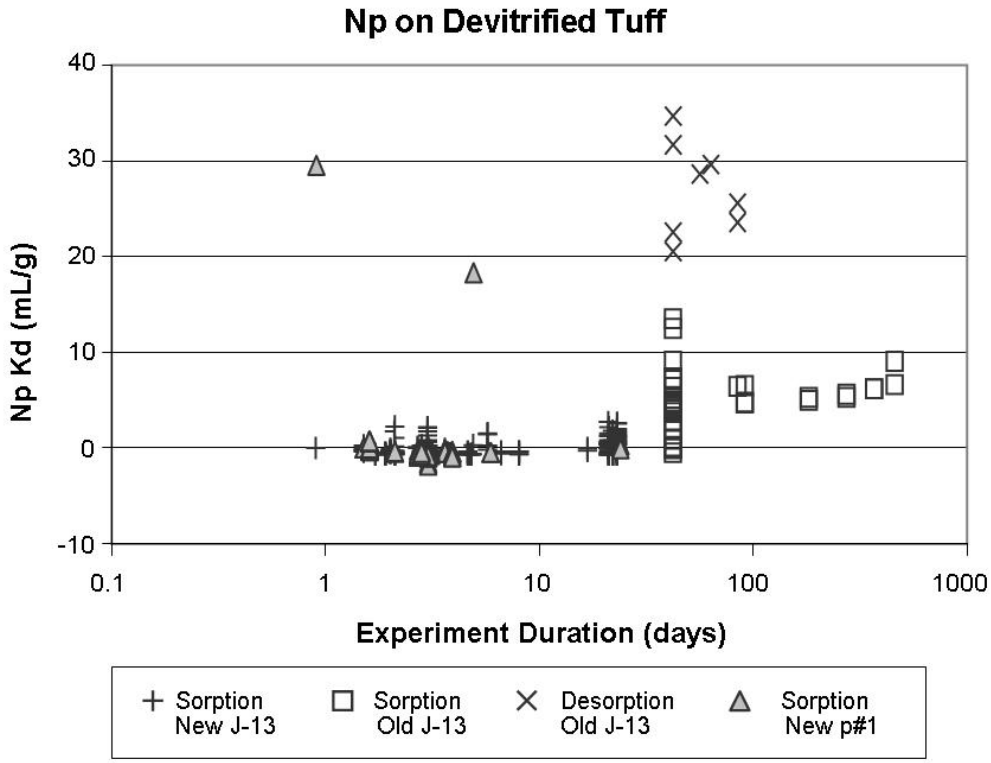

Sources: DTNs: LA0305AM831341.001 [DIRS 163789]; LA0407AM831341.004 [DIRS 170622].

NOTE: In the legend, 'old' stands for data collected before May 1989, 'new' stands for data collected after May 1989. Experiments oversaturated with Np_2O_5 have been omitted.

Figure A-16. Neptunium Sorption Coefficients on Devitrified Tuff versus Experiment Duration for Sorption (Forward) and Desorption (Backward) Experiments

The impact of variations in pH on neptunium coefficients on devitrified tuffs is shown in Figure A-17. There is a lot of scatter in the "new" data, and there do not appear to be clear positive or negative trends among these data points nor does there appear to be much difference between the results for J-13 well water and synthetic p#1 water. The "old" data points are more consistent and show very little dependence of the neptunium sorption coefficient on pH except at pH values less than 7.0.

To further investigate the potential impact of variations in water chemistry on neptunium sorption on devitrified tuff, a surface complexation model was developed using the hydrochemical code PHREEQC (see Section A6). In this model, a silica surface was used to represent devitrified tuff. Neptunium binding constants on silica were obtained from measurements by Turner et al. (1998 [DIRS 162989]). Other inputs required for the surface complexation models are discussed in Section A6. This surface complexation modeling study was performed to simulate the results of the experiment used for synthetic p#1 water using the same concentrations as for the volcanic portion of p#1 (Table A-2a), except the sodium and bicarbonate concentrations, which were modified to the values for synthetic p#1 water (Table A-2b). The results of the PHREEQC calculations are presented in Figure A-17. Note that the sorption coefficients calculated for J-13 well water are larger than those calculated for p#1 water. Although there is substantial scatter in the "old" data, the J-13 curve lies below the sorption coefficients obtained in "old" J-13 desorption experiments and above many of the

sorption coefficient values obtained in "old" J-13 sorption experiments. This result suggests the curve may reflect the equilibrium values of neptunium sorption coefficients on devitrified tuff better than the experimental data. In this interpretation, all the "new" J-13 sorption data points and many of the "old" J-13 sorption data points represent experiments that did not reach equilibrium. The same would be true for all the J-13 "old" desorption data points.

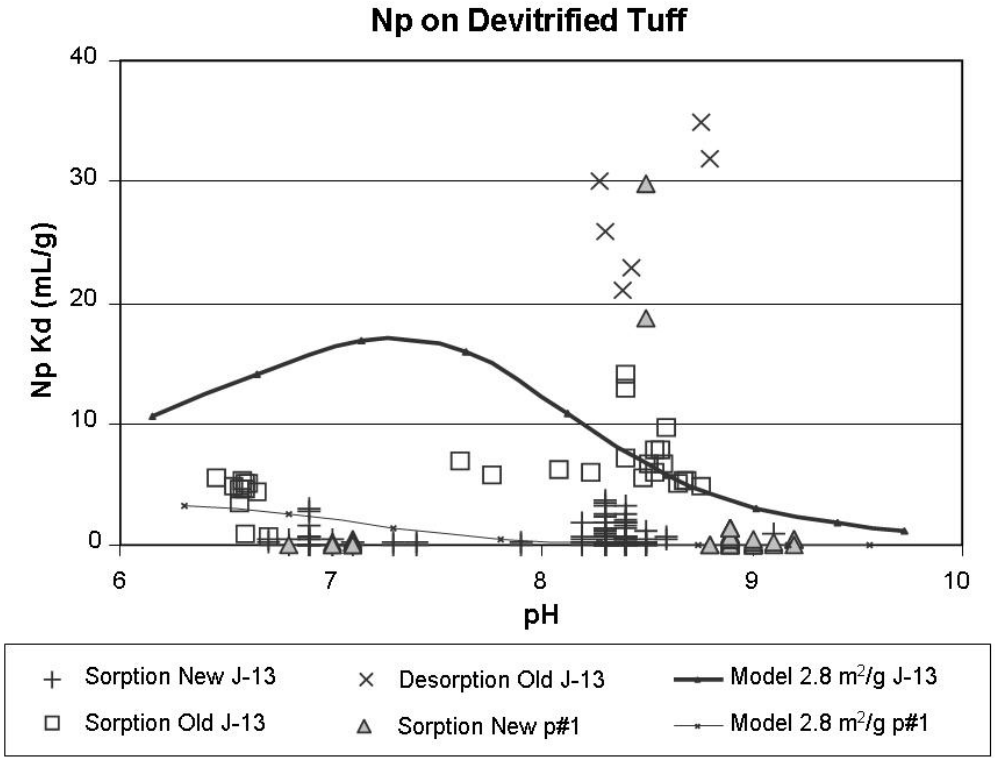

Sources: DTNs: LA0305AM831341.001 [DIRS 163789]; LA0407AM831341.004 [DIRS 170622], and Output DTN: LA0702MD831232.002, file *output_07.xls*, worksheets *Npsij13.pun.xls* and *Npsip1.pun.xls*

NOTE: In the legend, 'old' stands for data collected before May 1989, 'new' stands for data collected after May 1989. PHREEQC model results for J-13 well and p#1 waters are also plotted (Output DTN: LA0702MD831232.002).

Figure A-17. Neptunium Sorption Coefficients on Devitrified Tuff in J-13 Well and Synthetic p#1 Waters versus Solution pH in Sorption (Forward) and Desorption (Backward) Experiments

The neptunium sorption-coefficient probability distribution selected for devitrified tuff in the saturated zone is an exponential distribution with a range of 0 to 2 mL/g and a mean of 0.69 mL/g, and a standard deviation of 0.71 mL/g. The low end of the chosen range is selected based on the minimum value obtained in short-term experiments (up to 21 days). The upper end of the distribution was chosen as a minimum upper limit with a neptunium concentration near the solubility limit (Figure A-15). It is acknowledged that a higher limit could be selected for the upper end of the distribution based on the available experimental and modeling data.

A7.3.2 Zeolitic Tuff

Sorption coefficients on zeolitic tuff are shown as a function of calculated final solution concentration in Figure A-18. None of the final solutions were oversaturated with Np_2O_5. There

is very little evidence that neptunium sorption coefficients on zeolitic tuffs are dependent on the calculated final solution concentration in J-13 experiments (i.e., sorption isotherms are linear). However, it is clear that there is a dependence of sorption coefficient on water chemistry in the short-term experiments. If the solubility of neptunium in synthetic p#1 water is less than the solubility in actual p#1 water, this dependence on water chemistry may not be real.

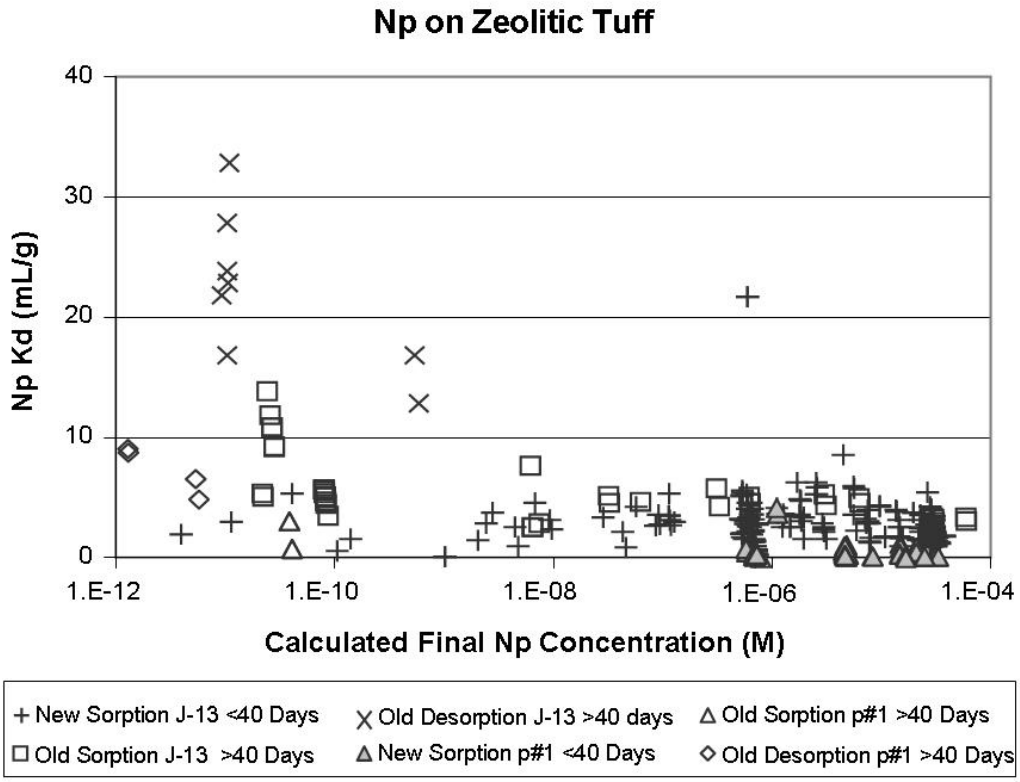

Sources: DTNs: LA0305AM831341.001 [DIRS 163789]; LA0407AM831341.004 [DIRS 170622].

NOTE: In the legend, 'old' stands for data collected before May 1989, 'new' stands for data collected after May 1989.

Figure A-18. Neptunium Sorption Coefficients on Zeolitic Tuff versus Calculated Final Neptunium Concentration in Solution

Neptunium sorption experiments carried out as a function of experiment duration are shown in Figure A-19. As with devitrified tuff, the kinetics of neptunium sorption on zeolitic tuff are relatively slow. Even at 100 days, the K_d values in sorption experiments are still smaller than the values obtained in desorption experiments.

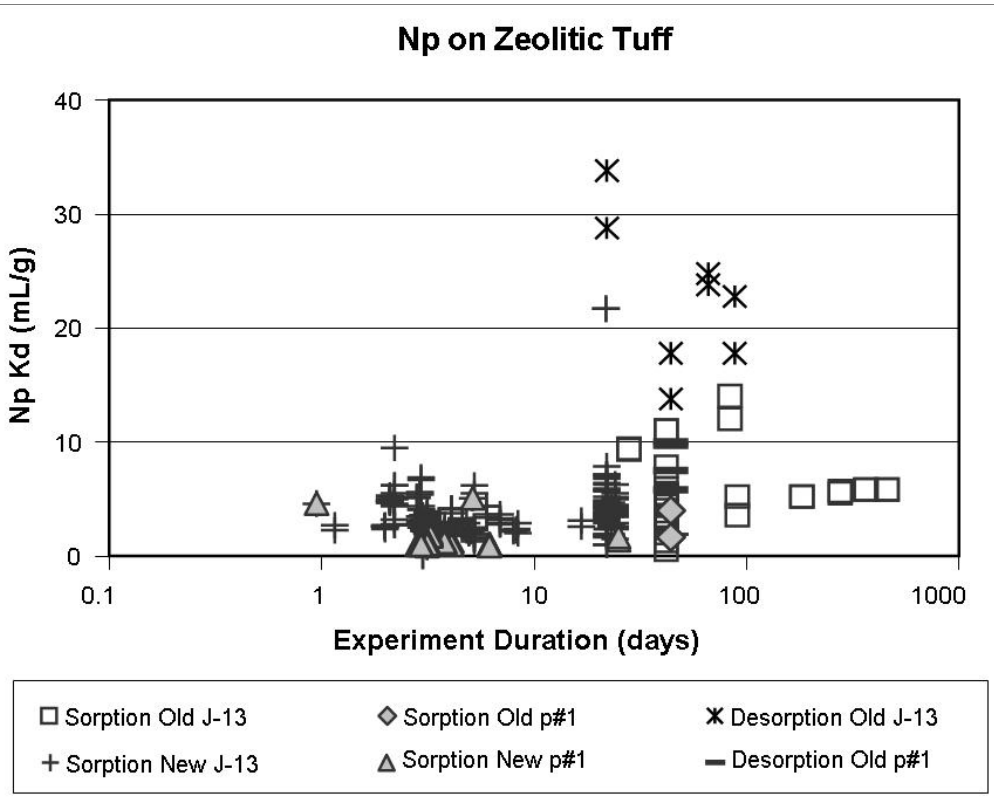

Sources: DTNs: LA0305AM831341.001 [DIRS 163789]; LA0407AM831341.004 [DIRS 170622].

NOTE: In the legend, 'old' stands for data collected before May 1989, 'new' stands for data collected after May 1989. Oversaturated experiments have been omitted.

Figure A-19. Neptunium Sorption Coefficients on Zeolitic Tuff versus Experiment Duration for Sorption (Forward) and Desorption (Backward) Experiments

The impact of variations in pH on neptunium coefficients for sorption on devitrified tuffs is shown in Figure A-20. There is a lot of scatter in the "new" data, and there do not appear to be clear positive or negative trends among these data points. It is interesting that zeolitic tuffs show a similar range of sorption coefficients as do devitrified tuffs in spite of the fact that zeolitic tuffs have approximately 10 times the surface area of devitrified tuffs. This suggests that neptunium cannot access the internal surface areas of the zeolites in the zeolitic tuffs. The neptunium sorption-coefficient probability distribution selected for zeolitic tuff in the saturated zone is a truncated normal distribution with a range of 0 to 6 mL/g, a mean of 2.88 mL/g, and a standard deviation of 1.47 mL/g. The low end of the chosen range is selected based on the minimum value obtained in short-term experiments (up to 21 days). The upper end of the distribution was chosen as a minimum upper limit with a neptunium concentration near the solubility limit (Figure A-18). It is acknowledged that a higher limit could be selected for the upper end of the distribution based on the available data.

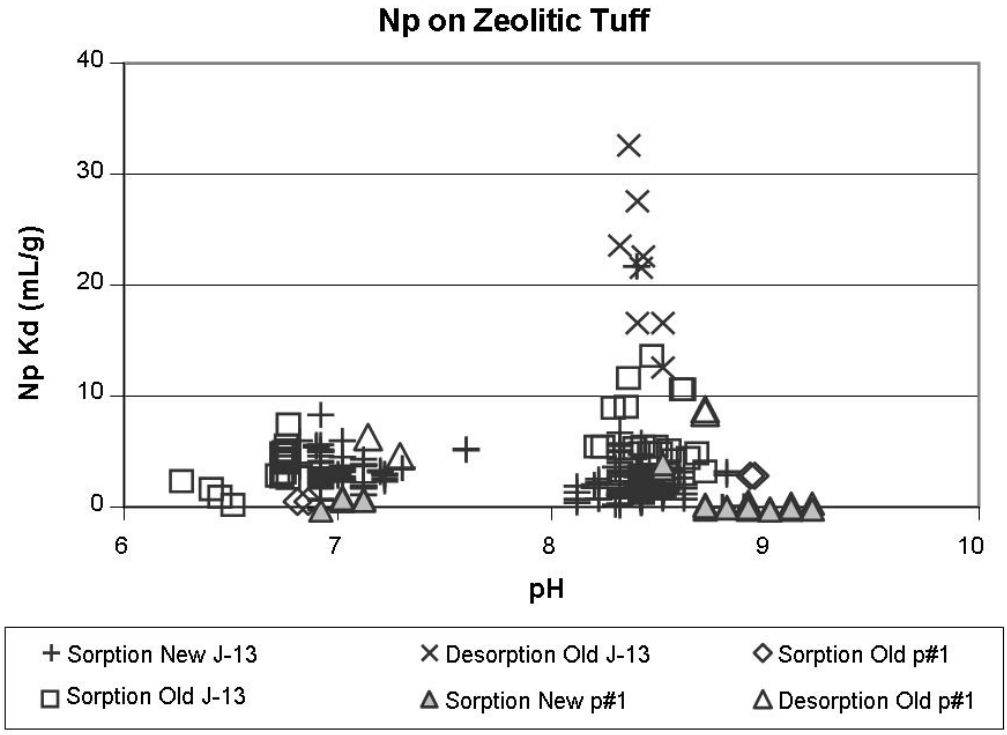

Sources: DTNs: LA0305AM831341.001 [DIRS 163789]; LA0407AM831341.004 [DIRS 170622].

NOTE: In the legend, 'old' stands for data collected before May 1989, 'new' stands for data collected after May 1989. Oversaturated experiments have been omitted.

Figure A-20. Neptunium Sorption Coefficients on Zeolitic Tuff in J-13 Well Water and Synthetic p#1 Water versus Solution pH in Sorption (Forward) and Desorption (Backward) Experiments

A7.3.3 Alluvium

Sorption coefficients have been measured in batch experiments from core obtained from three wells drilled into the alluvium (DTN: LA0302MD831341.003 [DIRS 163784]): Borehole NC-EWDP-10SA to the north, NC-EWDP-22SA in the middle, and NC-EWDP-19IM1A to the south, spaced between 4 to 5 km apart. Samples were taken below the water table from a 5-ft interval at two depths in wells NC-EWDP-19IM1A and NC-EWDP-10SA and at six depths in well NC-EWDP-22SA. For each core sample, batch experiments were run on three particle sizes: 500 to 2,000 μm, 75 to 500 μm, and < 75 μm. The K_d values observed on the third particle size fraction were noticeably larger than the other two size fractions, probably because of mineral sorting effects and the higher surface area per unit mass for the smaller size particles. The K_d values for this size fraction were not considered further. Several replicates of each batch experiment were run so that a sample standard deviation could be obtained for each size fraction. Twelve of the 20 samples had a sample coefficient of variation < 0.1; six had a coefficient of variation < 0.22; and two had a coefficient of variation < 0.7.

The cell size in the three-dimensional model is 250 m × 250 m near the water table in the alluvium. Hence, the K_d parameter in the model represents a mean value, and the uncertainty distribution needs to represent the uncertainty about the mean on this large scale, not the local variance of the small-scale experiments. To avoid overly weighting the 12 samples from well 22SA, the mean K_d value was evaluated for each well (i.e., the K_d values obtained from any one

well were similar and, thus, suggested some correlation). The coefficients of variation for these means were of the same order of magnitude as those for the samples (i.e., < 0.16), and so the small errors in any one experiment could be neglected. The three mean K_d values were taken to represent the best estimate of the K_d for any one cell in the FEHM model. According to the Law of Large Numbers, the means should be normally distributed; however, since the number of samples is small (i.e., 3), the Student-t distribution was used to correctly account for the error in estimating the standard deviation. The K_d value for neptunium were taken to be described by a *t* distribution with the following statistics: $\mu Np = 6.3$ mL/g, $\sigma Np = 0.81$ mL/g.

Although the *t* distribution was thought to correctly capture the spatial uncertainty, the question about the representativeness of the experiment does introduce a small amount of additional uncertainty. For example, other sources of uncertainty that may not have been completely represented in the experiments included potential competitive effects among radionuclides, different adsorption behavior between different oxidation states of the radionuclides, impact of climatic change, variability in water composition and rock types, and complexation by organic ligands. The probability that these uncertainties were not properly represented by the experiment was thought to be less than 10%. Nonetheless, to accommodate for this possibility, the tails of the distribution were extended from the approximate bounds of the *t* distribution ($\pm 3\sigma$) to the maximum and minimum experimental values observed. A 10% probability was assigned to these tails. This adjustment was implemented by using a piecewise-uniform cumulative distribution. For neptunium, the minimum experimentally observed value was 1.8 mL/g. Five percent probability was uniformly distributed between 1.8 mL/g and the lower bound of the *t* distribution at 4.0 mL/g. Since the *t* distribution had such little variation, it was reasonably represented by a uniform distribution; hence, 90% probability was uniformly distributed between 4.0 mL/g and the upper bound of the *t* distribution at 8.7 mL/g. The remaining 5% probability was uniformly distributed between 8.7 mL/g and the maximum experimentally observed value of 13 mL/g.

A7.4 PLUTONIUM

According to Nitsche et al. (1993 [DIRS 155218], p. 54), the solubility of plutonium in J-13 well water at 25°C and a pH of 8.4 is $2.9 (\pm 0.8) \times 10^{-7}$ M and is not very sensitive to pH over the range from 7.0 to 8.4. The solubility of plutonium in p#1 water at 25°C is $1.0 (\pm 0.1) \times 10^{-6}$ M for a pH of 8.5 and $4.5 (\pm 0.4) \times 10^{-7}$ M for a pH of 7.0 according to Nitsche et al. (1995 [DIRS 100163], p. 39). Thus, the solubility of plutonium in J-13 well water is somewhat lower than it is in p#1 water.

A7.4.1 Devitrified Tuff

The experimentally derived sorption coefficients for plutonium on devitrified tuff are plotted against the calculated final plutonium concentrations of the experiments in Figure A-21. The data points are separated into groups on the basis of when the experiments were carried out (before May 1989 = "old" and after May 1989 = "new"), water chemistry, experiment duration, and on whether the sorption coefficient was determined from a sorption or a desorption experiment. The plotted data indicate that the "new" and "old" data show similar ranges of K_d values, that the longer-term experiments generally yield higher sorption-coefficient values than the shorter-term experiments, and that desorption experiments yield higher sorption-coefficient

values than sorption experiments. These points are discussed in greater detail in the following paragraphs.

The maximum calculated final plutonium concentration plotted in Figure A-21 is slightly less than the solubility determined by Nitsche et al. (1993 [DIRS 155218], p. 54) for plutonium in J-13 well water. Thus, the plutonium sorption coefficients plotted in Figure A-21 reflect solutions that were undersaturated with the solid plutonium phase precipitated in the experiments reported by Nitsche et al. (1993 [DIRS 155218], p. 54).

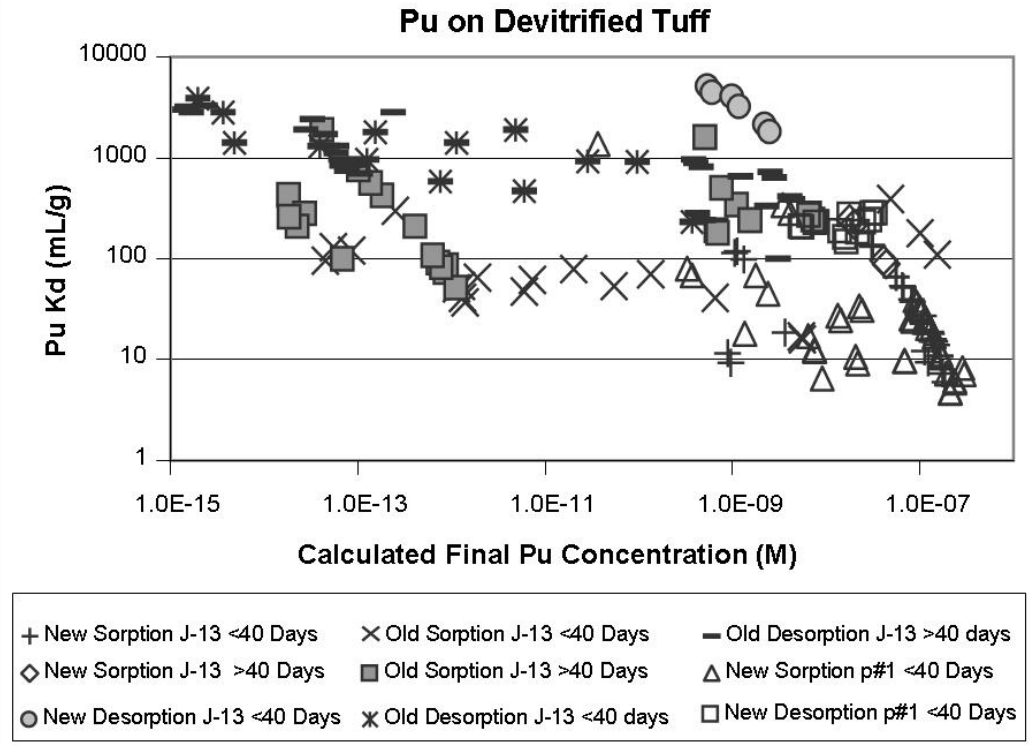

Sources: DTNs: LA0305AM831341.001 [DIRS 163789]; LA0407AM831341.005 [DIRS 170625].

NOTE: In the legend, 'old' stands for data collected before May 1989, 'new' stands for data collected after May 1989.

Figure A-21. Plutonium Sorption Coefficients on Devitrified Tuff versus Calculated Final Plutonium Concentration in Solution

The effect of the solution plutonium concentration on the sorption-coefficient value obtained is shown more clearly in Figure A-22. Data are plotted for two devitrified tuff samples that contain only trace amounts of secondary phases (e.g., clays, zeolites). In addition, plotted data are restricted to 21-day experiment durations and a pH value near 8.4. As is evident in the figure, within the errors of the analyses, the measured plutonium sorption coefficients are nearly independent of the final plutonium solution concentration.

The effect of experiment duration on the plutonium K_d value is shown in Figure A-23. As expected, the K_d values for sorption experiments increase with increasing duration, and the K_d values for desorption experiments decrease with increasing duration. However, the increase in the sorption values is much greater than the decrease in desorption values over the time frame of the experiments. This result may reflect the reduction of plutonium in the +5 and/or

+6 oxidation states to plutonium in the +4 oxidation state on the mineral surfaces present in devitrified tuff, as discussed in greater detail below. The trends in the sorption and desorption data points suggest they would converge to values somewhere between 100 mL/g and 1,000 mL/g. Based on the data plotted, such convergence would require more than 100 days. Note that the "old" sorption data points exceeding 1,000 mL/g are for samples that contain significant amounts of clay or zeolite. For this reason, these data are discounted in the derivation of the sorption-coefficient probability distribution.

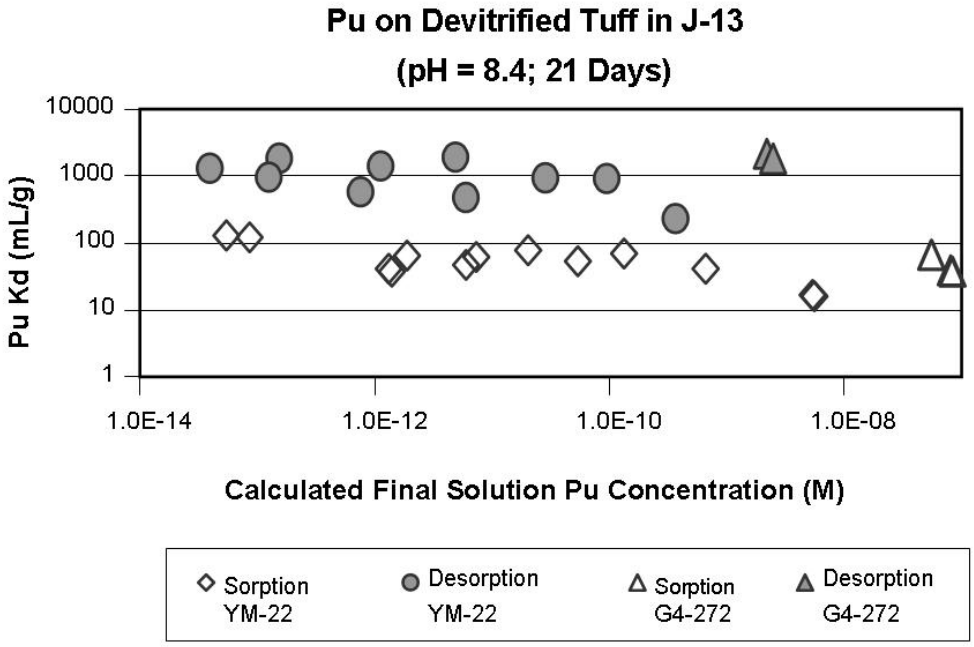

Sources: DTNs: LA0407AM831341.005 [DIRS 170625]; LA0305AM831341.001 [DIRS 163789].

Figure A-22. Plutonium Sorption Coefficients versus Calculated Final Plutonium Solution Concentration (M) for Experiments with Samples YM-22 and G4-272

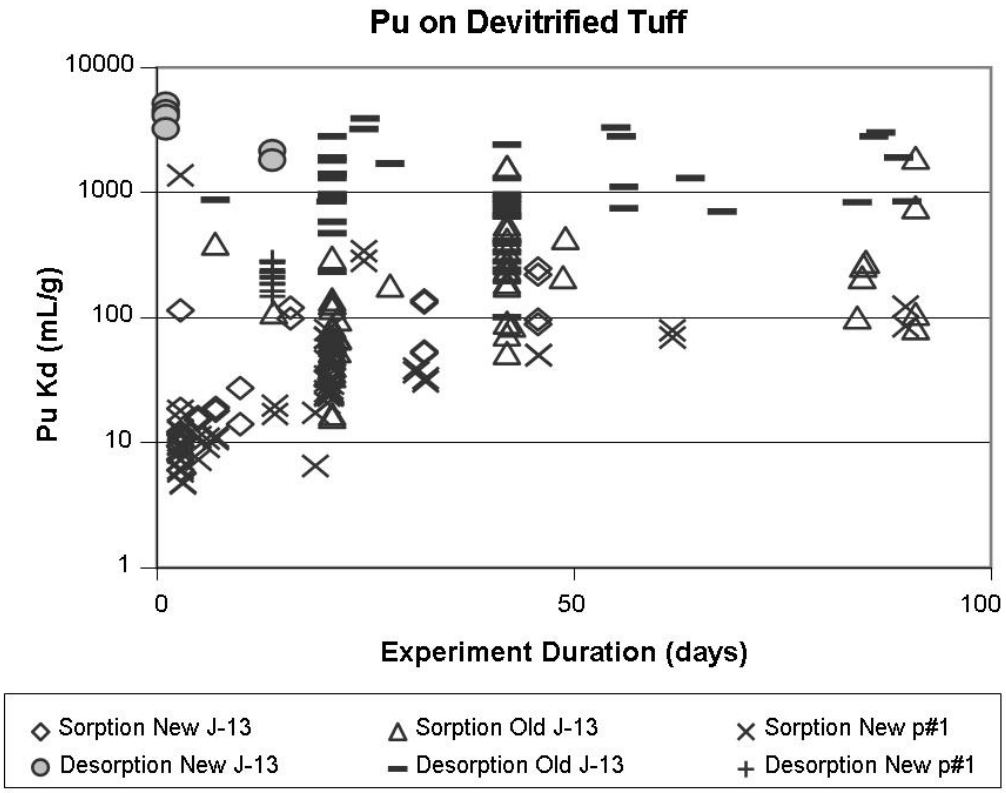

Sources: DTNs: LA0305AM831341.001 [DIRS 163789]; LA0407AM831341.005 [DIRS 170625].

Figure A-23. Plutonium Sorption Coefficients on Devitrified Tuff versus Experiment Duration for Sorption (Forward) and Desorption (Backward) Experiments

The impact of variations in pH on plutonium sorption coefficients on devitrified tuffs is shown in Figure A-24. There is a lot of scatter in the data, and there do not appear to be clear positive or negative trends in any of the data groupings.

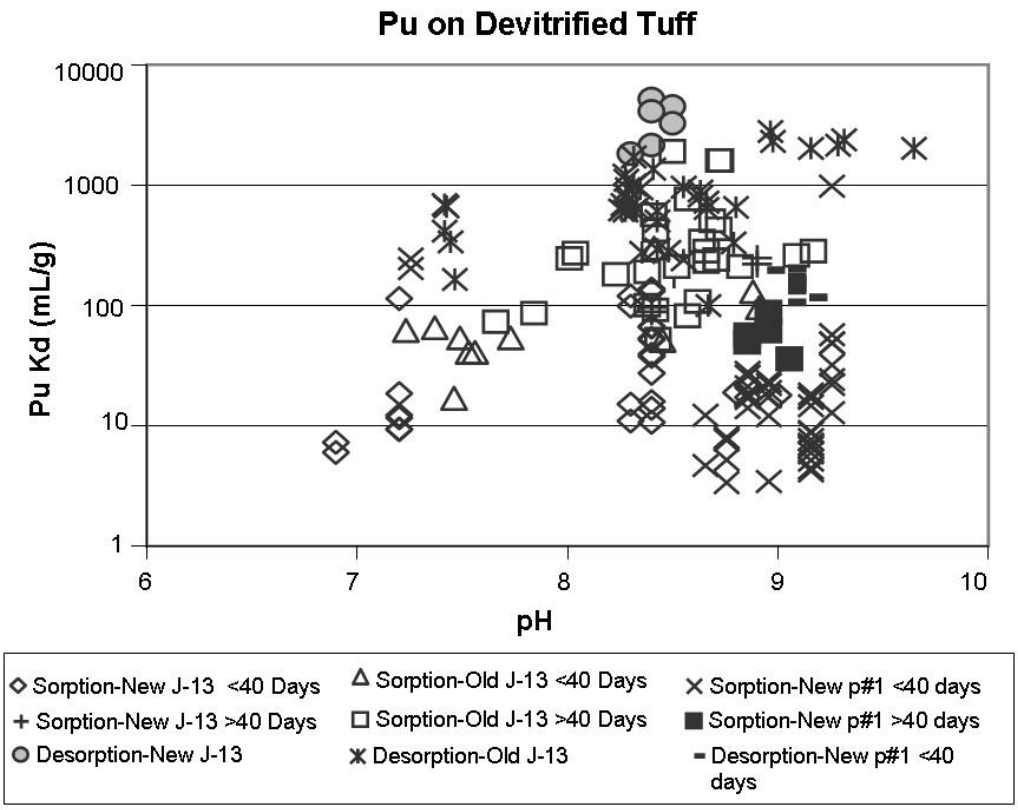

Sources: DTNs: LA0305AM831341.001 [DIRS 163789]; LA0407AM831341.005 [DIRS 170625].

NOTE: In the legend, 'old' stands for data collected before May 1989, 'new' stands for data collected after May 1989. Experiments lasting 40 days or more are plotted separately from experiments lasting less than 40 days.

Figure A-24. Plutonium Sorption Coefficients on Devitrified Tuff in J-13 Well Water and Synthetic p#1 Water versus Solution pH in Sorption (Forward) and Desorption (Backward) Experiments

The lack of clear trends is also evident when the results of short-term experiments (< 40 days) are removed from the data set. This outcome is shown in Figure A-25 in which only the longer-term data are plotted.

The impact of variations in the major ion composition of groundwaters is also shown in Figures A-24 through A-25. Although there is a limited set of experiments with synthetic p#1 water, the results are within the range of the results obtained in experiments with J-13 well water. Thus, there is no clear evidence of an impact of water chemistry variations on plutonium sorption coefficients in devitrified tuff.

A major factor not explicitly accounted for in the experimental program is the impact of variations in the Eh of Yucca Mountain groundwaters on plutonium sorption coefficients. The laboratory experiments upon which the data discussed in this section are based were invariably conducted under oxidizing conditions because the waters used in the experiments contained dissolved oxygen and were in contact with the atmosphere. Nitsche et al. (1993 [DIRS 155218], pp. 60 to 61) found that plutonium dissolved in J-13 well water is present predominantly in the +5 and +6 oxidation states. If plutonium in the +5 and +6 oxidation states behaves similarly to

neptunium +5 and uranium +6, respectively, as has been suggested by many investigators (e.g., Keeney-Kennicutt and Morse 1985 [DIRS 106313], pp. 2577 to 2578), then small values (< 10 mL/g) would be expected for plutonium sorption coefficients under oxidizing conditions (see the sections on neptunium and uranium). The fact that plutonium sorption coefficients measured under oxidizing conditions are up to 2 to 3 orders of magnitude larger than expected (Figure A-25) suggests that either plutonium +5 and +6 do not behave like neptunium +5, and uranium +6 in sorption reactions or plutonium is reduced to the +4 oxidation state on rock/mineral surfaces. Data presented by Keeney-Kennicutt and Morse (1985 [DIRS 106313], p. 2,577) support the latter alternative.

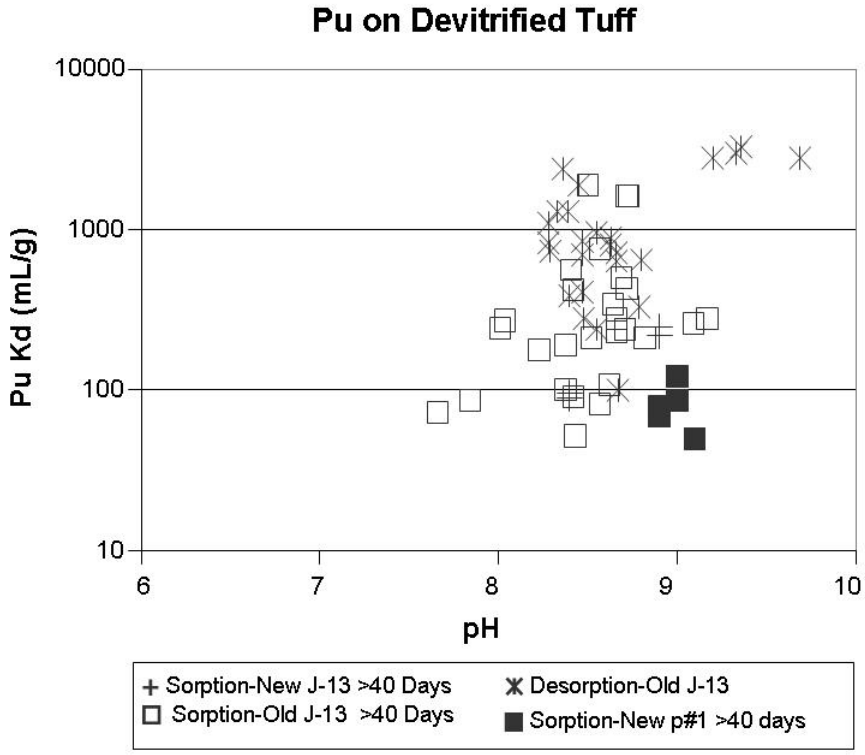

Sources : DTNs: LA0305AM831341.001 [DIRS 163789]; LA0407AM831341.005 [DIRS 170625].

NOTE: In the legend, 'old' stands for data collected before May 1989, 'new' stands for data collected after May 1989.

Figure A-25. Plutonium Sorption Coefficients on Devitrified Tuff in J-13 Well Water and Synthetic p#1 Water versus Solution pH in Sorption (Forward) and Desorption (Backward) Experiments with Durations Greater than 40 Days

The large range in plutonium sorption coefficients measured in devitrified tuffs (e.g., Figure A-25) could be explained if plutonium is present in more than one oxidation state on the rock/mineral surfaces in the devitrified tuffs. However, in the absence of definitive data on the oxidation state of plutonium on rock/mineral surfaces, the experimentally determined sorption-coefficient values will be used to derive the sorption coefficient probability distributions.

The plutonium sorption-coefficient probability distribution selected for devitrified tuff in the saturated zone is a beta distribution with a range of 50 to 300 mL/g, mean of 100 mL/g, and a

standard deviation of 15 mL/g. The low end of the chosen range is selected based on the minimum value observed in long-term experiments (> 40 days), but it also captures the potential impacts of variations in surface areas among samples used in the experiments, variations in water chemistry, and variations in plutonium concentrations up to the solubility limit. The upper end of the distribution was chosen as a minimum upper limit given the potential impacts of sorption kinetics in the long term. The fact that sorption coefficients derived from desorption experiments were, on average, greater in value than those obtained from sorption experiments (Figure A-25) indicates that equilibrium had not been reached. In longer time frames, the coefficients derived from desorption experiments may continue to decrease whereas the coefficients from sorption experiments continue to increase. The upper limit was selected in acknowledgement of this possibility. In addition, the impacts of variations in sample surface areas, waters chemistry, and plutonium solution concentrations were considered in choosing the upper limit value.

A7.4.2 Zeolitic Tuff

The experimentally derived sorption coefficients for plutonium on zeolitic tuff are plotted against the calculated final plutonium concentrations in Figure A-26. As before, the data points are separated into groups on the basis of when the experiments were carried out (before May 1989 = "old" and after May 1989 = "new"), water chemistry, experiment duration, and on whether the sorption coefficient was determined from a sorption or a desorption experiment. The plotted data indicate that there is no clear trend of plutonium K_d values with solution concentration. Most of the data from sorption experiments plot between sorption-coefficient values of 100 and 1,000 mL/g. A series of "old" experiments at concentrations between 10^{-7} and 10^{-9} M yielded sorption-coefficient values less than 100 mL/g. However, the same rock type, when used in "new" experiments, yielded a series of sorption-coefficient values > 100 mL/g. Why there is a difference of almost a factor of 10 between these two sets of data is not known with certainty. Part of the answer lies in the fact that, on average, the "old" data points represent shorter duration experiments than the "new" data points. However, other factors are likely involved. For example, the oxidation state of plutonium in the starting solution may play a role.

As with devitrified tuffs, the plutonium sorption coefficients for zeolitic tuff plotted in Figure A-26 reflect solutions that were undersaturated with the plutonium phase precipitated in the experiments conducted by Nitsche et al. (1993 [DIRS 155218], p. 54, and 1995 [DIRS 100163], p. 39).

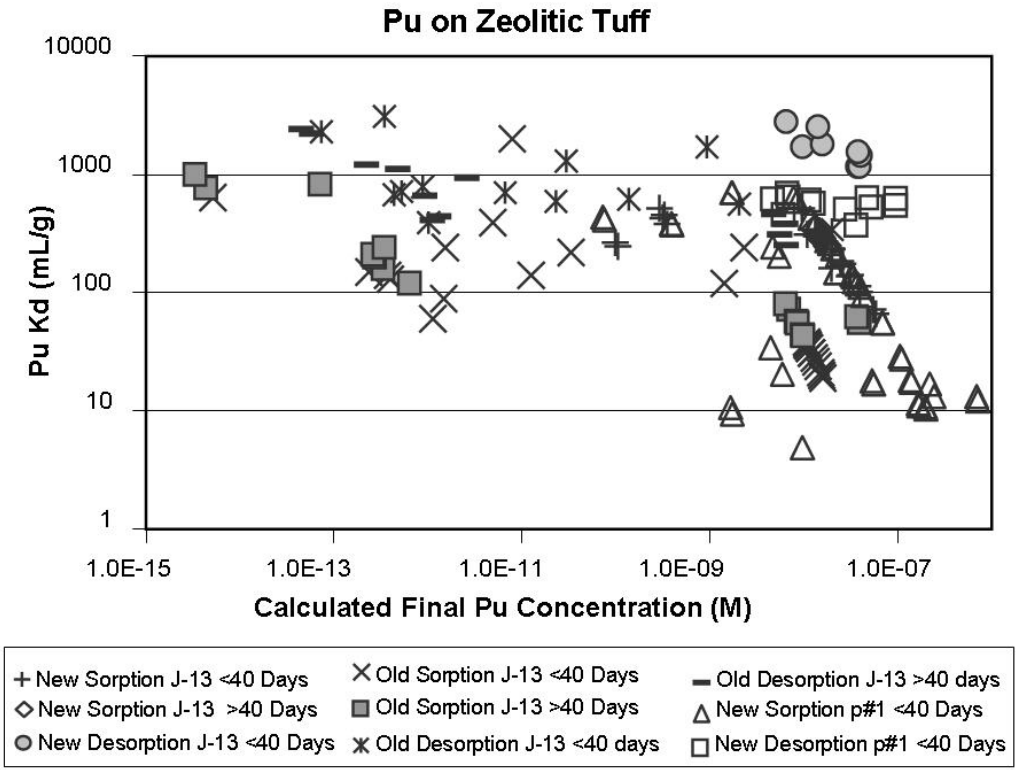

Sources: DTNs: LA0305AM831341.001 [DIRS 163789]; LA0407AM831341.005 [DIRS 170625].

NOTE: In the legend, 'old' stands for data collected before May 1989, 'new' stands for data collected after May 1989.

Figure A-26. Plutonium Sorption Coefficients on Zeolitic Tuff versus Calculated Final Plutonium Concentration in Solution

The effects of experiment duration on the plutonium K_d values for zeolitic tuff are shown in Figure A-27. As expected, the K_d values for sorption experiments increase with increasing duration and the values for desorption experiments decrease with increasing duration, at least in short-term experiments. Interestingly, the decrease in longer-term desorption experiments is not very pronounced. The trends in the sorption and desorption data points suggest they would converge to values somewhere between 100 and 1,000 mL/g. This result is similar to the range of values predicted for devitrified tuffs. Thus, the higher surface areas of zeolitic tuffs compared to devitrified tuffs (approximately 10 times) do not appear to result in higher sorption values. This effect was also observed by Pabalan et al. (1998 [DIRS 162987], p. 113) in experiments with uranium sorption on zeolite. The cause for the large range of values obtained at a given value for experiment duration is not known but may be due largely to variations in the oxidation state of plutonium in the starting solutions. However, variations in surface areas and surface chemistry among the samples used in the experiments must also contribute to the range observed.

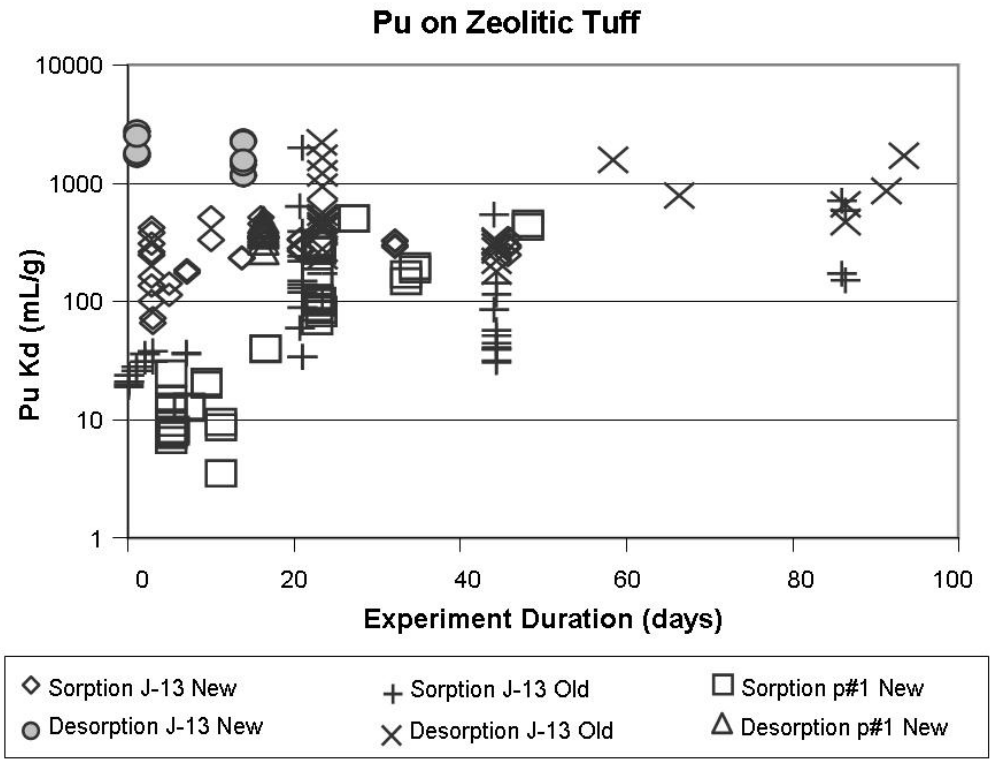

Source: DTNs: LA0305AM831341.001 [DIRS 163789]; LA0407AM831341.005 [DIRS 170625].

NOTE: In the legend, 'old' stands for data collected before May 1989, 'new' stands for data collected after May 1989.

Figure A-27. Plutonium Sorption Coefficients on Zeolitic Tuff versus Experiment Duration for Sorption (Forward) and Desorption (Backward) Experiments

The impact of variations in pH on plutonium sorption coefficients on zeolitic tuffs is shown in Figure A-28. Although there is a lot of scatter in the data, there do not appear to be clear positive or negative trends among any of the data groupings.

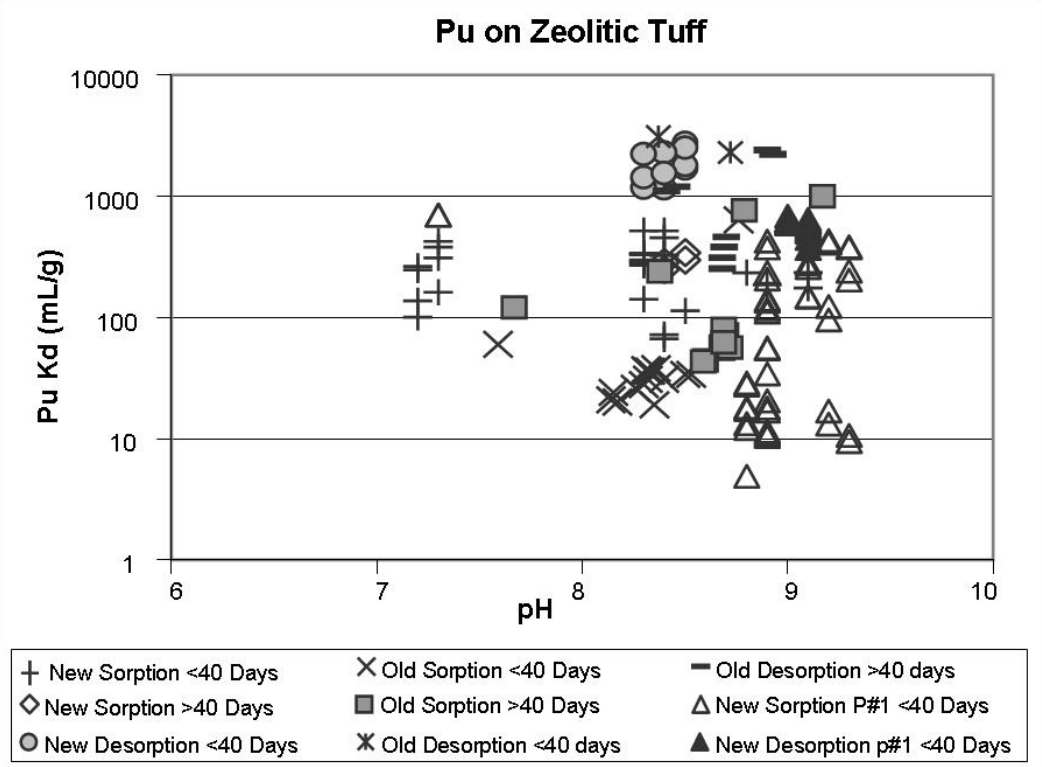

Source: DTNs: LA0305AM831341.001 [DIRS 163789]; LA0407AM831341.005 [DIRS 170625].

NOTE: In the legend, 'old' stands for data collected before May 1989, 'new' stands for data collected after May 1989.

Figure A-28. Plutonium Sorption Coefficients on Zeolitic Tuff in J-13 Well Water and Synthetic p#1 Water versus Solution pH in Sorption (Forward) and Desorption (Backward) Experiments

The impact of variations in the major ion composition of groundwaters is also shown in Figure A-28. Although there is a limited set of experiments with synthetic p#1 water, the results are largely within the range of the results obtained in experiments with J-13 well water. Thus, there is no clear evidence of an impact of water chemistry variations on plutonium sorption coefficients in devitrified tuff.

The plutonium sorption-coefficient probability distribution derived for zeolitic tuff in the saturated zone is the same as the distribution derived for devitrified tuff because the experimentally derived sorption-coefficient values show similar ranges as a function of variations in surface areas among samples used in the experiments, variations in water chemistry, and variations in plutonium concentrations up to the solubility limit.

A7.4.3 Alluvium

The probability distribution for devitrified tuff will be used as a default for the plutonium sorption-coefficient probability distribution in alluvium. Alluvium along the flow path is composed largely of disaggregated tuffaceous materials. Because it has been disaggregated, the surface area of alluvial material should be higher than that of devitrified tuff. In addition, clays and other secondary minerals are enriched in alluvial materials. These characteristics should result in higher sorption coefficients for plutonium in alluvial materials compared to intact devitrified tuff.

A7.5 PROTACTINIUM

Protactinium is very insoluble in waters of the type found at Yucca Mountain. The best estimates of protactinium solubility in these waters range from 10^{-15} to 10^{-13} M (Berry et al. 1989 [DIRS 144728], p. 346).

A7.5.1 Devitrified Tuff

The oxidation state of protactinium is +5 in groundwaters of the type found at Yucca Mountain (Cotton and Wilkinson 1980 [DIRS 101584], pp. 1,092 to 1,093). No sorption-coefficient data have been obtained for protactinium on devitrified tuffs from Yucca Mountain. Allard et al. (1983 [DIRS 162982], p. 12) have reported protactinium sorption-coefficient data for experiments with a silica sample having a surface area similar to that measured for devitrified tuffs. The solution composition used in the experiments was 0.01 M $NaClO_4$. The initial protactinium concentration used in all experiments was 4.0×10^{-12} M. Allard's data indicate that protactinium sorption coefficients vary substantially (approximately 2 orders of magnitude) as a function of pH, as shown in Figure A-29. The cause for this variation in sorption coefficients with pH is unknown. Over the pH range expected in SZ waters at Yucca Mountain (7 to 8.5), the sorption coefficients reported by Allard et al. (1983 [DIRS 162982], p. 12) range from approximately 7,500 to 20,000 mL/g. The results for 6-hour experiments were similar to the results for experiments lasting up to 6 weeks. Thus, sorption kinetics for protactinium sorption reactions appear to be fast. Allard et al. (1983 [DIRS 162982], p. 12) reported results for alumina that were very similar to the results they reported for silica.

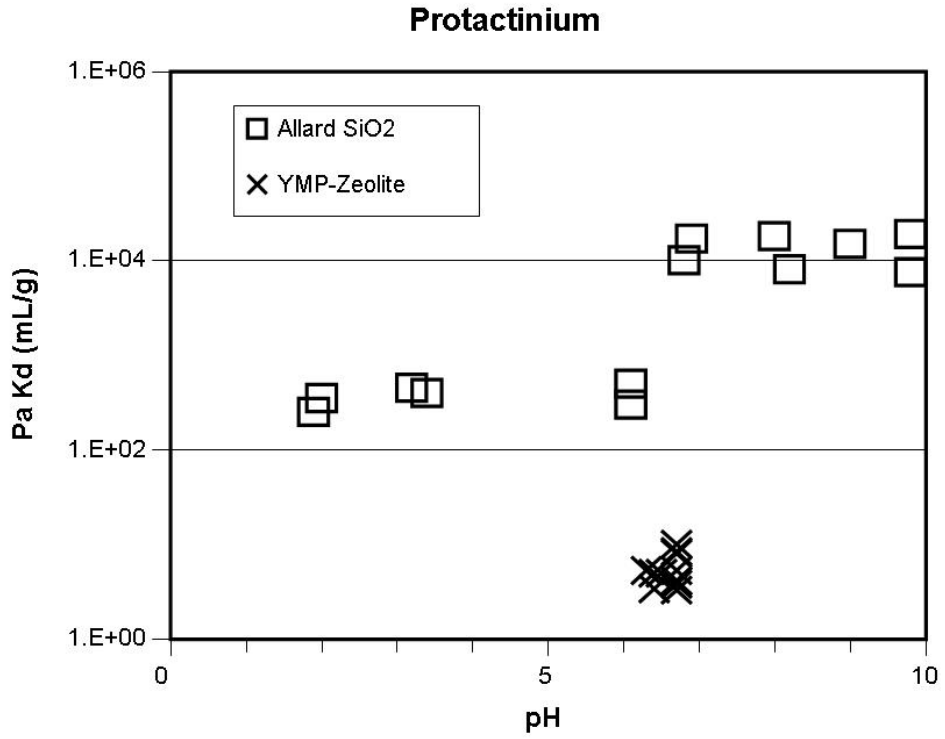

Source: DTN: LA0305AM831341.001 [DIRS 163789]; Allard et al. 1983 ([DIRS 162982], Figure 6]).

Figure A-29. Protactinium Sorption Coefficients versus pH

Hydrolysis reactions appear to dominate the solution chemistry of protactinium. The hydrolysis reactions of pentavalent protactinium in water are very complex even in relatively acidic solutions (Cotton and Wilkinson 1980 [DIRS 101584], pp. 1,091 to 1,093). In near-neutral solutions, the hydrolysis behavior of protactinium is essentially unknown. However, because hydrolysis reactions appear to dominate the solution behavior of protactinium, changes in the major ion chemistry of groundwaters are not expected to impact the sorption behavior of protactinium. Unfortunately, insufficient thermodynamic data are available to model protactinium sorption behavior using a surface complexation model.

The sorption-coefficient range for americium was used as a default for protactinium (i.e., 1,000 to 10,000 mL/g). This range is well within the range reported by Allard et al. (1983 [DIRS 162982], p. 12) for silica and alumina at values of pH > 7.0. As with americium sorption coefficients, a truncated normal distribution was selected with a mean of 5,500 mL/g and a standard deviation of 1,500 mL/g.

Corroboration of this range of sorption-coefficient values is provided by protactinium sorption experiments performed by Berry et al. (1989 [DIRS 144728], p. 347). These authors report a range of 1,000 to 1,000,000 mL/g for protactinium sorption coefficients for rock samples, including sandstone, shale, granite, and clay in contact with natural groundwaters.

A7.5.2 Zeolitic Tuff

Sorption coefficients for protactinium on zeolitic tuffs from Yucca Mountain in J-13 well water were reported by Rundberg et al. (1985 [DIRS 101355], p. 63). The reported sorption coefficients ranged from 3.3 to 10.1 mL/g (Figure A-29). The initial solution concentrations in the experiments ranged from 1×10^{-11} to 5×10^{-14} M. The initial solution concentration used by Allard et al. (1983 [DIRS 162982], p. 6) was in the low end of this range. Thus, initial solution concentration does not appear to explain the difference between the results of Allard et al. (1983 [DIRS 162982], p. 12) and the results on Yucca Mountain samples. It is likely that the results on Yucca Mountain samples reflect imperfect separation of liquid from solid phases after centrifugation.

The pH values of the final solutions in the experiments on Yucca Mountain samples were in the range of 6.3 to 6.7. These pH values are below the range expected in SZ waters at Yucca Mountain. Thus, the reported sorption coefficients do not directly apply to conditions in the saturated zone at Yucca Mountain. As shown in Figure A-29, there appears to be an adsorption edge at a pH close to 6.8, and sorption coefficients increase by approximately 2 orders of magnitude at values of pH > 6.8. The cause for this increase is not known but is likely related to hydrolysis reactions.

Because zeolitic tuffs have greater surface area than devitrified tuffs, the sorption-coefficient distribution for devitrified tuff is used as a default for zeolitic tuff. This approach will lead to conservative predictions of protactinium transport rates.

A7.5.3 Alluvium

The probability distribution for devitrified tuff will be used as a default for the protactinium sorption-coefficient probability distribution in alluvium. Alluvium along the flow path is composed largely of disaggregated tuffaceous materials. Because devitrified tuff makes up a major portion of the volcanic units exposed at the surface, it should be a major component in alluvium. In addition, clays and other secondary minerals are enriched in alluvial materials. The presence of these minerals should result in higher sorption coefficients in alluvial materials compared to intact devitrified tuff.

A7.6 RADIUM

The chemistry of the element radium is very similar to that of the element barium (Cotton and Wilkinson 1980 [DIRS 101584], p. 426). Because barium has a radioactive isotope that is more readily measured by gamma counting than the radium isotopes, barium was used to measure sorption coefficients for radium. A limited number of experiments were performed with radium to confirm its sorption behavior relative to barium.

Barite is the solubility-controlling solid for barium in Yucca Mountain groundwaters. PHREEQC modeling with the thermodynamic input data file PHREEQCDATA025.DAT (DTN: MO0604SPAPHR25.001 [DIRS 176868]) predicts that, at 25°C, the solubility limit with respect to barite (barium sulfate) is reached at a barium concentration in J-13 well water at 25°C of 1.05×10^{-6} M at a pH of 9.3 and 1.96×10^{-6} M at a pH of 4.6. For radium, the results are 3.37×10^{-7} M at a pH of 9.3 and 6.21×10^{-7} M at a pH of 4.6 (Output DTN: LA0702MD831232.002, File *output_07.xls*, worksheet *Usat.pun.xls*). The solubility of barium in p#1 water at 25°C is 7.49×10^{-7} M at a pH of 9.4 and 1.03×10^{-6} M at a pH of 4.67. For radium these values are 2.37×10^{-7} M at a pH of 9.4 and 3.24×10^{-7} M at a pH of 4.67 (Output DTN: LA0702MD831232.002, file *output_07.xls*, worksheet *Usatp1.pun.xls)*.

A7.6.1 Devitrified Tuff

The experimentally derived sorption coefficients for barium on devitrified tuff are plotted against the calculated final barium concentrations of the experiments in Figure A-30. The data points are separated into groups on the basis of when the experiments were carried out (before May 1989 = "old" and after May 1989 = "new"), water chemistry, experiment duration, and on whether the sorption coefficient was determined from a sorption or a desorption experiment.

The calculated final concentration of barium in the experiments with J-13 well water was below saturation with barite in all but one experiment (Figure A-30). The results for this one experiment will be omitted from further consideration. The calculated final barium concentrations in experiments with p#1 water are all lower than the barite saturation value of 2.0×10^{-7} M. Thus, oversaturation was not an issue in the barium sorption experiments with p#1 water. Similarly, the radium solution concentrations were all lower than the radium sulfate saturation value in J-13 well water. Thus, these experiments were undersaturated with radium sulfate.

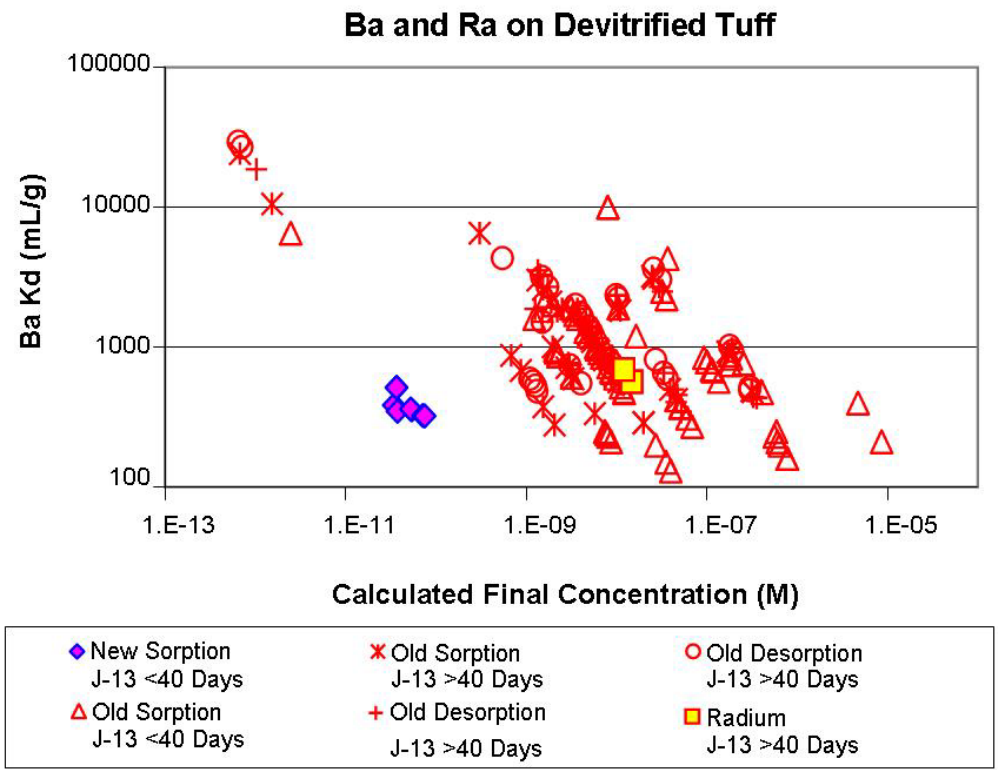

Sources: DTNs: LA0305AM831341.001 [DIRS 163789]; LA0407AM831341.001 [DIRS 170623].

NOTE: In the legend, 'old' stands for data collected before May 1989, 'new' stands for data collected after May 1989.

Figure A-30. Barium and Radium Sorption Coefficients on Devitrified Tuff versus Calculated Final Barium or Radium Concentrations in Solution

The data plotted in Figure A-30 show a general increase in sorption coefficient with decreasing concentration. This result suggests the isotherms for barium sorption onto devitrified tuff are nonlinear. The impact of this nonlinearity must be included in the sorption-coefficient probability distribution.

The effects of experiment duration on the barium K_d value for devitrified tuff are shown in Figure A-31. The large range in sorption coefficients obtained at a given duration reflects variations in grain size of the crushed-tuff samples used in the experiments, variations in solution concentrations, variations in surface chemistry, and analytical errors and artifacts. Experiments with crushed-tuff samples that include the fines (e.g., < 30 μm) often have sorption coefficients that are larger than samples from which the fines have been removed (e.g., 75–500 μm). This result is partly due to the higher surface area of samples with fines and partly due to mineral fractionation. Mineral fractionation can occur during the sieving process and cause the preferential concentration of very fine-grained minerals (e.g., clays) in the fine fraction.

Figure A-32 shows the effects of experiment duration on sorption coefficients for samples with the fines removed. The few sorption coefficients with values near 10,000 mL/g represent experiments with very low solution concentrations (Figure A-32). For the remaining experiments, the total range of sorption-coefficient values is substantially reduced. Further, it appears likely the range would converge to a range between 100 and 1,000 mL/g with increasing

duration. The horizontal trend among data points at durations other than 21 and 42 days suggests barium and radium sorption reactions are relatively fast.

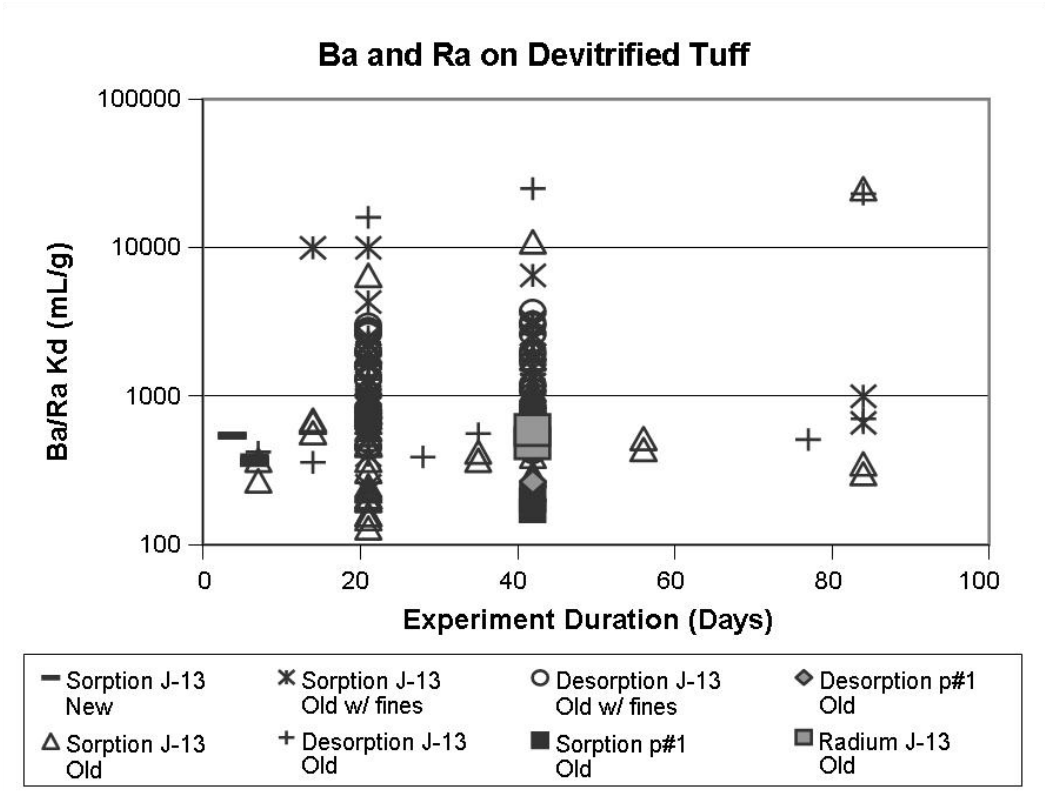

Sources: DTNs: LA0305AM831341.001 [DIRS 163789]; LA0407AM831341.001 [DIRS 170623].

NOTE: In the legend, 'old' stands for data collected before May 1989, 'new' stands for data collected after May 1989.

Figure A-31. Barium and Radium Sorption Coefficients on Devitrified Tuff versus Experiment Duration for Sorption (Forward) and Desorption (Backward) Experiments

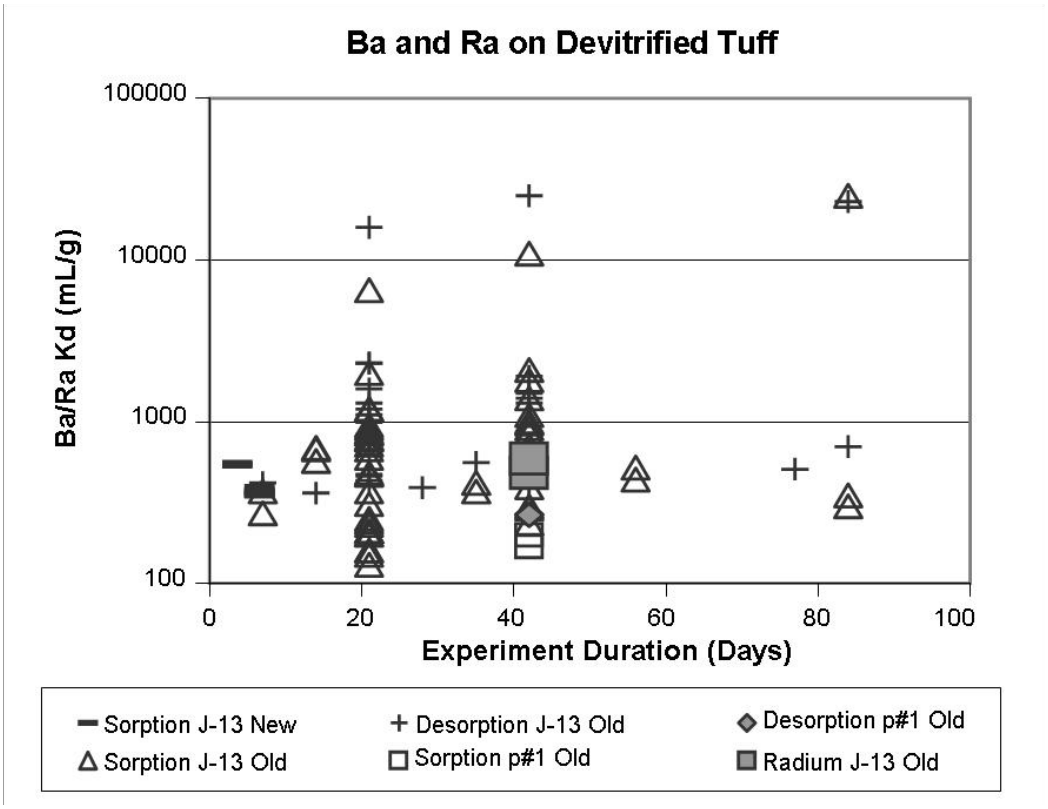

Sources: DTNs: LA0305AM831341.001 [DIRS 163789]; LA0407AM831341.001 [DIRS 170623].

NOTE: In the legend, 'old' stands for data collected before May 1989, 'new' stands for data collected after May 1989. Samples containing fines removed.

Figure A-32. Barium and Radium Sorption Coefficients on Devitrified Tuff with Fine Fraction Removed versus Experiment Duration for Sorption (Forward) and Desorption (Backward) Experiments

The impact of variations in the major ion composition of groundwaters is also shown in Figures A-31 and A-32. Although there is a limited set of experiments with p#1 water, the sorption coefficients obtained (at 42 days) fall at the low end of the range of results for J-13 well water. Thus, there is some impact of water chemistry, although it is substantially less than an order of magnitude.

The radium sorption-coefficient probability distribution derived for devitrified tuff in the saturated zone is a uniform distribution with a range of 100 to 1,000 mL/g. The low end of the chosen range was selected based on the minimum value observed in long-term experiments (> 40 days) and potential impacts of variations in water chemistry and surface areas among devitrified tuffs at Yucca Mountain. Because there are experiments within the data set that have solution concentrations close to saturation with a barium/radium sulfate, the effect of nonlinear isotherms is incorporated into the distribution. The upper end of the distribution was chosen as a minimum upper limit given the potential impacts of sorption kinetics, radium solution concentrations, and surface areas.

A7.6.2 Zeolitic Tuff

The experimentally derived sorption coefficients for barium and radium on zeolitic tuff are plotted against the calculated final barium or radium concentrations in Figure A-33. As before, the data points are separated into groups on the basis of when the experiments were carried out (before May 1989 = "old" and after May 1989 = "new"), experiment duration, and on whether the sorption coefficient was determined from a sorption or a desorption experiment. The plotted data indicate that there is no clear trend of barium K_d values with solution concentration. Essentially all the sorption coefficients exceed a value of 10,000 mL/g and some desorption experiments approach values of 1,000,000 mL/g. The radium results are in the range of the results for barium, confirming the similar sorption behavior of these two elements. As with devitrified tuffs, the barium and radium sorption coefficients for zeolitic tuff plotted in Figure A-33 reflect solutions that were undersaturated with barium and radium sulfate. The sorption coefficients obtained with p#1 water are well within the range defined by the experiments with J-13 well water. Thus, there does not appear to be a clear impact of variations in groundwater chemistry.

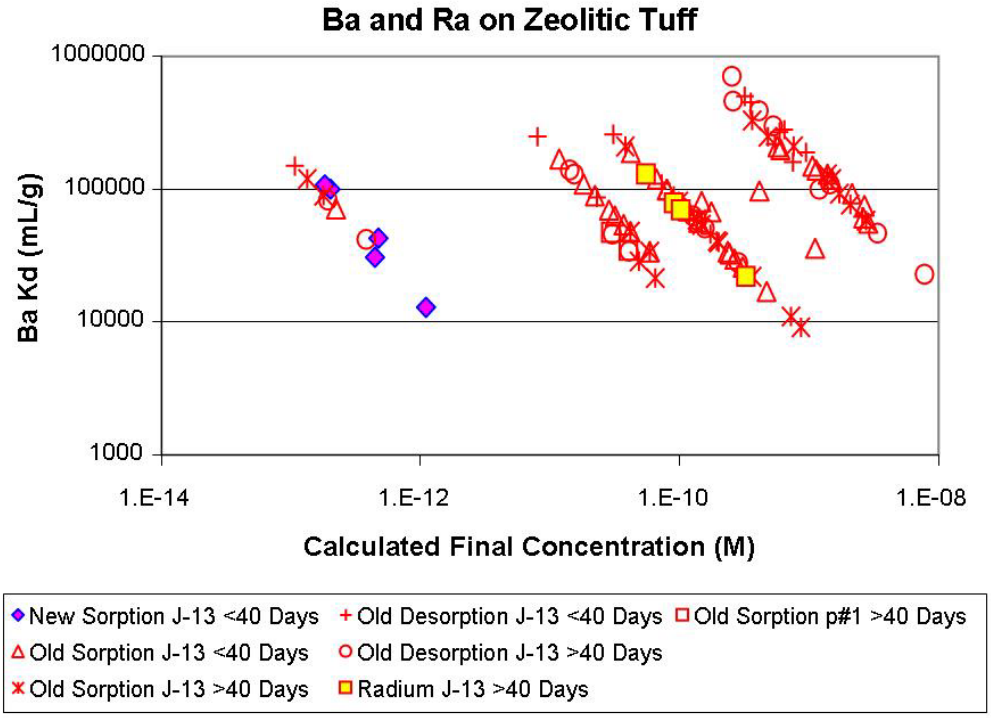

Sources: DTNs: LA0305AM831341.001 [DIRS 163789]; LA0407AM831341.001 [DIRS 170623].

NOTE: In the legend, 'old' stands for data collected before May 1989, 'new' stands for data collected after May 1989.

Figure A-33. Barium and Radium Sorption Coefficients on Zeolitic Tuff versus Calculated Final Barium or Radium Concentrations in Solution

The data plotted in Figure A-34 also indicate that there is no clear trend of barium K_d values with solution concentration. Data were obtained for a sorption isotherm on sample YM-38 (Figure A-34). As indicated by the exponent in the equation on the diagram, the calculated isotherm is essentially linear.

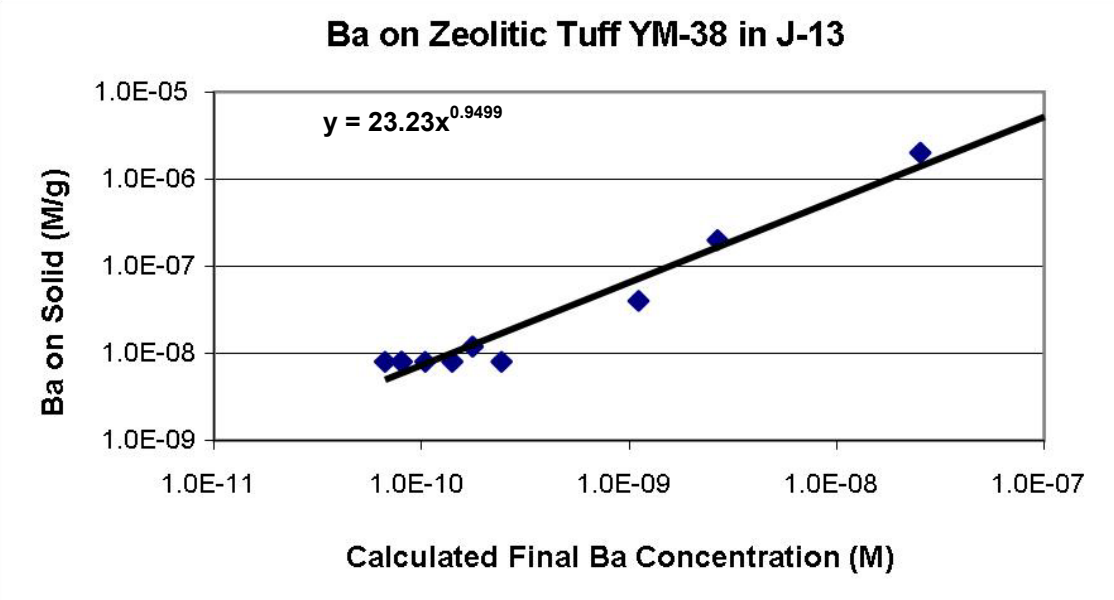

Source: DTN: LA0305AM831341.001 [DIRS 163789].

Figure A-34. Isotherm Diagram for Barium Sorption on Zeolitic Tuff Sample YM-38 in J-13 Well Water

The effects of experiment duration on the barium K_d values for zeolitic tuff are shown in Figure A-35. The barium and radium sorption reactions are quite fast. This characteristic is indicated by the fact that the range of values obtained in 6-day experiments (Figure A-35) is similar to the range of values obtained in 84-day experiments.

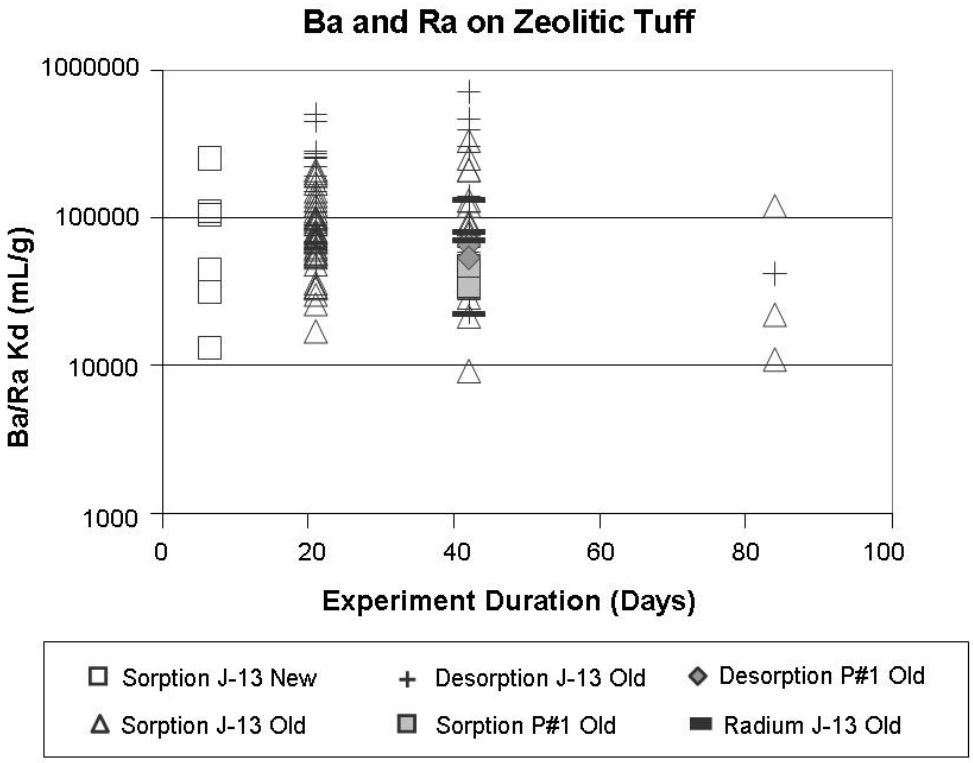

Sources: DTNs: LA0305AM831341.001 [DIRS 163789]; LA0407AM831341.001 [DIRS 170623].

NOTE: In the legend, 'old' stands for data collected before May 1989, 'new' stands for data collected after May 1989.

Figure A-35. Barium and Radium Sorption Coefficients on Zeolitic Tuff in J-13 Well Water versus Experiment Duration for Sorption (Forward) and Desorption (Backward) Experiments

The impact of variations in the major ion composition of groundwaters is also shown in Figure A-35. Although there is a limited set of experiments with synthetic p#1 water, the results are largely within the range of the results obtained in experiments with J-13 well water. Thus, there is no clear evidence of an impact of water chemistry variations on barium/radium sorption coefficients in zeolitic tuff.

The radium sorption-coefficient probability distribution derived for zeolitic tuff in the saturated zone is a truncated log-normal distribution with a range of 1,000 to 250,000 mL/g, a mean of 100,000 mL/g, and a standard deviation of 31,420 mL/g. The low end of the chosen range was selected based on the minimum value observed in long-term experiments (> 40 days) and potential impacts of variations in water chemistry and ion-exchange capacities among zeolitic tuffs at Yucca Mountain. The upper end of the distribution was chosen to address the potential for low radium solution concentrations and high ion-exchange capacities along the expected transport pathways.

Because zeolitic tuffs have greater surface area than devitrified tuffs, the sorption-coefficient distribution for devitrified tuff is used as a default for the radium sorption in the volcanic tuffs. This approach will lead to conservative predictions of radium transport rates.

A7.6.3 Alluvium

The probability distribution for devitrified tuff will be used as a default for the radium sorption-coefficient probability distribution in alluvium. Alluvium along the flow path is composed largely of disaggregated tuffaceous materials. Because devitrified tuff makes up a major portion of the volcanic units exposed at the surface, it should be a major component in alluvium. In addition, clays and other secondary minerals are enriched in alluvial materials. The presence of these minerals should result in higher sorption coefficients in alluvial materials compared to intact devitrified tuff.

A7.7 SELENIUM

Selenium has a high solubility limit in the type of groundwaters associated with Yucca Mountain. None of the sorption experiments carried out for selenium were oversaturated with a pure selenium phase.

A7.7.1 Devitrified Tuff

The experimentally derived sorption coefficients for selenium on devitrified tuff are plotted against the calculated final selenium concentrations of the experiments in Figure A-36. These data were all obtained prior to May 1989. The range of K_d values obtained in sorption experiments was 1.4 to 51.0 mL/g. The range of K_d values obtained in desorption experiments was 19.7 to 94.0. The K_d values obtained in sorption experiments do not show a clear correlation with final solution concentration (Figure A-36). In the case of K_d values obtained from desorption experiments, there is greater scatter in the data but also no clear correlation.

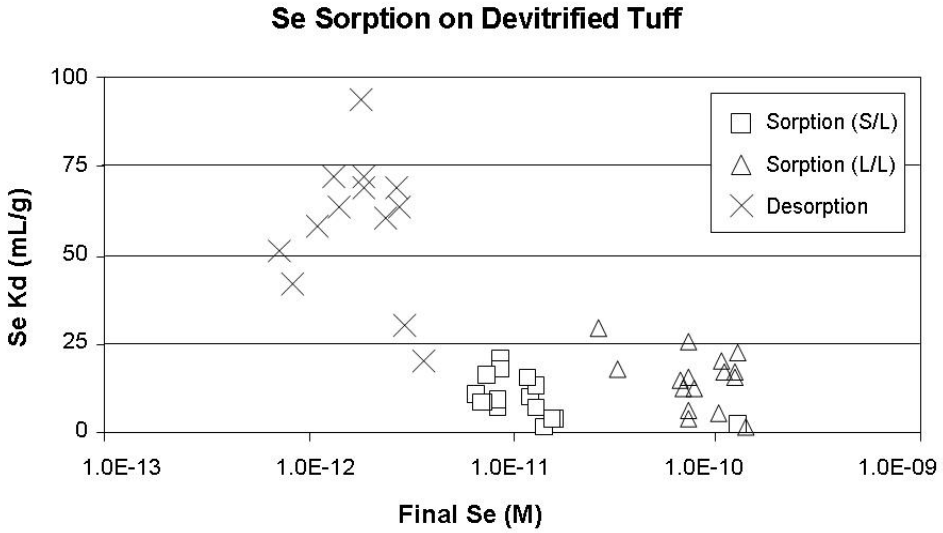

Source: DTN: LA0702AM831341.001 [DIRS 179306].

NOTE: S/L = Solid/Liquid, L/L = Liquid/Liquid (see text).

Figure A-36. Selenium Sorption Coefficients on Devitrified Tuff versus Calculated Final Selenium Concentration in Solution

The equilibration rate for selenium sorption reactions on tuff can potentially be gauged from a plot of sorption coefficients versus experiment duration as shown in Figure A-37. The normal expectation would be that for experiments of a given duration, K_d values from sorption experiments would be larger than those obtained from desorption experiments and would show an increase with experiment duration (i.e., a positive trend in Figure A-37). The opposite would be expected for K_d values obtained from desorption experiments (negative trend in Figure A-37). Unfortunately, there is too much scatter in the dataset to discern clear trends. However, the fact that K_ds obtained in desorption experiments are consistently larger in value than the K_ds obtained in sorption experiments is significant. It suggests desorption rates are slow relative to sorption rates.

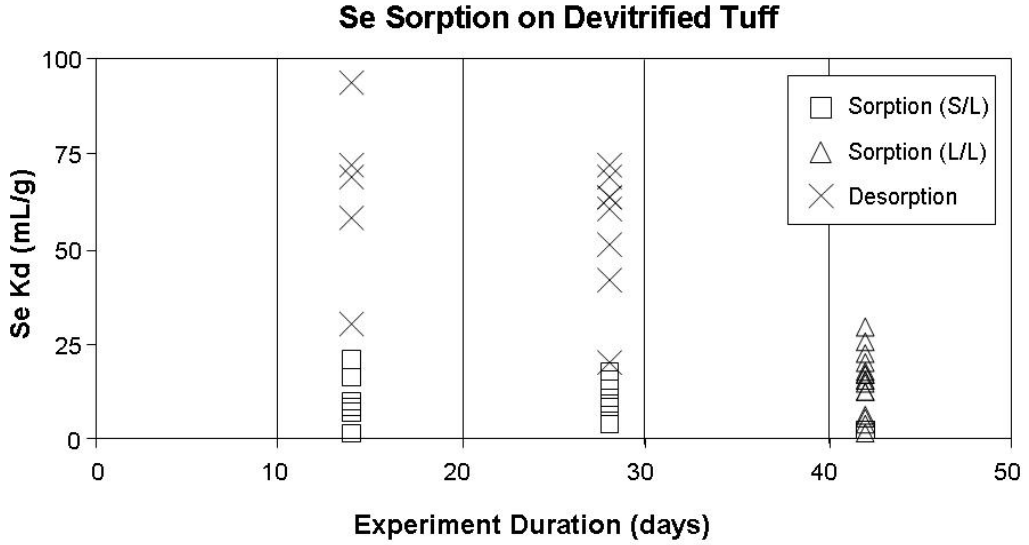

Source: DTN: LA0702AM831341.001 [DIRS 179306].

NOTE: S/L = Solid/Liquid, L/L = Liquid/Liquid (see text). Duration for sorption (forward) and desorption (backward) experiments.

Figure A-37. Selenium Sorption Coefficients on Devitrified Tuff versus Experiment

The effect of water chemistry on the sorption of selenium on devitrified tuffs is shown in Figure A-38. It is evident that there is no clear correlation between the measured selenium K_ds and water chemistry or ionic strength. In fact, experiments with deionized water and p#1 water resulted in very similar K_d values (Figure A-38).

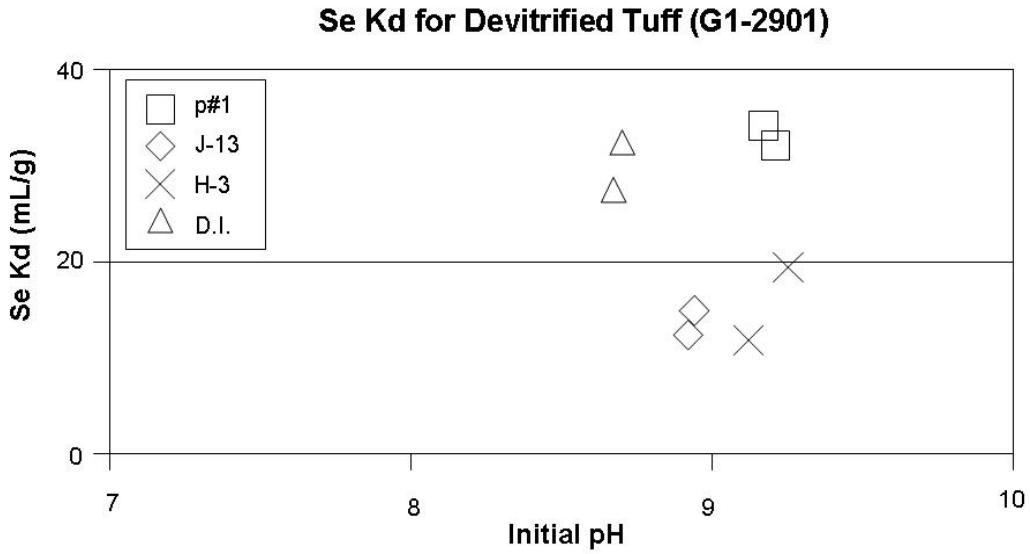

Source: DTN: LA0702AM831341.001 [DIRS 179306].

Figure A-38. Selenium Sorption Coefficients on Devitrified Tuff G1-2901 versus Initial Solution pH for Experiments using Four Different Water Compositions

The selenium sorption coefficient probability distribution derived for devitrified tuff in the saturated zone is a truncated log normal distribution with a mean value of 14.0, a standard deviation of 11.2, and range from 1 to 50 mL/g. The lower bound of the distribution was selected based on the minimum value observed in long-term experiments (> 40 days). The upper end of the distribution was selected as a minimum upper limit given the results of desorption experiments and potential impacts of variation in tuff surface areas.

A7.7.2 Zeolitic Tuff

The experimentally derived sorption coefficients for selenium on zeolitic tuff are plotted against the calculated final selenium concentrations of the experiments in Figure A-39. These data were all obtained prior to May 1989. The range of K_d values obtained in sorption experiments was 1.4 to 29.1 mL/g. The range of K_d values obtained in desorption experiments was 19.7 to 94.0. The K_d values obtained in sorption experiments do not show a clear correlation with final solution concentration. In the case of K_d values obtained from desorption experiments, there is greater scatter in the data but also no clear correlation.

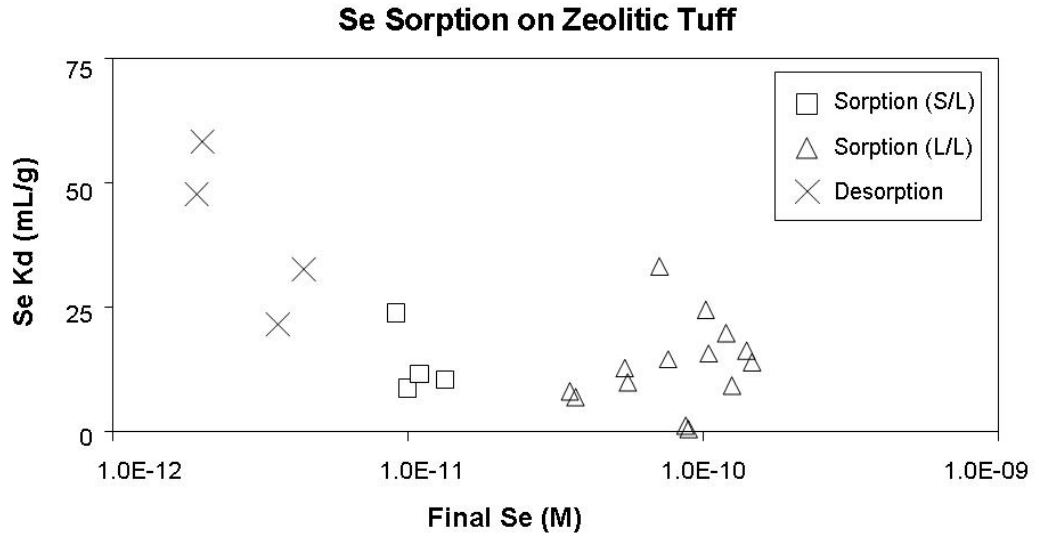

Source: DTN: LA0702AM831341.001 [DIRS 179306].

NOTE: S/L = Solid/Liquid, L/L = Liquid/Liquid (see text).

Figure A-39. Selenium Sorption Coefficients on Zeolitic Tuff versus Calculated Final Selenium Concentration in Solution

The equilibration rate for selenium sorption reactions on tuff can potentially be gauged from a plot of sorption coefficients versus experiment duration as shown in Figure A-40. As with selenium sorption on devitrified tuff, there is too much scatter in the dataset to discern clear trends. However, the fact that K_ds obtained in desorption experiments are consistently larger in value than the K_ds obtained in sorption experiments is significant. It suggests desorption rates are slow relative to sorption rates.

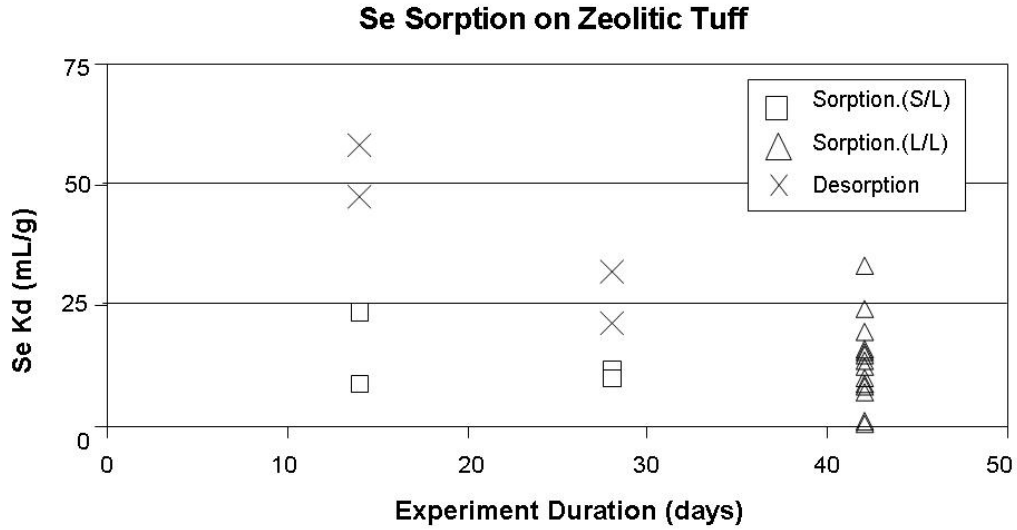

Source: DTN: LA0702AM831341.001 [DIRS 179306].

NOTE: S/L = Solid/Liquid, L/L = Liquid/Liquid (see text).

Figure A-40. Selenium Sorption Coefficients on Zeolitic Tuff versus Experiment Duration for Sorption (Forward) and Desorption (Backward) Experiments

The effect of water chemistry on the sorption of selenium on devitrified tuffs is shown in Figure A-41. It is evident that there is no clear correlation between the measured selenium K_ds and water chemistry or ionic strength.

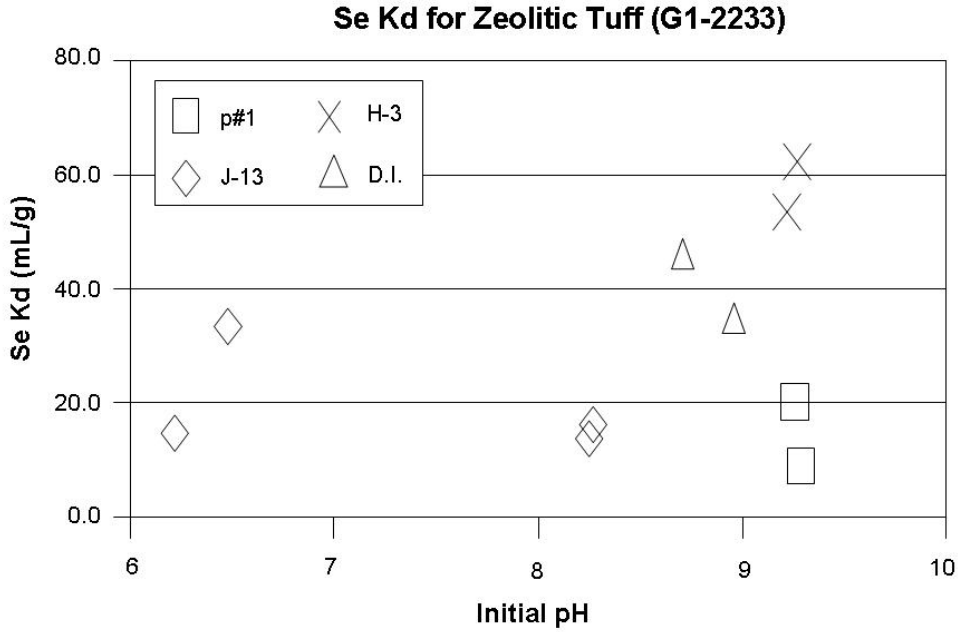

Source: DTN: LA0702AM831341.001 [DIRS 179306].

Figure A-41. Selenium Sorption Coefficients on Devitrified Tuff G1-2901 versus Initial Solution pH for Experiments Using Four Different Water Compositions

The selenium sorption coefficient probability distribution derived for zeolitic tuff in the saturated zone is a truncated log normal distribution with a mean value of 14.3, a standard deviation of 7.9, and range from 1 to 35 mL/g. The lower bound of the distribution was selected based on the minimum value observed in long-term experiments (> 40 days). The upper end of the distribution was selected as a minimum upper limit given the results of desorption experiments and potential impacts of variation in tuff surface areas.

A7.7.3 Alluvium

The probability distribution for devitrified tuff will be used as a default for the selenium sorption-coefficient probability distribution in alluvium. Alluvium along the flow path is composed largely of disaggregated tuffaceous materials. Because devitrified tuff makes up a major portion of the volcanic units exposed at the surface, it should be a major component in alluvium. In addition, clays and other secondary minerals are enriched in alluvial materials. The presence of these minerals should result in higher sorption coefficients in alluvial materials compared to intact devitrified tuff.

A7.8 STRONTIUM

PHREEQC modeling with the thermodynamic input data file PHREEQCDATA025.DAT (DTN: MO0604SPAPHR25.001 [DIRS 176868]) predicts that the solubility limit with respect to strontium is controlled by strontianite (strontium carbonate) in both J-13 and p#1 waters. The solubility of strontium obtained from PHREEQC modeling with the thermodynamic input data file *PHREEQCDATA025.DAT* (DTN: MO0604SPAPHR25.001 [DIRS 176868]) in J-13 well water at 25°C ranges from 2.51×10^{-5} M at a pH of 7.1 to 1.36×10^{-6} M at a pH of 8.5 and the solubility controlling phase is strontianite (strontium carbonate). The solubility of strontium in p#1 water is also controlled by strontianite and at 25°C ranges from 8.35×10^{-6} M at a pH of 7.4 to 8.74×10^{-7} M at a pH of 8.6 (Output DTN: LA0702MD831232.002, file *output_07.xls*, worksheets *Usat.pun.xls* and *Usatp1.pun.xls*).

A7.8.1 Devitrified Tuff

The experimentally derived sorption coefficients for strontium on devitrified tuff are plotted against the calculated final strontium concentrations of the experiments in Figure A-42. The data points are separated into groups on the basis of when the experiments were carried out (before May 1989 = "old" and after May 1989 = "new"), water type, and on whether the sorption coefficient was determined from a sorption or a desorption experiment. There are also data for a sorption isotherm on sample G1-2840.

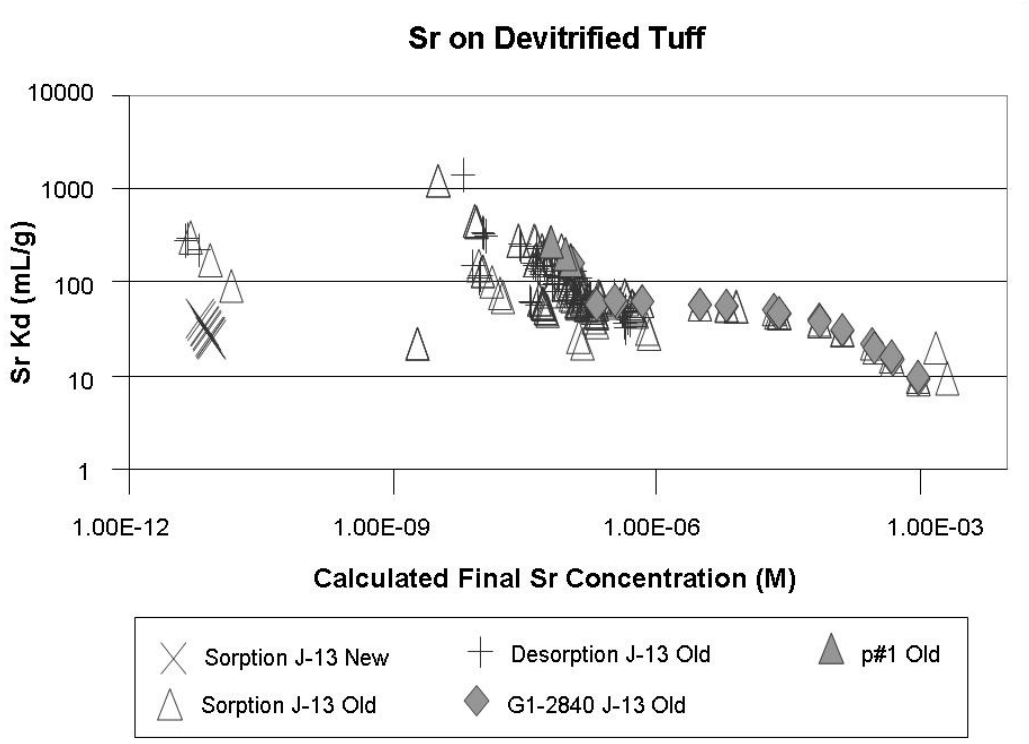

Source: DTNs: LA0305AM831341.001 [DIRS 163789]; LA0407AM831341.003 [DIRS 170626].

NOTE: In the legend, 'old' stands for data collected before May 1989, 'new' stands for data collected after May 1989.

Figure A-42. Strontium Sorption Coefficients on Devitrified Tuff versus Calculated Final Strontium Concentration in Solution

Most of the calculated final solution concentrations for the sorption experiments are below saturation with strontianite in J-13 well water. The data points with concentrations greater than 1.0×10^{-6} M reflect experiments that were oversaturated with strontianite. Thus, the sorption coefficients obtained in these experiments will not be used in the derivation of the strontium sorption-coefficient probability distribution. The calculated final strontium concentrations used in experiments with p#1 water are all lower than the saturation value. Thus, oversaturation was not an issue in the strontium sorption experiments with p#1 water.

A sorption "isotherm" was obtained for sample G1-2840 in J-13 well water. The "isotherm" was linear below a ^{85}Sr concentration of approximately 5×10^{-5} M as shown in Figure A-42. At higher concentrations, the final solutions were oversaturated with strontianite. Thus, these data points should not be used to construct an isotherm. Interestingly, if strontianite had precipitated in these experiments, it would be expected that the sorption coefficients would increase with increasing strontium concentrations. However, the data in Figure A-42 indicate sorption coefficients decreased with increasing solution concentrations. This suggests strontianite was not precipitated from solution for some reason. A possible explanation is that the nucleation or precipitation rates of strontianite are very slow relative to the duration of the experiments (21 days). Alternatively, strontianite could have nucleated but was sufficiently fine grained so that it remained with the solution phase during the process used to separate the solid and liquid phases in the experiments.

The K_d value in the linear portion of the "isotherm" in Figure A-42 is at the low end of the range of strontium sorption coefficients obtained with J-13 well and p#1 waters. This suggests isotherms for the other samples plotted in Figure A-42 would lie at higher K_d values compared to the "isotherm" for sample G1-2840. The sorption coefficients obtained in experiments with p#1 water fall in the middle of the range of values obtained for experiments with J-13 well water. Thus, there is little or no impact of variations in water chemistry on strontium sorption coefficients on devitrified tuff.

The effects of experiment duration on values of the strontium K_d for devitrified tuff are shown in Figure A-43. The large range in sorption coefficients obtained at a given duration reflects variations in grain size of the crushed-tuff samples used in the experiments, variations in solution strontium concentrations, variations in surface chemistry, and analytical error and artifacts. Experiments with crushed-tuff samples that include the fines (e.g., particle size < 30 μm) usually have sorption coefficients that are larger than samples from which the fines have been removed (e.g., particle sizes 75 to 500 μm). This result is partly due to the higher surface area of samples with fines and partly due to mineral fractionation. Mineral fractionation can occur during the sieving process and cause the preferential concentration of very fine-grained minerals (e.g., clays) in the fine fraction.

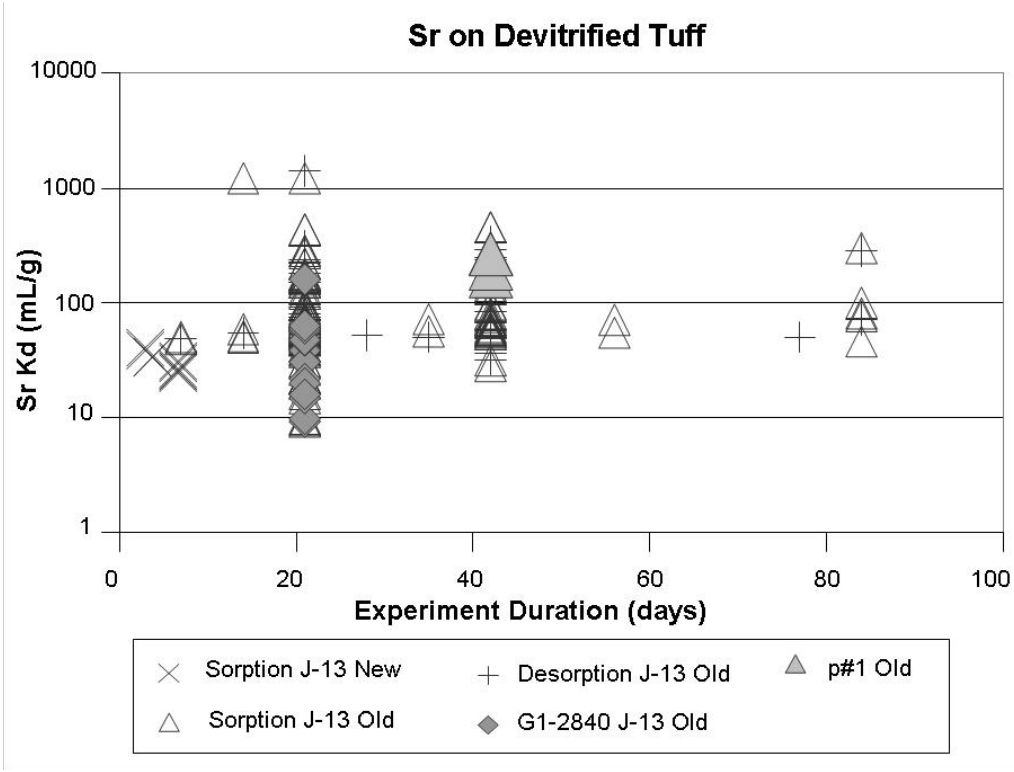

Sources: DTNs: LA0305AM831341.001 [DIRS 163789]; LA0407AM831341.003 [DIRS 170626].

NOTE: In the legend, 'old' stands for data collected before May 1989, 'new' stands for data collected after May 1989. Data points include experiments in which fines were not removed from the samples.

Figure A-43. Strontium Sorption Coefficients on Devitrified Tuff versus Experiment Duration for Sorption (Forward) and Desorption (Backward) Experiments

Figure A-44 shows the effects of duration on sorption coefficients for crushed-tuff samples with the fines removed. The total range of sorption-coefficient values is reduced compared to Figure A-43. Further, it appears likely this range would converge to values between 50 and 500 mL/g with increasing duration. The horizontal trend among data points at durations other than 21 and 42 days suggests strontium sorption reactions are relatively fast.

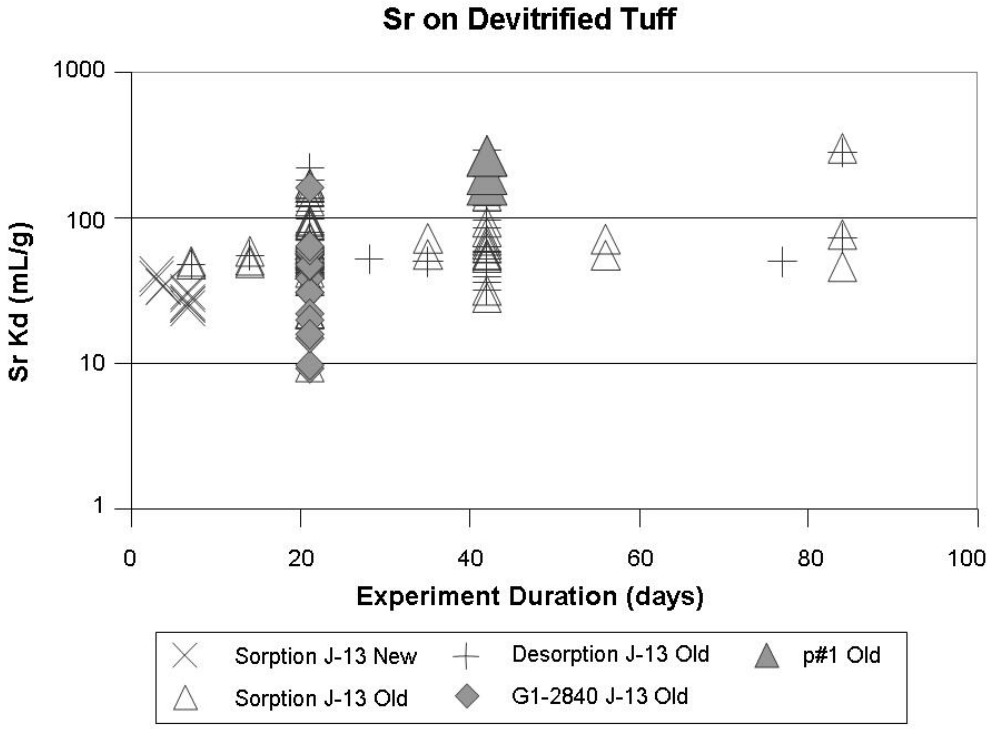

Source: DTNs: LA0305AM831341.001 [DIRS 163789]; LA0407AM831341.003 [DIRS 170626].

NOTE: In the legend, 'old' stands for data collected before May 1989, 'new' stands for data collected after May 1989. Samples containing fines fraction are removed from the figure.

Figure A-44. Strontium Sorption Coefficients on Devitrified Tuff versus Experiment Duration for Sorption (Forward) and Desorption (Backward) Experiments with Reduced Range

The strontium sorption-coefficient probability distribution derived for devitrified tuff in the saturated zone is a uniform distribution with a range of 20 to 400 mL/g. The low end of the chosen range was selected based on the minimum value observed in long-term experiments (> 40 days) and potential impacts of variations in water chemistry and surface areas among devitrified tuffs at Yucca Mountain. Because there are experiments within the data set that have solution concentrations close to saturation with a strontium carbonate, the effect of nonlinear isotherms is incorporated into the distribution. The upper end of the distribution was chosen as a minimum upper limit given the potential impacts of strontium solution concentrations and surface areas.

A7.8.2 Zeolitic Tuff

The experimentally derived sorption coefficients for strontium on zeolitic tuff are plotted against the calculated final strontium concentrations of the experiments in Figure A-45. The data points

are separated into groups on the basis of when the experiments were carried out (before May 1989 = "old" and after May 1989 = "new"), water type, whether or not the solid phase included fines, and whether the sorption coefficient was determined from a sorption or a desorption experiment.

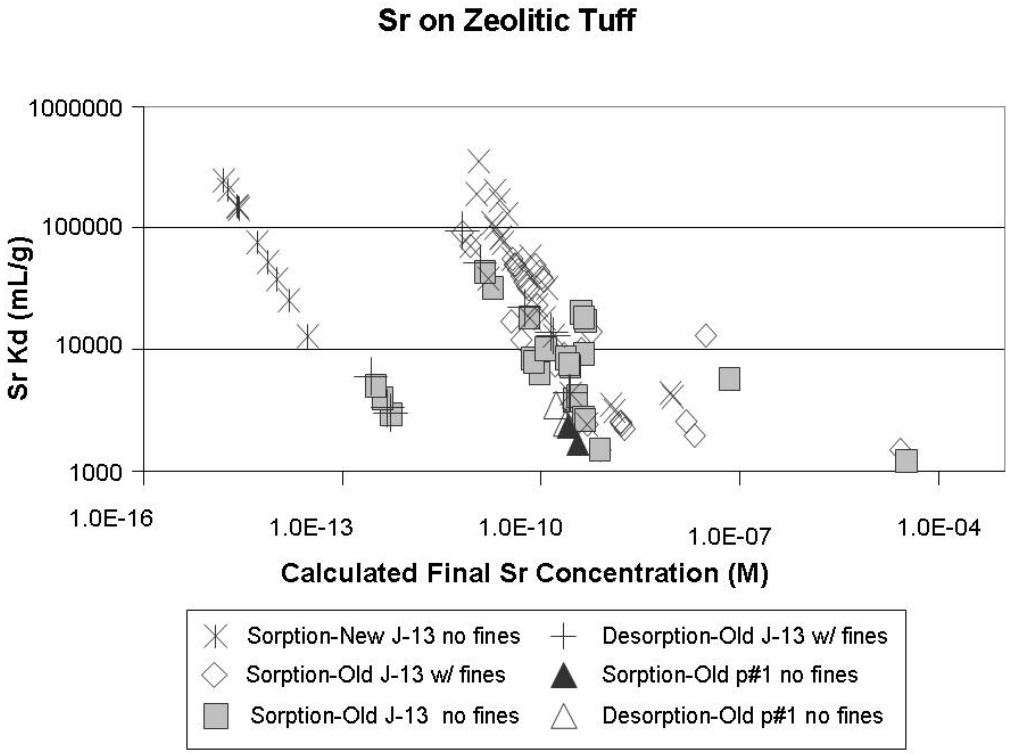

Sources: DTNs: LA0305AM831341.001 [DIRS 163789]; LA0407AM831341.003 [DIRS 170626].

NOTE: In the legend, 'old' stands for data collected before May 1989, 'new' stands for data collected after May 1989.

Figure A-45. Strontium Sorption Coefficients on Zeolitic Tuff versus Calculated Final Strontium Concentration in Solution

All except two of the calculated final solution concentrations were below the saturation level with strontianite. The calculated final strontium concentrations used in experiments with p#1 water are all lower than the saturation value. Thus, oversaturation was not an issue in most of the strontium sorption experiments.

The few sorption coefficients obtained with p#1 water tend to lie at the low end of the range of values shown in Figure A-45. This result suggests variations in water composition will have an impact on the strontium sorption coefficient for zeolitic tuff.

Sorption experiments were carried out at a number of different starting concentrations to obtain an isotherm for sample YM-38. As shown in Figure A-46, the sorption coefficients obtained in these experiments are not consistent with a simple relationship between strontium concentration and sorption coefficient. Nonetheless, the sorption coefficients plotted in Figure A-46 were obtained over a range of strontium concentrations. Thus, the concentration dependence of the sorption coefficient is included in the data set.

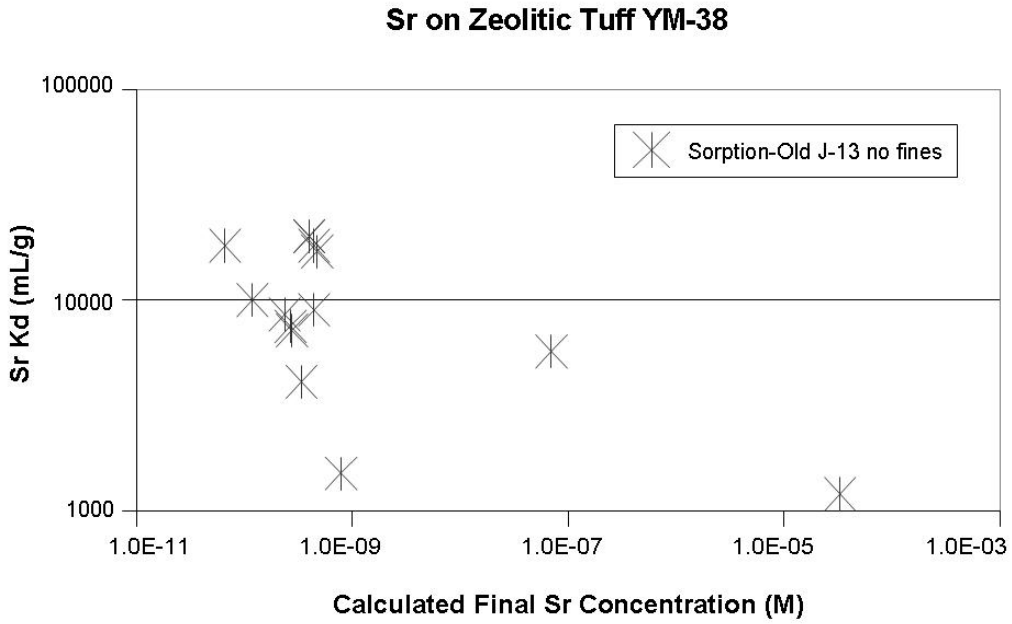

Sources: DTNs: LA0305AM831341.001 [DIRS 163789]; LA0407AM831341.003 [DIRS 170626].

NOTE: In the legend, 'old' stands for data collected before May 1989, 'new' stands for data collected after May 1989.

Figure A-46. Strontium Sorption Coefficients versus Calculated Final Solution Concentration (moles/L) for Sample YM-38 in J-13 Well Water

The effects of experiment duration on the values of strontium K_d for zeolitic tuff are shown in Figure A-47. The large range in sorption coefficients obtained at a given duration reflects variations in grain size of the crushed-tuff samples used in the experiments, variations in solution strontium concentrations, variations in surface chemistry, and analytical errors and artifacts. Experiments with crushed-tuff samples that include the fines (e.g., particle size < 30 μm) usually have sorption coefficients that are larger than samples from which the fines have been removed (e.g., particle sizes 75 to 500 μm). This result is partly due to the higher surface area of samples with fines and partly due to mineral fractionation. Mineral fractionation can occur during the sieving process and cause the preferential concentration of very fine-grained minerals (e.g., clays) in the fine fraction.

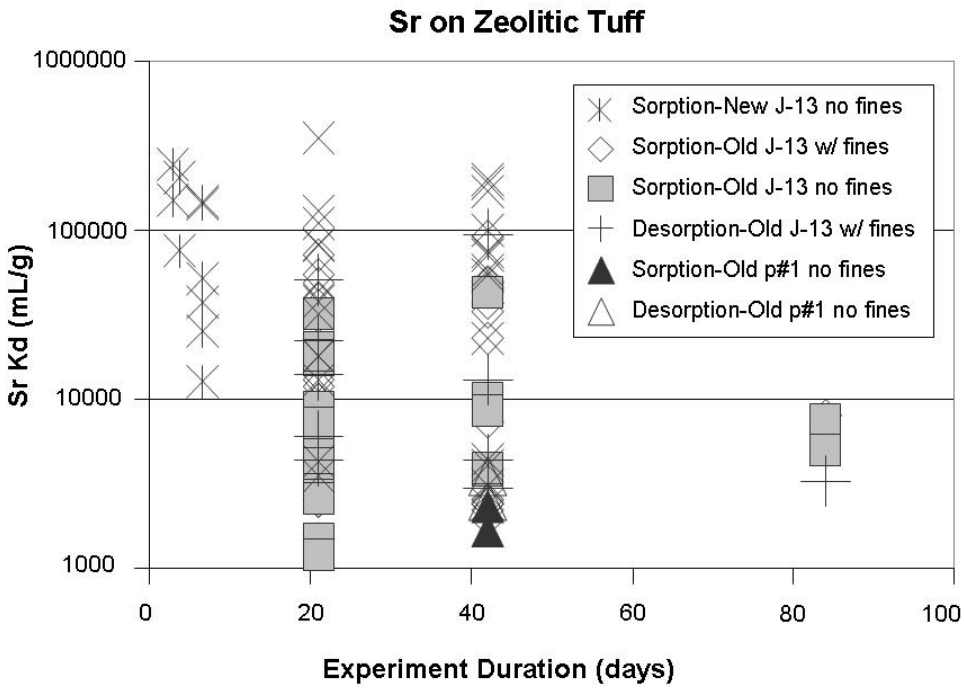

Sources: DTNs: LA0305AM831341.001 [DIRS 163789]; LA0407AM831341.003 [DIRS 170626].

NOTE: In the legend, 'old' stands for data collected before May 1989, 'new' stands for data collected after May 1989.

Figure A-47. Strontium Sorption Coefficients on Zeolitic Tuff versus Experiment Duration for Sorption (Forward) and Desorption (Backward) Experiments

Figure A-48 shows the effects of experimental duration on sorption coefficients for crushed-tuff samples with the fines removed. The total range of sorption-coefficient values is reduced slightly compared to Figure A-47. The rather limited range of values at 84 days is likely due to the limited number of experiments carried out at this duration. There is no clear trend of sorption-coefficient value with duration. This result likely reflects fast sorption kinetics.

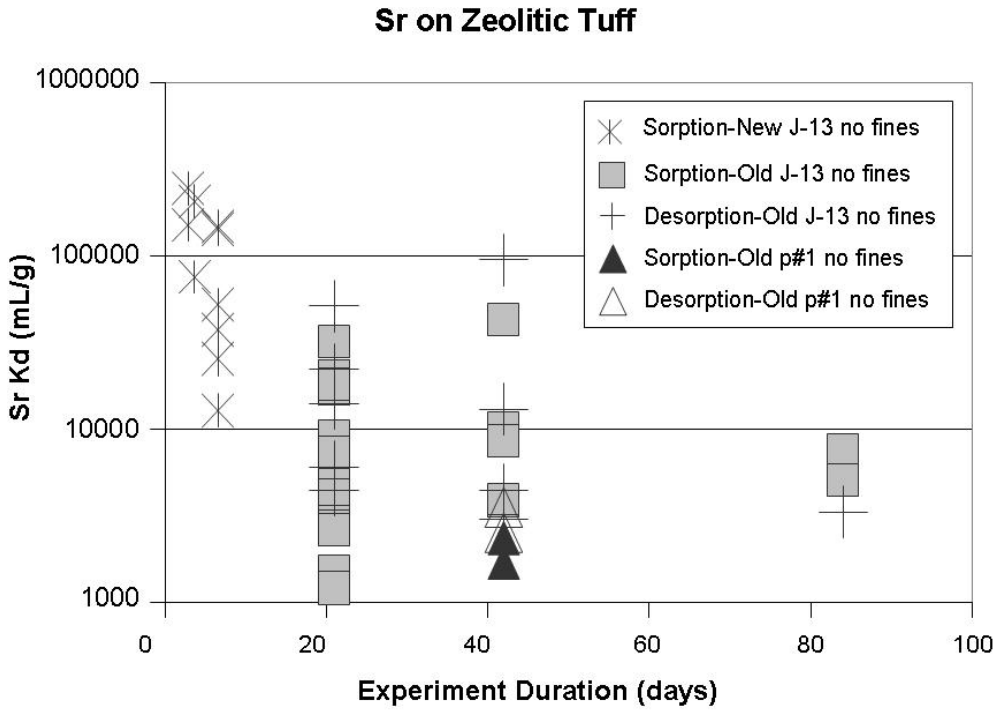

Sources: DTNs: LA0305AM831341.001 [DIRS 163789]; LA0407AM831341.003 [DIRS 170626].

NOTE: In the legend, 'old' stands for data collected before May 1989, 'new' stands for data collected after May 1989.

Figure A-48. Strontium Sorption Coefficients on Zeolitic Tuff with Fine Fraction Removed versus Experiment Duration for Sorption (Forward) and Desorption (Backward) Experiments

The strontium sorption-coefficient probability distribution derived for zeolitic tuff in the saturated zone is a cumulative distribution starting at 100 mL/g, with a value of 5,000 mL/g at 0.5 and a value of 90,000 mL/g at 1.0. The low end of the chosen range was selected based on the minimum value observed in long-term experiments (> 40 days) and potential impacts of variations in water chemistry and ion-exchange capacities among zeolitic tuffs at Yucca Mountain. Because there are experiments within the data set that have solution concentrations close to saturation with a strontium carbonate, the effect of nonlinear isotherms is included in the distribution. The upper end of the distribution was chosen as a minimum upper limit given the potential impacts of strontium solution concentrations and ion-exchange capacities.

A7.8.3 Alluvium

The probability distribution for devitrified tuff will be used as a default for the strontium sorption-coefficient probability distribution in alluvium. Alluvium along the flow path is composed largely of disaggregated tuffaceous materials. Because devitrified tuff makes up a major portion of the volcanic units exposed at the surface, it should be a major component in alluvium. In addition, clays and other secondary minerals are enriched in alluvial materials. The presence of these minerals should result in higher sorption coefficients in alluvial materials compared to intact devitrified tuff.

A7.9 THORIUM

The solubility of thorium dioxide in waters such as the saturated zone waters is estimated at 3.2×10^{-9} M at values of pH > 6.0 (Hummel et al. 2002 [DIRS 161904], p. 377).

A7.9.1 Devitrified Tuff

Experiments with Yucca Mountain tuffs were carried out with initial concentrations in the 1.0×10^{-7} to 6×10^{-8} M range. Thus, the experiments were initially oversaturated with thorium dioxide. The calculated final thorium concentrations shown in Figure A-49 indicate thorium sorption onto the rock sample brought the final solution concentrations below saturation with thorium dioxide in some cases but not all. The results of experiments oversaturated with thorium dioxide are of questionable value. For the remaining experiments, the sorption coefficients range from 1,213 to 23,800 mL/g. There are no data available for the effect of experimental duration on sorption-coefficient values for Yucca Mountain samples. However, Allard et al. (1983 [DIRS 162982], p. 10) reported that, over experiment durations of 6 hours to 6 weeks, time had little influence on the measured sorption coefficients for thorium on silica in 0.01 M $NaClO_4$. The starting concentrations reported by Allard et al. (1983 [DIRS 162982], p. 6) were below the saturation level for thorium dioxide.

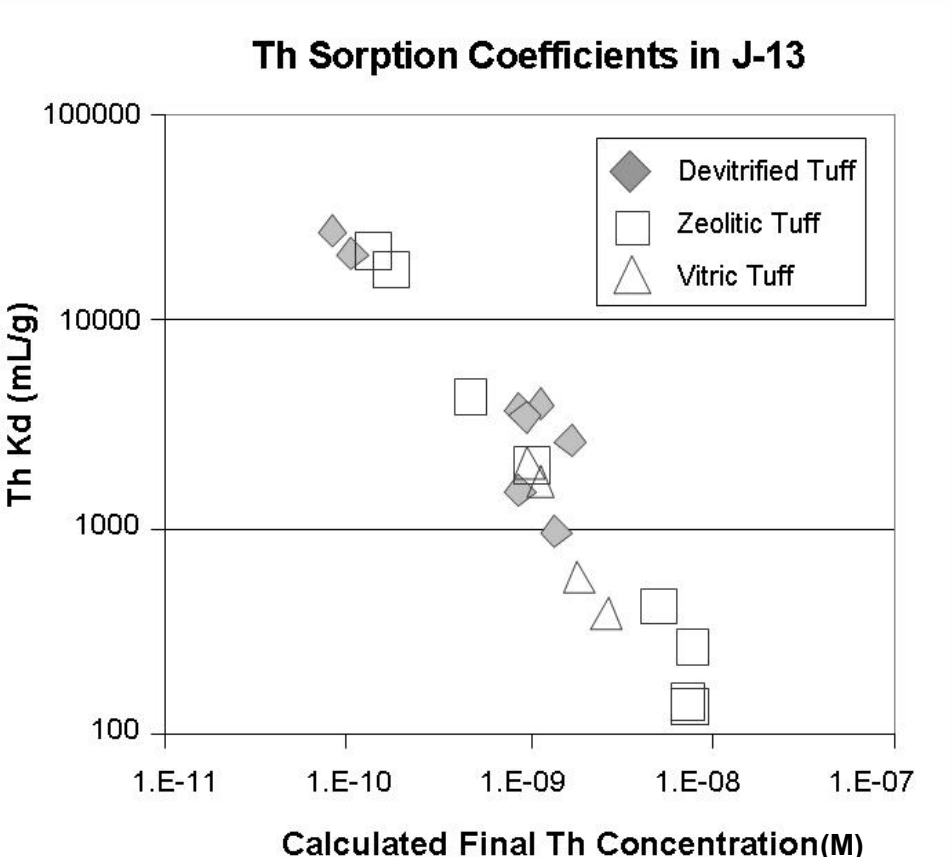

Source: DTN: LA0305AM831341.001 [DIRS 163789].

Figure A-49. Thorium Sorption Coefficients on Tuff versus Calculated Final Thorium Concentration in Solution

There are no data available to evaluate the impact of variations in water chemistry on thorium sorption coefficients. However, thorium forms primarily hydroxide complexes at near neutral pH in dilute solutions (Langmuir and Herman 1980 [DIRS 147527], p. 1753). Therefore, water chemistry is expected to have very little influence on thorium sorption-coefficient values in Yucca Mountain groundwaters. However, water chemistry (i.e., pH) does impact the solubility of thorium dioxide. This effect is the reason some of the experiments in Figure A-49 were oversaturated with thorium dioxide. As shown in Figure A-50, the lowest sorption coefficients were obtained at near-neutral pH values where J-13 well water was oversaturated with thorium dioxide.

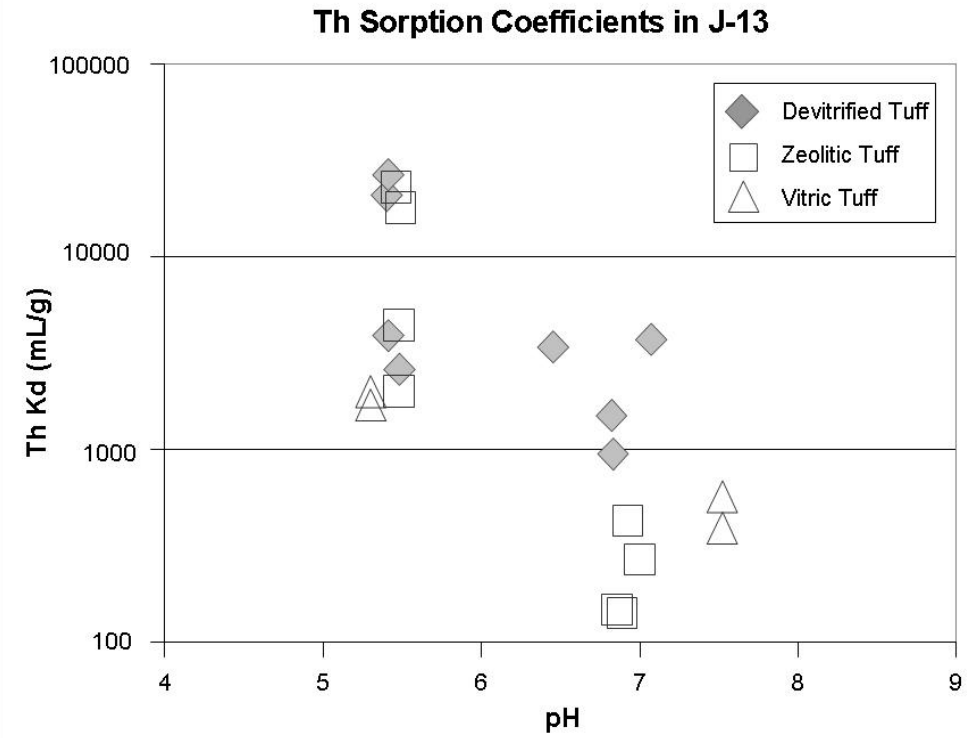

Source: DTN: LA0305AM831341.001 [DIRS 163789].

Figure A-50. Thorium Sorption Coefficients on Tuff versus pH

On the basis of the experimental data in Figures A-49 and A-50, the range of thorium sorption coefficients expected for devitrified tuffs in the saturated volcanic section at Yucca Mountain is 1,000 to 10,000 mL/g. This range is intended to reflect the range in surface areas found in devitrified tuffs in the saturated zone and the range in thorium concentrations expected during SZ transport. The lower end of the range reflects sorption coefficients at thorium concentrations near the solubility limit. The probability distribution type selected is a truncated normal distribution with a mean of 5,500 mL/g and a standard deviation of 1,500 mL/g, for a symmetric distribution and a min and max at ±3 σ.

A7.9.2 Zeolitic Tuff

Sorption coefficient data for zeolitic tuff are also plotted in Figures A-49 and A-50. Based on the available data, zeolitic tuffs have sorption coefficients for thorium that are similar to those obtained for devitrified tuffs.

On the basis of the data plotted in Figures A-44 and A-45, the range of thorium sorption coefficients selected for zeolitic tuffs in the saturated volcanic section at Yucca Mountain is 1,000 to 10,000 mL/g. The upper end of this range was selected to reflect the higher surface areas of zeolitic tuffs relative to devitrified tuffs. The probability distribution selected is a truncated normal distribution with a mean of 5,500 mL/g and a standard deviation of 1,500 mL/g.

A7.9.3 Alluvium

The probability distribution for devitrified tuff will be used as a default for the thorium sorption coefficient distribution in alluvium. Alluvium along the flow path is composed largely of disaggregated tuffaceous materials. Because it has been disaggregated, the surface area of alluvial material should be higher than that of devitrified tuff. In addition, clays and other secondary minerals are enriched in alluvial materials. These characteristics should result in higher sorption coefficients in alluvial materials compared to intact devitrified tuff.

A7.10 TIN

The solubility of tin in Yucca Mountain type groundwaters will most likely be controlled by hydrous tin oxide (SnO_2am). The solubility of hydrous tin oxide in SZ waters is estimated to range between 5.0×10^{-8} M at pH = 7.0 to 1.0×10^{-6} M at pH = 9 (Hummel et al. 2002 [DIRS 161904], p. 408).

A7.10.1 Devitrified and Zeolitic Tuff

The results for tin sorption experiments with devitrified and zeolitic tuff in J-13 and p#1 well waters are shown in Figure A-51. All the final solution concentrations were well below the saturation level with hydrous tin oxide. Thus, oversaturation was not an issue for any of the experimental results shown in Figure A-51. The fact that sorption coefficients measured for zeolitic tuff are not substantially larger than those measured for devitrified tuff (DTN: LA0702AM831341.001 [DIRS 179306]) suggests that the internal surface areas of zeolites in zeolitic tuffs are not accessible to tin species. There clearly is a trend in the dataset toward lower K_d values with higher final solution concentrations (similar to that discussed for americium). One explanation for these results is that this trend is due to imperfect separation of liquid and solid phases at the end of the sorption experiments—colloidal particles may have remained suspended in solution after centrifugation. This leads to a higher measured value of concentration in the solution and a lower value of K_d. It is also of note that the sorption coefficients for devitrified tuff in p#1 well water are larger than the coefficients obtained for devitrified tuff in J-13 well water (DTN: LA0702AM831341.001 [DIRS 179306]). Because colloids are less stable (DeGueldre et al. 2000 [DIRS 153651], p. 1,048) in ground waters with higher calcium and magnesium concentrations such as the p#1 water, the above explanation can also account for the differences between the results for J-13 and p#1 waters seen in Figure A-51. However, in the

absence of confirming information, the data with high K_d values in Figure A-51 are not given more weight than those with lower K_d values.

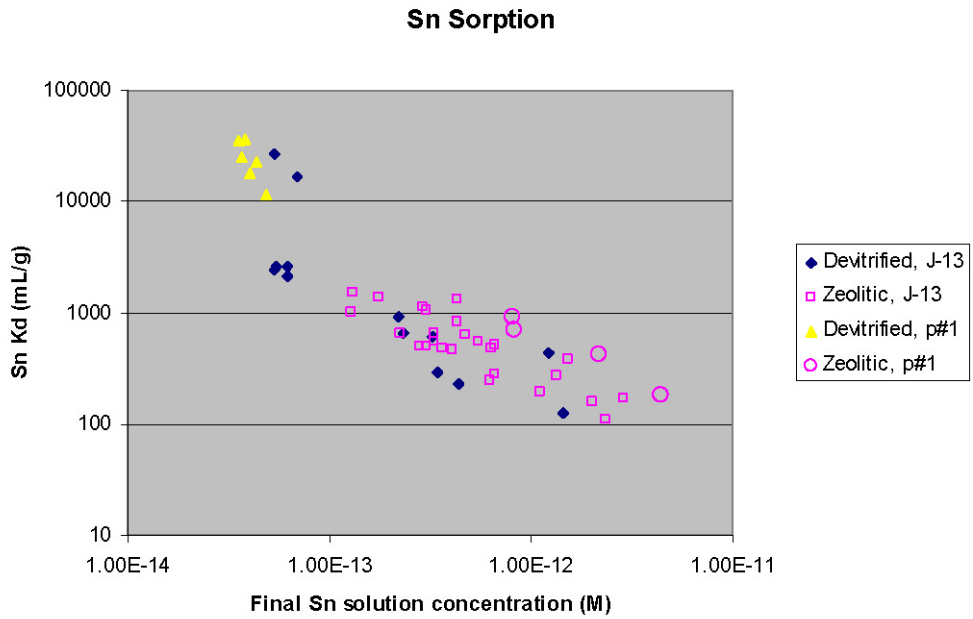

Source: DTN: LA0702AM831341.001 [DIRS 179306].

NOTE: Two of the data points from the source DTN for devitrified tuff with p#1 water are repeat measurements with similar reported results and are not included in this plot.

Figure A-51. Tin Sorption Coefficients on Tuff versus Calculated Final Tin Concentration in Solution

The data plotted in Figure A-52 shows little or no time dependence in the sorption coefficients measured for tin. This observation implies tin sorption reactions are relatively fast.

As noted above, the sorption coefficients measured for tin in p#1 water are equal to or greater than the sorption coefficients measured in J-13 well water. This suggests tin sorption coefficients are not greatly influenced by variations in water compositions. Although pH values were not reported for the experiments on Yucca Mountain tuffs, Ticknor et al. (1996 [DIRS 159212]) carried out tin sorption experiments on granitic rock samples with bulk compositions similar to Yucca Mountain tuffs. These authors found that pH variations do not have a major effect on tin K_d values measured on granite. The same conclusion likely applies to tuffs.

The amount of data available on tin sorption coefficients in Yucca Mountain tuffs is limited. Further, volcanic formations are composites incorporating both devitrified and zeolitic rock types in different proportions. Hence a single distribution is developed for the combined data set containing zeolitic and devitrified rock samples using J-13 and p#1 waters. The range of tin sorption coefficients in the saturated volcanic section at Yucca Mountain, presented in Figure A-51, is approximately 100 to 36,700 mL/g, and density of the data is higher at lower values. Hence the distribution selected is log uniform in the range of 100 to 36,700 mL/g. This is also the distribution selected for alluvium.

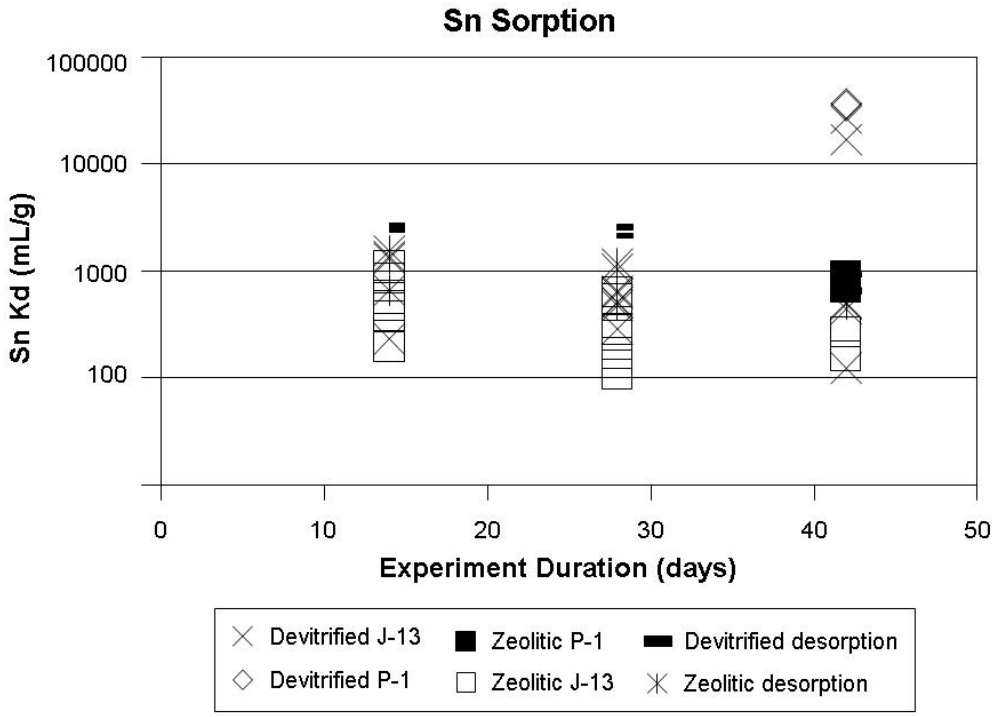

Source: DTN: LA0702AM831341.001 [DIRS 179306].

Figure A-52. Tin Sorption Coefficients on Tuff versus Experiment Duration

A7.10.2 Alluvium

The probability distribution for devitrified tuff will be used as a default for the tin sorption coefficient distribution in alluvium. Alluvium along the flow path is composed largely of disaggregated tuffaceous materials. Because it has been disaggregated, the surface area of alluvial material should be higher than that of devitrified tuff. In addition, clays and other secondary minerals are enriched in alluvial materials. These characteristics should result in higher sorption coefficients in alluvial materials compared to intact devitrified tuff.

A7.11 URANIUM

The solubility of uranium obtained from PHREEQC modeling with the file *PHREEQCDATA025.DAT* (DTN: MO0604SPAPHR25.001 [DIRS 176868]) in J-13 well water under oxidizing conditions ranges from 4.84×10^{-3} M at a pH of 4.61 to 2.12×10^{-4} M at a pH of 9.29 (Output DTN: LA0702MD831232.002 file *output_07.xls*, worksheet *Usat.pun.xls*). The solubility of uranium in p#1 water under oxidizing conditions ranges from 5.78×10^{-3} M at a pH of 4.67 to 8.43×10^{-4} M at a pH of 9.4 (Output DTN: LA0702MD831232.002, file *output_07.xls*, worksheet *Usatp1.pun.xls*). The solubility-controlling solid in both waters is schoepite.

A7.11.1 Devitrified Tuff

As shown in Figure A-53, the calculated final uranium concentrations in the sorption experiments were generally below saturation with schoepite. The sorption coefficients obtained in experiments with devitrified tuffs do not show a correlation with the calculated final uranium solution concentrations.

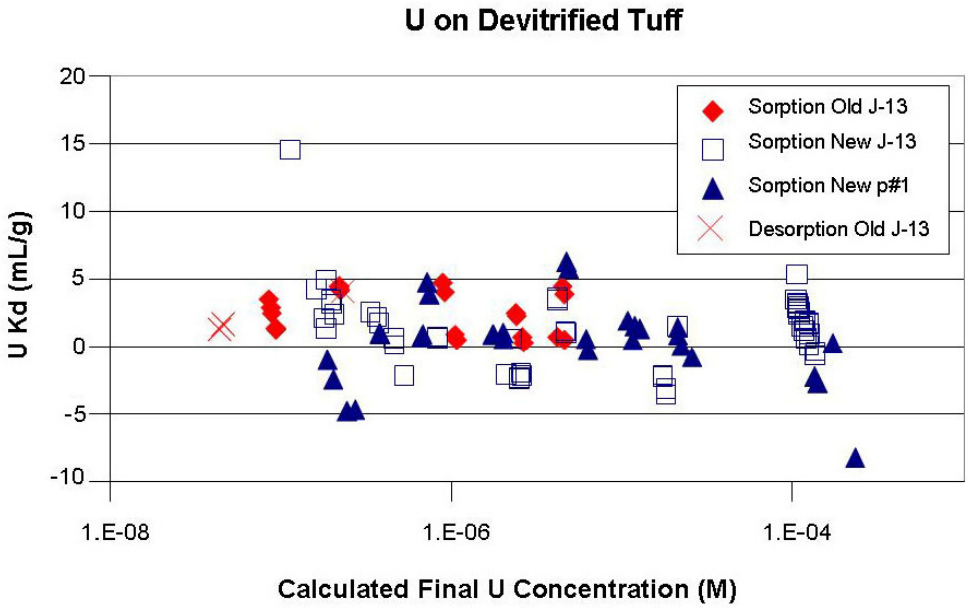

Sources: DTNs: LA0305AM831341.001 [DIRS 163789]; LA0407AM831341.006 [DIRS 170628].

NOTE: In the legend, 'old' stands for data from before PVAR, 'new' stands for after PVAR data.

Figure A-53. Uranium Sorption Coefficients on Devitrified Tuff versus Calculated Final Uranium Concentration in Solution

Sorption experiments carried out as a function of time are shown in Figure A-54. Beyond approximately 3 days, there is no clear correlation between the sorption coefficients obtained and the duration of the experiments. The data imply that uranium sorption reactions on devitrified tuffs must be relatively fast (i.e., they reach steady state in a few days).

The dependence of the uranium sorption coefficient on water chemistry was tested with experiments using two water compositions (J-13 well and synthetic p#1). The J-13 experimental data are shown as a function of pH in Figure A-55. The "old data" were obtained before May 1989 and the "new data" after May 1989. The difference between the two data sets is not significant. The range of values obtained at a given pH (e.g., 8.4) reflects experimental errors and natural variations in rock properties (e.g., surface area and mineral chemistry). It is not possible to discriminate between these possible causes with the available data. On the basis of the experimental data points, there does not appear to be a correlation between K_d values and pH. However, surface-complexation modeling with PHREEQC, using binding constants derived by Pabalan et al. (1998 [DIRS 162987], p. 124) for uranium on silica points to a clear pH dependence. Pabalan was the source for uranium binding constants on silica. The binding constants were used in surface complexation modeling calculations to evaluate the impact of

variations in water chemistry (e.g., pH, J-13 well versus p#1) on uranium sorption coefficients). As shown in Figure A-55, the two model curves reflect two different surface areas (2.8 and 5.6 m^2/g). The 2.8 m^2/g surface area is approximately an average value for devitrified tuffs at Yucca Mountain.

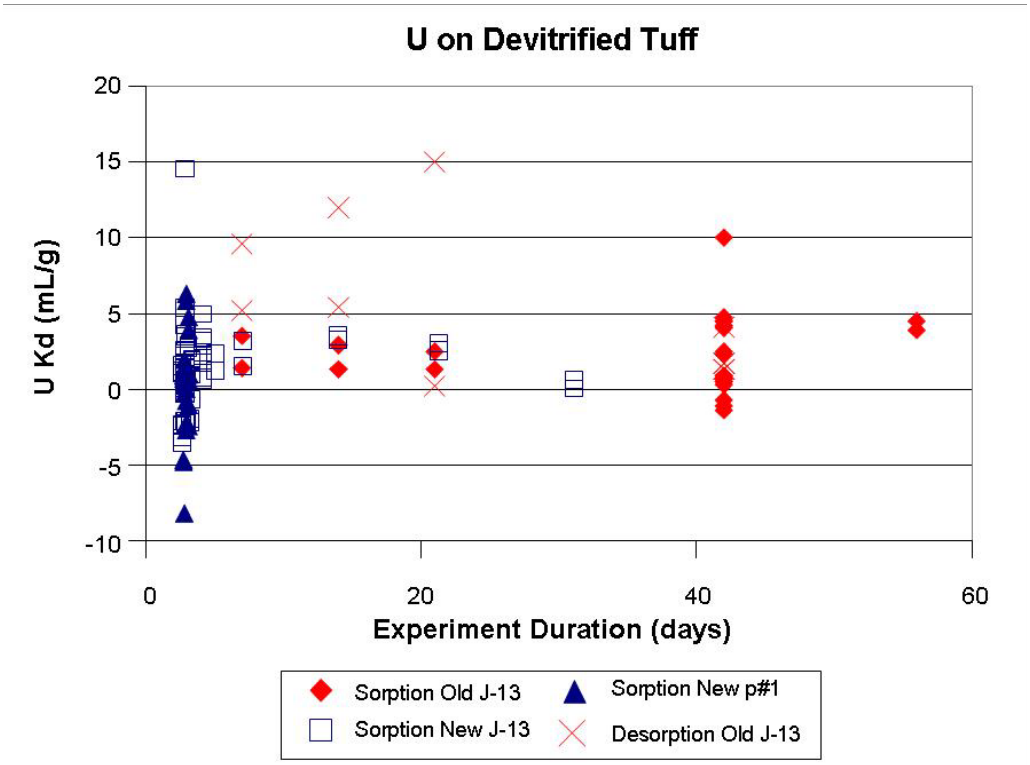

Sources: DTNs: LA0305AM831341.001 [DIRS 163789]; LA0407AM831341.006 [DIRS 170628].

NOTE: In the legend, 'old' stands for data collected before May 1989, 'new' stands for data collected after May 1989.

Figure A-54. Uranium Sorption Coefficients on Devitrified Tuff versus Experiment Duration for Sorption (Forward) and Desorption (Backward) Experiments

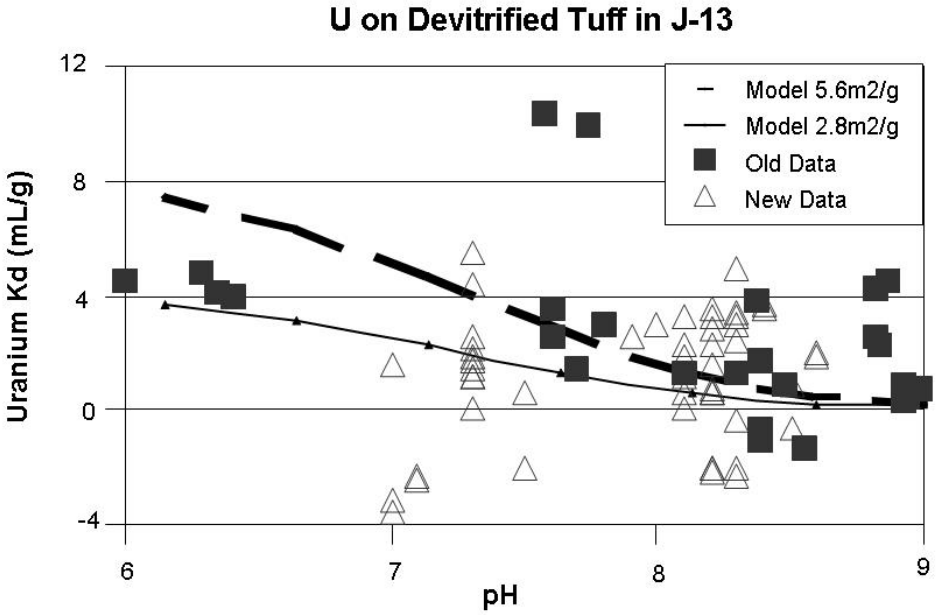

Sources: DTNs: LA0305AM831341.001 [DIRS 163789]; LA0407AM831341.006 [DIRS 170628].

NOTE: In the legend, 'old' stands for data collected before May 1989, 'new' stands for data collected after May 1989. Model curves are from the PHREEQC surface-complexation model (Output DTN: LA0702MD831232.002, file *output_07.xls*, worksheets *Udtj13.pun.xls* and *Udt2j13.pun.xls*).

Figure A-55. Uranium Sorption Coefficients on Devitrified Tuff versus pH

The sorption coefficients obtained in experiments with synthetic p#1 water are shown in Figure A-56. The data plotted have substantial experimental errors associated with them as indicated by the magnitude of some of the negative K_d values. These experimental errors result from counting statistics, the stability of counters over time, corrections made for adsorption to container walls, and the pH of the tracer solution added to the experiment. Taken at face value, the experimental data suggest a trend of increasing values of K_d with increasing pH. However, the surface complexation modeling predicts a decrease in the value of K_d with increasing pH, although the absolute K_d values are rather small.

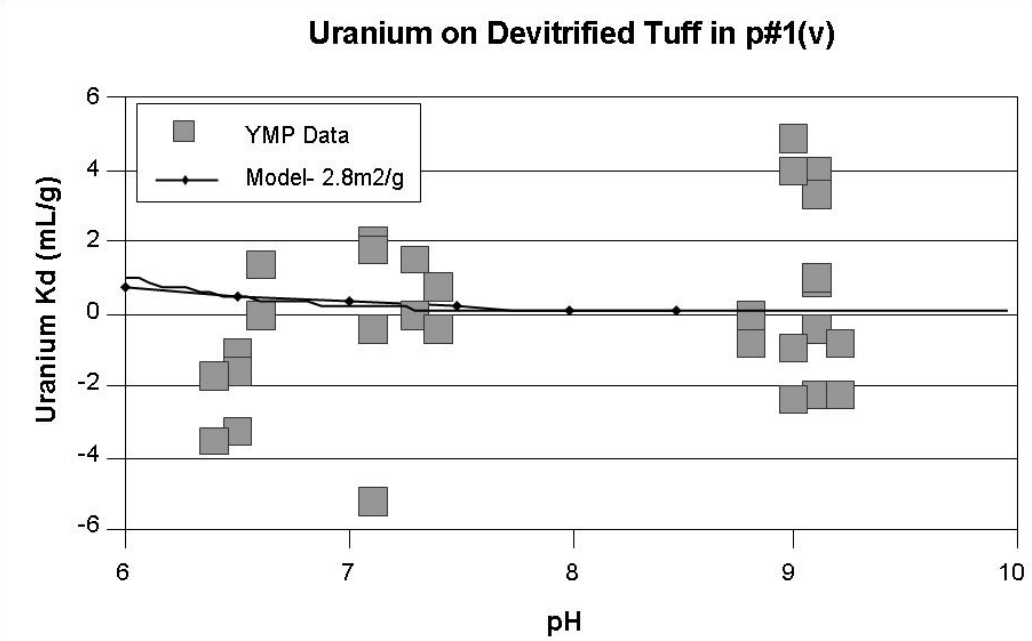

Sources: DTNs: LA0305AM831341.001 [DIRS 163789]; LA0407AM831341.006 [DIRS 170628].

NOTE: Model curve is from the PHREEQC surface-complexation model (Output DTN: LA0702MD831232.002, file *output_07.xls*, worksheet *Udtp1.pun.xls*).

Figure A-56. Uranium Sorption Coefficients on Devitrified Tuff in p#1 (Volcanics) Water versus pH

On the basis of the experimental data and model curves plotted in Figures A-55 and A-56, a truncated normal distribution was selected for the uranium sorption-coefficient probability distribution for devitrified tuff in the saturated volcanic section with a range of 0 to 4 mL/g, a median of 2 mL/g, and a standard deviation of 0.6 mL/g.

A7.11.2 Zeolitic Tuff

As shown in Figure A-57, the sorption coefficients obtained in experiments with zeolitic tuffs do not show a clear correlation with the calculated final uranium solution concentrations. The high end of the concentrations plotted is below saturation with a solid uranium phase.

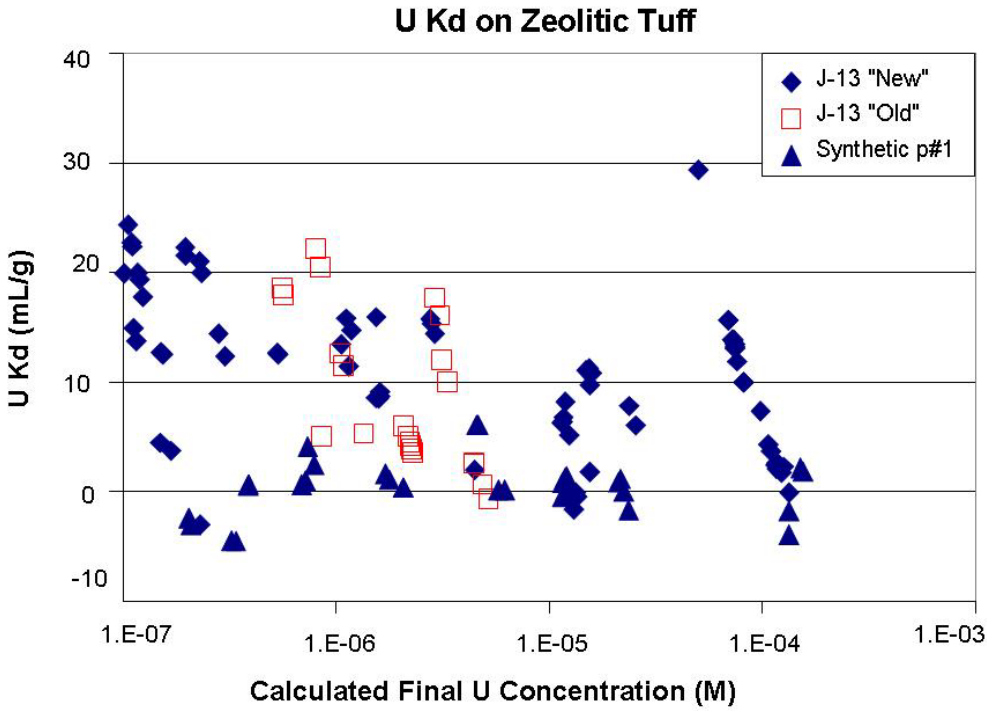

Sources: DTNs: LA0305AM831341.001 [DIRS 163789]; LA0407AM831341.006 [DIRS 170628].

NOTE : In the legend, 'old' stands for data collected before May 1989, 'new' stands for data collected after May 1989.

Figure A-57. Uranium Sorption Coefficients on Zeolitic Tuff versus Calculated Final Uranium Concentration in Solution

Uranium sorption experiments on zeolitic tuffs carried out as a function of time are shown in Figure A-58. Beyond a period of approximately 3 days, there is no clear correlation between the sorption coefficients obtained and the duration of the experiments. These data imply that uranium sorption reactions on zeolitic tuffs are relatively fast (i.e., they reach steady state in a few days).

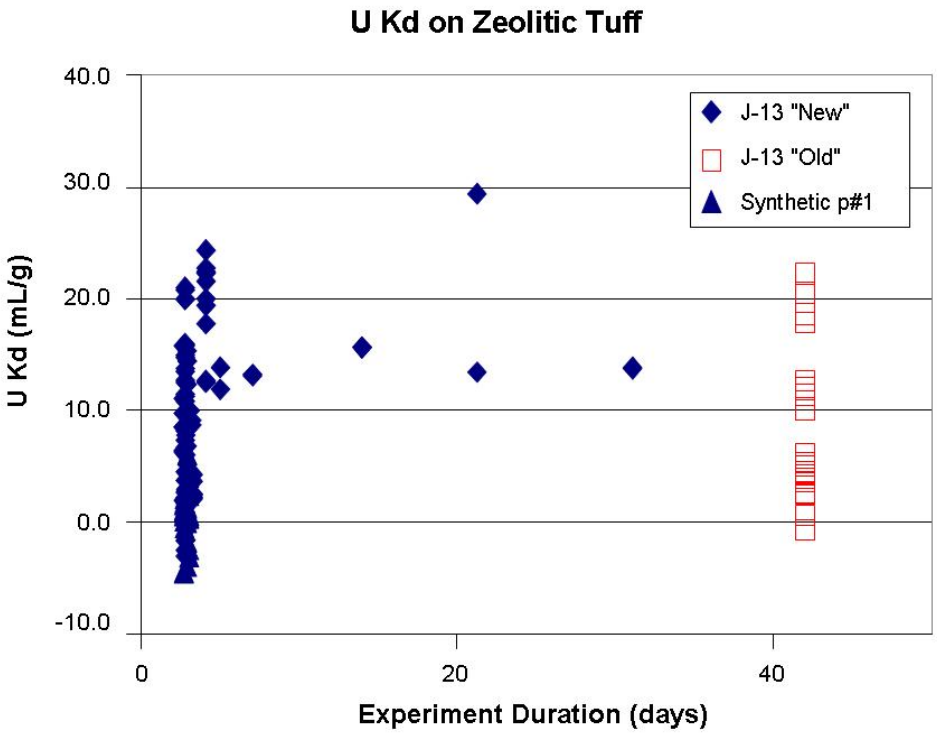

Sources: DTNs: LA0305AM831341.001 [DIRS 163789]; LA0407AM831341.006 [DIRS 170628].

NOTE: In the legend, 'old' stands for data before PVAR, 'new' stands for after PVAR data.

Figure A-58. Uranium Sorption Coefficients on Zeolitic Tuff as a Function of Experiment Duration

The dependence of the uranium sorption coefficient on water chemistry was tested with experiments using two water compositions (J-13 well and synthetic p#1). The J-13 data are shown as a function of pH in Figure A-59. The "old data" were obtained before May 1989 and the "new data" after May 1989. The difference between the two data sets is not statistically significant. The range of values observed at a given pH (e.g., 8.4) reflects variations in rock properties and experimental errors. The experimental errors result from such things as counting statistics, the stability of counters over time, the accuracy of corrections for adsorption to container walls, and other experimental artifacts. In some cases, the pH of the tracer solution added to the experiment seems to have an effect. Some of these errors are random (e.g., counting errors) and others (e.g., adsorption to container walls) may have a nonrandom bias. It is not possible to evaluate these errors separately with the available information. The distribution of data points in Figure A-59 does not indicate a correlation between the K_d and pH values.

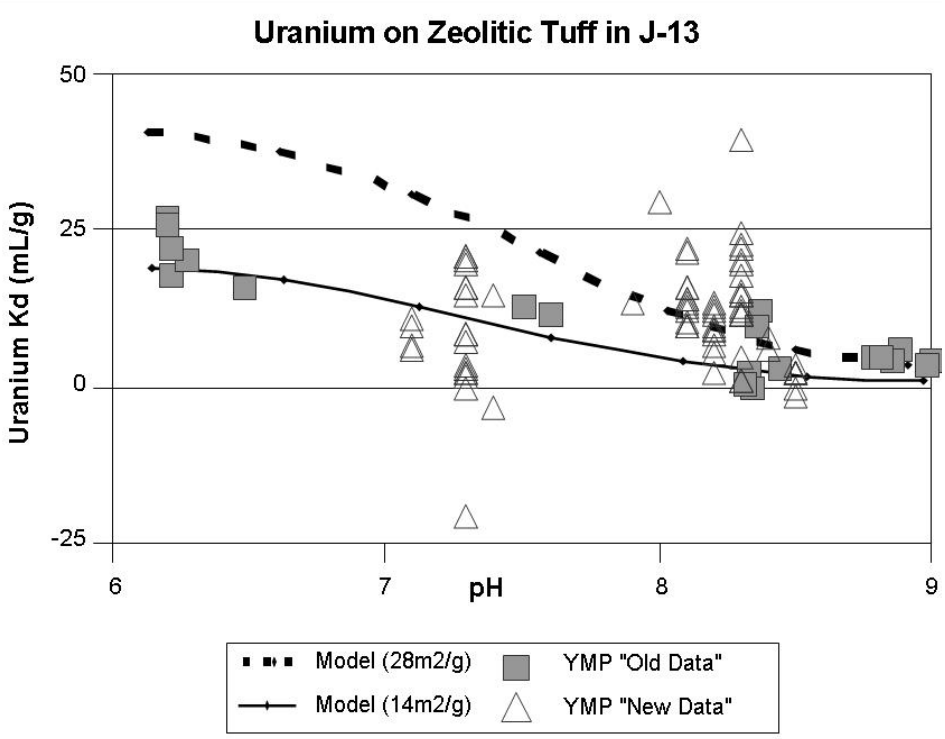

Sources: DTNs: LA0305AM831341.001 [DIRS 163789]; LA0407AM831341.006 [DIRS 170628].

NOTE: In the legend, 'old' stands for data collected before May 1989, 'new' stands for data collected after May 1989. Model curves derived with PHREEQC surface-complexation modeling are also shown (Output DTN: LA0702MD831232.002, file *output _07.xls*, worksheets *Uzeolitj13.pun.xls and Uzeolj13.pun.xls*).

Figure A-59. Uranium Sorption Coefficients for Zeolitic Tuff in J-13 Well Water Plotted as a Function of pH

Surface-complexation modeling was carried out with PHREEQC with the thermodynamic input data file *PHREEQCDATA025.DAT* (DTN: MO0604SPAPHR25.001 [DIRS 176868]) to provide a framework in which to interpret the experimental data. Binding constants for uranium on silica derived by Pabalan et al. (1998 [DIRS 162987], p. 124) were used in the modeling. Pabalan was the source for uranium binding constants on silica. The binding constants were used in surface complexation modeling calculations to evaluate the impact of variations in water chemistry (e.g., pH, J-13 versus p#1 on uranium sorption coefficients). The modeling results show a clear pH dependence (Figure A-59). The two model curves reflect two different surface areas. A surface area of 28 m^2/g was used because it is approximately an average value for zeolitic tuffs and because it is an order of magnitude larger than the average value used for modeling devitrified tuffs. A surface area of 14 m^2/g was also used to show the impact of change in surface area by a factor of 2.

The sorption coefficients obtained in experiments with synthetic p#1 water are shown in Figure A-60. The magnitudes of the negative K_d values plotted are similar to the magnitudes of the positive values plotted. Thus, the net values may be very close to zero. Taken at face value, the experimental data suggest a trend of increasing K_d values with increasing pH. However, the surface complexation modeling predicts a slight increase in K_d with decreasing pH, although the

absolute K_d values are rather small in agreement with the net values obtained from the experimental data.

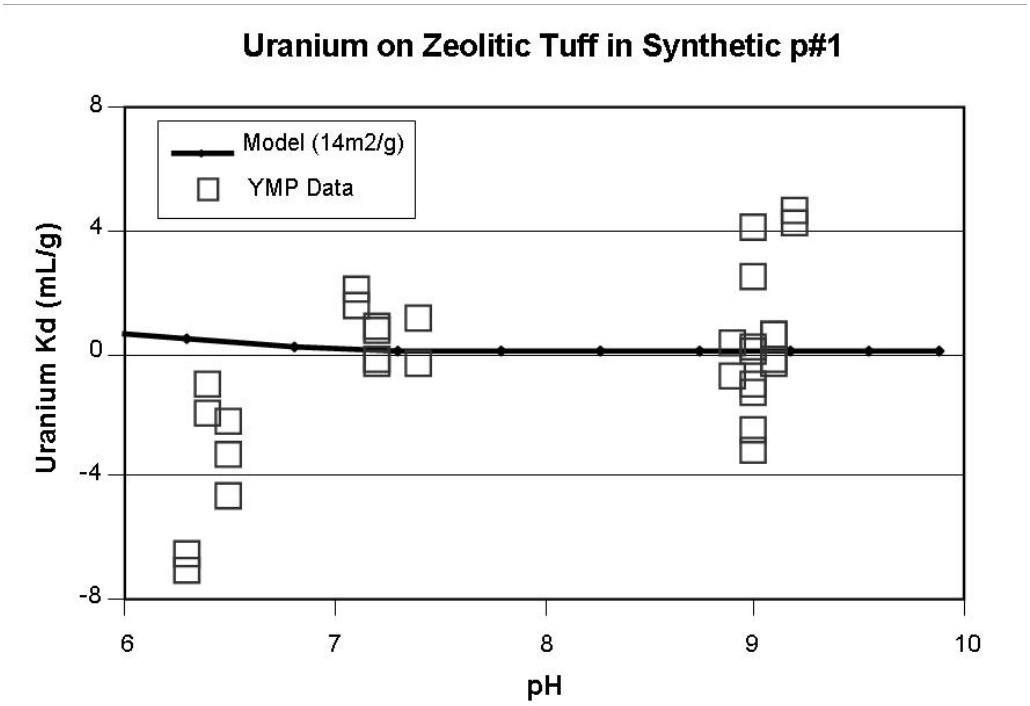

Sources: DTNs: LA0305AM831341.001 [DIRS 163789]; LA0407AM831341.006 [DIRS 170628].

NOTE: Model curves derived with PHREEQC surface-complexation modeling are also shown (Output DTN: LA0702MD831232.002, file *output_07.xls*, worksheet *Uzeop1.pun.xls*).

Figure A-60. Uranium Sorption Coefficients for Zeolitic Tuff in Synthetic p#1 Water as a Function of pH

On the basis of the experimental data and model curves plotted in Figures A-59 and A-60, a truncated normal distribution was selected for the uranium sorption-coefficient probability distribution for zeolitic tuff in the saturated volcanic section with a range of 5 to 20 mL/g, a median of 12 mL/g, and a standard deviation of 3.6 mL/g (Output DTN: LA0702AM150304.001). This distribution emphasizes the J-13 well water chemistry over the p#1 water chemistry.

A7.11.3 Alluvium

Sorption coefficients for uranium were measured in batch experiments on cores obtained from three wells (10SA, 22SA, and 19IM1A) drilled into the alluvium (DTN: LA0302MD831341.004 [DIRS 163785]). Following a procedure identical to that used for neptunium, described in Section A7.3.3 of this report, the K_d values for uranium were taken to be described by a *t* distribution with the following statistics: $\mu_U = 4.6$ mL/g, $\sigma_U = 0.58$ mL/g.

Although the *t* distribution was thought to capture correctly the spatial uncertainty, the question about the representativeness of the experiment does introduce a small amount of additional uncertainty, as discussed for the neptunium case in Section A7.3.3. Hence, a cumulative distribution was chosen for uranium. The minimum experimentally observed value was

1.7 mL/g. Five percent probability was uniformly distributed between 1.7 mL/g and the lower bound of the *t* distribution at 2.9 mL/g. Since the *t* distribution had such little variation, it was reasonably represented by a uniform distribution. Hence, 90% probability was uniformly distributed between 2.9 mL/g and the upper bound of the *t* distribution at 6.3 mL/g. The remaining 5% probability was uniformly distributed between 6.3 mL/g and the maximum experimentally observed value of 8.9 mL/g.

A8. SUMMARY

Sorption-coefficient probability distribution functions were derived for the radionuclides of uranium, cesium, neptunium, plutonium, americium, thorium, strontium, protactinium, and radium. These are summarized in Table A-4. Experimental and modeling results were used to constrain the distributions. In general, the approach used in the derivation of the distributions tended to underestimate the range and median or mean. This approach was used to provide some conservatism in the derivation given potential scaling uncertainties in the application of these distributions to transport calculations at the Yucca Mountain site.

Table A-4. Small-Scale Probability Distribution Functions for K_ds in the Saturated Zone Developed on the Basis of Laboratory Data from Core Samples

Species	Unit/Analysis	Distribution	Coefficients Describing Distribution (mL/g)
U	Zeolitic	Truncated Normal	Range = 5–20; μ = 12, σ = 3.6
	Devitrified	Truncated Normal	Range = 0–4; μ = 2, σ = 0.6
	Alluvium	Cumulative	(K_d, prob) (1.7, 0.) (2.9, 0.05) (6.3, 0.95) (8.9,1.0)
Np	Zeolitic	Truncated Normal	Range = 0 to 6; μ =2.88, σ = 1.47
	Devitrified	Exponential	Range = 0 to 2; μ = 0.69, σ = 0.71
	Alluvium	Cumulative	(K_d, prob) (1.8, 0.) (4.0, 0.05) (8.7, 0.95) (13, 1.0)
Pu	Zeolitic	Beta	Range = 50 to 300; μ = 100, σ = 15
	Devitrified	Beta	Range = 50 to 300; μ = 100, σ = 15
	Alluvium	Beta	Range = 50 to 300; μ = 100, σ = 15
Cs	Zeolitic	Exponential	Range = 4,000 to 42,000; μ = 16,942: σ = 14,930
	Devitrified	Truncated Normal	Range = 100 to 1,000; μ = 728, σ = 464
	Alluvium	Truncated Normal	Range = 100 to 1,000; μ = 728, σ = 464
Am	Zeolitic	Truncated Normal	Range = 1,000 to 10,000; μ = 5,500, σ = 1,500
	Devitrified	Truncated Normal	Range = 1,000 to 10,000; μ = 5,500, σ = 1,500
	Alluvium	Truncated Normal	Range = 1,000 to 10,000; μ = 5,500, σ = 1,500
Pa	Zeolitic	Truncated Normal	Range = 1,000 to 10,000; μ = 5,500, σ = 1,500
	Devitrified	Truncated Normal	Range = 1,000 to 10,000; μ = 5,500, σ = 1,500
	Alluvium	Truncated Normal	Range = 1,000 to 10,000; μ = 5,500, σ = 1,500

Table A-4. Small-Scale Probability Distribution Functions for K_ds in the Saturated Zone Developed on the Basis of Laboratory Data from Core Samples (Continued)

Species	Unit/Analysis	Distribution	Coefficients Describing Distribution (mL/g)
Sr	Zeolitic	Cumulative	(K_d, prob) (100,0) (5,000, 0.5) (90,000, 1.0)
	Devitrified	Uniform	Range = 20 to 400
	Alluvium	Uniform	Range = 20 to 400
Th	Zeolitic	Truncated Normal	Range = 1,000 to 10,000; μ = 5,500, σ = 1,500 (for a symmetric distribution and a min and max at ± 3 σ
	Devitrified	Truncated Normal	Range = 1,000 to 10,000; μ = 5,500, σ = 1,500 (for a symmetric distribution and a min and max at ± 3 σ
	Alluvium (same as devitrified)	Truncated Normal	Range = 1,000 to 10,000; μ = 5,500, σ = 1,500 (for a symmetric distribution and a min and max at ± 3 σ
Ra	Zeolitic	Truncated Log-Normal	Range = 1,000 to 250,000; μ =100,000, σ = 31,420
	Devitrified	Uniform	Range =100 to 1,000
	Alluvium	Uniform	Range =100 to 1,000
Se	Devitrified	Truncated Log-Normal	Range = 1 to 50; μ = 14.0; σ = 11.2
	Zeolitic	Truncated Log-Normal	Range = 1 to 35; μ = 14.3; σ = 7.9
	Alluvium	Truncated Log-Normal	Range = 1 to 50; μ = 14.0; σ = 11.2
Sn	Devitrified	Log Uniform	Range = 100 to 36,700
	Zeolitic	Log Uniform	Range = 100 to 36,700
	Alluvium	Log Uniform	Range = 100 to 36,700
C/Tc/I	Volcanics/Alluvium	Constant	Zero

Output DTN: LA0702AM150304.001, Tables 1 and 4.

μ = mean; σ = standard deviation.

A9. CORRELATIONS FOR SAMPLING OF SORPTION-COEFFICIENT PROBABILITY DISTRIBUTIONS

In the TSPA, SZ transport calculations are carried out separately for each radionuclide. The sorption-coefficient probability distribution for each radionuclide could be sampled independently in each transport calculation. However, such independent sampling could potentially lead to dose dilution. That is, independent sampling of the distributions could cause radionuclides to travel at independent rates such that the calculated dose at the accessible environment is not representative of maximum possible doses. Similarities in the chemical dependencies of sorption coefficients for the various radionuclides suggest transport rates in the saturated zone are likely to be correlated for some radionuclides. These correlations are summarized in Table A-5.

Correlations for sampling sorption coefficient probability distributions have been derived for the elements americium, cesium, neptunium, protactinium, plutonium, radium, strontium, thorium, and uranium. In order to derive the correlations, a rating system was first developed to rate the

impact of 6 different environmental variables on the sorption coefficient for a given element on each of the three major rocks types. The six variables are pH, Eh, water chemistry, rock composition, rock surface area, and radionuclide concentration. Most of these parameters are self-explanatory. Water chemistry refers to the major ion concentrations and silica. Rock composition refers to both the mineralogic composition of the rocks as well as the chemical composition of the minerals (e.g., zeolite compositions). The matrix containing the ratings is shown in Table A-5. The ratings are based on the sorption data and modeling presented in this appendix combined with professional judgment.

Table A-5. Ratings of Controls on Sorption Behavior

Element	pH	Eh	Water Chemistry	Rock Comp.	Surface Area	Radionuclide Concentration
Am (D)	2	No	3	4	1	ND
Am (Z)	2	No	3	4	1	ND
Am (V)	2	No	3	4	1	ND
Cs (D)	No	No	3	4	2	1
Cs (Z)	No	No	2	1	3	4
Cs (V)	No	No	3	4	2	1
Np (D)	2	(No)	1	4	3	5
Np (Z)	2	(No)	1	4	3	5
Np (V)	2	(No)	1	4	3	5
Pa (D)	2	No	ND	ND	1	ND
Pa (Z)	2	No	ND	ND	1	ND
Pa (V)	2	No	ND	ND	1	ND
Pu (D)	4	(No)	2	1	3	5
Pu (Z)	4	(No)	2	1	3	5
Pu (V)	4	(No)	2	1	3	5
Ra (D)	No	No	3	4	2	1
Ra (Z)	No	No	1	2	3	4
Ra (V)	No	No	3	4	2	1
Se (D)	2	(No)	1	4	5	3
Se (Z)	2	(No)	1	4	5	3
Se (V)	2	(No)	1	4	5	3
Sn (D)	2	No	4	3	1	(ND)
Sn (Z)	2	No	4	3	1	(ND)
Sn (V)	2	No	4	3	1	(ND)
Sr (D)	No	No	2	4	1	3
Sr (Z)	No	No	1	2	3	4
Sr (V)	No	No	2	4	1	3
Th (D)	2	No	3	ND	1	ND
Th (Z)	2	No	3	ND	1	ND

Table A-5. Ratings of Controls on Sorption Behavior (Continued)

Element	pH	Eh	Water Chemistry	Rock Comp.	Surface Area	Radionuclide Concentration
Th (V)	2	No	3	ND	1	ND
U (D)	2	(No)	1	5	4	3
U (Z)	2	(No)	1	5	4	3
U (V)	2	(No)	1	5	4	3

1 = High impact, 5 = Low impact. D = devitrified; Z = zeolitic; V = vitric.

NOTES: No = No impact under oxidizing conditions.
(No) = No impact under oxidizing conditions. However, rock composition may provide locally reducing environments for plutonium to sorb as plutonium IV. Ferrous iron-bearing minerals may provide such local microenvironments, for example.
ND = No data available.
(ND) For selenium, the radionuclide concentration dependence evident in the experimental data is attributed to an experimental artifact (i.e., colloids in the supernate).

The rating system presented in Table A-5 was used to develop correlations between the sorption coefficient probability distributions for the elements of interest, as shown in Table A-6. Identical parameter ratings resulted in a correlation of 100%. If the two highest rating were in the same parameters in the same order, a correlation of 75% was assigned. If the two highest ratings were in the same parameters but not in the same order, a correlation of 50% was assigned. If the three highest ratings were in the same parameters but not in the same order, a correlation of 25% was assigned. If the four highest ratings were in the same parameters but not in the same order, a correlation of 10% was assigned. For all other combinations, a correlation of 0% was assigned.

Table A-6. Correlations for Sampling Sorption Coefficient Probability Distributions

Element	Am (D)	Am (Z)	Am (V)	Cs (D)	Cs (Z)	Cs (V)	Np (D)	Np (Z)	Np (V)	Pa (D)	Pa (Z)	Pa (V)	Pu (D)	Pu (Z)	Pu (V)
Am(D)	100														
Am(Z)	100	100													
Am(V)	100	100	100												
Cs(D)	0	0	0	100											
Cs(Z)	0	0	0	10	100										
Cs(V)	0	0	0	100	10	100									
Np(D)	25	25	25	0	0	0	100								
Np(Z)	25	25	25	0	0	0	100	100							
Np(V)	25	25	25	0	0	0	100	100	100						
Pa(D)	75	75	75	0	0	0	0	0	0	100					
Pa(Z)	75	75	75	0	0	0	0	0	0	100	100				
Pa(V)	75	75	75	0	0	0	0	0	0	100	100	100			
Pu(D)	10	10	10	0	75	0	10	10	10	0	0	0	100		
Pu(Z)	10	10	10	0	75	0	10	10	10	0	0	0	100	100	
Pu(V)	10	10	10	0	75	0	10	10	10	0	0	0	100	100	100
Ra(D)	0	0	0	100	10	100	0	0	0	0	0	0	0	0	0
Ra(Z)	0	0	0	10	50	10	0	0	0	0	0	0	50	50	50
Ra(V)	0	0	0	100	10	100	0	0	0	0	0	0	0	0	0
Se(D)	0	0	0	0	0	0	0	0	0	0	0	0	0	0	0
Se(Z)	0	0	0	0	0	0	0	0	0	0	0	0	0	0	0
Se(V)	0	0	0	0	0	0	0	0	0	0	0	0	0	0	0
Sn(D)	75	75	75	0	0	0	25	25	25	75	75	75	10	10	10
Sn(Z)	75	75	75	0	0	0	25	25	25	75	75	75	10	10	10
Sn(V)	75	75	75	0	0	0	25	25	25	75	75	75	10	10	10
Sr(D)	0	0	0	25	10	25	50	50	50	0	0	0	0	0	0
Sr(Z)	0	0	0	10	50	10	0	0	0	0	0	0	50	50	50
Sr(V)	0	0	0	25	10	25	50	50	50	0	0	0	0	0	0
Th(D)	100	100	100	0	0	0	0	0	0	100	100	100	0	0	0
Th(Z)	100	100	100	0	0	0	0	0	0	100	100	100	0	0	0
Th(V)	100	100	100	0	0	0	0	0	0	100	100	100	0	0	0
U(D)	0	0	0	0	0	0	75	75	75	0	0	0	0	0	0
U(Z)	0	0	0	0	0	0	75	75	75	0	0	0	0	0	0
U(V)	0	0	0	0	0	0	75	75	75	0	0	0	0	0	0

Table A-6. Correlations for Sampling Sorption Coefficient Probability Distributions (Continued)

Element	Ra (D)	Ra (Z)	Ra (V)	Se (D)	Se (Z)	Se (V)	Sn (D)	Sn (Z)	Sn (V)	Sr (D)	Sr (Z)	Sr (V)	Th (D)	Th (Z)	Th (V)	U (D)	U (Z)	U (V)
Am(D)																		
Am(Z)																		
Am(V)																		
Cs(D)																		
Cs(Z)																		
Cs(V)																		
Np(D)																		
Np(Z)																		
Np(V)																		
Pa(D)																		
Pa(Z)																		
Pa(V)																		
Pu(D)																		
Pu(Z)																		
Pu(V)																		
Ra(D)	100																	
Ra(Z)	10	100																
Ra(V)	100	10	100															
Se(D)	0	0	0	100														
Se(Z)	0	0	0	100	100													
Se(V)	0	0	0	100	100	100												
Sn(D)	0	0	0	0	0	0	100											
Sn(Z)	0	0	0	0	0	0	100	100										
Sn(V)	0	0	0	0	0	0	100	100	100									
Sr(D)	25	10	25	0	0	0	0	0	0	100								
Sr(Z)	10	100	10	0	0	0	0	0	0	10	100							
Sr(V)	25	10	25	0	0	0	0	0	0	100	10	100						
Th(D)	0	0	0	0	0	0	75	75	75	75	0	0	100					
Th(Z)	0	0	0	0	0	0	75	75	75	0	0	0	100	100				
Th(V)	0	0	0	0	0	0	75	75	75	0	0	0	100	100	100			
U(D)	0	0	0	75	75	75	0	0	0	0	0	0	0	0	0	100		
U(Z)	0	0	0	75	75	75	0	0	0	0	0	0	0	0	0	100	100	
U(V)	0	0	0	75	75	75	0	0	0	0	0	0	0	0	0	100	100	100

Source: Output DTN: LA0702AM150304.001.

D = devitrified; Z = zeolitic; V = vitric.

INTENTIONALLY LEFT BLANK

APPENDIX B
COLLOID-FACILITATED TRANSPORT OF REVERSIBLY ATTACHED RADIONUCLIDES

The analysis presented in this appendix supports the model component of the saturated zone (SZ) transport model that deals with colloid-facilitated transport of radionuclides that are attached reversibly to the colloids, and in particular the adoption of the advection–dispersion equation to model colloid transport (Section 6.4.2.6). The results of this analysis do not form a direct input to the site-scale SZ transport model.

The radioisotopes of plutonium and americium can sorb either reversibly or irreversibly onto colloids with the relative percentages of these obtained from an analysis of waste form degradation and waste package corrosion processes occurring in the repository near-field environment as shown in *Saturated Zone Colloid Transport* (BSC 2004 [DIRS 170006], Section 6.3.). In general, the majority of the plutonium and americium sorbed onto colloids is irreversibly sorbed, with a typical percentage being 90% to 99% irreversible and 1% to 10% reversible as shown in *Waste Form and In-Drift Colloids-Associated Radionuclide Concentrations: Abstraction and Summary* (SNL 2007 [DIRS 177423], Section 6.3.3.2). Radionuclides that are irreversibly sorbed are typically embedded in the colloid or are so strongly sorbed onto the colloid that there is no possibility of detachment for typical transport time scales (thousands of years) through the saturated zone. On the other hand, reversibly sorbed colloids have measurable desorption rates. The irreversibly sorbed radionuclides are taken to transport in a manner identical to the colloids onto which they are sorbed. The colloid retardation factor distributions for irreversible colloids are developed in *Saturated Zone Colloid Transport* (BSC 2004 [DIRS 170006]), so only a brief description is provided here. The transport of the colloids is simulated using the advection–dispersion equation, and colloids are taken to not diffuse. Several field observations have suggested that a small percentage of colloids transport with essentially no retardation in groundwater (Kersting et al. 1999 [DIRS 103282], pp. 56 and 58; Penrose et al. 1990 [DIRS 100811], p. 228), whereas the majority undergoes either reversible or irreversible filtration, which can be described by a retardation factor, R_{col}. In this analysis, filtration is defined as the net effect of chemical sorption of the colloid onto the rock surface and the physical removal of colloids from the advective flow due to sieving and settling. The value of R_{col} is dependent on several factors such as colloid size, colloid type, and geochemical conditions (e.g., pH, Eh, and ionic strength). These factors are folded into the distribution of R_{col} that has been developed from field and experimental data collected under varying geochemical conditions with different colloid types and sizes as shown in *Saturated Zone Colloid Transport* (BSC 2004 [DIRS 170006] Section 6.4.2). Attachment rate constants, k_{att}, detachment rate constants, k_{det}, of colloids to the rock matrix and R_{col} distributions are related by:

$$R_{col} = 1 + \frac{k_{att}}{k_{det}} \qquad \text{(Eq. B-1)}$$

The attachment rate constant is also used to determine the fraction of the colloids that transport with no retardation. Specifically, colloids for which one over the attachment rate constant is smaller than the travel time through the system will transport with no retardation. The development of R_{col} distributions for the volcanics and the alluvium as well as the fraction of colloids that transport unretarded is documented in *Saturated Zone Colloid Transport* (BSC 2004 [DIRS 170006]).

The saturated zone transport simulations of radionuclides that are reversibly attached to colloids are conducted for radioisotopes of plutonium, americium, thorium, protactinium, and cesium (the rationale for selection of these radionuclides is given in *Waste Form and In-Drift Colloids-Associated Radionuclide Concentrations: Abstraction and Summary* (SNL 2007 [DIRS 177423], Section 6.3.3.1). Plutonium and americium inventories are split into reversibly and irreversibly sorbed fractions. For the reversibly sorbed transport simulations, radioisotopes of plutonium are transported as one group, radioisotopes of plutonium, thorium, and protactinium are transported as a second group, and cesium is transported as a third group. Americium, thorium, and protactinium are being treated as a single group based on the similarity in their absorption characteristics–each of these three radionuclides are strongly sorbed to surfaces generally involving the hydroxide group, and each of them displays a single valance state in solution and sorption (Allard et al. 1983 [DIRS 162982], pp. 9, 10, and 12). The radionuclides that are reversibly absorbed onto colloids are modeled using the K_c model, which represents the equilibrium partitioning of radionuclides between the aqueous phase and the colloidal phase with the distribution coefficient K_c (Robinson et al. 1997 [DIRS 100416], Equation 8-10, p. 8-35). The K_c model is a simplified colloid transport model that applies under the following conditions:

1. Contaminants sorb reversibly to the colloids in addition to interacting with the rock matrix and fractures

2. Colloids are isolated to the fracture and possess dispersive properties equivalent to that of an aqueous solute

3. Colloids interact reversibly with the rock surface

4. Colloids exist throughout the flow system.

Under these conditions, a transport equation for a contaminant attached to colloids can be written as:

$$R_{\text{col}} \frac{\partial C_c}{\partial t} = D_z \frac{\partial^2 C_c}{\partial z^2} - v \frac{\partial C_c}{\partial z} \qquad \text{(Eq. B-2)}$$

where

C_c	=	concentration of contaminants attached to colloids
R_{col}	=	a retardation factor that captures the details of colloid attachment/detachment and reversible filtration processes
v	=	porewater velocity
t	=	time
z	=	spatial coordinate
D_z	=	coefficient of longitudinal dispersion.

Equation B-2 represents a mass balance of solute sorbed to colloids, not to colloids alone.

The concentration of contaminants attached to the colloids is related to the aqueous contaminant concentration C using a linear relationship:

$$C_c = K_c C \quad \text{(Eq. B-3)}$$

where K_c is the distribution parameter relating the concentrations. As C and C_c are expressed as moles contaminant per unit fluid volume, K_c is a dimensionless parameter expressing the ratio of contaminant mass residing on colloids to the mass present in aqueous form. In terms of more commonly defined and measured quantities, K_c is the product of the distribution coefficient for contaminant sorbing onto colloids ($K_{d(\text{colloids})}$) and the concentration of colloidal material available for sorption-mass of colloids per unit fluid volume ($C_{d\ (\text{colloids})}$):

$$K_c = K_{d(\text{colloids})} C_{\text{colloids}} \quad \text{(Eq. B-4)}$$

The C_{colloids} term includes the concentration of colloids in the aqueous phase and sorbed to the rock. The transport equation for the contaminant transporting in the aqueous phase is given by:

$$R_f \frac{\partial C}{\partial t} = D_z \frac{\partial^2 C}{\partial z^2} - v \frac{\partial C}{\partial z} \quad \text{(Eq. B-5)}$$

where R_f is a retardation factor that captures details of radionuclide attachment/detachment. Substituting Equations B-3 into B-2 and adding to Equation B-5, the concentration of the contaminant in the aqueous phase for the fracture can be obtained:

$$\left(\frac{R_f + K_c R_{col}}{1 + K_c} \right) \frac{\partial C}{\partial t} = D_z \frac{\partial^2 C}{\partial z^2} - v \frac{\partial C}{\partial z} \quad \text{(Eq. B-6)}$$

The coupling between the fracture and matrix is identical to the case without colloids if there is no mobility of colloids into the rock matrix. Inspection of Equations B-5 and B-6 reveals that the forms of the transport equations are identical, with different constants in the accumulation loss term. Therefore, the solutions developed thus far need only be modified slightly to include colloid contaminant transport. To do this, a revised constant $\hat{R}_f$ is defined as follows:

$$\hat{R}_f = \frac{R_f + K_c R_{col}}{1 + K_c} \quad \text{(Eq. B-7)}$$

Using $\hat{R}_f$ accounts for colloidal transport using the advection–dispersion equation.

INTENTIONALLY LEFT BLANK

APPENDIX C
DERIVATION OF COMPOSITE UPSCALED K_d DISTRIBUTIONS

This appendix provides details of the study performed to derive composite distributions applicable on the scale of the computational grid used in the site-scale saturated zone (SZ) transport model for the radionuclides cesium, neptunium, plutonium, uranium, americium, thorium, protactinium, radium, selenium, strontium, and tin. The small-scale distributions developed in Appendix A (Table A-4) in conjunction with the analysis presented in this appendix led to the recommended composite distributions for K_ds (Table C-14) that form a technical product output of this report (Output DTN: LA0702AM150304.001). The data needed as inputs to the analysis presented in this appendix are treated as being "direct input" to the site-scale SZ transport model. These distributions will be used to simulate transport of radionuclides in the SZ site-scale model during the Total System Performance Assessment (TSPA) calculations. The distributions in alluvium for these radionuclides were taken to be the same as the small-scale distributions derived in Table A-4. Given the scope of the work presented here, simulations could not be carried out for all radionuclides, and a choice had to be made. The four radionuclides cesium, neptunium, plutonium, and uranium were chosen so as to approximately bracket the expected range of values. The distributions in volcanics for americium, thorium, protactinium, selenium, tin, strontium, and radium were taken to be the same as those in Table A-4. The distributions in volcanics for cesium, neptunium, plutonium, and uranium were upscaled using stochastic modeling (Section C1), and then modified to include additional uncertainties leading to composite distributions (Section C2) for use with the TSPA calculations.

The small-scale K_d distributions for these radionuclides were developed on the basis of laboratory data for samples on the scale of centimeters. This development is given in detail in Appendix A, and the small-scale K_d distributions are presented in Table A-4. In the TSPA calculations, radionuclide transport is modeled using a single value of K_d for grid blocks with dimensions 250 m × 250 m in the x and y directions. In the field, values of K_d are variable at a scale much smaller than the model scale. Thus, if a uniform single value of K_d is used to model sorption, it is important to use a value that effectively captures variability at the smaller scale and results in the same sorption behavior as if all the small-scale processes were represented explicitly. The factors that affect the sorption behavior of the rock matrix include mineral composition, groundwater chemistry, and the type of radionuclide. Mineral composition and groundwater chemistry are spatially variable at a scale smaller than 250 m. The mineral compositions of the volcanic rocks show systematic variability, represented by the mineralogical data summarized in Tables C-1 through C-4. Hence, in the volcanics, it was considered necessary to upscale the laboratory-scale K_d distributions to the model scale. Results of such upscaling to a 500-m size were available, conducted using stochastic modeling techniques. 500 m is the same order of magnitude as 250-m grid spacing used in the SZ transport model, and both are several orders of magnitude larger than the laboratory scale. As shown in Section C1.3.3, the upscaled distributions for uranium are not very sensitive to a variation of the correlation length from 4 m up to 1,000 m. The underlying mineralogical model and spatial correlations used in the upscaling process are same for the four radionuclides considered here. Also, comparing Tables C-4 and C-11 shows that upscaled distributions are considerably narrower than the starting experimental distributions. Hence, behavior similar to uranium can be expected for the other three radionuclides in regards to the lack of sensitivity to variations in spatial correlation length. Upscaled K_d distributions are further modified using expert judgment, as described in the next paragraph. Hence, the distributions upscaled to 500 m are considered adequate for the SZ transport model. This upscaling development is presented in Section C1. The results of this scaling analysis are presented in Table C-11.

Although the scaled distributions are thought to correctly capture the spatial uncertainty, other sources of uncertainty such as potential fast pathways, reducing conditions along potential transport pathways, higher concentrations of radionuclides during transport in the saturated zone than the ranges included in the analysis, and competition among radionuclides for sorption sites may not be completely represented in these distributions. To incorporate these other sources of uncertainty, expert judgment was used to develop subjective estimates on the appropriate range of the K_ds and percentile points for the distribution. This process is described in Section C2 of this appendix and the results are presented in Table C-14 and Figures C-7 to C-16. The K_d distributions presented in this table are the ones recommended for use in TSPA analysis.

C1. STOCHASTIC MODELING FOR UPSCALING OF K_d DISTRIBUTIONS IN THE VOLCANICS

The stochastic approach used to calculate effective values of K_d for a 500-m grid block is discussed here. The 500-m block was subdivided to the scale of 4 m. The effect of spatial heterogeneity in K_d values, the effect of upscaling, and the effect of mineralogy were incorporated. The approach included generating spatially heterogeneous distributions of K_d at a scale of 4 m, much smaller than 500 m and using the heterogeneous distributions to calculate effective K_d values. The heterogeneous distributions were generated by incorporating the effect of spatial variability in rock mineralogy. A stochastic approach was used to generate distributions of effective K_d values, and multiple K_d realizations were used to calculate effective K_d values. The input data used to generate the heterogeneous K_d distributions were derived from experimental data described in Appendix A.

C1.1 DEFINITION OF EFFECTIVE K_d

Effective K_d was defined as the value of K_d that would result in a radionuclide sorption behavior that is similar to the sorption behavior resulting from a heterogeneous distribution of small-scale K_d values. This concept is shown schematically in Figure C-1, in which a two-dimensional grid block with a uniform effective K_d produces radionuclide breakthrough behavior that is similar to that shown by the same grid block with four subgrid blocks with different K_d properties.

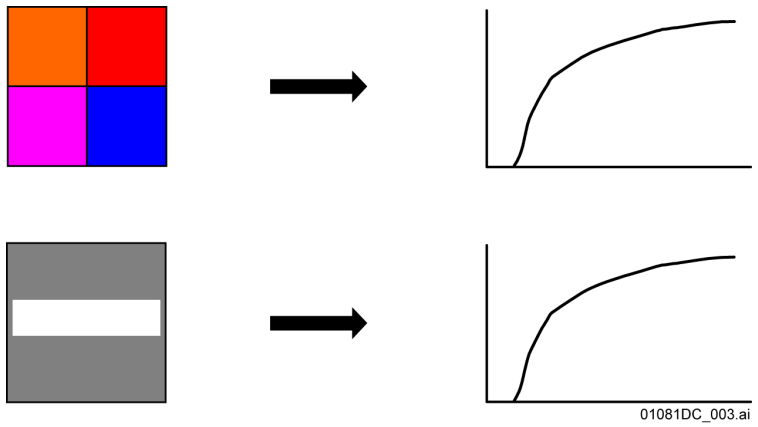

NOTE: For illustration purposes only.

Figure C-1. A Schematic Representation of the Definition of Effective K_d

With this definition, the following approach was used to compute an effective K_d. The retardation coefficient and K_d are related to each other by the following equation:

$$K_d = (\text{retardation coeff.} - 1)\frac{\text{Porosity}}{\text{Bulk Density}} \quad \text{(Eq. C-1)}$$

Thus, if the retardation behavior of a system is appropriately calculated, it can be used to calculate the effective K_d. Effective retardation behavior of a grid block for a particular radionuclide was determined by comparing two breakthrough curves (BTC) for the same grid block under identical flow conditions. One BTC was calculated using a dual-porosity transport in which the radionuclide can diffuse from fracture to matrix and get retarded in the matrix (Figure C-2a). The second curve was calculated with identical diffusion behavior but using no retardation in the matrix (Figure C-2b). In both calculations, retardation on fracture surface was not included. Using these two curves, effective matrix retardation was calculated by comparing the breakthrough times for 50% relative concentration. This concept is further explained schematically in Figure C-3 where relative behavior of two BTCs for a pulse input, with and without matrix sorption, is shown.

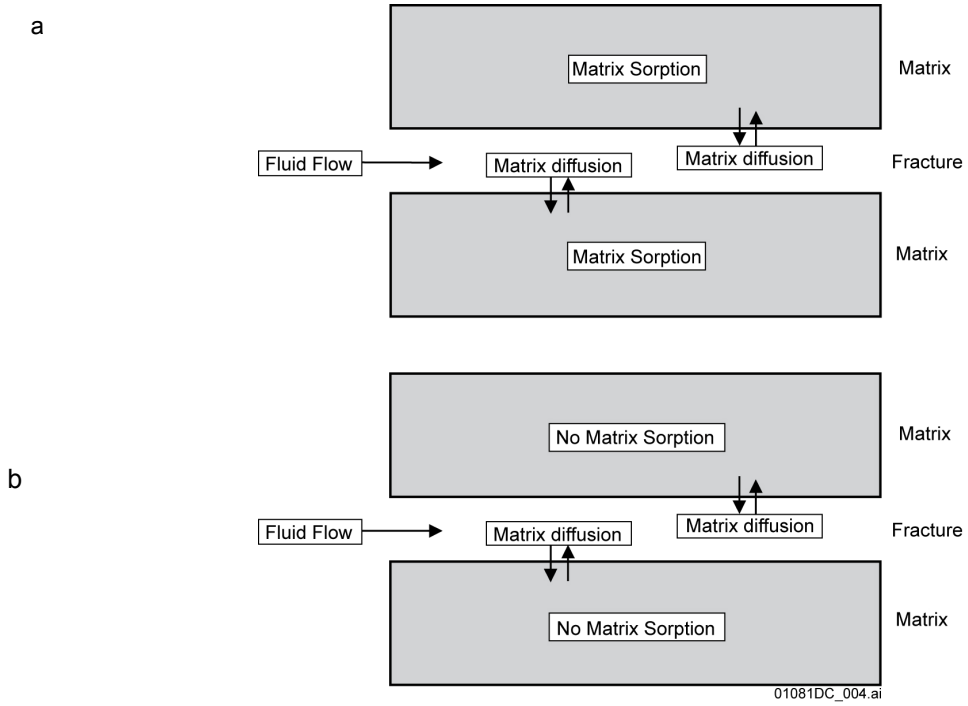

NOTE: For illustration purposes only.

[a]Transport with diffusion followed by matrix sorption.

[b]Transport with diffusion followed by no matrix sorption.

Figure C-2. The Processes during Transport of a Radionuclide in a Fractured Media

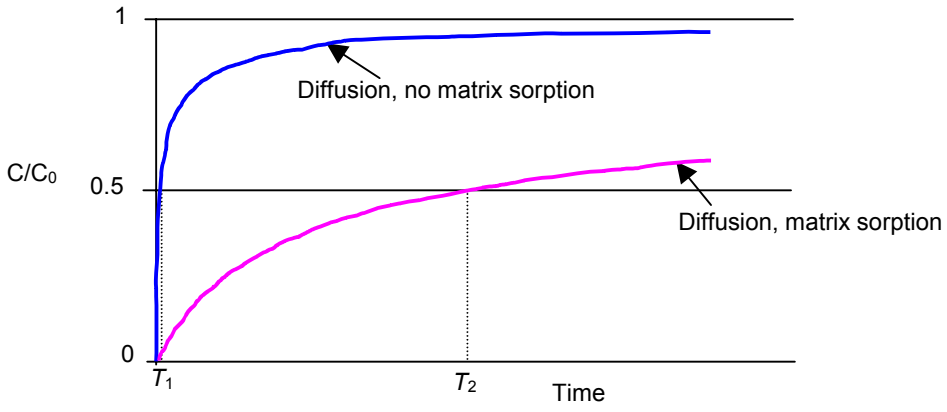

NOTE: For illustration purposes only.

Figure C-3. Representation of the Breakthrough Curves Used to Calculate Effective Matrix Retardation Behavior

The BTC for the case with no matrix sorption is much steeper than that for the case with matrix sorption. The times at which 50% breakthrough takes place are marked as T_1 and T_2 for the cases without matrix sorption and with matrix sorption, respectively. The effective retardation coefficient was calculated as the ratio of these two times:

$$\text{Effective Retardation } (r_{\text{eff}}) = \frac{T_2}{T_1} \qquad \text{(Eq. C-2)}$$

This definition of effective retardation was used to calculate effective K_d values using Equation C-1. Multiple values of effective K_d were calculated using multiple spatially heterogeneous realizations of K_d and subsequently were used to generate statistical distribution of effective K_d. The heterogeneous K_d distributions were generated using a geostatistical approach. Before describing the approach, a brief discussion on the method used to perform transport calculations follows.

C1.2 TRANSPORT CALCULATIONS

As mentioned earlier, a dual-porosity transport model was used to calculate the BTCs. The calculations were performed using the streamline particle-tracking macro '*sptr*' in FEHM (V2.20, STN: 10086-2.20-00 [DIRS 161725]). The dual-porosity transport model in the *sptr* macro is based on the analytical solution developed by Sudicky and Frind (1982 [DIRS 105043]) for contaminant transport in a system of parallel fractures. This solution takes into account advective transport in the fractures, molecular diffusion from the fracture into the porous matrix, and adsorption on the fracture surface as well as within the matrix. In this model, all of the above-mentioned processes except adsorption on the fracture surface are represented. The model includes the assumption that there is no sorption on fracture surfaces (see Table 5-1). Input files for the *sptr* macro were created using *cr8sptr.c* V2.0 (STN: 10927-2.0-00) (SNL 2002 [DIRS 163836]).

C1.2.1 Stochastic Realizations of K_d

As mentioned before, the value of K_d is dependent on multiple factors, including rock mineralogy and water chemistry, as well as spatial location. This dependence was taken into account when developing K_d realizations. As discussed in Appendix A3, effects of variations in groundwater composition on K_d values have been implicitly included in the small scale distributions given in Table A-4. A two-step process was used to capture dependence on rock mineralogy. First, spatial distributions of mineralogically dependent rock types were generated. Data on mineral abundance in rock were available from X-ray diffraction analysis of samples from multiple wells (Table C-1). The mineral abundance data provided the content of the following minerals: smectites, zeolites, tridymite, cristobalite, quartz, feldspar, volcanic glass, analcime, mica, and calcite.

Table C-1. List of Wells for Which Mineral Abundance Data Were Available

Data Description	DTN
Mineralogy, Borehole UE-25 a#1	MO0101XRDDRILC.002 [DIRS 163795]
Mineralogy, Borehole UE-25 UZ#16	LA000000000086.002 [DIRS 107144]; LAJC831321AQ98.005 [DIRS 109004]
Mineralogy, Borehole USW G-1	MO0101XRDMINAB.001 [DIRS 163796]
Mineralogy, Borehole USW G-2	MO0101XRDDRILC.002 [DIRS 163795]
Mineralogy, Borehole USW G-3/GU-3	MO0101XRDMINAB.001 [DIRS 163796]
Mineralogy, Borehole USW G-4	MO0101XRDMINAB.001 [DIRS 163796]
Mineralogy, Borehole USW SD-7	MO0408K8313211.000 [DIRS 171437]; LAJC831321AQ98.005 [DIRS 109004]
Mineralogy, Borehole USW SD-9	MO0408K8313211.000 [DIRS 171437]; LAJC831321AQ98.005 [DIRS 109004]
Mineralogy, Borehole USW SD-12	MO0408K8313211.000 [DIRS 171437]; LAJC831321AQ98.005 [DIRS 109004]
Mineralogy, Borehole USW WT-24	LASC831321AQ98.001 [DIRS 109047]; LADV831321AQ99.001 [DIRS 109044]
Mineralogy, Borehole H-6	MO0106XRDDRILC.003 [DIRS 163797]

DTN=data tracking number.

These mineral abundance data were used to determine prevalent mineralogic rock types. The rock type was labeled as zeolitic if the zeolitic abundance was greater than 20%, as vitric if glass abundance was greater than 80%, and as devitrified otherwise. Only the data that were part of the saturated zone extending from the water table to 200 m below the water table were used in the analysis. When mineralogic abundance data were converted to rock-type data with the above definition, it was observed that only zeolitic and devitrified rocks were present for the top 200 m of the saturated zone. The observed proportions of the rocks were 60% zeolitic and 40% devitrified. The data set also included information on the spatial location of rock samples. These data were used to calculate spatial correlation information through indicator semivariograms. Two directional semivariograms were calculated: one in the horizontal direction and another in the vertical direction using GSLIB (GSLIB V1.0GAMV3V1.201, STN: 10398-1.0GAMV3V1.201-00) (LBNL 2000 [DIRS 153099]). The semivariograms were used to calculate the spatial correlation parameters. Next, the spatial correlation parameters were used to generate multiple realizations of spatial distribution of rock types. The geostatistical

approach of sequential indicator simulations (GSLIB V2.0 MSISIM, STN: 10098-2.0MSISIMV2.0-00; SNL 2000 [DIRS 149114]) was used to generate the spatial distributions. Sequential indicator simulation is a powerful tool that can be used to generate stochastic realizations of parameters. It uses cumulative distribution functions (CDFs) of observed data as input and tries to estimate a discrete, nonparametric true CDF of a simulated parameter. An indicator is a variable used to show the presence or absence of any parameter qualitatively or quantitatively. For example, an indicator can be used to define the presence of a particular rock type at any spatial location. It can also be used to define whether the value of a parameter falls within a certain range of parameter values defined as cutoffs.

After the spatial distributions of rock types were generated, the small scale distributions were used to generate realizations of K_d *values*. Next, indicators were defined at four CDF cutoffs of 0.2, 0.4, 0.6, and 0.8. These cutoffs, along with the spatial correlation information, were then used to generate spatial distributions. Unlike mineral abundance data, spatial information on K_d observations was not available. As a result, no spatial correlation functions were available for K_d data. In the absence of any spatial correlation functions, the approach used was to generate spatial K_d distributions for a correlation length of 500m. The spatial distributions of K_d realizations were generated using the sequential indicator simulation approach. These spatial distributions of K_d values were generated for individual rock types. Distributions for each rock type were generated independent of other rock-type distributions. Finally, the rock type-specific K_d distributions and rock-type distributions were used to generate integrated K_d distributions. The approach used is explained schematically as follows:

- K_d distribution for rock type‘1’: $K_{\mathrm{dl}}^{1}, K_{\mathrm{d2}}^{1}, K_{\mathrm{d3}}^{1}, K_{\mathrm{d4}}^{1}, K_{\mathrm{d5}}^{1}, K_{\mathrm{d6}}^{1}, K_{\mathrm{d7}}^{1}, \ldots, K_{\mathrm{d}n}^{1}$
- K_d distribution for rock type ‘0’: $K_{\mathrm{dl}}^{0}, K_{\mathrm{d2}}^{0}, K_{\mathrm{d3}}^{0}, K_{\mathrm{d4}}^{0}, K_{\mathrm{d5}}^{0}, K_{\mathrm{d6}}^{0}, K_{\mathrm{d7}}^{0}, \ldots, K_{\mathrm{d}n}^{0}$
- Rock type distribution: 1, 0, 1, 1, 1, 0, 0,…, 1
- Combined K_d distribution: $K_{\mathrm{dl}}^{1}, K_{\mathrm{d2}}^{0}, K_{\mathrm{d3}}^{1}, K_{\mathrm{d4}}^{1}, K_{\mathrm{d5}}^{1}, K_{\mathrm{d6}}^{0}, K_{\mathrm{d7}}^{0}, \ldots, K_{\mathrm{d}n}^{1}$, where n is the number of grid points.

Sensitivity of the results to the correlation length was evaluated using uranium as an example by varying the correlation length and to understand the impact of varying the correlation length on effective K_d calculations. Four different values were used for correlation length. This range covers the entire spectrum from completely uncorrelated to fully correlated. Four values were used to represent the entire spectrum while not making the number of simulations excessively large:

- Correlation length equal to a single grid-block dimension (4 m) that represents spatially random realizations
- Correlation length equal to the correlation length used to generate permeability realizations (60 m)

- Correlation length equal to the large grid-block length (500 m)
- Correlation length equal to the correlation length used to generate rock-type data (1,000 m).

All of the listed values represent the expected possible range of correlation lengths for K_d values.

The approach explained above incorporates the effect of spatial heterogeneity and rock mineralogy on the spatial distribution of K_d. Multiple realizations for the spatial distribution of K_d values were generated with this approach.

C1.2.2 Stochastic Realizations of Permeability

Similar to the K_d distributions, spatial distributions of permeability were generated using the stochastic approach. GS2FEHM.C (V1.0, STN: 10923-1.0-00; SNL 2002 [DIRS 163837]) was used to create files for the "perm" macro needed as input to FEHM. These permeability realizations represented continuum distributions of permeability for fractured rocks.

C1.3 RESULTS

C1.3.1 Stochastic Realizations of K_d

Figures C-4 and C-5 show the semivariograms calculated from the rock-type data (converted from available mineral abundance data). The figures also show the correlation functions fit to the semivariograms. There is scatter in the data, but the fits are considered reasonable. The parameters for the model fit are shown in Table C-2.

These correlation parameters were used to generate spatial distributions of rock types. The sequential indicator simulation algorithm SISIM (GSLIB V2.0MSISIM), which is part of GSLIB, was used to generate these distributions. Five different rock-type realizations were generated using this approach. The proportions of zeolitic and devitrified rocks in the five output realizations are shown in Table C-3.

Spatial realizations for K_d were generated for four different radionuclides: uranium, neptunium, cesium, and plutonium. Neptunium to cesium covers the low to high K_d spectrum. The small-scale uncertainty distributions based on experimentally available data for these radionuclides (discussed in Appendix A) are given in Table C-4 (reproduced from Table A-4 for convenience).

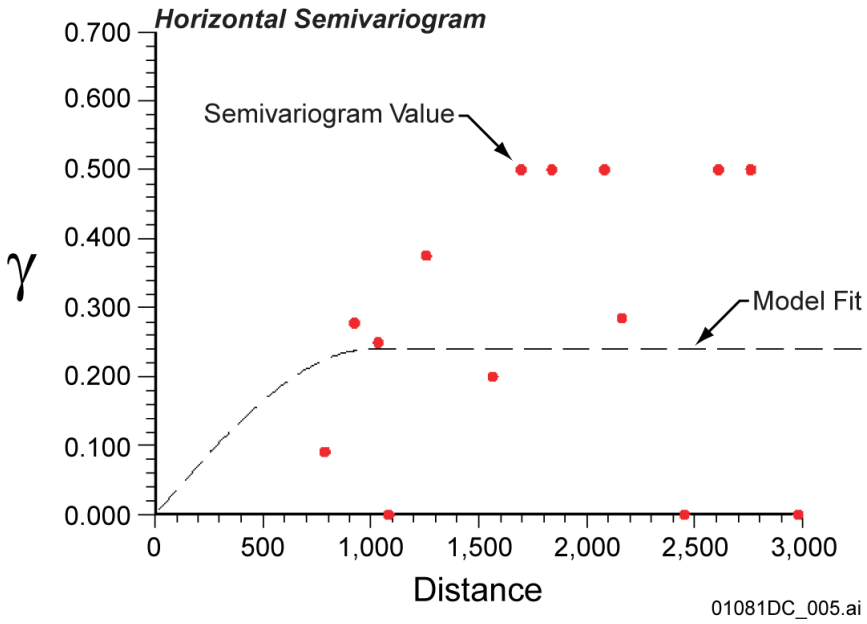

Output DTN: LA0309RP831321.001.
NOTE: The distance on the *x*-axis is in meters.

Figure C-4. Calculated Semivariogram and Model Fit in the Horizontal Direction

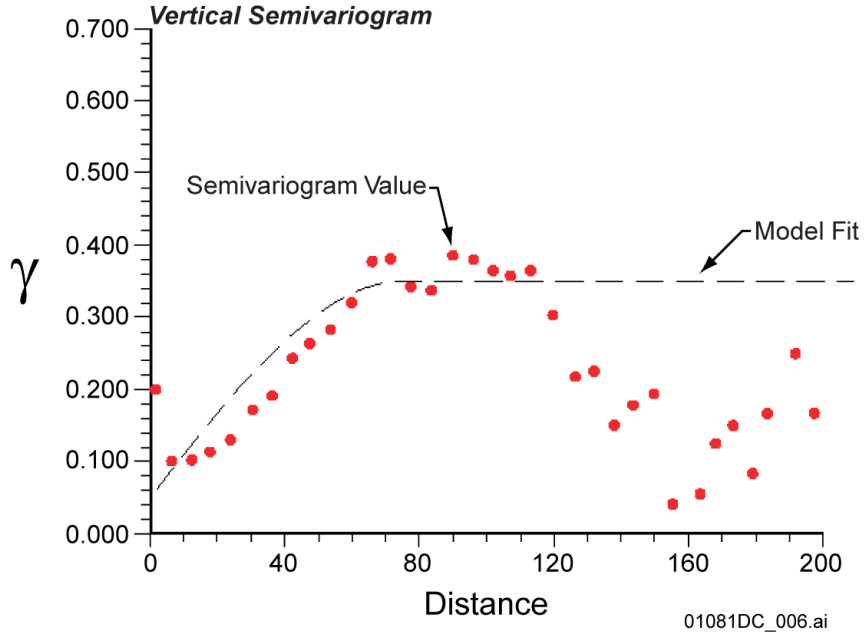

Output DTN: LA0309RP831321.001.
NOTE: The distance on the *x*-axis is in meters.

Figure C-5. Calculated Semivariogram and Model Fit in the Vertical Direction

Table C-2. Spatial Correlation Parameters for Mineralogic Rock Type Data

Direction	Range (m)	Sill
Horizontal	1,000	0.25
Vertical	75	0.35

Output DTN: LA0309RP831321.001.

Table C-3. Proportions of Zeolitic and Devitrified Rocks in Output Realizations

Realization	Zeolitic	Devitrified
1	0.6106	0.3894
2	0.5746	0.4254
3	0.6034	0.3966
4	0.5890	0.4110
5	0.6270	0.3730

Output DTN: LA0309RP831321.001.

Table C-4. Statistical Distributions of Experimentally Observed K_d Values

Radionuclide	Rock-type	Distribution	Mean (mL/g)	Standard Deviation (mL/g)	Minimum (mL/g)	Maximum (mL/g)
Uranium	Zeolitic	Truncated Normal	12.0	3.6	5.0	20.0
	Devitrified	Truncated Normal	2.0	0.6	0.0	4.0
Cesium	Zeolitic	Exponential	16,942.0	14,930.0	4,000.0	42,000.0
	Devitrified	Truncated Normal	728.0	464.0	100.0	1,000.0
Neptunium	Zeolitic	Truncated Normal	2.88	1.47	0.0	6.0
	Devitrified	Exponential	0.69	0.71	0.0	2.0
Plutonium	Zeolitic	Beta	100.0	15.0	50.0	300.0
	Devitrified	Beta	100.0	15.0	50.0	300.0

Source: Table A-4.

These distributions were used to derive the CDFs for each radionuclide for each rock type using software routine *calc_cdf.c* (*calc_cdf.c* V1.0, STN: 10924-1.0-00; SNL 2000 [DIRS 149117]). For each CDF, indicators were defined at four CDF cutoffs: 0.2, 0.4, 0.6, and 0.8. As mentioned earlier, in the absence of spatial data, correlation length was parameterized, and four different correlation lengths were used to generate stochastic realizations. This effect of correlation length was studied only for uranium. For other radionuclides, a correlation length of 500 m was used. Fifty different realizations were generated for each radionuclide and each rock type. Statistics of the output realizations were calculated and compared against the input data. The software routine *calc_cdf.c* was used to calculate the CDF from the statistical realizations. Tables C-5 through C-8 compare the mean CDFs (calculated from 50 realizations) with the input CDFs for the four cutoffs.

Finally, these rock-type specific K_d distributions were combined to generate distributions that were conditioned to the realizations of rock types. The procedure for doing this was outlined in Section C2.3.

Table C-5. Comparison of Input and Mean Output CDFs for Uranium

Zeolitic			Devitrified		
K_d (mL/g) Cutoff	Input CDF	Output CDF	K_d (mL/g) Cutoff	Input CDF	Output CDF
8.97	0.2	0.2047	1.49	0.2	0.2128
11.09	0.4	0.4014	1.84	0.4	0.4050
12.91	0.6	0.5964	2.15	0.6	0.5939
15.03	0.8	0.7918	2.50	0.8	0.7909

Output DTN: LA0309RP831321.004.

CDF = cumulative distribution function.

Table C-6. Comparison of Input and Mean Output CDFs for Cesium

Zeolitic			Devitrified		
K_d (mL/g) Cutoff	Input CDF	Output CDF	K_d (mL/g) Cutoff	Input CDF	Output CDF
4,929.3	0.2	0.2018	337.5	0.2	0.2026
9,478.5	0.4	0.4058	610.5	0.4	0.4079
14,613.3	0.6	0.5975	845.5	0.6	0.6012
24,896.8	0.8	0.8058	1,118.5	0.8	1.0

Output DTN: LA0309RP831321.001.

CDF = cumulative distribution function.

Table C-7. Comparison of Input and Mean Output CDFs for Neptunium

Zeolitic			Devitrified		
K_d (mL/g) Cutoff	Input CDF	Output CDF	K_d (mL/g) Cutoff	Input CDF	Output CDF
1.65	0.2	0.2018	0.12	0.2	0.2018
2.51	0.4	0.4059	0.30	0.4	0.4059
3.26	0.6	0.5976	0.51	0.6	0.5976
4.12	0.8	0.8058	0.93	0.8	0.8058

Output DTN: LA0309RP831321.002.

CDF = cumulative distribution function.

Table C-8. Comparison of Input and Mean Output CDFs for Plutonium

Zeolitic			Devitrified		
K_d (mL/g) Cutoff	Input CDF	Output CDF	K_d (mL/g) Cutoff	Input CDF	Output CDF
87.005	0.2	0.2054	87.005	0.2	0.2018
95.094	0.4	0.4229	95.094	0.4	0.4059
102.743	0.6	0.5852	102.743	0.6	0.5976
112.348	0.8	0.7855	112.348	0.8	0.8058

Output DTN: LA0309RP831321.003.

CDF = cumulative distribution function.

C1.3.2 Results of Breakthrough Curve Calculations Using the Particle-Tracking Algorithm

These multiple K_d realizations were used to compute BTCs and model the sorption behavior of each radionuclide. A two-step approach was used. In the first step, steady-state flow fields were computed for 50 different permeability realizations. The properties used for these calculations are shown in Table C-9.

Table C-9. Values of Properties Used in Flow and Transport Calculations

Property	Value
Matrix porosity	0.22 [a]
Rock bulk density	1,997.5 kg/m^3 [a]
Flowing interval porosity	0.001 [a]
Flowing interval spacing	19.49 m [a]
Hydraulic gradient	2.9×10^{-4} [b]

Sources: [a]Value chosen to fall within the range given in Table 4-2.
[b]DTN: LA0511SK831214.001[DIRS 175769] (data qualified in BSC 2006 [DIRS 180708]).

The steady-state flow fields were used in the particle-tracking calculations. In these calculations, 4,000 particles were released along one face of the model and were allowed to move under the influence of the steady-state flow field. The locations of the particle releases were determined by a flux-weighted placement scheme. As mentioned in Section C2.1, two sets of particle-tracking calculations were performed for each steady-state flow field. In the first set of calculations, the baseline BTC was calculated for transport with diffusion from fracture to matrix and no matrix sorption. In the second set of calculations, the BTC was calculated for transport with diffusion followed by sorption on the matrix. For these calculations, the stochastically generated K_d distributions were used. The values of the diffusion coefficient used for these calculations are shown in Table C-10.

Table C-10. Values of Diffusion Coefficients Used for the Particle-Tracking Calculations

Radionuclide	Diffusion Coefficient (m^2/s)
Anion (uranium)	3.2×10^{-11}
Cation (plutonium, cesium, neptunium)	1.6×10^{-10}

Source: DTN: LA0003JC831362.001 [DIRS 149557] (Data qualified in Appendix K).

These BTCs were used to calculate the effective K_d values using the procedure described in Section C2.1. The procedure was repeated for 50 realizations of K_d. The statistics of the calculated effective K_d values are provided in Table C-11. These calculations of stochastic realizations of K_d were performed using a correlation length of 500 m. As can be seen from the results, the effective K_d distributions are very narrow compared to the distributions of experimentally observed K_d values.

Table C-11. Statistics of Calculated Effective K_d Values

Radionuclide	Distribution	Mean	Standard Deviation	Minimum	Maximum
Uranium	Truncated Normal	6.61	0.61	5.39	8.16
Cesium	Truncated Normal	5,188.72	941.55	3,000.59	6,782.92
Plutonium	Truncated Normal	110.17	7.45	89.90	129.87
Neptunium	Truncated Normal	1.48	0.23	0.99	1.83

Output DTNs: LA0309RP831341.001; LA0309RP831341.002 ; LA0309RP831341.003; LA0309RP831341.004.

A comparison was made as to how well the calculated effective K_d values predicted the particle breakthrough behavior with respect to the breakthrough behavior predicted by the heterogeneous K_d field (from which the effective value was calculated). In these calculations, a uniform value of K_d equal to the effective K_d value was used. Figure C-6 shows the two BTCs for one of the K_d realizations. The effective value of K_d calculated for this realization was 7.32 (mL/g). As can be seen from the figure, the calculated effective K_d value captures the breakthrough behavior of the heterogeneous K_d field very well.

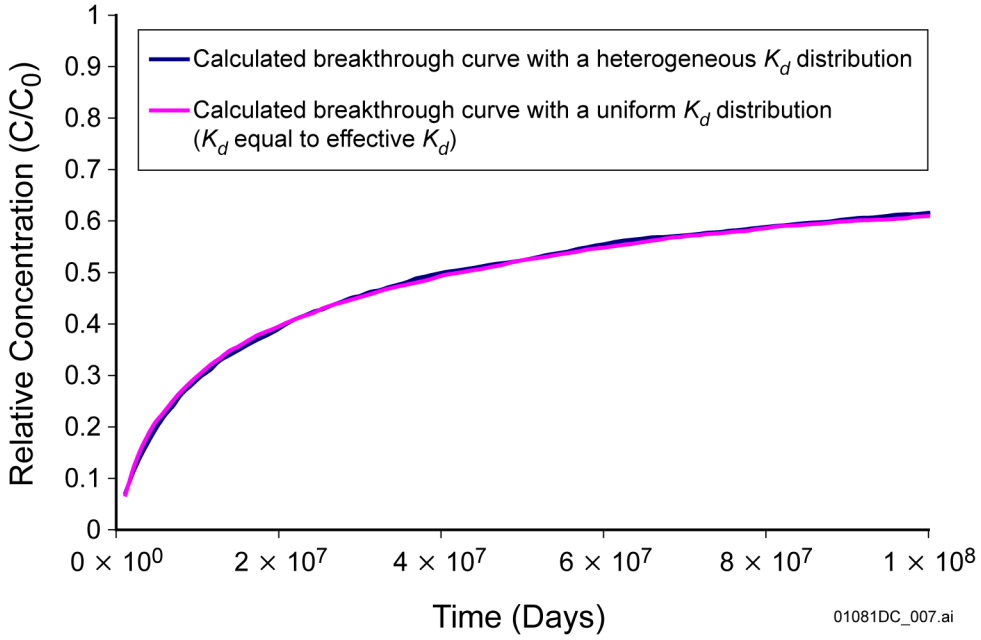

Output DTNs: LA0309RP831341.003; LA0309RP831341.004.

Figure C-6. Comparison of Breakthrough Behavior Predicted by the Calculated Effective K_d

C1.3.3 Effect of Correlation Length on Effective K_d Distributions of Uranium

As mentioned earlier, the correlation length used in generating the stochastic K_d realizations was parameterized because of the lack of the spatial information. The intent was to examine the effect of changes in correlation length on the distribution of effective K_d values. Once again, a similar procedure was followed to calculate effective K_d values. The heterogeneous K_d distributions generated by using different correlation lengths were used for these calculations. Table C-12 details the statistics of the calculated effective K_d values along with the correlation length used to generate the heterogeneous K_d distributions. As can be seen from the results, variation in the correlation length does not significantly affect the calculated statistics of effective K_d values.

Table C-12. Effect of Changes in Correlation Length on Effective K_d Distributions for Uranium

Correlation Length (m)	Mean K_d (mL/g)	Standard Deviation	Minimum	Maximum
4	6.71	0.49	5.70	8.13
60	6.79	0.47	5.42	8.14
500	6.61	0.61	5.39	8.16
1,000	6.58	0.62	4.46	7.85

Output DTN: LA0309RP831341.004.

C1.3.4 Effect of Variability in the Hydraulic Gradient

The effect of variability in the hydraulic gradient on calculated effective K_d values was studied. These calculations were performed only for uranium and used K_d realizations generated with a correlation length of 500 m. Two different values of hydraulic gradient were used: 8.7×10^{-4} (3 times mean hydraulic gradient) and 0.967×10^{-4} (one-third of mean hydraulic gradient). Steady-state flow fields were calculated with these hydraulic gradients and were subsequently used to calculate particle BTCs. The statistics of the resulting effective K_d values are compared with the ones for a mean hydraulic gradient of 0.14 in Table C-13. As can be seen from the results, a variability of an order of magnitude in hydraulic gradient has not significantly affected the effective K_d distributions.

Table C-13. Statistics of Calculated Effective K_d Values for Uranium for Different Hydraulic Gradients

Hydraulic Gradient	Mean K_d (mL/g)	Standard Deviation (mL/g)	Minimum (mL/g)	Maximum (mL/g)
0.967×10^{-4}	6.55	0.59	5.13	7.53
2.9×10^{-4}	6.61	0.61	5.39	8.16
8.7×10^{-4}	6.27	0.56	4.97	7.65

Source: DTN: LA0511SK831214.001 [DIRS 175769] (data qualified in BSC 2006 [DIRS 180708])

Output DTN: LA0309RP831341.004.

C1.4 SUMMARY OF STOCHASTIC MODELING

This study was performed to calculate distributions of effective K_d for uranium, neptunium, cesium, and plutonium. The effective K_d distributions were calculated through a stochastic approach in which multiple values of effective K_d were calculated. The value of effective K_d was determined by calculating effective retardation resulting from a spatially heterogeneous K_d field. The spatially heterogeneous K_d fields were calculated using a geostatistical approach. The factors affecting the spatial distribution of K_d, such as rock mineralogy and spatial heterogeneity, were taken into account while generating the heterogeneous K_d fields. As spatial data on K_d were not available, the correlation length used to generate the fields was parameterized. The observations of the study were as follows:

- The calculated effective K_d values reproduced the sorption behavior of the heterogeneous K_d field very well, validating the approach used to determine the effective K_d values.

- The distributions of calculated effective K_d fields were much narrower than the distributions used as the input. This is to be expected because, in any upscaling study, as the scale gets larger, the variability in effective parameter values gets smaller.

- Variability in correlation length did not significantly affect the effective K_d distributions for uranium.

- Variability in hydraulic gradient did not significantly change the effective K_d distributions.

C2. DEVELOPMENT OF COMPOSITE K_d DISTRIBUTIONS

In the TSPA calculations, radionuclide transport is modeled using a single value of K_d for grid blocks with dimensions 250 × 250 m in the x and y directions. In the field, values of K_d are variable at a scale much smaller than the model scale. Thus, if a uniform single value of K_d is used to model sorption, it is important to use a value that effectively captures variability at smaller scale and results in the same sorption behavior as if all the small-scale processes were represented explicitly. Given the scope of the work presented here, simulations could not be carried out for all radionuclides in both the alluvium and the volcanics, and a choice had to be made. The distributions in alluvium were taken to be the same as the small-scale distributions derived in Table A-4 for all radionuclides. The distributions in volcanics for americium, thorium, protactinium, strontium, and radium were also taken to be the same as those in Table A-4. The distributions in volcanics for selenium and tin were also taken to be the same as those in Table A-4. The distribution in volcanics and alluvium for the radionuclides americium, thorium, and protactinium are plotted in Figure C-7. The distribution in volcanics and alluvium for the radionuclide strontium is plotted in Figure C-8. However, in volcanics, the distributions for cesium, neptunium, plutonium, and uranium were generalized using stochastic modeling (Section C1) to a scale of 500 m, and then modified to include additional uncertainties leading to composite distributions for use with the TSPA calculations.

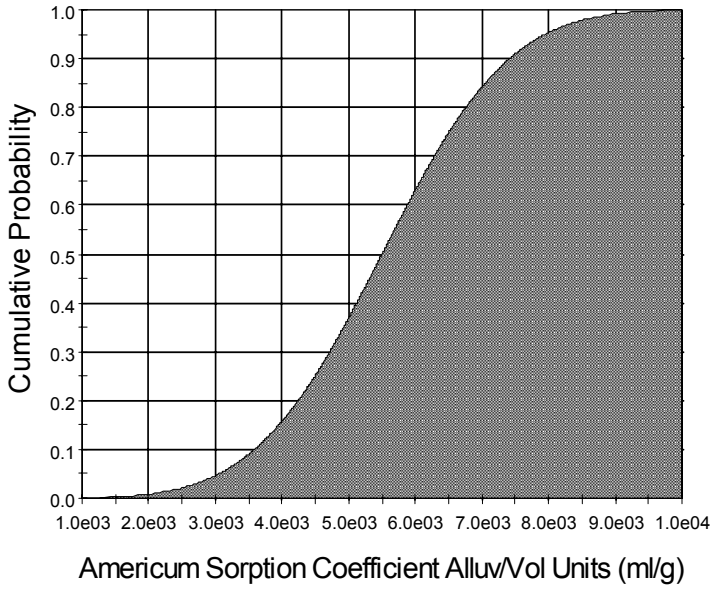

Output DTN: LA0702AM150304.001.

Figure C-7. Plot of Composite Cumulative Probability Distribution for Americium, Thorium, and Protactinium in Volcanics and Alluvium

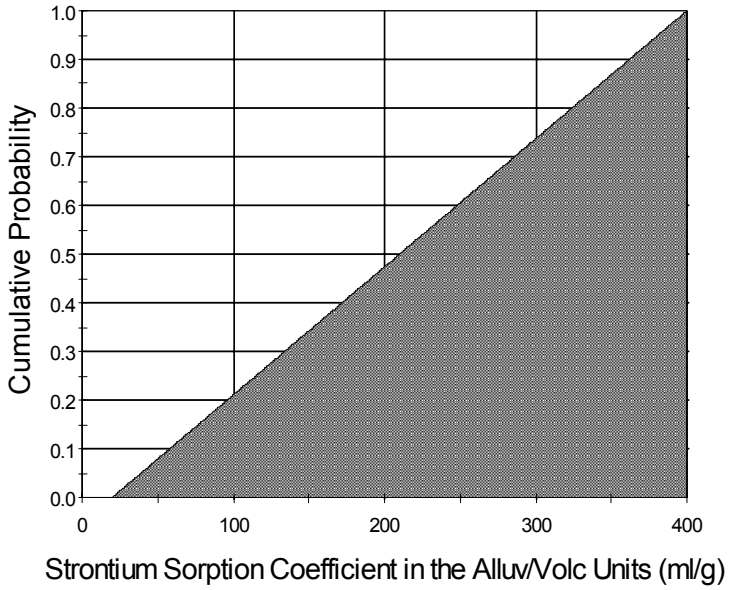

Output DTN: LA0702AM150304.001.

Figure C-8. Plot of Composite Cumulative Probability Distribution for Strontium in Volcanics and Alluvium

As can be seen by comparing Tables C-11 and A-4, the stochastically derived upscaled K_d distributions in the volcanics are narrow compared to the small-scale distributions. Although the scaled distributions are thought to correctly capture the spatial uncertainty, other sources of uncertainty may not be completely represented in these distributions. Other sources of uncertainty in the volcanics may include potential fast pathways (e.g., along faults) through devitrified tuff, the existence of reducing conditions along potential transport pathways, higher concentrations of radionuclides during transport in the saturated zone than the ranges included in the analysis, and competition among radionuclides for sorption sites.

To incorporate these other sources of uncertainty in the volcanics, the methods and approach for the development of parameter distributions documented in *Guidelines for Developing and Documenting Alternative Conceptual Models, Model Abstractions, and Parameter Uncertainty in the Total System Performance Assessment for the License Application* (BSC 2002 [DIRS 158794], Section 4.2) was implemented. In implementing this process, the subject matter expert (SME) who developed the small-scale K_d distributions worked with the parameter team lead to assess the impact of these other sources of uncertainty on the recommended distributions. Because the observational data was limited, the SME worked with the parameter team lead and several experts in uncertainty analysis to develop subjective estimates on the appropriate range of the K_ds and percentile points for the distribution.

The outcome of this process was that the SME judged that the scaled distributions did not completely capture the full range of K_d uncertainty. The SME judged the full range of the scaled distribution extended to the minimum and maximum values of the small-scale distribution to create the range for the composite distribution. In this composite distribution 5% to 30% of the full distribution was assigned to the tails of the composite distribution. The resulting recommended composite distributions are piece-wise uniform distributions that incorporate both

the scaled distributions and the small-scale distributions. These composite distributions are given in Table C-14 and their plots are presented in Figures C-9 through C-16. The following paragraphs detail the development of these distributions for uranium, neptunium, plutonium, and cesium.

For uranium in volcanics, the minimum small-scale value was 0 mL/g. Five percent probability was uniformly distributed between 0 mL/g and the lower bound of the scaled distribution at 5.39 mL/g. Since the scaled distribution had such little variation, it is reasonably represented by a uniform distribution; hence, 90% probability was uniformly distributed between 5.39 mL/g and the upper bound of the upscaled distribution at 8.16 mL/g. The remaining 5% probability was uniformly distributed between 8.16 mL/g and the maximum small-scale experimentally observed value of 20 mL/g. This distribution is shown schematically in Figure C-9. The distribution for uranium in alluvium is shown in Figure C-10.

Table C-14. Recommended Composite Distribution for K_ds in Volcanics and Alluvium

Species	Unit/Analysis	Distribution	Coefficients describing distribution (mL/g)
Uranium	Composite (Volcanics)	Cumulative	(K_d, prob) (0, 0.) (5.39, 0.05) (8.16, 0.95) (20, 1.0)
	Alluvium	Cumulative	(K_d, prob) (1.7, 0.) (2.9, 0.05) (6.3, 0.95) (8.9,1.0)
Neptunium	Composite (Volcanics)	Cumulative	(K_d, prob) (0, 0) (0.99, 0.05) (1.83, 0.90) (6, 1.0)
	Alluvium	Cumulative	(K_d, prob) (1.8, 0.) (4.0, 0.05) (8.7, 0.95) (13, 1.0)
Plutonium	Composite (Volcanics)	Cumulative	(K_d, prob) (10, 0.) (89.9, 0.25) (129.87, 0.95) (300, 1.0)
	Alluvium (Devitrified)	Beta	μ = 100, range = 50 to 300, σ = 15
Cesium	Composite (Volcanics)	Cumulative	(K_d, prob) (100, 0.) (3,000.59, 0.05) (6,782.92, 1.0)
	Alluvium (Devitrified)	Truncated Norm	range = 100 to 1,000,μ = 728, σ = 464
Amercium/ Thorium/ Protactinum	Volcanics and Alluvium	Truncated Norm	range = 1,000 to 10,000,μ = 5,500, σ = 1,500
Strontium	Volcanics and Alluvium	Uniform	range = 20 to 400
Radium	Volcanics and Alluvium	Uniform	range = 100 to 1,000
Selenium	Volcanics	Truncated Log Normal	range = 1 to 35; m= 14.3; s= 7.9
	Alluvium	Truncated Log Normal	range = 1 to 50; m= 14.0; s= 11.2
Tin	Volcanics	Truncated Log Uniform	range = 100 to 36,700
	Alluvium	Truncated Log Uniform	range = 100 to 36,700
Carbon/ Technetium/ Iodine	Volcanics and Alluvium	Constant	Zero

Output DTN: LA0702AM150304.001.

NOTE: Development of the distributions is based on Tables A-4 and C-11.

μ = mean; σ = standard deviation.

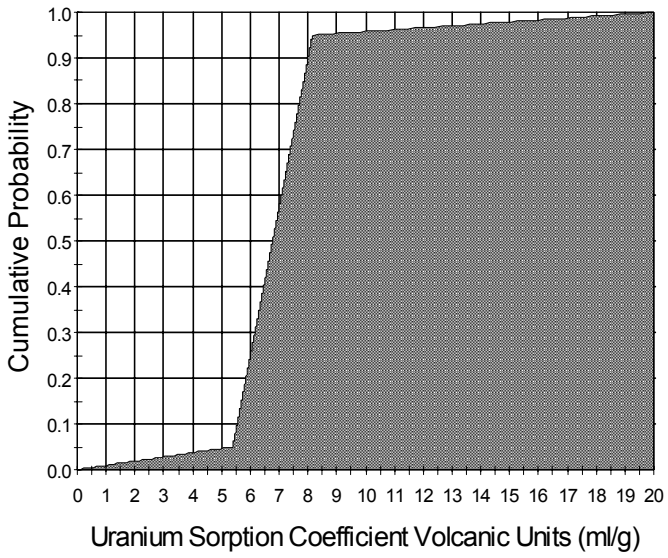

Output DTN: LA0702AM150304.001.

Figure C-9. Plot of Composite Cumulative Probability Distribution for Uranium in Volcanics

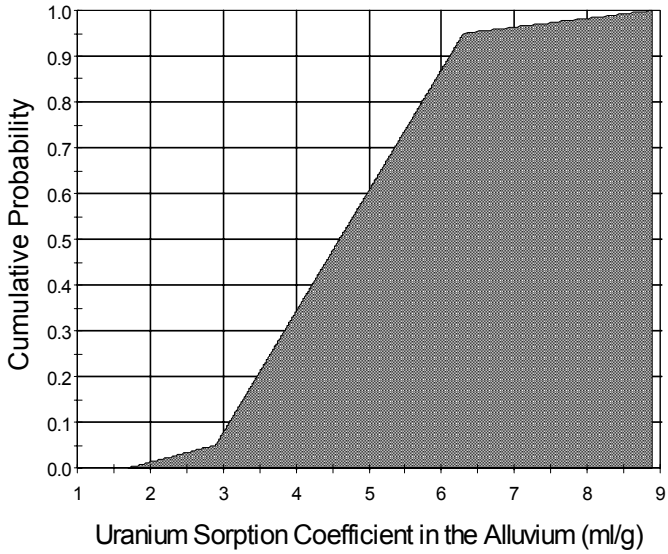

Output DTN: LA0702AM150304.001.

Figure C-10. Plot of Composite Cumulative Probability Distribution for Uranium in Alluvium

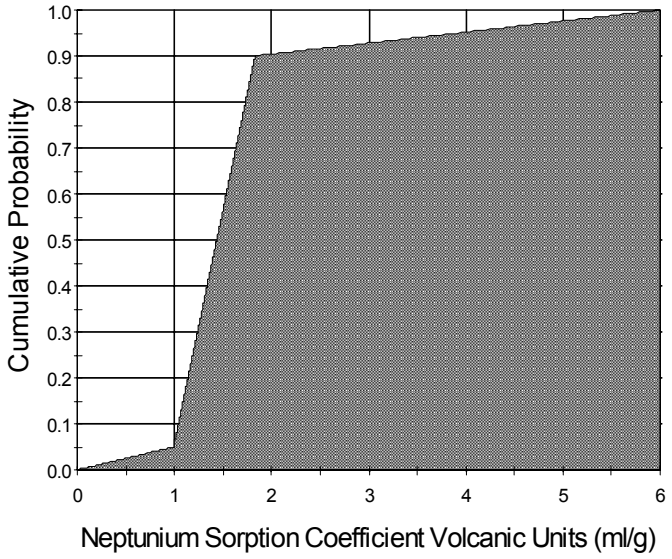

Output DTN: LA0702AM150304.001.

Figure C-11. Plot of Composite Cumulative Probability Distribution for Neptunium in Volcanics

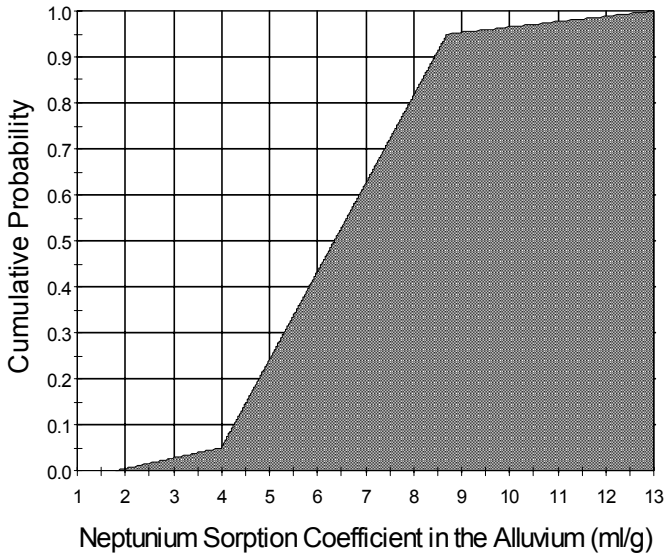

Output DTN: LA0702AM150304.001.

Figure C-12. Plot of Composite Cumulative Probability Distribution for Neptunium in Alluvium

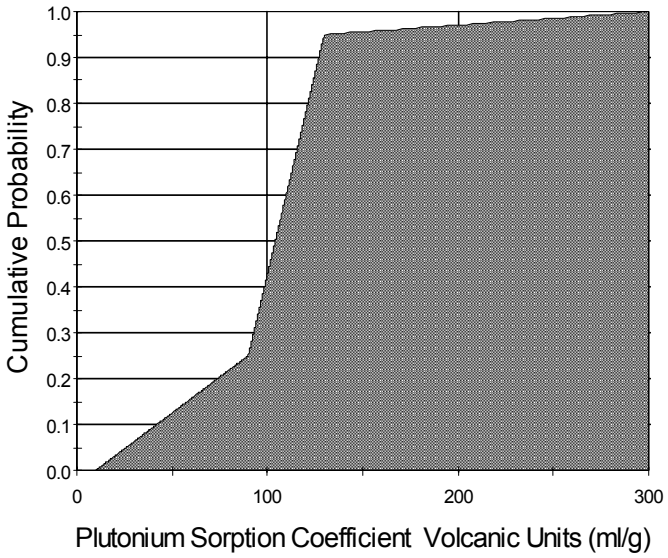

Output DTN: LA0702AM150304.001.

Figure C-13. Plot of Composite Cumulative Probability Distribution for Plutonium in Volcanics

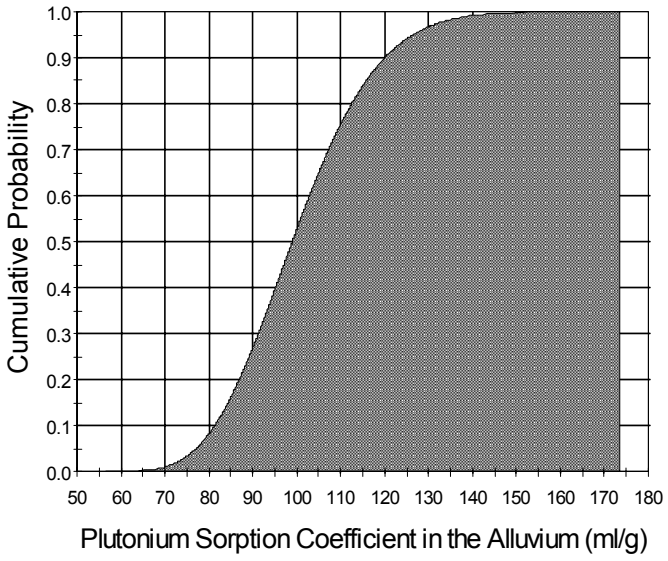

Output DTN: LA0702AM150304.001.

NOTE: The range of values for X-axis given in Table C-14 goes up 300; however, this plot is cut-off at 174. At higher values on x-axis, the curve cannot be distinguished from the horizontal y = 1 line.

Figure C-14. Plot of Composite Cumulative Probability Distribution for Plutonium in Alluvium

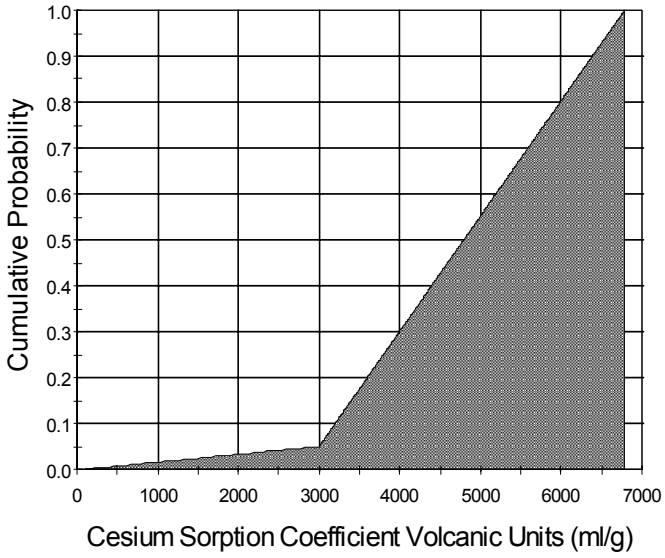

Output DTN: LA0702AM150304.001.

Figure C-15. Plot of Composite Cumulative Probability Distribution for Cesium in Volcanics

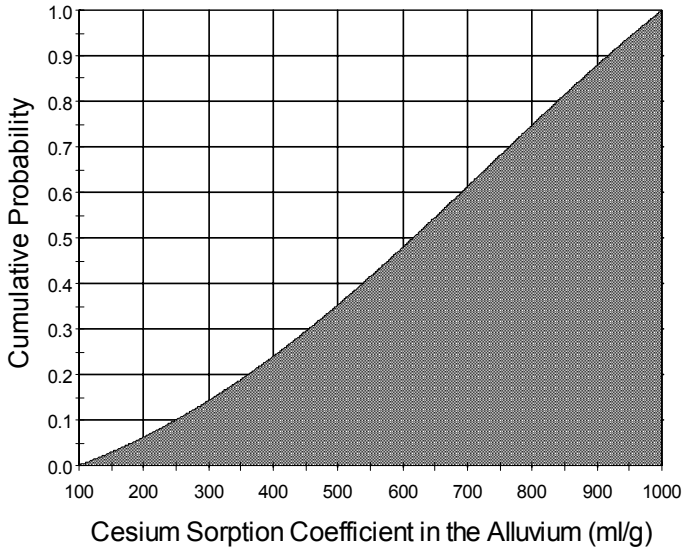

Output DTN: LA0702AM150304.001.

Figure C-16. Plot of Composite Cumulative Probability Distribution for Cesium in Alluvium

For neptunium in volcanics, the minimum small-scale value was 0 mL/g. Five percent probability was uniformly distributed between 0 mL/g and the lower bound of the scaled distribution at 0.99 mL/g. Since the scaled distribution had such little variation, it is reasonably represented by a uniform distribution; hence, 85% probability was uniformly distributed between 1 mL/g and the upper bound of the upscaled distribution at 1.83 mL/g. The remaining 10%

probability was uniformly distributed between 1.83 mL/g and the maximum small-scale experimentally observed value of 6 mL/g. This distribution is shown schematically in Figure C-11. The distribution for neptunium in alluvium is shown in Figure C-12.

For plutonium in volcanics, the minimum small-scale value was 50 mL/g. Twenty-five percent probability was uniformly distributed between 10 mL/g and the lower bound of the scaled distribution at 89.9 mL/g. Since the scaled distribution had such little variation, it is reasonably represented by a uniform distribution; hence, 70% probability was uniformly distributed between 89.9 mL/g and the upper bound of the upscaled distribution at 129.87 mL/g. The remaining 5% probability was uniformly distributed between 129.87 mL/g and the maximum small-scale experimentally observed value of 300 mL/g. This distribution is shown schematically in Figure C-13. The distribution for plutonium in alluvium is shown in Figure C-14.

For cesium in volcanics, the minimum small-scale value was 100 mL/g. Five percent probability was uniformly distributed between 100 mL/g and the lower bound of the scaled distribution at 3,000.59 mL/g. Since the scaled distribution had such little variation, it is reasonably represented by a uniform distribution; hence, the remaining 95% probability was uniformly distributed between 3,000.59 mL/g and the upper limit of the scaled distribution at 6,782.92 mL/g. This distribution is shown schematically in Figure C-15. The distribution for cesium in alluvium is shown in Figure C-16.

APPENDIX D
JUSTIFICATION OF LOCAL EQUILIBRIUM APPROACH FOR MODELING RADIONUCLIDE TRANSPORT IN THE SATURATED ZONE

The analysis presented in this appendix provides a part of the basis for the disposition of the alternative conceptual model "Sorption reactions are not instantaneous" (Table 6.6-1b, Item #1). The results of this analysis do not form a direct input to the site-scale SZ transport model.

To assess whether the sorption kinetics process needs to be included in the transport model, column test data, under flow rates pertinent to the Yucca Mountain flow system, are used to calculate Damköhler numbers to determine if kinetic effects are important (Triay et al. 1997 [DIRS 100422]). The Damköhler number can be used to determine whether the local equilibrium approach is valid. If valid, kinetic effects can be neglected, and equilibrium models that are computationally much more efficient can be used. Plutonium kinetics is examined in this analysis since plutonium sorption kinetics has been shown to be slower than the other radionuclides in the inventory (see Appendix A). Therefore, if the local equilibrium approach is valid for plutonium, it should be valid for the other radionuclides in the inventory.

The Damköhler number is defined as the rate constant, k (1/time), multiplied by a representative residence time, T,

$$Da = k * T \qquad \text{(Eq. D-1)}$$

where k is a first order reaction rate constant.

In Equation D-1, the rate constant quantifies the reaction timescale of the system whereas the residence time quantifies the transport timescale. By multiplying these parameters together, Da provides a basis for evaluating which timescale dominates a system. For cases in which the reaction timescale is much faster than the transport timescale, Da is large and the local equilibrium approach is valid.

Bahr and Rubin (1987 [DIRS 144539], p. 440, Equation 12) demonstrate that the mass balance equation describing solute transport can be separated into an equilibrium and a kinetic component. The smaller the kinetic component, the more accurate are the retardation factors based on the local equilibrium approach.

For evaluation of sorption behavior, separate Damköhler numbers, Da_{att} and Da_{det}, can be computed for attachment and detachment of the sorbing contaminant using k_{att} and k_{det}, which are the attachment and detachment rate constants for plutonium sorbing onto the mineral surfaces. The magnitude of the kinetic component is inversely proportional to the total Damköhler number. As the sum of the two Damköhler numbers becomes larger, the equilibrium approximation becomes more appropriate. Bahr and Rubin (1987 [DIRS 144539], p. 450) found that equilibrium was well approximated when the sum of the two Damköhler numbers is greater than 100 and reasonably well estimated when the sum is greater than 10.

Valocchi (1985 [DIRS 144579], p. 813, Figure 2) had a similar result, although he used only the reverse rate k_{det} to compute a Damköhler number. Valocchi's approach is utilized in this study since a single, first-order rate best fit the column experiments. Because the Valocchi's approach utilizes one Damköhler number, which results in lower Da numbers than the Bahr and Rubin method, the Bahr and Rubin criteria of 10 and 100 can also be used with the Valocchi approach.

As seen from Equation D-1, to estimate the Damköhler number for the SZ transport model, the reaction rate constants for plutonium sorption must be determined. This determination is done by using laboratory data from column experiments. The general idea behind the calculation is to fit a first-order reaction rate constant to ^{239}Pu column data (DTN: LA0302HV831361.001 [DIRS 163783]). This rate constant, along with a conservative travel time through the fractured volcanics, can be used to estimate a Damköhler number. The Damköhler number indicates whether kinetics is important in a system. A sample calculation is presented below.

1. Determine the pore volume, *PV,* of the column:

   The pore volume of the column is necessary to calculate the residence time of each column experiment. The pore volume can be calculated by determining the mean breakthrough time for tritium, which is a conservative tracer:

   PV = 0.5 concentration breakthrough of tritium

   Pore volume for sample G4-268 devitrified tuff with J-13 well water (as given in Table A-2, J-13 well water has geochemical composition in the range of values adopted for the SZ transport model) and radionuclides ^{3}H and ^{239}Pu equals 7 mL (DTN: LA0401PR831361.001 [DIRS 166726]).

   With the pore volume and flow rate, the residence time *RT* for each column experiment can be calculated:

   RT of Each Column = *PV*/Flow rate:

   Column 1: RT = (7 mL)/(2.89 mL/hr) = 2.42 hr
   Column 2: *RT* = (7 mL)/(1.12 mL/hr) = 6.25 hr
   Column 3: *RT* = (7 mL)/(0.4 mL/hr) = 17.5 hr.

2. Determine the steady-state fractional recoveries concentrations of plutonium in the column for the different flow rates:

   For each column experiment, the plutonium fractional recovery plateaus at significantly less than 1.0. The value at which the recovery plateaus is used to determine the kinetic sorption rate of plutonium.

   Steady-state concentrations of plutonium at different flow rates:

   Column 1: 2.89 mL/hr: *Fractional Recovery* C/C_0 = 0.67
   Column 2: 1.12 mL/hr: *Fractional Recovery* C/C_0 = 0.31
   Column 3: 0.4 mL/hr: *Fractional Recovery* C/C_0 = 0.06.

3. Determine the kinetic rate constants that fit the plutonium column data:

   The steady-state fractional recovery versus residence time data was used to obtain the first-order kinetic reaction rate constant (k_{att}). The first-order kinetic rate law (e^{-kt}) yields a result of k_{att} = ~0.2 hr^{-1}. This result is obtained directly from rearrangement of the first-order rate law expression: k_{att} =absolute value(ln(frac. rec.))/*RT*.

   To calculate the *Da* number, a reverse kinetic rate is needed. Using a representative value of K_d for plutonium in devitrified tuff of 100 mL/g (Section A7.4.1), $k_{det} = k_{att}/100 = 0.002$ hr^{-1} is obtained.

4. Estimate a travel time through the system:

   Time to first breakthrough for neptunium reported in *Saturated Zone Flow and Transport Model Abstraction* (SNL 2007 [DIRS 181650]), Figure 6-32) is about 100 years. Hence, a conservative value of 10 years is used for travel time through the fractured volcanics in the saturated zone.

5. Calculate the Damköhler number:

$$Da = k_{det} * (\textit{Travel time through the system}) = 175 \qquad \text{(Eq. D-2)}$$

Valocchi found that equilibrium is well estimated for $Da > 100$ (1985 [DIRS 144579], p. 813, Figure 2).

Based on this analysis, the local equilibrium approach is valid for plutonium transport in the saturated zone of Yucca Mountain.

It should be noted that colloid-facilitated transport could not be ruled out as an explanation for the early breakthrough of ^{239}Pu in the column experiments used in this analysis. The kinetic interpretation of these column studies is also consistent with a colloid transport interpretation where the sorption and desorption rate constants are equivalent to colloid filtration and detachment rate constants. Another possible explanation for the early ^{239}Pu breakthrough in the column experiments is that microbial growth or other processes in the columns may have resulted in localized reducing conditions that caused some of the injected Pu(V) to be reduced, sorb strongly to microbial colloidal material, and be transported faster than the portion of plutonium sorbed onto the rock matrix. However, if the early plutonium breakthroughs in the column experiments were a result of colloid-facilitated transport of a portion of the plutonium, then the sorption rate constants for the soluble plutonium fraction would have to be greater than those obtained assuming that all the plutonium was soluble. This scenario would only strengthen the conclusion that the equilibrium approximation is valid for soluble plutonium over large time scales.

INTENTIONALLY LEFT BLANK

APPENDIX E
TRANSPORT SIMULATIONS WITH THE HIGHER WATER TABLE

The analysis presented in this appendix supports screening assessment of the alternative conceptual model that deals with the effect of water table rise due to future climate conditions (Table 6.6-1a, Item #4). The results of this analysis do not form a direct input to the site-scale saturated zone (SZ) transport model.

Simulations were performed for the estimated wetter, glacial-transition climatic conditions in which the groundwater flux through the saturated zone is greater than present conditions by a factor of 3.9, as given in *Saturated Zone Flow and Transport Model Abstraction* (SNL 2007 [DIRS 181650], Table 6-4[a]). In that work, the base case SZ site-scale flow model, adapted with a higher water table (DTN: SN0702T0510106.006 [DIRS 179575]), was used to conduct particle-tracking simulations for a nonsorbing species and for neptunium. Multiplying the recharge and the values of permeability for all hydrogeologic units by a factor of 3.9 (SNL 2007 [DIRS 181650], Tables 6-4[a]) approximates the higher groundwater flux rates. The expected values for parameters associated with radionuclide transport are applied in these simulations.

The green line in Figure E-1 shows the results of the transport simulation with the higher water table and estimated groundwater flow under future glacial-transition climatic conditions for a nonsorbing species. The red line in Figure E-1 shows the result obtained from the base case transport model but with the infiltration recharge and the model permeabilities scaled by a factor of 3.9. For comparison, the blue line in Figure E-1 shows the simulated breakthrough curve (BTC) using the simplified approach utilized in the TSPA abstraction of radionuclide transport in the saturated zone as shown in *Saturated Zone Flow and Transport Model Abstraction* (SNL 2007 [DIRS 181650], Section 6.5). This simplified approach uses the simulated BTC from the SZ site-scale flow model with the present water table configuration and scales that BTC to shorter transport times using the groundwater flux multiplier of 3.9 for future glacial-transition climatic conditions. All of the simulated BTCs presented in Figures E-1 and E-2 are for transport from beneath the proposed repository to the 18-km regulatory limit of the accessible environment. Figure E-2 shows similar results for the transport of neptunium using the two alternative approaches. Neptunium exhibits a small amount of sorption in the matrix of volcanic units and a moderate amount of sorption in the alluvium.

Differences in the simulated transport times for these alternative approaches to climate change in the saturated zone are primarily attributable to differences in the hydrogeologic units encountered along flow paths from beneath the repository. Flow paths in the saturated zone pass through a considerably longer length of the upper volcanic confining unit in the adapted site-scale SZ model with the higher water table. The upper volcanic confining unit has significantly lower permeability than the underlying units of the Crater Flat Tuff, leading to longer transport times along these flow paths. In addition, the relatively slower groundwater flow rates in the upper volcanic confining unit allow greater matrix diffusion, leading, in turn, to even longer transport times. There is also greater flow path length through the porous alluvium near the water table to the south and east of the repository in the adapted model with the higher water table. The porous nature of the alluvium also leads to longer simulated transport times through this medium.

Comparison of the two approaches shown in Figures E-1 and E-2 indicates that the model with the higher water table results in longer simulated transport times for both the nonsorbing species and for neptunium. The simplified approach of scaling the BTCs from the SZ site-scale flow

model with the present water table elevations produces more rapid transport in the saturated zone under wetter glacial-transition climatic conditions relative to the adapted model that incorporates water table rise associated with future conditions. Consequently, the results of these simulations tend to verify the assumption that the flux scaling approach to simulation of climate change is conservative with regard to radionuclide transport in the saturated zone, relative to the more realistic situation in which water table rise is included in the modeling.

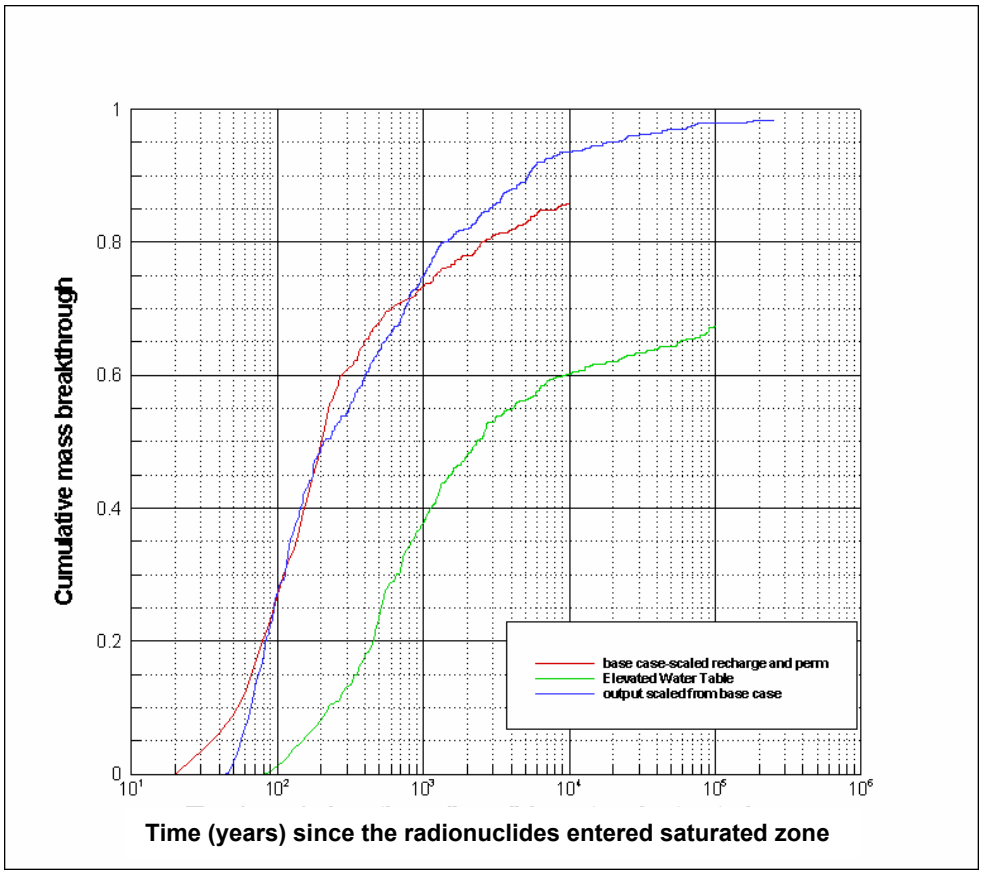

Output DTN: LA0703SK150304.011.

NOTES: Mass BTCs and median transport times are for an instantaneous source and do not include radionuclide decay. Particle source location was a point near the middle of the repository footprint. The red line is the saturated zone BTC at 18 km for future glacial-transition climatic conditions, represented by scaling the recharge and permeabilities by a factor of 3.9 from transport simulation for present-day climatic conditions. The blue line is the output of the base case scaled by a factor of 3.9. The green line is the saturated zone BTC at 18 km for future glacial-transition climatic conditions that have been simulated with the higher water table model.

Figure E-1. Breakthrough Curves for Nonsorbing Radionuclides for Future Glacial-transition Climatic Conditions Using Two Alternative Approaches

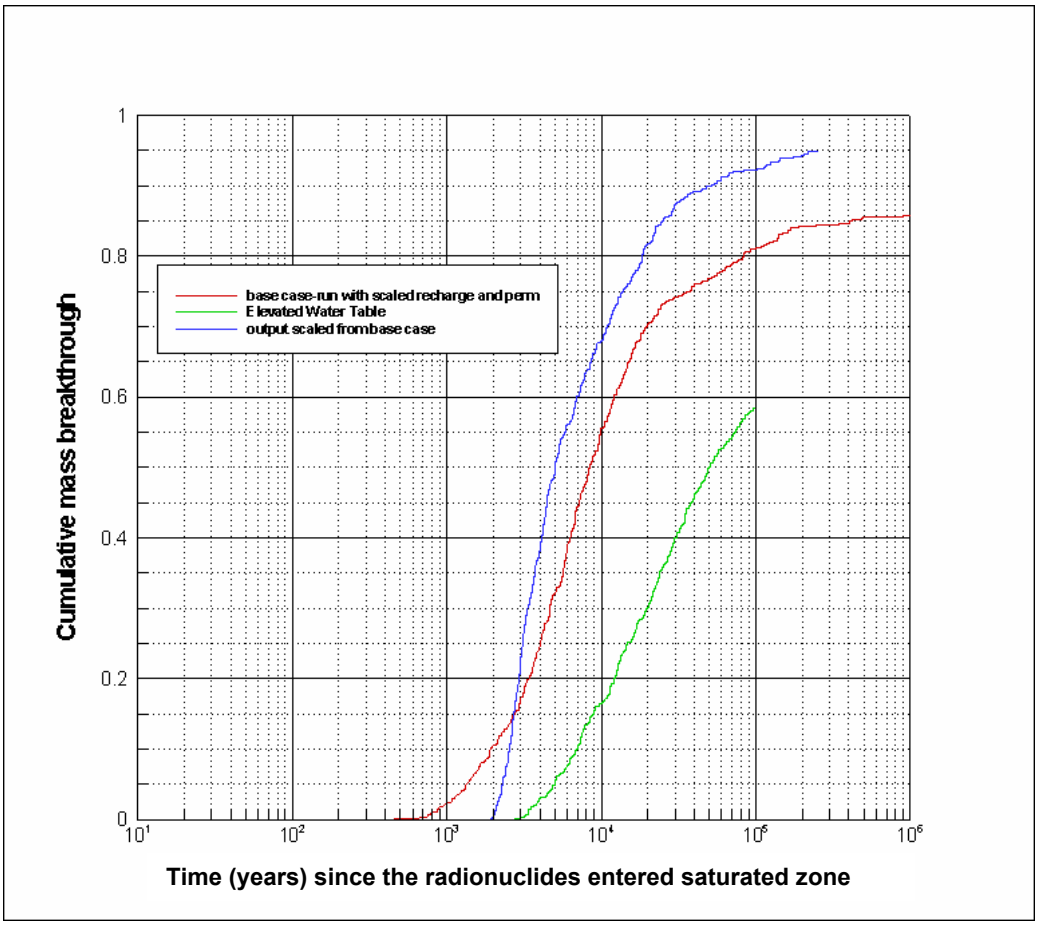

Output DTN: LA0703SK150304.011.

NOTE: Mass BTCs and median transport times are for an instantaneous source and do not include radionuclide decay. Particle source location was a point near the middle of the repository footprint. The red line is the saturated zone BTC at 18 km for future glacial-transition climatic conditions, represented by scaling the recharge and permeabilities by a factor of 3.9 from transport simulation for present-day climatic conditions. The blue line is the output of the base case scaled by a factor of 3.9. The green line is the saturated zone BTC at 18 km for future glacial-transition climatic conditions that have been simulated with the higher water table model.

Figure E-2. Breakthrough Curves for Neptunium for Future Glacial-transition Climatic Conditions Using Two Alternative Approaches

INTENTIONALLY LEFT BLANK

APPENDIX F
REDOX MEASUREMENTS IN SATURATED ZONE WATERS

The purpose of this appendix is to discuss analytical data obtained on redox conditions in groundwaters along potential flow paths from the repository to the accessible environment. The data and analysis presented in this appendix support the rationale for the assumption that for the development of sorption coefficient distributions, groundwater conditions are oxidizing in the site-scale saturated zone (SZ) transport model (Table 5-1, Item #2). The field measurements of redox conditions involve a number of experimental difficulties that are discussed later in this appendix. These data are not used as direct input to the site-scale SZ transport model. However, these data are included here because they show a potential for occurrence of greater retardation of radionuclides than currently included in the SZ transport model. The important question to be answered with all these data is "What redox conditions will radionuclides be subject to during transport in oxidizing groundwaters in the saturated zone?" The data and analysis presented in this appendix indicate a rather broad range of measured Eh values for oxidizing saturated zone waters. The broadness in the range of measured Eh values may be due in part to natural phenomena such as the mixing of oxidizing and reducing groundwaters, in part to a lack of equilibrium between the platinum electrode and the redox-sensitive species in groundwater, and in part to borehole construction and pumping effects.

Variations in the oxidation/reduction (i.e., redox) potential in the saturated zone along potential transport pathways can have significant impacts on the rates at which redox-sensitive radionuclides are transported from the potential repository. Technetium and the actinide elements neptunium, plutonium, and uranium can each assume several oxidation states depending on redox conditions. The redox conditions along potential transport pathways determine the oxidation states that these radioelements assume in groundwater and in/on solid phases. The lower oxidation states of these elements (e.g., +4) have higher retardation coefficient values (Lieser and Mohlenweg 1988 [DIRS 106684], Figure 4) and are, therefore, transported at slower rates than these elements in higher oxidation states (e.g., +5 and +6).

Redox potential is basically the voltage of groundwater. The sources for this voltage are oxidation/reduction reactions (i.e., reactions in which electrons are transferred) that occur naturally in aquifers. A redox potential can be measured in groundwater with an inert probe (e.g., platinum electrode). The potentials measured in the field with a probe are referred to as oxidation/reduction potential measurements. They are usually referenced to a silver/silver chloride (Ag/AgCl) reference electrode. By convention, the standard hydrogen electrode (SHE) has been assigned a voltage of zero at standard conditions. When field oxidation/reduction potential measurements referenced to the Ag/AgCl reference electrode are normalized to the standard hydrogen electrode scale, the measurements are called Eh values. The interpretation of redox potentials measured in oxidizing waters with a platinum electrode can often be complicated to an absence of equilibrium among the redox reactions that occur in groundwaters (Lindberg and Runnels 1984 [DIRS 106685]). However, for the purposes of predicting radionuclide transport, it is generally sufficient to determine whether groundwaters along potential flow paths have redox potentials greater or less than certain critical values. These critical values are those potentials at which neptunium, plutonium, technetium, and uranium are predominantly in their lower (e.g., +4) or higher (i.e., +5, +6, and or +7) oxidation states (a discussion of these critical values is not included here).

F1. DISCUSSION OF DATA

Redox conditions in groundwaters can be characterized by the measurement of various parameters including oxidation/reduction potential (ORP/Eh), dissolved oxygen, and the concentrations of redox-sensitive constituents such as ferrous iron (Fe^{2+}), total iron (Fe_{total}), total manganese (Mn_{total}), nitrate (NO_3^-), nitrite (NO_2^-), ammonium (NH_4^+), sulfide (HS^-), sulfate (SO_4^{2-}), as well as other less well known constituents such as different oxidation states of antimony, arsenic, and selenium. The Yucca Mountain Project (YMP) has made measurements of many of these parameters in groundwaters pumped from boreholes along potential flow paths from the repository. Locations of many of these wells are shown schematically in Figure F-1. The results are discussed in this appendix.

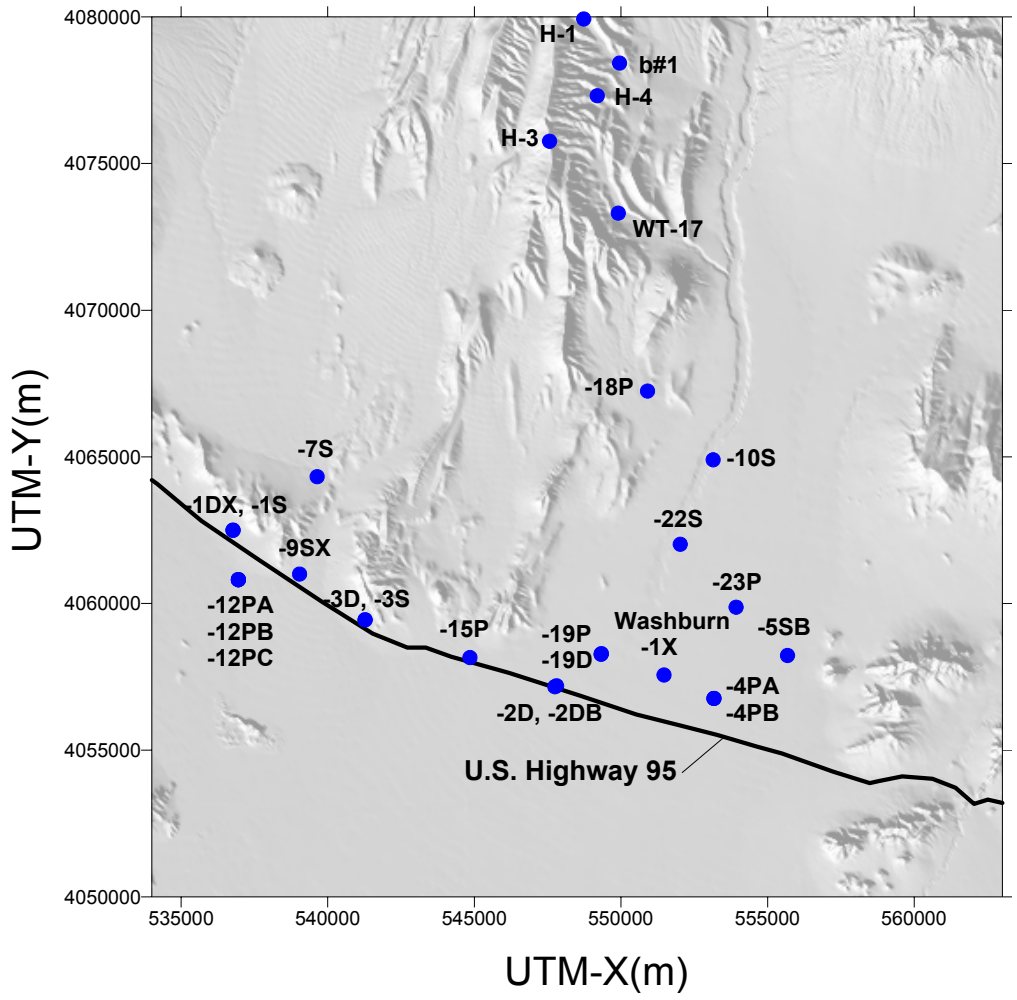

Source: DTN: GS010908312332.002 [DIRS 163555], *312411MEAN.doc*

Figure F-1. Locations of the Wells Sampled for Redox Analysis

In addition to the problem of disequilibrium conditions among different redox reactions in the natural system, there are other factors that can complicate the analysis of redox conditions in aquifers. These factors include borehole construction effects, pumping effects, and analytical

problems and errors. The data on redox parameters must be evaluated in light of these factors before the potential impacts on radionuclide transport can be discussed.

F1.1 BOREHOLE CONSTRUCTION EFFECTS

Borehole construction effects include the use of chemicals and materials during the drilling of a borehole, the use of steel casings and screens below the water table, improper sealing of casing against a borehole wall, and contaminants added to the boreholes during or after construction. After borehole construction has been completed, a borehole is generally "developed" to clean out the bulk of any chemicals and materials that may remain in the borehole from construction activities. In addition, when groundwater from a given borehole is to be sampled, at least three borehole volumes of groundwater are purged from the borehole prior to sampling the water. These activities are designed to remove chemicals and materials that were used in borehole construction, remove contaminants that may have entered the borehole after construction, and minimize any potential impacts from the corrosion of steel casing materials.

As a check on whether or not the borehole development and purging activities have produced the desired results, groundwater pumped during purging is routed through a flow-through cell at the surface that allows continuous measurement of water quality parameters (temperature, pH, conductivity, dissolved oxygen, and Eh). Water sampling is begun once three borehole volumes have been purged from the borehole and the water quality parameters have stabilized (i.e., the values have reached a plateau). This procedure helps to avoid most of the potential impacts of borehole construction and contamination. However, the results of sampling of the same boreholes over a period of years suggest that some borehole construction effects take a long time to clean out. This issue is discussed in greater detail in a following section.

Improper sealing of the casing against the borehole wall can impact redox measurements by allowing mixing of waters from different flow zones. These may include waters that have been in contact with the atmosphere. Hydraulic measurements (i.e., heads) are generally used as a guide to detecting borehole sealing problems.

F1.2 PUMPING EFFECTS

Pumping effects primarily involve the impact of the removal of groundwater from an aquifer. When an aquifer is pumped, water may be produced from more than one horizon even if the borehole is properly sealed. These different horizons may contain waters with different redox properties. Depending on how many producing horizons there are in the packed-off interval and how much each horizon produces, water pumped to the surface could represent a mixture. For example, if some horizons contain water with dissolved oxygen while other horizons contain water with dissolved metals but no dissolved oxygen, the mixture could contain dissolved oxygen and dissolved metals. These mixtures are generally unstable. If the mixture were allowed to stand, the redox-sensitive metals would eventually be oxidized and could precipitate out of solution. If the residence time of water in the pump circuit is sufficiently long, it is possible that the metals could precipitate from the mixed water as it is pumped to the surface. Filtration of these waters before analysis could result in lower metal concentrations than were present at the source. Problems such as these make it difficult to unambiguously interpret redox parameter measurements on groundwaters from some boreholes.

Pumping groundwater from depth to the surface usually involves a decrease of water pressure. The pressure decreases generally result in some degassing, forming bubbles in the water discharge line. Such degassing can reduce the concentrations of dissolved gases such as carbon dioxide and oxygen in the groundwater. A decrease in the concentration of carbon dioxide in a given groundwater generally leads to a higher pH. Thus, pH values measured at the surface in a flow-through cell may not reflect the pH values of in situ groundwater.

Another potential pumping effect involves air leakage from gas-actuated pumps. These pumps operate on gas pressure delivered to the pump from the surface. If the air hoses or the pump assembly leak air into the water column, measurements of dissolved oxygen, pH, and other parameters could be impacted. The YMP has addressed this problem either by using an electric pump or by using a gas other than air (e.g., argon or nitrogen) to pump water from boreholes prior to sampling.

F1.3 PROBLEMS AND ERRORS ASSOCIATED WITH ANALYTICAL MEASUREMENTS

Problems and errors associated with analytical measurements include inadequate analytical equipment, analytical equipment failure, improper standards, poor analytical technique, sample contamination, and recording or transcribing errors. Inadequate analytical equipment for redox potential measurements (ORP/Eh) in oxidizing waters is a problem well known in the analytical community (Langmuir 1997 [DIRS 100051], p. 414) and is primarily the result of poorly poised solutions. The term "poised" refers to the concentration of redox-sensitive species in solution. When these concentrations are very low, the corresponding exchange currents on the platinum electrode are very low. Under these conditions, the platinum electrode may respond to impurities in the platinum metal or other impurities (e.g., organic species) from either the natural groundwater system or introduced by borehole construction activities.

Another measurement difficulty arises from the fact that some redox-sensitive species in solution are not very electroactive. That is, they (e.g., dissolved oxygen, nitrite, and nitrate; Stumm and Morgan 1981 [DIRS 100829], p. 493) do not result in exchange currents on a platinum electrode that properly reflect their concentration in solution. In effect, the measured platinum electrode potentials primarily reflect those redox-sensitive species in solution that are electroactive on platinum. Further, disequilibrium conditions among electroactive redox couples in solution can result in mixed potentials. These are potentials that are some combination of the potentials that would be measured if each electroactive redox couple were present in the absence of others.

Another problem associated with the analytical equipment used in measurements of redox couples is sensitivity. In effect, the detection limits of the available field equipment are higher than are required for the analysis of various important redox-sensitive species in Yucca Mountain groundwaters. For example, in oxidizing groundwaters the concentrations of Fe^{2+} are commonly below the detection limits of the available field analytical equipment. This limits the number of redox couples available to define the redox state of Yucca Mountain groundwaters.

Problems with analytical equipment failure, improper standards, poor analytical technique, sample contamination, and recording or transcribing errors can generally be resolved by fixing the problem once it is recognized. The use of detailed technical procedures has been one

approach used to minimize the potential impacts of these problems and thus minimize potential errors.

F2. INTERPRETATION OF REDOX DATA

F2.1 OXIDIZING GROUNDWATERS

Platinum electrode (i.e., Eh) measurements on oxidizing groundwaters from the Yucca Mountain area are plotted against dissolved oxygen measurements in Figure F-2. Oxidizing groundwaters are here defined as those having more than 1.0 mg/L dissolved oxygen. According to Stumm and Morgan (1981 [DIRS 100829], p. 492), dissolved oxygen is not electroactive on a platinum electrode. That is, the exchange current for the dissolved oxygen/H_2O couple on platinum does not properly reflect the concentration of dissolved oxygen in solution. To test this idea, Eh values were calculated for the dissolved oxygen/H_2O couple based on the following reaction (Langmuir 1997 [DIRS 100051], p. 409):

$$O_2(g) + 4H^+ + 4e^- = 2H_2O \quad \text{(Eq. F-1)}$$

This reaction corresponds to the following equation for Eh (in volts) at 25ºC (Langmuir 1997 [DIRS 100051], p. 409):

$$Eh = 1.23 + (0.0592/4)*(\log pO^2[H^+]4) \quad \text{(Eq. F-2)}$$

Using a Henry's Law constant of 1.26×10^{-3} M/bar (Langmuir 1997 [DIRS 100051], p. 409) in water and an atomic weight of oxygen of 31.999 g/M, this equation yields the calculated Eh values shown in Figure F-2 for the various measured dissolved oxygen values. Clearly, the calculated Eh values do not correspond well to the measured Eh values.

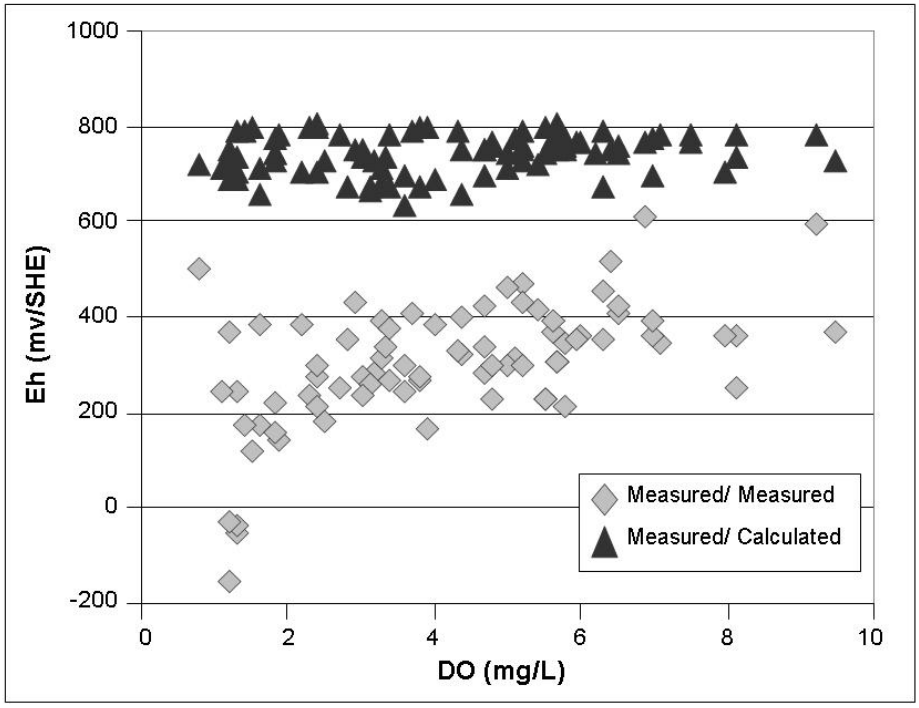

Source: DTN: LA0206AM831234.001 [DIRS 160051].

NOTE: Calculated Eh values obtained from measured dissolved oxygen concentrations are also plotted against measured dissolved oxygen concentrations.

Figure F-2. Measured Eh Values Relative to the Standard Hydrogen Electrode versus Measured Values of Dissolved Oxygen

According to Stumm and Morgan (1981 [DIRS 100829]), the cause for the low exchange currents on platinum is likely the fact that four electron transfers must occur in sequence to produce the equilibrium potential and one of these transfer reactions is very slow. It has been suggested (Stumm and Morgan 1981 [DIRS 100829], p. 462) that the Eh values measured with a platinum electrode in waters containing dissolved oxygen may actually reflect the concentration of one of the reaction intermediates (i.e., hydrogen peroxide). However, this explanation is difficult to test without analyses of the concentration of the reaction intermediates in groundwater. To our knowledge, these analyses have not been performed on Yucca Mountain groundwaters.

The differences between measured and calculated Eh values in Figure F-2 likely reflect a combination of phenomena. First, the Eh measurements reported in Figure F-2 do not all represent the same equilibration time. During the field measurements, the platinum electrode was in contact with groundwater for as little as 25 minutes or as long as 345 minutes depending on the site (i.e., borehole). At the shorter measurement times, Eh values were generally increasing with time when the measurements were stopped. Thus if the shorter time measurements had been allowed to go as long as 345 minutes, a larger value would have been obtained for Eh in most cases.

A plot of measurement time and measured Eh in oxidizing groundwaters (i.e., dissolved oxygen> 1.0 mg/L) is shown in Figure F-3. Although there is a lot of scatter in the data, repeat measurements on water from the same borehole generally show an increase in measured Eh value with increased measurement time. The example shown with an arrow is from Borehole NC-EWDP-19IM1, zone #5, which was first measured in November 2001 (low Eh value) and measured again in October 2003 (high Eh value).

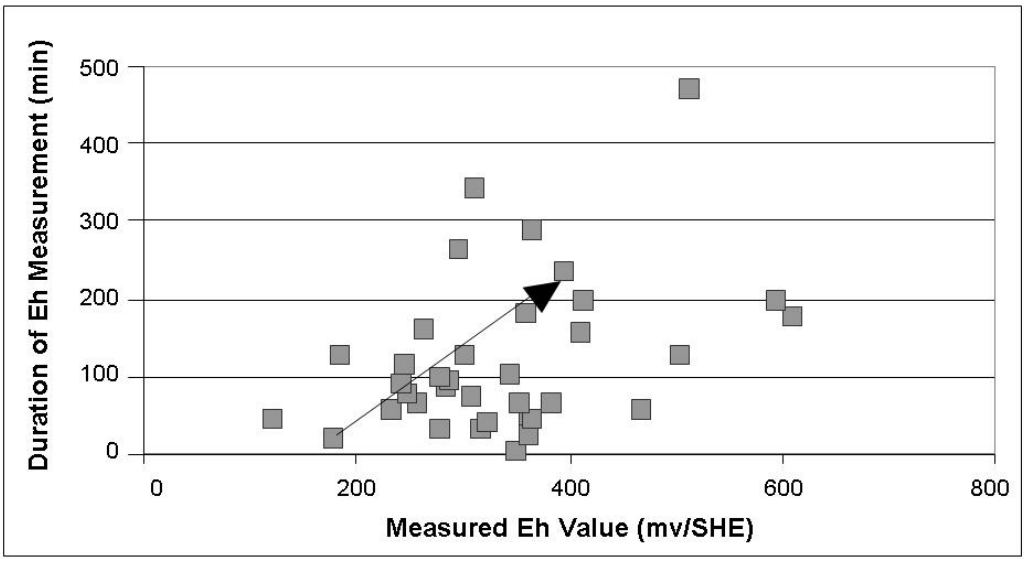

Source: DTN: LA0206AM831234.001 [DIRS 160051].

NOTE: Arrow shows example of repeat analyses.

Figure F-3. Plot of Duration of Field Measurement (in minutes) versus Measured Eh Value in mv Relative to the Standard Hydrogen Electrode for Oxidizing Waters

Second, the measured Eh values likely reflect the presence of other redox-sensitive constituents in the groundwaters that are more electroactive on platinum than the dissolved oxygen/H_2O couple. To test this concept, Eh values were calculated for groundwaters on the basis of various redox couples. The couples considered here include Mn^{2+}/MnO_2, $Fe^{2+}/Fe(OH)_3$, and NO_2^-/NO_3^-. For the Mn^{2+}/MnO_2 couple, the following reaction can be written assuming pyrolusite is the solubility-controlling solid under oxidizing conditions at 25ºC (Langmuir 1997 [DIRS 100051]; p. 417):

$$MnO_2 \text{ (pyrolusite)} + 4H^+ + 2e^- = Mn^{2+} + 2H_2O \qquad \text{(Eq. F-3)}$$

This reaction corresponds to the following equation for Eh (in volts) at 25ºC (Langmuir 1997 [DIRS 100051], p. 417):

$$Eh = 1.23 + (0.0296)*\log([H^+]^4/[Mn^{2+}]) \qquad \text{(Eq. F-4)}$$

The Eh values calculated with this equation are plotted against measured pH values in Figure F-4. The calculated values are based on the assumption that all the manganese measured in the water samples is Mn^{2+}. This assumption is reasonable in that Mn^{4+} is highly insoluble and would tend to precipitate out of solution. However, this assumption would bias the calculated values to somewhat lower values compared to values that would be obtained if only Mn^{2+}

concentrations were used. As shown in the figure, the calculated Eh values are generally equal to or larger than the Eh values measured with the platinum electrode, although they are consistently smaller in value than those calculated on the basis of the dissolved oxygen/H_2O couple. The measured Eh values that plot close to the Eh values calculated on the basis of the Mn^{2+}/MnO_2 couple is consistent with the idea that the platinum electrode is reacting to this couple in some of the groundwaters. In Figure F-4, measured Eh values less than 0.0 mv/SHE either represent mixed waters (see below) or they represent reducing groundwaters that were contaminated with dissolved oxygen during the pumping activities.

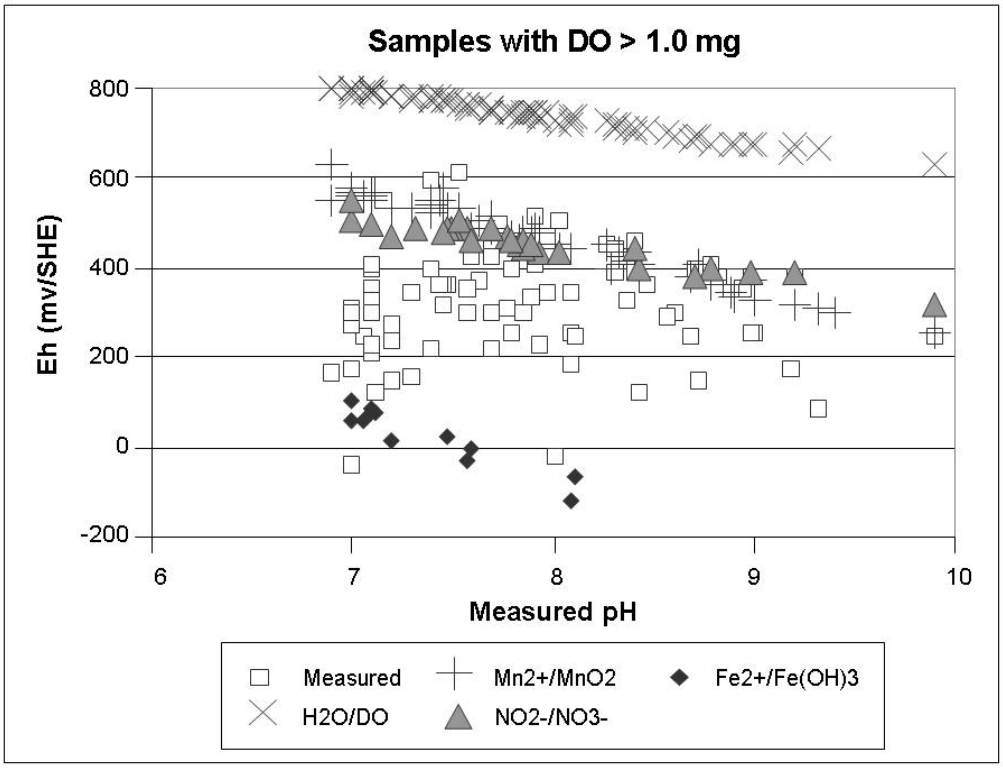

Source: DTNs: LA0206AM831234.001 [DIRS 160051]; LA0206AM831234.002 [DIRS 163852]; LA9907AM831234.009 [DIRS 149209]; LA9907AM831234.011 [DIRS 149212]; LAAM831311AQ98.007 [DIRS 149520]; LAAM831311AQ98.010 [DIRS 149522].

Figure F-4. Measured pH Values versus Measured Eh Values and Eh Values Calculated From the Dissolved Oxygen/H_2O, Mn^{2+}/MnO_2, NO^-_2/NO^-_3, and $Fe^{2+}/Fe(OH)_3$ Couples in Oxidizing Groundwaters (Dissolved Oxygen > 1.0 mg/L)

There are a number of reasons why the calculated Eh values might be larger than the measured values plotted in Figure F-4. First, as noted above, measured Eh values often do not reflect steady-state values. That is, with increased measurement times, the measured values tend to increase toward higher values. Second, Equation F-3 may not be the appropriate equation for calculating the control of Mn^{2+} concentrations in all the groundwaters. That is, the Mn^{2+} concentration may be controlled by a phase other than MnO_2. This is very likely the case for measured Eh values that are < 100 mv but it may also be true for some of the waters with higher measured Eh values. In these cases, the Mn^{2+} concentration in groundwater may be controlled by equilibria involving phases such as MnO_x, Mn_2O_3, and $MnCO_3$; solid solutions containing these components; and/or by manganese adsorption reactions on other solid phases (e.g., clays,

zeolites, feldspars, silica phases). Measurements with negative Eh values in combination with dissolved oxygen values greater than 1 mg/L may reflect mixing of waters with different redox properties in the wellbore. Third, the thermodynamic data on which the calculated Eh values are based may not be accurate.

The lack of consistency between Eh values calculated on the basis of the dissolved oxygen/H_2O and Mn^{2+}/MnO_2 couples, as shown in Figure F-4, is not without precedent. According to Stumm and Morgan (1981 [DIRS 100829]; Figure 7.12), a similar situation exists in seawater where the Eh value calculated on the basis of dissolved oxygen is higher (740 mv/SHE) than the values calculated from the Mn^{2+}/MnO_2 couple (598 mv/SHE).

The Eh values calculated from the NO_2^-/NO_3^- couple are not subject to uncertainty regarding the identity of the equilibrium solid phase. However, the calculated values (Figure F-4) are sensitive to experimental artifacts and errors and measured pH values. The concentrations of nitrite measured in most groundwaters in the Yucca Mountain area are in the range of 0.01 to 0.02 mg/L. This is close to the detection limit of the techniques used in the analysis of nitrite. Further, nitrite is present in the environment as preservatives in meat products and other foods. Thus, contamination is always a potential problem.

These factors could bias the Eh values calculated on the basis of the NO_2^-/NO_3^- couple to lower values. This is reflected in the fact that the Eh values calculated on the basis of the NO_2^-/NO_3^- couple are consistently less than the values calculated based on the dissolved oxygen concentrations in the oxidizing groundwaters (Figure F-4). The NO_2^-/NO_3^- couple is apparently not electroactive on platinum electrodes (Stumm and Morgan 1981 [DIRS 100829], p. 493). Thus, the measured Eh values plotted in Figure F-4 most likely do not reflect the NO_2^-/NO_3^- couple.

For the $Fe^{2+}/Fe(OH)_3$ couple, the following reaction can be written assuming amorphous $Fe(OH)_3$ is the solubility controlling (Langmuir 1997 [DIRS 100051], p. 417):

$$Fe(OH)_3\ (am) + 3H^+ + e^- = Fe^{2+} + 3H_2O \qquad \text{(Eq. F-5)}$$

This reaction corresponds to the following equation for Eh (in volts) at 25ºC (Langmuir 1997 [DIRS 100051], p. 417):

$$Eh = 0.975 + (0.0592)*\log([H^+]^3/[Fe^{2+}]) \qquad \text{(Eq. F-6)}$$

Most of the groundwaters analyzed for this study did not contain measurable Fe^{2+}. Those that did plot at the low end of the range of measured Eh values (Figure F-4). This suggests the platinum electrode may be responding to ferrous iron in at least some of the water samples. Many of the water samples analyzed had concentrations of Fe^{2+} and total iron below the detection limit (i.e., <0.01 mg/L). Theoretical Eh values were not calculated for these samples. However, in Figure F-4, these samples would plot somewhere between the highest values calculated on the basis of the $Fe^{2+}/Fe(OH)_3$ couple and the Eh values calculated on the basis of the dissolved oxygen/H_2O couple.

Many of the water samples analyzed contained measurable concentrations of total iron. These total iron concentrations most likely reflect colloidal ferric iron particles less than 0.45 microns

in diameter (i.e., less than pore size of filters used in analysis). The origin of these particles is not certain. They could be naturally occurring colloids that were pumped from the producing horizon(s), or they could be artifacts from well construction and/or pumping activities. The fact that the platinum electrode Eh values range between the calculated Eh values for the $Fe^{2+}/Fe(OH)_3$ couple and those calculated for the more oxidizing Mn^{2+}/MnO_2 and NO_2^-/NO_3^- couples suggests the ferric iron particles may have been formed through the oxidation of dissolved ferrous iron present in the pumped water. In this scheme, the large range in measured Eh values reflects the extent to which ferrous iron in water pumped from depth was oxidized prior to coming in contact with the platinum electrode at the wellhead.

At the dissolved oxygen concentrations found in most of these waters and under equilibrium conditions, the amount of ferrous iron in the waters should be well below the detection limit of the techniques used in the analysis. This suggests the waters containing measurable total iron result from a mixing process. Because the oxidation rate of ferrous iron is relatively fast in neutral to alkaline solutions (Stumm and Morgan 1981 [DIRS 100829], p. 465), such a mixing process would have to occur during the pumping event. The components of the mixture could be naturally occurring, or they could be artifacts of borehole construction and/or pumping activities.

It is considered unlikely that waters containing dissolved oxygen could be kept isolated from waters containing dissolved metals over aquifer thicknesses of 10 to 30 ft (i.e., packed-off interval lengths) in porous media over rather long (i.e., kilometer scale) flow paths. Recharge waters generally contain 8 to 9 mg/L of dissolved oxygen. As these waters flow downgradient, some of this dissolved oxygen may be consumed in oxidation reactions. However, some groundwaters appear to have retained nearly all of their dissolved oxygen as they moved downgradient (Figure F-2). These waters would have to remain separated from the waters containing dissolved metals from the time they were recharged. How waters with such distinctive redox characteristics could have remained separated from each other in alluvium is very difficult to understand.

This leads to consideration of the possibility that either the metals or the dissolved oxygen concentrations in the waters reflect borehole construction or pumping artifacts. In the case of the metals, obvious sources of reduced (i.e., ferrous) iron are steel casings and screens. Where the borehole casing material is polyvinyl chloride or where there is no casing below the water table, metallic iron could have been introduced into the aquifers during drilling (i.e., from steel drilling equipment). Pumps and their fittings are another potential source of reduced iron.

If the iron present in groundwaters containing dissolved oxygen is an artifact of borehole construction activities, these groundwaters should show progressively lower iron concentrations when sampled over time as the "contaminants" are cleared from the well. The data shown in Table F-1 offer a possible example of this scenario. These are water quality data collected in 2002 and 2003 from Borehole NC-EWDP-22S, which was constructed in 2002 with PVC casing. The data collected in 2003 show lower ferrous and total iron concentrations along with higher dissolved oxygen and nitrate concentrations when compared with data collected in 2002. Manganese and nitrite concentrations show less consistent trends for the two sampling rounds with one unusually high manganese value (0.168 mg/L) obtained in 2002. Because Eh values were not measured in 2002, no comparison can be made for this parameter.

Table F-1. Water Quality Data for Samples from Borehole NC-EWDP-22S

Well Number	Date Measured	Casing Type	Fe^{+2} (mg/L)	Fe (total) (mg/L)	Mn (total) (mg/L)	Nitrate (mg/L)	Nitrite (mg/L)	Dissolved Oxygen (mg/L)
NC-EWDP-22S-1	9/11/2002	PVC	0.02	0.10	0.017	7.5	0.008	1.3
NC-EWDP-22S-1	8/5/2003	PVC	N/M	N/M	N/M	N/M	N/M	7.1
NC-EWDP-22S-2	9/10/2002	PVC	0.01	0.15	0.023	4.2	0.008	N/M
NC-EWDP-22S-2	8/12/2003	PVC	0.00	0.06	0.027	8.9	0.014	5.4
NC-EWDP-22S-3	9/10/2002	PVC	0.00	0.20	0.168	6.6	0.013	1.7
NC-EWDP-22S-3	9/9/2003	PVC	0.00	0.01	0.035	10.3	0.009	4.8
NC-EWDP-22S-4	9/9/2002	PVC	0.00	0.19	0.029	3.4	0.017	1.3
NC-EWDP-22S-4	9/23/2003	PVC	0.00	0.05	0.017	7.1	N/M	5.3

Source: DTN: LA0410AM831232.002 [DIRS 180743].
N/M = not measured.

The possibility that high dissolved oxygen concentrations are artifacts is considered a less likely general explanation for the disequilibrium conditions observed. Boreholes with multiple completions (i.e., packed-off intervals at different depths) such as NC-EWDP-22S (Table F-1) produce waters from the deepest zones that have a similar dissolved oxygen concentration (5.5 mg/L) as those produced from the shallower zones (5.0 to 7.1 mg/L). It is difficult to understand how waters in the deepest zone could be in contact with the atmosphere unless the cone of depression around the pump reached the pump entry port. Pumping procedures ensured that this situation was avoided in nearly all cases. On the other hand, dissolved oxygen could have been introduced into the pumping circuit in boreholes that do not penetrate very far below the water table (e.g., NC-EWDP-18P). When these boreholes are pumped, water that has been at or near the water table may be drawn into the pumping circuit and mixed with waters containing metals that originate from flow zones deeper in the borehole.

To summarize, the Eh values measured with a platinum electrode in waters containing dissolved oxygen generally do not correspond to Eh values calculated on the basis of the measured dissolved oxygen concentrations. In many cases, the platinum electrode appears to have responded to iron and possibly manganese concentrations in the groundwaters. Further, it appears likely that these metal concentrations are artifacts of borehole construction and/or pumping activities.

The important question to be answered with all these data is "What redox conditions will radionuclides be subject to during transport in oxidizing groundwaters in the saturated zone?" The data plotted in Figure F-4 indicate a rather broad range of measured Eh values for oxidizing saturated zone waters. The broadness in the range of measured Eh values may be due in part to natural phenomena such as the mixing of oxidizing and reducing groundwaters, in part to a lack of equilibrium between the platinum electrode and the redox-sensitive species in groundwater, and in part to borehole construction and pumping effects.

The ubiquitous presence of dissolved oxygen in these waters suggests these waters will be oxidizing overall. However, if the radionuclides-of-interest respond to the presence of dissolved oxygen in the same way as the Mn^{2+}/MnO_2 and NO^{-}_2/NO_3^{-} couples, the redox potentials will be less than those calculated on the basis of the dissolved oxygen/H_2O couple. The range of Eh

values calculated on the basis of the Mn^{2+}/MnO_2 and NO^{-}_2/NO_3^- couples could be used to estimate the redox potential that would be experienced by the radionuclides-of-interest.

The range of Eh values that these radionuclides would experience during transport can be further narrowed by noting that the range of pH values measured in saturated zone waters is in part an artifact of borehole construction and pumping activities. For example, cement was used in the construction of some boreholes. Cement used below the water table can leach alkaline solutions into the groundwater causing increased pH. More generally, waters brought to the surface from the saturated zone often outgas carbon dioxide and probably other gases during pumping. Outgassing is evidenced by bubbles that appear in water flowing through the discharge line. The loss of carbon dioxide causes an increase in the measured pH of the pumped waters (i.e., the waters that pass through the flow-through cell). These effects imply the range of pH values of groundwaters in the aquifer is smaller than the range indicated by the values measured in the flow-through cell at the wellhead.

In the case of J-13, the in situ pH value is near 7.0 while the value obtained under normal atmosphere is 8.4. If it is assumed other groundwaters show similar changes in pH values between the aquifer depth and the surface, it is likely in situ pH values would be in the range of 7.0 to 8.0. Further, if it is assumed the redox conditions to which radionuclides would be exposed in oxidizing saturated zone groundwaters are represented by the ranges of Eh values calculated from the Mn^{2+}/MnO_2 and NO_2^-/NO_3^- couples, the redox potentials would range from approximately 400 to 500 mv/SHE at pH = 8.0 to 500 to 600 mv/SHE at pH = 7.0. If for some reason the Eh values calculated from the Mn^{2+}/MnO_2 and NO_2^-/NO_3^- couples are not representative of saturated zone conditions, the range in redox potentials could be as high as 750 to 800 mv/SHE (i.e., the range calculated for the dissolved oxygen/H_2O couple).

F2.2 REDUCING GROUNDWATERS

The situation is different for reducing waters. In these waters, dissolved oxygen concentrations are low (less than 1.0 mg/L) and dissolved metal concentrations are higher than in oxidizing waters. Under these conditions, the platinum electrode does provide useful information on the redox potential of groundwaters largely because exchange currents are larger. The exchange currents are larger because the concentrations of electroactive species in solution are larger. Conversely, Eh values calculated on the basis of dissolved metal concentrations are less definitive in these waters because the identities of the phases that control these concentrations are less obvious.

The boreholes in which reducing conditions have been found in groundwaters in the Yucca Mountain area include boreholes (Figure F-1) on or near Yucca Mountain (H-1, H-3, H-4, 25b#1, WT-17), a borehole in alluvium to the east of Fortymile Wash (NC-EWDP-5SB), and a group of boreholes to the west of Fortymile Wash (NC-EWDP-1D, 3S, 7SC). The boreholes on Yucca Mountain that contain reducing waters are relatively deep holes that penetrate the Tram Member of the Crater Flat Tuff. This member includes a volcanic unit that contains pyrite (FeS_2). The pyrite is apparently a primary (i.e., volcanic) constituent of this unit (Castor et al. 1994 [DIRS 102495]). It is thought to have been eroded from the volcanic conduit during the eruption that produced the ash flow. The presence of pyrite in this unit is a likely source of the reducing conditions observed in the groundwaters pumped from these boreholes.

The equilibrium reaction between Fe^{2+} and FeS_2 (pyrite) can be represented with the following equation (Langmuir 1997 [DIRS 100051]; p. 417):

$$2SO_4^{2-} + Fe^{2+} + 16H^+ + 14e^- = FeS_2(\text{pyrite}) + 8H_2O. \quad \text{(Eq. F-7)}$$

The following equation is used to calculate Eh values for the Fe^{2+}/FeS_2 couple at 25ºC (Langmuir 1997 [DIRS 100051]; p. 417):

$$Eh = 0.362 + 0.00423 \log [Fe^{2+}][SO_4^-]^2[H^+]^{16}. \quad \text{(Eq. F-8)}$$

The Eh values, measured in these boreholes and the Eh values calculated on the basis of the Fe^{2+}/FeS_2 couple, are plotted against measured pH in Figure F-5. Although the measurements show a similar trend to that shown by the calculated values, the calculated trend is displaced to somewhat lower Eh values. The trend in calculated Eh values based on the $Fe^{2+}/Fe(OH)_3$ couple seems to correspond more closely to the trend in the measured values. In either case, the measured and calculated values indicate reducing conditions in these wells.

The sample that lies above the main trend in Figure F-5 (more than 400 mv) represents a water with an oxidizing Eh value and a low dissolved oxygen concentration. This sample likely represents a mixture of oxidizing and reducing waters. Such mixtures could originate in open boreholes or boreholes with multiple screens that are not packed off. For example, if a water with 2.0 mg/L ferrous iron and no dissolved oxygen from one horizon were mixed with a water with 6.0 mg/L dissolved oxygen and no ferrous iron from another horizon in a ratio of 10:1, the dissolved oxygen would eventually oxidize the ferrous iron so that the mixture would contain little or no dissolved oxygen or ferrous iron. However, the total iron concentration could remain elevated if insufficient time had passed for the oxidized iron to precipitate out of solution prior to analysis.

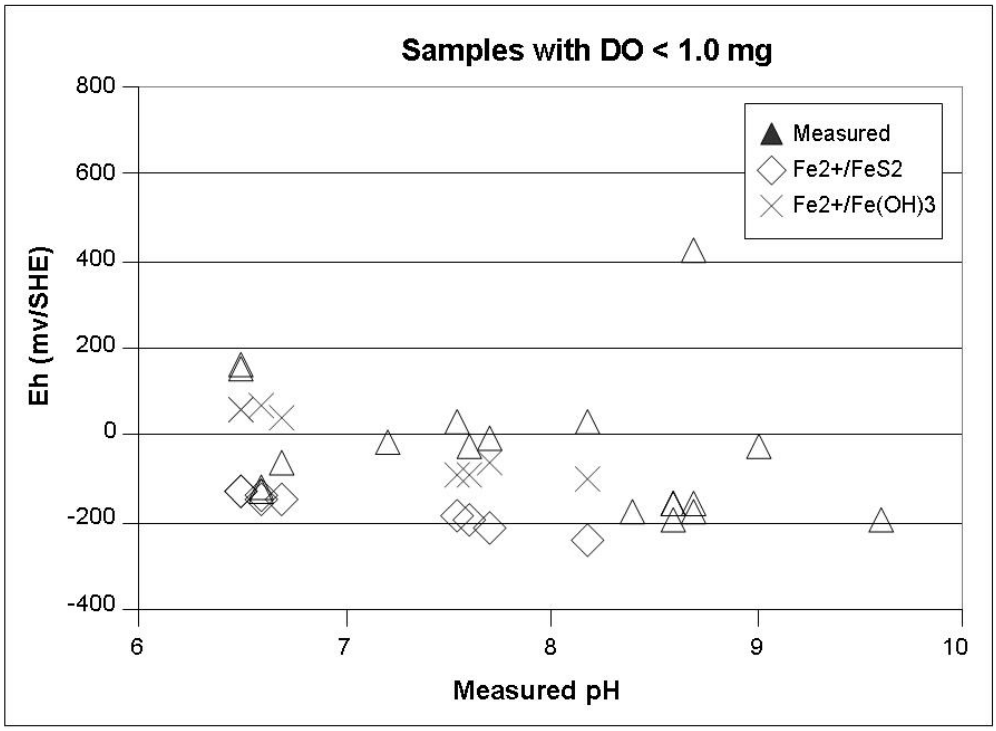

Source: DTNs: LA0206AM831234.001 [DIRS 160051]; LA0206AM831234.002 [DIRS 163852]; LA9907AM831234.009 [DIRS 149209]; LA9907AM831234.011 [DIRS 149212]; LAAM831311AQ98.007 [DIRS 149520]; LAAM831311AQ98.010 [DIRS 149522].

Figure F-5. Measured Eh Values versus pH Values and Measured pH Values versus Eh Values Calculated on the Basis of the Fe^{2+}/FeS_2 (pyrite) Couple

It is very important to recognize that the presence of reducing conditions in more than one borehole located directly to the east of the repository footprint (e.g., WT-17 and b#1) suggests there may be a volume of rock east of the repository footprint that contains reducing groundwaters. This volume could be a substantial barrier to the transport of redox-sensitive radionuclides in the saturated zone as discussed in the following section.

The groundwaters showing reducing conditions in boreholes to the east and west of Fortymile Wash near the southern boundary of the site include Boreholes NC-EWDP-1D, 3S, 5SB, 7SC, 12PA and 12 PB. Borehole NC-EWDP-1D is known to contain pyrite based on core descriptions provided by Nye County. The other boreholes may also contain pyrite although core descriptions are not available to test this possibility.

F3. IMPLICATIONS FOR RADIONUCLIDE TRANSPORT

The discussion in this section is intended to provide a general consideration of the impact of redox conditions on radionuclide transport based on available laboratory and field data than has been acquired to date. The general conclusions to be drawn from the data and the discussion presented in this appendix are: a) measuring redox potentials is a very sensitive undertaking and the results have to be interpreted with caution taking into account the various experimental difficulties discussed in this appendix, and b) despite these problems, there are abundant measurements taken in the saturated zone that indicate saturated zone waters along the predicted

transport path are primarily oxidizing. A few 'islands' of reducing areas lie along the transport path and, if modeled as such in the saturated zone transport abstraction, they would result in higher radionuclide retardation along the transport path.

The TSPA calculations for saturated zone transport use a stochastic approach in which many separate realizations are obtained to provide statistically meaningful results. In each realization for saturated zone transport, a single value is used for the sorption coefficient of each radionuclide for the volcanic section, and another single value is used for the alluvium section (independent values are used for colloid-facilitated transport). The site-scale SZ transport model (Section 5, Table 5-1) assumes redox conditions oxidize along all the potential transport pathways from the repository to the accessible environment. Thus, variations in redox conditions in the saturated zone are not explicitly addressed in the TSPA calculations. This is consistent with the fact that the bulk of the redox measurements obtained on groundwaters in volcanic and alluvial aquifers indicate the presence of oxidizing conditions (i.e., conditions in which the radioelements technetium, neptunium, plutonium, and uranium are in their highest oxidation states). However, there are some volumes of rock in which reducing conditions exist in critical locations important to radionuclide transport. One of these volumes is located directly east of the repository footprint.

Data presented by Lieser and Mühlenweg (1988 [DIRS 106684]) indicate that retardation coefficients for neptunium under reducing conditions are three orders of magnitude higher than they are under oxidizing conditions. Similar differences in retardation coefficient values under reducing versus oxidizing conditions are likely for plutonium, technetium, and uranium. The conditions in most of the boreholes containing reducing groundwaters are sufficiently reducing so that neptunium, plutonium, technetium, and uranium will be predominantly in the +4 oxidation state in these waters. Thus, the site-scale SZ transport model assumes conditions that could be significantly less retarding than those that actually occur in the field for these radionuclides, making the model significantly conservative in regards to the predicted travel times of these radionuclides. Explicit consideration in the transport calculations of the reducing conditions present in the saturated zone directly east of the repository could result in much longer travel times for redox-sensitive radionuclides. Similarly, the reducing conditions observed in boreholes to the east and west of Fortymile Wash suggest redox-sensitive radionuclides will have much longer transport times through these areas than those that may be predicted by the current TSPA calculations.

INTENTIONALLY LEFT BLANK

APPENDIX G
RADIONUCLIDE SORPTION PARAMETERS FROM BATCH AND COLUMN TRANSPORT EXPERIMENTS IN SATURATED ALLUVIUM AND DISCUSSION OF EARLY BREAKTHROUGH BEHAVIOR IN COLUMN EXPERIMENTS

G1. INTRODUCTION

The data and analysis presented in this appendix support the screening assessment of the alternative conceptual model that deals with the treatment of sorption reactions as being instantaneous (Table 6.6-1b, Item #1) in the site-scale saturated zone (SZ) transport model. The results of this analysis do not form a direct input to the site-scale SZ transport model.

The saturated alluvium south of Yucca Mountain is expected to serve as a natural barrier to the migration of radionuclides from the repository to the accessible environment. The alluvium consists primarily of materials of volcanic origin, with some enrichment of clays and zeolites relative to the volcanic tuffs at Yucca Mountain.

This appendix describes a series of experiments conducted to better characterize the radionuclide retardation potential of the saturated alluvium. The objectives of the experiments were to:

- Evaluate the retardation potential of alluvium for ^{129}I, ^{99}Tc, ^{237}Np, and ^{233}U by determining distribution coefficients (K_d; mL/g) in batch sorption and desorption experiments using alluvium samples and water collected from boreholes in saturated alluvium along potential flow pathways to the accessible environment.

- Determine the retardation behavior of these radionuclides in column transport experiments using the same water and alluvium as in some of the batch experiments, and to determine whether the sorption parameters measured in batch experiments can be used to predict column transport behavior.

In addition to presenting the experimental results and interpretations, this appendix provides an explanation of apparent inconsistencies between results from batch sorption and column transport experiments. Specifically, the early breakthrough of a portion of the radionuclide mass in some column transport experiments is discussed in light of results from batch sorption experiments that suggest that much later breakthrough times should have been observed in the column experiments.

G2. EXPERIMENTAL APPROACH

All batch sorption, desorption, and column transport experiments were conducted under ambient conditions (room temperature and in contact with atmosphere). Two separate sets of experiments were conducted. The first set was carried out using alluvium samples from boreholes drilled in Phase 1 of the Nye County early-warning drilling program (NC-EWDP-1X, 2D, 3S, 9SX, 19D). Groundwater from Borehole 3S was used in experiments with samples from Boreholes 1D, 2D, 3S, and 9SX while groundwater from Borehole 19D was used in experiments with alluvium samples from 19D. ^{129}I, ^{99}Tc, and ^{237}Np were used in these experiments; ^{233}U was not used until the second set of experiments. Column transport experiments were conducted using ^{237}Np along with tritiated water, which served as a nonsorbing tracer. Groundwater from Borehole 3S and alluvium material from Borehole 2D were used in these column experiments. Because groundwater from Borehole 3S may not be representative of in situ conditions (the water obtained from 3S may have contained organic materials used in well construction), the results obtained in experiments with samples from Boreholes 1X, 2D, 3S, and 9S were not used

in the derivation of sorption coefficient probability distributions. However, the results from the batch sorption and column transport experiments using these materials are discussed in this appendix because they exhibit similar qualitative sorption behavior to other sets of alluvium batch and column experiments.

A second set of experiments was carried out using alluvium samples from Phase II Nye County Boreholes NC-EWDP-10SA, 19M1A, and 22SA and groundwater from different zones in NC-EWDP-19D (Zones 1 and 4) and NC-EWDP-10SA. ^{129}I, ^{99}Tc, ^{237}Np, and ^{233}U were used in these experiments. In addition to batch sorption experiments conducted for all four radionuclides, desorption experiments were carried out for ^{233}U. Also, four column transport experiments were conducted using ^{237}Np, and three were conducted using ^{233}U. The ^{237}Np column experiments were carried out using water and alluvium from Borehole 19D. The flow rates in these experiments were varied to span a range of over one order of magnitude. The ^{233}U column experiments were conducted using different combinations of alluvium and water from the three Phase II wells, and all experiments were conducted at the same flow rate. Four scoping column transport experiments (not reported to the Technical Data Management System) were also conducted using ^{129}I and ^{99}Tc, but they are not presented in this appendix because they were conducted only to confirm the nonsorbing nature of these radionuclides that was observed in the batch experiments.

G3. EXPERIMENTAL RESULTS

G3.1 NEPTUNIUM BATCH SORPTION RESULTS FROM FIRST SET OF EXPERIMENTS

The alluvium samples used and their preparation methods for the first set of ^{237}Np batch sorption experiments are presented in Table G-1. The water compositions used in the experiments are shown in Table G-2. The results of ^{129}I and ^{99}Tc batch sorption experiments are not presented here because they indicated no significant sorption of either radionuclide. The compositions of Boreholes NC-EWDP-03S and NC-EWDP-19D (1 and 2) water were similar. Groundwater from Borehole NC-EWDP-03S had a lower dissolved oxygen concentration, a lower Eh, and a higher organic carbon concentration than the Borehole 19D groundwater. Thus, groundwater from Borehole 3S is more reducing than groundwater from Borehole 19D. Because there is not a high degree of variability in the groundwater compositions in the alluvium south of Yucca Mountain, particularly with respect to expected sorption radionuclide sorption behavior, the 3S and 19D groundwaters are considered to adequately represent the groundwater compositions in the alluvial flow system.

Alluvium samples were characterized primarily by quantitative X-ray diffraction and N_2-Brunauer-Emmett-Teller surface area measurements (Table G-3). Samples selected for use in the batch sorption tests represented different boreholes, intervals, sieving methods, and particle sizes.

The mineralogy of the alluvium used in the experiments is summarized in Table G-3. The amount of organic carbon in the samples was negligible. Trace amounts of calcite and hematite were detected in some samples. Alluvium from Borehole NC-EWDP-03S contained a considerable amount of calcite. Dry sieved samples were used for all the experiments except for

a column experiment with material from Borehole NC-EWDP-19D. The sieving technique (wet versus dry) had only a minor effect on the mineral composition of the 75- to 500-μm fraction of the 19D sample.

Table G-1. Boreholes and Sample Preparation Methods

Borehole Location	Depth (ft BLS)	Sample Preparation Method	Particle Size Fraction (wt %)		
			75 to 2,000 μm	75 to 500 μm	< 75 μm
2D	395 to 400	A	—	59	41
2D	400 to 405	A	—	60	40
2D	405 to 410	A	—	56	44
2D	410 to 415	A	—	56	44
9S	145 to 150	A	—	66	34
9S	150 to 155	A	—	62	38
9S	155 to 160	A	—	61	39
9S	160 to 165	A	—	61	39
3S	60 to 65	A	—	54	46
3S	65 to 70	A	—	64	36
3S	70 to 75	A	—	59	41
3S	75 to 80	A	—	66	44
1X	390 to 395	B	40	39	21
1X	395 to 400	B	71	19	10
1X	400 to 405	B	33	45	22
1X	405 to 410	B	51	33	16
19D	405 to 425	A	ND	ND	ND
19D	405 to 425	C	100	0	0
19D	405 to 425	C	0	0	100

Source: Ding et al. 2003 [DIRS 164737)].

NOTES: A) Grind, crush, and dry sieve; B) Collect 75- to 2,000-μm particle materials by dry sieving without grinding or crushing, followed by process A; C) Collect 75- to 2,000-μm particle materials by dry sieving without grinding or crushing processes, follow with washing out the fine particles and collecting particle size range 75- to 2,000-μm materials by wet sieving.

BLS = below land surface; ND = not determined.

Table G-2. Borehole NC-EWDP-03S and NC-EWDP-19D Water Composition

Species	Concentration (mg/L)		
	3S (449 ft BLS)	19D1 (412 to 437 ft + 490 to 519 ft BLS)	19D2 (412 to 437 ft BLS)
Na^+	141	69.4	73.2
K^+	2.99	3.61	3.92
Li^+	0.26	0.087	0.081
Ca^{2+}	0.94 ± 0.01	7.59	7.70
Mg^{2+}	0.14	0.65	0.69
Mn^{2+}	< 0.002	0.0088	< 0.0001
$Fe^{2+/3+}$	0.02	0.09	< 0.01
Al^{3+}	0.34	0.05	0.002

Table G-2. Borehole NC-EWDP-03S and NC-EWDP-19D Water Composition (Continued)

Species	Concentration (mg/L)		
	3S (449 ft BLS)	19D1 (412 to 437 ft+ 490 to 519 ft BLS)	19D2 (412 to 437 ft BLS)
SiO_2	48.4	58.0	58.4
F^-	3.24	1.78	1.96
Cl^-	8.68	5.61	6.52
NO_3^-	0.28	4.18	4.84
SO_4^{2-}	50.0	23.0	23.8
HCO_3^-	261	168	146
CO_3^{2-}	ND	0	17.9
Alkalinity ($CaCO_3$)	193	ND	ND
PH	8.67	8.11	9.02
Eh (mv/SHE)[a]	190	ND	ND
Dissolved Oxygen	0.02	ND	ND
Total Organic Carbon	1.5	<0.6	0.67
Ionic strength (mol/kg)	0.007	0.004	0.005

Source: DTN: LA0705MD150304.001 [DIRS 181309].

[a] SHE is the reference electrode for reporting Eh data. $Eh(SHE)_{sample} = Eh(SHE)_{measured\ for\ sample} + [((285-2.0*(T-25))-Eh(SHE)_{measured\ for\ 7.0\ buffer}]$.

BLS=below land surface; ND=not determined; SHE=standard hydrogen electrode.

Table G-3. Mineral Abundance and Surface Areas for Selected Alluvium Samples Used in Neptunium Sorption Tests

Alluvium				Quantitative Mineral Abundance for Alluvium Samples (wt %)											Surface Area (m^2/g)	Sample Number
Sieve Method	Bore-hole	Depth (ft BLS)	PS (μm)	Smec-tite	Clino-ptilolite	Kao-linite	Mica	Tridy-mite	Cristo-balite	Quartz	Feld-spar	Calcite	Hema-tite	Total		
Dry	2D	410 to 415	75 to 500	2±1	4±1	1±1	trace	3±1	16±1	18±1	54±8	—	1±1	99±8	1.97	1
	9Sx	160 to 165	75 to 500	6±2	3±1	—	trace	1±1	18±1	14±1	58±8	—	Trace	100±8	2.80	2
	3S	75 to 80	75 to 500	1±1	13±1	1±1	1±1	—	10±1	17±1	53±8	4±1	—	100±8	3.67	3
	19D	405 to 425	75 to 500	5±2	7±1	1±1	Trace	3±1	13±1	20±2	52±8	Trace	Trace	101±9	7.60	4
	2D	410 to 415	<75	4±1	7±1	1±1	1±1	5±1	14±1	17±1	53±8	—	1±1	103±8	4.27	5
	2D	395 to 400	<75	10±3	13±1	1±1	Trace	4±1	13±1	11±1	47±7	1±1	Trace	100±8	5.55	6
	9S	155 to 160	<75	19±6	3±1	Trace	1±1	4±1	14±1	12±1	50±7	—	Trace	103±9	5.69	7
	3S	60 to 65	<75	7±2	13±1	2±1	1±1	1±1	11±1	12±1	44±7	9±1	Trace	100±8	11.94	8
Wet	19D	405 to 425	75 to 2,000	4±1	5±1	1±1	1±1	3±1	16±1	16±1	49±7	—	1±1	96±8	5.42	9
	19D	405 to 425	<75	48±14	6±1	1±1	1±1	2±1	5±1	8±1	29±4	1±1	—	101±15	73.65	10
	3S	65 to 70	<75	30±9	21±2	1±1	2±1	Trace	2±1	5±1	25±4	12±1	—	98±10	37.49	11

Sources: LA0401MD831322.001 [DIRS 180903], LA0401MD831322.002 [DIRS 180904], LA0401MD831322.003 [DIRS 180905], LA0412MD831341.001 [DIRS 180906].

NOTE: Surface area measurements were conducted using MONOSORB N_2-Brunauer-Emmett-Teller Single Point Surface Area Analyzer.

BLS = below land surface; PS = particle size; "—" = not detected; Trace = amount at less than 0.5 wt %.

G3.1.1 Kinetics of Np(V) Sorption onto Alluvium

Kinetic experiments, using the experimental conditions described in Table G-4, were conducted to examine the interaction of Np(V) and alluvium. The initial sorption kinetics were fast, as can be seen in Figure G-1. After one day of contact between solid and solution, the amount of Np(V) adsorbed onto alluvium changed little with time in all four tests. The effects of different waters and concentrations of Np(V) on the kinetic processes of reaction between Np(V) and alluvium were not systematically evaluated, but they appeared to be of less importance than the alluvium characteristics.

Table G-4. Experimental Conditions for Testing Kinetics of Np(V) Sorption to Alluvium

Test	Alluvium			Neptunium(V) Initial Concentration	Water Used
	Borehole	Depth (ft BLS)	Particle Size (μm)		
Test 1	2D	410 to 415	75 to 500	1×10^{-7} mol/L	NC-EWDP-3S
Test 2	9S	160 to 165	75 to 500	1×10^{-7} mol/L	NC-EWDP-3S
Test 3	3S	75 to 80	75 to 500	1×10^{-7} mol/L	NC-EWDP-3S
Test 4	19D	405 to 425	75 to 2,000	1×10^{-6} mol/L	NC-EWDP-19D1

BLS = below land surface.

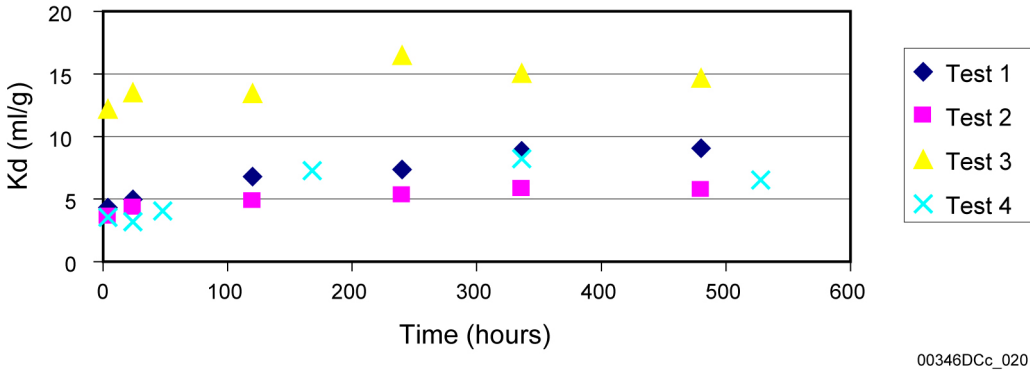

Sources: DTNs: LA0109MD831341.001 [DIRS 156870], Table S01139.002 ; LA0412MD831341.004 [DIRS 181078].

Figure G-1. Sorption Kinetics of ^{237}Np to Yucca Mountain Alluvium

G3.1.2 Range of K_d Values for Np(V)

The experimentally determined K_d values for all the alluvium samples listed in Table G-1 are presented in Figure G-2. The solid-solution contact period for these tests was two weeks. The water used for Borehole NC-EWDP-19D alluvium test was Borehole NC-EWDP-19D1 groundwater. The water used for all other experiments was Borehole NC-EWDP-3S groundwater. The results suggest that the K_d of Np(V) in alluvium differs from sample to sample and ranges from about 4 to 500 mL/g. The particle size of the sample appears to play an important role with respect to K_d value. In general, the smaller the particle size, the larger the K_d value. Alluvium samples from near the surface of Boreholes NC-EWDP-2D and NC-EWDP-3S boreholes have a large adsorption capacity for Np(V).

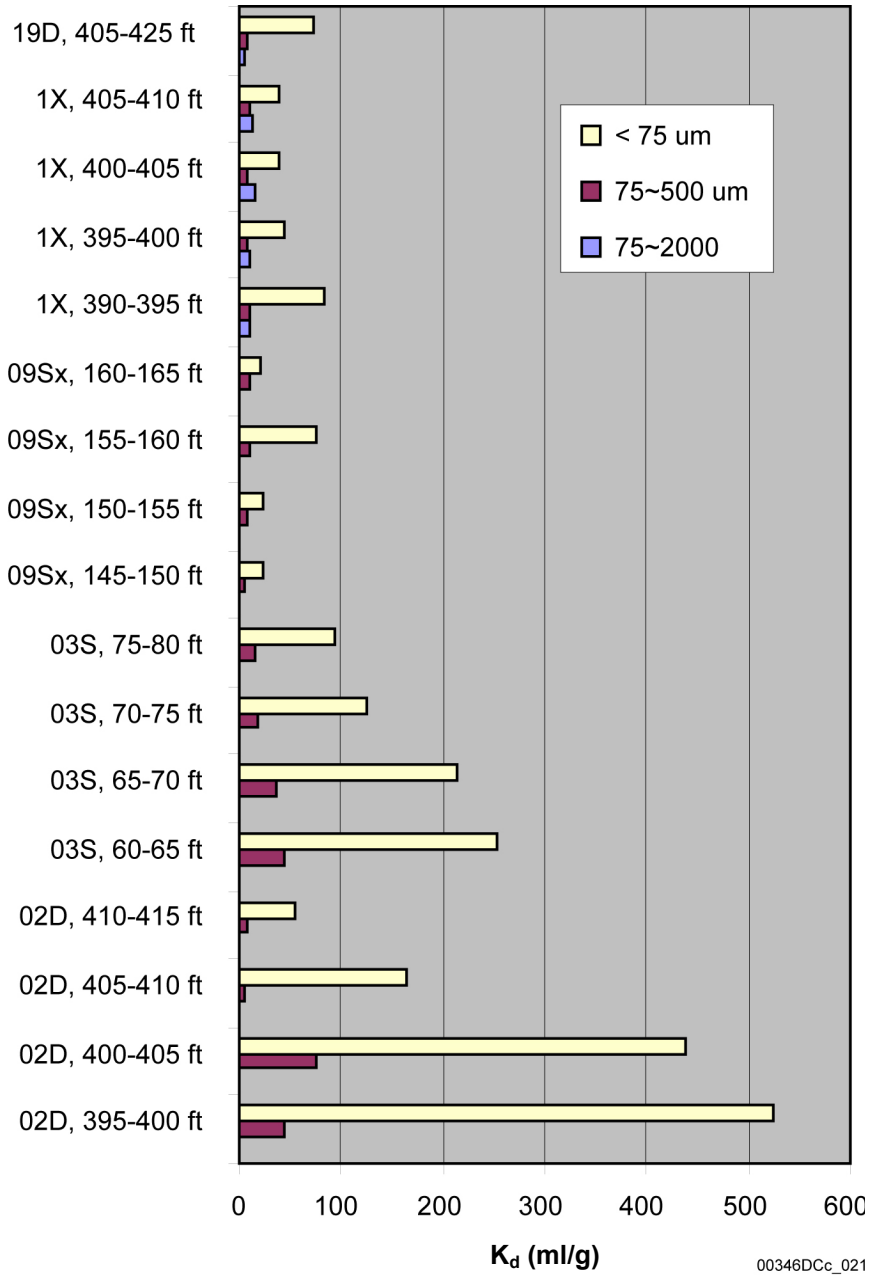

Source: DTN: LA0401MD831341.001 [DIRS 180906].

Figure G-2. Batch K_d Values for Np(V) in Different Intervals and Size Fractions

G3.1.3 Effect of Groundwater Chemistry on Np(V) K_d Values

Adsorption experiments were conducted using ^{237}Np with alluvium and groundwater from the same boreholes (NC-EWDP-03S and NC-EWDP-19D). The K_d values obtained for a given sample with the two different waters were similar (Figure G-3).

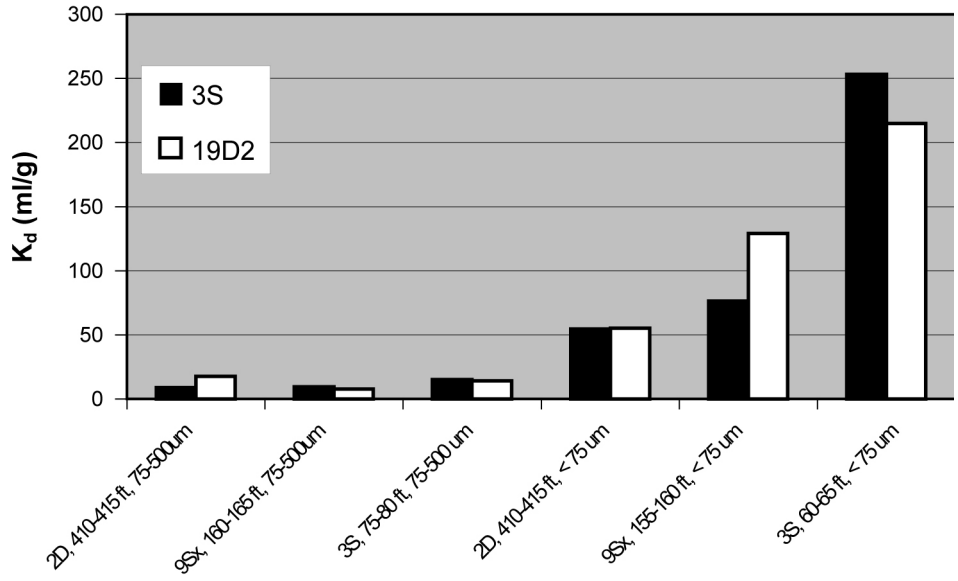

Sources: DTNs: LA0401MD831341.001 [DIRS 180906], LA0412MD831341.002 [DIRS 180908].

NOTE: The initial concentration of Np(V) was 1×10^{-6} M. The liquid to solid ratio for all experiments was 20 mL/g. The testing period was 2 weeks.

Figure G-3. Batch K_d Values for Np(V) in Waters from Boreholes NC-EWDP-3S and NC-EWDP-19D

G3.1.4 Effects of Ionic Strength on ^{237}Np K_d Values

The adsorption of ^{237}Np in alluvium from Borehole NC-EWDP-19D was examined under various ionic strengths. The original ionic strength of Borehole NC-EWDP-19D water was 0.004, but this was modified by adding NaCl. The K_d of ^{237}Np did not change significantly with increasing ionic strength (Figure G-4). These results suggest that the reaction mechanism is dominated by surface complexation rather than ion exchange. An additional experiment (not shown) indicated a much larger K_d value in deionized water than in the Borehole 19D water, suggesting a possible role of carbonate in suppressing neptunium sorption in the Borehole 19D water (carbonate was not present in significant quantities in the deionized water).

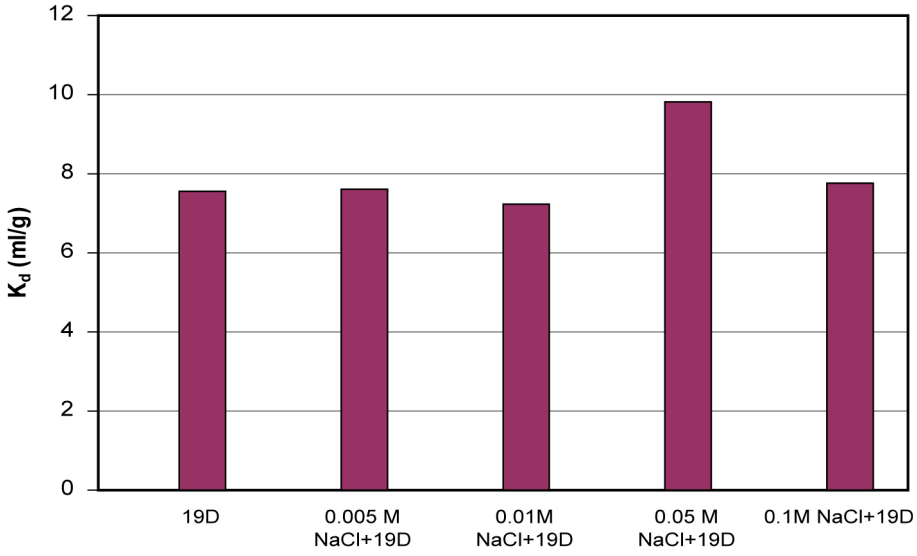

Source: DTN: LA0412MD831341.003 [DIRS 180911].
NOTE: Equilibration period is two weeks.

Figure G-4. Batch K_d Values for ^{237}Np in Solutions with Different Ionic Strengths

G3.1.5 ^{237}Np K_d Values in Relation to Surface Area and Secondary Mineral Content

Surface reactions (e.g., sorption) depend on the surface properties of the sorbent material (e.g., surface area). In general, the larger the surface area of the sample, the larger will be the K_d value obtained under the same experimental conditions. Clays and zeolites have larger surface areas than do minerals such as quartz and feldspar. Thus, alluvium containing more clay and zeolites would be expected to have larger K_d values.

Experiments were conducted to examine the relationships between surface area, the amount of secondary minerals (combined amounts of smectite and clinoptilolite), and the K_d values of ^{237}Np in alluvium. The results of these experiments are presented in Figure G-5.

Figure G-5 shows that the ^{237}Np K_d values were positively correlated with the amount of smectite and clinoptilolite in the samples and also with the surface area of the samples. However, two samples with extremely high K_d values did not have extremely high smectite and clinoptilolite contents, and they also did not have the highest surface areas. Thus, while neptunium sorption is positively correlated with surface area and mineralogy, trace amounts of minerals such as amorphous iron and manganese oxides, which were not identified by quantitative x-ray diffraction (XRD), may ultimately exert significant influence on neptunium K_d values in the alluvium. Studies of sorption of neptunium, plutonium, and americium onto the vitric tuffs of Busted Butte indicated that sorption increases with increasing levels of smectite, iron, and manganese oxides in the rock (Turin et al. 2002 [DIRS 164633]).

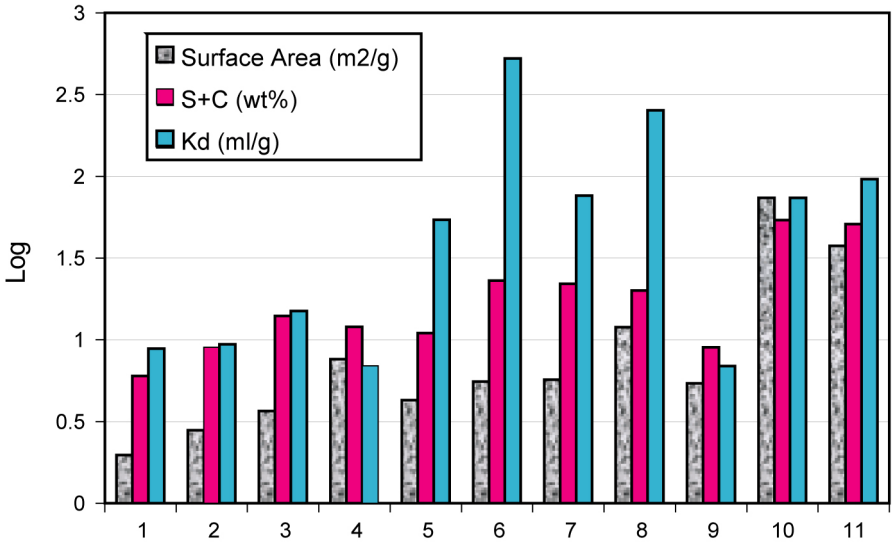

Sources: DTNs: LA0401MD831322.001 [DIRS 180903], LA0401MD831322.002 [DIRS 180904]], LA0401MD831322.003 [DIRS 180905], LA0412MD831341.001 [DIRS 180906], LA0412MD831341.001 [DIRS 180906].

NOTE: Surface area units = m^2/g, S = smectite (wt %); C = clinoptilolite (wt %), K_d units = mL/g. The Y axis represents the log-values of the three variables as shown in the legend of graph. The X-axis represents the Sample Identification Numbers reported in the last column of Table G-3.

Figure G-5. Surface Area, Combined Smectite and Clinoptilolite, and K_d Values for Np(V)

G3.2 NEPTUNIUM AND URANIUM RESULTS FROM SECOND SET OF SORPTION AND DESORPTION EXPERIMENTS

The alluvium samples used in the second set of batch sorption experiments were dry sieved for most experiments. Groundwater used in the experiments was obtained from Boreholes NC-EWDP-19D (Zones 1 and 4) and NC-EWDP-10SA. The chemical composition of Borehole NC-EWDP-19D waters is summarized in Table G-5.

The mineralogy of the alluvium used in the experiments was determined by quantitative XRD (Table G-6). The major phases in the alluvium samples are silica (i.e., quartz, tridymite, cristobalite), K-feldspar, and plagioclase. The amount of smectite and clinoptilolite in the alluvium differs for the different samples. Among these samples, the sum of the smectite and clinoptilolite in Borehole NC-EWDP-22SA is larger than in NC-EWDP-19IM1A or NC-EWDP-10SA.

G.3.2.1 Batch K_d Values for ^{129}I, ^{99}Tc, ^{233}U, and ^{237}Np in Alluvium

Under ambient conditions, measured K_d values were not statistically distinguishable from zero for ^{129}I and ^{99}Tc sorption onto the alluvium, and the reproducibility of the K_d measurements was poor (Figure G-6). These results are consistent with earlier results for these two radionuclides in experiments involving alluvium and groundwater from the Phase I Nye County wells.

Table G-5. Chemical Composition of NC-EWDP-19D Waters

Species	Concentration (mg/L) in Zone 1	Concentration (mg/L) in Zone 4
pH	8.3	8.9
Na^+	79	107
K^+	3.6	3.4
Ca^{2+}	5.9	0.96
Mg^{2+}	0.56	0.035
SiO_2	59	60
F^-	1.8	2.4
Cl^-	6.3	5.8
SO_4^{2-}	23	18
HCO_3^-	190	211

Source: DTN: GS011108312322.006 [DIRS 162911].

NOTE: pH and Eh were measured in the laboratory under the conditions of the batch sorption and column transport experiments.

Table G-6. Quantitative X-ray Diffraction Results of Alluvium Used in Second Set of Experiments

	Samples (75 to 500 μm fraction, dry sieve)					
	NC-EWDP-19IM1A		NC-EWDP-10SA		NC-EWDP-22SA	
Minerals	725 to 730[a, b]	785 to 790	665 to 670[b]	695 to 700	522 to 525[b]	660 to 665
Smectite	6.9[b]	6.2	5.7[b]	2.6	8.3[b]	4.7
Kaolinite	1.2	1.3	0.8	0.5	2.0	1.1
Clinoptilolite	7.7[b]	8.5	7.0[b]	4.1	14.3[b]	7.9
Tridymite	7.6	7.9	3.5	2.3	8.5	10.2
Cristobalite	5.8	6.4	7.0	5.9	5.6	7.2
Quartz	19.2	16.1	14.0	6.0	12.8	17.3
K-Feldspar	23.7	25.8	29.7	32.5	22.7	25.0
Plagioclase	25.0	26.5	30.5	40.7	19.1	21.2
Biotite	1.0	3.0	3.1	2.5	2.4	2.1
Hematite	0.7	0.7	0.8	2.4	1.0	2.5
Total	98.8	102.3	102.3	99.6	96.7	99.2

Source: DTN: LA0401MD831322.002 [DIRS 180904].

[a]Interval below land surface (feet).

[b]Samples selected to conduct kinetic adsorption of ^{233}U.

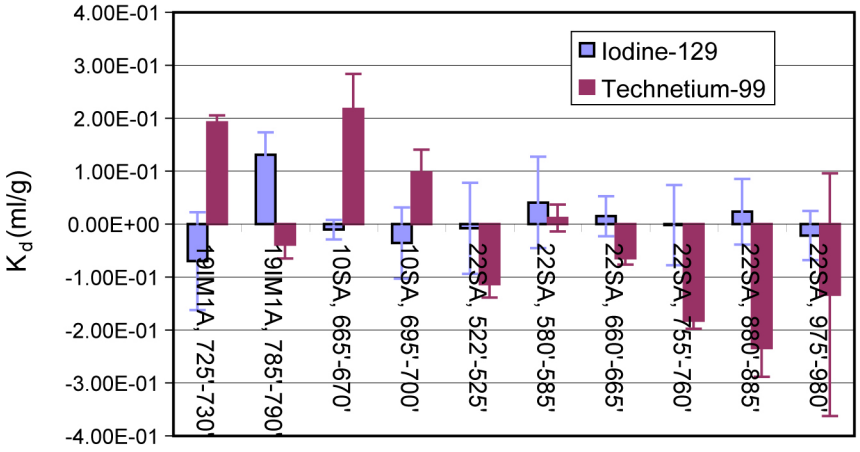

Sources: DTNs: LA0302MD831341.001 [DIRS 164956]; LA0302MD831341.002 [DIRS 164957].

NOTE: Experiments terminated after two weeks. Liquid to solid ratio (L/S) of the experiments is 20 mL/g. Borehole NC-EWDP-19D Zone 1 water was used for the experiments with alluvium from Boreholes NC-EWDP-19IM1A and NC-EWDP-22SA, and Borehole NC-EWDP-10 S water was used for the experiments with alluvium from Borehole NC-EWDP-10SA. Data for particle sizes from 75 to 500 μm are plotted.

Figure G-6. Batch K_d Values for ^{129}I and ^{99}Tc in Alluvium

The K_d values of ^{237}Np and ^{233}U in the alluvium were found to differ from sample to sample depending on the depths and types of the alluvium tested (Figure G-7). The K_d values range between 3 and 13 mL/g for ^{237}Np and about 3 to 9 mL/g for ^{233}U. The sorption capacity of alluvium for ^{237}Np is larger than that for ^{233}U. Unlike K_d measurements for ^{129}I and ^{99}Tc, the reproducibility of ^{237}Np and ^{233}U sorption measurements was good.

To test if ^{233}U sorption is a function of water composition, adsorption experiments were performed with ^{233}U using water from Borehole NC-EWDP-19D Zones 1 and 4. The K_d values of ^{233}U measured in Zone 4 water were lower than those for Zone 1 (Figure G-8).

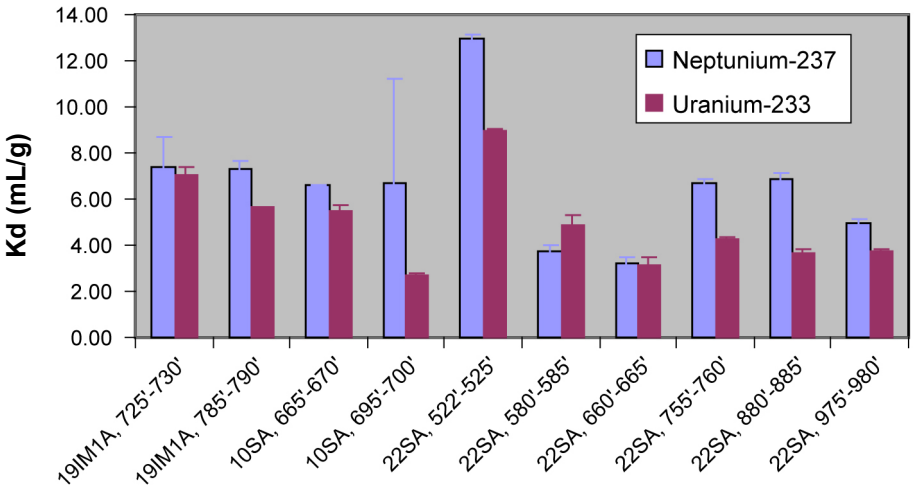

Sources: DTNs: LA0302MD831341.003 [DIRS 163784], LA0302MD831341.004 [DIRS 163785].

NOTE: L/S = 20 mL/g. NC-EWDP-19D Zone 1 water was used for the experiments with alluvium from NC-EWDP-19IM1A and NC-EWDP-22SA, and NC-EWDP-10S water was used for the experiments with alluvium from NC-EWDP-10SA. Data for particle sizes from 75 to 500 μm are plotted.

Figure G-7. K_d Values for ^{237}Np and ^{233}U in Alluvium

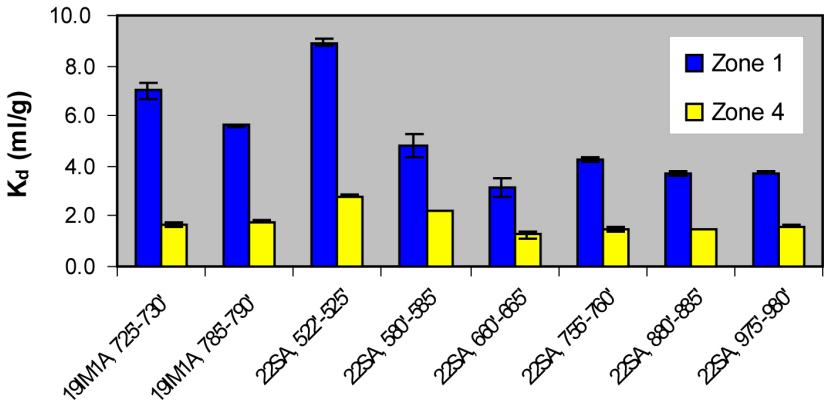

Sources: DTNs: LA0302MD831341.004 [DIRS 163785], LA0408MD831341.001 [DIRS 180913].

NOTE: Experiments terminated after two weeks. Liquid to solid ratio (L/S) of the experiments was 20 mL/g. Data for particle sizes from 75 to 500 μm are plotted.

Figure G-8. Batch K_d Values for ^{233}U in NC-EWDP-19D Zone 1 and Zone 4 Waters

G3.2.2 Uranium Sorption and Desorption Kinetics in Alluvium

Sorption kinetics of ^{233}U was measured in three alluvium samples (composition of these samples is shown in Table G-6). After one day of exposure, the amount of ^{233}U adsorbed onto alluvium changed little during the remainder of the tests. Thus, the equilibration rate for the uranium sorption reaction is relatively fast (Figure G-9). Higher K_d values from the NC-EWDP-22SA sample may be the result of higher smectite and clinoptilolite content (composition of these samples is shown in Table G-6).

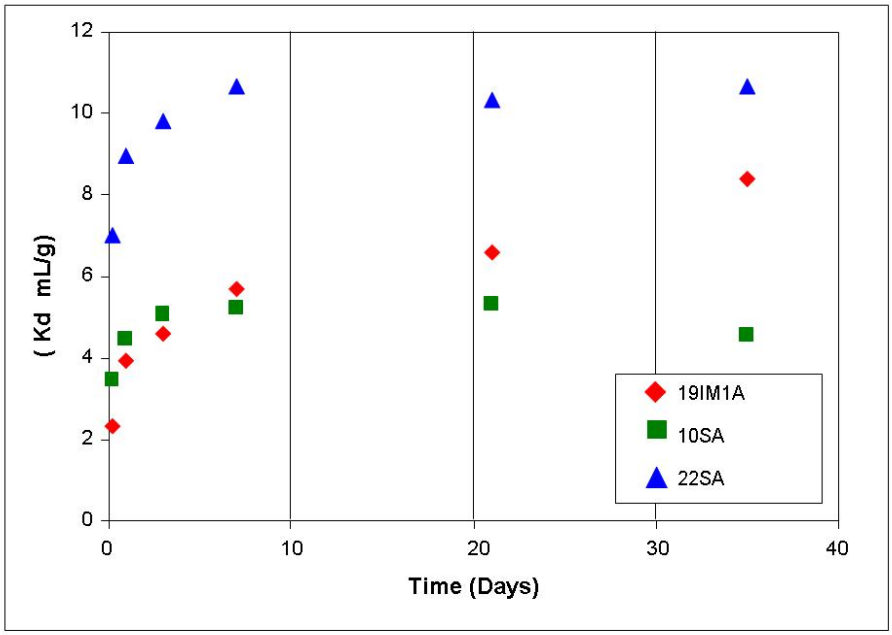

Source: DTNs: LA0408MD831341.002 [DIRS 180727], LA0408MD831341.003 [DIRS 180728], LA0408MD831341.004 [DIRS 180729].

NOTE: Experiments terminated after two weeks. Liquid to solid ratio (L/S) of the experiments is 20 mL/g. NC-EWDP-19D Zone 1 water was used for the experiments with alluvium from NC-EWDP-19IM1A and NC-EWDP-22SA, and NC-EWDP-10S water was used for the experiments with alluvium from NC-EWDP-10SA.

Figure G-9. Batch K_d Values for ^{233}U onto Alluvium as a Function of Time

Multi-step batch desorption experiments of sorbed ^{233}U were conducted (Figure G-10). Most of the uranium desorbed from the alluvium samples was desorbed during the first step. Less uranium was desorbed in subsequent desorption steps. A large fraction (30% to 50%) of the sorbed ^{233}U remained sorbed on the solid phase even after three desorption steps. These results suggest that the ^{233}U desorption kinetics were relatively slow and that they were slowing down as the experiments progressed.

Continuous-flow ^{233}U desorption experiments were conducted after the end of some of the sorption experiments. The alluvium material containing sorbed ^{233}U was removed from the test tubes used in the batch experiments and placed in a small "column," where it was then subjected to a continuous flow of fresh water. The total duration of the experiment was about 5.5 days, including a ~2.5-day flow interruption just after 100 mL eluted. Thus there was approximately 36 hrs of flow at ~3 mL/hr before and after the flow interruption. The effluent from the column was analyzed for ^{233}U. The results showed that the release of sorbed ^{233}U slowed down after first 100 mL of groundwater had contacted the alluvium (Figure G-11), but release continued at a finite rate for the remainder of the experiment. As seen in Figure G-11, the fraction desorbed jumped after the flow interruption, indicating net desorption; net resorption would have resulted in a decrease in the fraction desorbed after the flow interruption.

The concentrations of eluted ^{233}U near the end of the experiment were very close to the detection limit for most of the time after the flow interruption. These results suggest that desorption of the sorbed ^{233}U was quite slow. Simple linear extrapolation of the trends at the end of the

experiments suggests that the total desorption after 15 more days of flow (bringing the experiment duration up to 3 weeks) would have been comparable to or slightly larger than the total desorption measured after three weeks in the multistep batch desorption experiments shown in Figure G-10.

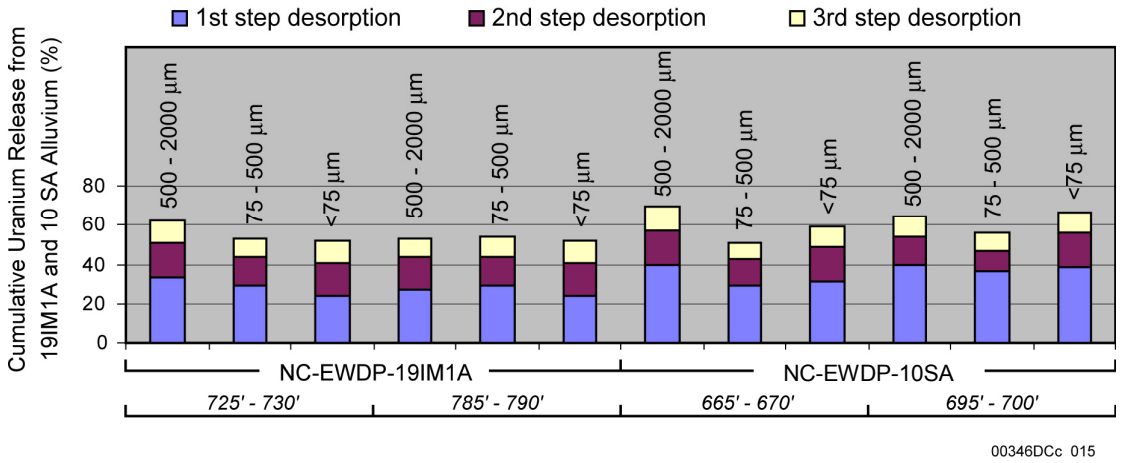

Source: DTN: LA0408MD831341.005 [DIRS 180917].

NOTE: The period for each desorption step was one week. L/S ratio for desorption is about 20 mL/g.

Figure G-10. Cumulative Release of Sorbed ^{233}U from NC-EWDP-19IM1A and NC-EWDP-10SA Alluvium

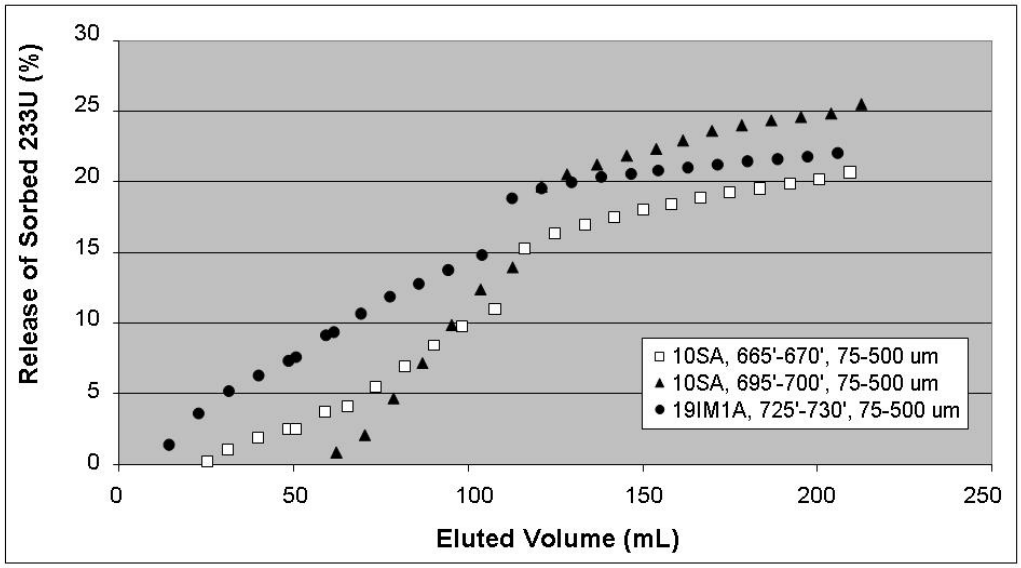

Source: DTN: LA0410MD831341.006 [DIRS 182089].

NOTE: The flow rate is 3 mL/h. NC-EWDP-19D Zone 1 water was used for NC-EWDP-19IM1A sample, 10 S water was used for NC-EWDP-10SA samples.

Figure G-11. Release of Sorbed ^{233}U as a Function of Eluted Volume of Groundwater

G4. COLUMN TRANSPORT EXPERIMENTS

G4.1 NEPTUNIUM COLUMN TRANSPORT EXPERIMENTS

Two sets of column experiments were performed to investigate Np(V) transport behavior in saturated alluvium under flowing conditions. Tables G-7 and G-8 list individually the columns used and conditions in the two studies. In all the column experiments, tritium (^{3}HHO) was used as a nonsorbing tracer. Water from NC-EWDP-03S was used in the experiments in columns 1 and 2, and water from NC-EWDP-19D was used in the experiments in columns 3, 4, and 5. The alluvium used to pack the columns was wet sieved in all cases to remove fine particles that would clog the columns. The latter set of experiments was reported by Ding et al. (2003 [DIRS 164737]).

Table G-7. Np(V) Column Study (I)

	Columns 1 and 2
Geologic Medium	Alluvium in Well NWDP-03S
Interval (ft. BLS)	65 to 70
Particle Size (μm)	75 to 500
Water Used	−03S
pH range	8.5 to 9.0
Diameter, cm	1.0
Length of column (cm)	60
Porosity in column	0.44 (Col. 1), 0.45 (Col. 2)
Flow rate (mL/h)	2 (reduced to 0.5 mL/h late in the test)

Source: DTN: LA0409MD831341.004 [DIRS 180925], LA0409MD831341.005 [DIRS 180926].
BLS=below land surface.

Table G-8. Np(V) Column Study (II)

	Column 3	**Column 4**	**Column 5**
Geologic Medium	Alluvium in Well NWDP-19D	Alluvium in Well NWDP-19D	Alluvium in Well NWDP-19D
Interval (ft. BLS)	405 to 425	405 to 425	405 to 425
Particle Size (μm)	75 to 2,000	75 to 2,000	75 to 2,000
Water Used	19D	19D	19D
pH range	8.4 to 8.7	8.4 to 8.7	8.4 to 8.7
Diameter, cm	2.5	2.5	2.5
Length of column (cm)	45	45	45
Porosity in column	0.38	0.37	0.34
Flow rate (mL/h)	10, 0.6 (2 tests)	3	10

Source: DTNs: LA0408MD831341.007 [DIRS 180927], LA0409MD831341.001 [DIRS 180928], LA0409MD831341.002 [DIRS 180929], LA0409MD831341.003 [DIRS 180930].
BLS=below land surface.

Figure G-12 shows the breakthrough curves (BTCs) of neptunium from columns 1 and 2, and Figure G-13 shows the BTCs of neptunium from columns 3, 4, and 5. The reproducibility of the two identical experiments in columns 1 and 2 (Figure G-12) is quite good, particularly with

respect to the timing of the peak neptunium concentration and the general shape of the BTCs. It is interesting to note that the 2 mL/hr experiments in columns 1 and 2 and the 10 mL/hr experiment in column 3 each exhibited effective K_d values (associated with the peak neptunium concentration) that were 12 to 14 times lower than the batch K_d values measured on the same alluvium, and they also had comparable mean water residence times (~10.5 hr in columns 1 and 2, and ~8.5 hr in column 3). Furthermore, the effective K_d value associated with the peak neptunium concentration in the column 4 experiment, conducted at a flow rate of ~3 mL/hr and having a mean water residence time approximately 3.3 times longer than the 10 mL/hr experiment in column 3, was about a factor of 4 larger than the K_d value in the column 3 experiment but was still lower than batch K_d value by a factor of ~3. The 0.6 mL/hr experiment conducted in column 3 was not carried out long enough to detect neptunium breakthrough, and therefore it was not possible to estimate an effective K_d value in this experiment. However, the fact that there was no breakthrough at the elution volume corresponding to the peak concentration in the 3 mL/hr experiment indicates that the trend of increasing K_d values with experiment time scale was at least qualitatively preserved in the 0.6 mL/hr experiment. This apparent trend is revisited in Section G5.4.

The 10-mL/hr experiment in column 5 was intended to be a duplicate of the 10-mL/hr experiment in column 3, which was terminated prematurely because of equipment problems. However, this experiment had an abnormally high background alpha activity, which made it impossible to see the tailing behavior that occurred in the other experiments (and suppressed the peak concentration after background subtraction). The earlier breakthrough and peak concentration in this experiment relative to the 10-mL/hr experiment in column 3 may be related to the fact that column 5 had a significantly greater hydraulic conductivity (by about 35%) than column 3. This higher hydraulic conductivity suggests that there were fewer fine grains and, hence, less surface area and probably less clay and zeolite material in column 5 than in column 3 (despite the fact that the same alluvium material and same sieving method was used).

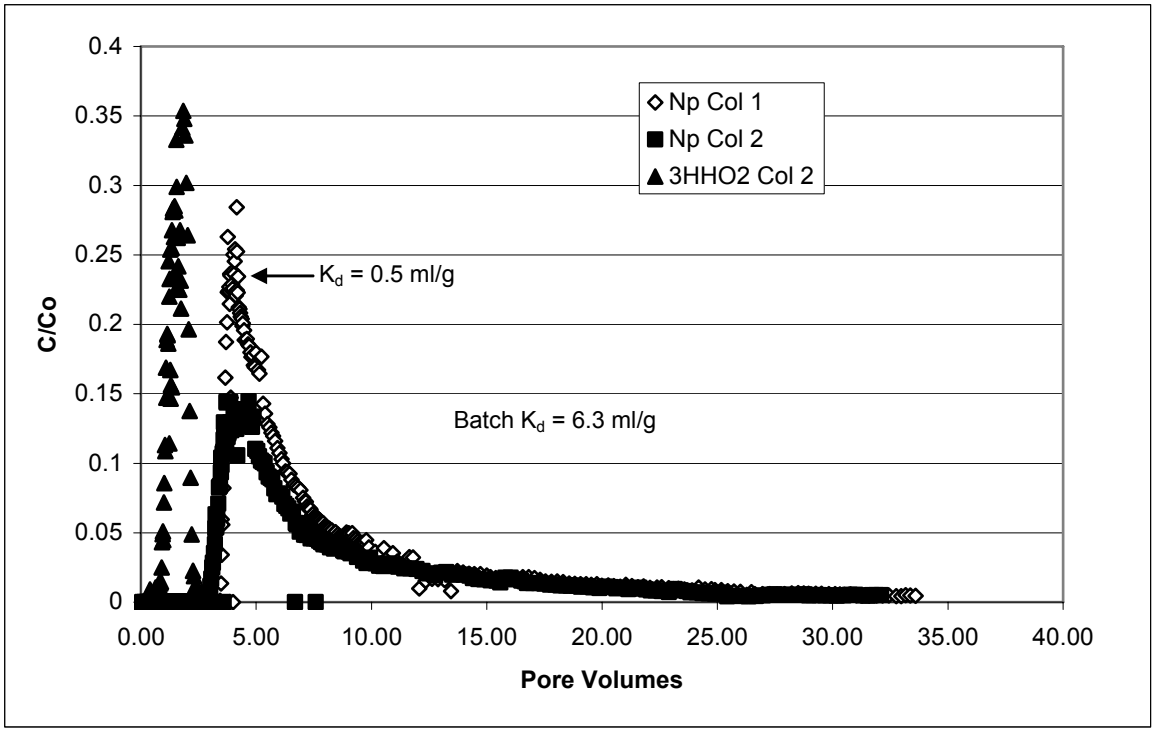

Source: DTNs: LA0409MD831341.004 [DIRS 180925], LA0409MD831341.005 [DIRS 180926].

Figure G-12. Tritiated Water and Neptunium Breakthrough Curves in Columns 1 and 2

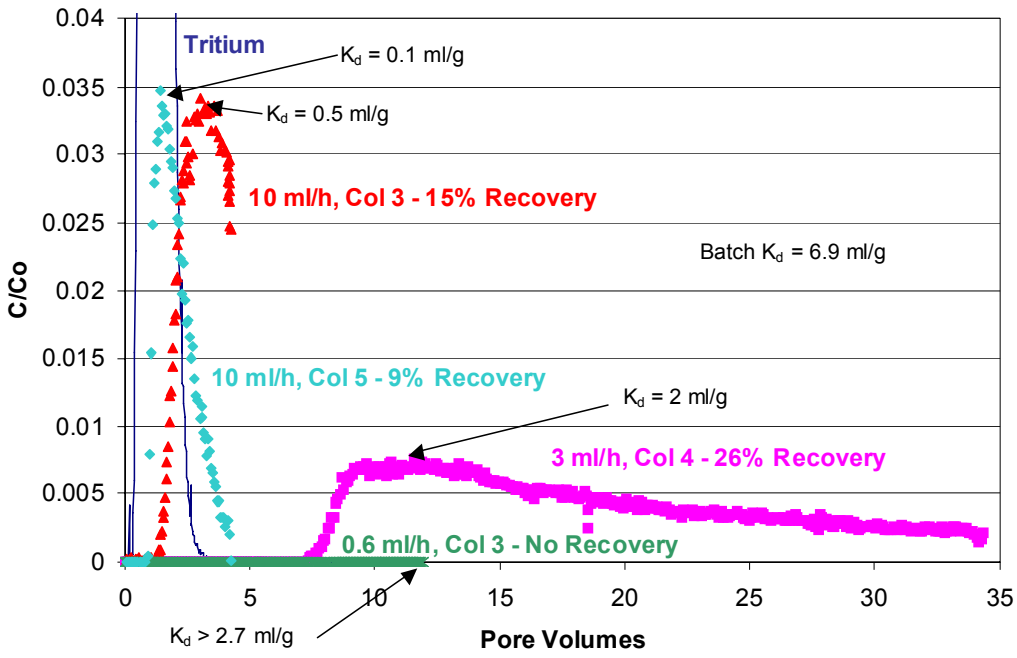

Source: DTNs: LA0408MD831341.007 [DIRS 180927], LA0409MD831341.001 [DIRS 180928], LA0409MD831341.002 [DIRS 180929], LA0409MD831341.003 [DIRS 180930].

NOTE: Column 5 had a significantly higher hydraulic conductivity than column 3, and the tail of the BTC was truncated because of an artificially high background concentration (which was subtracted from the measured concentrations).

Figure G-13. Neptunium Breakthrough Curves in Columns 3, 4, and 5

The 0.6-mL/hr experiment shown in Figure G-13 was conducted in column 3 after the 10-mL/hr experiment. The column was flushed until no more neptunium eluted prior to injecting the neptunium at a rate of 0.6 mL/hr. As Figure G-13 shows, there was no breakthrough of neptunium after ~12.5 pore volumes had been eluted in the 0.6-mL/hr test. The K_d value corresponding to a breakthrough at 12.5 pore volumes is approximately 2.7 mL/g for the column in which this test was conducted. Thus, all of the neptunium in the 0.6-mL/hr test had an effective K_d value of greater than 2.7 mL/g. This test is significant because the linear flow velocity in the column was 43 m/yr, which is in the range of estimates of linear flow velocities over all assumed flow porosities in the alluvial aquifer (9.9 to 77.1 m/yr) as given in *Saturated Zone In-Situ Testing* (SNL 2007 [DIRS 177394], Table 6.5.5).

Figure G-13 indicates that higher flow rates result in a lower effective K_d value for at least a portion of the neptunium traveling through the columns. However, despite the early breakthroughs in the experiments at the two higher flow rates, the recoveries of neptunium were still quite low (less than 40%), suggesting slow desorption rates for most of the neptunium in the columns. Furthermore, the long tails in these experiments suggest a wide range of desorption rates for neptunium. The minimum possible K_d value in the lowest flow rate column test (2.7 mL/g) agrees better with the batch studies (K_d = 6.9 mL/g) than the K_d values for the earliest arriving neptunium in the higher flow rate tests.

The observed differences in neptunium transport as a function of flow rate cannot be explained by a single rate-limited sorption reaction. It is likely that multiple reactions with multiple rates were occurring in the columns because of multiple sorption sites. An approach to modeling these experimental results is discussed later in this appendix. The column experiments reveal that reactive transport processes in heterogeneous alluvium, even at a relatively small scale, are quite complicated and not amenable to simple transport models, at least when flow velocities are high.

G4.2 URANIUM COLUMN TRANSPORT EXPERIMENTS

Continuous-flow column experiments involving ^{233}U were conducted at room temperature and under ambient conditions at an initial elution rate of 10 mL/hr. The elution rate was decreased first to 5 mL/hr and then very quickly to 3 mL/hr as the experiments progressed (DTN: LA0401MD831361.001 [DIRS 166696]). Experimental conditions are presented in Table G-9. The ^{233}U BTCs relative to ^{3}HHO are shown in Figure G-14. In all cases, a small fraction of the uranium broke through at almost the same time as the ^{3}HHO, but the vast majority of the uranium mass was significantly retarded. Total uranium recoveries ranged from 26% to 65% of the uranium injected. The long tails and incomplete recoveries observed in the column experiments indicate that some of the ^{233}U was slow to desorb from the columns within the time frame of the experiments. These experiments have not yet been quantitatively interpreted to obtain estimates of uranium sorption parameters, but the modeling approach discussed later in this appendix is capable of qualitatively explaining the observed behavior.

Table G-9. Uranium Column Experiments

	Column #1	**Column #2**	**Column #3**
Geological Medium	19IM1A	10SA	22SA
Interval (ft. BLS)	725 to 730	665 to 670	522 to 525
Particle Size (μm)	75 to 2,000	75 to 2,000	75 to 2,000
	Column #1	**Column #2**	**Column #3**
Water Used	19D Zone 1	10S	19D Zone 1
pH range	8.4 to 8.7	8.2 to 8.5	8.4 to 8.7
Diameter, cm	2.5	2.5	2.5
Dry alluvium packed in column (g)	374.61	356.59	390.72
Water weight after the saturation (g)	89.82	102.4	85.98
Porosity in column	0.41	0.44	0.39
Pore volume at which flow rate change to 5 ml/hr	2.2	1.8	2.3
Pore volume at which flow rate change to 3 ml/hr	2.7	2.3	2.9

Source: DTN: LA0401MD831361.001 [DIRS 166696].

NOTE: The length of columns 1, 2, and 3 are 45, 47, and 45 (cm), respectively. The flow rate for all three columns is 10 mL/h.

BLS=below land surface.

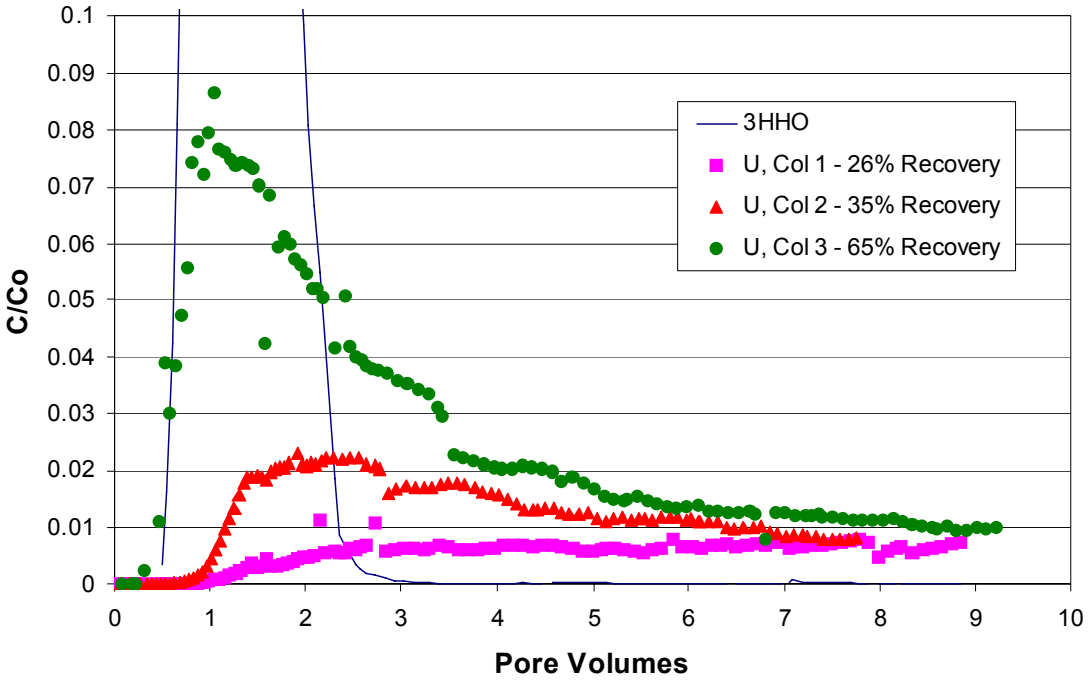

Source: DTN: LA0401MD831361.001 [DIRS 166696].

NOTE: The total recovery of ^{3}HHO was greater than 90% in all experiments. The flow rate was 10 mL/h. Table G-9 gives the pore volume values at which flow rate was changed for each column.

Figure G-14. ^{233}U Breakthrough Curves in the Three Alluvium Column Experiments

G5. ANALYSIS OF EARLY COLUMN BREAKTHROUGH BEHAVIOR OF ^{237}NP AND ^{233}U TRANSPORT AND FLOW-RATE DEPENDENCE OF ^{237}NP COLUMN TRANSPORT

The site-scale SZ transport model described in the body of this report uses the "local equilibrium approach" (Section 6, Table 6.6-1), treating the dissolved and sorbed solutes as being locally in equilibrium. The partitioning is taken to vary linearly with solution concentration and is described by a partition coefficient (the ratio of sorbed solute mass per unit mass of solid to solute concentration in solution at equilibrium), or K_d value, which can vary spatially in the flow system depending on the local rock type and groundwater chemistry. The local equilibrium approach results in a linear retardation factor (the ratio of radionuclide travel time to groundwater travel time) that is directly proportional to the K_d value. As discussed in Appendix A, the uncertainty and variability in K_d values due to uncertainty and variability in rock mineralogy, water chemistry, and other factors are accounted for in the site-scale SZ transport model through the use of K_d probability distributions that are based on experimental batch sorption data and equilibrium geochemical modeling.

The combination of the delay in first arrival time relative to a nonsorbing tracer and the long tails and incomplete recoveries of the responses shown in Figure G-14 are inconsistent with linear first-order adsorption and desorption kinetics. The dependencies of both the first and peak arrival times on flow rate or column residence time are also inconsistent with linear first-order kinetics. Figure G-15 shows a representative range of responses that are described by linear first-order adsorption and desorption kinetics. If the adsorption rate is slow enough relative to the flow rate through the column, some of the radionuclide mass will pass through the column with essentially no retardation because the residence time is insufficient for all the mass to sorb. The mass that does sorb gives rise to a long tail in the BTC. As the reaction rate or the residence time in the column increases, more of the mass sorbs, and eventually the BTC transitions to the classical retarded response associated with linear equilibrium sorption behavior. Slow kinetics broadens the peak of the response curve relative to fast kinetics, but after some critical residence time in the column is reached, the peak always occurs at the time corresponding to the peak associated with local equilibrium conditions.

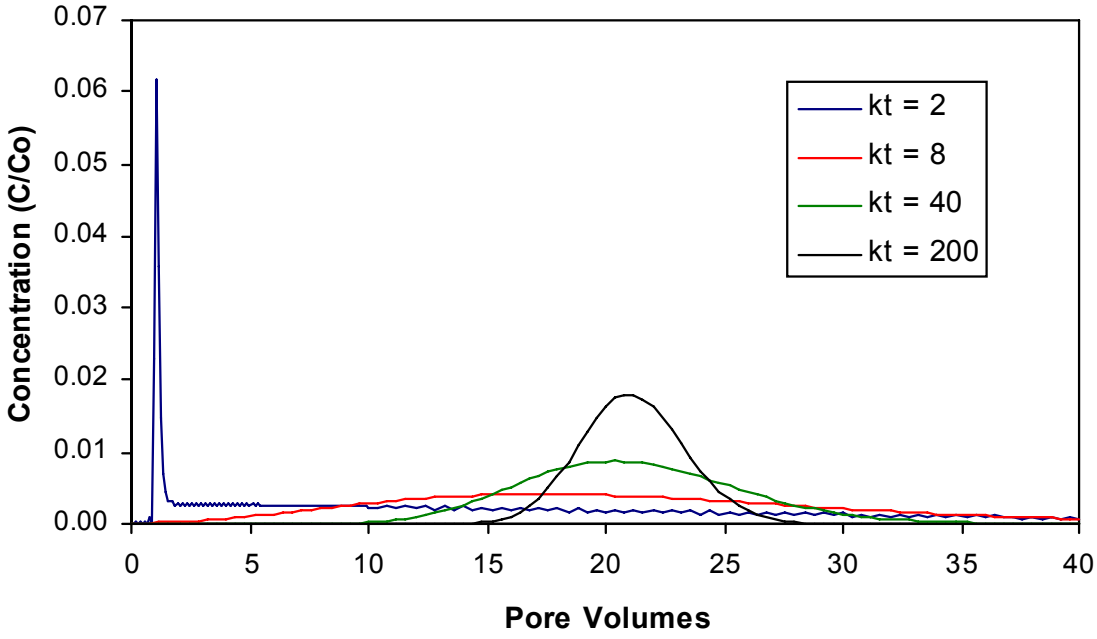

Source: DTN: LA0408PR831341.001 [DIRS 181187], *Kinetics_Relap*, tab Figure

NOTE: Breakthrough curves generated using RELAP (RELAP V2.0, STN: 10551-2.0-00) (LANL 2002 [DIRS 159065]). The retardation factor for all four cases is 21.

Figure G-15. Predicted Breakthrough Curves as a Function of the Product of Adsorption Rate Constant (k) and Nonsorbed Residence Time in the Column (t)

The initial portions of the responses in Figure G-15 look like classical delays due to equilibrium sorption behavior, but the low mass fractions associated with this early-arriving mass and the long tails are not consistent with equilibrium sorption. Some researchers have suggested using a hybrid equilibrium and slow kinetics approach that implicitly assumes two types of sorption sites: a weaker equilibrium sorption site that affects all the tracer mass (imposing a fixed delay on all the mass) and a stronger, but kinetically controlled sorption site that can significantly delay a substantial fraction of the tracer mass and result in a long tail. This type of analysis could

explain reasonably well any of the individual responses shown in Figure G-13, but it cannot explain the different responses as a function of residence time in the columns because a different equilibrium K_d value and different sorption and desorption rate constants are needed to explain each response. Multiple first-order linear adsorption and desorption reactions (with each successive reaction having a rate that approximately results in equilibrium sorption behavior at each successive column residence time) would likely improve the ability to match the responses of Figure G-13, but it would probably still be necessary to adjust the rate constants somewhat at each residence time. This adjustment is inherently unsatisfactory because one would expect all of the responses of Figure G-13 to be attributable to a single set of sorption characteristics given that the column material and water chemistry were the same in all the experiments.

G5.1 ADSORPTION RESIDENCE TIME DISTRIBUTION APPROACH

One approach to explaining the responses of Figure G-13 is to treat the sorption process as being the result of a *distribution* of residence times that solute molecules spend adsorbed to the immobile surfaces in the column. This approach is essentially equivalent to assuming that multiple adsorption sites of varying sorption strengths exist on the adsorbent. Even for pure crystalline minerals, one might expect a relatively broad distribution of adsorption residence times caused by edge, corner, or "hole" defect sites, or by element substitutions in crystal lattices. Different adsorption residence times might also be expected for "internal" versus "external" surface area in porous granular materials that are otherwise quite homogeneous. Thus, it seems quite reasonable to expect that the distribution of adsorption residence times (i.e., adsorption site strength) for a complex heterogeneous mixture of materials such as Yucca Mountain alluvium will be very broad.

Assuming a random spatial distribution of different adsorption sites, the sorption process can be simulated by randomly sampling the adsorption residence time distribution either each time a solute molecule collides with an immobile surface or, more practically, for every specified increment of time the solute spends in the solution phase in the column. Adsorption kinetics can be defined by specifying the number of times the distribution is sampled per unit time spent in solution and/or by specifying a distribution with a finite probability of near-zero residence times. For a given distribution, the adsorption kinetics will increase as the distribution is sampled more frequently per unit time spent in the solution phase. Similarly, for a given number of random samples of a distribution, the kinetics will increase as the probability of a near-zero residence time decreases for each sampling event.

These principles can be illustrated by considering a simple binary adsorption residence time distribution, such that there is a 50% probability that there will be no adsorption (zero adsorption time) and a 50% probability of an adsorption time of one time unit. Clearly, if this distribution is sampled twice per unit time increment spent in the solution phase in the column (i.e., nonsorbed time increment), the adsorption kinetics will be twice as fast as when the distribution is sampled only once per nonsorbed time increment. That is, only 25% of the solute mass will pass through the column without sorption if the distribution is sampled twice during transport through the column (0.5×0.5), while 50% of the mass will pass through without sorbing if the distribution is sampled only once during transport through the column. Furthermore, in the case of sampling the distribution twice, 25% of the solute mass will have an adsorption time of two time units and 50% will have an adsorption time of 1 time unit, while in the case of sampling the distribution

only once there will be no mass with an adsorption time of two time units and 50% with an adsorption time of one unit. The same results can be obtained by defining two different distributions that are each sampled only once per nonsorbed time increment in the column. For instance, consider another distribution given by residence time of 0.0 for probability less than 0.25, residence time of 1 for probability between 0.25 and 0.75, and residence time of 2 for probability greater than 0.75. This distribution yields the same results for a single random sample as two random samples of the first distribution. Thus, adsorption kinetics can be defined by both the number of random samples per unit nonsorbed time and/or by the shape of the distribution. Furthermore, it follows that for any given number of random samples of an adsorption time distribution, another distribution can be defined that yields the same kinetics after sampling the distribution either a *multiple* or a *divisible factor* of the number of times that the first distribution is sampled.

Another key point is that, for sufficiently long nonsorbed residence times in the column, the effective retardation factor will always be equal to one plus the ratio of the area under the adsorption distribution (in time units) to the nonsorbed residence time increment associated with each random sample of the distribution. For the first distribution described above, the retardation factor will be two if each random sample of the distribution is associated with one unit of nonsorbed residence time. On the other hand, if the distribution is sampled twice for each unit of nonsorbed residence time, the retardation factor will be three because the distribution will be sampled once for each *half unit* of nonsorbed residence time (i.e., 1 + 1/0.5). A retardation factor of three will also be obtained if the second distribution described above is sampled once for each unit of nonsorbed residence time because the area under the distribution is two time units (i.e., 1 + 2/1). The retardation factor increases linearly with the number of times a distribution is sampled per unit nonsorbed residence time and with the area under the distribution.

Batch sorption experiments, in principle, can also be simulated using this same adsorption residence time distribution approach. Given that the approach is based on associating a randomly sampled adsorption residence time with some number of collision events between solute molecules and adsorbent surfaces, the number of times a distribution is randomly sampled per unit of nonsorbed residence time should scale approximately with the collision frequency. The collision frequency, in turn, should scale with the adsorbent surface area to solution volume ratio in an experiment (assuming that all surface area is equally accessible and the temperature is approximately the same in all experiments). Thus, if a batch sorption experiment is conducted using a surface area to volume ratio of 1 cm^{-1}, and a column experiment is conducted using the same material, but with a surface area to volume ratio of 10 cm^{-1}, the adsorption time distribution corresponding to the material should be sampled 10 times more often per unit of nonsorbed residence time in the column experiment than in the batch experiment.

G5.2 ANALYSIS USING AN EXCEL SPREADSHEET

Three Excel spreadsheets were set up to simulate batch adsorption, batch desorption, and column transport experiments, respectively, using the adsorption residence time distribution approach. Briefly, these spreadsheets work as follows.

Batch Adsorption Spreadsheet–1,000 "particles" are assumed to represent all the solute mass in a batch sorption experiment. Each particle starts out in the solution phase. The time that each

particle spends in the solution phase is given by $t = -t_{ads}*\ln(P)$, where t_{ads} is the characteristic mean time spent in the solution phase between adsorption events and P is a random number generated from a uniform distribution having a minimum of 0 and a maximum of 1. These randomly sampled times approximate a first-order collision frequency with a collision rate constant of $1/t_{ads}$.

After each particle is "sorbed," another uniformly distributed random number between 0 and 1 is generated and substituted for P into the following empirically developed equation to determine the particle adsorption time:

$$t = A\left(10^{BP^C} + 10^{DP^E} - 1\right) \quad \text{(Eq. G-1)}$$

where, A, B, C, D, and E are user-adjustable parameters. This general form of the residence time distribution is used because it can be readily manipulated (by changing the values of A, B, C, D, and E) to simulate a wide range of possible adsorption/desorption behaviors, including behavior that is consistent with the column transport results of Figure G-13, as will be shown later.

Each particle alternates between the solution phase and the solid phase, with the solution and adsorption residence time distributions being alternately sampled. The fraction of particles sorbed at any given time is taken to be the fraction of solute mass sorbed at that time. The spreadsheet can be used to manually generate an adsorption kinetics curve by plotting the fraction of solute particles that are sorbed as a function of time.

Note that the adsorption process can be specified to have a maximum number of particles that are "strongly" sorbed in any given experiment. This limitation is accomplished by specifying a maximum number of particles that can have an adsorption residence time associated with a probability greater than a specified number. For instance, it can be specified that only 100 particles can be adsorbed at any given time with an adsorption residence time given by $P > 0.95$. When additional particles try to sorb after 100 particles already occupy these "strong" sorption sites, they sorb according to a modified distribution where the parameter (E in Equation G-1) is decreased by a specified amount.

Desorption Spreadsheet—The desorption spreadsheet requires the following information from the adsorption spreadsheet:

- The number of particles that are sorbed at the end of the adsorption experiment,
- The value of P (in Equation G-1) associated with each sorbed particle at the end of the sorption experiment, and
- The parameters A through E of Equation G-1.

This information is used to generate a desorption kinetics curve that gives the fraction of particles originally sorbed that become desorbed as a function of time after stopping the adsorption experiment. It is assumed that there is no "memory" of adsorption residence times between the adsorption and desorption phases; that is, if a particle has already spent x hours adsorbed during the adsorption experiment, the adsorption residence time in the desorption experiment is not decreased by x hours when the time associated with the P value is obtained

from Equation G-1. It is also assumed that there is no re-adsorption of desorbed particles – the spreadsheet simply calculates the amount of time each particle spends sorbed to surfaces before desorbing.

Column Transport Spreadsheet–Column transport is simulated as follows:

- 2,500 particles are used to represent the solute mass that transports through a column.
- The residence time for each particle in the solution phase is determined by randomly sampling a normal distribution that has mean given by the mean fluid residence time in the column and a standard deviation given by $\sqrt{2\tau^2/\mathrm{Pe}}$, where τ = mean fluid residence time in column, and Pe = Peclet number = L/α, where L = column length and α = longitudinal dispersivity.
- The user specifies the number of times the adsorption residence time distribution should be sampled during each particle's movement through the column assuming that the particle spends the mean amount of time in the solution phase. The spreadsheet adjusts the number of times the distribution is sampled (rounded to the nearest integer) based on the ratio of the actual particle residence time in the solution phase to the mean time. When applying the sorption behavior observed in a batch experiment to a column experiment, the "collision frequency" (the number of times the adsorption residence time distribution is sampled per unit time in the solution phase) in the batch experiment should be adjusted for the column experiment based on the ratio of the mass to volume ratios in the two experiments. The spreadsheet contains cells for calculating this conversion.
- Once the number of times to sample the adsorption residence time distribution is determined for each particle, the distribution is sampled that number of times (same process as in the batch adsorption spreadsheet), and the adsorption residence times are added to the solution phase residence time to determine the overall particle residence time in the column.
- The "breakthrough curve" for the solute in the column experiment is determined from the distribution of 2,500 particle residence times in the column.

The use of 1,000 particles for the sorption experiments and 2,500 particles for the column experiments in the Excel spreadsheets is less than optimal, particularly in the case of the column transport simulations, but the spreadsheet implementation of the above algorithms makes it impractical to exceed these numbers by much. Also, the column transport spreadsheet cannot accommodate more than 250 samplings of the adsorption residence time distribution for any given particle. These limitations could be eliminated by implementing the above algorithms in a computer software code (e.g., Fortran or C), but the spreadsheets are adequate for demonstrating and testing the approach and for qualitatively explaining the column transport results of Figure G-13.

G5.3 ANALYSIS OF BATCH EXPERIMENTS

Before addressing the column results, it is worthwhile to demonstrate the ability of the generalized adsorption residence time distribution approach to mimic first-order adsorption and desorption kinetics. Figure G-16 shows the adsorption residence time distribution that results from first-order desorption kinetics (an "inverse" exponential distribution) with a mean adsorption residence time of 5 hours (i.e., a desorption rate constant of 0.2 hr−1). Mathematically, this distribution is given by $t = -\ln(1-P)/k_{des}$, where t = adsorption time, P = probability (0 to 1, the dependent variable on the x-axis), and k_{des} is the desorption rate constant (hr^{-1}). Figure G-16 also approximates this residence time distribution using Equation G-1 with A = 0.001, B = 4.2, C = 0.265, D = 4.5, and E = 10 (Distribution 1).

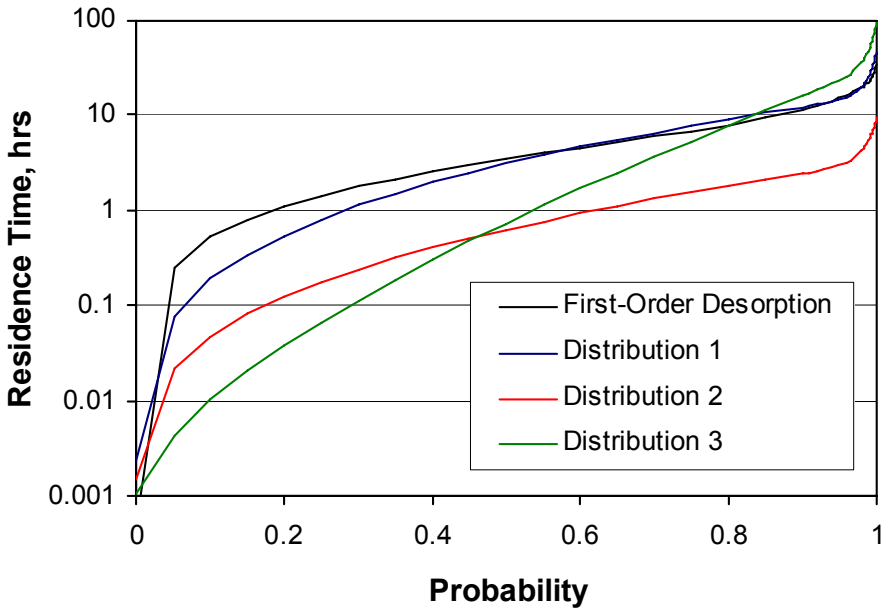

Source: DTN: LA0408PR831341.001 [DIRS 181187], *Desorption*, tab Desorption.

NOTE: Distribution 1 is an approximation of the first-order desorption distribution, distribution 2 is an approximation to a first-order desorption distribution with a rate constant of 1 hr^{-1}, and distribution 3 has the same area under the curve as distribution 1, but with an effective adsorption rate about 4 times lower.

Figure G-16. Adsorption Residence Time Distribution Corresponding to First-order Desorption with a Rate Constant of 0.2 hr^{-1}, and Three Distributions Defined by Equation G-1

Figure G-17 shows the predicted column transport behavior as a function of nonsorbed residence time in the column when Distribution 1 of Figure G-16 is sampled 4 times per hour of nonsorbed time (corresponding to an adsorption rate constant of 4 hr^{-1}). Breakthrough curves are shown for the same products of rate constant and nonsorbed residence time as in Figure G-15. It is apparent that the spreadsheet BTCs and the curves of Figure G-15 are in reasonably good agreement. The primary difference between the two sets of curves is that the unretarded solute mass associated with the kt = 2 curve (the early spike in concentration) is much lower in Figure G-17 than in Figure G-15. Also, the spreadsheet BTCs are much more jagged because they are generated from a relatively small number of particle residence times.

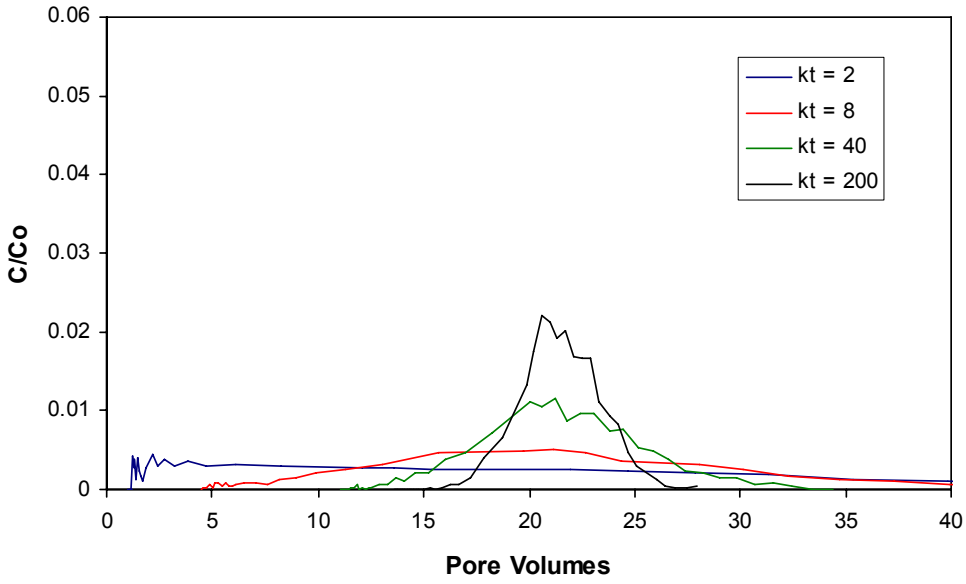

Source: DTN: LA0408PR831341.001 [DIRS 181187], *Column_Transport*, tab T0.5 5-5.

NOTE: The products of the adsorption rate constant and the nonsorbed residence time associated with each BTC are listed in the legend. These products are the same as those associated with the BTCs of Figure G-15.

Figure G-17. Breakthrough Curves Computed by Spreadsheet Analysis When Residence Time Distribution 1 from Figure G-16 is Sampled Four Times per Hour of Nonsorbed Residence Time in the Column

Another test of the spreadsheet's ability to simulate first-order adsorption and desorption kinetics is to determine whether it predicts the same BTCs when the nonsorbed residence time is changed but the product of the rate constant and nonsorbed residence time are kept the same (and the ratio of the adsorption and desorption rate constants are also kept the same). A higher adsorption rate was achieved by sampling the adsorption residence time distribution 5 times more frequently than in the slower case (20 times per hour). A higher desorption rate was achieved by changing the values of B, C, and D in Equation G-1 to 3.5, 0.32, and 3.8 (respectively), which lowered the distribution 1 curve in Figure G-16 such that the mean adsorption time was 1 hour instead of 5 hours but preserved the shape of the curve (i.e., distribution 2 in Figure G-16). Thus, both the adsorption and desorption rates were effectively increased by a factor of 5, resulting in no net change in their ratio. Figure G-18 shows that the BTCs for these two cases are in very good agreement when they are plotted as a function of pore volumes.

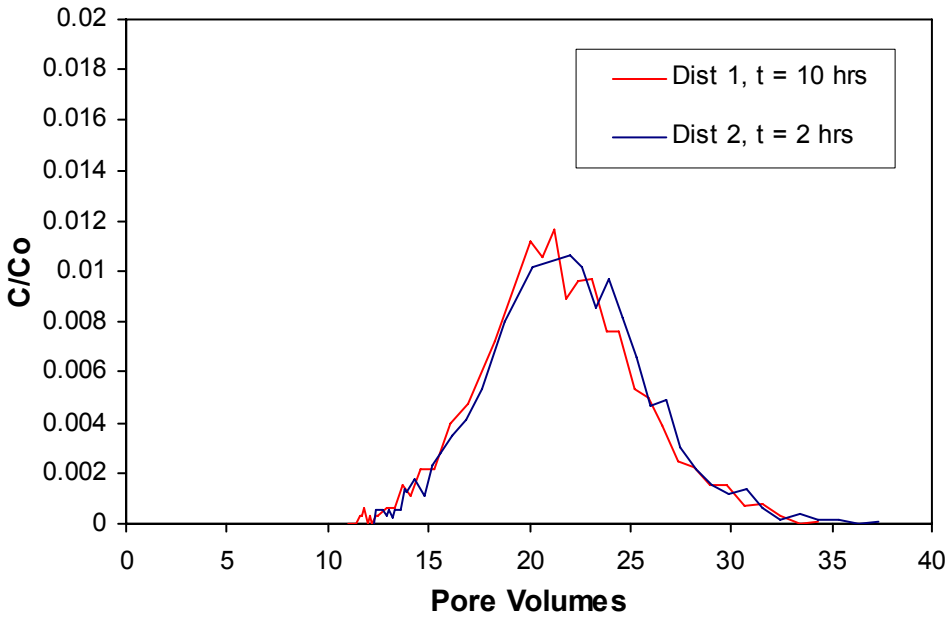

Source: DTN: LA0408PR831341.001 [DIRS 181187], *Column_Transport*, tab T 21-1.

Figure G-18. Breakthrough Curves Obtained by Sampling Distribution 2 Five Times More Frequently than Distribution 1 but with the Nonsorbed Residence Time in the Column Being Five Times Longer for Distribution 1

A final test of the column transport spreadsheet is to see if the same BTC can be obtained by altering the adsorption residence time distribution to have a lower probability of greater residence times while maintaining the same overall area under the curve and decreasing the column flow rate. Distribution 3 in Figure G-16 has the same area under the curve as distribution 1, but the probability associated with larger residence times is smaller, and the probability associated with shorter residence times is greater. This greater probability of shorter residence times is offset by having larger residence times at the high end of distribution 3 (to make the areas under the curves equal). From the above discussion, the net effect of a shift from distribution 1 to distribution 3 while maintaining the same distribution sampling frequency should be to decrease both the effective adsorption and desorption rates. Figure G-19 shows that, in fact, very similar column BTCs are obtained using distributions 1 and 3 with the same sampling frequency when the flow rate is about a factor of 4 greater for distribution 1 (indicating that the effective adsorption and desorption kinetics are about 4 times faster for distribution 1). The peaks occur at the same number of pore volumes because the areas under the two distributions are the same, and hence their effective retardation factors are the same.

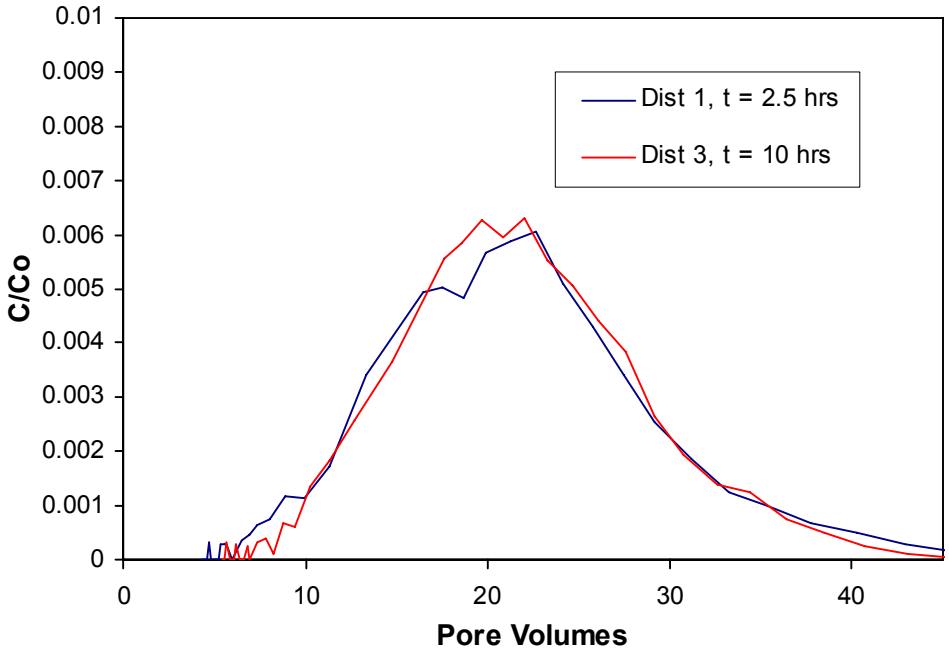

Source: DTN: LA0408PR831341.001 [DIRS 181187], *Column_Transport*, tab T2.5-5.

Figure G-19. Breakthrough Curves Obtained by Sampling Distribution 1 and Distribution 3 at the Same Frequency (four times per hour) with the Nonsorbed Residence Time in the Column Being Four Times Longer for Distribution 3

G5.4 QUALITATIVE SIMULATION OF EARLY COLUMN BREAKTHROUGH BEHAVIOR

An adsorption residence time distribution such as that shown in Figure G-20 can now be considered. This distribution was selected to yield adsorption and desorption rates that, when the distribution is sampled once every two hours of nonsorbed residence time, are qualitatively similar to those observed for uranium and neptunium in batch experiments. The shape of the distribution is motivated primarily by the uranium desorption data of Figure G-11, which do not exhibit first-order kinetic desorption behavior but rather indicate that a fraction of the sorbed uranium desorbs very rapidly while the remainder of the uranium desorbs much more slowly. Figure G-21 shows the adsorption rate curve associated with the distribution of Figure G-20, and Figure G-22 shows two desorption rate curves generated after two different time periods of adsorption. Clearly, desorption is predicted to be faster after a shorter adsorption time period, which can be attributed to the fact that there is less opportunity for solute molecules to come in contact with "strong" sorption sites during shorter adsorption times. This aspect of predicted desorption behavior has not been experimentally verified, but the analysis suggests that measuring desorption rates after different periods of adsorption might be a good strategy. Figures G-21 and G-22 are qualitatively similar to Figures G-9 and G-11.

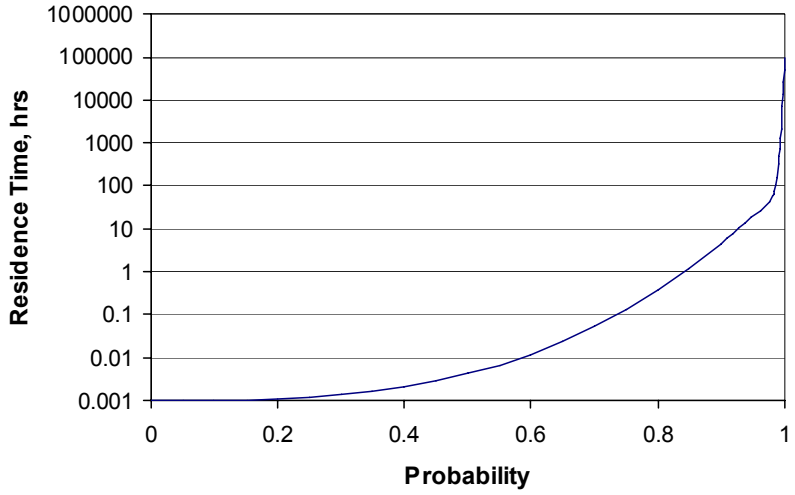

Source: DTN: LA0408PR831341.001 [DIRS 181187], *Desorption*, tab Desorption.

Figure G-20. Adsorption Residence Time Distribution That Has a Low Probability of Very Long Residence Times (i.e., a Small Fraction of Very Strong Adsorption Sites)

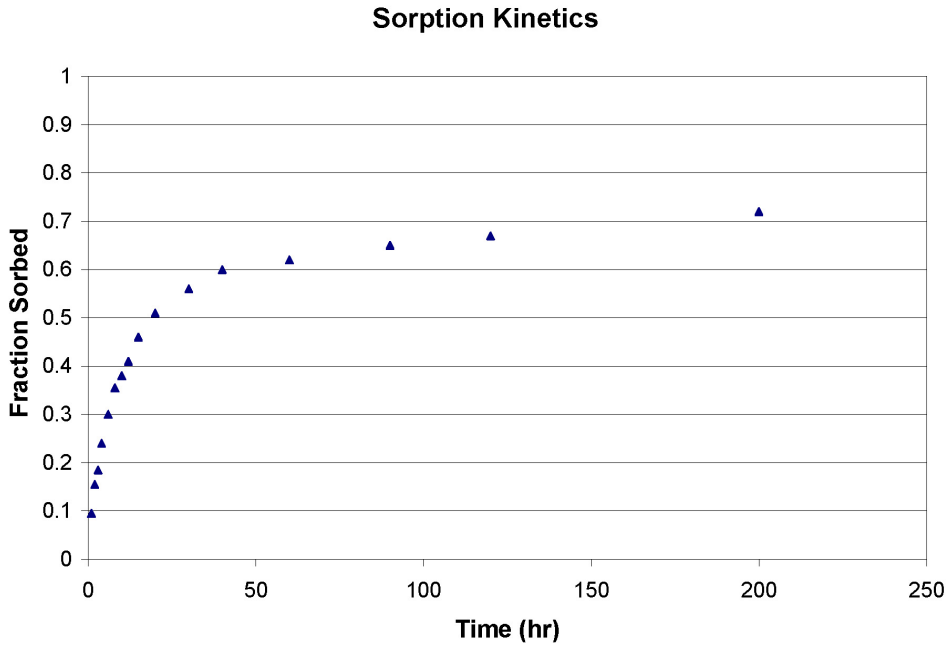

Source: DTN: LA0408PR831341.001 [DIRS 181187], *Desorption*, tab Tab 200 hrs SORP.

Figure G-21. Percent of Solute Sorbed as a Function of Time in a Simulated Batch Sorption Experiment Using the Adsorption Residence Time Distribution of Figure G-20 at a Sampling Frequency of Once Every 2 Hours

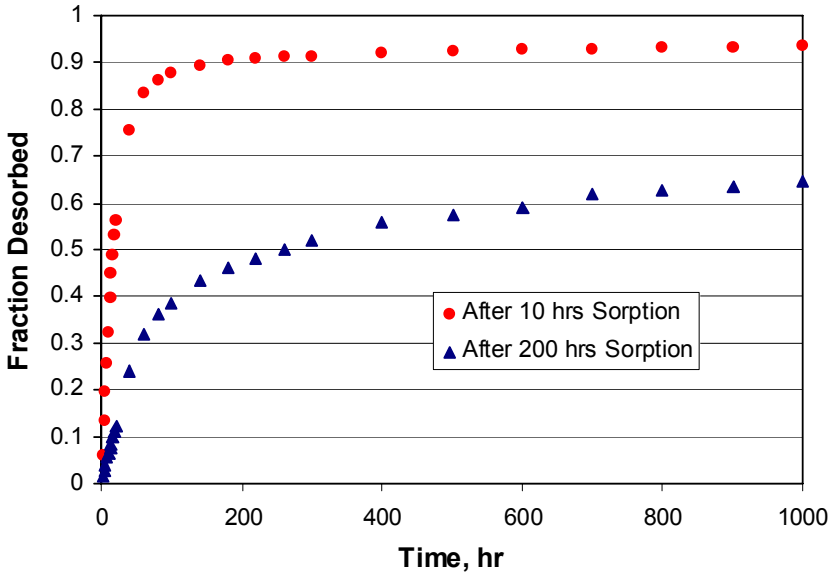

Source: DTN: LA0408PR831341.001 [DIRS 181187], *Desorption*, tab Tab 200 hrs SORP.

NOTE: Figure G-21 is the corresponding simulated adsorption experiment.

Figure G-22. Fraction of Solute Desorbed as a Function of Time in Simulated Desorption Experiments Initiated After 10 Hours and 200 Hours of Sorption, Respectively, Using the Adsorption Residence Time Distribution of Figure G-20

When the distribution of Figure G-20 is used in the simulation of column transport experiments, the BTCs of Figure G-23 are obtained at the three different relative flow rates listed in the figure as a function of pore volumes eluted. For these simulations, the adsorption time distribution was sampled 10 times for every hour of nonsorbed residence time in the column. This is an appropriate frequency given the surface area to volume ratios used in the batch and column experiments described earlier in this appendix and the sampling rate of once every two hours used to generate the batch adsorption curve of Figure G-21. The predicted column transport behavior shown in Figure G-23 compares favorably with the neptunium transport behavior shown in Figure G-13. The increasing delay in the first arrival time of neptunium and the decreasing fractional recovery as flow rates decrease can be attributed to the greater probability of encountering "strong" sorption sites (sites with long adsorption residence times) as the nonsorbed residence time in the column increases. In particular, the retardation factors (or effective K_d values) associated with the peak concentration of neptunium in Figure G-23 follow the same increasing trend with mean water residence time that was discussed in Section G4.1 and shown in Figure G-13. Although the experimental BTCs have somewhat sharper leading fronts at the lower flow rates than the curves estimated from the analysis, the shapes of the curves in Figures G-23 and G-13 are qualitatively quite similar. This qualitative agreement between analysis and experiment could probably be improved by employing a more rigorous fitting exercise.

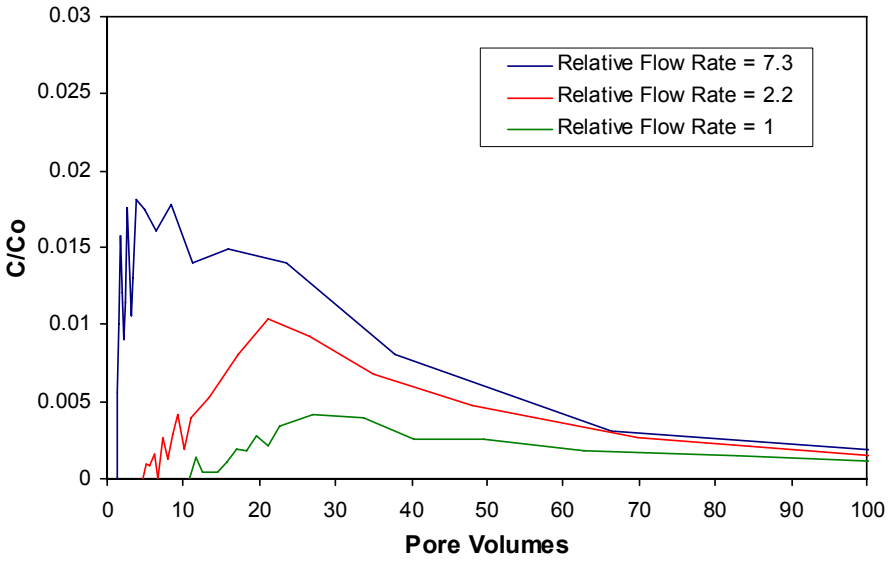

Source: DTN: LA0408PR831341.001 [DIRS 181187], *Column_Transport*, tab Tau 22.

NOTE: Simulated fractional recoveries are 0.55, 0.36, and 0.17 for the three BTCs at 100 pore volumes. These BTCs are qualitatively comparable to those for neptunium in Figure G-13.

Figure G-23. Simulated Breakthrough Curves as a Function of Relative Flow Rate for a Solute with an Adsorption Residence Time Distribution Given by Figure G-20

In conclusion, the generalized adsorption residence time approach is consistent with the column transport behavior of Figure G-13 (as well as Figures G-12 and G-14) as well as with the batch sorption and, particularly, the desorption experimental results that have been obtained for uranium and neptunium on Yucca Mountain alluvium. A wide range of adsorption residence times, with a small fraction of very large residence times, is necessary to obtain this agreement with experimental results, but such a distribution seems quite reasonable given the heterogeneous nature of the alluvium used in the batch and column transport experiments. The approach is very flexible in that it can be made entirely consistent with a more-traditional first-order sorption kinetics while offering the ability to describe much more complex adsorption and desorption behavior such as that observed experimentally for neptunium and uranium.

G6. IMPLICATIONS FOR SATURATED ZONE RADIONUCLIDE TRANSPORT

The adsorption residence time distribution analysis approach for radionuclide transport in the SZ near Yucca Mountain has very favorable implications for TSPA. The approach provides a reasonable explanation for why early breakthroughs sometimes occur in laboratory column experiments (i.e., the residence time is insufficient for all the radionuclide mass to come in contact with strong sorption sites). According to this approach, radionuclide solute retardation over long time and distance scales in the field should always be greater than in shorter-duration laboratory column experiments. Furthermore, this analysis suggests that the use of the local equilibrium approach in the SZ radionuclide transport model with K_d distributions derived from laboratory batch sorption experiments should provide reasonable transport predictions in the SZ because both the predicted and observed effective K_d values in the laboratory column experiments increase and approach batch K_d values as mean water residence times increase. In

fact, the analysis and data suggest that the use of batch K_d values in transport predictions could ultimately result in underprediction of radionuclide retardation in the SZ because of the implied existence of very strong sorption sites with very slow desorption rates that are not effectively interrogated in batch sorption experiments.

APPENDIX H
QUALIFICATION OF SORPTION DATA

H1. QUALIFICATION OF SORPTION DATA

The qualification of DTNs: LA0305AM831341.001 [DIRS 163789] and LA0310AM831341.001 [DIRS 165865] is documented here in accordance with SCI-PRO-001, *Qualification of Unqualified Data*. This qualification provides a desired level of confidence that the data are suitable for their intended use, which is limited to the subject of this work product (SZ radionuclide transport) for use in total system performance assessment (TSPA). The qualification is based on corroboration of data and technical assessment. The plan for the qualification of this data is presented at the end of this appendix.

H1.1 CORROBORATING DATA

One important aspect of the data qualification process is corroboration of unqualified data with qualified data. If it can be shown that unqualified sorption coefficient experiments on a given water/rock combination and under a specified set of experimental parameters produced sorption coefficient data that are equivalent to data obtained under a qualified quality assurance (QA) program using a similar set of rock/water combinations and experimental parameters, the concordance of the two data sets can be used to support the qualification of the unqualified data set.

Sorption coefficients are subject to a range of factors including some associated with the solid phase, some associated with the liquid phase (groundwater or pore water), and some associated with the element-of-interest. The two main factors associated with the solid phase include mineralogy and surface area. Mineralogy includes mineral type and mineral composition, particularly for minerals that sorb primarily by ion exchange. The factors in the liquid phase that can influence sorption behavior are different for different elements-of-interest. For example, for alkali and alkaline earth elements of interest (i.e., barium, cesium, strontium, and radium), the concentrations of alkali and alkali earth elements in solution (e.g., calcium, phosphorus, sodium, and magnesium) are important factors. For an element such as uranium, pH, and alkalinity are important factors. Factors associated with the element-of-interest include concentration in solution and complexation behavior.

In comparing an unqualified dataset with a qualified dataset for a given element-of-interest, it is important that the factors that can control sorption behavior are at the same or similar values in both datasets unless it can be shown that a given factor does not control sorption behavior for the element-of-interest.

Two examples are cited of comparisons of qualified and unqualified datasets for elements-of-interest, the first is barium representing radionuclides that sorb by ion exchange and the second is uranium representing radionuclides that sorb by surface complexation. The first example is for barium sorption coefficients on zeolitic tuff in J-13 well water. Qualified and unqualified data points for sorption coefficients and final solution concentrations are shown in Figure H-1. The same water composition was used in both the unqualified and the qualified experiments. Thus, differences in water composition are not an issue in comparisons of the two datasets. The differences in final solution concentrations did not influence the sorption coefficient ranges for the two datasets because the isotherms for barium sorption on zeolitic tuff in J-13 well water are essentially linear as shown in Figure A-34. Differences in experimental

duration did not influence the sorption coefficient ranges because the barium sorption reactions are fast, as discussed in Section A7.6.2. The fact that the ranges in sorption coefficient values are very similar for the two datasets provides confidence that the experimental procedures used to obtain the unqualified data were appropriate and equivalent to those used to obtain the qualified dataset.

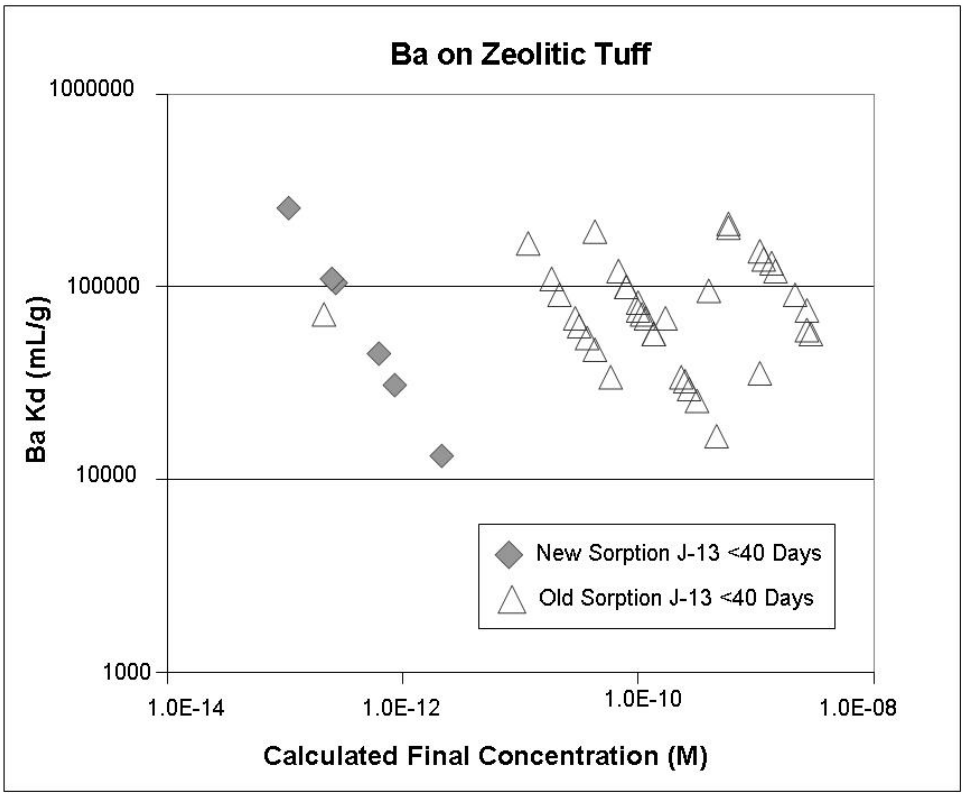

Source: DTNs: LA0305AM831341.001 [DIRS 163789]; LA0407AM831341.001 [DIRS 170623] (corroborating data).

NOTE: In the legend, 'old' stands for data before PVAR, 'new' stands for data after PVAR.

Figure H-1. Barium Sorption Coefficient on Zeolitic Tuff in J-13 Well Water versus Calculated Final ^{133}Ba Solution Concentration

The second example of a comparison of qualified and unqualified datasets involves uranium sorption on devitrified tuff in J-13 well water. Qualified and unqualified data points for sorption coefficients and pH are shown in Figure H-2. The same water composition was used in both the unqualified and the qualified experiments. Thus, differences in water composition are not an issue in comparisons of the two datasets. The differences in final solution concentrations did not influence the sorption coefficient ranges for the two datasets because the uranium sorption coefficients are not sensitive to final solution concentrations as shown in Figure A-53. Differences in experimental duration did not influence the sorption coefficient ranges because the uranium sorption reactions on devitrified tuff are fast, as discussed in Section A7.9.1. The fact that the ranges in uranium sorption coefficient values are similar for the two datasets, excluding the outlier with a K_d = 10 mL/g, provides confidence that the experimental procedures used to obtain the unqualified data were appropriate and equivalent to those used to obtain the qualified dataset.

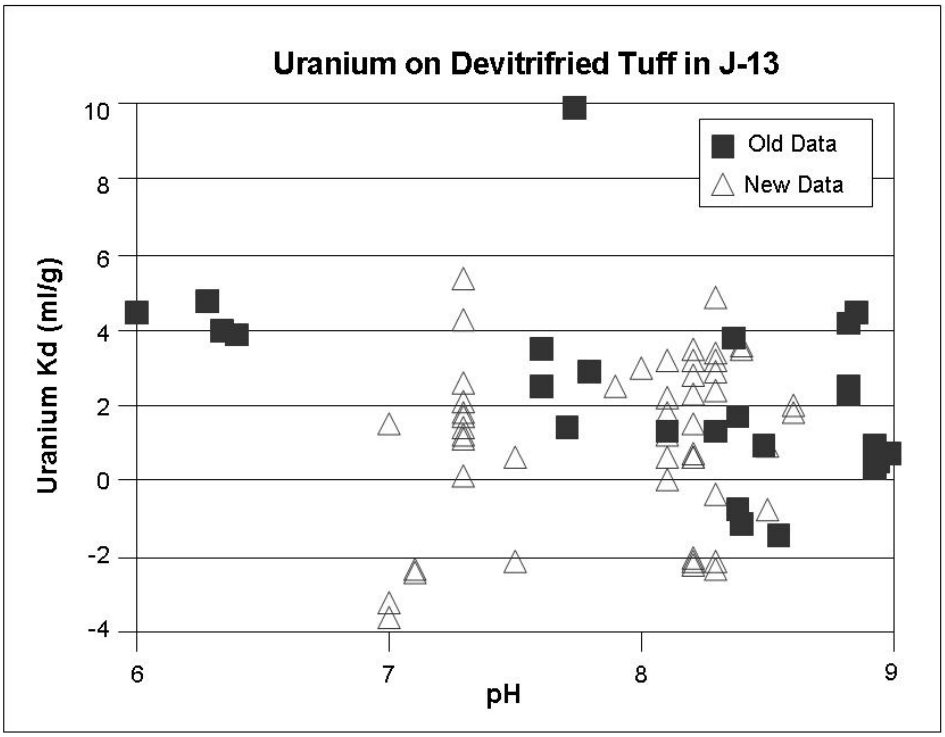

Source: DTNs: LA0305AM831341.001 [DIRS 163789]; LA0407AM831341.006 [DIRS 170628] (corroborating data).
NOTE: In the legend, 'old' stands for data before PVAR, 'new' stands for data after PVAR.

Figure H-2. Uranium Sorption Coefficient on Devitrified Tuff in J-13 Well Water versus pH

H1.2 TECHNICAL ASSESSMENT

The Los Alamos National Laboratory (LANL) studies of the sorptive behavior of tuff and transport of radionuclides through tuff were performed under the Nevada Nuclear Waste Storage Investigations (NNWSI) project that was managed by the Nevada Operations Office of the DOE. These investigations were performed under the Los Alamos QA program for the NNWSI, with the Materials Science and Technology Division quality assurance organization responsible for the planning and implementation of the Los Alamos QA program.

Los Alamos National Laboratory Quality Assurance Plan And Procedures For The Nevada Nuclear Waste Storage Investigations (LA-9331-MS) is a collection of the quality assurance documents that provides a detailed account of the Los Alamos NNWSI QA program, including the Quality Assurance Program Plan, the Quality Assurance Program Index and Procedures, work plans, and the detailed procedures developed for the Yucca Mountain Project (YMP).

The QA program developed for the NNWSI at Los Alamos was outlined in the Quality Assurance Program Plan and was structured to meet the requirements of NQA-1 and 10 CFR 50 ([DIRS 176567], Appendix B), as applied to the evaluation of major geologic formations with regard to their suitability as locations of permanent repositories for high-level radioactive wastes.

Quality Assurance Program Index (TWS-QI-1 and TWS-CMBQA-QP-02) is a cross-reference between basic requirements standards NQA-1 and 10 CFR 50 [DIRS 176567] showing where

these requirements are addressed in the Los Alamos Quality Assurance Manual (QAM) and YMP implementing procedures. The QAM was the primary compliance document for this work unless otherwise stated in the Quality Assurance Program Plan or in the specific procedure documents written for NNWSI.

Work plans were the primary planning documents covering the Los Alamos technical activities for the NNWSI. These work plans were written to provide an adequate description of the scope and purpose of the task. They include, directly or by reference, the QA requirements with regard to data validity and documentation. Review boards that consisted of, at a minimum, a management member, a QA member, and an independent technical reviewer who was experienced and competent in the field under review but had no direct program responsibility, approved the work plans as well as the acceptance of final documents. The work plan TWS-CNC-WP-03, *Tuff Experiments-Sorption Ratios and Migration Measurements* described the scope of work; provided an overview of how batch sorption studies were to be performed; defined which procedure to be used to control the experiments; and detailed performance, equipment, QA, and work documentation requirements for the radioactivity measurements. TWS-CNC-DP-05, *Sorption, Desorption Ratio Determinations of Geologic Materials by a Batch Method* was used to control the experiments in the same process as used in LANL-INC-DP-86, *Sorption and Desorption Determinations by a Batch Sample Technique for the Dynamic Transport Task* to control the qualified K_d data.

Training requirements for personnel were delineated in the QAM by QMR 1, *Quality Assurance Management and Planning* and QMI 1-1, *Quality Program Management*.

Measuring and testing equipment that require calibration was controlled in accordance with the applicable sections of the QAM (QMR 9 and QMI 9-1). The only equipment used for these experiments that required calibration were the balances and gamma counters. These were controlled in accordance with procedures QMR 9 *Control and Calibration of Standards and Measuring and Testing Equipment* and QMI 9-1 *Acquisition and Calibration Control of Standards and Measuring and Testing Equipment*. *Quality Assurance Audit of Los Alamos National Laboratories (LANL) Nevada Nuclear Waste Storage Investigations (NNWSI) Project* (LANL 1984 [DIRS 171444]) (performed July 16 through 18, 1984) verified that the control of measuring and test equipment was adequate. There were no problems found with the measuring and test equipment program. *Audit of Los Alamos Scientific Laboratories Quality Assurance Program Plan for Nevada Nuclear Waste Storage Investigations* (Los Alamos Scientific Laboratories 1979 [DIRS 171445]) (conducted May 1 to 3, 1979) also found that the measuring and test equipment program was satisfactory.

Corrective actions for significant conditions adverse to quality were provided in accordance with QMR 12, *Corrective Action,* of the QAM. Compliance with the QA program was verified by periodic audits that were planned, documented, and carried out in accordance with QMI 15-1, *Quality Audits,* of the QAM.

H1.3 SUMMARY

The programs in place at the time these sorption experiments were performed and the fact that the audits mentioned above did not identify anything that would affect the quality of the data lend support to the conclusion that the data collection methodology and equipment used were appropriate for the type of data under consideration. Corroborating information available for barium and uranium also show the equivalence of the unqualified and qualified data, supporting the adequacy of the unqualified data set. Furthermore, the uncertainty distributions for sorption coefficients generally span a range that is one order of magnitude or more (see Table C-14). The corroborating data comparisons suggest that differences between the unqualified and qualified data are much less than the inherent uncertainty. Therefore, the unqualified data are justified for use in supporting the sorption coefficient distributions to be used in TSPA.

Data Qualification Plan

Complete only applicable items.

QA: QA
Page 1 of 1

Section I. Organizational Information

Qualification Title

Qualification of sorption data, DTNs: LA0305AM831341.001 AND LA0310AM831341.001

Requesting Organization

LANL

Section II. Process Planning Requirements

1. List of Unqualified Data to be Evaluated

Barium Sorption Coefficient on Zeolitic Tuff in J-13 Water (DTN: LA0305AM831341.001 [DIRS 163789]), and Uranium Sorption Coefficient on Devitrified Tuff in J-13 Water (DTN: LA0310AM831341.001 [DIRS 165865])

2. Type of Data Qualification Method(s) [Including rationale for selection of method(s) (Attachment 3) and qualification attributes (Attachment 4)]

Method: Corroborating Data (Method 4), Technical Assessment (Method 5)

Rationale:

a. Corroborating data are available for comparison with the unqualified data set(s).
b. Inferences drawn to corroborate the unqualified data can be clearly identified, justified, and documented.

Qualification Process Attributes:

5. Quality and reliability of the measurement control program under which the data were generated
10. Extent and quality of corroborating data

3. Data Qualification Team and Additional Support Staff Required

Sharad Kelkar, Arend Meijer

4. Data Evaluation Criteria

1. Data to be compared shall have the same range as the corroborating data. The differences between the unqualified and the corroborating data are less than the inherent uncertainty which is one order of magnitude.
2. The technical adequacy of equipment and procedures used to collect and analyze the data.

5. Identification of Procedures Used

SCI-PRO-001 Rev1

6. Plan coordinated with the following known organizations providing input to or using the results of the data qualification

N/A

Section III. Approval

Qualification Chairperson Printed Name	Qualification Chairperson Signature	Date
Sharad Kelkar	Sharad Kelkar	5/16/2007
Responsible Manager Printed Name	**Responsible Manager Signature**	**Date**
Stephanie Kuzio		5/16/2007

SCI-PRO-001.1-R1

APPENDIX I
QUALIFICATION OF COMPOSITIONS OF WATERS FROM UE-25 J-13 AND UE-25 P#1(CARBONATE)

I1. INTRODUCTION

I1.1 PURPOSE

This report documents the findings of the data qualification team assembled to evaluate selected unqualified hydrology data that were used in the characterization of transport processes in the saturated zone (SZ) at Yucca Mountain, Nevada. These data are qualified for inclusion in this report, which supports total system performance assessment (TSPA) model/analysis for the license application. This activity has been planned and implemented in accordance with SCI-PRO-001, *Qualification of Unqualified Data*. The plan for the qualification of this data is presented at the end of this appendix.

I1.2 QUALIFICATION TEAM

Chairperson Sharad Kelkar has 25 years experience in the area of flow and transport through geological media. He has been a member of the Hydrology, Geochemistry, and Geology group at Los Alamos National Laboratory (LANL) since 1985. In 2002, Mr. Kelkar began his ongoing role as a principal scientist with the Yucca Mountain Project (YMP), where he is responsible for documentation in support of the license application for the repository. Mr. Kelkar has contributed to the YMP in the development of the code FEHM that forms a basis for the flow and transport modeling for the SZ. He has also worked on geothermal energy programs at LANL. Prior to his association with LANL, he worked on laboratory and field testing and engineering analysis in support of petroleum production (Terra Tek Inc., Salt Lake City, Utah, 1982 to 1985) and laboratory and field testing in support of gas recovery programs (Institute of Gas Technology, Chicago, Illinois, 1979 to 1982). Mr. Kelkar received his M.S. degree in Petroleum Engineering from the University of Texas at Austin (1979) for measurements of poro-elastic properties of rocks at elevated pressures and temperatures. Mr. Kelkar received his M.S. degree in Nuclear Physics from the University of Bombay (1974). In addition, Mr. Kelkar has done extensive course-work in hydrology and minerals engineering at the University of California, Berkeley.

Team member: Dr. James Houseworth's professional experience includes groundwater and surface water hydrology and petroleum reservoir engineering. He has provided, over a twelve-year period, technical and management support for performance assessment and site characterization efforts at Yucca Mountain, Nevada, which is being studied by the DOE as a disposal site for high-level radioactive waste. This includes unsaturated zone flow and transport analyses in fractured rock to support performance assessment of the potential repository system and analyses to support construction and testing activities at Yucca Mountain. In addition, he has eight years experience in characterization of petroleum reservoirs including laboratory core analysis methods to determine single and multiphase flow properties and reservoir simulation. Other experience includes numerical modeling of mixing and stratification in surface water reservoirs and the design of outfalls for the discharge of waste heat from nuclear power plants and municipal sewage effluent. Dr. Houseworth received his Ph.D. in 1984 in Environmental Engineering Science from the California Institute of Technology, his M.S. in 1978 in Environmental Engineering Science from California Institute of Technology and his B.S. in 1977 in Environmental Engineering Science from California Institute of Technology.

I1.3 DESCRIPTION OF THE DATA TO BE QUALIFIED

The data that were evaluated and documented in this qualification report are published in *Groundwater Chemistry Along Flow Paths Between a Proposed Repository Site and the Accessible Environment* (Ogard and Kerrisk 1984 [DIRS 100783]). These data are shown in Table I-1.

Table I-1. Compositions of Waters from UE-25 J-13 and UE-25 p#1

Chemical Constituent	UE-25 J-13 Well Water	UE-25 p#1 (Carbonate) Water (mg/L)
Ca^{2+}	11.5	87.8
Mg^{2+}	1.76	31.9
Na^{+}	45	171
K^{+}	5 .3	13.4
SiO_2	64.2	37.3
Cl^{-}	6.4	37
F^{-}	2.1	3.5
SO_4^{2-}	18.1	129
HCO_3^{-}	143	698
pH	6.9	6.7

Source: Ogard and Kerrisk 1984 [DIRS 100783] data.

I2. QUALIFICATION METHOD AND EVALUATION CRITERIA

The method used to qualify the data in this report is corroborating data (SCI-PRO-001, Attachment 3, Method 2). The confidence in the data is in question because data collection procedures are unavailable for review.

A comparison of the unqualified data and available qualified corroborating data will be conducted to determine that the unqualified data is acceptable and confidence in the data is established.

The following data qualification attributes will be used:

1. Extent and quality of corroborating data

2. Agreement between the data being qualified and the corroborating data

3. The importance of the data to showing that the proposed U.S. Department of Energy repository design meets the performance objectives of 10 CFR 63 [DIRS 180319].

I3. EVALUATION RESULTS

The compositions reported by Ogard and Kerrisk (1984 [DIRS 100783]) for J-13 well and p#1 waters were used in the analysis presented in Appendix A because many of the sorption coefficient experiments used in this analysis were performed in the early 1980s. Thus, to make the comparisons of experimental data and model results more direct, the Ogard and Kerrisk (1984 [DIRS 100783]) data were used in the analysis. The Ogard and Kerrisk (1984

[DIRS 100783]) data were used as limiting cases to set bounding ranges for concentrations of various constituents, which were then used as inputs for the PHREEQC modeling for extrapolating sorption coefficient data (described in Appendix A) to pH and geochemical compositions for which sufficient laboratory measurements were not available. The results of this modeling, in conjunction with the experimental data, inform the process of expert judgment to arrive at the uncertainty distributions for sorption coefficients for americium (Appendix A7.1), neptunium (Appendix A7.3), plutonium (Appendix A7.4), and uranium (Appendix A7.9). As such, the recommended distributions for sorption coefficient are expected to be weakly to moderately sensitive to the limits of compositional values that were input to the surface complexation modeling.

The composition of water from well J-13 as reported by Ogard and Kerrisk (1984 [DIRS 100783]) and the corroborating data from DTN: MO0006J13WTRCM.000 [DIRS 151029] are given in Table I-2. As noted in *Saturated Zone Site-Scale Flow Model* (SNL 2007 [DIRS 177391], Section A7.3.1), the uncertainty in concentration of major anions and cations is on the order of 10% for most species and 15% for F^-. Uncertainties add up–when comparing two items with uncertainty of 10% each, the total is 20%. As the Ogard and Kerrisk (1984 [DIRS 100783]) data do not have specific values of uncertainty given, it is also taken to have the same level of uncertainty as the other data. Thus, the data from the two sets can be expected to agree within 20% of each other for all the constituents except for F^-, which should agree within 30% of each other. As seen in Table I-2, there is remarkably good agreement between the two data sets. It is seen that for a number of constituents, the two data sets agree within the experimental uncertainty given in column 3. For those constituents where data differences fall somewhat outside the data uncertainty (Ca_2^+, Mg_2^+, K^+, SiO_2), the differences are still within the 20% limit. Thus the Ogard and Kerrisk (1984 [DIRS 100783]) data for the composition of the water sample from UE-25 J-13 meet the qualification requirements.

Table I-2. Comparison of Composition of Water from UE-25 J-13

Chemical Constituent	Concentration (mg/L) [a]	Concentration ± Uncertainty (mg/L) [b]	% Difference Absolute Value(100*(Column2 − Column3)/Column2)
Ca^{2+}	11.5	13 ±0.99	13
Mg^{2+}	1.76	2.01±0.21	14
Na^+	45	45.8±2.29	2
K^+	5 .3	5.04±0.61	5
SiO_2	64.2	60.97±1.85	5
Cl^-	6.4	7.14±0.61	12
F^-	2.1	2.18±0.29	4
SO_4^{2-}	18.1	18.4±1.03	2
HCO_3^-	143	128.9±8.6	10
PH	6.9	7.41±0.44	7

Sources: [a] Ogard and Kerrisk 1984 [DIRS 100783] data.
[b] Corroborating Data DTN: MO0006J13WTRCM.000 [DIRS 151029].

The composition of water from UE-25 p#1 (carbonate) as reported by Ogard and Kerrisk (1984 [DIRS 100783]) and the corroborating data from DTN: MO0006J13WTRCM.000 [DIRS 151029] are given in Table I-3. The corroborating data set is verified and qualified per

SCI-PRO-001. As noted in *Saturated Zone Site-Scale Flow Model* (SNL 2007 [DIRS 177391], Section A7.3.1), the uncertainty in concentration of major anions and cations is on the order of 10% for most species and 15% for F^-. Thus the data from the two sets can be expected to agree within 20% of each other. As shown in Column 4 of the Table I-3, this holds for all the constituents except Cl^-. The Ogard and Kerrisk (1984 [DIRS 100783]) value for Cl^- is somewhat higher than this range. However, because the data are used for setting limits on the range of compositional values, this is considered acceptable. Thus, the Ogard and Kerrisk (1984 [DIRS 100783]) data for the composition of the water sample from UE-25 p#1(carbonate) meet the qualification requirements.

Table I-3. Comparison of Compositions of Water from UE-25 p#1(Carbonate)

Chemical Constituent	Corroborating Data (mg/L) [a]	Concentration (mg/L) [b]	% Difference Absolute Value(100*(Column2 − Column3)/Column2)
Ca^{2+}	100	87.8	12
Mg^{2+}	39	31.9	18
Na^+	150	171	14
K^+	12	13.4	12
SiO_2	41	37.2	9
Cl^-	28	37	32
F^-	N/D	3.5	N/A
SO_4^{2-}	160	129	19
HCO_3^-	694	698	0.5
PH	6.6	6.7	1.5

Sources: [a] Corroborating Data DTN: MO0007MAJIONPH.011 [DIRS 151524].
[b] Ogard and Kerrisk 1984 [DIRS 100783] data.

I4. RESULTS

The qualification team determined, based on the discussions above, that the referenced data are both reasonable and appropriate for the application. This evaluation did not produce any new data.

I5. CONCLUSION

The data qualification effort documented in this report was performed in accordance with the requirements of the approved data qualification plan included in this appendix. The approved qualification method, corroborating data, was implemented as required. As a result of this qualification evaluation, these data are qualified for inclusion in this report.

Data Qualification Plan

Complete only applicable items.

QA: QA

Page 1 of 1

Section I. Organizational Information

Qualification Title

QUALIFICATION OF COMPOSITIONS OF WATERS FROM UE-25 J-13 AND UE-25 P#1(CARBONATE)

Requesting Organization

LANL

Section II. Process Planning Requirements

1. **List of Unqualified Data to be Evaluated**

Chemical Constituent	UE-25 J-13 Water	UE-25 p#1 (Carbonate) Water (mg/L)
Ca^{2+}	11.5	87.8
Mg^{2+}	1.76	31.9
Na^{+}	45	171
K^{+}	5 .3	13.4
SiO_2	64.2	37.3
Cl^{-}	6.4	37
F^{-}	2.1	3.5
SO_4^{2-}	18.1	129
HCO_3^{-}	143	698
pH	6.9	6.7

Compositions of Waters from UE-25 J-13 and UE-25 p#1, from Groundwater Chemistry Along Flow Paths Between a Proposed Repository Site and the Accessible Environment (Ogard and Kerrisk 1984 [DIRS 100783]).

2. **Type of Data Qualification Method(s)** [Including rationale for selection of method(s) (Attachment 3) and qualification attributes (Attachment 4)]

Method: SCI-PRO-001REV3, Method 2- Corroborating Data

Rationale:

a. Corroborating data are available for comparison with the unqualified data set(s).

b. Inferences drawn to corroborate the unqualified data can be clearly identified, justified, and documented.

Qualification Attributes: Attachment 4, Items 10 and 12.

3. **Data Qualification Team and Additional Support Staff Required**

Sharad Kelkar, James Houseworth

4. **Data Evaluation Criteria**

Data to be qualified shall fall within 20% of the corroborating data.

5. **Identification of Procedures Used**

SCI-PRO-001 Rev3

6. **Plan coordinated with the following known organizations providing input to or using the results of the data qualification**

N/A

Section III. Approval

Qualification Chairperson Printed Name	Qualification Chairperson Signature	Date
Sharad Kelkar	Sharad Kelkar	7/23/2007
Responsible Manager Printed Name	Responsible Manager Signature	Date
Stephanie Kuzio for	Kim Rehfeldt	7/23/07

SCI-PRO-001.1-R1

INTENTIONALLY LEFT BLANK

APPENDIX J
URANIUM AND NEPTUNIUM EFFECTIVE K_d VALUES FROM LONG-TERM DESORPTION EXPERIMENTS

J1. INTRODUCTION

This appendix describes a series of experiments conducted to further evaluate the radionuclide retardation potential of the saturated alluvium at Yucca Mountain. These experiments represent new work that effectively extends the experimental investigations presented in Appendix G. In that appendix, it was postulated that the apparent increase in the retardation of uranium and neptunium in column transport experiments as water residence times increased was a consequence of radionuclides having a greater probability of encountering stronger sorption sites as the transport time through the column increased.

The experiments discussed in this appendix were conducted to better quantify the distribution of alluvium sorption site strengths postulated in Appendix G and to estimate effective partition coefficients (K_d values) that are consistent with these distributions. These effective K_d value estimates serve to corroborate the K_d distributions presented in Appendix A, which are based almost exclusively on batch sorption experiments that did not effectively sample strong sorption sites or slow desorption kinetics. The resulting estimates of uranium and neptunium effective K_d values are not used to alter the distributions of Appendix A because this would result in inconsistencies between the K_d distributions for these nuclides and for all the other nuclides that do not have similar experimental data. It could also result in inconsistencies between K_d distributions in the saturated volcanics and alluvium, as similar long-term desorption experiments were not conducted using volcanic rocks. Such inconsistencies could result in unrealistic *relative* K_d values and retardation factors for different radionuclides and/or for volcanics and alluvium in the SZ transport model.

The effective K_d values presented in this appendix serve to show that Appendix A K_d distributions should tend to underpredict radionuclide retardation factors if strong sorption sites and slow desorption behavior are accounted for. This behavior could also serve as an explanation for the smaller K_d values obtained from some of the column experiments presented in Appendix G relative to batch sorption K_d values. Consideration of strong sorption sites and slow desorption behavior will ultimately result in K_d values that are predicted to be larger than batch sorption K_d values if the explanation is extrapolated to longer time and distance scales.

Uranium and neptunium interactions with alluvium were investigated in long-term laboratory desorption studies involving alluvium and water collected from boreholes along potential flow pathways between the proposed repository and the accessible environment. In addition to estimating effective K_d values from the long-term desorption data, the experiments were designed to provide a preliminary evaluation of the effects of water chemistry and alluvium secondary mineralogy on the estimated K_d values.

J2. EXPERIMENTAL APPROACH

The alluvium used in the experiments is from drill cuttings obtained from NC-EWDP-19IM1A, NC-EWDP-22SA and NC-EWDP-10SA at depth intervals of 740.0 to 745.0 ft, 557.5 to 560 ft, and 680 to 685 ft below ground surface, respectively. These boreholes are located along a ~7.6-km stretch of Fortymile Wash that essentially encompasses the maximum plausible transport distance in saturated alluvium between the repository horizon and the accessible environment. Alluvium samples were sieved to obtain size distributions, and the size range

between < 75 to 2,000 μm was proportionally recombined. The bulk mineralogies of the three recombined alluvium samples, as determined by quantitative X-ray diffraction, are listed in Table J-1. Experiments with the 19IM1A and 22SA alluvium were conducted using a low carbonate groundwater (shallow zone from NC-EWDP-19D, referred to as Zone 1) and a high carbonate groundwater (deep zone from NC-EWDP-19D, referred to as Zone 4). The objective of the paired experiments using groundwater from Zone 1 and Zone 4 of 19D was to investigate the effect of uranyl and neptunyl carbonate complex formation on sorption and long-term desorption. Experiments using 10SA alluvium were conducted with water from the same borehole as the alluvium. The groundwater was filtered using a 0.2-μm filter before use. Major ion chemistry, including total inorganic carbon, pH, and ionic strength of the waters used in the experiments, is provided in Table J-2.

The $^{233}U(VI)$ tracer solutions were prepared by diluting a $^{233}U(VI)$ (as $UO_2(NO_3)_2$ in dilute HNO_3) stock solution obtained from Isotope Products Laboratories in the groundwaters described above. The $^{237}Np(V)$ tracer solutions were prepared by diluting a $^{237}Np(V)$ (as NpO_2^+ in HCl) stock solution obtained from Los Alamos National Laboratory in distilled water to make a stock solution of 2×10^{-4} mol/L ^{237}Np. Lower concentrations of neptunium tracer solutions were made by dilution of the 2×10^{-4} mol/L ^{237}Np stock solution with the groundwaters described above. The final concentrations of each of the $^{233}U(IV)$ and $^{237}Np(V)$ tracer solutions are given in Table J-3. The studies described herein were performed at ambient laboratory temperature and pressure (~23°C and ~0.8 bars, respectively) and the groundwater/tracer solutions used in the experiments were assumed to be in equilibrium with the ambient atmosphere (oxidizing conditions, 0.033% CO_2).

Desorption rates were determined by long-term desorption of uranium and neptunium from the alluvium samples after a relatively quick adsorption contact period. For the sorption phase of the experiments, the alluvium was brought into contact with a tracer solution containing one of the radionuclides of interest (^{233}U or ^{237}Np). The radionuclide was batch sorbed to the alluvium for two weeks, and the supernatant was decanted and either centrifuged or filtered to remove fine particles before being analyzed for radionuclide concentration (using a 2500TR Packard liquid scintillation counter) to determine the partition coefficient (ratio of sorbed radionuclide per unit mass of solid to nonsorbed radionuclide per unit volume of solution, or K_d value, mL/g). A partition coefficient implies a linear sorption isotherm, which should provide a good approximation of the sorption isotherm at the relatively low concentrations used in the experiments and the even lower concentrations that would likely occur in the saturated zone. Also, isotherm nonlinearity is expected to be a second-order effect compared to sorption heterogeneity due to variability in mineralogy and water chemistry in the alluvium.

After the sorption measurements were conducted, the radionuclide-bearing alluvium and tracer-free groundwater from the same borehole/zone used in the sorption phase of the experiments were added to a small column and placed on a rocking shaker to maximize alluvium-solution contact. Tracer-free groundwater was then eluted through the column and collected in fractions. The activity in the samples was measured using a Packard 2500TR liquid scintillation counter. The groundwater zone, sorption period, tracer solution concentration, and liquid-to-solid ratio used for the experiments are listed in Table J-3.

Table J-1. Quantitative X-ray Diffraction Results for Alluvium Used in Long-term Uranium and Neptunium Desorption Experiments

Mineral Phase	Well NC-EWDP-19IM1A (wt %)	Well NC-EWDP-22SA (wt %)	Well NC-EWDP-10SA (wt %)
Quartz	15.3	10.1	8.7
Plagioclase	23.0	28.4	26.0
K-Feldspar	24.4	17.5	30.6
Clinoptilolite	7.6	12.0	11.6
Mica	1.3	1.0	1.8
Kaolinite	0.5	0.2	0.4
Cristobalite	5.8	5.9	8.1
Tridymite	4.1	4.3	1.6
Opal-CT	13.6	—	—
Hematite	0.4	0.6	0.5
Smectite	4.6	19.4	8.0
Total	100.6	99.4	97.4

Source: DTN: LA0705CS150304.001 [DIRS 181762].

Table J-2. Major Ion Chemistry of Groundwaters Used in Long-term Uranium and Neptunium Desorption Experiments

Species	Concentration (mg/L) in NC-EWDP-19D Zone 1 (411' to 431' BLS) [a]	Concentration (mg/L) in NC-EWDP-19D Zone 4 (720' to 795' BLS) [a]	Concentration (mg/L) in NC-EWDP-10SA (662' to 700' BLS) [b]
Temperature (°C)	32	31	29.7
pH	8.6	8.85	7.8
Na^+	91.50	107.30	40.6
K^+	3.70	3.40	6.12
Ca^{2+}	3.70	0.92	13.8
Mg^{2+}	0.31	0.03	2.45
SiO_2	22.0	18.7	55.3
F^-	2.0	2.7	2.0
Cl^-	6.10	5.60	7.0
SO_4^{2-}	22.0	18.7	19.6
HCO_3^-	189	212	129
CO_3^{2-}	12.8	12.5	0
Ionic Strength (M)[c]	0.0048	0.0054	0.0035

Sources: DTNs: [a]GS011108312322.006 [DIRS 162911]; [b]GS040108312322.001 [DIRS 179422].

NOTES: [c]Calculated from major ion chemistry.

BLS = Below Land Surface.

Table J-3. Experimental Parameters Used in Uranium and Neptunium Batch Sorption and Long-term Desorption Column Experiments

Alluvium/Groundwater	Sorption Period (days)	Desorption Period (days)	Radionuclide	Tracer Solution Concentration (M)	Liquid:Solid (mL/g)
19IM1A/19D Zone 1[a]	14	134	^{233}U	1×10^{-6}	7.55:1
19IM1A/19D Zone 4[b]	14	120	^{233}U	1×10^{-6}	7.52:1
22SA/19D Zone 1[c]	14	14	^{233}U	1×10^{-6}	7.38:1
22SA /19D Zone 4[d]	14	120	^{233}U	1×10^{-6}	7.47:1
10SA/10S[e]	14	14	^{233}U	1×10^{-6}	7.35:1
19IM1A/19D Zone 1[f]	14	59	^{237}Np	3×10^{-6}	1.76:1
19IM1A/19D Zone 4[g]	14	57	^{237}Np	3×10^{-6}	1.76:1
22SA/19D Zone 1[h]	14	59	^{237}Np	3×10^{-6}	1.73:1
22SA/19D Zone 4[i]	14	57	^{237}Np	3×10^{-6}	1.31:1

Sources: DTNs: [a]MO0608DOEU19Z1.000 [DIRS 180720]. [b]MO0608DOEU19Z4.000 [DIRS 180719]. [c]MO0608DOEU22Z1.000 [DIRS 180718]. [d]MO0608DOEU22Z4.000 [DIRS 180717]. [e]MO0608DOEUS10S.000 [DIRS 180721]. [f]MO0608DOE19MZ1.000 [DIRS 180723]. [g]MO0608DOENP2Z4.000 [DIRS 180724]. [h]MO0608DOENPSZ1.000 [DIRS 180725]. [i]MO0608DOENPMZ4.000 [DIRS 180726].

J3. DATA INTERPRETATION

Effective K_d values were calculated for uranium and neptunium from the 14-day sorption data and long-term column desorption data based on estimates of sorption and desorption rate constants obtained from the experiments. Long-term column desorption data for uranium can be found in DTNs: MO0608DOEUS10S.000 [DIRS 180721]; MO0608DOEU19Z4.000 [DIRS 180719]; MO0608DOEU19Z1.000 [DIRS 180720]; MO0608DOEU22Z1.000 [DIRS 180718]; MO0608DOEU22Z4.000 [DIRS 180717]). Long-term column desorption data for neptunium can be found in DTNs: MO0608DOENPSZ1.000 [DIRS 180725]; MO0608DOENPMZ4.000 [DIRS 180726]; MO0608DOENP2Z4.000 [DIRS 180724]; MO0608DOE19MZ1.000 [DIRS 180723]. In the remainder of this appendix, K_d refers to partition coefficients estimated from the 14-day sorption phase of the experiments, and $K_{d,eff}$ refers to partition coefficients estimated from the column desorption data.

Desorption (reverse reaction) rate constants (K_r) were calculated for each eluted sample from the desorption experiments using Equation J-1, which assumes that desorption is a first-order kinetic process and that radionuclide concentrations in the aqueous phase are low enough that the sorption rate is negligible compared to the desorption rate. This approach allows for the possibility that the alluvium may contain sorption sites having a wide range of sorption affinities and hence a wide range of desorption rate constants.

$$K_r = \frac{V}{S}\frac{dC}{dt} + q\frac{C}{S} \qquad \text{(Eq. J-1)}$$

where

K_r = desorption reaction rate constant (g/hr)
V = amount of desorption solution in column (g)

C = activity in solution (CPM/ml (or gram of solution))
S = activity on sorbed on solid (CPM/g)
t = time (hr)
q = volumetric flow rate (ml/hr).

Sorption rate constants were estimated as the product of the K_d value measured at the end of the 14-day sorption period (K_d = S/C) and the average desorption rate constant (K_r) over the entire column desorption experiment. Sorption rate constants could not be estimated during the sorption phase of the experiments because the amount of radionuclide sorbed was not measured at intermediate times during the 14-day sorption period—it was measured only at the end of the period. Average K_r values over the entire desorption experiment were estimated in three different ways:

1. The K_r values for each eluted sample were multiplied by the fraction of radionuclide desorbed for that sample, and the sum of the resulting values was divided by the total fraction of radionuclide sorbed prior to desorption to obtain a weighted average. The fraction remaining sorbed at the end of the desorption experiment was assumed to have a desorption rate constant equal to one-half the numerical average of the last 5 instantaneous desorption rate constant measurements, and this value was weighted by the fraction remaining sorbed at the end of the experiment. Mathematically:

$$K_{r,avg}(1) = \frac{\sum_{i}(f_i - f_{i-1})K_{ri} + f_{final}\dfrac{\sum_{N-4}^{N} K_{ri}}{10}}{f_0} \qquad \text{(Eq. J-2)}$$

where

f_i = fraction of radionuclide sorbed after desorption sample i
f_{final} = fraction of radionuclide sorbed at end of desorption experiment
f_0 = fraction of radionuclide sorbed prior to desorption
K_{ri} = desorption rate constant associated with desorption sample i
N = number of desorption samples collected.

2. The desorption experiment was divided into four mass fraction "bins" (assumed to correspond to different sorption sites), and a numerical average desorption rate constant was calculated for each bin. The last bin was associated with the fraction remaining sorbed at the end of the experiment, and the rate constant for this bin was taken to be the average from the last 5 desorption samples divided by 2. The three other bins had identical mass fractions, equal to the total mass fraction desorbed during the experiment divided by 3. The overall average desorption rate constant was calculated as the weighted average rate constant from each of the four bins; i.e.,

$$K_{r,avg}(2) = \frac{\sum_{j=1}^{3} \frac{(f_0 - f_{final})}{3} \left[\frac{\sum_{i=a_j}^{b_j} K_{ri}}{(b_j - a_j)} \right] + f_{final} \frac{\sum_{N-4}^{N} K_{ri}}{10}}{f_0} \quad \text{(Eq. J-3)}$$

where

j = bin number
a_j = sample number associated with first sample in bin j
b_j = sample number associated with last sample in bin j.

3. As with #2, the desorption experiment was divided into four mass fraction "bins" (assumed to correspond to different sorption sites), and a numerical average desorption rate constant was calculated for each bin. The bins and average desorption rate constants in each bin were calculated the same as in #2. However, the overall average desorption rate constant was calculated as the geometric mean of the four rate constants from each bin; i.e.,

$$K_{r,avg}(3) = \left(\prod_{j=1}^{3} \left[\frac{\sum_{i=a_j}^{b_j} K_{ri}}{(b_j - a_j)} \right] \left(\frac{\sum_{N-4}^{N} K_{ri}}{10} \right) \right)^{0.25} \quad \text{(Eq. J-4)}$$

Minimum and maximum sorption rate constants ($K_{f\min}$, $K_{f\max}$) were calculated for each experiment using the batch sorption K_d value and the minimum and maximum of the three $K_{r,avg}$ values calculated above.

$$K_{f\max} = K_d K_{r\max} \text{ and } K_{f\min} = K_d K_{r\min} \quad \text{(Eq. J-5)}$$

where

$K_{f\min}$, $K_{f\max}$ = minimum or maximum forward reaction rate constant (mL/hr)
K_d = two-week sorption partition coefficient (mL/g)
$K_{r\min}$, $K_{r\max}$ = minimum or maximum reverse reaction rate constant (g/hr) calculated from Equations J-2 to J-4.

The sorption rate constants calculated in this way provided estimates of upper and lower bounds to bracket the effective sorption rate constant in each experiment. Previous kinetic sorption experiments for uranium (DTNs: LA0408MD831341.002 [DIRS 180727], LA0408MD831341.003 [DIRS 180728], LA0408MD831341.004 [DIRS 180729], LA0302MD831341.004 [DIRS 163785]) and neptunium (DTNs: LA0302MD831341.003 [DIRS 163784], LA0109MD831341.001 [DIRS 156870]) indicated that the sorption rate of these radionuclides is relatively fast with respect to the two-week sorption period. The sorption rate constants calculated using the above indirect method yielded values that were consistent with these sorption kinetics experiments.

The forward (K_f) rate constants estimated above and the reverse (K_r) rate constants calculated for each desorption sample were used to estimate a K_d value associated with each sample. The overall $K_{d,eff}$ value for the entire experiment was then calculated in two ways that are similar to the first two methods used to calculate the $K_{r,avg}$ values above:

1. The calculated K_d value for each sample was multiplied by the fraction of total radionuclide mass that was collected in that sample. The K_d value associated with the mass fraction remaining sorbed at the end of the experiment was calculated using the average K_r value for the last 5 samples collected in the experiment divided by 2. The sum of the products of the K_d values and fractions were then divided by the total fraction of radionuclide that had sorbed during the sorption phase of the experiment to obtain an estimate of $K_{d,eff}$. Mathematically,

$$K_{d,eff}(1) = \frac{\sum_i (f_i - f_{i-1}) \frac{K_f}{K_{ri}} + f_{final} \left(K_f \Big/ \frac{\sum_{N-4}^{N} K_{ri}}{10} \right)}{f_0} \qquad \text{(Eq. J-6)}$$

2. The desorption experiment was divided into four mass fraction "bins," and a K_d value was calculated for each bin using the numerical average desorption rate constant calculated for that bin. The first three bins had identical mass fractions, equal to the total mass fraction desorbed during the experiment divided by 3. The last bin was associated with the fraction remaining sorbed at the end of the experiment, and the K_d value for this bin was calculated using the average K_r value for the last 5 samples collected in the experiment divided by 2. The $K_{d,eff}$ value was calculated as the weighted average K_d value from each of the four bins; i.e.,

$$K_{d,eff}(2) = \frac{\sum_{j=1}^{3} \frac{(f_0 - f_{final})}{3} \left(K_f \Big/ \frac{\sum_{i=a_j}^{b_j} K_{ri}}{(b_j - a_j)} \right) + f_{final} \left(K_f \Big/ \frac{\sum_{N-4}^{N} K_{ri}}{10} \right)}{f_0} \qquad \text{(Eq. J-7)}$$

For each of these methods, a minimum and maximum $K_{d,eff}$ value was calculated using $K_{f\,\min}$ and $K_{f\,\max}$, respectively, in place of K_f in Equations J-6 and J-7. Thus, a total of four K_d values were calculated; two as lower bounds using $K_{f\,\min}$ and two as upper bounds using $K_{f\,\max}$. The smallest and largest of these four values were taken to be the range of $K_{d,eff}$ values associated with a given experiment.

It should be noted that the $K_{d,eff}$ values calculated this way represent only an approximation to the "true" $K_{d,eff}$ values associated with a given radionuclide, alluvium sample, and water chemistry. The approximate nature of these estimates is a result of the fact that desorption experiments were stopped before desorption from the alluvium was complete and also because the sorption rate constants were not measured directly and they could have been different for the sorption sites with different affinities. The desorption rates were clearly decreasing with time in the experiments, so using the average value of the desorption rate constant over the last 5 collected

samples divided by 2 as an estimate of the desorption rate constant associated with the radionuclide fraction remaining sorbed at the end of each experiment seemed a reasonable, and probably conservative, approach to take. Although the error or bias associated with the indirect estimates of the sorption rate constants could not be directly assessed, an explicit kinetic model (implemented with an unqualified Fortran code) was developed to corroborate the experimentally derived rates. The model was used to simulate four sorption/desorption reactions simultaneously to determine if the sorption and desorption rate constants estimated from the four-bin approach described above yielded reasonable approximations to the fraction sorbed versus time in the experiments.

The predictions of the explicit kinetic model using both $K_{f\,\min}$ and $K_{f\,\max}$ as the sorption rate constants were in reasonably good agreement with the experimental curves, although some experiments deviated from the model predictions more than others. The model was also used to fit the data for each experiment with K_f and K_r values allowed to vary for each of the four sorption site bins. The resulting best-fitting values of K_f and K_r for each site bin were then used to calculate a K_d value for each site. Both an unweighted and a weighted average of these K_d values (weighted by the fraction of radionuclide associated with each of the site bins at the end of the sorption phase of the simulated experiments) were calculated to obtain estimates of the overall $K_{d,eff}$ value resulting from the best-fitting model. Although the Fortran code used to implement the explicit kinetic model was not qualified for use to support Yucca Mountain licensing activities, it was used corroboratively to establish that the minimum $K_{d,eff}$ values obtained directly from the experimental data serve as reasonably good lower bounds for the "true" $K_{d,eff}$ values for the radionuclide, alluvium, and water combinations tested. However, the maximum estimated $K_{d,eff}$ values may not serve as good upper bounds because of the possibility that some of the radionuclide fraction remaining sorbed at the end of the experiments had much smaller desorption rate constants than were assumed in the calculations. In this case, the true $K_{d,eff}$ values would be larger than the maximum estimated $K_{d,eff}$ values.

J4. EXPERIMENTAL RESULTS

J4.1. URANIUM (VI) LONG-TERM DESORPTION

J4.1.1 Range of $K_{d,eff}$ Values for Uranium (VI)

The 14-day uranium batch sorption K_d and the minimum and maximum $K_{d,eff}$ values for each of the uranium long-term desorption experiments are given in Table J-4. The discrete values are obtained by method 1 above ($K_{d,eff}(1)$, Equation J-6) and the binned values are obtained by method 2 above ($K_{d,eff}(2)$, Equation J-7). The overall range of $K_{d,eff}$ values for uranium differs between the different alluvial/groundwater combinations and ranges from 5 to 281 mL/g (discrete + binned). The length of the desorption period has a significant influence on the $K_{d,eff}$ value; generally the longer the desorption period, the higher the $K_{d,eff}$ value for a particular alluvium/groundwater combination (determined by calculating $K_{d,eff}$ values at different times during the desorption period). This dependence on desorption time period suggests that a fraction of the uranium remaining sorbed at the end of a desorption experiment has a significantly greater $K_{d,eff}$ value than twice the $K_{d,eff}$ value of the last uranium that desorbed (the assumption used in the $K_{d,eff}$ calculations).

J4.1.2 Explicit Kinetic Model Simulations of Uranium (VI) Sorption/Desorption

The unweighted and weighted average $K_{d,eff}$ values calculated using the K_f and K_r values resulting from the best fit of the experimental desorption curve are provided in Table J-4. In all but two cases, the $K_{d,eff}$ estimates obtained from the model results fell in the range of the low and high estimates or above the high estimate obtained directly from the data using the $K_{f\min}$ and $K_{f\max}$ values and the binned K_r values.

Figure J-1 shows the experimental data curve, fit, and predictive models for uranium desorption from 19IM1A alluvium in 19D Zone 4 groundwater. For this alluvium/groundwater combination, the weighted and unweighted $K_{d,eff}$ values calculated from the K_f and K_r values resulting from the best fit of the experimental data curve are greater than the high estimate obtained directly from the data using the $K_{f\min}$ and $K_{f\max}$ values and the binned K_r values (Table J-4).

The $K_{d,eff}$ values obtained from the explicit kinetic model are quite uncertain because of the flattening of the desorption curves at the end of the experiments (e.g., Figures J-1 and J-2). This flattening causes the fits to be relatively insensitive to the desorption rate constant associated with the strongest sorption site. For many of the experiments, a reasonably good fit to the late-time data could be achieved with a desorption rate constant for the strongest site that varied from some upper limit to nearly zero. Because a desorption rate constant of zero implies an infinite $K_{d,eff}$ value, the actual $K_{d,eff}$ values could be much larger than the values listed in Table J-4.

Table J-4. Effective $K_{d,eff}$ Values from Uranium Long-term Desorption Experiments and Explicit Kinetic Model

NC-EWDP Well No.	Groundwater	14-Day Batch Sorption K_d (mL/g)	$K_{d,eff}$(1) (mL/g) Discrete [a]		$K_{d,eff}$(2) (mL/g) Binned [b]		$K_{d,eff}$ (mL/g) Explicit Kinetic Model [c]	
			Min	Max	Min	Max	Unweighted	Weighted
19IM1A	19D-Zone 1	5.22	65.83	280.72	62.57	266.81	401.40	475.15
19IM1A	19D-Zone 4	1.36	4.70	11.26	4.56	10.93	26.27	29.28
22SA	19D-Zone 1	9.96	36.14	80.03	45.01	99.69	29.15	22.29
22SA	19D-Zone 4	3.25	10.30	55.75	9.74	52.72	11.29	7.19
10SA	10S	5.17	17.98	23.62	17.63	23.16	25.69	44.13

Source: DTN: LA0702CS150304.004 [DIRS 181311].

NOTE: The length of the desorption period affects the value of the $K_{d,eff}$. Generally, the longer the desorption period, the higher the $K_{d,eff}$ value for a particular sample (see Table J-3 for desorption period).

[a] Calculated using Equation J-6.
[b] Calculated using Equation J-7.
[c] The $K_{d,eff}$ was obtained from the 4 sorption and desorption rate constants that yielded a reasonable fit to the desorption data using the explicit kinetic model. The Fortran code used to implement the kinetic model is not qualified for use to support licensing, so the results are for corroborative purposes only.

J4.1.3 Effects of Groundwater Chemistry on Uranium (VI) K_d and $K_{d,eff}$ Values

Paired experiments using groundwater from Zone 1 and Zone 4 of 19D were used to investigate the effect of uranyl carbonate complex formation on sorption and long-term desorption of uranium. The NC-EWDP-19D Zone 4 groundwater used in the coupled experiments with the NC-EWDP-19IM1A and NC-EWDP-22SA alluvium has a higher bicarbonate concentration than the NC-EWDP-19D Zone 1 groundwater.

The $K_{d,eff}$ values in Table J-4 indicate that results are consistent with results obtained from 14-day batch sorption experiments in that $K_{d,eff}$ values tend to be higher for experiments using the lower carbonate 19D Zone 1 water. The range of $K_{d,eff}$ values for uranium in the 19IM1A alluvium in the lower carbonate 19D Zone 1 water is 63 to 281 mL/g (discrete + binned), and the range of $K_{d,eff}$ values for uranium in the same alluvium using the 19D Zone 4 water is 5 to 11 mL/g. The same trend is observed in the paired 22SA alluvium experiments. These results suggest that the presence of higher carbonate concentrations in the groundwater decreases the sorption of U(VI) presumably due to the formation of negatively charged uranyl carbonate complexes in solution. The $K_{d,eff}$ values in the Zone 1 groundwater were greater than in the Zone 4 groundwater even when the desorption experiments were carried out for much longer times in the Zone 4 water (which should have given the Zone 4 experiments a bias toward larger $K_{d,eff}$ values).

J4.1.4 Effects of Smectite + Clinoptilolite Content on Uranium (VI) K_d and $K_{d,eff}$ Values

The mineralogy of the NC-EWDP-19IM1A, NC-EWDP-22SA, and NC-EWDP-10SA alluvium used in the experiments was determined by quantitative X-ray diffraction (Table J-1). The major phases in the alluvium samples are silica (i.e., quartz, tridymite, cristobalite), K-feldspar, and plagioclase. The amount of smectite and clinoptilolite in the alluvium differs between samples. Between these samples, the sum of the smectite and clinoptilolite percentages in NC-EWDP-22SA is larger than in NC-EWDP-19IM1A or NC-EWDP-10SA.

This result can be used in conjunction with the $K_{d,eff}$ values obtained from long-term desorption of uranium from the samples to determine if clay and zeolite minerals have a significant influence over uranium $K_{d,eff}$ values. The range of $K_{d,eff}$ values for uranium in the 19IM1A alluvium in the 19D Zone 4 groundwater is 5 to 11 mL/g, and the range of $K_{d,eff}$ values for uranium in the 22SA alluvium in the same groundwater is 10 to 56 mg/L. These ranges indicate a positive correlation between uranium $K_{d,eff}$ values and the amount of smectite and clinoptilolite minerals present in the alluvium. The results are inconclusive for the comparison between 19IM1A and 22SA alluvium in 19D Zone 1 groundwater due to the termination of the 22SA Zone 1 experiment after only 14 days of desorption (as opposed to the 134-day desorption period for the 19IM1A Zone 1 experiment).

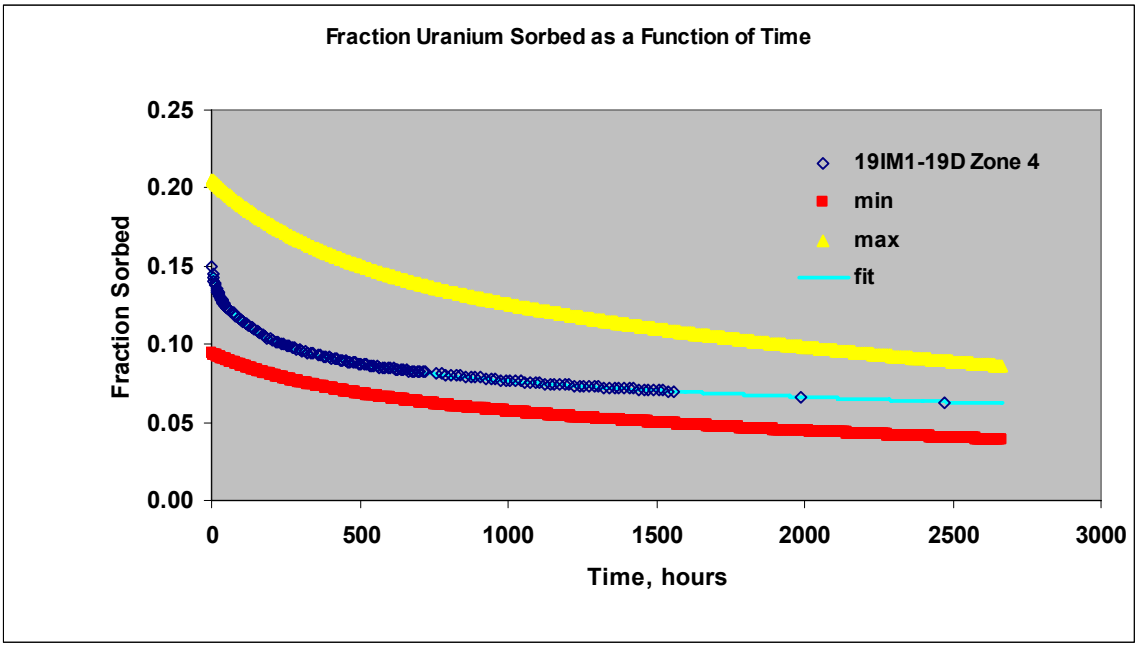

Source: DTN: LA0702CS150304.003 [DIRS 181312].

NOTES: The red and yellow curves were calculated with the explicit kinetic model using a single $K_{f,min}$ or $K_{f,max}$ value (calculated from Equation J-5) in conjunction with the average K_r values from each of the 4 mass fraction bins assumed in the binned approach. The blue model curve (fit) was generated using the explicit kinetic model and allowing K_f and K_r to vary for each of the 4 mass fraction bins to obtain a best fit to the experimental data.

Figure J-1. Fraction of Uranium Sorbed to 19IM1A Alluvium in 19D Zone 4 Groundwater as a Function of Time

J4.2 NEPTUNIUM LONG-TERM DESORPTION

J4.2.1 Range of Effective $K_{d,eff}$ Values for Neptunium (V)

The 14-day neptunium batch sorption K_d and the minimum and maximum $K_{d,eff}$ values for each of the neptunium long-term desorption experiments are given in Table J-5. The discrete values are obtained by method 1 above ($K_{d,eff}(1)$, Equation J-6) and the binned values are obtained by method 2 above ($K_{d,eff}(2)$, Equation J-7). The overall range of $K_{d,eff}$ value for neptunium differs between the different alluvial/groundwater combinations and ranges from 40 to 458 mL/g (discrete + binned).

J4.2.2 Explicit Kinetic Model Simulations of Neptunium (VI) Sorption/Desorption

The K_f and K_r values resulting from the best fit of the experimental data curve were used to calculate the unweighted and a weighted average $K_{d,\,eff}$ values listed in Table J-5. In all but one case, the $K_{d,eff}$ estimates obtained from the model results fell between the low and high estimates or above the high estimate obtained directly from the data using the $K_{f\,\mathrm{min}}$ and $K_{f\,\mathrm{max}}$ values and the binned K_r values.

The experimental data curve and fit and predictive models for neptunium desorption from 19IM1A alluvium in 19D Zone 1 groundwater are shown in Figure J-2. For this alluvium/groundwater combination, the $K_{d,eff}$ calculated from the K_f and K_r values resulting from the best fit of the experimental data curve are above the high estimate obtained directly from the data using the $K_{f\min}$ and $K_{f\max}$ values and the binned K_r values (Table J-5). The same uncertainties associated with the uranium $K_{d,eff}$ values obtained from the explicit kinetic model also apply to the neptunium $K_{d,eff}$ values obtained from this model.

Table J-5. $K_{d,eff}$ Values from Neptunium Long-Term Desorption Experiments and Explicit Kinetic Model

NC-EWDP Well No.	Groundwater	14-Day Batch Sorption K_d (mL/g)	$K_{d,eff}$ (mL/g) Discrete[a]		$K_{d,eff}$ (mL/g) Binned[b]		$K_{d,eff}$ (mL/g) Explicit Kinetic Model[c]	
			Minimum	Maximum	Minimum	Maximum	Unweighted	Weighted
19IM1A	19D-Zone 1	10.12	99.77	242.15	96.55	234.35	255.40	281.72
19IM1A	19D-Zone 4	5.75	40.12	128.27	41.49	132.66	117.08	83.59
22SA	19D-Zone 1	23.31	160.10	463.94	158.06	458.02	309.59	175.47
22SA	19D-Zone 4	17.87	109.42	332.95	108.57	330.35	42.81	33.49

Source: DTN: LA0702CS150304.002 [DIRS 181313].

NOTE: The length of the desorption period affects the value of the $K_{d,eff}$. Generally, the longer the desorption period, the higher the $K_{d,eff}$ value for a particular sample (see Table J-3 for desorption period).
[a]Calculated using Equation J-6.
[b]Calculated using Equation J-7.
[c]$K_{d,eff}$ was obtained from the four sorption and desorption rate constants that yielded a reasonable fit to the desorption data using the explicit kinetic model. The Fortran code used to implement the kinetic model is not qualified for use to support licensing, so the results are for corroborative purposes only.

J4.2.3 Effects of Groundwater Chemistry on Neptunium (V) K_d and $K_{d,eff}$ Values

Paired experiments using groundwater from Zone 1 and Zone 4 of 19D were used to investigate the effect of neptunyl carbonate complex formation on sorption and long-term desorption of neptunium. The NC-EWDP-19D Zone 4 groundwater used in the coupled experiments with the NC-EWDP-19IM1A and NC-EWDP-22SA alluvium has a higher bicarbonate concentration than the NC-EWDP-19D Zone 1 groundwater.

The $K_{d,eff}$ values in Table J-5 indicate that results are consistent with results obtained from 14-day batch sorption experiments in that the $K_{d,eff}$ values tend to be higher for experiments using the lower carbonate 19D Zone 1 water. The range of $K_{d,eff}$ values for neptunium in the 19IM1A alluvium in the lower carbonate 19D Zone 1 water is 97 to 242 mL/g (discrete + binned), and the range of $K_{d,eff}$ values for neptunium in the same alluvium using the 19D Zone 4 water is 42 to 133 mg/L. The same trend is observed in the paired 22SA alluvium experiments. These results suggest that the presence of higher carbonate concentrations in the groundwater decreases the sorption of Np(V) presumably due to the formation of negatively charged neptunyl carbonate complexes in solution.

J4.2.4 Effects of Smectite + Clinoptilolite Content on Neptunium (V) K_d and $K_{d,eff}$ Values

As was the case for uranium, the alluvium mineralogy of Table J-1 can be used in conjunction with the $K_{d,eff}$ values obtained from long-term neptunium desorption experiments to determine if clay and zeolite minerals have a significant influence over neptunium $K_{d,eff}$ values. The range of

$K_{d,eff}$ values for neptunium in the 19IM1A alluvium in the 19D Zone 1 groundwater is 97 to 242 mL/g, and the range of $K_{d,eff}$ values for neptunium in the 22SA alluvium in the same groundwater is 158 to 464 mg/L. The same trend is observed for the 19IM1A and 22SA alluvium in 19D Zone 4 groundwater (i.e., greater sorption and slower desorption associated with higher smectite + clinoptilolite content). The range of $K_{d,eff}$ values in Table J-5 indicate a positive correlation between neptunium $K_{d,eff}$ values and the amount of these minerals present in the alluvium.

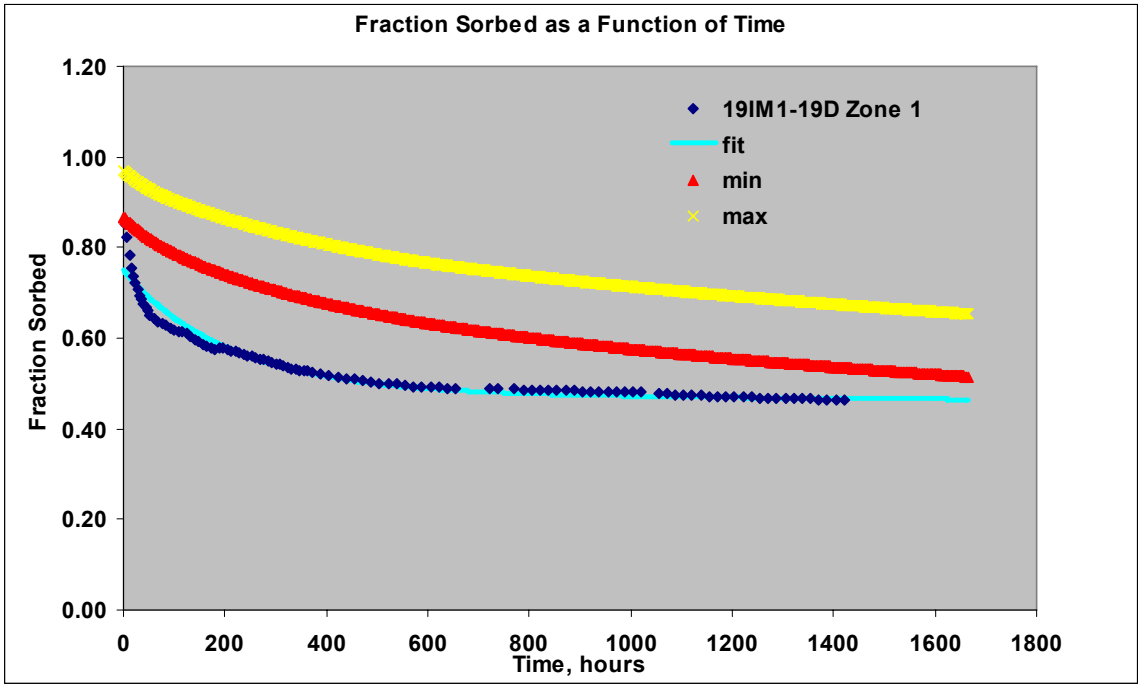

Source: DTN: LA0702CS150304.001 [DIRS 181314].

NOTE: The red and yellow curves were calculated with the explicit kinetic model using a single $K_{f,min}$ or $K_{f,max}$ value (calculated from Equation J-5) in conjunction with the average K_r values from each of the 4 mass fraction bins assumed in the binned approach. The blue model curve (fit) was generated using the explicit kinetic model and allowing K_f and K_r to vary for each of the 4 mass fraction bins to obtain a best fit to the experimental data.

Figure J-2. Fraction of Neptunium Sorbed to 19IM1A Alluvium in 19D Zone 1 Groundwater as a Function of Time

J5. CONCLUSIONS

The long-term uranium and neptunium desorption experiments described in this appendix show quite convincingly that (1) there are a variety of sorption sites on Yucca Mountain alluvium having varying sorption affinities and (2) the K_d values obtained from batch sorption experiments tend to be biased low because they do not account for the slower desorption rates associated with the higher affinity sorption sites. The $K_{d,eff}$ values estimated from the desorption experiments are not factored into the development of the uranium and neptunium K_d distributions of Appendix A. Use of the $K_{d,eff}$ would introduce inconsistencies relative to the K_d distributions for other radionuclides and also for uranium and neptunium in the saturated volcanics (for which similar desorption experiments have not been conducted). However, the $K_{d,eff}$ values serve to show that

the K_d distributions from Appendix A should tend to underpredict radionuclide retardation factors if strong sorption sites and slow desorption behavior are accounted for. The experimental results also suggest that the explanation for smaller effective K_d values observed in some column experiments as compared to batch sorption K_d values (Appendix G) will ultimately result in K_d values that are predicted to be larger than batch sorption K_d values if the explanation is extrapolated to long enough time and distance scales.

Additionally, the desorption experiments demonstrated that both uranium and neptunium sorb more strongly and desorb more slowly in solutions with lower carbonate/bicarbonate concentrations and onto alluvium with higher smectite and clinoptilolite contents. These observations are not factored explicitly into the uranium and neptunium K_d distributions of Appendix A, although the batch experiments upon which the distributions are based had similar variations in water chemistry and alluvium mineralogy. The $K_{d,eff}$ values presented in this appendix indicate that the Appendix A distributions have plenty of margin at the lower end to account for the possibility of unfavorable uranium and neptunium sorption conditions (high carbonate water, low smectite/clinoptilolite alluvium) present in alluvium flow pathways.

APPENDIX K
QUALIFICATION OF DIFFUSION COEFFICIENTS INPUT TO PARTICLE TRACKING IN STOCHASTIC MODELING FOR UPSCALING OF K_d DISTRIBUTIONS IN THE VOLCANICS

K1. PURPOSE

This report documents the findings of the data qualification team assembled to evaluate selected unqualified hydrology data that were used in the characterization of transport processes in the saturated zone at Yucca Mountain, Nevada. These data are qualified for inclusion in this report, which supports total system performance assessment (TSPA) model/analysis for the license application. This activity has been planned and implemented in accordance with SCI-PRO-001, *Qualification of Unqualified Data*. The data qualification plan is presented at the end of this appendix.

K2. QUALIFICATION TEAM

Chairperson Sharad Kelkar has 25 years experience in the area of flow and transport through geological media. He has been a member of the Hydrology, Geochemistry, and Geology group at LANL since 1985. In 2002, Mr. Kelkar began his ongoing role as a principal scientist with the Yucca Mountain Project (YMP), where he is responsible for modeling, analysis and documentation in support of the license application for the repository. Mr. Kelkar has contributed to the YMP in the development of FEHM, the code that forms a basis for the flow and transport modeling for the saturated zone. He has also worked on geothermal energy programs at Los Alamos National Laboratory (LANL). Prior to his association with LANL, he worked on laboratory and field testing and engineering analysis in support of petroleum production (Terra Tek Inc., Salt Lake City, Utah; 1982 to 1985) and laboratory and field testing in support of gas recovery programs (Institute of Gas Technology, Chicago, Illinois, 1979 to 1982). Mr. Kelkar received his M.S. degree in Petroleum Engineering from the University of Texas at Austin (1979) for measurements of poro-elastic properties of rocks at elevated pressures and temperatures. Mr. Kelkar earned his M.S. degree in Nuclear Physics from the University of Bombay (1974). In addition, Mr. Kelkar has done extensive coursework in hydrology and minerals engineering at the University of California, Berkeley.

Dr. Mei Ding earned a Ph.D. in 1998 in Geochemistry from the Utrecht University, the Netherlands, an M.S. in 1994 in Water Quality Management from the International Institute for Hydraulic and Environmental Engineering, the Netherlands, an M.S. in 1987 in Coordination Chemistry from Central South University and Technology, China, and a B.S. in 1984 in Analytical Chemistry from Central South University and Technology, China. Dr. Mei Ding has worked on the YMP for over seven years, and she has served as co-originator for saturated zone laboratory transport testing, and provided technical support for performance assessment and site characterization efforts as contributor for the saturated zone transport model report, and as technical reviewer and checker for *KTI (Key Technical Issues) of K_ds in Saturated Alluvial*. Dr. Ding's professional experience includes laboratory-scale solute (radioactive and nonradioactive) adsorption and desorption experiments. In addition to her Yucca Mountain work, Dr. Mei Ding has served as the co-originator for an existing OST&I project addressing radionuclide retardation in Yucca Mountain alluvial and volcanics. She is also the principal investigator for "Pu(VI) reduction by metallic iron/aluminum in the presence of alpha-radiolysis by-product in Waste Isolation Pilot Plan brines", and principal investigator for "Chemical environments and latent debris effects on the Post-Loss-Of-Coolant-Accident (LOCA) (funded by the NRC)," and the co-principal investigator for "the data assessment team for Water Stewardship Program at LANL."

K3. DESCRIPTION OF THE DATA TO BE QUALIFIED

Data evaluated and documented in this qualification report are from DTN: LA0003JC831362.001 [DIRS 149557]. These data are shown in Table K-1.

Table K-1. Values of Diffusion Coefficients Used for Particle-tracking Calculations in Stochastic Modeling for Upscaling of K_d Distributions in the Volcanics

Radionuclide	Diffusion Coefficient (m^2/s)
Anion (uranium)	3.2×10^{-11}
Cation (plutonium, cesium, neptunium)	1.6×10^{-10}

Source: DTN: LA0003JC831362.001 [DIRS 149557].

K4. QUALIFICATION METHOD AND EVALUATION CRITERIA

The method used to qualify the data in this report is corroborating data (SCI-PRO-001, Attachment 3, Method 2). The confidence in the data is in question because data collection procedures are unavailable for review.

A comparison of the unqualified data and available qualified corroborating data will be conducted to determine that the unqualified data is acceptable and confidence in the data is established.

The team conducted the comparison by considering the importance of the data to showing that the proposed U.S. Department of Energy repository design meets the performance objectives.

The following data qualification attributes will be used:

1. Extent and quality of corroborating data
2. Agreement between the data being qualified and the corroborating data
3. The importance of the data to showing that the proposed U.S. Department of Energy repository design meets the performance objectives of 10 CFR 63 [DIRS 180319].

K5. EVALUATION RESULTS

The corroborating data, shown in Table K-2, are taken from DTN: SN0310T0502103.009 [DIRS 168763]. Details of this analysis are presented in *Saturated Zone Flow and Transport Model Abstraction* (SNL 2007 [DIRS 181650], Section 6.5.2.6). As discussed there, and in Section 4.1.2.10, this range was developed based on experimental data and theoretical considerations influencing the process of matrix diffusion in porous media.

Table K-2. Range of Values of Diffusion Coefficients Used for Corroboration

	Diffusion Coefficient (m^2/s)
Lower Limit	5×10^{-12}
Upper Limit	15×10^{-10}

Source: DTNs: LA0003JC831362.001 [DIRS 149557], SN0310T0502103.009 [DIRS 168763].

The values of diffusion coefficients given in Table K-1 are within the range prescribed for comparison.

K6. CONCLUSION

The qualification team determined, based on the discussions above, that the referenced data are both reasonable and appropriate for the application. This evaluation did not produce any new data. The data qualification effort documented in this report was performed in accordance with the requirements of the approved Data Qualification Plan included in this appendix. The approved qualification method, corroborating data, was implemented as required. As a result of this qualification evaluation, these data are qualified for use in the report.

YMP

Data Qualification Plan

Complete only applicable items.

QA: QA
Page 1 of 1

Section I. Organizational Information

Qualification Title

Qualification of diffusion coefficients input to particle tracking in Stochastic Modeling For Upscaling Of K_D Distributions in the Volcanics

Requesting Organization

LANL

Section II. Process Planning Requirements

1. List of Unqualified Data to be Evaluated

of Diffusion Coefficients Used for the Particle-Tracking Calculations

Anion (Uranium): 3.2 x 10-11 m2/s
Cation (Plutonium, Cesium, Neptunium): 1.6 x 10-10 m2/s
Source DTN: LA0003JC831362.001 [DIRS 149557].

2. Type of Data Qualification Method(s) [Including rationale for selection of method(s) (Attachment 3) and qualification attributes (Attachment 4)]

Method: Corroborating Data

Rationale:

a. Corroborating data are available for comparison with the unqualified data set(s).
b. Inferences drawn to corroborate the unqualified data can be clearly identified, justified, and documented.

Qualification Attributes: Extent and quality of corroborating data

3. Data Qualification Team and Additional Support Staff Required

Sharad Kelkar, Mei Ding

4. Data Evaluation Criteria

Data to be qualified shall fall within the range of the corroborating data.

5. Identification of Procedures Used

SCI-PRO-001 Rev1

6. Plan coordinated with the following known organizations providing input to or using the results of the data qualification

N/A

Section III. Approval

Qualification Chairperson Printed Name	Qualification Chairperson Signature	Date
Sharad Kelkar	Sharad Kelkar	5/16/2007
Responsible Manager Printed Name	Responsible Manager Signature	Date
Stephanie Kuzio		5/16/2007

SCI-PRO-001.1-R1

APPENDIX L
QUALIFICATION OF UNQUALIFIED EXTERNAL SOURCES

This appendix presents the qualifications of external unqualified data used as direct input in Table 4-1, "Input Data and Technical Information."

L1. SURFACE AREA DATA FROM ALLARD ET AL. 1980 [DIRS 104410] AND EXPERIMENTAL DATA FOR THE BINDING OF AMERICIUM ON SILICA BY BEALL ET AL. 1986 [DIRS 162983]

Data Qualification Methods: SCI-PRO-001, Attachment 3, Method 5.

Data Qualification Attributes: SCI-PRO-001, Attachment 4, Attributes 1, 3, and 8.

Discussion: These data were used for calculating americium sorption coefficient over the range of geochemical conditions expected to occur at the Yucca Mountain repository. The calculations were conducted using the geochemical code PHREEQC V2.3 (STN: 10068-2.3-01 [DIRS 157837]). Site-specific americium sorption coefficient data are available only for J-13 well water. To evaluate the impact of variations in groundwater compositions on americium sorption coefficients, a surface complexation modeling exercise was carried out. In order to model americium surface complexation reactions with PHREEQC, one or more surface species must be selected along with appropriate binding constants for these species. The surface species and binding constants were obtained through an inverse approach where experimental data for the binding of americium on silica presented by Beall et al. (1986 [DIRS 162983]) were fit with a surface complexation model using the surface area reported by Allard et al. (1980 [DIRS 104410]). Two americium surface species and their binding constants were derived in fitting the data. These species and binding constants were then used to evaluate the water compositional dependence of americium sorption coefficients on silica.

The americium sorption coefficient data presented by Beall et al. were published in a paper titled "Americium Speciation and Distribution Coefficients in a Granitic Water," published in Scientific Basis for Nuclear Waste Management IX, a symposium held September 11, 1985, in Stockholm, Sweden. Dr. Beall is a Professor of Chemistry at Texas State University. He received his Ph.D. in Physical Chemistry from Baylor University and has more than 20 years of experience in research and development. The surface area measurement on silica was published in a paper titled "The sorption of Actinides in Igneous Rocks," published in the journal *Nuclear Technology* (Volume 49, pp. 474 and 480). Articles submitted to this journal are peer reviewed. Dr Allard is a professor of Chemistry/Environmental Sciences at Orebro University, Sweden; and a member of the Royal Swedish Academy of sciences, and has extensive background in radiochemistry and measurement of sorption coefficients on silicate rocks.

Decision: The americium sorption coefficient data is deemed reliable and appropriate for use in modeling americium sorption behavior in Yucca Mountain samples.

L2. SORPTION COEFFICIENT DATA FOR PROTACTINIUM ON SILICA IN A SIMPLE ELECTROLYTE BY ALLARD ET AL. 1983 [DIRS 162982]

Data Qualification Methods: SCI-PRO-001, Attachment 3, Method 5.

Data Qualification Attributes: SCI-PRO-001, Attachment 4, Attributes 1, 3, and 8.

Discussion: The available data on site-specific sorption coefficients for protactinium are very limited. Further, the available data were not obtained under conditions (i.e., pH values) expected in the saturated zone. These data were obtained over a range of pH values that is directly applicable to the saturated zone at Yucca Mountain. The protactinium sorption coefficient data presented by Allard et al. (1983 [DIRS 162982]) were published in a paper titled, "Sorption Behavior of Actinides in Well-defined Oxidation States," published by the Swedish Nuclear Fuel and Waste Management Company (SKB). The work of SKB is well respected in the international nuclear waste community. Dr Allard is a professor of Chemistry/Environmental Sciences at the Orebro University, Sweden; and a member of the Royal Swedish Academy of sciences, and has extensive background in radiochemistry and measurement of sorption coefficients on silicate rocks.

Decision: The protactinium sorption coefficient data is deemed reliable and appropriate for use in modeling americium sorption behavior in Yucca Mountain samples.

L3. SURFACE SPECIES AND BINDING CONSTANTS FOR URANIUM SORPTION ON SILICA BY PABALAN ET AL. 1998 [DIRS 162987]

Data Qualification Methods: SCI-PRO-001, Attachment 3, Method 5.

Data Qualification Attributes: SCI-PRO-001, Attachment 4, Attributes 1, 3 and 8.

Discussion: Site-specific sorption coefficient data for uranium have been obtained for the major rock types and a range of water compositions. To obtain a more complete understanding of the relationship between uranium sorption and variations in water composition, modeling calculations were carried out using the code PHREEQC. As part of the input to the PHREEQC surface complexation model, surface species must be selected along with appropriate binding constants for these species. The paper by Pabalan et al. (1998 [DIRS 162987]) was published in a volume titled, "Adsorption of Metals by Geomedia" by the Academic Press. This volume presented state-of-the-art understanding of the sorption behavior of metals in geomedia at the time it was published. Dr. Pabalan received his Ph.D. from University of California at Berkeley, and has published extensively in the field of geochemistry. The work described in the paper was carried out by the authors while at the Center for Nuclear Waste Regulatory Analysis (CNWRA) under contract with the U.S. Nuclear Regulatory Commission (NRC). CNWRA conducts its work under NQA-1 base QA program and is accepted by the NRC.

Decision: The uranium surface species and binding constants reported by Pabalan et al. (1998 [DIRS 162987]) are judged to be reliable and appropriate for use in modeling uranium sorption behavior on silica.

L4. SURFACE SPECIES, BINDING CONSTANTS, AND SITE DENSITY FOR NEPTUNIUM SORPTION ON SILICA BY TURNER ET AL. 1998 [DIRS 162989]

Data Qualification Methods: SCI-PRO-001, Attachment 3, Method 5.

Data Qualification Attributes: SCI-PRO-001, Attachment 4, Attributes 1, 3, and 8.

Discussion: Site-specific sorption coefficient data for neptunium have been obtained for the major rock types and a range of water compositions. To obtain a more complete understanding of the relationship between neptunium sorption and variations in water composition, modeling calculations were carried out using the code PHREEQC. As part of the input to the PHREEQC surface complexation model, surface species must be selected along with appropriate binding constants for these species and site densities. The article by Turner et al. (1998 [DIRS 162989]) was peer reviewed prior to being published. The work described in the paper was carried out by the authors while at CNWRA under contract with the NRC. CNWRA conducts its work under NQA-1 base QA program and is accepted by the NRC.

Decision: The neptunium surface species and binding constants reported by Turner et al. (1998 [DIRS 162989]) is judged to be reliable and appropriate for use in modeling neptunium sorption behavior in the Yucca Mountain flow system.

L5. DERIVED ACIDITY CONSTANTS FOR SILICA SURFACES BY DIXIT AND VAN CAPPELLEN 2002 [DIRS 162985]

Data Qualification Methods: SCI-PRO-001, Attachment 3, Method 5.

Data Qualification Attributes: SCI-PRO-001, Attachment 4, Attributes 1, 3, and 8

Discussion: As part of the input to the PHREEQC surface complexation model, acidity constants are required for the chosen solid surface (silica). These acidity constants quantify the binding of hydrogen ions to the solid surface. The article by Dixit and Van Cappellen (2002 [DIRS 162985]) was peer reviewed prior to being submitted to the journal, *Geochimica et Cosmochimica Acta*. The journal is published by The Geochemical Society, which is a premier source of information to the international geochemical community. Dr. van Cappellen earned a PhD from Yale University and is a Professor of Geochemistry at Utrecht University, Netherlands.

Decision: The surface acidity constants reported by Dixit and Van Cappellen (2002 [DIRS 162985]) are judged to be reliable and appropriate for use in PHREEQC surface complexation modeling on silica.

L6. BINDING CONSTANT FOR SODIUM ON SILICA SURFACES BY MARMIER ET AL. 1999 [DIRS 162986]

Data Qualification Methods: SCI-PRO-001, Attachment 3, Method 5.

Data Qualification Attributes: SCI-PRO-001, Attachment 4, Attributes 3 and 8.

Discussion: In modeling surface complexation reactions, competition among species in solution for surface sites, and in particular, competition from the major cations in solution, must be considered. In order to include such competitive effects, binding constants for the major cations on the chosen surface (silica) are required. The article by Marmier et al. (1999 [DIRS 162986]) was peer reviewed prior to being published in *Journal of Colloid and Interface Science*, which is a premier source of information to the international surface science community

Decision: The binding constant for sodium on silica reported by Marmier et al. (1999 [DIRS 162986]) is judged to be reliable and appropriate for use in PHREEQC surface complexation modeling on silica.

APPENDIX M
QUALIFICATION OF DTN: SN0705FLUORINE.001, REVISION 1

M1. DATA SET TO BE QUALIFIED

The data set to be qualified is DTN: SN0705FLUORINE.001 [DIRS 182006], which contains the fluoride analytical data for fluoride, for the depth interval 381 to 1,197 m below ground surface, collection date 02/09/1983, as reported by Benson and McKinley (1985 [DIRS 101036], Table 1) for UE-25p#1. Benson and McKinley (1985 [DIRS 101036], Table 1) reported values for two samples from borehole UE-25-p#1; one representing the depth range 381 to 1,197 m, and the other 1,297 to 1,805 m. The shallower sample is of interest here because the flow paths developed in Section 6.5 are shallow.

M2. METHOD OF QUALIFICATION AND EVALUATION CRITERION

The method of qualification is Method 2 of SCI-PRO-001, Attachment 3: Corroborating Data. This method was used because corroborating data are available. The evaluation criterion used was: if the value to be qualified falls within one standard deviation of the mean of the representative measurements used for corroboration, the value will be accepted as qualified for use as an input for PHREEQC modeling documented in Appendix A.

M3. IDENTIFICATION OF REPRESENTATIVE MEASUREMENTS USED FOR CORROBORATION

Saturated Zone Site-Scale Flow Model (SNL 2007 [DIRS 177391], Tables A4-3 and B4-1) summarizes data sources from approximately 240 boreholes near Yucca Mountain, including the borehole locations (SNL 2007 [DIRS 177391], Figures A6-5 and B6-3). Analyses of groundwater from these 240 samples are also shown in *Saturated Zone Site-Scale Flow Model* (SNL 2007 [DIRS 177391], Tables A6-1 and B4-2). Fluoride data from these samples were used for corroboration if they met the following criteria:

1. Water was sampled from a Tertiary volcanic (not alluvial) unit

2. Data do not duplicate other results

3. Sample location is along a flowpath in, near, or downgradient from Yucca Crest (the Yucca Mountain repository footprint). This region is approximately bounded to the north by the repository site, to the south by US Highway 95, to the east by Fortymile Wash, and to the west by Crater Flat.

Forty samples meet these criteria, as summarized in Table M-1. The mean and standard deviations of fluoride concentration of these samples are 2.5 and 1.2 mg/L.

M4. EVALUATION RESULTS

The value to be qualified, 3.4 mg/L, meets the criterion set by the data qualification plan included in this appendix by falling within the range of 2.5 to 2.5 plus 1.2 mg/L. Therefore, DTN: SN0705FLUORINE.001 [DIRS 182006] is qualified for use as an input for PHREEQC modeling documented in Appendix A.

Table M-1. Fluoride Concentrations in Groundwater Collected from Tertiary Volcanic Rocks in the Vicinity of Yucca Mountain

Sample #	Well Name	Hydrochemical Subarea	Geologic Unit[a]	F (mg/L)	Original Data Sources[b]
35	J-13	Fortymile Wash - North	Tpt, Tct, Tlr	2.4	GS930308312323.001 [DIRS 145530]
36	J-12	Fortymile Wash - North	Tpt	2.1	GS930308312323.001 [DIRS 145530]
37	JF#3	Fortymile Wash - North	Tv	1.6	GS930908312323.003 [DIRS 145404]
38	H-6(bh)	Solitario Canyon Wash	Tcb/Tct	4.7	GS930308312323.001 [DIRS 145530]
39	H-6(Tct)	Solitario Canyon Wash	Tct	3.9	GS930308312323.001 [DIRS 145530]
40	H-6(Tcb)	Solitario Canyon Wash	Tcb	4.7[c]	GS930308312323.001 [DIRS 145530]
42	WT-10	Solitario Canyon Wash	Tpt	3.7	LA0311EK831232.001 [DIRS 166068]
43	G-2	Yucca Mountain - Crest	Tpt, Tac	1.0	LA0311EK831232.001 [DIRS 166068]
47	H-1(Tcp)	Yucca Mountain - Crest	Tcp	1.2	GS930308312323.001 [DIRS 145530]
48	H-1(Tcb)	Yucca Mountain - Crest	Tcb	1.0	GS930308312323.001 [DIRS 145530]
49	H-5	Yucca Mountain - Crest	Tcb/Tct	1.4	GS930308312323.001 [DIRS 145530]
51	H-3	Yucca Mountain - Crest	Tct	5.5	Benson and McKinley 1985 [DIRS 101036]
52	G-4	Yucca Mountain - Central	Tct	2.5	GS930308312323.001 [DIRS 145530]
53	B#1(Tcb)	Yucca Mountain - Central	Tcb	1.6 [c]	GS930308312323.001 [DIRS 145530]
54	B#1(bh)	Yucca Mountain - Central	Th/Tct	1.6	GS930308312323.001 [DIRS 145530]
55	H-4	Yucca Mountain - Central	Tcb/Tct	4.6	GS930308312323.001 [DIRS 145530]
58	c#1	Yucca Mountain - Southeast	Tcb/Tct	2.1	Benson and McKinley 1985 [DIRS 101036]
59	c#3	Yucca Mountain - Southeast	Tcb/Tct	2.0	Benson and McKinley 1985 [DIRS 101036]
61	c#2	Yucca Mountain - Southeast	Tcb	2.1	Benson and McKinley 1985 [DIRS 101036]
62	p#1(v)	Yucca Mountain - Southeast	Tuff	3.4	Benson and McKinley 1985 [DIRS 101036]
64	WT-17	Yucca Mountain - Southeast	Tcp	2.0	GS980908312322.008 [DIRS 145412]
65	WT#3	Yucca Mountain - Southeast	Tcb	2.3	GS980908312322.008 [DIRS 145412]
66	WT#12	Yucca Mountain - Southeast	Tpt/Tac	3.1	SNL 2007 [DIRS 177391], Table A6-1
68	GEXA Well 4	Crater Flat	Tv	3.2	SNL 2007 [DIRS 177391], Table A6-1
69	VH-1	Crater Flat	Tcb	2.7	GS930308312323.001 [DIRS 145530]
70	VH-2	Crater Flat - Southwest	Tv	1.1	LA0311EK831232.001 [DIRS 166068]
75	NC-EWDP-01S Zone 1	Crater Flat - Southwest	Tertiary welded tuff	0.6 [c]	GS010308312322.003 [DIRS 154734]
76	NC-EWDP-01S Zone 2	Crater Flat - Southwest	Tertiary welded tuff	0.6 [c]	GS010308312322.003 [DIRS 154734]
77	NC-EWDP-01S	Crater Flat - Southwest	Tertiary welded tuff	0.6	GS010308312322.002 [DIRS 162910]

Table M-1. Fluoride Concentrations in Groundwater Collected from Tertiary Volcanic Rocks in the Vicinity of Yucca Mountain (Continued)

Sample #	Well Name	Hydrochemical Subarea	Geologic Unit[a]	F (mg/L)	Original Data Sources[b]
78	NC-EWDP-12PA	Crater Flat - Southwest	Tertiary reworked tuff	4.1	GS011108312322.006 [DIRS 162911]
79	NC-EWDP-12PB	Crater Flat - Southwest	Tertiary reworked tuff	4.2	GS011108312322.006 [DIRS 162911]
84	NC-EWDP-9SX Zone 3	Yucca Mountain - South	Tertiary tuff	2.2	GS010308312322.003 [DIRS 154734]
85	NC-EWDP-9SX Zone 4	Yucca Mountain - South	Tertiary tuff	2.1	GS010308312322.003 [DIRS 154734]
87	NC-EWDP-3S Zone 2	Yucca Mountain - South	Tertiary tuff and sediments	3.0	GS010308312322.003 [DIRS 154734]
88	NC-EWDP-3S Zone 3	Yucca Mountain - South	Tertiary tuff and sediments	4.2	GS010308312322.003 [DIRS 154734]
89	CIND-R-LITE	Yucca Mountain - South	Tv	2.5	LA0311EK831232.001 [DIRS 166068]
205	NC-EWDP-07SC Zone 3	Crater Flat - Southwest	Tmr	0.8[c]	LA0612RR150304.003 [DIRS 179438]
206	NC-EWDP-07SC Zone 4	Crater Flat - Southwest	Tmr	0.8	LA0612RR150304.003 [DIRS 179438]
213	NC-EWDP-16P composite	Yucca Mountain - South	Tmr	2.7	LA0612RR150304.003 [DIRS 179438]
214	NC-EWDP-18P composite	Yucca Mountain - South	Tpts	2.5	LA0612RR150304.003 [DIRS 179438]
215	NC-EWDP-19D Zones 5-7	Yucca Mountain - South	Tpt, Tpts, Tge	2.2	LA0612RR150304.003 [DIRS 179438]
221	NC-EWDP-IM1 Zone 5	Yucca Mountain - South	Tpt	2.1	LA0612RR150304.003 [DIRS 179438]
236	NC-EWDP-24P	Yucca Mountain - South	Tcb	2.2	LA0612RR150304.003 [DIRS 179438]
237	NC-EWDP-27P	Yucca Mountain - South	Tpt	3.7	LA0612RR150304.003 [DIRS 179438]
238	NC-EWDP-28P	Yucca Mountain - South	Tma, Tmabt	2.1	LA0612RR150304.003 [DIRS 179438]
239	NC-EWDP-29P	Yucca Mountain - South	Tpc, Tpbt4	2.1	LA0612RR150304.003 [DIRS 179438]

Source: SNL 2007 [DIRS 177391], Appendices A and B. Fluoride data from Tables A6-1 and B4-2. Sample numbers, well names, hydrochemical subareas to which sampled wells are assigned (based on geographic and geochemical similarities), and geologic units for the sampled depth intervals are listed in Tables A4-3 and B4-1.

NOTE: Gray-shaded row is the data being corroborated.

[a] Geologic units: Tac—Tertiary Calico Hills Formation, Tcb—Tertiary Bullfrog Member of Crater Flat tuff, Tcp—Tertiary Prow Pass Member of Crater Flat tuff, Tct—Tertiary Crater Flat tuff, Tge—Prevolcanic Tertiary sedimentary rocks, Th—Tertiary tuffaceous beds of Calico Hills, Tlr—Tertiary Lithic Ridge tuff, Tma—Tertiary Ammonia Tanks tuff, Tmabt—Tertiary pre-Ammonia Tanks bedded tuff, Tmr—Tertiary Rainier Mesa tuff, Tpbt4—pre-Tiva Canyon Tuff bedded tuff, Tpc—Tertiary Tiva Canyon tuff, Tpt—Tertiary Topopah Spring Member of Paintbrush tuff, Tpts—Tertiary pre-Topopah Spring sedimentary rocks, Tv—Tertiary volcanic rocks.

[b] For samples 35 to 89, the original data sources listed in this column are as listed in Table A4-3 of LANL 2007. For samples 205 to 239, data are from DTN: LA0612RR150304.003 [DIRS 179438].

[c] These samples are listed in this table because the samples meet the selection criteria. However, they are not included in the calculated mean and standard deviation because they are considered duplicates of the locations represented by other samples in this table.

Data Qualification Plan

Complete only applicable items.

QA: QA

Page 1 of 1

Section I. Organizational Information

Qualification Title

Qualification of Fluorine Abundance Data from UE-25 p#1 taken February 9, 1983

Requesting Organization

Los Alamos National Laboratory

Section II. Process Planning Requirements

1. List of Unqualified Data to be Evaluated

Data contained in DTN: SN0705FLUORINE.001 Revision 1

ROW#	FLUORINE ABUNDANCE mg/L	LOCATION	DATE
1	3.4	UE-25 p #1	02/09/1983

2. Type of Data Qualification Method(s) [Including rationale for selection of method(s) (Attachment 3) and qualification attributes (Attachment 4)]

Corroborating data (SCI-PRO-001, Attachment 3, Method 2)
Rationale for selection of method
a. Corroborating data are available for comparison with the unqualified data set.
b. Inferences drawn to corroborate the unqualified data can be clearly identified, justified, and documented.
Qualification Attributes: Extent and quality of corroborating data

3. Data Qualification Team and Additional Support Staff Required

Sharad Kelkar, Qualification Chairperson
Peter Persoff

4. Data Evaluation Criteria

Representative fluoride concentrations in groundwaters will be identified. The range, mean, and standard deviation corresponding to these measurements will be calculated. The data in SN0705FLUORINE.001 will be accepted as qualified for the purpose of use in MDL-NBS-HS-000010 Rev 03 if the value in that DTN falls within one standard deviation of the mean of the corroborating values.

5. Identification of Procedures Used

SCI-PRO-001 Qualification of Unqualified Data
SCI-PRO-006 Models

6. Plan coordinated with the following known organizations providing input to or using the results of the data qualification

This plan is not coordinated with any organization other than Performance Assessment, Natural Systems.

Section III. Approval

Qualification Chairperson Printed Name	Qualification Chairperson Signature	Date
Sharad Kelkar	Sharad Kelkar	7/18/07
Responsible Manager Printed Name	Responsible Manager Signature	Date
Stephanie Kuzio for	Kenneth Rehfeldt	7/18/2007

SCI-PRO-001.1-R1